TELSTAR I

400p.

NASA SP-32
VOLUME 1
JUNE 1963

Contents: 13 analyses

NATIONAL AERONAUTICS AND SPACE ADMINISTRATION
GODDARD SPACE FLIGHT CENTER

Preface

NASA Special Publication SP-32 is being published in accordance with the cooperative agreement executed on July 27, 1961 between the National Aeronautics and Space Administration and the American Telephone and Telegraph Company for the development and experimental testing of active communications satellites.

This report consists of four volumes. The first three are composed of papers originally published together as a regular issue of the Bell System Technical Journal. The fourth volume, to be published at a later date, will contain pertinent papers contributed by various authors at the NASA Goddard Space Flight Center; the General Post Office of the United Kingdom; the Centre National d'Etudes des Telecommunications, France; and Telespazio, Italy.

Contents:

Contents, Part 1*

*Contents for Parts 2 and 3 of this issue will be found in front of each of these parts.

The *Telstar* Experiment

By A. C. DICKIESON

(Manuscript received February 6, 1963)

The papers that follow describe in depth the satellite and ground systems designed for the Telstar experiment and give the results to date. The purpose of this introduction is to set the scene in which the project was undertaken and to state some general conclusions.

Bell System interest in satellite communication had been aroused when in 1955, Dr. John R. Pierce published calculations showing the possible usefulness of satellites to communication. Dr. Pierce discussed the relations among power, bandwidth, antenna gain, and orbit parameters. Sputnik in 1957 started the procession of man-made satellites.

In 1960, with the launching of a large aluminum-coated balloon by the National Aeronautics and Space Administration, the famous Echo experiments[1] were conducted between a transmitting and receiving station set up by Bell Telephone Laboratories at Holmdel, New Jersey, and a companion station at Goldstone, California, designed and operated by Jet Propulsion Laboratory.

The Echo experiments produced the first two-way telephone conversations via satellite. They also confirmed predictions of the radio path loss to be encountered, the stability of the radio medium, and the low noise picked up by a well designed antenna pointing at the sky.

These results were studied at Bell Laboratories in the context of the Bell System's long-term interest in overseas communication. The first New York-London commercial voice circuit was established by long-wave radio in 1927 and was followed by short-wave (HF) circuits in 1929. Over the years, a network of some 240 radio circuits has been constructed, connecting the United States to 140 countries.

By the end of the late 1940's it had become evident that the frequency space available in the HF range was not sufficient to support the volume

of worldwide communication that was developing. It was clear also that because of physical limitations inherent in the very nature of the radio transmission medium, the reliability and quality of the resultant telephone circuits would leave something to be desired.

At this time the development of repeatered, multi-channel submarine cable was pressed forward. The first transatlantic cable of this type was placed in service in 1956,[2] followed in rapid succession by many others. The submarine cable network is expanding rapidly, providing high quality and reliable communication service.

The Echo experiments opened the possibility of applying microwave radio relay technology to transoceanic links. The line-of-sight transmission characteristic of microwaves had prevented their use over the oceans until the possibility of a "microwave repeater in the sky" appeared.

As we studied the problem of satellite communication, it became apparent that we had most of the tools to do the job in the fruits of previous research and development in widely scattered fields. Transistors and diodes, solar cells, low-noise maser amplifiers, long-lived traveling-wave tubes, horn-reflector antennas, FM-feedback receivers — these and other essential tools were available.

It was recognized that there was a long step in development needed to fit these essential but separate elements into a coordinated working system. Also, numerical knowledge of the characteristics and magnitude of radiation in the Van Allen belt was not adequate as a basis for design of a long-lived satellite.

It was decided, therefore, to design and build an experimental satellite communication system. To this end, the A.T.&T. Co. entered into a cooperative agreement with NASA; A.T.&T. to design and construct a satellite and NASA to launch it into space, with A.T.&T. paying its own costs plus reimbursing NASA for the cost of launching and for certain tracking and telemetry services.

In setting the objectives for the experiment, the desideratum was the simplest experiment that would answer the really critical questions, leaving until a later round of design the optimization of trade-offs and the development and construction of a commercial operating system. Thus, the objectives were:

1. To look for the unexpected.

2. To demonstrate the transmission of multichannel two-way telephony, television, data and facsimile via satellite.

3. To build a very large ground station antenna and find out how to point its extremely sharp beam very accurately at the satellite.

4. To gain a firm understanding of the problems of measuring orbital parameters and predicting satellite positions.

5. To gain a better numerical knowledge of the character and intensity of radiation in the Van Allen belt.

6. To face the problems of designing for long life and reliability of electronic equipment for operation in the space environment.

It was decided to install a microwave repeater in the satellite. While the passive reflector of the Echo type has advantages, calculations indicated that the transmitter power required for television bandwidths would be excessive unless balloons of a size well beyond the present state of the art were used.

Study of available boosters led to the Delta configuration of the Thor as the simplest and most reliable rocket for these purposes. Its relatively limited lifting capacity set a bound of about 180 pounds for a useful orbit. This was established as: apogee 3450 miles, perigee 575 miles, inclination to equator 45°. The apogee is high enough to give good mutual visibility between northeastern United States and western Europe. Calculations for a working worldwide system indicate the desirability of circular orbits at 6000–8000 mile elevations; however, these were not achievable with the Delta vehicle.

The weight restriction now forced the decision to install only a single, one-way amplifier in the satellite, rather than two. This permits one full-band signal to be sent one way, or two (or more) narrow-band signals to be sent two ways. Also, the solar cell power supply capacity was limited to less than that required to operate all of the electronic circuits continuously. It was necessary, therefore, to use a nickel-cadmium storage battery to handle the peak loads, with means to turn the amplifier on and off by command from the ground.

If the satellite presented one face to the earth at all times, it would be possible to use directional antennas, with consequent gain in signal strength. While such arrangements exist as concepts, it was not practicable to apply them in this experiment. It was decided to stabilize the position of the satellite by spinning it around one axis, like a child's top. This fitted well into the Delta vehicle; the third stage of the Delta is a solid-fuel rocket which is spun during firing for reasons of stability and equalization of thrust. The payload is thus spinning at the time of ejection.

It was decided that the satellite antennas should receive and transmit circularly polarized waves, so as not to require polarization tracking by the ground system. Consideration of the geometrical relations between the earth and the spinning satellite in an inclined, elliptical orbit indi-

cated the desirability of omnidirectional antennas if communication is to be maintained unhampered at all times and places. Such a design is not possible; thus the design objective was to achieve the broadest coverage obtainable. Calculations indicated that with the antenna pattern attainable and with the satellite launched with its spin axis perpendicular to the sun line, its aspect with respect to locations in the northern hemisphere would be satisfactory for long periods.

To gain more numerical understanding of the distribution of radiation in the Van Allen belt, it was decided to include a rather complicated array of sensors and measuring devices in the satellite. Clearly, to return this information to earth required radio telemetry. Parts of some and all of other orbits are not visible from the BTL stations. Thus it was made part of the cooperative agreement with the National Aeronautics and Space Administration that their Minitrack stations around the world would collect telemetry from the satellite. For this reason, the telemetry frequency was chosen in the band around 136 mc for which the Minitrack stations were already equipped.

The necessity to turn the communication repeater on and off (because of power capacity limitations) established a need for a radio command channel. Further consideration of the over-all problem indicated the desirability of additional command capability. Since it seemed likely that it might be desirable for some Minitrack stations to issue commands, it was decided to use a frequency near 120 mc for this purpose, and to use a command format for which the Minitrack stations were equipped.

The choice of frequencies for the communications repeater was more complicated. Previous research had indicated that the preferred frequencies lie between 1000 and 10,000 mc. In the United States, and generally in the rest of the world, these frequencies have all been allocated for various terrestrial uses. The newcomer, satellite communication, has to work its way into this established pattern. This presents a complex international question which is not yet resolved.

In the meanwhile, though, it seemed most practical to assume that at least initially satellite communication of the Telstar type would have to share frequencies with terrestrial systems; hence it became important to examine the conditions of compatibility. After considerable study,[3] and consultation with various foreign communication agencies, it was concluded that for a start it was most practical to share frequencies with the point-to-point, common carrier microwave relay systems. These are the frequency bands 3700–4200 mc and 5925–6425 mc.

It was decided to use the 4000-mc band for the down direction, from satellite to ground, so as to minimize the deleterious effects of rain on the

received signal and noise. The 6000-mc band is used for the up direction. The wide frequency separation between the two directions simplifies sharing of the ground antenna and minimizes interference effects in the satellite. The A.T.&T.Co. applied for and received from the Federal Communications Commission research-experimental licenses for satellite and ground stations.

Sharing of frequencies with terrestrial systems had an effect on the choice of the site for the ground station. A location in the northeast part of the United States was wanted, so as to minimize the great circle distance to western Europe. Separation from large cities and from existing or probable microwave radio relay stations operating in the 4000- or 6000-mc bands was desirable.

Fairly flat ground was desired for the installation of initially one, and later several, large antennas. For best protection against interference, the site should be ringed by hills. Finally, the site should have road access, power, water, and living facilities nearby. All of these were found at a location near Andover, Maine.

Study of the over-all system parameters lead to the conclusion that a large ground antenna with minimum power in the satellite was the economical choice. Research work at the Bell Laboratories Holmdel Radio Research Laboratory had culminated in the construction of a horn-reflector antenna with 400 square feet of aperture. This was used very successfully in the Echo experiments. The particular virtue of the horn-reflector type is that it has very low side lobes; hence it does not pick up extraneous noise from the ground when it is pointed even a few degrees above the horizon. Besides being very broad-band, it can be designed so that the receiving equipment does not move with elevation motions of the horn.

It was decided to design and build a horn-reflector antenna with 3600 square feet of aperture. The very sharp beam of such an antenna would stretch our ability to point it accurately at the satellite. To preserve the accuracy of the antenna, and to permit it to operate in all kinds of weather (including the 90 inches of snow to be expected in Maine), an air-inflated covering or radome was added.

Study of the antenna-pointing problem led to the conclusion that the satellite should radiate a low-level microwave signal whenever the communications transmitter is turned on. This has two uses. It permits very precise tracking of the satellite, and hence accurate determination of its orbit. Also, it facilitates the design of an autotrack system that automatically optimizes the pointing of the ground antenna once its beam is placed on the satellite.

It was decided to design for tape-controlled pointing of the antenna, as well as for slaving to a small, precise autotracking dish. The objective was to acquire knowledge of the advantages and limitations of several methods of antenna pointing.

To receive telemetry at 136 mc, and to transmit commands at 120 mc, it was decided to construct a directional antenna with autotrack capability. This would lock on to the 136-mc telemetry carrier normally radiated from the satellite. The relatively broad beam (about 20°) of this antenna facilitates finding the satellite in space, even with quite crude orbit prediction. It was decided to arrange for slaving of the precision tracker to the command antenna, so that we could go through the sequence of acquiring the satellite with the 20° command antenna, having it direct the 2° beam of the precision tracker to the right position, and then have the precision tracker give instructions to the horn-reflector antenna.

To make the most of the very good noise performance of the horn-reflector antenna, the communications receiver was designed to use a traveling-wave maser operating in liquid helium. Also, to improve the breaking point of the receiver, (i.e., to permit the receiver to reach deeper into noise for very weak signals) the technique of FM-feedback is used. This method was invented at Bell Telephone Laboratories some years ago, and was applied very successfully in the Echo experiment.

Thus the main outlines of the Telstar experiment were established. The plans were discussed in considerable detail with the communication agencies in England, France and Germany. All three decided to build ground stations to work with Telstar; the German station was planned for operation in 1963 or 1964, while the British and French set it as an objective to be ready on or near the time of the first Telstar satellite launching. In the meanwhile, NASA discussions led to the agreement that the Bell System, British and French stations would be equipped to operate with Project Relay, along with other stations such as those planned in Italy, Brazil, and elsewhere. To simplify the hardware situation at the ground stations, it was agreed to have Project Relay use the same frequency plan as Telstar for the downward direction.

GENERAL CONCLUSIONS

The Telstar satellite was launched in the early morning of July 10, 1962. On the first pass usable from Andover, demonstrations were made of speech and television transmission. These transmissions were carried on between distinguished audiences in Washington, D.C., and

Andover, Maine. Also the first transmission of a telephoto picture was achieved. The procedure was also televised for the national networks. In the midst of this program, word was received that the French station at Pleumeur-Bodou was receiving picture and sound perfectly. The British station at Goonhilly was receiving the signal, but was not able to utilize it because of a turnover in polarization at the antenna.

On the next pass, six two-way telephone circuits were set up through the Telstar system, and various people in Washington and Andover talked to people around the United States. Also, high-speed data messages were sent successfully. On the next day, television signals were received from Pleumeur-Bodou and Goonhilly.

In the next several months, in addition to more than 250 technical tests covering every aspect of transmission, there were some 400 demonstrations. These included multi-channel telephony, telegraphy, data, telephoto and other facsimile transmissions. Transatlantic television was demonstrated 47 times, and on 5 of these occasions the transmission was in color. At the same time, a great deal of telemetry data were received, covering conditions in the Van Allen belt, temperatures, degradation of the solar cell plant, spin rate, voltages, etc.

During the fourth week of November, 1962, the command channel began to act erratically. Increasing difficulty was encountered in having it accept commands. Since it seemed possible that control might be lost, arrangements were made to leave the telemetry on continuously rather than switching it on and off. Also, the traveling-wave tube was not energized at all, lest loss of control should leave this heavy drain on continuously and thereby ruin the batteries. After the 1242nd orbit on November 23, 1962, the command channel ceased responding.

It was known from previous studies[4] that radiation may produce important effects on transistors. Telstar telemetry data indicated that the density of electrons of high energy was much higher than had been anticipated. The working hypothesis was formed that the command circuit failure was caused by radiation damage to certain of the transistors in the command decoder. Careful study of previous data indicated that one of the two command decoders had failed in August of 1962.

During November, our command stations in the northern hemisphere were addressing the Telstar satellite near the perigee of its orbit, while it was traversing the worst part of the Van Allen belt. The possibility existed that the radiation damage effects would be less serious while the satellite was nearer apogee. Thus attempts were made to command the satellite from the Minitrack station at Johannesburg, South Africa, but without success.

In the meanwhile, laboratory tests had pointed to certain transistors as being the most likely sources of trouble. Special codes were devised to take advantage of certain circuit features that would permit by-passing these particular transistors. On December 20, 1962, one of these modified codes was successfully transmitted to the satellite. In subsequent operations, all voltages were removed from the command decoders. As had been predicted, this action allowed recovery of the transistors. On January 4, 1963, during orbit 1628, public demonstrations of live television to and from Europe were concluded. Telstar by then was responding properly to all normal commands.

On February 14, 1963, there began to be indications that the operation of the command system was beginning to degrade again. The satellite began to take longer and longer to respond to the normal command codes. By February 20, it did not respond to the normal codes. During this period, the response to the modified codes was solid.

On February 21, the satellite misinterpreted a command and operated the relay that disconnects most of the electronic system from the power plant. Since then to the present writing (March 18), the Telstar satellite has not responded to even the modified commands.

The results of the Telstar experiments are given in detail in the following papers. Two general conclusions can be drawn:

1. Design of a second-generation Telstar satellite could be approached by Bell Telephone Laboratories with confidence as an engineering project. Where uncertainties exist, they have to do with the conditions existing in space.

2. Problems of the ground station are clearly understood. The usual design trade-offs and optimizations can be made with real understanding. The second-generation ground station will be considerably simpler than the first experimental station at Andover.

REFERENCES

1. B.S.T.J., Project Echo issue, **40,** July, 1961.
2. B.S.T.J., Transatlantic Cable issue, **36,** January, 1957.
3. Curtis, H. E., Interference between Satellite Communication Systems and Common Carrier Surface Systems, B.S.T.J., **41,** May, 1962, p. 921.
4. Peck, D. S., Blair, R. R., Brown, W. L., and Smits, F. M., Surface Effects of Radiation on Transistors, B.S.T.J., **42,** January, 1963, p. 95.

The Research Background of the *Telstar* Experiment

By A. B. CRAWFORD, C. C. CUTLER, R. KOMPFNER, and L. C. TILLOTSON

(Manuscript received March 5, 1963)

For several years before the launch of the Telstar satellite, research effort was directed toward an experiment with an active satellite capable of relaying a broadband communication channel. The intention was to utilize and test a number of novel techniques which had become available, to explore those areas in which the current technology was lacking, and to demonstrate the feasibility of this means of communication. This paper describes some of this work, the background of facts and beliefs on the basis of which a number of important choices were made, and the general state of the radio art upon which the Telstar program was built.

I. INTRODUCTION

The Telstar satellite communications experiment, like all achievements in technology and engineering, has many roots. Some of these roots are as broad and old as science itself; others are rather recent and include modern rockets, missile guidance, and general space technology. Other more modest but essential roots grew from an early appreciation of the potential of satellite communication and the steps taken in the area of communication technology to foster its growth.

Bell Telephone Laboratories interest in the possibility of using artificial earth satellites for communication purposes began in 1955 with the publishing of the article on "Orbital Radio Relays"[1] by J. R. Pierce. It is significant, however, that some of the research which was relevant to the success of the satellite predated this publication by a decade or more.

The material presented here consists of a summary of scientific and technological knowledge and advances which were important to the satellite program. It also contains the pertinent parts of a memorandum dated August 24, 1959, which summarizes the background and views

that led to work toward a particular sort of experimental communication satellite. This memorandum expresses better than could be done retrospectively the thinking that led to the course of research activity which followed.

Bell Laboratories activities which followed the publication of Pierce's article and which culminated in the Telstar satellite experiment can be divided into five rather distinct periods of approximately one year each:

(*i*) 1958 Preliminary studies
(*ii*) 1959 Initiation of research and development programs
(*iii*) 1960 Experimentation and verification
(*iv*) 1961 Intensive development
(*v*) 1962 System construction and test.

The year 1958 was one for imagination and invention. The activities consisted principally of paper studies of the many system possibilities which were made possible by satellites, and resulted in a number of memoranda and published papers[2,3,4,5] which provided guide-lines for subsequent activities. Systems proposed in Bell Telephone Laboratories were conservative by many standards but relatively realistic if we judge by the fact that most of the factors which have so far proven to be important to the problem were well evaluated at that time. The most notable exceptions have been the unforeseen radiation hazard and the degradation of two-wire circuits with echo suppression by delay, which has dampened an early enthusiasm for 24-hour "stationary" satellites.

During 1959 several research and development programs were initiated which led directly to the Telstar experiment. An ad-hoc group containing people from many disciplines throughout the organization was formed to initiate activities in the areas which needed attention. It is principally the early work of this group which is described in this paper.

By 1960 laboratory work was well under way on several of the problems. During the year, the Project Echo experiment[6] was carried out and provided valuable experience with many of the elements inherent in a satellite communication system. Prototype models of the traveling-wave tube used in the Telstar satellite were built and put on life test, and life tests on batteries and other components were also started. Discussions with others working in the field led to an appreciation of the environmental problems and the necessity of radiation shielding. During this time, studies of radiation damage to solid-state devices were undertaken in cooperation with Brookhaven Atomic Energy Laboratories, which led to the design of the radiation-sensing package

and the radiation protection used on the satellite. A general electrical-mechanical configuration of the satellite was also proposed, although many important problems remained to be worked out.

Early in 1961 intensive development of the satellite began and is described elsewhere in this issue. The present paper discusses the more important parts of the research program which preceded the development project.

II. RESEARCH LEADING TO THE STATE-OF-THE-ART

If the Telstar satellite had been built using the state-of-the-art of a decade ago, it would have been a very different satellite. The evaluation of the sky noise temperature, the development of the low-noise maser amplifier, the appreciation of the low-noise properties of the horn-reflector antenna, and the solving of the problem of demodulation of large-index frequency modulation using feedback combined to reduce the power requirement on the satellite by two or three orders of magnitude (about 20 db in effective noise temperature and 5 db in FM threshold improvement). Similarly, advances in solid-state electronics reduced power requirements, size and weight enormously. In the following pages, we will outline some of the more significant parts of the general research activities which produced the state-of-the-art upon which the Telstar satellite was built, and we then will describe work done more recently, specifically to implement satellite communication. Less attention will be given to a number of areas which were of vital importance to the success of the experiment, such as the development of solid-state electronics, microwave electronics and large computers, since these are covered in other papers.

2.1 *Low-Noise Receivers*

Research leading to the understanding of the effective temperature of the sky has gone on intermittently for several decades and has yielded important results, culminating in the determination of the now well known relationships[7] of sky noise temperature vs frequency and elevation angle. These relationships were vital to the choice of frequencies for space communication, and the realization that these very low effective sky noise temperatures existed revealed the possibility of utilizing the properties of masers and low-noise antennas.

Most work on antennas in the past has been directed toward producing high area efficiency in terms of the gain or directivity of the antenna, properties which are not uniquely related to the noise properties. How-

ever, the horn-reflector antenna,[8,9] developed for terrestrial microwave relay systems, was found to have an effective noise temperature of only one to two degrees Kelvin.[10]

The low-noise character of sky-directed antennas would be of little use were it not for the extremely low-noise microwave amplifiers which came into being just as satellite communications became a possibility. The microwave maser amplifier,[11] having a noise temperature of two or three orders of magnitude lower than the best previously existing amplifiers, grew out of a decade or more of physical research in microwave molecular spectroscopy and paramagnetic resonance in solids. The parametric amplifier, similarly, was the product of years of work in solid-state physics and nonlinear circuit theory.[12,13]

Research and development in these three low-noise areas were greatly stimulated by the prospect of satellite relays. Research on atmospheric absorption and radiation, particularly in the presence of high humidity and rainfall, was intensified because of this prospect.[14] Traveling-wave masers played key roles in both the Echo[15] and Telstar experiments; those used in the Telstar Project were among the first masers with truly broadband capability. Antenna development (larger horns and Cassegrainian antennas) was likewise spurred by the fact that new low-noise and large-size requirements had to be met.

2.2 *Electron Devices*

Perhaps the most remarkable contribution to the state-of-the-art came from solid-state physics. Few components used in the satellite or on the ground are not at least in part the product of research in this area of physics. The maser and parametric amplifier have already been mentioned. All of the active elements in the satellite, except the traveling-wave tube, are solid-state devices, none of which was beyond an early state of development a decade ago. The availability of the reactance diode used in the frequency multipliers and the high-frequency transistor could scarcely have been more timely.[13]

Microwave tube development was likewise timely. Five years before the Telstar experiment there were no CW microwave tubes of adequate power for ground station operation, and the long life and reliability required in space were just beginning to be obtained. These efforts, directed toward more conventional applications, were almost directly applicable to the space problem.

Development in other areas, such as missile tracking and computers, as well as the chemistry of plastics and adhesives, also helped to provide

a state-of-the-art conducive to the development of satellite communications; but it is perhaps more appropriate to consider those problems which were newly posed by the new prospect. These problems ranged from satellite components and construction to considerations of celestial mechanics and geography necessary to establish probability statistics of mutual visibility between stations.

III. THE SATELLITE RESEARCH PROGRAM

In the face of a bewildering variety of options, it was necessary in 1959 to settle on a particular plan of action which would define the next nearest goal and the steps needed to attain it. This plan had to be sufficiently concrete to make it possible to identify the various problems and to help in getting people interested in solving them; at the same time it had to be flexible to allow for unexpected discoveries and developments.

Such a plan, embodying much of the thinking of Bell Laboratories at that time, was presented in an unpublished company memorandum dated August 24, 1959. In view of the influence of this memorandum on the subsequent course of events, we feel that the readers' interests are best served by reproducing below the relevant parts of this memorandum,* including even those parts about which we might feel differently now. It will be seen that while a number of important choices and decisions were made at a relatively early date and were adhered to subsequently, there were other choices, such as the traveling-wave tube power level, the modulation bandwidth and the choice of frequencies, which had to be changed to meet new requirements.

An important change in outlook has resulted from tests of the effect of long delays and echo suppressors on telephone users. The degradation due to delay has not been precisely defined over the total range of interest in satellite communications, but present evidence strongly favors an approach which minimizes the delay. Thus our initial enthusiasm for a 24-hour system as an ultimate goal has been considerably dampened, and the low-altitude system, proposed in the memorandum as the first experiment, has become more attractive.

The fact that the document reproduced here was a plan, a program of action only and conditioned by the time it was written, should be kept clearly in mind by the reader.

* Only sections which are pertinent to the subsequent activities and which led to the Telstar experiment are included here.

Active Satellite Repeaters: Interim Report I

By L. C. TILLOTSON

ABSTRACT

An experiment employing an active repeater in orbit at an altitude of about 2500 miles is discussed. The system would provide an experimental circuit having a bandwidth of 5 mc and suitable for TV or multiplex telephony between the U.S.A. and Europe for periods of up to 30 minutes. Broadband frequency modulation would be used to ease power requirements on board the satellite. Possible interference between the space system and existing services is discussed briefly. Some of the problems which must be solved before such a system can be considered feasible are outlined.

Active versus Passive Repeaters

As the title indicates, we are here concerned primarily with active repeaters. This comes about in part because passive repeaters are already receiving considerable attention at Bell Telephone Laboratories* and in part by the writer's conviction that passive satellites are best for military systems, particularly if the orbiting body is chosen for its immunity to enemy action, and that active satellite repeaters will be more useful in civilian activities.

For long-haul point-to-point service, a repeater in a synchronous (24-hour) equatorial orbit is very attractive. The main disadvantages, in addition to the large distances involved, are the $\frac{1}{4}$-second round trip delay and the fact that the satellite is not visible near the north and south poles. The latter is more important to military than to civilian communications. An unoriented passive reflector at this altitude is prohibitively large. On the other hand, if it is to be successful, an active repeater must be built from *reliable* components. Herein lies the challenge....

Frequency Allocations

Space-borne repeaters will obviously have to compete with other types for frequency allocations. This problem could be considerably reduced if bands presently assigned to the common carriers are also used for common carrier activities in space, the only real difference being that the satellite radio repeaters would be located on very high altitude platforms. If a given frequency band is to be used for space and earth-based repeaters simultaneously, several possible interference paths must be studied and controlled.† These are:

* Both passive and active satellite repeaters are considered at some length a memorandum by C. C. Cutler dated 1/12/59. Many of the proposals in this memorandum are based in part on this work. [Later published, Ref. 5.]

† Since we also propose to use the same frequency for several satellite repeaters, relying upon spatial separation and antenna discrimination for protection, this subject must also be investigated but it is not part of the present consideration.

1. Interference to earth-based receivers caused by satellite-borne transmitters.
2. Interference to earth-based receivers caused by space system ground-terminal transmitters.
3. Interference to space system ground-terminal receivers by earth-based transmitters....

Proposed Experiment

A system with a 5-mc baseband and a snr of 40 db which uses a repeater circulating in a 2500-mile polar orbit could provide a TV circuit to Europe with a common visibility time from Holmdel and Paris of up to 30 minutes. The communication system parameters are listed in Fig. 2 [Table I in this

TABLE I—ACTIVE SATELLITE REPEATER SYSTEM PARAMETERS
(Fig. 2 of 8/24/59 memorandum)

Experimental path	USA (Holmdel)—Europe (Paris)
Satellite, altitude	2500 miles
orbit	circular polar
period	2 hours 55 minutes
velocity	14,450 mph (4 mps)
Mutual visibility time, best pass	approx. 30 minutes $7\frac{1}{2}°$ above horizon
Maximum range to satellite	4600 miles
Maximum path loss	130 db
Minimum range to satellite	2500 miles
Minimum path loss (reference value)	125 db
Ground antenna effective area	1700 ft² (60-foot dish)
Temperature of ground receiver	30° Kelvin
Noise in 10-mc band	−144 dbw
Power of ground transmitter	1 kw
Satellite antenna	isotropic −3 db
Temperature of satellite receiver	3000° Kelvin
Noise in 100-mc band	−114 dbw
Power of satellite transmitter	1 watt
With satellite at *maximum* range:	
Margin relative to system objective	−1 db
Margin about FMFB threshold (C/N = 12 db)	2 db
Modulation	Large-index FM
Improvement factor	21 db
Baseband	5 mc
RF band (30 db down)	104 mc
Radio frequency	6 kmc
S/N for TV, p.t.p. signal to rms noise	48 db
Noise in message channel	38 dba at zero level
Number of message channels	500 to 1000

paper]; possible repeater arrangements are described in a later section entitled "Satellite Microwave Repeaters".

The philosophy used in the design of the experiment is as follows:

(*i*) *Minimum requirements on the propulsion and guidance equipment used to inject the payload into orbit.* Thus the satellite is assumed to be either completely unoriented and hence tumbling through space or, at most, spin-stabilized, and hence precessing only very slowly. This choice must be determined by further study of the satellite antenna and orbit injection problems.

(*ii*) *Minimum possible payload size and weight.* This is achieved mostly by limiting the experiment to a single one- or two-way channel and by using a receiver which trades bandwidth for snr in an advantageous manner. This makes it possible to keep the satellite transmitter power down to one watt. Special care will also need to be taken in the design of the microwave tube to achieve maximum efficiency. Since one of the larger components of the payload weight will be solar cells and storage batteries, this will be reflected directly in the total weight of the package.

(*iii*) *The space-borne apparatus must be compatible with our long-range objectives.** Since the path loss to an unoriented satellite at 2500 miles altitude is nearly equal to that for a 22,300-mile attitude-stabilized repeater with a 19-db antenna, the satellite electronics can be essentially the same at both altitudes. This is very desirable since even a "minor" change in the design of long-life apparatus may mean starting over.

(*iv*) *The space-borne apparatus must have maximum possible life.* Almost every design parameter must be considered here. Some of the most important are:

(a) *Low transmitter power.* Tubes in the one- to ten-watt power range have a longer operational life than those in the 100- to 1,000-watt range. As shown in a memorandum† by D. A. Chisholm et al, tube life decreases rapidly as cathode current density is raised. High-power tubes call for high cathode current densities. It is expected that a one-watt TWT can be built with a cathode current density not to exceed 50 ma/cm^2. Such a tube would have an "expected" life of 10 to 20 years. Low power is also important in the satellite because waste heat dissipation is a problem at best.

(b) *Only one microwave tube per repeater channel and maximum use of solid-state devices operated in a conservative manner.*

(c) *Simplest possible repeater circuit arrangements consistent with a useful communication capability.* It seems clear that components left out will never cause trouble. However, this must be achieved by straightforward design rather than by resorting to "trick" circuits which make repeater performance unduly sensitive to component characteristics.

(d) *The space electronics must not quickly become obsolete because of advances in the art.* We propose a "straight-through" repeater having a

* Soon after this memorandum was issued, experiments with delay on a two-wire telephone circuit indicated that there is a very serious problem in the use of a synchronous satellite in two-way telephony.

† Contents of this memorandum are presented in Ref. 16.

bandwidth of 100 mc and providing a minimum cnr of 15 db at the earth-based receiver....

Satellite Microwave Repeaters

Although there are many possible apparatus arrangements which could be used for satellite repeaters, there are only two broad categories. The first type puts out what it receives, but at higher level and perhaps shifted in frequency. This is essentially a broadband straight-through amplifier which will handle any signal within the range of its performance characteristics. Such an arrangement has two outstanding advantages.

(*i*) Great changes in ground-based apparatus, modulation techniques, etc., can be made with no reaction on the satellite repeater. This will help to avoid obsolescence caused by advances in the state of the art, which is an important consideration when development of very reliable apparatus which takes years to complete is being started.

(*ii*) Since the signal handling at the satellite is simple, i.e., just amplification, simple circuit arrangements and relatively few components can be used. In spaceborne apparatus this is a vital consideration, at least for the present.

The second type processes the signal during its passage through the repeater. Examples are: demodulating-remodulating repeaters, or receivers and transmitters connected back to back; pulse-regenerating repeaters, receivers which employ a correlation detector feeding a local transmitter; and very advanced types which include on-board computers for error correction, key stream generation, path selection (antenna pointing), orbit parameter control, etc. The disadvantages of this type are rather obvious:

(*i*) We must decide the system mode of operation in considerable detail before launching. Any important change will require a new satellite.

(*ii*) Most of these schemes require an untenable amount of complication in on-board apparatus.

Since even the simplest schemes will require a major effort to achieve adequate reliability in the space environment, we shall consider only the simplest possible versions of each of the two basic repeater types.

Straight-Through IF Repeater

Two variations of a possible IF type repeater are shown in Figs. 8 and 9 [Figs. 1 and 2 in this paper]. In type I the IF amplifier, up and down converter, frequency shift oscillator and local (microwave) oscillator, would all be realized by using solid-state devices. Since a real microwave transistor is doubtful, especially on the required time scale, local oscillator power would need to be obtained by harmonic generation from a transistor oscillator operating at several hundred megacycles. Of course, if all this can be achieved, the repeater will require only one microwave tube. If not, then repeater type II, shown on Fig. 9 [Fig. 2], is a possibility. This arrangement exploits the bandwidth of the TWT to provide a microwave oscillator at a different frequency, but at the same time it is being used as a

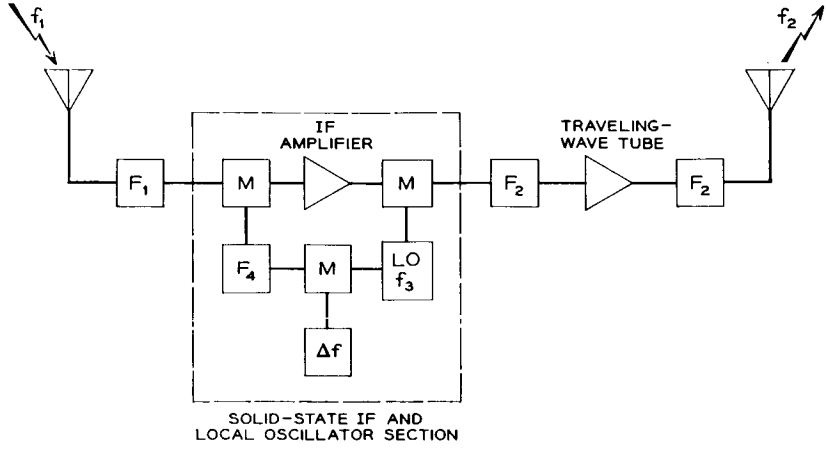

Fig. 1 — IF repeater type I (Fig. 8 of 8/24/59 memorandum).

signal amplifier. There are intermodulation troubles here, too, but the local oscillator power can be kept 20 db or more below the signal power, which should be very helpful in solving this problem.

At present, the most likely choice appears to be an IF repeater of type I or II, as shown in Figs. 8 and 9 [Figs. 1 and 2]....

Satellite Repeater Design

(*i*) *Life.* While launching costs are expected to decrease markedly as the operation moves from R and D into an operational phase and as more effi-

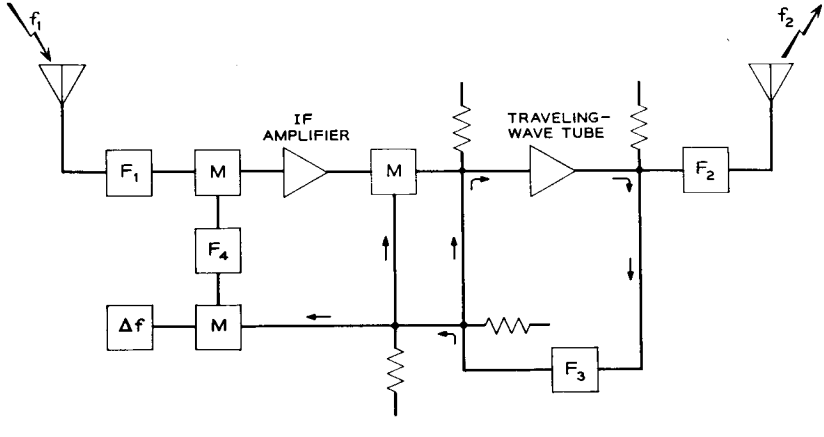

Fig. 2 — IF repeater type II (Fig. 9 of 8/24/59 memorandum).

cient propulsion systems become available, the cost of placing a repeater in orbit seems likely to remain as a major item of expense. Even if this were not so, it would still be important that the repeater last as long as possible in order to avoid cluttering up space with unusable derelicts. Hence, both for economic and political reasons, a long-life repeater appears essential. It is suggested that our goal be the same as for undersea cables — 20 years. More knowledge of the space environment than we now possess is likely to be required before such an ambitious goal can be achieved, but it is not too early to define our objective. Also, in order to make the first experiment appear successful, from both economic and psychological points of view, the first satellite should not be launched until it has a high expectancy of living at least one year.

(*ii*) *Size and Weight.* Clearly, both size and weight should be held down, but not at the price of compromising on performance. The successful launching of a device which then fails to operate will avail us less than nothing. An over-all weight in the vicinity of 100 pounds and a surface area of 20 square feet for solar cells appears reasonable from both the propulsion and electronic subsystem viewpoints. As propulsion systems with greater capabilities become available, they can be used to launch a multichannel repeater or several satellites at one time, or both. The basic repeater design can remain unchanged, if it is right in the first place. For example, the experimental single-channel one-way repeater discussed above could be used to build up a multichannel two-way repeater....

* * *

About the time the memorandum reproduced above was written, work was started on a number of problems defined therein in several places, both within the Research Division and in other Divisions of Bell Telephone Laboratories. Since much of this work is treated in considerable detail in this issue and elsewhere, we shall treat each topic with only the amount of detail appropriate to this historical introduction.

3.1 *Project Echo*

Early in 1959 preparation was begun for the Project Echo experiment,[6] and this work dominated our satellite communication activity for a time. Interest in the passive satellite was spurred by realization of the magnitude of the job of building an adequate active satellite, and the desire to gain early experience with systems. It was also believed that a system based on passive satellites might be created before the reliability of active satellites could be proven.

Bell Laboratories cooperated with the National Aeronautics and Space Administration, Jet Propulsion Laboratories, Naval Research Laboratories and others in formulating and carrying out the communication part of the Echo experiment. For this purpose a ground station with transmitter, receiver and satellite-tracking facility was established at

Holmdel, New Jersey. As is now well known, single-channel two-way voice communication, facsimile transmission, etc., were demonstrated over transcontinental paths; transmission characteristics were measured; and valuable operational experience was obtained using the 100-foot aluminized balloon reflector. This work spurred large ground station tracking and control and receiver development, and contributed valuable assurance that there were no propagation anomalies except for atmospheric refractive effects at low elevation angles. Experience with the large horn-reflector antenna with its complement of low-noise components, experience with orbit prediction and tracking, and experience with wide-index feedback FM demodulators were of considerable value in subsequent design of the much larger ground station used for the Telstar experiment. Portions of the ground station constructed for Echo were also eventually used in connection with the Telstar experiment.[17]

3.2 *Satellite Electronics*

The most critical component of the spacecraft itself was considered to be the traveling-wave tube. Fortunately, the development of tubes for terrestrial microwave relay systems had recently demonstrated as much as a five-year life span for such tubes, and their use in missile systems had shown that they could be made light and rugged enough. To design and build a tube for particular performance objectives — frequency, gain and power level — and with an aim toward even longer life, was no trivial task, and it was felt that at least a two-year lead time would be needed. To complicate the matter, the assignment of frequencies for an experiment with communication satellites could not be rushed. Consequently, some long guesses had to be made, and work on a one-watt tube at 6000 megacycles was started because this seemed a most likely possibility. The eventual change to two watts at 4000 megacycles was not so great as to void much of the work that was done. A full account of this work is presented elsewhere in this issue.[16]

Experience with an experimental light-route radio relay gave confidence that the solid-state devices and microwave circuitry used therein could be adapted to the design of a broadband repeater in space, and there was considerable experience upon which to draw. Several repeater circuit configurations were considered, and the straight-through IF configuration was favored because it made more straightforward use of existing circuitry.

3.3 *Satellite Power Supply*

Since the satellite power supply accounts for an appreciable part of the total satellite weight, it was essential that the most efficient design be used. While several schemes, including nuclear reactors and isotope power supplies, had been proposed, the only feasible means (1959–1960) was to use solar cells and a storage battery, together with a solid-state converter to change the low battery voltage to the various potentials required by the electronic circuitry. Study of the solid-state power converter, which was started at this time, benefited from considerable related experience with dc-to-dc converters for terrestrial microwave systems and for various military applications. The main problem was one of reliability. How this was obtained is described elsewhere in this issue.[18]

A storage battery of suitable design was not available; existing cells suffered from a lack of control during the manufacturing process and from a tendency to leak. There was also considerable question about cell life under continuous deep cycling and the effects of a long continued overcharge. Some of the early results obtained from a fundamental investigation started at this time have been published.[19,20,21] Early work on solar cells consisted mostly of radiation damage studies, since this was expected to be the most crucial problem; considerations were also given to temperature control and mounting arrangements.

3.4 *The Satellite Antenna*

The satellite antenna posed a difficult problem because of the conflicting mechanical and electrical requirements. Since the satellite diameter would inevitably be many wavelengths at the operating frequency, severe shadowing would occur if a nondirectional antenna was mounted near the surface. Erection of extensible arms in space had proven risky at best; and even if this were achieved, a sufficiently flexible low-loss microwave transmission line was not available.

A solution to the electrical problem was to divide the spherical satellite into two parts, separated by a radial transmission line which fed a circumferential slot radiatior. This antenna configuration was studied analytically and checked experimentally and found to produce a pattern acceptable for a spin-stabilized satellite.[22] However, this basic structure, consisting of two hemispheres insulated from each other by a small slot, posed severe mechanical and thermal problems in the satellite design. A multiplicity of closely spaced "boxes" fed in-phase by an array of

coaxial cables and arranged to radiate circular polarization[23] provided an acceptable solution which was adopted in the development models of the Telstar satellite.

3.5 *The Satellite Structure*

Since it was desired to build a satellite which would have a long useful life, and there was no assurance of being able to provide attitude control, it was important that the satellite not be dependent upon orientation relative to the sun or the earth. For this reason an approximately spherical shape was chosen, and solar cells were distributed more or less uniformly so that the power generated would not depend upon solar aspect.

The early work was on a larger framework than used on the Telstar satellite, because continuous operation was envisaged, but work on the structure, heat flow and vibration damping paved the way for the later design.[24]

3.6 *Mutual Visibility Problems*

A crucial factor in the design of satellite communication systems is the problem of mutual visibility statistics. It was easy to derive a first-order approximation to the operational statistics for particular ground terminals and satellite orbit. To get a more general solution was a good mathematical problem which was solved in an interesting fashion.[25] It is clear from this work that a practical real-time, low-altitude satellite system for use between the United States and Europe should use polar, or at least steeply inclined, orbits at an altitude of several thousand miles. Other orbits are more suitable for other paths, and it appears that a global system would make good use of both polar and equatorial orbits. Before the radiation hazard was appreciated, it was thought that a 2,500-mile orbital altitude represented a logical compromise between the many factors involved, but to ease the radiation problem, and for other reasons, higher altitudes are now favored. The 24-hour synchronous satellite was, of course, expected to be much better from this point of view, but was ruled out of early consideration because of the more severe technical problems.

3.7 *The Delay and Echo Problem*

A most interesting research problem has been that of the delay and echoes inherent in long two-wire telephone circuits. The literature of a generation ago has a lot to say on this subject, and set a limit on the largest acceptable delay in a two-way, two-wire telephone circuit.

Heretofore, it has not been too difficult to stay within such a limitation, but it was soon clear that any double-hop, low-altitude system or single-hop synchronous satellite system would exceed this standard by a considerable amount. Early (1959) and simple experiments indicated that delay alone (in four-wire circuits) was not a problem, but that eliminating the echo in the presence of a delay up to 0.6 second was not a trivial problem.

It was soon apparent that this problem strongly involved user psychology as well as some severe technological problems. Circuits were devised which worked very well with some individuals and very poorly with others. Accordingly, in addition to work on specific apparatus for echo suppression, a user preference testing program was inaugurated. Tests were conducted over several years using a number of echo suppression techniques, including those of competitive companies. The user reaction to circuits with the best available echo suppressors and delays corresponding to only a single 24-hour satellite link is of serious concern in commercial telephony. This question still remains a fruitful area of research.[26]

3.8 *The Ground Station Antenna*

During the early planning for an active satellite experiment, it became evident that a low-noise antenna larger than any then in existence would be required. Design, construction, and test of the 20 × 20-ft horn reflector for Project Echo were sufficiently advanced to make clear that such an antenna would also be acceptable for use with an active satellite. Hence, plans were initiated for a 60 × 60-ft horn-reflector antenna of similar design. It was suggested by the mechanical designers that a conical horn might ease some of the structural problems. As a result of this suggestion, an analysis and an experimental check were made of the gain and pattern of such an antenna[27] which showed that performance equal to that of the older rectangular horn-reflector antenna could be obtained.

With antennas of the size contemplated, it is desirable that steering (autotrack) information be derived from the antenna itself. Prior research on waveguide modes provided a solution to this problem[28] and a multimode autotrack system was developed which contributed greatly to the Telstar operation.[29]

3.9 *Modulation*

A large number of possible modulation methods were considered for both passive and active satellites. During the Project Echo experiment

amplitude modulation, phase modulation, single-sideband and frequency modulation (FM) were used. When complexity, power requirements on the satellite, and frequency spectrum limitations were all considered, it was not difficult to settle on wide-index FM as the most desirable. FM seemed desirable even for spectrum conservation because the relative freedom from interference greatly reduces the required geographical separation of stations sharing the same band.

The desirability of FM was greatly enhanced by the promised advantage of feedback in reducing the receiver threshold power.[30] Early attempts to use feedback demodulation failed to demonstrate the expected advantage, because of the seeming conflict between the IF band-shape requirements of the noise elimination and feedback stability criteria. A considerable amount of rather difficult theoretical and experimental work was necessary to resolve this difficulty, and the improvement obtained,[31,32,33] first for Project Echo and later in the broadband Telstar receiver, was very near the amount expected on more intuitive grounds.

IV. TRANSITION FROM THE RESEARCH TO THE DEVELOPMENT PHASE

Up to 1960, Bell Laboratories activity in satellite communication centered in an ad hoc group representing many parts of the organization. No large expenditure had been committed, and in fact it was not known at this date when, if ever, a satellite for other than government purposes would be launched. The work was undertaken because of a firm conviction of its eventual importance to the Bell System and because it posed problems which the technical staff found interesting and challenging. It was made possible by the freedom granted to the research groups to enter new areas which they found promising, long before it was possible to evaluate the commercial importance of the new field of activity.

Where does research end and development begin? It must be clear to the reader that there is as much "development" described in the foregoing paragraphs as there is research. However, there came a time in the course of events when a clear-cut change in the nature of the effort took place. Prior to the fall of 1960, "research," motivated primarily by the desire to solve crucial and interesting problems, dominated the Bell System activities in this field. After the fall of 1960, the activities were dominated by the dedication and commitment to produce a working experimental system in the shortest possible time. This paper covers only the earlier effort when activities were based on a hope rather than

a commitment, were directed toward components more than toward a system, and before most of the people who made the Telstar experiment work had become involved. In the two years that followed, a number of important changes in the plan took place, and the pace accelerated many fold. The earlier contributions seem pale beside the later achievement, but small as the beginnings were, they played an important part in getting the Telstar satellite program under way.

REFERENCES

1. Pierce, J. R., Orbital Radio Relays, Jet Propulsion, **25,** April, 1955, pp. 153–157.
2. Pierce, J. R., and Kompfner, R., Transoceanic Communication by Means of Satellites, Proc. I.R.E., **47,** March, 1959, pp. 372–380.
3. Pierce, J. R., and Cutler, C. C., Interplanetary Communication, Advances in Space Science, **1,** Academic Press, Editor Fredrich I, Ordway III, New York, 1959, pp. 55–109.
4. Tillotson, L. C., Active Satellite Repeaters, Signal, **14,** No. 11, July, 1960, pp. 48–50.
5. Cutler, C. C., Radio Communication by Means of Satellites, Advances in Ballistic Missile and Space Technology, Proc. Fourth AFBMD/STL Symposium, **3,** Pergamon Press, 1961, pp. 254–271.
6. B.S.T.J., **40,** July, 1961, entire issue.
7. Hogg, D. C., Effective Antenna Temperature Due to Oxygen and Water Vapor in the Atmosphere, J. Appl. Phys., **30,** September, 1959, pp. 1417–1419.
8. Friis, H. T., and Beck, A. C., U. S. Patent 2,236,393, filed 3/1/39, issued 3/25/41.
9. Crawford, A. B., Hogg, D. C., and Hunt, L. E., A Horn-Reflector Antenna for Space Communication, B.S.T.J., **40,** July, 1961, p. 1095.
10. DeGrasse, R. W., Hogg, D. C., Ohm, E. A., and Scovil, H. E. D., Ultra-Low Noise Antenna and Receiver Combination for Satellite and Space Communication, Proc. Nat. Elect. Conf., **15,** 1959, p. 370.
11. DeGrasse, R. W., Schulz-DuBois, E. O., and Scovil, H. E. D., The Three-Level Solid-State Traveling-Wave Maser, B.S.T.J., **38,** March, 1959, p. 305.
12. Manley, J. M., and Rowe, H. E., Some General Properties of Nonlinear Elements — Part I, General Energy Relations, Proc. I.R.E., **44,** July, 1956, pp. 904–913.
13. Uhlir, A., Jr., The Potential of Semiconductor Diodes in High-Frequency Communications, Proc. I.R.E., **46,** June, 1958, p. 1099.
14. Hogg, D. C., and Semplak, R. A., The Effect of Rain on the Noise Level of a Microwave Receiving System, Proc. I.R.E., **48,** December, 1960, p. 2024.
15. DeGrasse, R. W., Kostelnick, J. J., and Scovil, H. E. D., The Dual Channel 2390 mc Traveling-Wave Maser, B.S.T.J., **40,** July, 1961, p. 1117.
16. Bodmer, M. G., Laico, J. P., Olsen, E. G., and Ross, A. T., Satellite Traveling-Wave Tube, B.S.T.J., this issue, Part 3.
17. Jakes, W. C., Jr., Participation of the Holmdel Station in the *Telstar* Project, B.S.T.J., this issue, Part 2.
18. Bomberger, D. C., Feldman, D., Trucksess, D. E., Brolin, S. J., and Ussery, P. W., The Spacecraft Power Supply System, B.S.T.J., this issue, p. 943.
19. Thomas, U. B., The Oxides and Hydroxides of Nickel, Their Composition, Structure, and Electrical Properties, presented to the Electro-Chemical Society, Ottawa, Canada, October, 1958.
20. Thomas, U. B., Battery Considerations for a Communication Satellite, presented at the American Rocket Society Energy Conversion for Space Power Conference, Santa Monica, California, September, 1960, published in Progress in Astronautics and Rocketry, **3,** ARS series, Chapter 34, 1961, pp. 497–514.

21. Thomas, U. B., Kinetic Basis for the Operating Characteristics of Sealed Nickel-Cadmium Batteries, presented at the Third International Symposium on Batteries, Bournemouth, England, October, 1962, published in the Proceedings.
22. Bugnolo, D. S., A Quasi-Isotropic Antenna in the Microwave Spectrum, I.R.E. Trans. on Antennas and Propagation, AP-10, No. 4, July, 1962, p. 377.
23. Bangert, J. T., Engelbrecht, R. S., Harkless, E. T., Sperry, R. V., and Walsh, E. J., The Spacecraft Antennas, B.S.T.J., this issue, p. 869.
24. Hrycak, P., Koontz, D. E., Maggs, C., Stafford, J. W., Unger, B. A., and Wittenberg, A. M., The Spacecraft Structure and Thermal Design Considerations, B.S.T.J., this issue, p. 973.
25. Sinden, F. W., Geometric Aspects of Satellite Communication, I.R.E. Trans. on Space Electronics and Telemetry, **6,** September–December, 1960, p. 146.
26. News Feature in the Bell Laboratories Record, Simulating Speech through Space, **38,** August, 1960, pp. 296–298.
27. Li, Tingye, and Turrin, R. H., Performance Characteristics of a Conical Horn-Reflector Antenna, presented at URSI Spring Meeting, Washington, D.C., April 30 to May 3, 1962.
28. Miller, S. E., Multimode Automatic Tracking Antenna System, Patent No. 2,931,033, filed 7/19/55, issued 3/29/60.
29. Cook, J. S., and Lowell, R., The Autotrack System, B.S.T.J., this issue, Part 2.
30. Chaffee, J. G., The Application of Negative Feedback in Frequency-Modulation Systems, B.S.T.J., **18,** July, 1939, pp. 385–403.
31. Ruthroff, C. L., FM Demodulators with Negative Feedback, B.S.T.J., **40,** July, 1961, p. 1149.
32. Enloe, L. H., Decreasing the Threshold in FM by Frequency Feedback, Proc. I.R.E., **50,** January, 1962, pp. 18–30.
33. Ruthroff, C. L., and Bodtmann, W. F., Design and Performance of a Broadband FM Demodulator with Frequency Compression, Proc. I.R.E., **50,** No. 12, December, 1962, pp. 2436–2445.

The *Telstar* Satellite System

By D. F. HOTH, E. F. O'NEILL, and I. WELBER

(Manuscript received March 15, 1963)

This paper describes the Telstar system and discusses the over-all system design. System considerations, the orbit selection and frequency allocation considerations are covered. A general description of the Telstar satellite and Andover, Maine, ground station provides background for companion articles in this series. Finally, the transmission performance is given with some discussion of system parameters.

I. INTRODUCTION

The Telstar system consists of the active communication satellite repeater in orbit and ground facilities to work with it. The satellite was designed and built by Bell Telephone Laboratories and launched by the National Aeronautics and Space Administration (NASA) under the terms of a cooperative agreement. Bell Laboratories built the ground station at Andover, Maine, and furnished launch support equipment at Cape Canaveral. The station at Holmdel, New Jersey,[1] originally built for the Echo project, was modified to work with the Telstar system. Participating European stations were constructed at Goonhilly Downs in England, Pleumeur-Bodou in France, and Fucino in Italy by telecommunications agencies in the respective countries.

This paper gives a general description of the Telstar satellite system. It starts with a discussion of the over-all system design. This is followed by a more detailed discussion of the factors affecting the choice of the orbit and of the operating frequencies. The satellite, the Andover ground station, and the equipment at Cape Canaveral are next described and, finally, certain important transmission parameters are presented.

II. SYSTEM OBJECTIVES

The system was designed to meet the following objectives:

(1) To demonstrate broadband microwave transmission through an active satellite.

In its Telstar I, Vol. I Jun. 1963
P 765-799 refer (See N64-10868 02-01)

Specifically, this included the transatlantic transmission of high-quality television with sound, or the equivalent of 600 one-way telephone channels. It was also desired to test the transmission of a limited number of two-way telephone channels using a common amplifier in the satellite. A further transmission objective was to demonstrate that other services, such as data, telegraphy and telephoto, could be sent through the satellite.

(2) To test the operation of a ground station capable of transmitting to, and receiving from, the satellite while tracking it.

This involved the simultaneous operation of a high-power broadband transmitter and an ultra-low-noise receiver through a common horn-reflector antenna. An important aspect of the ground station tests was the trial of several means of acquisition and tracking of the satellite, and the steering of the antenna by both programmed and autotrack methods.

(3) To obtain data on the space environment and its effect on the satellite.

For this purpose, equipment is carried to measure particle radiation in space, as well as temperatures, voltages and other conditions in the satellite. Telemetry is provided to relay this information to the earth.

III. GENERAL SYSTEM CONSIDERATIONS AND FEATURES

A satellite communications system differs in major respects from other kinds of radio communications systems, and hence the various constraints faced by the designer differ in nature or emphasis. In this section, the major constraints which influenced the design of the Telstar system and the way in which they affected the system parameters are discussed in a general way. Major system features are given. Subsequent sections will discuss these matters in more detail.

The principal factors affecting the choice of the parameters of the Telstar system were the following:

(1) In order to provide mutual visibility across the Atlantic for periods of useful length, it was necessary to place the satellite in an orbit above 2000 miles. On the other hand, the weight which could be launched into a satisfactory orbit with available launch vehicles was limited.

(2) It was necessary to choose operating frequencies at which the sky noise and atmospheric absorption would be low and where sufficient bandwidth for television and other broadband services could be obtained. It was also necessary to consider interference between the satellite system and other radio services.

(3) Because of the long distances involved, radio path losses are very great. In addition, the effective radiated power of the satellite was limited by the primary power obtainable within the weight restrictions and because of the impracticality of using directive antennas in the satellite. The signal power received at the ground antenna, therefore, is very weak compared with levels normally received in overland radio relay systems.

(4) It was desired to design a satellite with a high probability of surviving the launch and which would last as long as possible in the space environment. This consideration affected the design and weight of the satellite in many ways, including selection of reliable components, rugged construction and protection against particle radiation.

All of these factors interact with each other and, as a result, there is no uniquely logical order in which the design choices can be developed in a step-by-step manner. Probably the choice of operating frequencies is the best starting point.

Considerations of bandwidth, propagation and radio noise narrow the choice of operating frequencies to the region between one and ten gigacycles, as will be discussed in more detail in a later section. These factors, together with hardware considerations and problems of coordination with other radio services, led to operation in the 3700–4200-mc and 5925–6425-mc common-carrier bands. The low power received at the ground led to the choice of the lower frequency band for the down path because these frequencies are better from the standpoints of radio propagation and noise.

At the operating frequencies chosen, noise from the sky is very low (as much as 20 db lower than that radiated by the earth into terrestrial microwave antennas) and thus very weak signals can be used. Advantage could be taken of this by using a low-noise ground antenna and a helium-cooled maser amplifier at the input to the ground receiver. A horn reflector was chosen because it has very low gain a few degrees off the main beam and thus would pick up very little noise from terrestrial sources. To further improve reception, it was decided to build at Andover the largest, and thus highest-gain, horn-reflector antenna that could be designed with confidence that it could be steered accurately enough to track the satellite. This antenna has a 3600-square-foot aperture.

Even with the low-noise antenna and maser, it was necessary to employ every possible technique for achieving high quality transmission with weak signals. This led to the choice of wide-swing frequency modulation for the down path, since it permits good baseband signal-to-noise ratios with poor radio-frequency carrier-to-noise ratios. The use of a frequency compression demodulator (also referred to as an FM feedback

receiver) permits operation with lower carrier-to-noise ratios than is possible with a conventional FM detector. For satellite simplicity and other reasons, FM was also chosen for the up path. The satellite amplifies the signal but does not alter the modulation.

The Andover ground station provides adequate transmission performance for the down link out to a range of more than 8000 nautical miles with a satellite effective radiated power of 2 watts. A 2-kw transmitter on the same antenna provides similar performance for the up link.

If antenna gain could be used in the satellite, the actual RF power could be less than 2 watts and this could be traded for other simplifications in the satellite or ground station, or for improved transmission performance. There are a number of possible techniques for achieving this, including the use in the satellite of earth pointing attitude stabilization along with a directive antenna, steerable phased arrays or provision for switching several directive antennas. These possibilities were discarded for various reasons, including the state of the art, the time it would have taken to develop them, and the desire for a simple satellite. Instead, an antenna system which is nearly isotropic is employed. To minimize the effects of nulls on communication, the satellite is spin stabilized around the axis of symmetry of the antenna system.

A traveling-wave tube was chosen for the satellite output amplifier, since it could provide sufficient power with good efficiency and because it would provide a wide bandwidth. Prior experience with missile-borne traveling-wave tubes had demonstrated that they could be made rugged enough to withstand a rocket launch. All other circuits employ solid-state devices.

Solar cells were chosen as the only practical source of primary power for the satellite. To supply the power required for the communication equipment directly from the solar cells would mean more cells and thus more weight than was possible within the weight and size limitations on the satellite. Therefore, a nickel-cadmium storage battery charged by the solar cells supplies the communications equipment during operation. Command circuits are provided to turn off the communications equipment so the batteries can be charged and to perform a number of other functions.

Facilities for measuring trapped particle radiation and its effect on solid-state devices are provided. Telemetry provides information on the condition of the satellite and on the results of the radiation experiment. The satellite is approximately spherical, with a diameter of 34 inches, and weighs approximately 170 pounds.

The launch vehicle was a major factor in the Telstar experiment.

Very early in the planning of the project, consideration was given to possible vehicles which might be capable of putting a sufficient payload into a satisfactory orbit. For reasons of availability and reliability, the NASA Delta vehicle was chosen. Since it could not launch the payload into a high enough circular orbit, an elliptical orbit with an apogee of about 3000 nautical miles and a perigee of about 500 nautical miles was chosen. The orbit is inclined 45° to the equator. When apogee is over the North Atlantic, there are several good periods of mutual visibility between Europe and Andover daily.

Table I lists the major parameters of the Telstar system.

IV. ORBIT SELECTION

As indicated in the preceding section, it was necessary to place the satellite in a high enough orbit to give satisfactory periods of mutual visibility across the Atlantic. The problem is illustrated by Fig. 1.* It shows lunes of mutual visibility for communication between Andover, Maine, and either Goonhilly Downs in England or Pleumeur-Bodou in France, assuming minimum antenna elevation of 7.5°. For a particular height, the subsatellite point on the earth's surface must be within the corresponding lune if the satellite is to be mutually visible. As the height gets lower, the lune becomes smaller. At the same time, the orbit period becomes shorter so that the subsatellite point moves more rapidly over the earth. The net result is fewer and shorter useful passes. The lune would vanish at 475 nm height.

The inclination of the orbit also affects visibility, since the satellite never passes over regions whose latitudes are higher than the inclination. Thus, only part of the visibility lune may actually be useful for communication. The best choice of orbit inclination depends on the particular points on the earth between which communication is desired; for the points of principal interest here a high inclination is best. Thus, for the Telstar satellite, an orbit was desired with the highest altitude and inclination possible with the available launch vehicle and launch location.

The launch vehicle used is a major factor in any satellite experiment. Rockets capable of orbiting significant payloads do not exist in such variety that the problem can be approached with a set of requirements on *them* as an end result. On the contrary, it is almost inevitable that an available vehicle must be found and the experiment framed within its capability. This, in effect, limits the achievable orbits and sets weight and size limits on the satellite.

---

* For a more complete discussion of satellite visibility, see Ref. 2.

TABLE I — PRINCIPAL FEATURES OF THE *Telstar* SYSTEM

TRANSMISSION

- Signals handled
  - Television
  - 600 one-way telephone channels (simulated by noise)
  - 12 two-way telephone channels
- Modulation — FM
- RF bandwidth
  - Ground station — 25 mc
  - Satellite — 50 mc
- Frequencies
  - Communication up — 6389.58 mc
  - Communication down — 4169.72 mc
  - Beacon — 4079.73 mc
  - Telemetry and beacon — 136.05 mc
  - Command — about 123 mc
- Polarization
  - Microwave channels — circular
  - VHF beacon — linear
  - Command — circular

SATELLITE

- Size, shape, and weight — 34-inch sphere, 170 pounds
- Orbit
  - Perigee 514.21 nm
  - Apogee 3051.37 nm
  - Inclination 44.8°
- Launch — Delta vehicle from Cape Canaveral
- Repeater configuration — IF type: amplifies, shifts frequency, does not alter modulation
- Communications antennas — approximately isotropic, circularly polarized
- RF power output — 2 watts
- Power plant
  - Silicon n-on-p solar cells — shielded
  - Ni-Cd storage battery
- Stabilization
  - Spin with axis normal to plane of ecliptic
  - Magnetic torquing coil control
- Radiation experiments — proton and electron
  - Flux in several energy ranges
  - Radiation damage to special solid-state devices

ANDOVER GROUND STATION

- Communications antenna
  - 3600 square foot horn reflector
  - Inflated radome
  - Pointing by tape drive, autotrack, slave to precision tracker
- Communications transmitter — 2 kw
- Communications receiver — maser input, frequency compression demodulator
- Noise temperature — 32° K at zenith

The capabilities of the possible launch vehicles were analyzed. The most readily available was the Delta vehicle used by NASA for the Echo launch and planned to be the vehicle for many other space experiments. It was also believed to be reliable, as has since been borne out by a long succession of successful launches. The initial weight objective

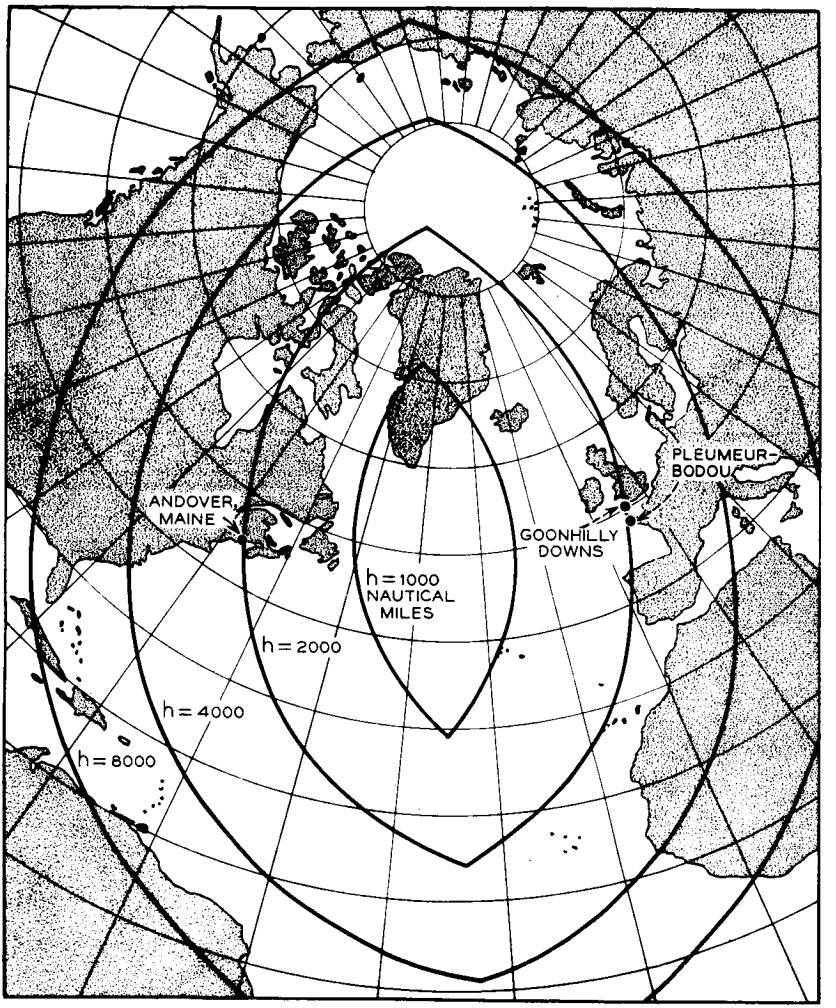

Fig. 1 — Useful regions for various heights above surface of earth.

for the Telstar spacecraft was 125 pounds, but as the real problems of design were met and solved, it became apparent that the satellite would weigh about 170 pounds. With this weight, analysis indicated that the Delta vehicle, launched from Cape Canaveral, would achieve a circular orbit only about 1000 nautical miles high with 42° inclination. This would result in only about three passes per day, typically only five minutes long, with mutual visibility across the Atlantic.

In spite of this disadvantage, the availability and reliability of the

Delta made it an attractive vehicle. Therefore, attention was turned to the possibilities of an elliptical orbit. By accepting a low perigee, an apogee much higher than 1000 miles could be achieved. If the apogee were located well north of the equator, satisfactory periods of mutual visibility could be achieved across the North Atlantic. Table II shows the orbit parameters chosen, together with those actually achieved.

Fig. 2 shows the suborbital track of the Telstar satellite for the first 24 hours after launch. With a period of 158 minutes, the satellite completes nine orbits in 23 hours, 42 minutes, accounting for the near retracing of the first track on the tenth orbit. Those periods when the satellite was mutually visible across the Atlantic are shown by heavy solid lines. Additional time when it was visible from Andover only are shown by light solid lines. Other periods are shown dashed.

It will be noted from the table that the initial apogee was south of the equator — not the best position from the standpoint of visibility. However, the line of apsides advances about 2° per day, and after launch the apogee moved in a northerly direction. It reached its northernmost point in about 50 days and then started to move southward. This gave a period of about three months during which visibility was good, followed by a period of poor visibility. Fig. 3 shows visible time per day when the satellite is at least 7.5° above the horizon. Initially, there were three or four passes per day, each lasting 10–20 minutes, during which the satellite could be used for transatlantic communication. Seven weeks later, with the apogee in its best position, there were four or five passes daily, each lasting 20–40 minutes.

Another orbit parameter is spin-axis orientation. For optimum output from the solar power plant and favorable heat balance, it was desired to have the spin axis perpendicular to the sun line. If this attitude is to be maintained as the earth carries the satellite with it around the sun, the axis must also be normal to the ecliptic plane. The desired inclination of the orbit was achieved by dog-leg maneuvers during the launch. Thus, while the orbit plane is inclined 45° to the equator, the direction

TABLE II — ORBIT OF THE *Telstar* SATELLITE

	Proposed	Actual Orbit (NASA Minitrack)
Perigee	500 nm	511.9 nm
Apogee	3000 nm	3043.2 nm
Inclination	45.43°	44.8°
Period	156.47 min.	157.6 min.
Initial apogee latitude	8.59°S	11.92°S
Apsidal advance	2.02°/day	1.98°/day

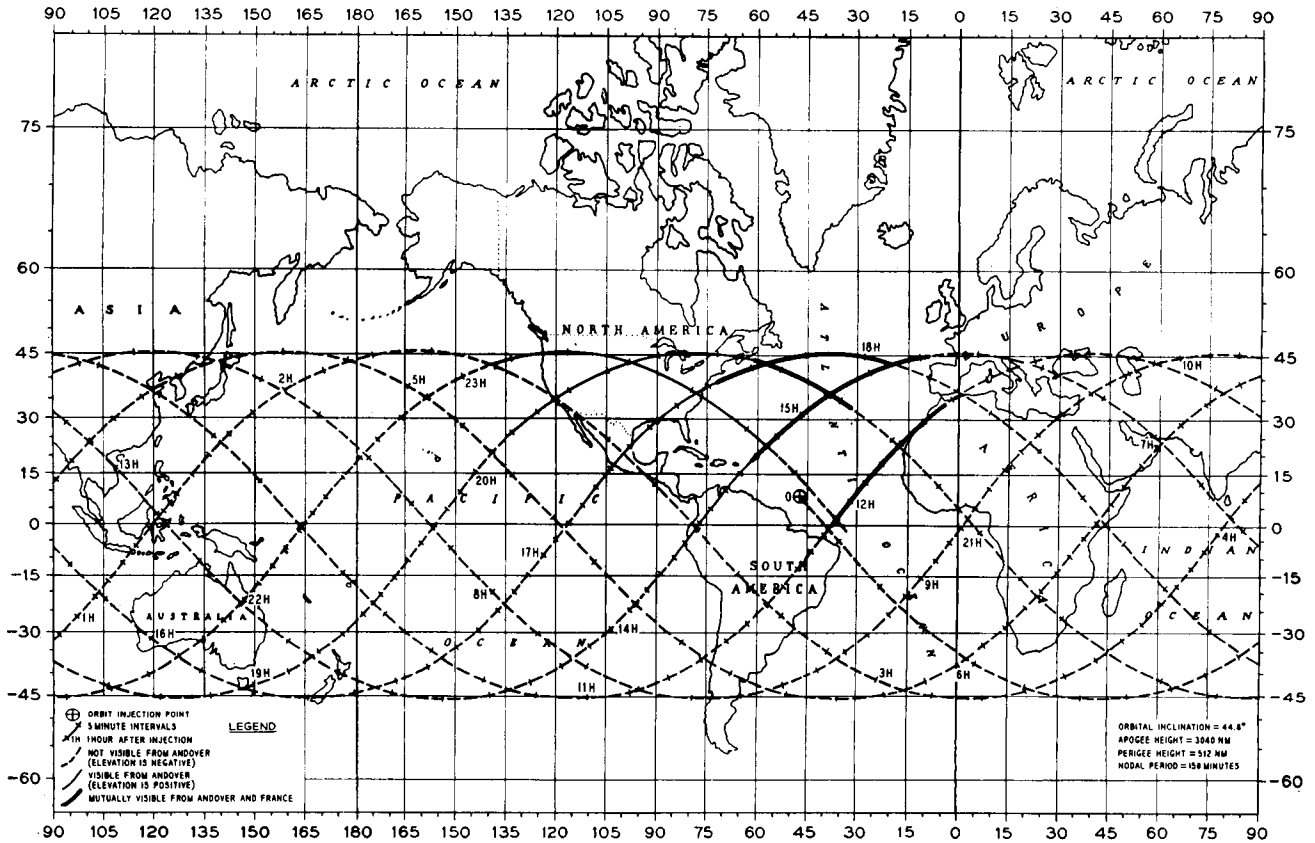

Fig. 2 — Suborbital tracks and mutual visibility for first 24 hours.

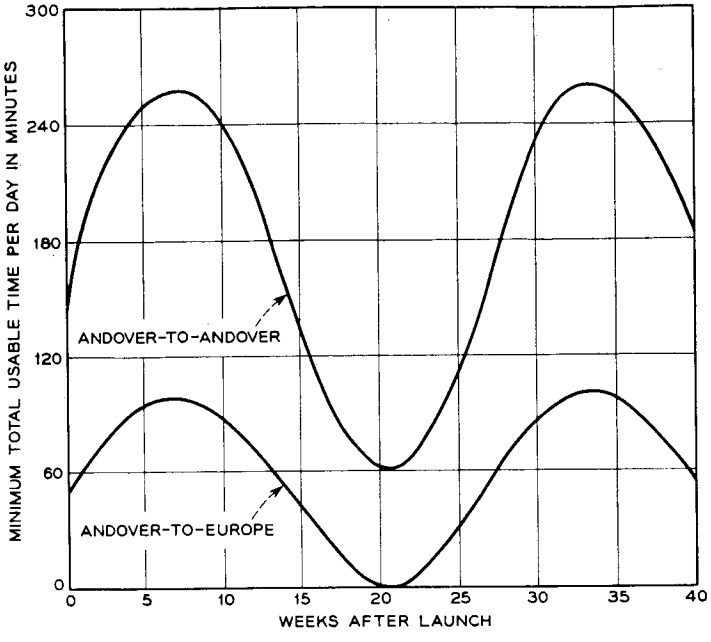

Fig. 3 — Minimum usable time per day.

of the final thrust of the third-stage rocket, and hence the orientation of the spin axis, was at a higher inclination to the equator — actually 67°. By choosing the time of launch, the 23° inclination of the earth's axis with respect to the ecliptic plane was added to this, resulting in a spin-axis attitude almost perpendicular to the ecliptic plane. The axis precesses with time because of the torque created by the residual magnetic moment of the satellite in the earth's field. To correct this precession, a magnetic torquing coil is provided in the satellite which can be turned on from time to time to control the position of the spin axis.

The elliptical orbit of the Telstar satellite is also desirable for the radiation experiment, since it covers a large part of the inner Van Allen belt and, with its apogee in northerly or southerly positions, it passes through a portion of the outer Van Allen belt.

V. CHOICE OF OPERATING FREQUENCIES

The frequencies used by the Telstar system include those required for the communications channel and for a microwave beacon used in tracking. They also include VHF channels for transmitting commands

to the satellite and for the VHF beacon and telemetry. The VHF channels were chosen to fit in with the facilities of NASA Minitrack stations.

Factors in the choice of the communications frequencies included propagation, noise, and interference within the satellite system and with other services. These were considered not only with respect to the experiment, but also from the point of view of later commercial systems. These factors lead to the choice of frequencies in the region between one and ten gigacycles.

5.1 *Propagation and Noise*

The 1- to 10-gc region is the same part of the spectrum commonly used for terrestrial radio relay systems, but the critical transmission factors are different. Radio relay systems are subject to severe selective fading due to multipath effects. When enough margin is provided for fading, atmospheric absorption is unimportant except at the upper edge of the band. Radio relay antennas, since they are pointed horizontally, receive thermal noise from the earth, and this puts a floor on the effective noise temperature of the system. On the other hand, in satellite systems, selective fading is nonexistent, except at very low elevation angles of the ground antennas. Noise received from the sky in favorable parts of the spectrum is much lower than thermal noise from the earth, so that low-noise amplifiers such as the solid-state maser can be used effectively.

Receiving system noise temperatures of satellite ground stations can be made very low compared with the approximately 300°K temperature of the earth. For example, the Andover station has an effective temperature, excluding sky noise, of about 30°K. Thus, sky noise temperatures in the tens of degrees are significant.

At one gigacycle, cosmic noise can be as high as 30°K and becomes greater at lower frequencies.[3] Above one gigacycle, sky noise due to air, water vapor and rain increases as frequency increases. Noise due to air and water vapor alone is worst at low antenna elevation angles. For an elevation of 7.5°, it is about 15°K at 1 gc and 30–60°K at 10 gc. More serious is the effect of rain. Zenith measurements at 6 gc have produced values in excess of 100°K during very heavy rainfall.[4] Unpublished data indicate that, for the same rain conditions, noise will generally be higher for low antenna elevation angles. The effect is highly dependent on frequency with the lower frequencies showing less noise.

When a radome is used, as at the Andover station, there is an additional source of noise during rain due to reflection and absorption from the wet radome. Particularly with high antenna elevation angles,

this may be the most important source of added noise. More data on this effect are needed, but they are not expected to alter conclusions regarding the choice of frequencies.

Not only is the noise temperature of the sky increased by rain, but the signal is attenuated because the raindrops scatter and absorb it. This effect is also strongly dependent on frequency, since it depends on the size of the raindrops measured in wavelengths. At 4 gc, a rainfall of five inches per hour causes about 0.2 db excess attenuation per mile of rainstorm traversed.[5] At 6 gc, the increase is about 1.5 db per mile of rainstorm. Although this rate of fall is very high, it does occur quite often for short periods during thunderstorms. The core of a thunderstorm may be some five miles in diameter. Thus it can be seen that excess attenuations of some 1 db at 4 gc and 7 db at 6 gc are indeed likely to occur a small fraction of the time, and lesser increases will occur more often. At frequencies higher than 6 gc, the excess attenuation will be higher — for instance, as much as 50 db at 11 gc.

5.2 *Frequency Allocation Considerations*

Frequencies in the 1- to 10-gc range are allocated internationally by the Radio Regulations resulting from the Administrative Radio Conference (Geneva, 1959) to a variety of services. Allocations differ in the three regions of the world recognized in the Geneva frequency tables, and there are numerous footnotes to the tables and reservations to the convention calling attention to national deviations from the tables. Furthermore, in the United States, there are further distinctions, particularly between government and nongovernment allocations.

It may be difficult for satellite communications systems to share frequencies with some of these services. For example, radio location and navigation services generally use very high power transmitters and very sensitive receivers, and hence may both cause interference to, and receive interference from, sharing services. Radio astronomy by its very nature uses very sensitive receivers, and would be vulnerable to interference from sharing services. The frequencies allocated to space research are scarcely wide enough to support a commercial satellite system on a world-wide basis.

Consideration of the variety of services in the 1- to 10-gc region led to the conclusion that the frequency space necessary for the Telstar satellite communications system could best be found by sharing with common-carrier radio relay systems. Specifically, these bands are 3700–4200 mc* and 5925–6425 mc. These bands are included in the October 22,

* In Europe, the band 3700–3800 mc is presently used for other services.

1962 "Draft Proposals of the United States of America for the Extraordinary Administrative Radio Conference for Space Radio Communication," to be presented at the conference scheduled by the International Telecommunications Union to be held at Geneva, Switzerland starting October 7, 1963.

5.3 *Coordination with Existing Terrestrial Systems*

When satellite systems share the same frequency bands with radio relay systems, it is necessary to consider four separate interference paths:

(1) satellite system ground transmitter to radio relay receivers,
(2) radio relay transmitters to satellite system ground receivers,
(3) radio relay transmitters to satellite receivers, and
(4) satellite transmitters to radio relay receivers.

The first two interferences are peculiar to the ground station sites and can be controlled by properly engineering the exposures between the satellite ground stations and radio relay routes.[6] The last two interferences must be considered on a world-wide basis, since they involve radio relay stations anywhere within view of the satellites with which frequencies are shared. These interferences must be kept acceptably small by agreement as to permissible parameters for both satellite and radio relay systems. Studies show that such coordination is possible with reasonable parameters of the terrestrial and satellite communications systems.[7]

Radio-frequency channel arrangements for the 4-gc and 6-gc common-carrier bands are given by C.C.I.R. Recommendations No. 278 and 280 (Los Angeles, 1959)* and are shown in Fig. 4. The microwave frequencies finally chosen for the Telstar system are indicated, with ground-to-satellite transmission at 6-gc and satellite-to-ground transmission at 4-gc. The high end of each band was chosen because, at least in the United States, it has been the custom to build up radio relay routes from the low-frequency end of the band and because, as previously mentioned, other services use the 3700–3800-mc band in Europe. While the frequency-sensitive factors favor 6-gc for the up direction and 4-gc for the down direction, the balance is not so overwhelming that the opposite choice is impractical. In the future it may be desirable to double satellite frequency usage by operating both ways simultaneously.

VI. THE *Telstar* SATELLITE

The Telstar satellite is a microwave repeater that receives signals from the earth, amplifies them and retransmits to the earth. The trans-

* These two recommendations were modified at the Plenary Meeting of the C.C.I.R. at Geneva, 1963, but the frequency arrangements are unchanged.

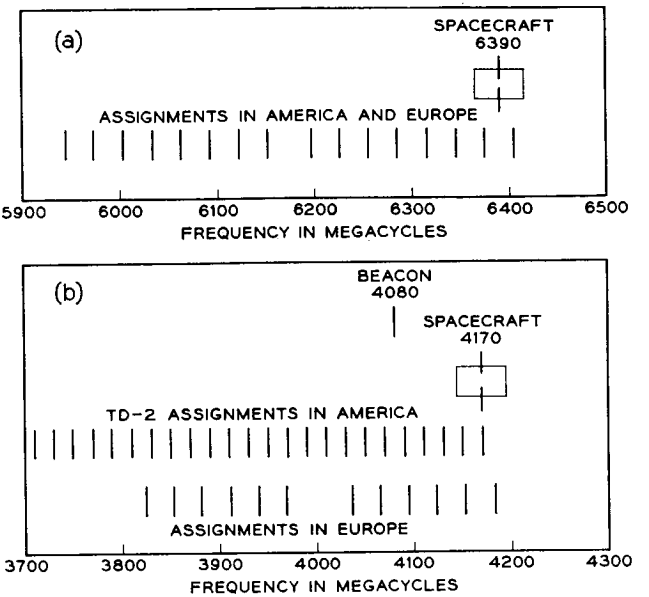

Fig. 4 — Frequency plan: (a) 6-gc common-carrier assignments, (b) 4-gc common-carrier assignments.

mission through the satellite is shown in Fig. 5. FM radio signals with a carrier at 6390 mc are received in an antenna, converted to 90 mc and amplified in an IF amplifier which supplies most of the repeater gain. The signals are then converted up to 4170 mc, amplified in a traveling-wave tube (TWT) and radiated from a separate antenna at a level of 2 watts. The beat frequency tones for the converters originate in crystal oscillators operating at about 16 mc. These frequencies are multiplied in a series of transistor and varactor doublers to the required microwave frequencies.

An interesting feature is the use of the TWT to amplify the up-converter local oscillator tone as well as the signal. This is done by combining the tone with the signal in a filter before the TWT, amplifying them together and then separating the tone from the signal in a separation filter at the TWT output. The separation filter is deliberately made "leaky" to the 4080-mc tone so that part of it is radiated as the microwave beacon for precision tracking. The 6300-mc down-converter tone is obtained by combining the 4080-mc up-converter tone with 2220 mc obtained from a separate oscillator and multiplying chain.

The primary power for the satellite is obtained from solar cells.

Silicon n-on-p cells were chosen because of their greater resistance to radiation. Radiation effects were further reduced by shielding the cells with 30 mils of synthetic sapphire. Fifty groups of cells are connected in parallel, each group containing 72 cells in series for a total of 3600 cells. The power required to operate the communication circuits, especially the TWT, is greater than the average output of the cells. A nickel-cadmium storage battery is provided to carry the peak load and also to permit operation during eclipse. The output of this battery is normally in the range of 24–27 volts. This is regulated to 16 volts, which is used directly for most of the solid-state circuits, or converted in dc-to-dc converters to the higher voltages needed for the TWT.

Since the satellite cannot be operated continuously because of power limitations, it is turned on and off by radio commands from the earth. The commands are transmitted at about 123 mc, which is received through a VHF antenna on the satellite. The command signals are amplified in command receivers, decoded, and used to operate relays which turn the communications repeater on and off. Commands are also used to turn the radiation experiment off and on, to switch between two telemetry encoders, to actuate the magnetic torquing coil and to turn the main power off and on. Duplicate command receivers and decoders are included for reliability.

The satellite transmits a continuous beacon signal at 136 mc from

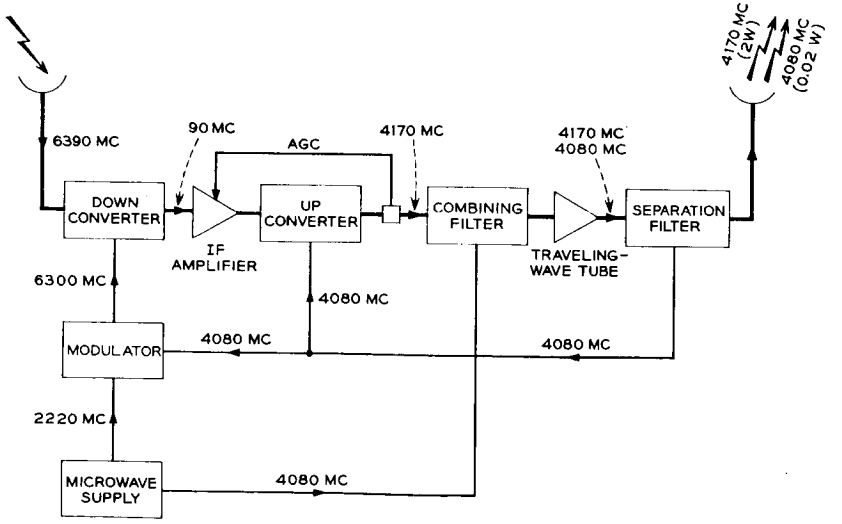

Fig. 5 — Telstar communications repeater

the same antenna used to receive commands. This is used for acquisition and coarse tracking. In addition to its use as a tracking beacon, the 136-mc signal is used as a carrier for telemetry to ground receivers. One hundred and twelve different items are measured each minute and the data transmitted to the ground by low-frequency modulations on this carrier. Measurements include information on temperatures, pressure, currents, and voltages, the state of several relays, RF power transmitted from the satellite and received signal strength at the satellite, as well as the results of the radiation experiment.

The radiation experiment is an important part of the Telstar spacecraft electronics. This experiment measures the flux of protons and electrons at several energy levels and the cumulative effect of the incident radiation on several specially designed semiconductor devices.

An external view of the satellite is shown in Fig. 6. It is a nearly spherical structure, $34\frac{1}{2}$ inches in diameter, weighing 170 pounds. It spins about an axis which is vertical in the picture. While the satellite was placed in orbit with the spin axis nearly perpendicular to the ecliptic plane, it is designed to operate, although on a reduced cycle, with the spin axis in any relation to the sun. For this reason, the solar cells are distributed approximately uniformly about the sphere.

Two equatorial bands of rectangular ports make up the microwave communications antennas. The smaller ports receive signals from the earth at 6390 mc and the larger ports transmit at 4170 mc. The design of the ports and the L-shaped diagonal probes is such that circularly polarized signals of opposite sense are received and transmitted in a nearly isotropic pattern. The pattern and circular polarization permit transmission through the satellite from all aspects without polarization tracking or loss due to cross polarization. Using opposite senses of circular polarization for the up and down paths helps to isolate the receiver from the transmitter both in the satellite and in the ground station.

The VHF command and telemetry antenna is a helical structure. It is also nearly isotropic, but is linearly polarized. Sensors for measuring solar aspect, radiation in the Van Allen belts, and the effects of this radiation, are located at several points on the outer surface. Three mirrors on the outer shell are used to reflect sunlight to the earth. Optical equipment at Holmdel, N. J., is used to observe these flashes and aid in the determination of the spin-axis orientation.

The outer structure consists of an aluminum skin on a magnesium frame. Within this outer shell and frame, a hermetically sealed cylindrical canister containing practically all the electronic circuits is suspended by nylon laces. This laced suspension provides thermal isolation from

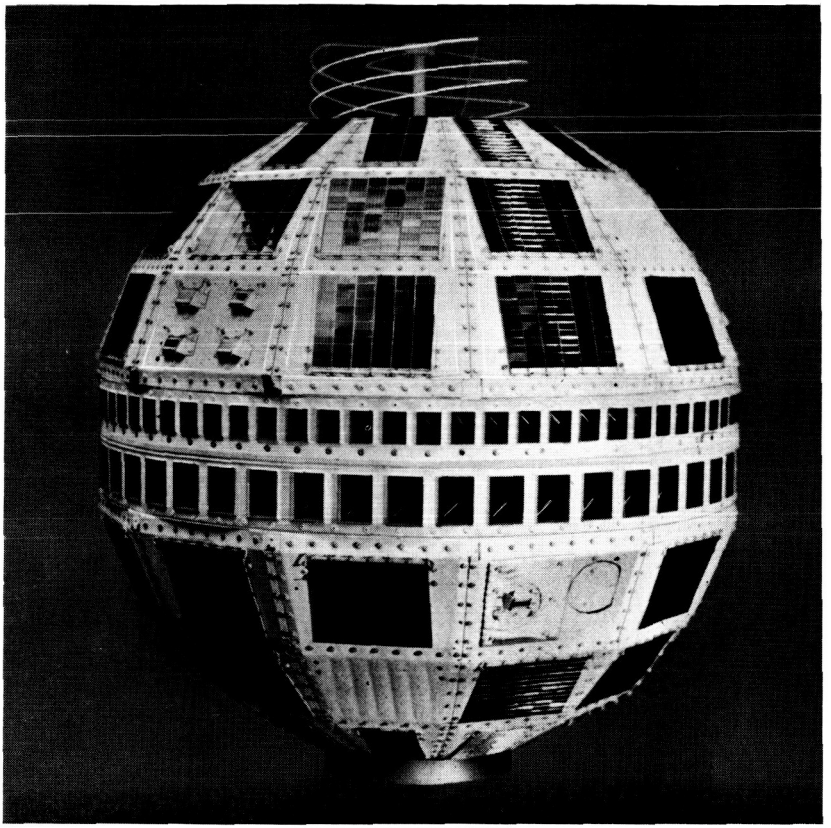

Fig. 6 — The Bell System's experimental communications satellite as it appeared before launch.

the outer shell and effectively attenuates the higher-frequency components of vibration experienced during the launch.

The circuits and subassemblies in the canister are individually encased in polyurethane foam, and the entire interior of the canister assembly is foamed as a unit and the covers welded on. The foam provides a lightweight support for the electronics and greatly reduces the effects of vibration on the subassemblies. It is extremely difficult, though not impossible, to make a repair if a failure should occur after the final foaming and welding operation. The principal reliance is on achieving a reliable unit before this step is taken.

Six complete flyable models were constructed in addition to a prototype and several special-purpose development models.

VII. THE ANDOVER GROUND STATION

The Andover ground station provides means for transmitting to and receiving from the Telstar satellite. The station includes the communications antenna, associated transmitting and receiving equipment, and means for steering the antenna to follow the satellite.

A separate microwave precision tracker is used for orbit determination. A VHF command tracker is used for acquisition and coarse tracking and for transmission of commands to and reception of telemetry from the satellite. The station has computers for the data processing involved in tracking and orbit determination and to reduce experimental data.

7.1 *The Andover Site*

In selecting the site for the Andover ground station, a location was picked which would be suitable for commercial operation as well as for the experiment. Several factors were taken into consideration,[8] principal among which were proximity to Europe and freedom from interference, existing or potential. Obviously, a site in the northeastern United States would best satisfy the first criterion.

Computations indicated that if interference was to be kept to tolerable levels, TD-2 and TH stations operating close to satellite frequencies should be at least 150 miles away if their antennas are aimed directly at the ground station. Average terrain was assumed. For other orientations of the radio relay antennas, a minimum of 40 miles was used. These values are believed to be quite conservative.[6]

Using these criteria, a number of areas in the northeastern states were selected as possibilities. Of these the one in western Maine was most promising. A siting team explored this area and selected the Andover site. Profile studies were made to existing and proposed radio relay stations and showed that interference at the Andover site would be negligible. Subsequent interference measurements confirmed this conclusion.

The location of the station is shown in Fig. 7. It is situated in western Maine close to the New Hampshire border. The site is nearly as close to Europe as is possible in the United States and is well removed from existing and potential radio relay routes. On the other hand, it is close enough to existing radio relay telephone and television routes for economical interconnection.

The connecting link consists of a four-hop system with two sections of TD-2 and two sections of TJ (11 gc) to enter the site. By using TJ for the sections closest to the site, and utilizing frequencies at the low

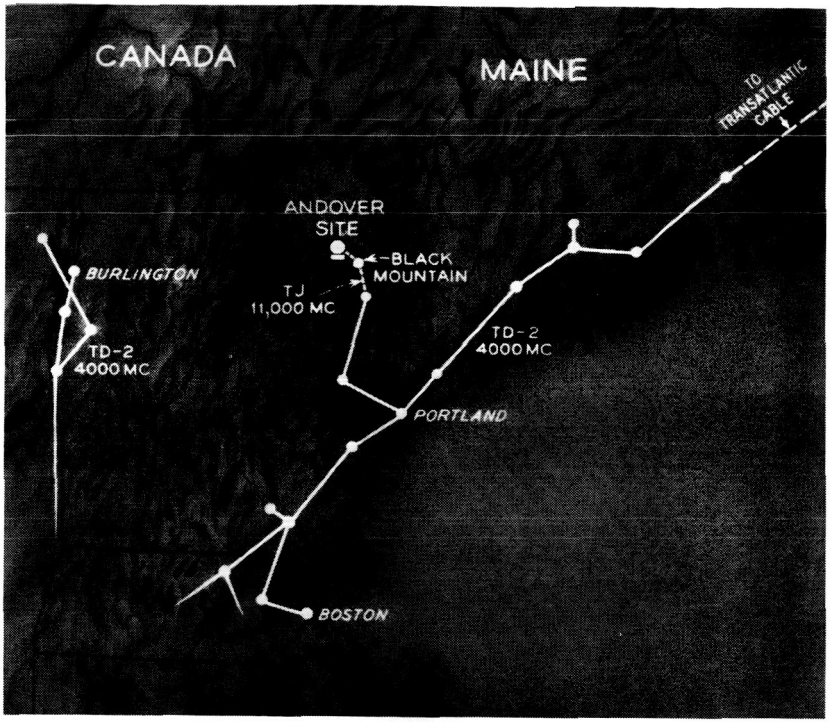

Fig. 7 — Map showing Andover site.

end of the TD-2 band, interference from the entrance link into the ground receiver has been completely avoided.

Fig. 8 is a general aerial view of the Andover site. The station is located in a wide shallow valley about 8 to 10 miles in diameter. The situation is such that additional shielding is obtained in almost all directions by surrounding hills. These are not high enough, however, to interfere significantly with the visibility of the satellite. The profile of the optical horizon from the site of the antenna is shown in Fig. 9. The tower in the foreground of Fig. 8 is for the last station of the radio entrance link. This tower houses, in addition to the TJ repeater, an electrical model of the satellite for calibrating the ground station.

A close-up aerial view of the station is shown in Fig. 10. The station is situated on a tract of about 1100 acres on top of a low rounded hill at an elevation of about 900 feet in the center of the valley. This area is large enough to permit future expansion for commercial operation. The most prominent feature of the station is the large inflated radome that

Fig. 8 — Aerial view of site.

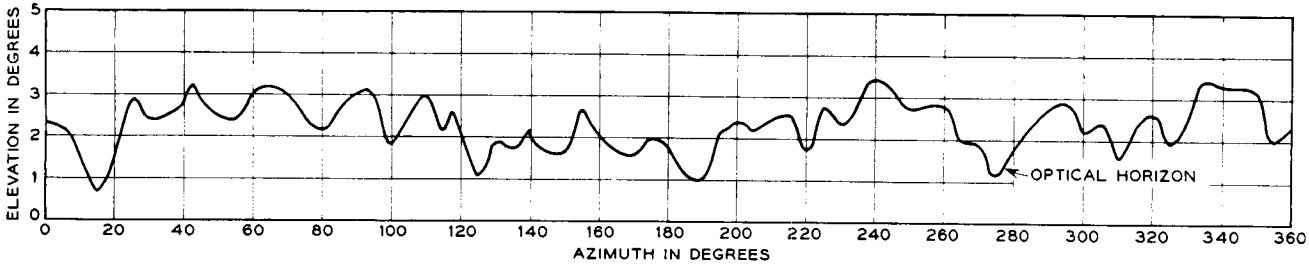

Fig. 9 — Optical horizon at Andover.

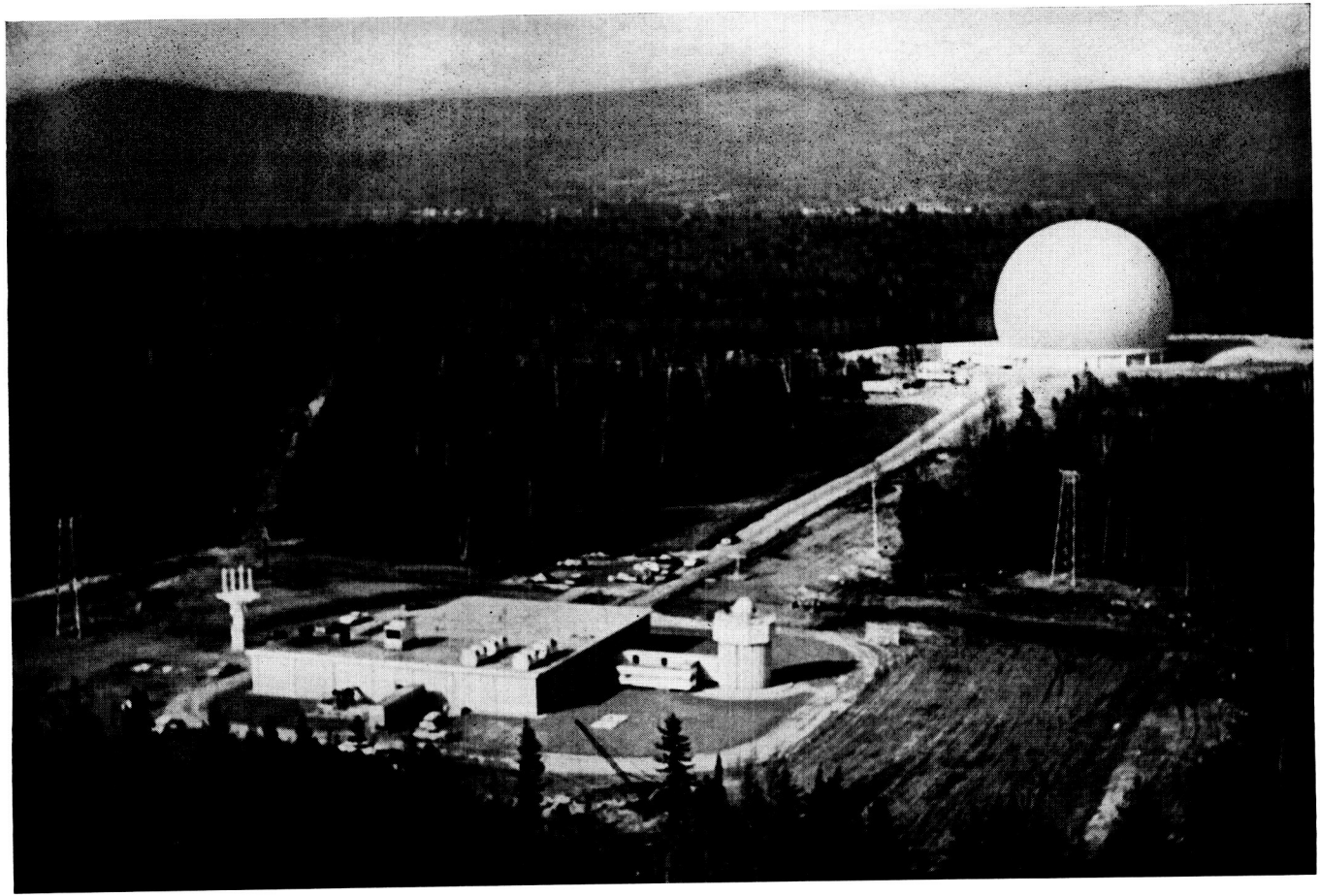

Fig. 10 — Close-up aerial view of Andover site.

shelters the horn antenna. It is made of rubberized Dacron and is 210 feet in diameter and 165 feet high. The control building in the foreground houses the equipment for terminating the telephone and television circuits brought into the station by the entrance link. It contains the equipment for making transmission tests through the satellite, as well as the heating plant for the station and diesel generators for power. Flanking the control building on the right is the precision tracking antenna on a concrete pylon and, on the left, the quad-helix command tracker antenna.

7.2 *Ground Station Transmission Plan*

A general transmission plan of the station is shown in Fig. 11. Tests or demonstrations that originate at other locations are received at 11 gc and demodulated to baseband in the control building. The link from the control building to the large horn is by video pairs. This is carried to equipment rooms on the antenna structure through slip rings. The baseband signals are used to frequency modulate the 6390-mc ground transmitter, which is connected to the horn through diplexing equipment. Incoming signals from the satellite at 4170 mc are connected to the radio receiver through the diplexer and demodulated to baseband in the equipment room and then transmitted to the control building by video pairs.

7.3 *Horn-Reflector Antenna*

The communications antenna at Andover is a much enlarged version of similar antennas widely used on Bell System microwave relay routes. A horn reflector of this type with a 20 × 20 foot aperture was used at Holmdel in the Echo experiments. Fig. 12 shows a model of the Andover antenna.* For structural reasons, the horn at Andover is conical rather than pyramidal, as was the case in the smaller versions. The antenna rotates in azimuth on two concentric rails and in elevation about the axis of the conical feed horn on two large bearings. Two equipment rooms are carried on the structure. The maser is in the upper room near the apex of the horn.

This configuration has several advantages over other possible forms. It is very broadband, presents an excellent impedance to the transmitter, and the parabolic surface is efficiently illuminated. Most im-

* Since the antenna was built under the radome and has never been exposed, it has not been possible to obtain a really satisfactory picture of the actual hardware.

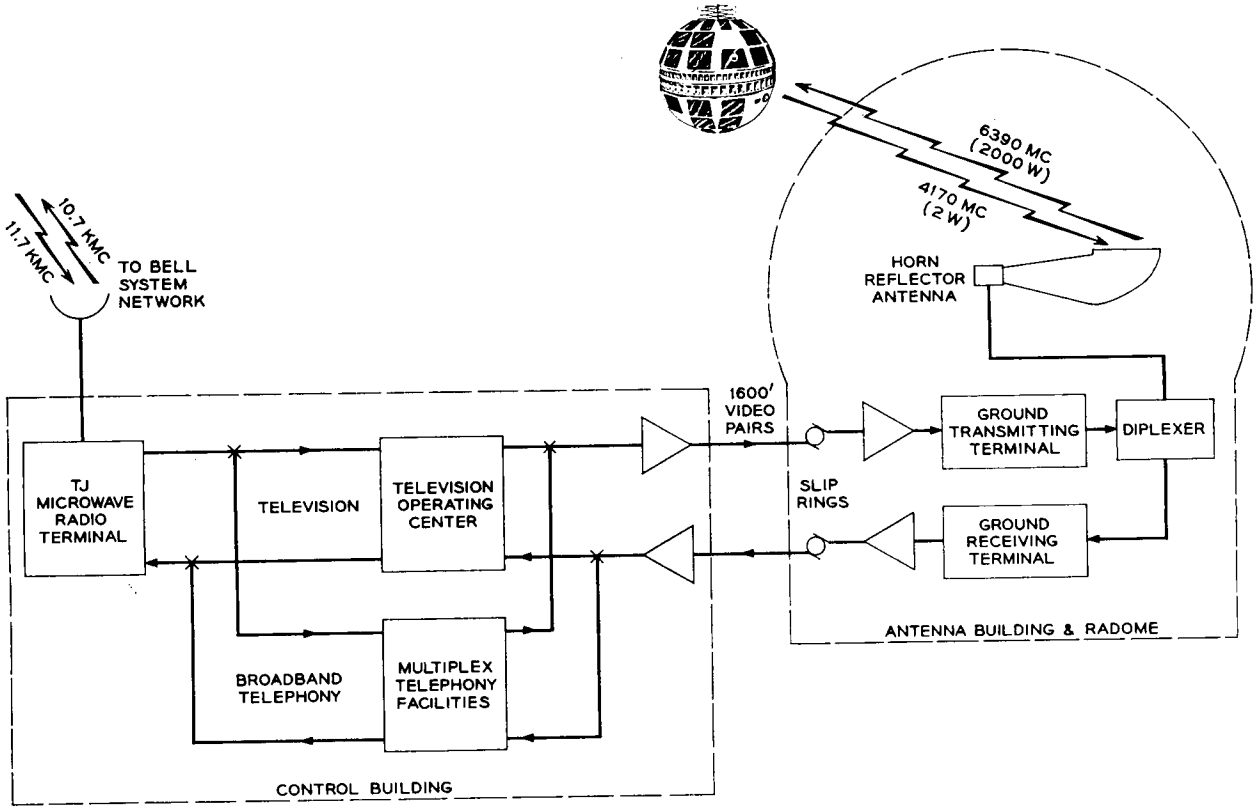

Fig. 11 — General transmission plan — Andover.

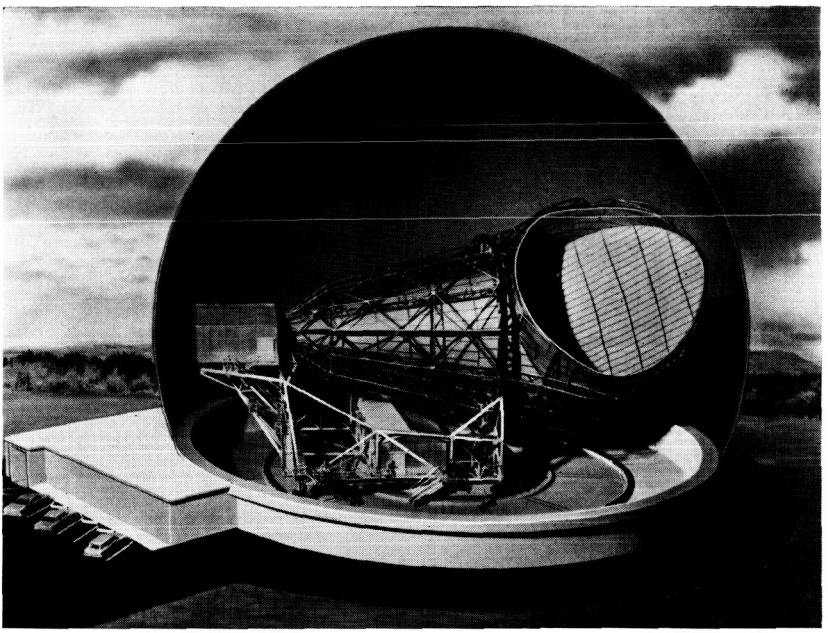

Fig. 12 — Model of Andover, Maine, antenna.

portant, however, for the present application, the antenna has very low side and back lobes and may be connected to the receiver with short, low-loss connections resulting in a low system noise temperature.

Table III gives the principal physical and performance characteristics of the Andover horn. The details of performance are covered in later papers in this series. The precision achieved on the critical parabolic surfaces is such that operation at frequencies considerably higher than 6000 mc is possible. Pointing calibration was made by tracking radio stars. The structural distortions indicated by these calibrations are corrected for in the electronic antenna direction system. The corrections are known with sufficient accuracy that, with good ephemeris data, the antenna beam may be pointed at the satellite within a small fraction of a beamwidth.

All connections to the antenna are made through slip rings located around a pintle bearing at the azimuth axis. This permits free rotation of the antenna. Cooling water, power and control leads are also carried through rotating joints and slip rings in the pintle bearing.

TABLE III — HORN-REFLECTOR ANTENNA

Structural Characteristics		
Aperture	3600 square feet	
Length	177 feet	
Weight	380 tons	
Reflector accuracy	0.060 inch (1 sigma)	
	Azimuth	Elevation
Tracking and Slewing		
Maximum tracking velocity	1.5 deg/sec	1.5 deg/sec
Maximum slewing velocity	1.5 deg/sec	1.5 deg/sec
Maximum acceleration	1.3 deg/sec^2	3.0 deg/sec^2
Error during acceleration	0.26° per deg per sec^2	
	4170 mc	6390 mc
Performance		
Gain	58 db	61 db
Beamwidth (3-db points)	0.23 degree	0.16 degree

7.4 *Transmitter and Receiver*

The ground transmitter, shown in Fig. 13, provides an FM signal of 2000 watts maximum with a peak deviation of ±10 mc. The FM deviator and modulator amplifier stages are modified versions of TH radio transmitting equipment. The output stage is a power amplifier using a high-power traveling-wave tube.

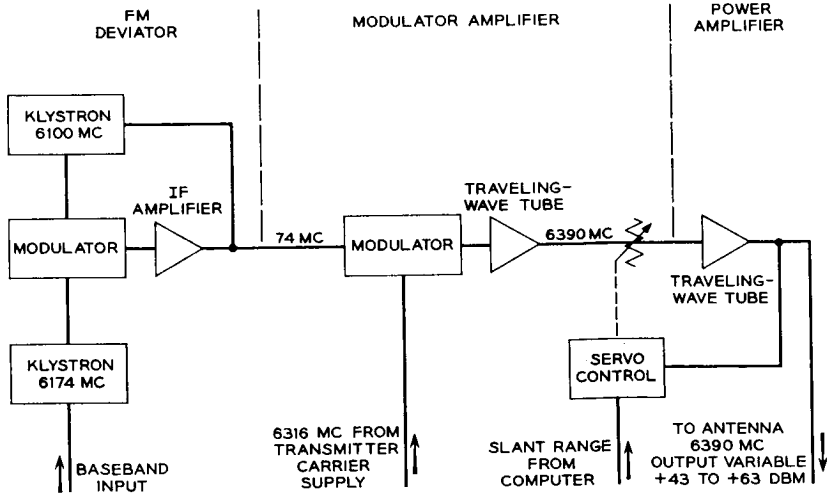

Fig. 13 — Block diagram — ground transmitter.

The center frequency is 6390 mc when the transmitter is used for television or other straight-away tests. It can be shifted ±5 mc for two-way message experiments. The servo control shown can be used to vary the output power to maintain a prescribed received power at the satellite. This is used in two-way telephone tests, where approximately equal carrier levels at the satellite are desired.

A block diagram of the receiver is shown in Fig. 14. Signals received through the antenna are first amplified 40 db by a traveling-wave ruby maser. They are then converted to a 74-mc IF frequency, where most of the receiver gain is obtained. The signals are then shifted back to the 6-gc band for demodulation in a frequency compression detector. This detector permits the baseband signal-to-noise advantage of wide-deviation FM to be realized without the loss in threshold level that would be suffered in a conventional detector of the same bandwidth. An effective compression of the noise band is achieved by feeding back part of the baseband output to a voltage-controlled local oscillator. The local oscillator follows the deviations of the incoming signal, and in this way the IF frequency deviations applied to the discriminator are reduced by the feedback factor. An improvement in threshold of 4–5 db is obtained by the feedback receiver. A standard FM detector operating at 74 mc may also be used.

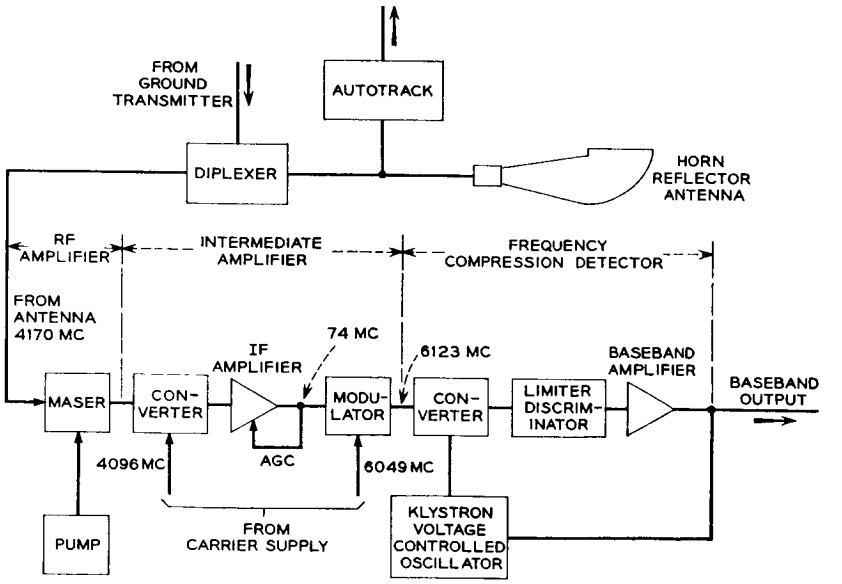

Fig. 14 — Block diagram — ground receiver.

The transmitter and receiver are located physically in the upper equipment room of the antenna structure. Unlike a conventional center-fed parabolic dish, the horn antenna allows for considerable equipment to be mounted at the feed. This has been used to good advantage at Andover, where feeder losses are kept to a minimum by locating the transmitter power stage and the maser close to the antenna feed.

7.5 *Tracking Equipment*

The tracking system at Andover consists of four parts. These are the: (1) command tracker and its control, (2) precision tracker and control, (3) horn-reflector antenna and control, and (4) computers. This is more elaborate than would be required for a commercial system. However, the flexibility that this arrangement provides is very useful in evaluating methods for future systems. Fig. 15 shows the four parts of the system and their interrelation.

The computer (IBM 1620) is programmed to derive drive tapes from any one of three different sources of information: (1) azimuth, elevation and time data from previous passes, (2) orbital elements, (3) X-Y-Z topocentric coordinates obtained from NASA. The drive tapes can be used to position all three antennas to the predicted position of the satellite. A different mode of operation which does not depend on accurate drive tapes is as follows.

The command tracker, with its wide beam of 20°, picks up the 136-mc beacon as the satellite rises above the horizon. When autotrack has been obtained with this antenna, the satellite is located to within 1°. If the telemetry indicates that the satellite is in satisfactory condition, the command sequence is started. By means of the three sequenced commands at 123 mc, the repeater in the satellite is turned on. At this time, the satellite transmits the 4080-mc beacon. With the precision tracker slaved to the command tracker, it can now acquire the microwave beacon with its 2° beam and autotrack. In this mode the precision tracker locates the satellite to within 0.02°. The horn antenna can then be slaved to the precision tracker and acquire the microwave beacon with its 0.2° beam and autotrack. Once this is accomplished, the horn can continue to autotrack without further aid.

The step-by-step procedure as outlined above is just one of many possible modes of operation. With good pointing information, the horn can be directed to acquire and then autotrack the satellite without going through the steps outlined above. This has been done on many occasions at Andover, and it is expected that a commercial system would be operated on this basis.

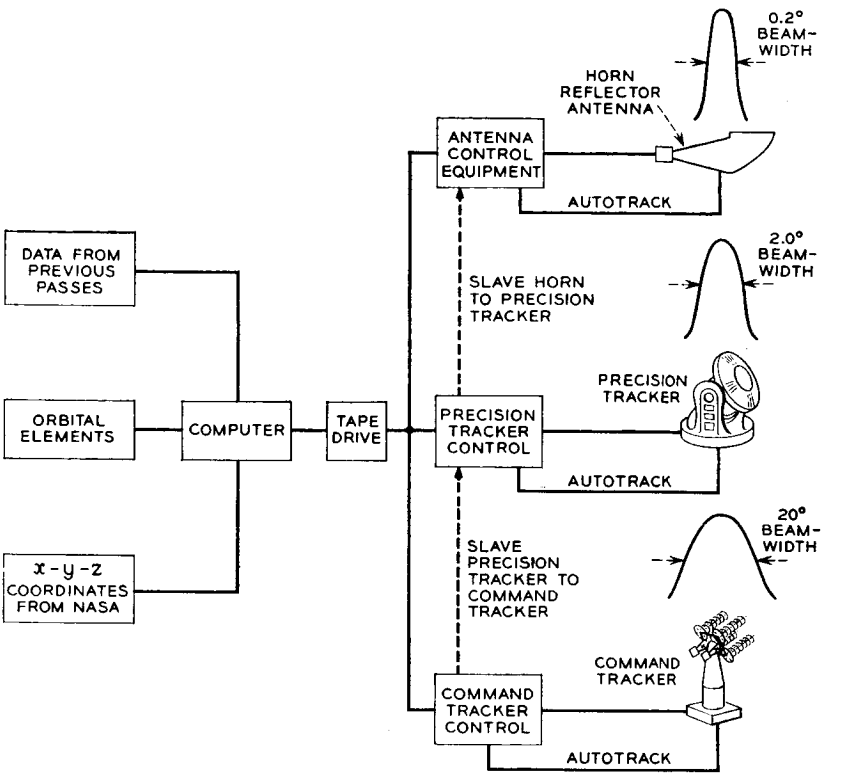

Fig. 15 — Block diagram of tracking system.

VIII. FACILITIES AT CAPE CANAVERAL

Special facilities were provided at Cape Canaveral for testing the satellite. Test equipment was located in three vans adjacent to Bell Laboratories' guidance facility and on the gantry. A command tracker like the one at Andover was provided. Compatibility of the radio frequency systems in a prototype model of the satellite with other systems involved in launching was verified about two weeks before launch. The flyable model was tested daily from the time of its arrival at the Cape and after mating with the third stage of the rocket, after spin balancing and on the gantry up to the time of launch. From lift-off, the satellite was tracked and telemetry monitored. During the following months, the facilities were used to augment Andover by receiving telemetry and, in some cases, by sending commands.

IX. TRANSMISSION PERFORMANCE

The broadband signals transmitted through the Telstar satellite were television and 600 telephone channels simulated by noise loading. In addition, the performance with 12 two-way voice channels was evaluated as well as performance with data and other special signals. Performance objectives for signals of these types have been established by the Bell System and the CCIR. Because of limitations imposed by the rocket on weight and, therefore, power, some compromise was necessary and the objectives were not met in all cases. However, the quality of these signals, when transmitted through the satellite link, is reasonably close to the objective for commercial service.

9.1 *Over-all Performance*

Table IV shows the performance with the satellite at a range of 5000 nm for the three main types of service considered: TV, 600-channel one-way telephony, and twelve-channel two-way telephony.

For TV transmission the audio signal is transmitted by frequency modulating a subcarrier located at 4.5 mc. This limits the bandwidth available for picture transmission to 3 mc. Other techniques for transmitting the sound would remove this limitation.

Two-way telephony is achieved by transmitting two carriers from two ground stations through the satellite simultaneously. These carriers are separated by ten megacycles with the carrier from Andover 5 mc above the normal center frequency and the carrier from Europe 5 mc below. Because of the lack of isotropy in the satellite antenna pattern, the two carriers may be received by the satellite with a 6-db level difference. Under this condition, compression in the TWT will cause the

TABLE IV — PERFORMANCE OF *Telstar* SYSTEM

Television	
Bandwidth	3 mc
Peak-to-peak signal to rms noise (unweighted)	41 db
Peak audio signal to rms noise	56 db
600-Channel One-Way Message	
Top telephone channel noise	49 dbrn 0*
Improvement with pre-emphasis	3 db
Noise in top telephone channel with pre-emphasis	46 dbrn 0
Twelve-Channel Two-Way Message	
Noise in top channel	45 dbrn 0

* Measured with 3A noise meter with C message weighting. 0 dbrn equals 1 picowatt at 1000 cycles.[9]

weaker carrier to be transmitted 10 db below maximum output power. The 45 dbrn 0 given in Table IV is based upon this weaker carrier power.

At 5000 nm, the quality achieved for TV transmission would be judged to be a slight picture impairment. Also under these conditions, the amount of noise in the poorest telephone channel would be 6 db more than the tentative CCIR objectives for a commercial grade circuit. For an experimental system, this performance is considered reasonable. The important consideration is that measured performance was consistent with actual parameters of the system, and that no unexplained degradations occurred.

9.2 *Fluctuation Noise*

The controlling parameter in a system such as this is noise. Table V shows the fluctuation noise performance for the ground-to-satellite and satellite-to-ground paths.

It will be noted from the Table V that the carrier-to-noise ratio in the down path is 15 db. Even with this low carrier-to-noise ratio, high quality performance is obtained by means of wide deviation FM. How-

TABLE V — FLUCTUATION NOISE

Up Path: Andover to satellite	
Maximum transmitted power (2 kw)	63 dbm
Ground waveguide losses	1 db
Ground antenna gain	61 db
Path loss (5000 nm)	187 db
Satellite antenna gain	0 db
Received carrier power	−64 dbm
Satellite antenna feed loss	2 db
Satellite receiver noise figure*	16.5 db
Noise power in 25-mc band	−83.5 dbm
Carrier-to-noise ratio in 25-mc band	17.5 db
Down Path: Satellite to Andover	
Satellite power (2 watts)	33 dbm
Path loss (5000 nm)	184 db
Satellite antenna gain	0 db
Ground antenna gain	58 db
Received carrier power	−93 dbm
System noise (50°K, 25-mc bandwidth)	−108 dbm
Carrier-to-noise ratio in 25-mc band	15 db

* The noise figure of the satellite as measured by a noise lamp is 13.5 db ±1 db. However, the noise does not have a flat spectrum over the band of interest and this number applies in the region where the noise is flat. Measurements made of the system noise spectrum using narrow-band analyzers indicate a satellite noise figure in the flat region of 15 db ±2 db. If the noise spectrum around the carrier is integrated over a 20-mc band, then an equivalent noise figure of 16.5 db ±2 db is obtained.

ever, at 10 db carrier-to-noise ratio a conventional FM receiver will start to rapidly degrade the demodulated signal. The carrier-to-noise ratio in the down path, being 15 db, is only 5 db above this threshold. Therefore, a frequency compression demodulator has been used in the Telstar system. This technique improves the threshold by about 5 db, allowing adequate margin against the onset of breaking. At 5000 nm range and with 50°K system noise temperature, the breaking margin due to the down link is 10 db. The ground to satellite path also contributes to the over-all system noise and reduces the breaking margin. With 2 kw radiated from the ground at 5000-nm range, the carrier to noise ratio at the satellite is 17.5 db. At this range for both the up and down path, the effect of the up path is to reduce the over-all carrier-to-noise ratio and the breaking margin by about 2 db. Most of the time the range is shorter and the performance is better.

A number of other factors may reduce the carrier-to-noise ratio and degrade the breaking margin. These are noncircular polarization, satellite antenna pattern, ground antenna mispointing and rain.

To the extent that the antennas at both ends of the link do not have circular polarization but are somewhat elliptic, i.e., have an axial ratio other than unity, there will be some loss of signal. The axial ratio of the Andover ground antenna system is in the order of 0.5 db and that of the satellite is 2 db in the equatorial plane. Maximum loss due to these axial ratios is about 0.1 db. When the satellite is viewed at angles 30° or more from the spin axis, the axial ratio may be as much as 4 db, but even under these conditions, the loss due to this effect is only 0.25 db.

The satellite antenna has essentially 0-db gain in the equatorial plane. It is down about 6 db at an angle $\pm 60°$ from the equator. The pattern is quite smooth around the spin axis with a ripple of about ± 1 db. This is adequate to maintain the signal above the FM threshold, especially since an unfavorable aspect and maximum range will rarely coincide.

The signal loss due to antenna mispointing is less than 0.1 db. This is due to the use of the vernier autotrack, which is capable of maintaining the antenna beam to within 0.005° of the satellite's position.

It has been observed that system noise temperature can increase to 130°K in the presence of heavy rain. This can be ascribed to the increase in sky noise and the effect of the wet radome. The degradation of carrier-to-noise ratio under these conditions is 4 db compared to conditions on a clear day with the antenna at zenith. With the system parameters described and the margin available, operation above threshold is still possible.

TABLE VI — FM DEVIATIONS

Video	
TV bandwidth	3 mc
Peak-to-peak frequency deviation (picture)	14 mc
Peak-to-peak frequency deviation (picture + aural subcarrier)	16.8 mc
Bandwidth of audio channel	8 kc
Peak-to-peak frequency deviation (audio on 4.5-mc aural subcarrier)	100 kc
600-Channel Noise Loading	
Peak frequency deviation due to noise loading signal	10 mc
RMS frequency deviation due to noise loading signal	1.77 mc
RMS frequency deviation per telephone channel	72 kc
Twelve-Channel Two-Way Message	
Baseband signal	60–108 kc
Peak frequency deviation for twelve channels	1 mc
RMS frequency deviation per channel	16 kc

9.3 *FM Deviations*

Based upon the fluctuation noise indicated in Table V, the required modulation indices were determined. These are given in Table VI.

9.4 *Amplitude and Phase Distortion*

The presence of amplitude and phase distortion causes transmission degradation which adds to that caused by thermal noise. This form of distortion does not affect the breaking margin, but adds to the noise at baseband. The most important forms of nonlinear distortions are envelope delay distortions[10] and differential gain. In a two-link radio relay system such as Telstar, this distortion can be made small compared to thermal noise. In the allocation of system impairments, the total for intermodulation noise is 36 dbrn at the 0-db transmission level. Fig. 16

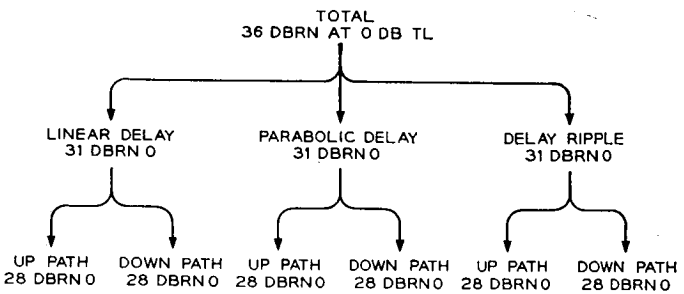

Fig. 16 — Allocation of intermodulation noise.

TABLE VII — DELAY DISTORTION OBJECTIVES

Frequency with respect to carrier — mc	±2	±4	±6	±8	±10
Linear delay distortion — nanoseconds	1.2	2.4	3.6	4.8	6
Parabolic delay distortion — nanoseconds	1.1	4.5	10	18	28
Delay Ripple					
Ripple periodicity — mc	0.3	0.6	1.5	3.0	6	15
Peak delay ripple — nanoseconds	30	15	6	3	1.5	1.5

indicates how this total is divided among the various sources. Assuming the parameters indicated previously for the 600-channel noise loading signal and the use of pre-emphasis,* Table VII indicates the delay distortion objectives. The figures indicated in Table VII apply to both the up-path and down-path equally.

The differential phase would be 4.2° if the objectives in Table VII are met. For N.T.S.C. color the requirement is 5°, so that this set of performance objectives is consistent. The performance measured for television and the 600 telephone channel simulated noise load indicates that these objectives have been met.

X. CONCLUSIONS

The Telstar system has demonstrated that wideband communications by means of an active satellite is feasible and that performance is predictable on the basis of system parameters. A ground station system has been tested and shown to be operable under a wide range of weather conditions and with a variety of tracking techniques. A large amount of data on the space environment has been gathered and analyzed and has added valuable information concerning the conditions which a satellite must withstand. The satellite, the Andover ground station, and the radiation experiment are discussed in more detail in companion papers.

REFERENCES

1. Jakes, W. C., Jr., Participation of Bell Telephone Laboratories in Project Echo and Experimental Results, B.S.T.J., **40**, July, 1961, pp. 975–1028; see also other papers in this Project Echo issue.
2. Rinehart, J. D., and Robbins, M. F., Characteristics of the Service Provided by Communications Satellites in Uncontrolled Orbits, B.S.T.J., **41**, September, 1962, pp. 1621–1670.
3. Pierce, J. R., and Kompfner, R., Transoceanic Communication by Means of Satellites, Proc. I.R.E., **47**, March, 1959, pp. 372–380.
4. Hogg, D. C., and Semplak, R. A., The Effect of Rain and Water Vapor on

* The pre-emphasis assumed starts at 3 mc with 6 db per octave slope and continues until a total of 10 db of pre-emphasis is reached.

Sky Noise at Centimeter Wavelengths, B.S.T.J., **40,** September, 1961, pp. 1331–1348.
5. Hathaway, S. C., and Evans, H. W., Radio Attenuation at 11 kmc and Some Implications Affecting Relay System Engineering, B.S.T.J., **38,** January, 1959, pp. 73–98.
6. Curtis, H. E., Interference between Satellite Communication Systems and Common Carrier Surface Systems, B.S.T.J., **41,** May, 1962, pp. 921–944.
7. Preparatory documents for Xth C.C.I.R. Plenary Assembly, particularly those submitted by the United States and the United Kingdom for Study Group IV.
8. Caserta, Nino, Engineering Considerations in the Selection of Andover, Maine, as the Location for the Bell System's Satellite Ground Station, A.I.E.E. Conference Paper, 62–328.
9. Cochran, W. T., and Lewinski, D. A., A New Measuring Set for Message Circuit Noise, B.S.T.J., **39,** July, 1960, pp. 911–932.
10. Bennett, W. R., Curtis, H. E., and Rice, S. O., Interchannel Interference in FM and PM Systems under Noise Loading Conditions, B.S.T.J., **34,** May, 1955, pp. 601–636.

A General Description of the *Telstar* Spacecraft

By R. H. SHENNUM and P. T. HAURY

(Manuscript received February 6, 1963)

The Telstar spacecraft design is discussed with emphasis on the electronics system. The description includes early planning, starting with frequency allocation considerations, and carries the program through electrical and mechanical design, construction and evaluation of the electronics system. The content is aimed at a broad introduction, depending on companion papers for many details of the spacecraft design.

I. INTRODUCTION

A description of the Telstar spacecraft presented in this paper is developed chronologically so that the reader may understand how each of the decisions influenced the design and construction which followed. Foremost in practical considerations affecting the satellite design was the selection of the Delta vehicle to launch the spacecraft.

II. BACKGROUND

Another paper of the series[1] outlines the needs for an orbit which would reach the vicinity of 3000 nautical miles apogee with a perigee of at least 500 nautical miles. The capability of the Delta vehicle to put a satellite into such an orbit, with the restriction of a launch from the Atlantic Missile Range and the desired inclination of the orbit plane to the equator of 45°, limited the permissible weight of the spacecraft to the order of 180 pounds. This weight limit was a severe restriction to incorporation of many ideas which were proposed early in the development. The second characteristic of the Delta which was influential in the Telstar spacecraft design was the existence of only two fairings and the decision not to undertake the development of a new one. The larger of the two, which had been tested repeatedly in satellite launchings and was large enough for our purposes, was selected as one which would be suitable for the spacecraft, as described in Section IX. The third aspect

of the Delta which was influential in planning the Telstar system was the need for spin stabilization of the third stage, which is a solid fuel motor without radio guidance. Typical spin rates of 200 revolutions per minute are used for this third stage and, while it would have been possible to despin the satellite after injection into orbit, it was judged desirable to utilize the spin for stabilization. In this way, the weight which would otherwise have been associated with a despin mechanism was saved. The detailed development of the structure of the frame, the shape of the spacecraft, and other mechanical aspects are treated in another paper in this issue.[2]

III. FREQUENCY ALLOCATION

Project Telstar was planned from the first as being primarily a communications experiment. However, other scientific experiments were also a very important part of the early planning. The selection of the frequency assignments used in Project Telstar is mentioned in Ref. 1. As discussed in that paper, some early thinking was based upon the assumption that new frequencies exclusively for the use of satellite communications could be assigned, and that interferences into and out of the ground receiver and transmitter, respectively, would be eliminated. It became apparent as the project developed, however, that such frequencies for exclusive use were not to be available for the Telstar experiment, so plans were developed for joint use of the 4-gc and 6-gc common-carrier bands with existing land-based microwave equipment. Both of these bands are in the broad spectral region where galactic noise is almost negligible compared to signals expected to be received at the ground station, and where atmospheric absorption is not a serious matter. The 4-gc band is, however, in the more favorable region and was chosen for the spacecraft microwave transmitter. The actual frequencies to be used were so chosen that they coordinated in the 4-gc region with existing TD-2 system assignments in this country and abroad, and in the 6-gc band with the TH system assignments, which are the same throughout the world. As seen in Fig. 1, the 16 satellite channels either coincide with existing common-carrier frequencies or fall approximately midway between bands. Concurrent work by H. E. Curtis was reported earlier.[3] His proposed frequency allocation plan, though very similar in most respects, resulted in frequencies slightly different from those actually used in the Telstar plan.

Although the Telstar repeater was conceived from the beginning as a single broadband amplifier, it was considered necessary that the frequencies used would be consistent with those which would later be

assigned to multichannel communications satellite systems. Allocations were studied and based on both six and eight channels allocated in each of the 500-mc* bands at 4 and 6 gc, respectively. The final choice of frequencies for the Telstar plan was based on an assignment which permits the eventual existence of eight broadband channels. In addition to the selection of frequencies for the broadband amplifier, a microwave beacon was an important part of the planning. Fig. 1 is a diagram giving the allocations both in the U. S. and in Europe in the 4- and 6-gc common-carrier bands and showing the location of the eight up and eight

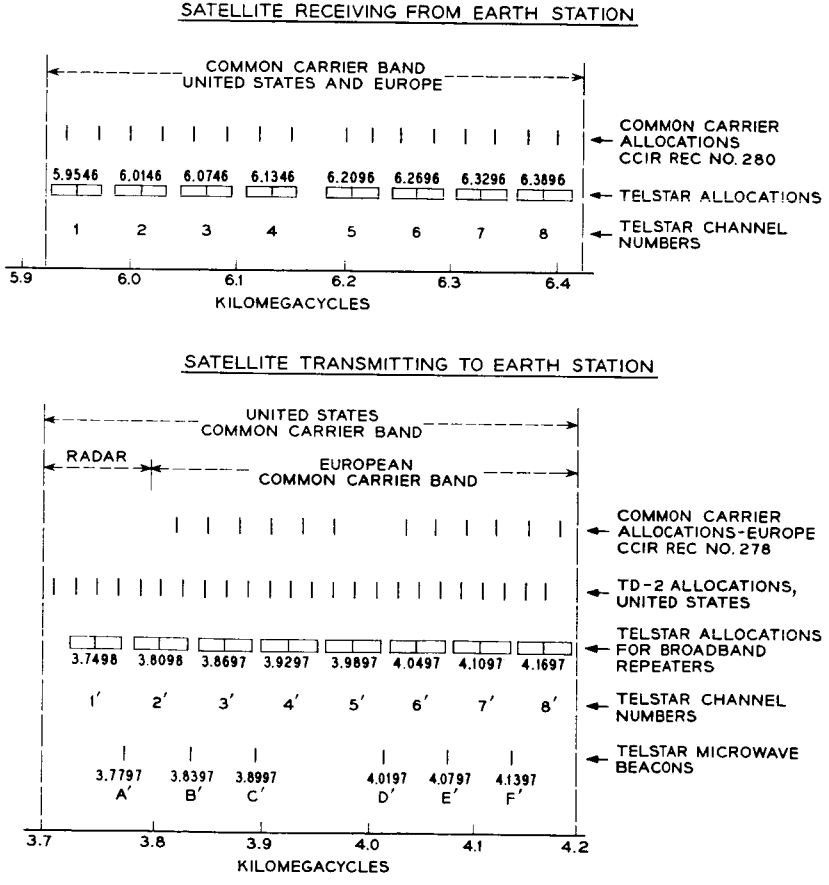

Fig. 1 — Frequency allocations

* Abroad, the 4-kmc band is narrower than the U. S. 500-mc assignment, as seen in Fig. 1.

down channels which are recommended for satellite use, as well as the frequencies for the associated microwave beacon tones. Channels 8 and 8′ with beacon E′ were used for Project Telstar.

To minimize the amount of electronic equipment in the spacecraft, the microwave beacon was obtained from the pump frequency of the up-conversion process. Consequently, the separation between the microwave beacon and the center of the broadband channel determined the midfrequency of the intermediate-frequency amplifier. The state of the art of transistor amplifiers for intermediate frequency use with proposed bandwidth of 50 mc dictated a center frequency above that which typically had been used for land-based microwave equipment. Preliminary designs of IF amplifiers which existed at the time of the beginning Telstar program made possible a center frequency of as high as 100 mc. The last constraint which was introduced into the calculations, and the one which in the final analysis proved to be the most limiting, was the requirement that the down conversion and the subsequent up conversion be accomplished by use of a pair of frequencies obtained from a coherent microwave carrier supply, with a single crystal-controlled oscillator producing both local oscillator signals. As will be noted in the discussion to follow, this last-stated objective was not to be attained, and an alternate method was adopted.

Fig. 2 shows a block diagram of the microwave carrier supply originally planned, with levels and frequencies sufficiently accurate for engineering purposes satisfying the previously stated requirements. This basic block diagram is readily expandable to obtain all necessary frequencies for an 8-channel system from a single crystal oscillator. Calculations by R. W. Hatch in unpublished work show that the noise associated with a non-

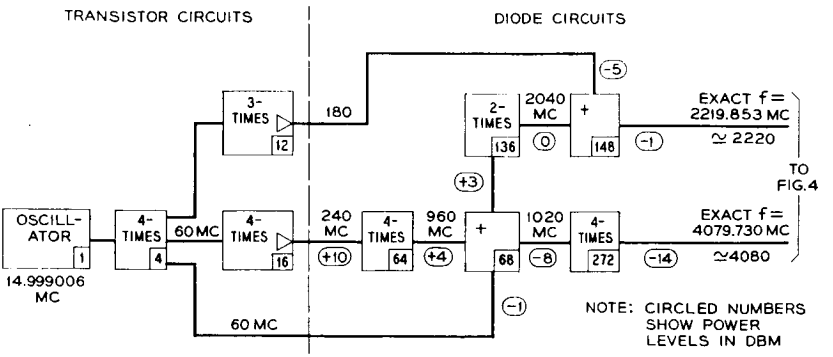

Fig. 2 — Single oscillator microwave carrier supply originally proposed.

coherent microwave carrier supply is not a major contributor to the over-all system noise. Despite the fact that it would have been desirable to eliminate this small noise contribution, the schedule of the Telstar program did not permit carrying to completion the circuitry indicated in Fig. 2. The decision was made about midway through the program (Aug., 1961) to implement the microwave carrier supply along the lines shown in Fig. 3, where two separate crystals are used. The resulting frequencies are the same as those in Fig. 2 to the first six significant figures. Better coordination with the existing land-based microwave systems could have been obtained by use of the two-oscillator approach. However, other parts of the program were so far advanced that a frequency change at that time was not possible.

IV. THE ELECTRICAL REQUIREMENTS OF THE MICROWAVE RECEIVER

The over-all signal-to-noise performance is summarized in a preceding paper.[1] Parts of this will be repeated and expanded in this discussion in order that an over-all description of the satellite proper may be contained within this paper. Data given here will supply the details necessary for the understanding of the block diagram of the communications repeater shown in Fig. 4. The nominal planned received signal for mid-range operation at the input to the converter is −60 dbm. There is an allocation of loss of 2 db between this point and the antenna, so that the nominal signal received into the antenna is −58 dbm. The IF amplifier operates with a midfrequency of approximately 90 mc and has a bandwidth requirement at the 1-db points of ±25 mc about this midfrequency. The automatic gain control was specified to operate over a signal range of approximately +5 to −12 db. The traveling-wave tube

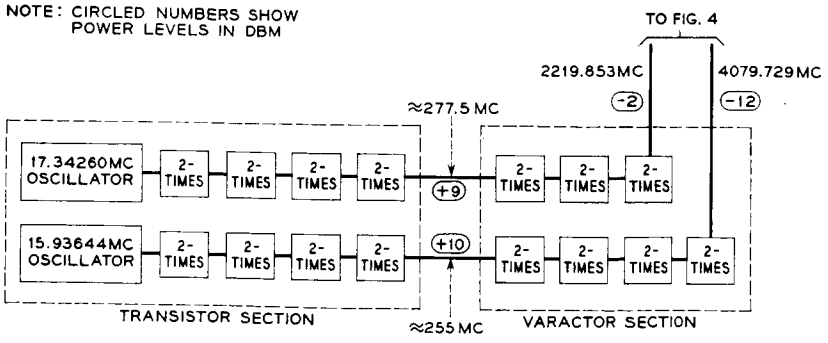

Fig. 3 — Final microwave carrier supply.

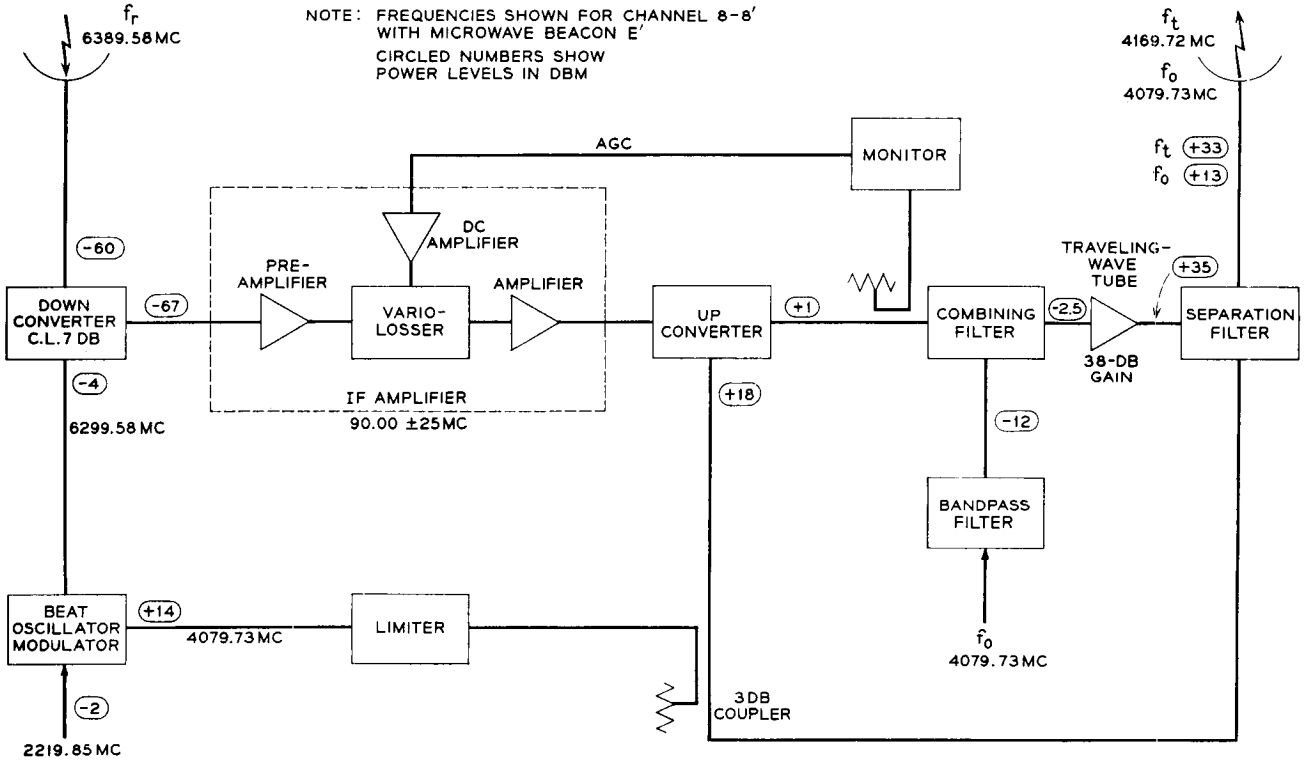

Fig. 4 — Telstar satellite amplifier simplified block diagram.

(TWT), the only electron tube in the Telstar satellite, amplifies two signals simultaneously. One, the main broadband signal with approximately 50 mc potential bandwidth, is required at an operating point in the tube at which the gain is 37.5 db and the power output is +35 dbm. The second signal at the output of the tube is 13 db lower than this main signal (i.e., +22 dbm), and under the condition of simultaneous existence of the two signals, separated in level by 13 db, the gain for the low-level signal is 35 db. The circuitry thus operates in a reflex mode such that the 4080-mc signal, which is one of the outputs of the microwave carrier supply, is combined with the main signal in the combining filter, amplified through the traveling-wave tube, and in the separation filter is largely transmitted back into the microwave repeater for use as the pump frequency in the up-conversion process. Part of the 4080-mc signal is also combined in the beat-oscillator modulator with a second output from the microwave carrier supply to produce the beat oscillator frequency for the down-conversion process. As will be discussed later, a small part of this 4080-mc signal at the output of the TWT is directed by the separation filter directly to the microwave transmitting antenna, where it is radiated to the earth station and used by the precision tracker and system autotrack for acquisition and tracking of the satellite. The radiated signal strength of the 4080-mc beacon at the output of transmitting antenna was required to be at a minimum power level of +13 dbm. The circuit design of the microwave repeater with its TWT in this dual-amplification mode with two signals widely separated in level was based on analytical predictions and early experimental work which was done by P. R. Wickliffe and reported in unpublished work. The experimental work was performed at 6 gc with traveling-wave tubes which were of sufficiently similar structure to the tube proposed for use in the Telstar repeater circuit that it was felt reasonable to extrapolate the results to the 4-gc operation.

V. THE ELECTRICAL DESIGN OF THE COMMUNICATIONS REPEATER

The operating levels of the communications repeater are given in the block diagram of Fig. 4. The design requirements have been discussed in the preceding section. This section describes briefly the realization of the system satisfying these requirements. The down-conversion system, consisting of down converter and its associated filters and beat oscillator signal from the microwave carrier supply, is in broad principle similar to those used in earlier land-based microwave systems.[4] The physical structure is, however, quite different and is based on operation of the

received signal and beat oscillator signal in orthogonal modes in a round waveguide. This is described in detail in another paper in this issue.[5] The noise figure and conversion loss, 12.5 db and 7 db respectively, resulting from this configuration, are both within the ranges which have been obtained at this frequency and bandwidth by earlier experimenters. However, the level of the beat oscillator signal (−4.0 dbm) to the down converter is substantially below that normally used. This low oscillator signal level was, of course, used because of the necessity to conserve power and to operate at the lowest practical level; however, small changes in power level are not troublesome with the regulation schemes provided. Similar statements concerning power levels can be made about almost every other block within the communications repeater.

The IF amplifier and associated automatic gain control will be described in considerable detail later in this issue.[5] The IF amplifier has a common-emitter doublet input stage working into a resistive load. The bandwidth of the IF amplifier is 50 mc, while the noise figure is 4.5 db. The 90-mc signal is amplified using broad-band common-emitter transistors with local shunt feedback. The amplifier is so designed that, should one of these transistors open circuit, the feedback network would operate to continue to provide a fairly flat transmission path without excessive loss.

The last two stages of the amplifier are common-base circuits. These circuits provide linear amplification at output power levels up to +6 dbm. A 20-db return loss is maintained at the output over the 50-mc frequency band. The maximum gain of the IF amplifier is 87 db. The gain of the amplifier is controlled using two similar resistive T-network diode variolossers. Each gives approximately 15 db of control range, more than satisfying the original requirement for a 17-db range.

The AGC variolossers are driven by a dc amplifier requiring four transistors. These are arranged in a differential input stage followed by two common-emitter stages. The sensing for the AGC is a measure of the signal output of the up converter, in contrast to the more usual method of monitoring the output of the IF amplifier. Since the up converter operates with relatively low pump power, its output is subject to some variations caused by temperature changes and aging. The action of the AGC compensates for these variations and ensures constant input to the TWT.

The up-converter is a balanced diode modulator in which the 90-mc signal is shifted to a frequency band centered at 4170 mc. It was designed for temperature stability and minimum susceptibility to fluctuations in

beat oscillator power. Consequently, the conversion gain of the device is low — only about 2 db.

The 4170-mc signal passes through a filter-monitor combination. The monitor is part of the AGC circuit, which ensures that the level of the signal fed to the TWT is constant. The monitor contains two separate diodes, mounted in the waveguide in a configuration designed to minimize directivity. The time and temperature stability of the monitor is better than ± 0.25 db.

The TWT amplifier is unusual for its high efficiency. A single-reversal permanent magnet is used for beam focusing in place of the customary straight field magnet such as that used in TH radio.[6] In addition to saving weight, this arrangement gives a substantial reduction in the associated magnetic dipole of the spacecraft, which must be neutralized by the addition of small magnets on the surface of the satellite to limit interaction with the earth's magnetic field. A net magnetic moment for the satellite of 1 ampere-turn meter squared was attained.

Some of the design parameters of the traveling-wave tube are given in Table I. It is of interest to note that the voltages and currents have been chosen to give maximum over-all efficiency, including the heater power, rather than maximum electronic efficiency. In the present design, lowering the collector voltage below the helix voltage increases the efficiency appreciably. The TWT is operated in the nearly linear region, where the output power is about 1.25 db below the saturation output power. This is done both to assure stability of the over-all circuit and to reduce intermodulation. The anode voltage is kept above the helix voltage to provide ion pumping. Further details describing the tube have been included in another article in this issue.[6]

The final microwave carrier supply provides local signals at approximately 4080 mc and 2220 mc. These frequencies are derived from crystal oscillators which drive transistors and varactor-multiplier chains as shown in Fig. 3. The two paths are similar except for the output stages, so only the one with the larger multiplication is discussed. The

TABLE I

Helix voltage	1500 volts
Anode voltage	1750 volts
Collector voltage	750 volts
Cathode current	17.5 milliamperes
Output power (saturated)	4.5 watts
Heater power	1.5 watts
Collector power	13 watts
Gain (saturated)	36.5 decibels

nominal 4080-mc (microwave-beacon frequency) path starts with a solid-state Pierce oscillator at about 15.9 megacycles. To ensure maximum short-term stability, the oscillator is operated at a high level. Since the crystal is driven hard, it is necessary to have crystals that are free from unwanted resonances at this operation level over the whole temperature range likely to be encountered. The long-term stability is determined mainly by the temperature characteristic of the crystals. All units manufactured met the specified limit of five parts per million, and in the Telstar satellite the microwave beacon has a stability of better than one part per million from 0 to 60°C. It is expected that the effect of aging will be of the order of one part per million per year.

The output of the oscillator is fed to a doubler stage and then the signal is alternately passed through transistor-doubler stages and amplifier stages until a frequency of 255 mc is reached. Temperature compensation is provided to the last four stages, keeping the output constant to 0.2 db over a range from $-10°$ to $+50°$C.

The 255-mc signal from the last transistor doubler is passed to a three-stage varactor multiplier using conventional lumped circuits. The output from these circuits is fed into a coaxial doubler, which connects the 4080-mc signal through a transducer into the combining network that feeds the traveling-wave tube. The units performed well and the entire harmonic-generator system showed less than 1.5 db variation in level over the temperature range 0 to 50°C.

VI. TELEMETRY AND COMMAND

The need for a telemetry system arises from three types of required measurements:

(a) communications experiment data such as transmitted and received signal strengths, and states of several relays;

(b) general "housekeeping" data such as temperatures, pressure in canister, currents and voltages of subsystems;

(c) radiation experiment measurements related both to integrated damage to solar cells and transistors and to counts of electrons and protons in several energy bands.

To simplify the telemetry in a way which is consistent with the design of the entire electronics system, it was decided to use a one-per-minute frame rate, which is very slow compared to normal industry standards. A tabulation of the necessary measurements in the three categories previously listed indicated that 118 channels would provide the required

data. The final channel assignment is described in some detail in another paper of this series.[7] The channels are approximately equally divided into the three categories which were listed earlier. Because of the needs of the radiation experiment for high accuracy, it was decided to use a PCM system with 7 bits, giving slightly better than 1 per cent basic coding accuracy and an over-all accuracy including the effect of gating of approximately 1 per cent. While most of the channels are sampled in analog fashion and converted to digital form, direct digital counts are used in much of the radiation particle counting, in order to increase the accuracy of the measurements. This is described in detail by Ref. 8 of this issue. The modulation scheme utilized to impress the telemetry information on the 136.05-mc VHF beacon (the power output of which is +23 dbm) involves two stages of modulation. The PCM signal is first changed to a frequency-shift form of modulation with frequencies of 3225 and 2775 cps representing the binary 1 and 0, respectively. This is then amplitude-modulated onto the 136.05-mc carrier. This form of modulation was utilized to keep the major sidebands far enough removed from the 136.05-mc carrier that it would be possible to utilize the carrier for tracking purposes in the presence of the telemetry signal. The percentage modulation was limited to 50 per cent to limit the sideband amplitudes and hence to ease tracking problems.

The need for a command system was established when the decision was made to operate the TWT only part time and to depend upon energy stored in a nickel-cadmium battery for the operation of the tube. The solar plant, when new, delivered slightly under 15 watts. This is expected to fall to two-thirds this value in a two-year period. With all the subsystems in the satellite operating simultaneously, the required power is more than twice that which is available from the new, undamaged solar plant. The command system provides sequential turn-on and turn-off of three voltages for the traveling-wave tube. The sequencing is controlled from the ground in order to permit the simplest possible satellite electronics system. In addition to the five commands which are utilized for TWT operation, commands are provided to turn the telemetry off and on and to switch or reverse the current in an orientation loop provided to correct spin-axis orientation, should this be required. Commands are also provided for test purposes to evaluate the operation of the two separate redundant command systems. Finally, it is possible to control a battery-cutoff relay which is provided to protect the nickel-cadmium cells from excessive discharge.

The command code structure was chosen to be consistent with that in use by the National Aeronautics and Space Administration Minitrack

network, (in order that the far-flung Minitrack stations would have command capability). The 15 command signals are at a frequency of approximately 123 mc and are modulated in a pulse-duration manner which is described in detail in Ref. 8. The block diagram, Fig. 5, shows the association of the command and telemetry and beacon systems, coupled through a diplexer to a common VHF antenna.

VII. ANTENNAS

Separate microwave antennas (pictured in Fig. 6) are used for the 6390-mc reception and the 4170-mc retransmission of the broadband microwave signal. The receiving antenna, the upper of the two equatorial units, consists of 72 boxes or ports which are coupled together with matched amplitude and phase so that the pattern of the antenna around the equatorial region of the satellite varies about 2 db peak-to-peak, as shown in Fig. 7(a). The antenna has reasonably uniform properties for an angle of $\pm 60°$ about the equator, leaving at either pole a cone with

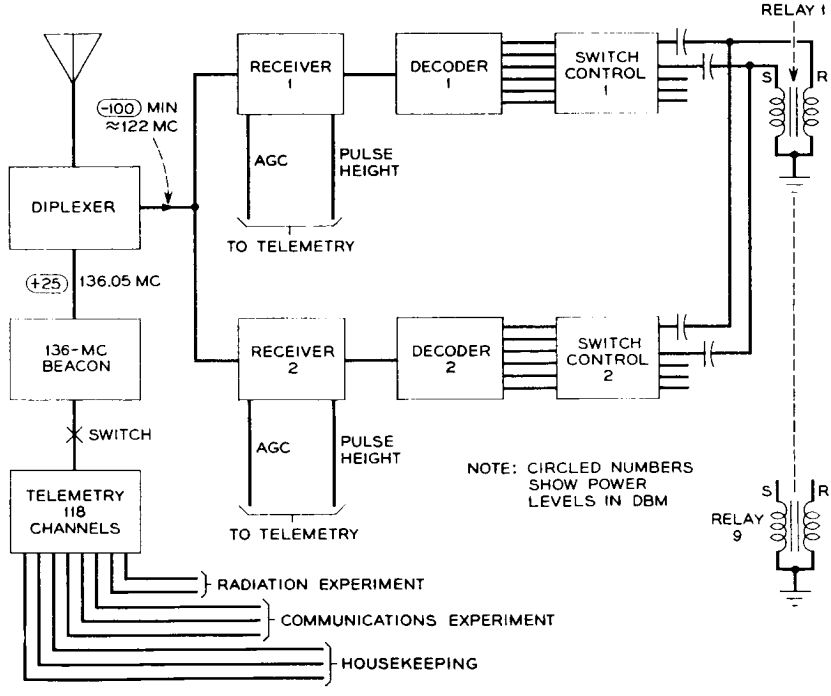

Fig. 5 — Telstar command and telemetry.

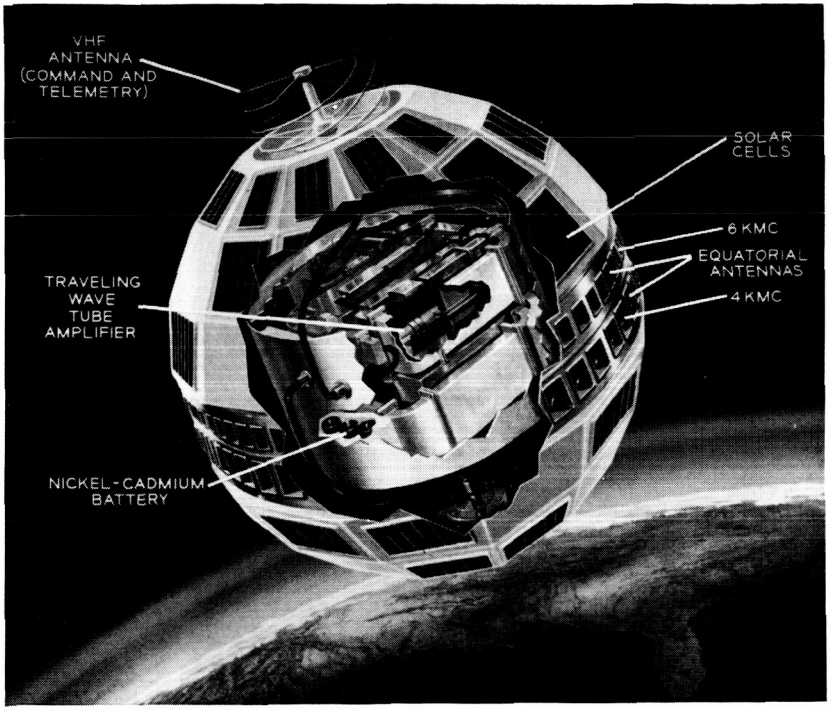

Fig. 6 — Spacecraft, showing antennas.

a half angle of 30° containing deep nulls. The details of the antenna are described by Ref. 9. The goal of the design was to produce a circularly polarizing antenna having a near isotropic pattern.

The microwave transmitting antenna is very similar to the one used for reception. It consists of 48 apertures, again equalized for amplitude and phase, and has radiation properties similar to those just described for the receiving antenna. The transmission loss between the receiving antenna and the down converter is approximately 2 db, while the loss between the output of the traveling-wave tube and the radiating apertures of the transmitting antenna is about 1.5 db. Contributing to these losses are the coaxial cables which couple the electronics canister to the radial power splitter and the cables which connect the outputs of the power splitters as antenna feeds to the hybrids. The transmitting and receiving power splitters are respectively 6-way and 9-way, which couple to as many hybrids. Each hybrid further subdivides by a factor of eight to couple to the individual ports of the respective antennas.

The VHF antenna is used both for transmission of the 136.05-mc

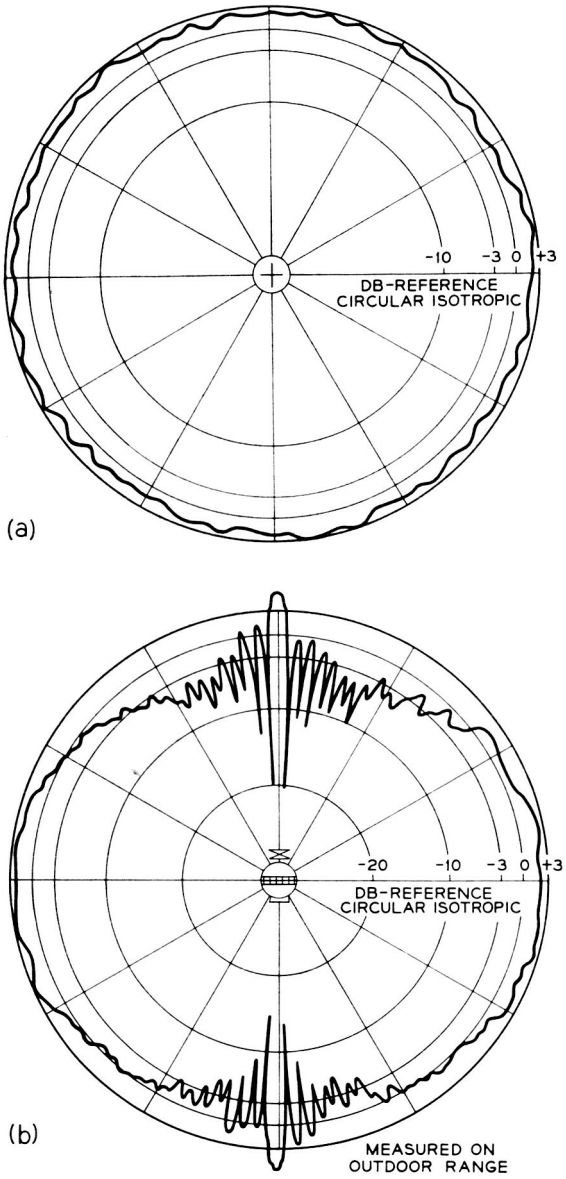

Fig. 7 — Antenna patterns at 6390 mc: (a) equatorial aspect; (b) polar aspect.

beacon signal, which is amplitude modulated with telemetry information upon command, and the reception of command signals at approximately 123 mc. The antenna is a quadrafilar helical unit which in free space produces a circular polarized signal over a wide angle. The half angle of the zone at each pole, where antenna gain is in excess of 6 db below the gain of an isotropic radiator, is approximately 20° (upper) or 10° (lower), as shown in Fig. 8(b).

The placement of this antenna close to the spacecraft as shown in Fig. 6 results in nearly linear polarization, since the proximity of the large metallic surface produces an image to cancel one component of the wave. The reasons for mounting this antenna close to the sphere are discussed in Section XI.

VIII. BATTERY AND POWER SUPPLY

The Telstar battery consists of 19 series-connected nickel-cadmium cells. Each cell has a nominal capacity of six ampere-hours and weighs eight ounces unmounted. The battery was made of 19 individual cells having essentially matched characteristics. The main voltage regulator is designed for satisfactory operation with maximum loads with an 18-cell battery, so there is series redundancy of one cell.

The main regulator provides -16 volts, regulated to ± 2 per cent. A minimum-loss design was of the greatest importance, and an efficiency of between 80 and 92 per cent is obtained as the output is varied from a light load to full load. There are two outputs from the regulator. The first output, feeding most of the solid-state circuits, has a ripple of less than 1 millivolt, rms. The other output is connected to the TWT supply.

The TWT supply is an unregulated dc-to-dc converter which provides heater, collector, helix and anode voltages for the tube. To conserve the life of the traveling-wave tube it is important that the voltages be applied and removed in a controlled time sequence. This is accomplished by commands from the ground which actuate magnetic latching relays within the satellite. Separate transformers for the high-voltage potentials are consequently required and are shown in Fig. 9. By use of new techniques in the oscillator portion of the converter it has been possible to achieve an efficiency as high as 70 per cent. The complete design of the regulator and converter is covered in another paper in this issue.[10]

IX. OVER-ALL STRUCTURE

As noted earlier, the structure of the Telstar satellite was determined largely by conditions inherent in the choice of the launch vehicle as

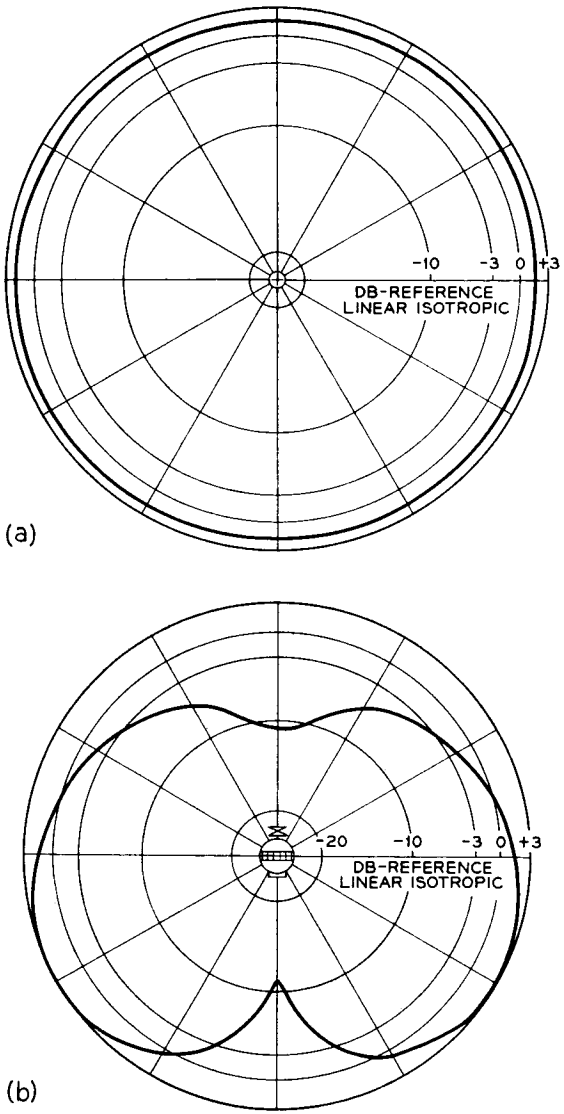

Fig. 8 — VHF antenna patterns: (a) equatorial aspect; (b) polar aspect.

well as fundamental decisions regarding the mission objectives. All studies and designs have been based on the use of the highly reliable Delta three-stage combination. Preliminary studies were directed toward an essentially spherical design with a diameter of about 27 inches and a weight of about 90 pounds. This early objective was a design that could

be accommodated in the low-drag fairing of the Delta vehicle. As more detailed examination of the electronics assembly progressed, it became apparent that the carlier proposals could not be attained within a reasonable schedule. It was then decided to examine the possibility of using a second nose fairing, originally developed for another program. This so-called "bulbous" fairing encloses more efficiently the volume needed for a spherical payload structure. With this alternative, a diameter of about 34 inches was made possible.

Concurrent with selection of the bulbous fairing, investigation was carried out on considerations of spacecraft weight versus orbital parameters. From this, it was established by engineers with NASA and

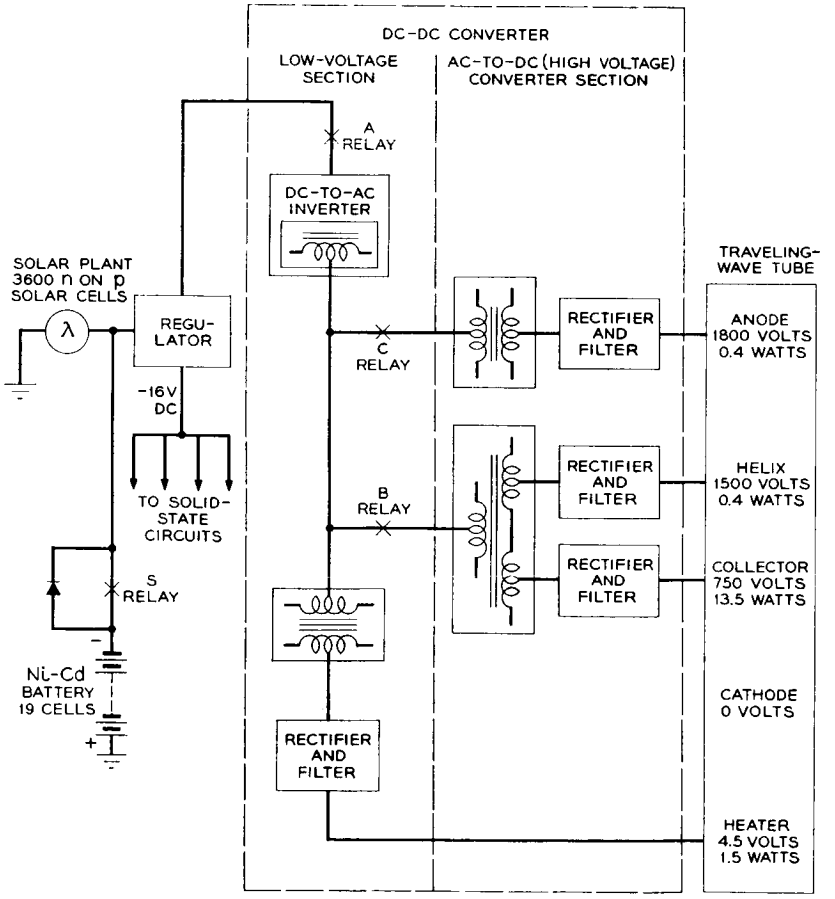

Fig. 9 — Power system.

Douglas Aircraft that a maximum payload of 180 pounds could be launched into an orbit consistent with the over-all objectives of the Telstar experiment. From design information available at that time, a maximum weight of 175 pounds was set as the limit for the Telstar spacecraft. Actual weights of six models completed for possible launch have ranged from 170.94 pounds for the model launched to 175.4 pounds.

The Telstar spacecraft structure was also influenced by the choice of spin stabilization, for which the reasons have already been discussed. The principal problems in this method are those related to dynamic and static balance of the payload about the spin axis and the requirement that the spin axis be that of major moment of inertia. As in most such designs, this is achieved by symmetry about the spin axis of the primary structure and judicious placement of masses not having natural balance by symmetry. Residual imbalance is, of course, removed by measurement and addition of trim weights as a final step in construction. In the satellite design, the major difficulty in optimizing the structure for spin stabilization was that of obtaining a low enough ratio of pitch to spin moments of inertia. A design requirement of 0.95 maximum was established and was attained with some compromise in performance of the VHF helical antenna. This antenna was to have been mounted on a telescoping mast and erected on firing a charge by closure of switches actuated by payload separation. Although the combined weight of mast and antenna was less than one pound, the effect on pitch moment was the deciding factor. The final mounting, although sacrificing 3 db in antenna performance, resulted in a more reliable design with an over-all saving in weight and an adequate ratio of pitch to spin moments. Mechanical and electrical testing were also simplified by this change.

In addition to spin-axis balance, the nearly spherical symmetry of Telstar is important in other respects. Foremost in these was the objective of near isotropy in the solar cell arrays.[2] The sphere-like outer shell permits placement of solar cell groups such that a reasonably uniform electrical output is obtained regardless of the relative orientation to the sun. The surfaces on which the solar cells are mounted are planar sections or facets rather than spherical sections. In this way all solar cells on a facet are illuminated to the same degree for maximum efficiency. The larger facets contain complete 72-cell groups (38 in number) while the 12 facets near each pole contain half-groups of 36 cells. The 24 half-groups combine in pairs to provide 12 complete groups, bringing the total to 50 groups providing 3600 cells. Facets not used for solar cell mounting and all other exposed outer surfaces are coated

with a plasma spray of aluminum oxide to effect the desired thermal balance.[2] Three facets carry optical mirrors for spin rate and orientation measurements by means of ground-based optical telescopes.[11]

The last factor to be discussed, wherein the choice of launch vehicle exerted particular influence, is related to the launch environment. Specifications covering shock and vibration tests had been effectively standardized for Delta missions and were invoked by NASA in the Telstar program. The severity of the tests for qualification of the prototype is 50 per cent greater than that for acceptance of models designated for launching. Included are random and sinusoidal vibration tests in three axes on all models. The prototype qualification tests also include constant acceleration and shock tests.[12] Levels of vibration input normal to the plane of the attachment fitting range from 2.3 g to 21 g between 5 and 2000 cps, with special requirements from 550–650 cps. In the latter range, a level of 40 g is used to simulate the resonant burning peculiar to the third-stage rocket. In order to isolate the sensitive electronics assemblies from the effects of shock and vibration, an isolation mounting comprising many strands of nylon cord was used. This support was designed to have a natural frequency of 40–45 cps, where the expected "g" input is of the order of 1.5 g along the spin axis. Maximum "g" levels experienced by the electronics assemblies due to qualification testing approach 20 g at resonance of the lacing support, while the higher-level inputs at frequencies above 50 cps are effectively damped, with occasional spikes of 5 to 10 g on the electronics section.

A simplified cross section showing relative positions of the major parts of the spacecraft is shown in Fig. 10. As shown, the electronics assembly occupies a large central volume of the structure. It is, in fact, a single assembly which is constructed and tested separately before insertion into the outer frame. All of the electronics subassemblies are contained in this "package" with the exception of portions of the radiation experiment, which had to be assembled close to detectors with which they were associated. The electronics package accounts for 85 pounds or essentially one-half the total spacecraft weight. Attached near the top and bottom of the cylindrical package are lacing rings through which the nylon lacing supports are stitched. The outer frame is a welded structure of magnesium tubing with an exterior skin of very thin aluminum panels. Whenever possible, these lightweight metals have been applied throughout for optimum utilization of their strength, weight, and heat conductivity, as applicable. Fabrication techniques and finishing problems were also of considerable importance.

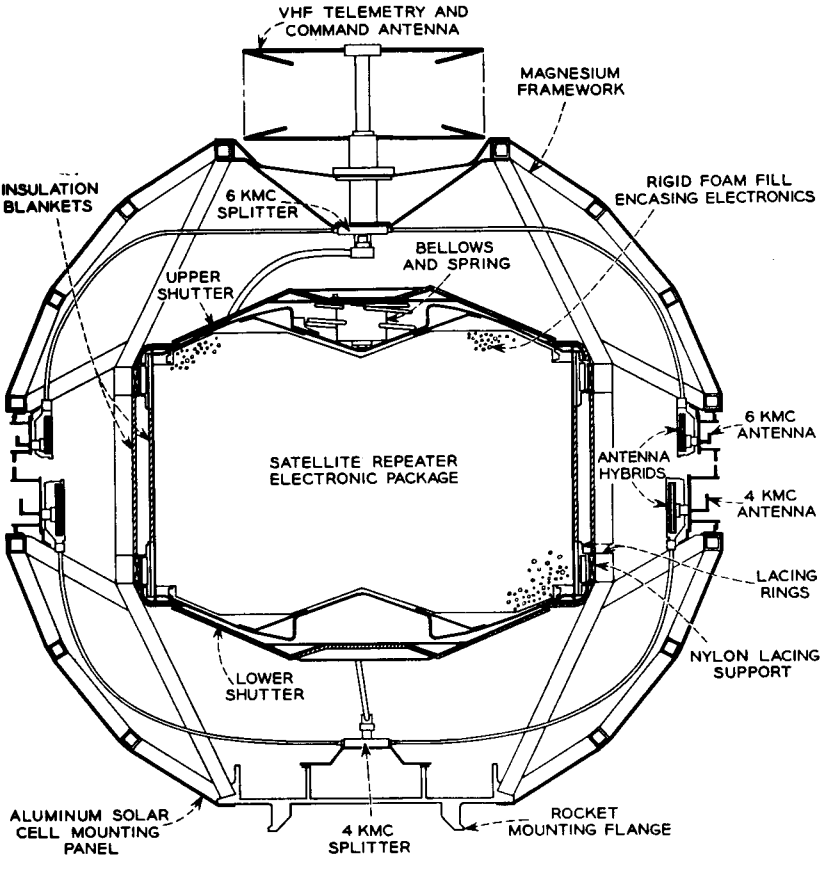

Fig. 10 — Cross section of spacecraft.

X. THE ELECTRONICS PACKAGE

The environment to be encountered during many months in orbit, as well as the conditions of launch, had strong influence on the design of the electronics package. The effects of high vacuum and Van Allen belt radiation on organic materials commonly used in electronic equipment were of particular concern. For this reason, many materials expected to be used in Telstar satellite designs were tested for the effects of radiation and vacuum. However, time did not permit adequate and conclusive tests on all such materials, especially since high-vacuum tests cannot be accelerated, but only extrapolated. This factor, coupled with the presence of high TWT voltages, led to the decision to enclose

the electronics in a hermetically sealed container which would carry an atmosphere into space. In this way, it could be assured that outgassing of organic materials would not contaminate finishes critical to thermal balance or solar cell operation. Also, any immediate hazard of high-voltage ionization and breakdown at low pressure was removed. While these were the primary objectives of the sealed container, fortuitous gains were improvement of shielding against electron radiation and completely valid tests of thermal characteristics on the laboratory bench.

Mention has been made of shock and vibration levels sustained by the electronics package during launch. In order that these inputs would not be further amplified by self-resonances within the electronics assembly, a somewhat radical approach was taken. In addition to the generally accepted procedure of encapsulating individual circuit packages, it was decided to fill the voids in the over-all assembly with polyurethane foam of the same type as that used for individual assemblies. This final encapsulation provided the major mechanical support for the TWT amplifier and waveguide components as well as for the transistorized units mounted with them. With the additional foam, the design of supporting brackets and testing for their adequacy could be minimized, if not ignored. Also, the retention of interconnecting wires prior to final encapsulation was essentially unnecessary. Consonant with this use of rigid foam is the avoidance of connectors except where essential to assembly and testing. All subassemblies are constructed with their wiring pigtailed from the units and color-coded. Interconnections are made with crimped sleeves covered over by heat-shrunk plastic tubing. The final assembly with foam fill in place might be equated to "launching" in the shop. However, repair, though difficult, is not impossible and the technique is believed to be consistent with the reliability objectives inherent in the program.

XI. THERMAL DESIGN WITHIN THE ELECTRONICS PACKAGE

Because of the almost complete filling of the electronics package with the rigid foam, appreciable heat transfer by gas convection cannot be expected. Hence, it was necessary to rely entirely on conductive heat transfer to remove power dissipated within the package to its outer walls, whence it could be radiated off. The comparatively massive waveguide structure (see Fig. 11), supplemented by heat conducting straps to attach it to the package cylinder wall, is the primary means of removing the heat. This was of particular significance at the TWT amplifier with a peak dissipation of 13 watts. Also, the chassis of a number of units, which accounted for the major part of the remaining dissipation,

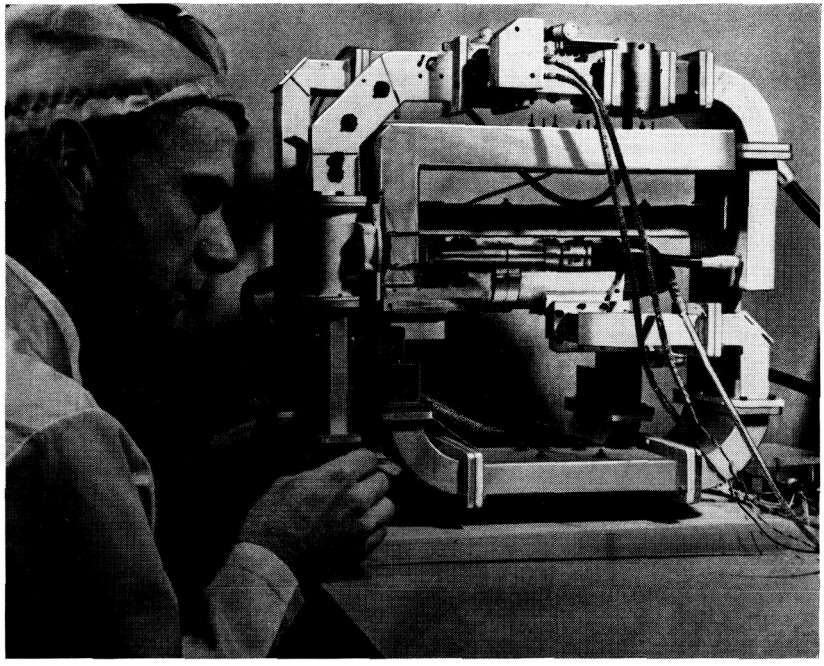

Fig. 11 — Waveguide structure.

were firmly attached to the waveguide structure. The power supply regulator was bonded directly to the cylinder wall, as were the cells of the nickel-cadmium battery. This treatment of the battery cells was most important, since during periods of overcharge almost all of the solar plant output may be dissipated in the battery as heat. Placing the cells in intimate contact with the cylinder wall avoided wide excursions in temperature at the cells. Similarly, the intimate bonding of all heat producing assemblies through the waveguide and package container avoided any significant localized heating, even with the peak dissipation associated with operation of the microwave repeater.

To verify the adequacy of the thermal design of the electronics package, an electrical analog was constructed of appropriate resistive and capacitive components and fed with currents corresponding to the various heat sources. The schematic of the analog circuit is shown in Fig. 12 with a table of current feed (temperature check) points. Continuously operating sources were separated from switched loads to permit precise simulation of operation in successive orbital passes. The electrical analog permitted evaluation in minutes of thermal charac-

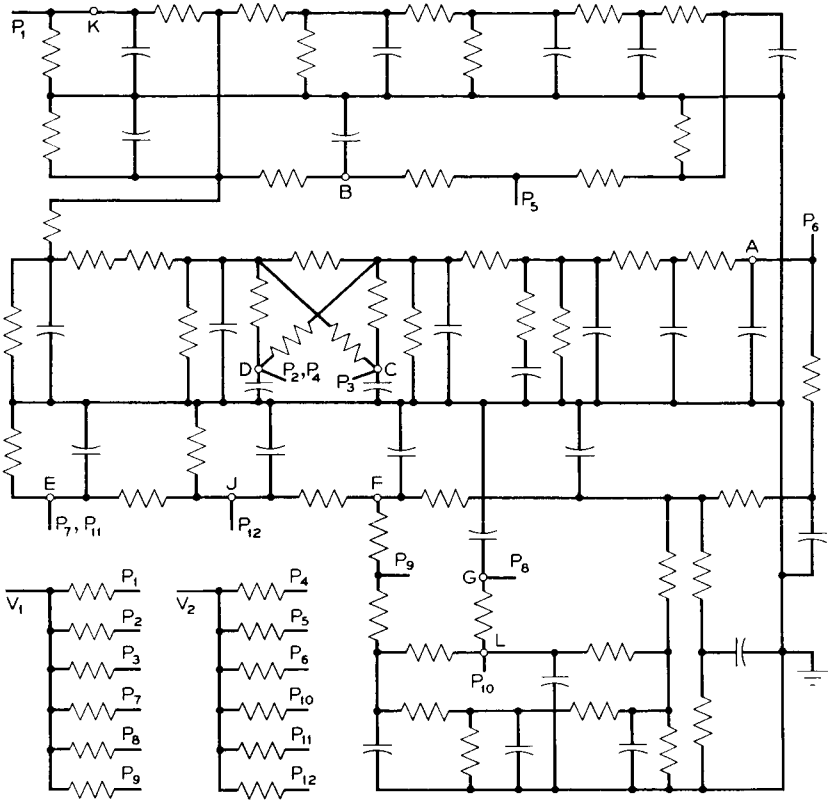

ANALOG POINT	TEMPERATURE MEASURED	ANALOG POINT	TEMPERATURE MEASURED
A	NEAR TWT COLLECTOR	F	COMMAND RECEIVER
B	IF AMPLIFIER	G	COMMAND SWITCH CONTROL
C	VHF BEACON TRANSMITTER	J	TELEMETRY
D	BEAT OSCILLATOR SUPPLY	K	COMMAND DECODER
E	POWER SUPPLY REGULATOR	L	DC-DC CONVERTER

NOTES

1. CIRCUIT GROUND CORRESPONDS TO CANISTER OF ELECTRONIC PACKAGE
2. V_1 FEEDS CONTINUOUS LOADS AND V_2 FEEDS LOADS SWITCHED BY COMMANDS

Fig. 12 — Electrical analog of thermal characteristics.

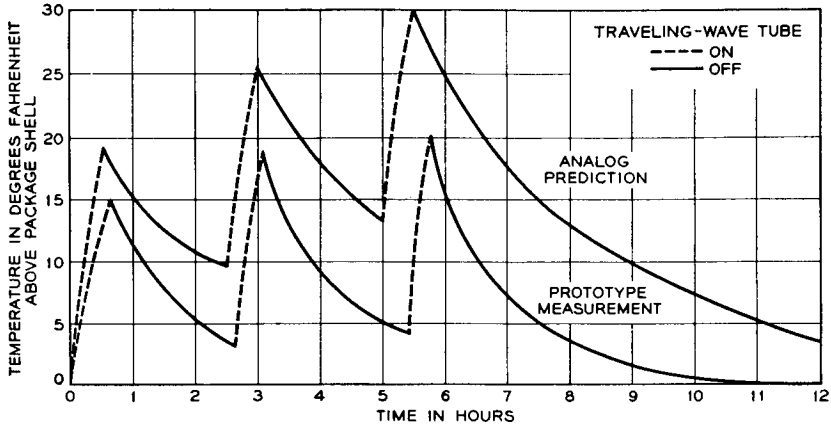

Fig. 13 — Predicted vs measured thermal performance of prototype spacecraft.

teristics actually realized in days (50 milliseconds = 1 hr.). Fig. 13 shows a comparison of results obtained at the TWT amplifier with the analog measurements to actual data obtained in thermal vacuum testing of the prototype model. The greater temperature rise shown by the analog data is indicative of the conservative approach taken in simplification of the analogous form. Temperature rises indicated by the analog, though consistently higher than actually realized, were within the objectives and confirmed the adequacy of the design.

XII. SUBASSEMBLIES FOR THE ELECTRONICS PACKAGE

Some further details of the design of the electronics package are of interest. The progress of the assembly before final encapsulation is shown at three stages in Fig. 14. Top and bottom views of the completely assembled unit are shown in Fig. 15. To reduce weight, the waveguide portions are constructed entirely of magnesium with silver plating to improve electrical performance. A layout was achieved which, if laid straight, would exceed 13 feet of 1″ × 2″ waveguide, but in which only 1 foot is simple waveguide and is not functional as a filter or other such component. In addition to the waveguide, 16 electronic units and 19 nickel-cadmium cells are assembled in the package. These are tabulated in Table II together with their approximate weights.

The total weight of waveguide components is 9.9 pounds while the TWT amplifier adds 7.1 pounds. The complete sealed container for the electronics weighs 13.9 pounds, and the foam for the final encapsulation varies in weight from 7 to 8 pounds.

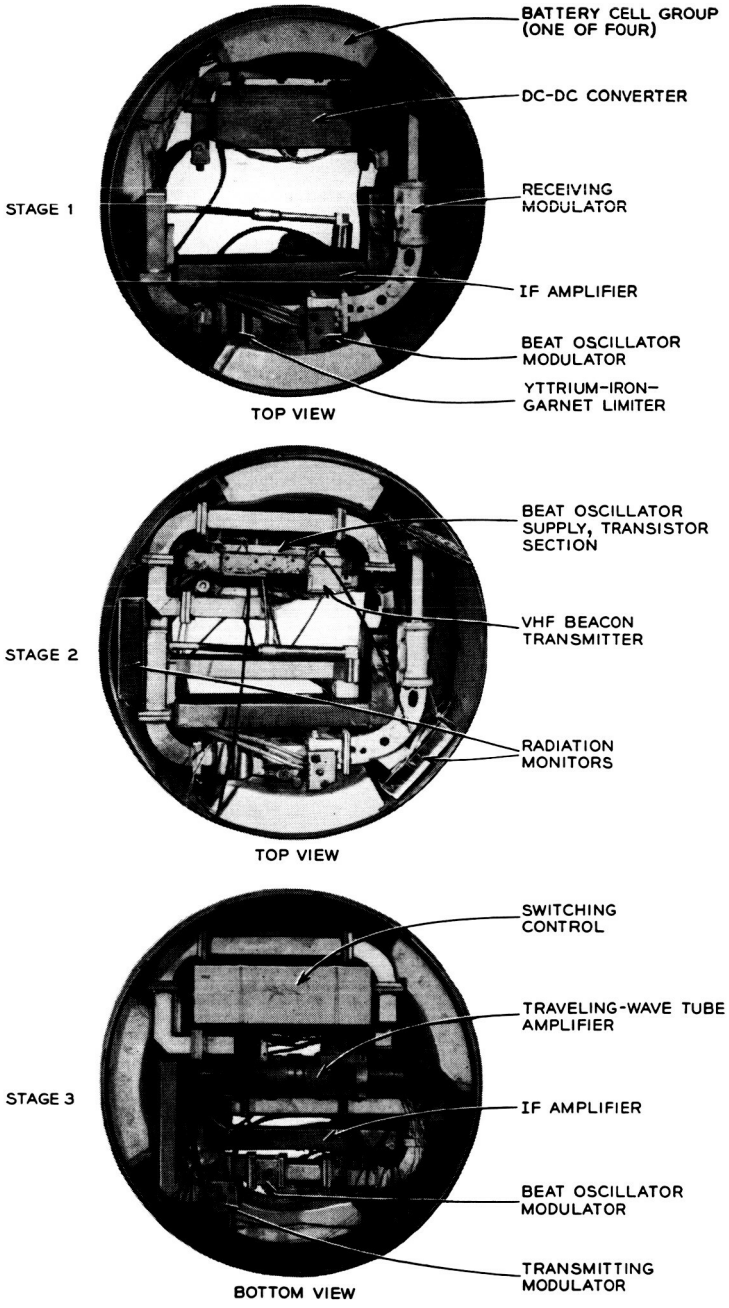

Fig. 14 — Assembly of electronics package.

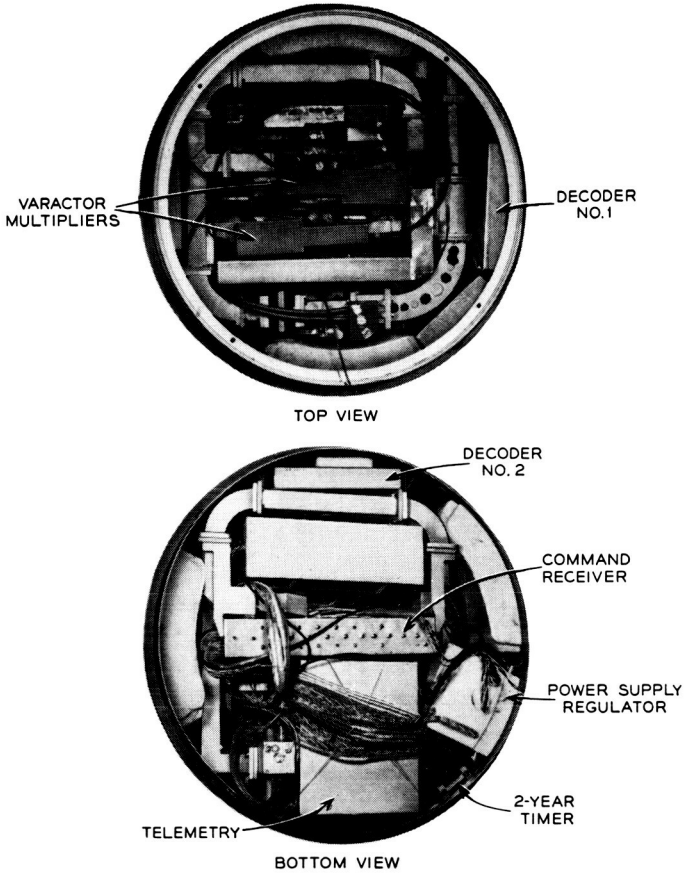

Fig. 15 — Completely assembled electronics package.

The designs of the individual units are quite varied in detail but fall into three principal categories:

(a) For high-frequency circuits such as the IF amplifier and beat oscillator supply, a fabricated aluminum chassis is used in conjunction with epoxy-glass boards for mounting. After wiring and testing, the structure is encapsulated with certain areas of the chassis exposed. Electrical shielding is then completed by a 0.003-inch aluminum cover. Cover and chassis are gold-plated to facilitate soldering the shield to the exposed chassis. A view of the IF amplifier before encapsulation and shielding is shown in Fig. 16.

(b) The second type is devoted to circuits lending themselves to modular construction, such as the decoder in Fig. 17. Small modules

TABLE II

Unit	Approximate Weight (lbs)
1. IF amplifier and AGC	1.2
2. B.O. supply	0.9
3. Varactor multipliers (2)	0.63
4. Command receiver	1.32
5. Command decoders (2)	1.98
6. Command switch control (2)	2.26
7. VHF beacon transmitter	0.9
8. Telemetry	8.5
9. Power supply regulator	4.0
10. DC-to-DC converter	2.92
11. Ni-Cd battery (19 cells)	11.25
12. Radiation particle counters (2)	1.65
13. Two-year timer	0.57

are encapsulated separately and grouped on unit boards to perform the more complex functions. After interconnection, board and modules are again encapsulated.

(c) The last type is best described as a free-form construction to accommodate components too varied in size and shape for strict organization. One or more insulating mounting boards are used with a single step of encapsulation completing the unit. One of three boards from the power supply regulator pictured in Fig. 18 is typical of these.

XIII. CANISTER FOR THE ELECTRONICS PACKAGE

The container for the electronics package is made of $\frac{1}{16}$-inch 1100-type aluminum. The cylindrical section is fabricated of sheet with a seam

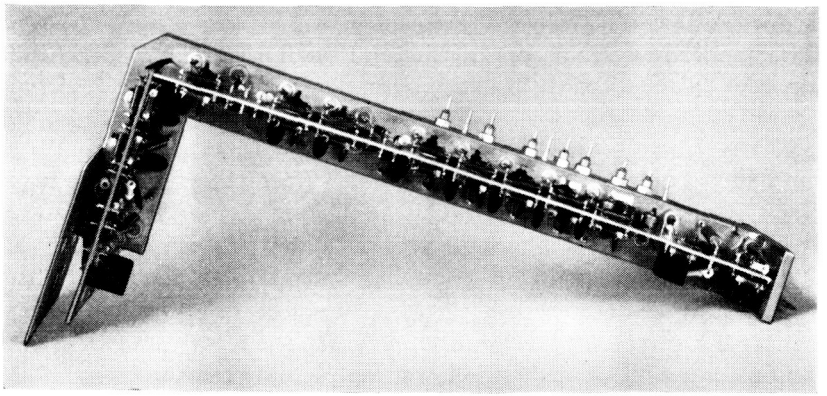

Fig. 16 — IF amplifier.

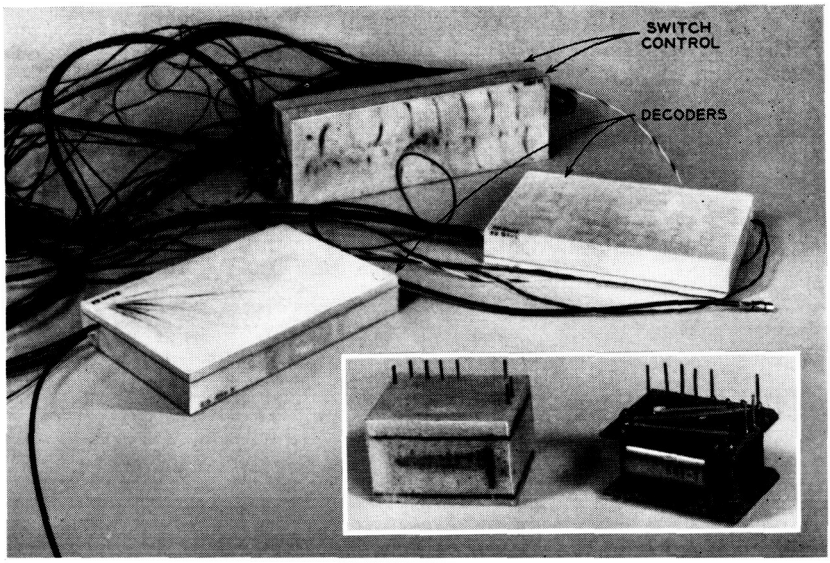

Fig. 17 — Modular construction — decoders and switch control.

weld, reinforced penetrations being provided at six locations for the electrical feed-throughs. The completed cylinder is gold-plated and polished on the exterior, after which glass-seal headers and coaxial feed-throughs are soldered into the penetrations. A helium leak check is made on each solder or glass seal before and after assembly and wiring. After foaming and temperature testing of the wired package, the top and bottom are closed by identical aluminum domes welded into place on an automatic argon-arc welding machine. A leak test is then made of the completed electronic package. Based on the reservoir of gas contained in the voids of the package assembly, a permissible leak rate of 8×10^{-5} standard cc/sec was computed for a 2-year life. The equipment used was sensitive enough to detect leaks in the order of 10^{-6} standard cc/sec or about two orders down from the permissible leak. Argon is used to make this test, since helium cannot be introduced into the package (helium would penetrate the glass envelope of the TWT and cause noise in the transmitted signal). As a final step the argon is also removed and replaced by carbon dioxide to minimize the chances of high-voltage breakdown inherent in the readily ionized argon. The final pinch-off, at slightly below atmospheric pressure, is also tested for leak by monitoring rise in pressure in a known evacuated volume.

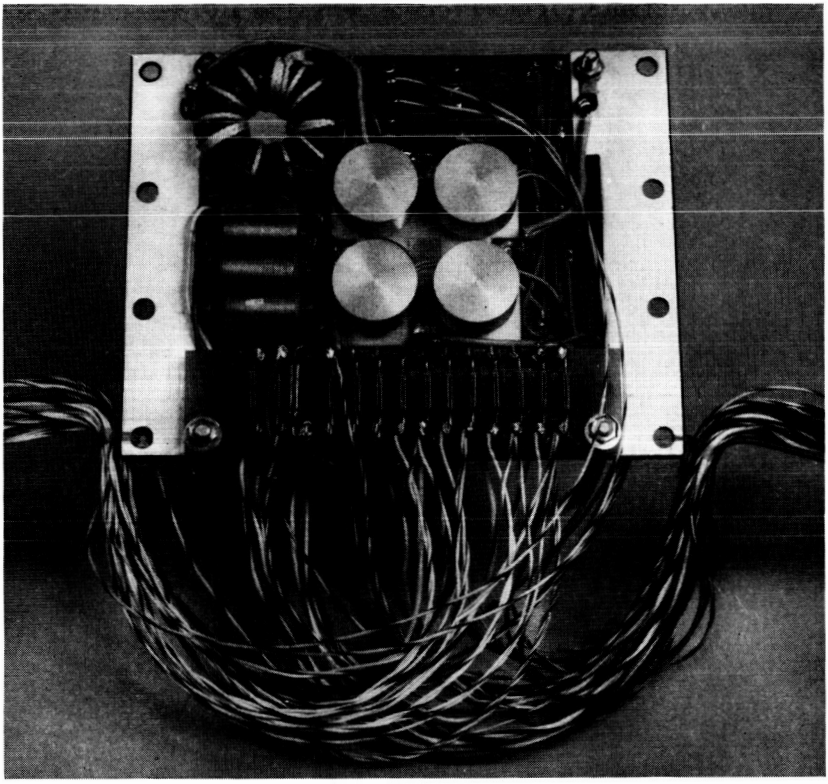

Fig. 18 — Free-form construction — portion of power supply regulator.

XIV. CONCLUSION

This paper has described the planning and general design of the Telstar satellite and attempts to give the reader an over-all picture of what the satellite contains. Several companion papers give very detailed descriptions of the various subassemblies and parts of the satellite. Another paper[13] discusses the importance of a reliable construction program. The relative simplicity and established performance of the circuit and equipment approaches described were basic to the development plan. Long life can best be attained, we believe, by a straightforward design based on a minimum of duplication and tried and proven design principles. The success of the Telstar program demonstrates the validity of this approach.

XV. ACKNOWLEDGMENTS

As in any corporate effort, many people made significant contributions to those phases of work described in this paper. The leadership and guidance of Messrs. A. C. Dickieson and E. F. O'Neill in the planning and early system layout are particularly worthy of mention.

REFERENCES

1. Hoth, D. F., O'Neill, E. F., and Welber, I., The *Telstar* Satellite System, B.S.T.J., this issue, p. 765.
2. Hrycak, P., Koontz, D. E., Maggs, C., Stafford, J. W., Unger, B. A., and Wittenberg, A. M., Spacecraft Structure and Thermal Design Considerations, B.S.T.J., this issue, p. 973.
3. Curtis, H. E., Interference between Satellite Communication Systems and Common Carrier Surface Systems, B.S.T.J., **41**, May, 1962, p. 921.
4. Sproul, P. T., and Griffiths, H. D., The TH Broadband Radio Transmitter and Receiver, B.S.T.J., **40**, November, 1961, p. 1521.
5. Davis, C. G., Hutchison, P. T., Witt, F. J., and Maunsell, H. I., The Spacecraft Communications Repeater, B.S.T.J., this issue, p. 831.
6. Bodmer, M. G., Laico, J. P., Olsen, E. G., and Ross, A. T., The Satellite Traveling-Wave Tube, B.S.T.J., this issue, Part 3.
7. Chapman, R. C. Jr., Critchlow, G. F., and Mann, H., Command and Telemetry Systems, B.S.T.J., this issue, p. 1027.
8. Brown, W. L., Buck, T. M., Medford, L., Thomas, E. W., Gummel, H. K., Miller, G. L., and Smits, F. M., The Spacecraft Radiation Experiments, B.S.T.J. this issue, p. 899.
9. Bangert, J. T., Engelbrecht, R. S., Harkless, E. T., Sperry, R. V., and Walsh, E. J., The Spacecraft Antennas, B.S.T.J., this issue, p. 869.
10. Bomberger, D. C., Brolin, S. J., Feldman, D., Trucksess, D. E., and Ussery, P. W., The Spacecraft Power Supply System, B.S.T.J., this issue, p. 943.
11. Courtney-Pratt, J. S., Hett, J. H., and McLaughlin, J. W., Optical Measurements on the *Telstar* satellite to Determine the Orientation of the Spin Axis and the Spin Rate, to be published.
12. Delchamps, T. B., Jonasson, G. C., and Swift, R. A., The Spacecraft Test and Evaluation Program, B.S.T.J., this issue, p. 1007.
13. Shennum, R. H., and Reid, E. J., The Design and Construction of the Electronics Package, B.S.T.J., this issue, Part 3.

The Spacecraft Communications Repeater

By C. G. DAVIS, P. T. HUTCHISON, F. J. WITT, and H. I. MAUNSELL

(Manuscript received January 28, 1963)

This paper describes the electrical characteristics of the waveguide components, the solid-state circuits and the traveling-wave tube used in the microwave communications repeater. The reflex-circuit method of obtaining local oscillator signals for the modulators and certain circuit stability problems are discussed.

I. INTRODUCTION

This paper describes the communications repeater portion of the Telstar satellite. This repeater receives the weak, −60 dbm nominal, FM signal from the earth at a center frequency of 6389.58 mc, shifts the frequency to 90 mc for amplification by transistors, shifts the frequency to 4169.72 mc for further amplification by the traveling-wave amplifier, and reradiates the signal at a minimum power of 33 dbm. The signals are received and transmitted through separate circularly polarized antennas which are nearly isotropic.[1] The satellite also radiates, for tracking purposes, a very stable microwave beacon signal at a frequency of 4079.73 mc and at a power of greater than 13 dbm. The bandwidth of the repeater is 50 mc, although to date only 25 mc has been used in the experiments because of bandwidth limitations of the maser in the ground receiver.

II. CIRCUIT OPERATION

The block diagram of the communications repeater, excluding power supply, is shown in Fig. 1; the numbers circled at various points in the circuit show the power levels in dbm. Fig. 1 shows exact frequencies, but for simplicity approximate frequencies will be used in the text. The signal path through the repeater is as follows.

The signal from the ground station is received by the nearly isotropic 6-gc antenna and is applied to the down converter at a nominal level of −60 dbm. A down converter shifts the center frequency to 90 mc where

In its Telstar, Vol. I Jun. 1963 p 831-867
(See N64-10868 02-01)

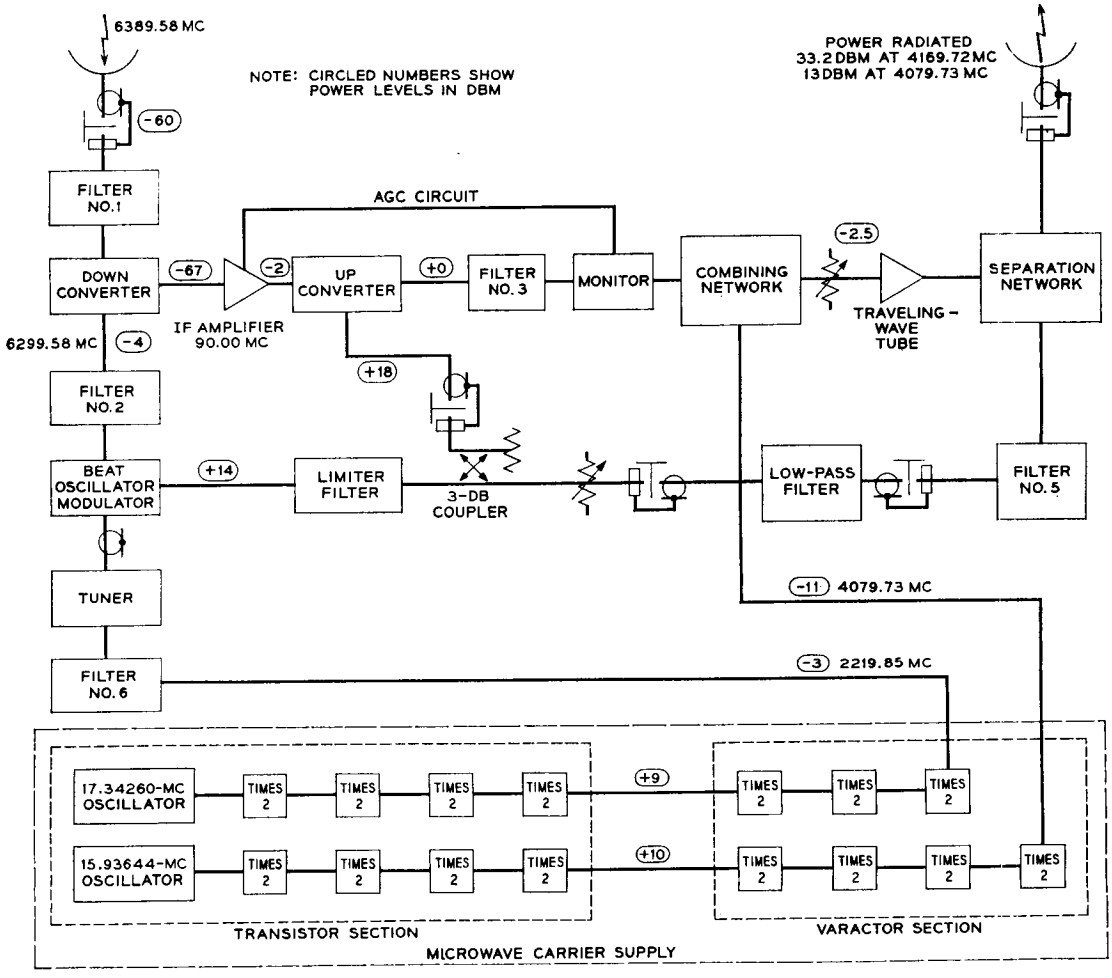

Fig. 1 — Communications repeater.

the signal undergoes gain of about 65 db in a 14-stage transistor amplifier. The signal is then applied to a balanced up converter which shifts the center frequency to 4170 mc. Varactor diodes are used in the up converter, so it provides some conversion gain. Filter 3 in the output of the up converter allows only the sum frequency (4080 + 90) mc from the up converter to pass into the monitor section. Silicon diodes in the monitor provide a dc output voltage which is a monotonic function of the power input to the monitor. This dc voltage, after amplification, controls the gain of the IF amplifier by changing the current through variolosser diodes in the IF amplifier. Because this automatic gain control (AGC) detector, the monitor, operates at 4 gc, the AGC loop includes the up converter and keeps the input power to the traveling-wave tube essentially constant as the input signal at 6390 mc varies from −55 to −72 dbm. Variations in the input signal are due to changes in satellite slant range and lack of isotropy in the receiving antenna. These variations are usually much less than 17 db when the transmitted power at 6390 mc is programmed. Ripple in the antenna pattern combined with spinning of the satellite causes the received signal to be amplitude modulated at frequencies of several hundred cycles per second. The frequency response of the AGC circuit is fast enough to smooth the amplitude modulation caused by the ripple in antenna gain.

After the signal passes through the monitor section, it is applied through a combining network to the traveling-wave tube (TWT). A card attenuator preceding the TWT is used so that small adjustments in tube drive can be made after the AGC adjustments have been completed. At the operating point selected for the tube, the gain for the 4170-mc signal is 37.5 db and the resulting power output is 35 dbm. The 4170-mc output of the TWT is applied to the transmitting antenna through a separation network which has an insertion loss of only 0.2 db at this frequency. However, the insertion loss of the transmitting antenna and connecting cables is 1.6 db, so the radiated power is 33.2 dbm.

The 4080-mc pump for the up converter is derived from a crystal oscillator at approximately 15.9 mc, followed by transistor and varactor frequency doublers. In order to obtain sufficient power for this up-converter pump, a special reflex circuit[2] using the TWT amplifier with a combining and a separation network is used, as shown in Fig. 1. In addition to furnishing the pump for the up converter, the 4080-mc amplified output of the TWT provides the microwave beacon needed for precision tracking and provides the pump for the beat oscillator (BO) modulator. The BO modulator furnishes the 6300-mc local oscillator for the down converter by combining the pump signal at 4080 mc with a signal at

2220 mc. The latter is also derived from a crystal oscillator and a series of frequency doublers. The yttrium-iron-garnet (YIG) limiter is used to ensure stability of the BO modulator under conditions of increased power at 4080 mc, conditions which exist when no 6-gc signal is transmitted to the satellite.

The gain of the TWT for the beacon signal is less than that for the communications signal, because the latter signal drives the tube into partial saturation: see Fig. 2. This graph shows the relationship of the power outputs at 4080 and 4170 mc when the 4080-mc input is constant and the 4170-mc input is varied. Three sets of curves also show the sensitivity of the tube to changes in the main regulator supply voltage; -16 volts is normal.* A circuit in the AGC amplifier changes the drive at 4170 mc to reduce the output variations if the supply voltage changes. Because two signals are amplified by the TWT, it is necessary to operate the tube about 1.5 db below saturation to reduce intermodulation to an acceptable level.

The reflex circuit is an electrically efficient way of obtaining sufficient power levels needed at 4080 and 6300 mc, but it introduces additional closed paths in the circuit, with the resulting possibility of instability. These closed paths are hereafter called feedback paths or loops, although the names are misleading because they are not used to improve circuit linearity or to realize the usual advantages of negative feedback. In this circuit, the feedback paths are undesirable by-products of the reflex method of obtaining the local oscillator signals for the converters.

The AGC circuit controls the gain of the IF amplifier so that the input signal power to the satellite is amplified by the proper amount to hold the power into the TWT constant. An increase in signal level of 3 db means a decrease in IF gain of 3 db with a corresponding 3-db decrease in noise drive to the TWT. The noise level to the TWT is low enough that noise amplification is linear, and that output noise increases almost linearly with a decrease in input signal so long as the signal falls within the AGC range.

When the input signal is removed, the gain of the IF amplifier is maximum and the noise drive to the TWT is enough to give a radiated noise power of 31 dbm in a 50-mc bandwidth. This noise will not cause trouble in any communications system unless the system uses the same frequency and has a very high-gain antenna pointed almost at the satellite. Sup-

* The variations in power output predicted from Fig. 2 are very pessimistic, because these data are shown for variations of ± 3 per cent in supply voltage. The predicted variation at the end of 2 years is less than ± 1 per cent, unless radiation damage is extensive.

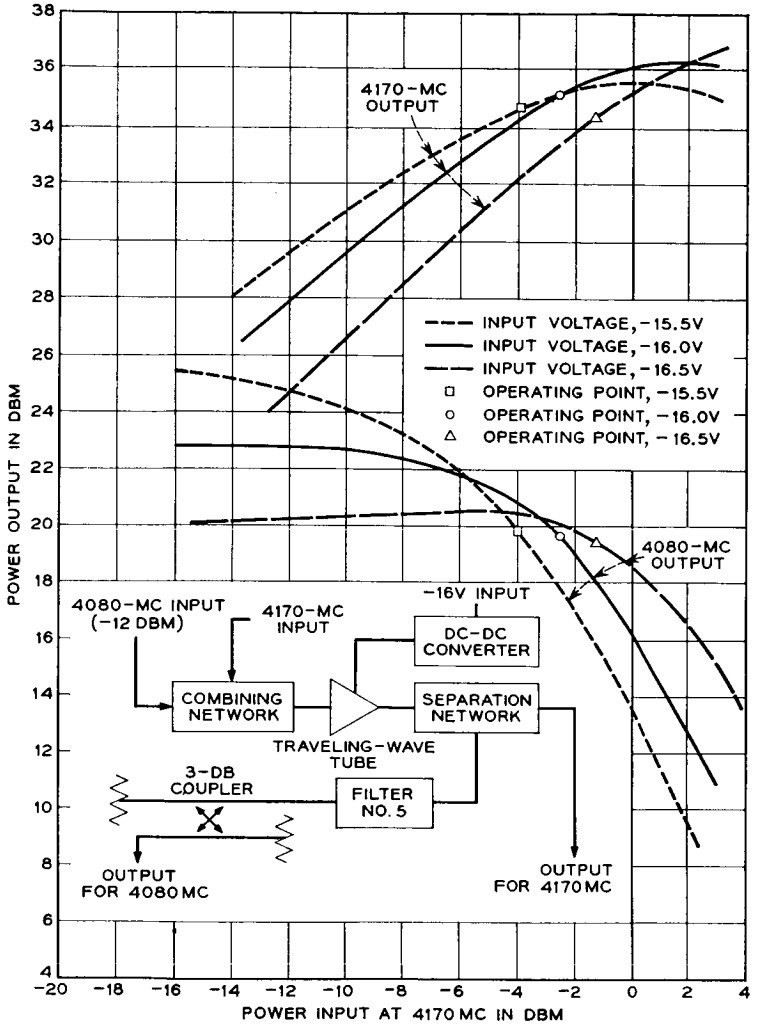

Fig. 2 — Operating characteristics for the traveling-wave amplifier.

pose, for example, there were two Telstar satellites in view, one turned on and in use, and the other turned on but having no input signal. The satellite not in use can increase the noise temperature of the Andover ground receiver by a maximum of only 2.2°K while the horn is pointing more than 3° away from the "noisy" satellite, and this would occur only when the slant range to the satellite is at its minimum possible distance of

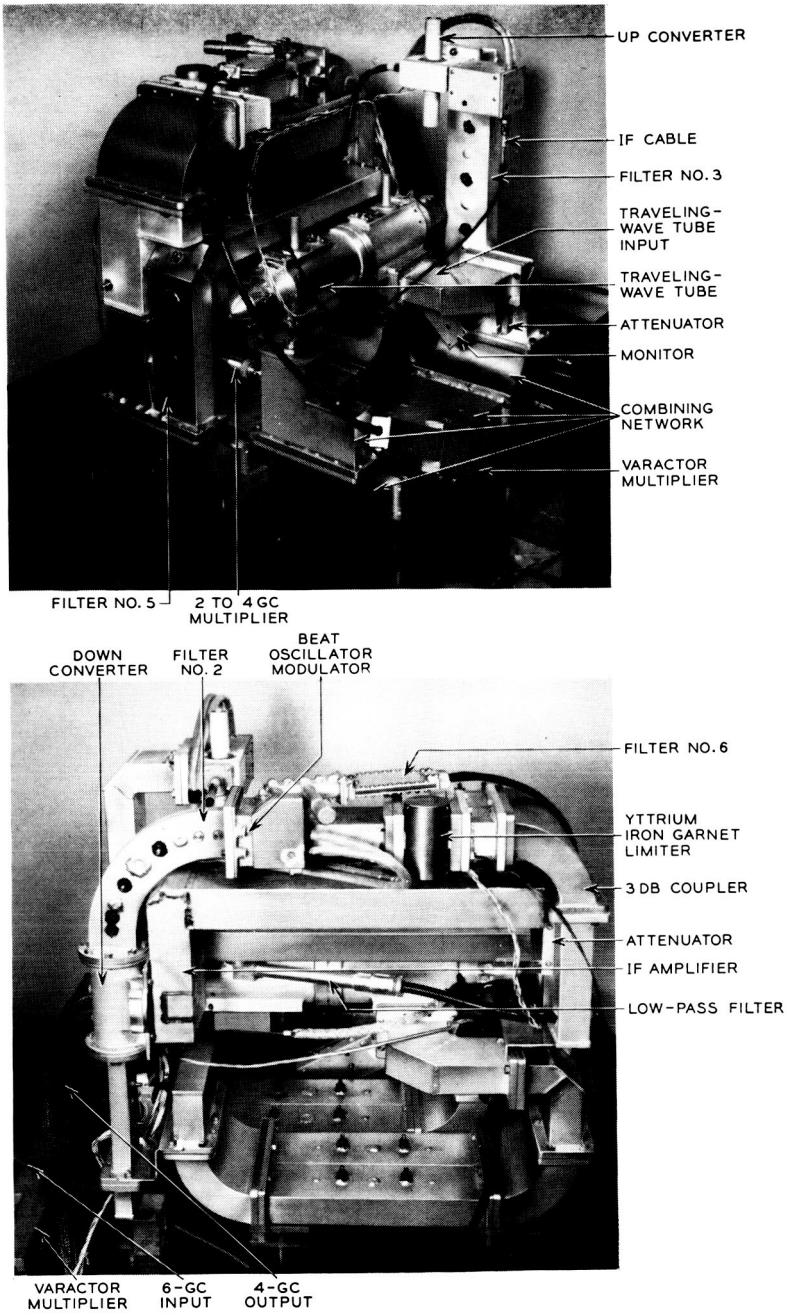

Fig. 3 — (a, b) Pictorial views of the repeater.

600 miles.[3] For a "normal" range of 2500 miles, the noise contribution from the "noisy" satellite when it is more than 3° from the beam of the ground antenna is less than 0.12°K.

When the spacecraft has no input signal, the TWT is not driven as hard as when a normal signal is used, so the microwave beacon power increases 2 db over its normal level. This extra power is advantageous, since the no-signal-input condition usually occurs when the ground tracking antennas are trying to acquire the satellite.

III. SUBASSEMBLY DESCRIPTIONS

In this section the various subassemblies of the repeater are described. The characteristics and unique features of the subassemblies are covered, but the descriptions are not intended to be design sections. Two views of the communications repeater, Figs. 3(a) and 3(b), show all the important subassemblies. All waveguide parts are made of magnesium; the 4-gc parts use WR187 guide, and the 6-gc parts use reduced-height WR137 guide. All subassemblies were tested before and after they were subjected to vibrational forces in excess of these expected in launch. The repeater must operate over a temperature range of 0° to 50°C, so all units were tested over at least this range.

3.1 *Down Converter*

The down converter shifts the 6390-mc broadband signal to an intermediate frequency centered at 90 mc. Fig. 4 shows the internal configuration of the down converter. The received signal passes through a waveguide filter into a circular cylindrical cavity in which two diodes are mounted. Inside the cavity, the signal power divides equally between the two diodes. The 6300-mc local oscillator signal is coupled into the opposite end of the cavity from a second waveguide filter; the principal axes of the two waveguides are at right angles to ensure isolation between the two frequencies present in the cavity. Input matching is provided at the signal input by the three screws which penetrate into the cavity as shown in the illustration. Two screws mounted in the waveguide close to the cavity are used to tune the local oscillator input.

The IF connection to each diode is decoupled to microwave signals by means of an RF choke which consists of two quarter-wavelength radial transmission lines. The resonant frequencies of the two lines are staggered to obtain high insertion loss over a wide bandwidth. The position of each choke along the IF output line is so chosen that an RF short circuit appears at the waveguide wall. The two IF output lines are parallel connected through coupling capacitors to the input of the IF ampli-

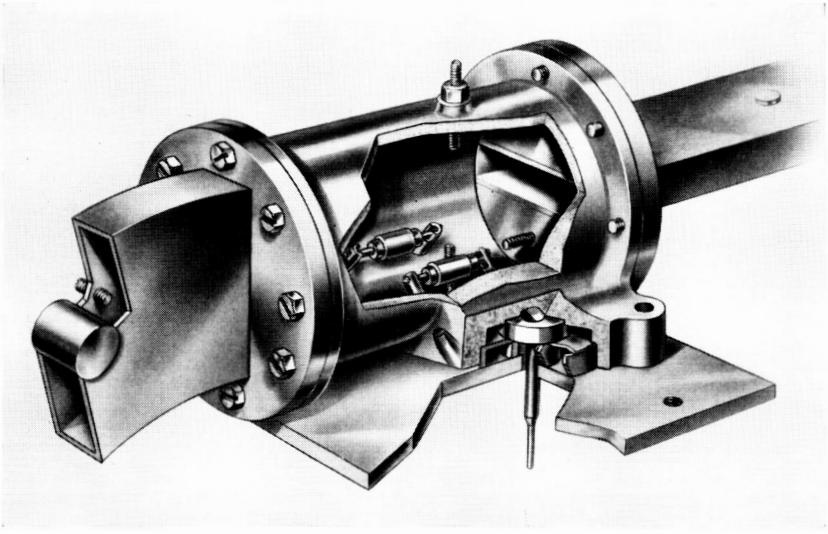

Fig. 4 — Internal structure of the down converter.

fier which is mounted directly onto the down converter. However, separate dc connections are made to the two IF output lines so that each diode may be forward biased for optimum performance.

It was experimentally determined that a good noise figure could be obtained most readily when the down converter was tuned to have a relatively narrow-band input match. The down converter is narrow banded by the presence of the resonant tuning screw placed between the two diodes, which reduces the bandwidth to about 120 mc. Narrow banding the down converter lessens the importance of the combination-frequency products generated by the modulator. With the down converter working into an IF amplifier with a noise figure of 4.5 db, the receiver noise figure is 12.5 db. Some improvement in noise figure would be obtained by increasing the level of the local oscillator signal; however, this would decrease the long-term stability and cause the properties of the down converter to be noticeably dependent on the exact level of the local oscillator signal. In the final design, the down-converter conversion loss is less than 7 db.

3.2 *IF Amplifier and AGC Circuit*

The IF amplifier provides the bulk of the amplification in the repeater, helps determine the repeater bandwidth,* and in conjunction with the

* One end of the receiver passband is determined by a high-pass filter at the input to the up converter.

microwave level monitor and the direct-coupled AGC amplifier provides automatic gain control.

Fig. 5 shows the levels encountered throughout the IF circuit. Note that the gain of the IF amplifier is adjusted by two variolossers whose losses are controlled by the output current of the AGC amplifier. The monitor for the AGC system is placed at the output of the up converter; thus the AGC system controls the input level to the traveling-wave tube.

3.2.1 *IF Amplifier*

Fig. 6 shows diagrammatically the basic design of the, IF amplifier, which uses diffused-base germanium pnp transistors throughout. Three different transistor IF amplifier configurations are employed.

The low-noise input stage consists of a common-emitter — common-emitter "doublet."[4] This configuration utilizes a large portion of the available power gain of the input transistor and thereby minimizes the effect on the over-all noise figure of the noise generated by the other transistors in the IF amplifier. A simple equalizer network is used at the output of the second transistor to compensate for the rolloff in gain of the doublet in the IF band. As one can see from Fig. 3(b), the input of the IF amplifier is physically located next to the down converter. A transformer with a 1:2 turns ratio is used between the down converter and the doublet to provide the proper mismatching for optimum noise figure. Averaged over the 65- to 115-mc band, the IF amplifier noise figure is 4.5 db, and the input impedance is about 30 ohms. The power gain of the doublet plus equalizer network is about 13 db.

To achieve the desired IF gain with a minimum number of stages while still realizing satisfactory aging and temperature performance characteristics, the common-emitter circuit with frequency-sensitive shunt feedback[4,5,6] is used for the large majority of IF amplifier stages. Frequency shaping is achieved by means of an RL network connected between base and collector. Consider the third transistor stage of Fig. 6. Resistor R_1 determines the low-frequency gain, and inductor L effectively removes the feedback at high frequencies and thereby plays the role of a broadbanding element. Resistor R_2 damps the resonance which occurs between the inductor L and the capacitive reactance presented by the transistor. Through adjustment of R_1, R_2 and L, gain and bandwidth can be exchanged; and the gain-bandwidth product is given approximately by f_T, the frequency at which the common-emitter short-circuit current gain is unity. The gain for each common-emitter shunt-feedback stage is approximately 8 db.

The principal requirement which dictates the selection of an IF out-

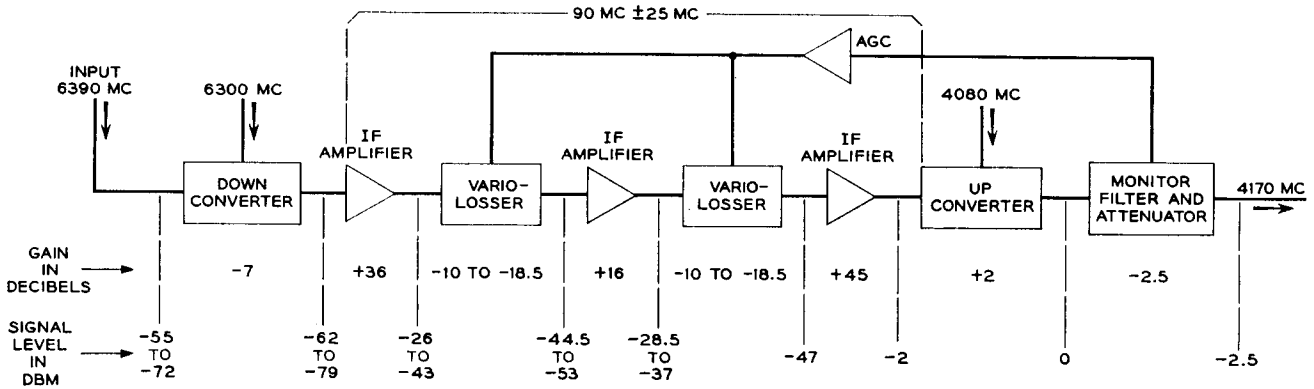

Fig. 5 — Level diagram of the IF amplifier.

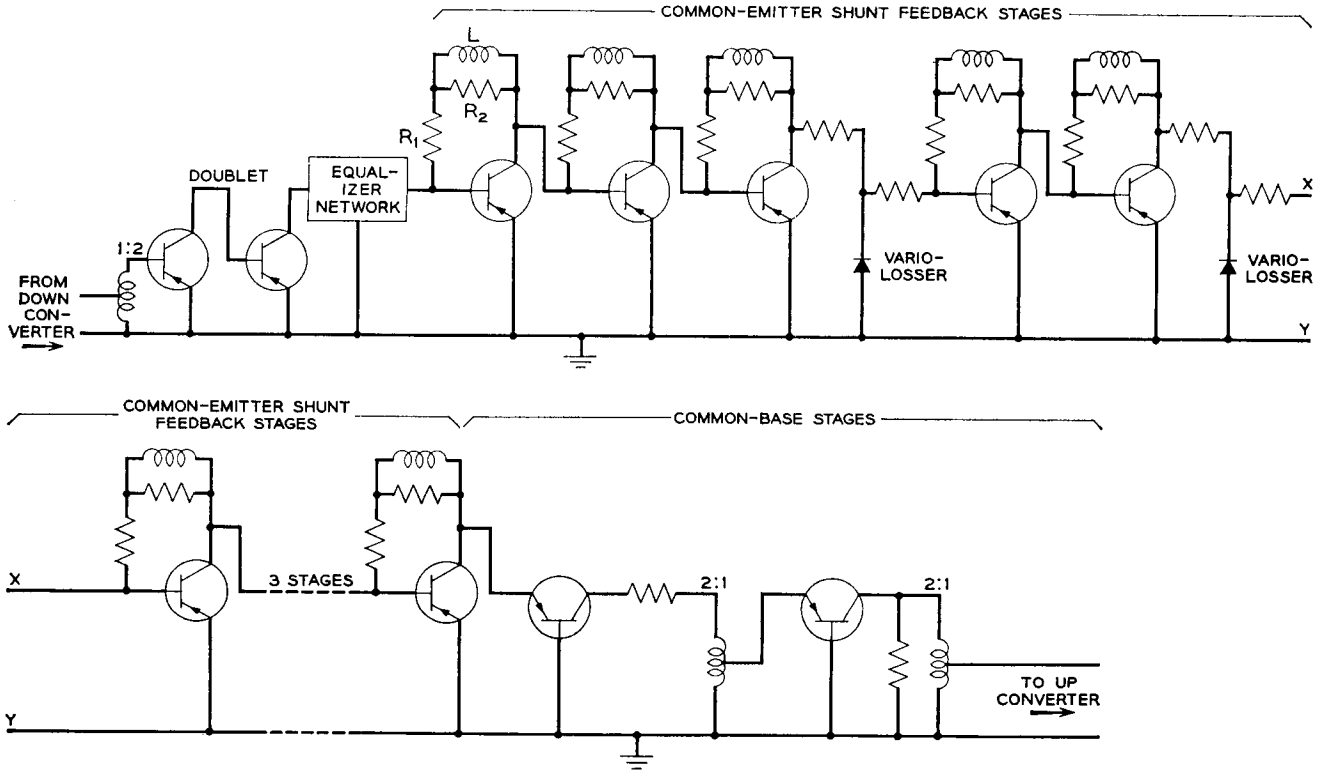

Fig. 6 — Basic circuits in the IF amplifier.

put stage configuration is that the desired undistorted output power should be achieved with minimum expenditure of dc power. For this reason the common-base configuration, with its inherently linear transfer characteristic, is used for the output stage and its driver. Two transformers, each with a 2:1 turns ratio, are used for current step-up between the common-base stages and at the output of the amplifier. Through the use of these transformers, each common-base stage provides about 5.5 db of power gain. The up converter, which is driven through a length of 75-ohm coaxial cable by the IF amplifier, must be driven by a generator with resistive impedance. An output return loss in excess of 20 db is achieved over the IF band. The output stage is capable of delivering up to +6 dbm into a 75-ohm resistive load.

The transmission characteristic of the complete IF amplifier with the variolossers set in the minimum loss condition is shown in Fig. 7. Note that over the 0° to 60°C temperature range the midband gain (nominally 87 db) changes 10 db and the tilt over the band varies from +1.5 db to −2.0 db. Delay slope over the band is less than 7 ns and AM-to-PM conversion is less than 0.4 degree per db. The circuit operates from a negative 16-volt supply and has a current drain of 90 milliamperes.

Conventional high-frequency wiring techniques are applied, and because of the inherent stability and low gain per stage of the configurations used, no interstage shielding is necessary.

3.2.2 *Variolossers*

The variolossers consist of a T-network containing two series resistors and a shunt low-capacitance germanium alloy diode used as a variable

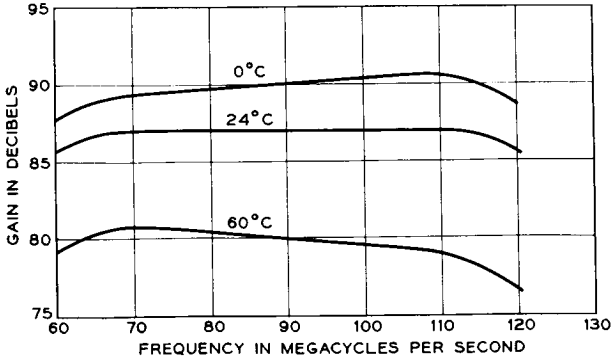

Fig. 7 — Transmission characteristics of the IF amplifier.

element. The resistors are large enough that they essentially mask out the reactive input and output impedances of the adjacent common-emitter shunt-feedback stages. They are small enough, however, to assure a low minimum loss for the variolossers. The loss of the variolossers is controlled by varying the direct current through the shunt diodes.

The placement of the variolossers in the IF amplifier is a compromise. If located too near the input, they cause too severe a degradation of noise figure during stronger input signal conditions. Placement too near the output of the amplifier will result in distortion due to rectification of the IF signal by the variolosser diodes.

The loss range of each variolosser is 15 db, and the minimum loss (relative to directly cascaded common-emitter shunt-feedback stages) is about 5 db. For the full 15-db loss variation at any temperature, the frequency distortion is less than 0.5 db; over the 0° to 60°C temperature range, the frequency distortion is negligible compared with that caused by other parts of the IF amplifier. The control current of 0 to 8 milliamperes flows through the two variolosser diodes. This current, which is a monotonic function of variolosser loss, is telemetered back to earth as an indication of the received signal strength at the satellite.

3.2.3 *AGC Amplifier and Loop Performance*

The AGC amplifier is a direct-coupled amplifier which provides control current for the variolosser diodes proportional to the difference between the dc output from the waveguide monitor and a dc reference voltage. The amplifier, which uses diffused-base silicon npn transistors, is shown diagrammatically in Fig. 8. In addition to providing high gain

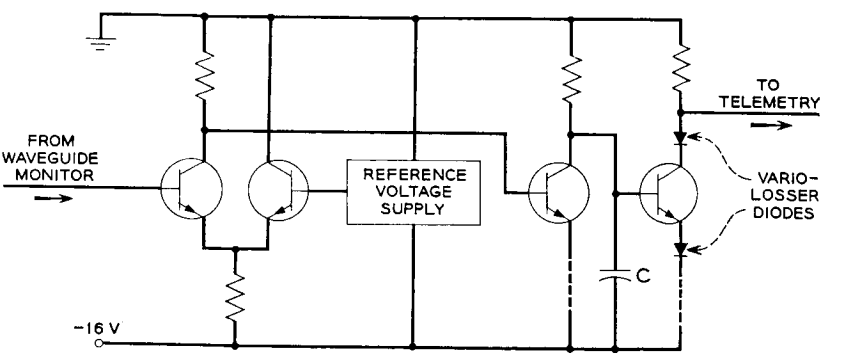

Fig. 8 — The AGC amplifier.

with low drift, the amplifier also has an adjustable feature which programs the reference voltage in accordance with variations in power supply voltage. Since the TWT uses the same power supply, the net effect of this feature is a compensation of the power supply dependence of the TWT overload characteristic through variation of TWT input level; see Fig. 2.

The differential input stage is followed by a common-emitter stage. One variolosser diode is driven from the emitter of the output stage and the other from the collector of that same stage; thus approximately equal currents flow through each variolosser diode. This diode-driving technique and the use of high-frequency transistors in the AGC amplifier (f_T = 250 mc) results in the frequency response of the AGC loop being controlled almost exclusively by capacitor C.

As has been mentioned previously, the AGC loop includes not only the IF amplifier, but also the up converter. Thus, the input level to the TWT is held relatively constant for variation in received signal strength, down converter loss, IF amplifier gain, and up converter gain. The dependence of TWT input level on received signal level is shown in Fig. 9. For received signal levels ranging between −55 and −72 dbm over a temperature range of 0 to 60°C, the input level to the TWT tube varies less than ±0.8 db.

Since the satellite is spinning and because the radiation pattern of the receiving antenna has ripples, the dynamic regulation of the AGC system must be effective for frequencies as high as 500 cps. The dynamic regulation of the AGC system is shown in Fig. 10 for several received signal levels.

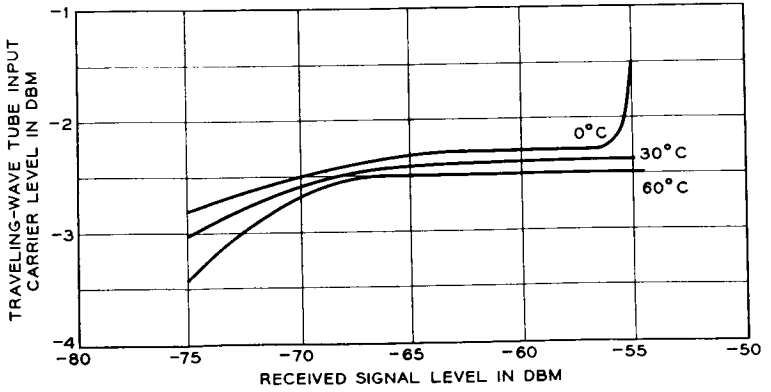

Fig. 9 — Tightness of the AGC system.

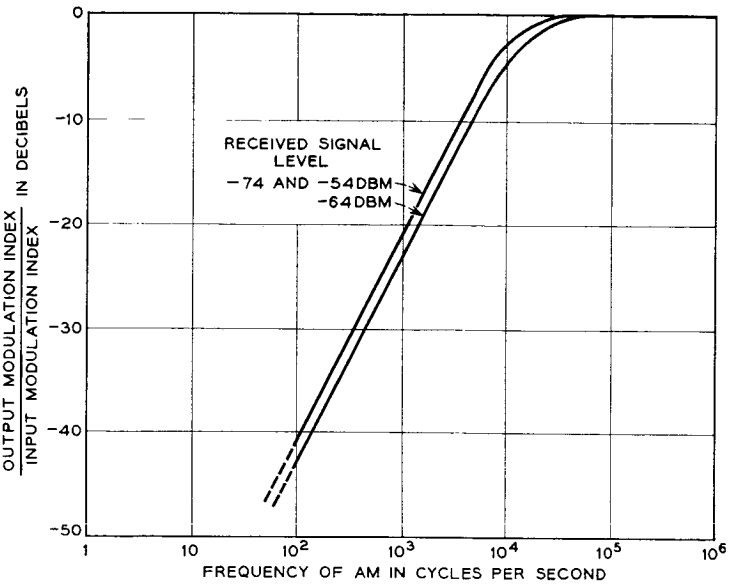

Fig. 10 — Dynamic regulation of the AGC system.

3.3 *Up Converter*

The output of the IF amplifier is connected through a short coaxial lead to the up-converter assembly, where the signal first passes through a high-pass filter. The over-all transmission characteristic of the filter is flat over the frequency band 65 mc to 115 mc, but has a minimum of 40-db rejection at frequencies below 50 mc. The up converter is a balanced diode modulator which was designed for good temperature stability and for low susceptibility to rapid fluctuations in the pump power level. To meet the special requirements imposed on the design of the converter, the diodes are operated in forward conduction and a conversion gain of about 2 db is obtained.

The up converter is designed around a hybrid junction; the output arm is waveguide, while the other three arms are coaxial, as shown in Fig. 11. Two of the arms containing the diodes also house matching transformers and second-harmonic rejection filters. The IF output leads are fed through hollow center conductors within the crystal arms and then through the center of a shorted coaxial stub. These leads are parallel coupled through capacitors to the input network and high-pass filter circuit mounted in the shielding can on the side of the up converter. DC bias voltages for the diodes are developed across self-bias resistors;

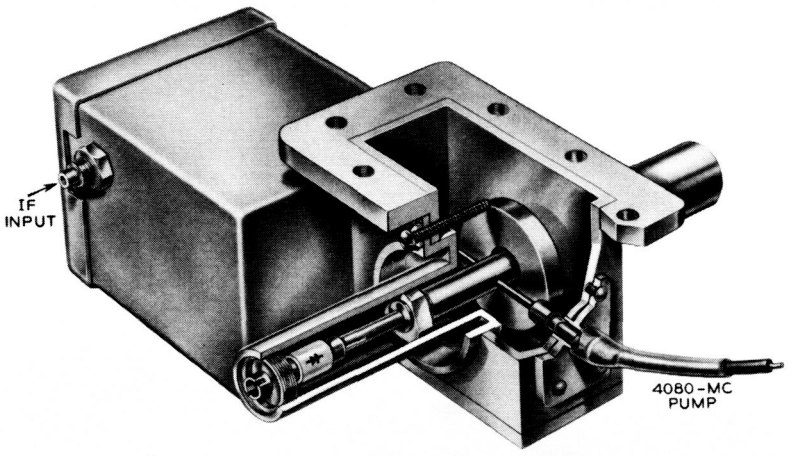

Fig. 11 — Internal structure of the up converter.

these voltages serve the secondary function of indicating the level of the pump signal for telemetry purposes. The waveguide filter on the output of the up converter is critically positioned to reflect the image frequency in correct phase to reinforce the modulator signal output power. Since the circuitry is adjusted to have a flat transmission characteristic, the return loss of the IF input to the up converter varies from 7 to 18 db over the 65- to 115-mc band.

The return loss at the microwave ports is in excess of 20 db. An important characteristic of the up converter is the relationship between the pump input level and the signal output level shown in Fig. 12. This relationship is vital to the AM stability of the circuit, a problem that will be discussed later in this article. Equally important is the absence of the pump signal at the output. Means are provided to adjust the balance of the converter to obtain a minimum loss of 30 db between the pump input and the signal output arm at normal operating levels.

3.4 *Waveguide Monitor*

The 4170-mc signal from the up converter passes through a filter and a monitor which consists of two similar diode mounts inserted one-quarter wavelength apart in a waveguide. Each diode, as shown in Fig. 13, is supported between two chucks, one on the end of the center conductor, the other in the center of a four-arm spider mounted in a die-

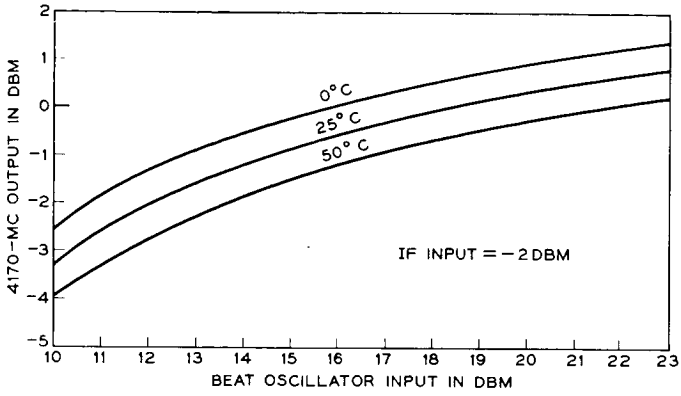

Fig. 12 — Operating characteristics of the up converter.

lectric support within the waveguide. The dc voltage developed across the diode appears between the center conductor and the outside conductor of the crystal mount, both parts being insulated from the waveguide itself. On the center conductor, a bucket-type choke determines the RF susceptance in series with the crystal.

The diode mounts are tested separately. To accommodate variations of the individual crystals, the position of the center conductor choke is varied until the impedance measured at the waveguide input and referred to the plane of the diode is found to be purely resistive. After the two diode mounts have been sealed and have passed their acceptance tests, they are mounted in the waveguide and load resistors and video-frequency decoupling components are added before foaming and final testing. No tuning or adjustment of the entire assembly is necessary.

The output voltage used for AGC purposes is derived by connecting the two diodes in series. Separation of the mounts by a quarter-wavelength along the waveguide ensures a design that is not too sensitive to the nature of the output termination. This eliminates the need for a directional coupler in this part of the circuit, thus simplifying the electronics package and reducing its size. The input-output characteristic of the monitor is shown in Fig. 14, where it will be seen that changes with temperature are relatively small. The monitor has a 20-db return loss into the waveguide input; its insertion loss is 1.5 db.

3.5 *Combining Network*

The function of the combining network is to provide a common connection to the TWT for both the communication and microwave beacon

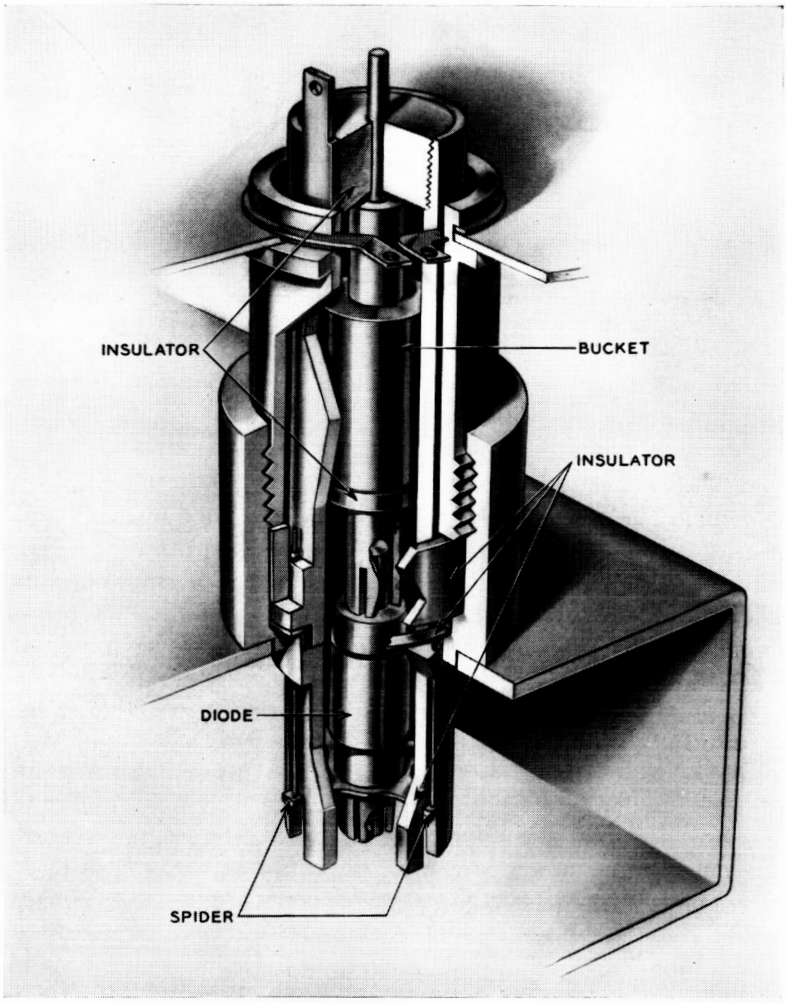

Fig. 13 — Internal structure of the monitor.

signals and at the same time provide isolation between these two inputs. This network consists of two 3-db couplers of the Riblet type,[7] two identical bandpass waveguide filters tuned to 4080 mc, and a matched termination; see Fig. 15.

The 4080-mc beacon signal input to filter B from coupler B lags the beacon signal input to filter A by 90° because of the nature of the coupler. The relative phase of the two signals is unaltered as the signals go

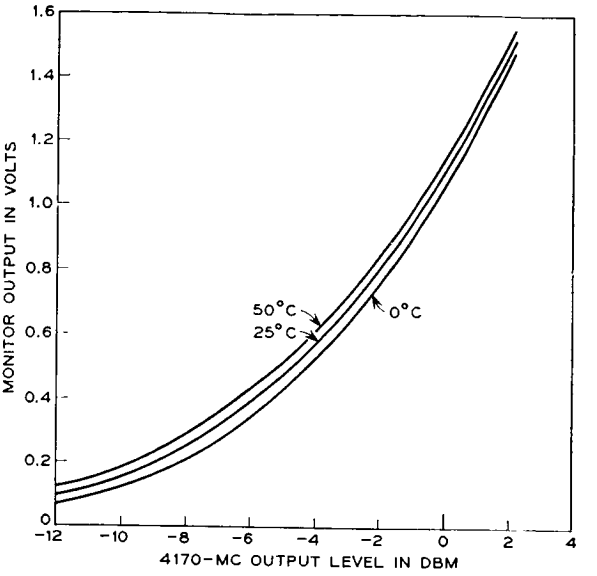

Fig. 14 — Voltage-power relations in the monitor.

through the identical two-section filters. At the output port, the signal from filter A is delayed 90° by coupler A, so at this point it is in phase with the signal from filter B. At the communications input port, the two equal-magnitude 4080-mc signals are 180° out-of-phase because the signal from filter B undergoes a 90° lag in going through coupler A, and it already lagged the output of filter A by 90°. Because of the cancellation of two 4080-mc signals at the 4170-mc input port, the only loss in the microwave beacon signal in this unit is due to the small ohmic losses.

The input signal at 4170 mc enters coupler A, and the nature of the coupler makes the input signal to filter B lag the input signal to filter

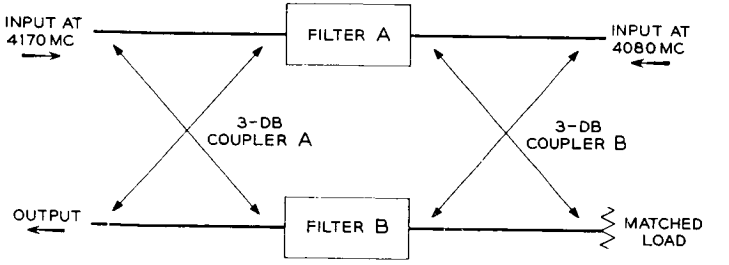

Fig. 15 — The combining network.

A by 90°. The relative phase of these signals is unchanged, as they are almost completely reflected from the filters which are tuned to 4080 mc. Thus, the phase relationship of the signals entering coupler A from the filter side is such that the two signals at the 4170-mc input port are 180° out of phase and the two signals at the output port are in phase. The isolation between the two input ports is greater than 30 db; the insertion loss at 4170 mc is 0.2 db; and the insertion loss at 4080 mc is 0.3 db.

3.6 *Separation Network*

The separation network, shown in Fig. 16, is similar to the combining network in that it comprises two 3-db couplers, two identical waveguide filters, and a matched termination. Because its filters are tuned to 4170 mc, signals near this frequency go through the separation network in the same manner that the signal at 4080 mc goes through the combining network. The filters are relatively broadband, so twenty per cent of the signal at 4080 mc leaks through the filters to the transmitting antenna, and eighty per cent is reflected from the filters. The behavior of the separation network to the reflected 4080-mc signal is similar to the behavior of the combining network to the 4170-mc signal. The 4080-mc signal level at the output port connected to the antenna is 7 db below the input signal. The insertion loss of the network in the band 4145 to 4195 mc is less than 0.2 db.

3.7 *Traveling-Wave Amplifier*

The type M4041 TWT is the only vacuum tube in the satellite. Since this tube is described in a separate paper,[8] only the circuit aspects are discussed here. The purpose of the tube is to provide power amplification for both the communications and microwave beacon signals. The operating characteristics of the tube, including the combining net-

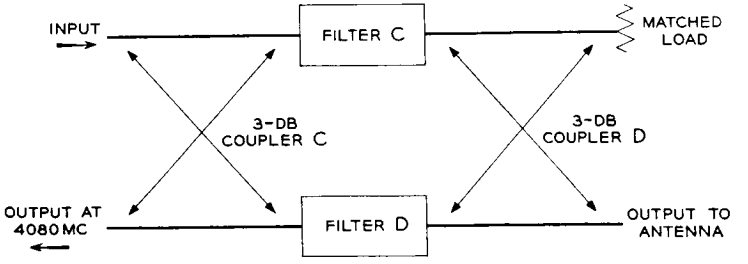

Fig. 16 — The separation network.

work, the separation network, and filter 5, are shown in Fig. 2. These filters are included in the circuit associated with Fig. 2 so the impedances seen by the tube will closely approximate those seen under actual operating conditions. The operating point was chosen well below the saturation power level of 36.5 dbm for four reasons.

First, operation in the near-linear region of the tube reduces the effect of amplitude changes in the communications signal causing amplitude changes in the microwave beacon signal. The circuit instability associated with this condition is discussed later in this paper.

Second, near-linear operation reduces the phase jitter of the microwave beacon signal. Stability of the beacon is important because both the precision tracker and the vernier autotrack systems phase lock on the signal. Even when the output load on the tube and the impedance of the source feeding the tube are perfectly matched, the power output is frequency sensitive. This means that when the communications signal is frequency modulated, the microwave beacon is amplitude and phase modulated. When the load impedance (the antenna) causes a reflection which is frequency sensitive, the above effect is made worse. Both types of modulation are decreased by operating below saturation. From the standpoint of the phase-locked tracking systems on the ground, the amplitude modulation is much less serious than the phase modulation.

The third reason for operating the TWT below saturation is the frequency characteristics of the up and down converters, the IF amplifier, and the monitor. None of these units has a perfectly flat frequency response, so an FM communications signal causes the instantaneous power drive to the tube to vary. This causes phase modulation (through AM to PM conversion) of the beacon and communications signals.

Finally, near-linear operation is desirable to reduce intermodulation of signals when the satellite is used for two-way communications experiments. This is true regardless of any effects on the microwave beacon.

The M4041 tube has very low AM-to-PM conversion when operated below saturation, so the first of the four reasons determines the operating point. With the operating point shown in Fig. 2, the net phase jitter or deviation of the microwave beacon as measured with the precision tracker[9] was less than the $\pm 5°$ "noise level" in the measuring equipment.

3.8 *Waveguide Limiter*

Because the level of the 4080-mc signal from the TWT varies with the level of 4170-mc signal, a waveguide limiter is used to stabilize the level of the 4080-mc signal at the input to the BO modulator. The lim-

iter comprises a half-height, half-wavelength waveguide cavity with a carefully oriented yttrium-iron-garnet (YIG)[10] single-crystal sphere supported in a dielectric material close to the side wall. The cavity is formed from two inductive irises; the reduced waveguide height improves the ratio of the volume of the YIG sphere to that of the cavity and appreciably reduces the size and weight of the permanent magnet required to bias the YIG sphere.

The sphere is highly polished to reduce the insertion loss to less than 0.75 db for operation below the limiting threshold. The power limiter is of the subsidiary resonance type. With the correct external magnetic field, above a critical power level a subsidiary resonance appears in the YIG crystal which is caused by the generation of spin waves at one-half the applied microwave frequency. With increasing power input, the power out of the device remains essentially constant because the excess RF energy goes into the generation of the spin waves or is reflected from the limiter.

The magnet is designed to produce a field of about 1200 gauss across a 0.4-inch gap. It consists of two truncated cones of magnetic material and two soft-iron pole pieces. The outer case, which is used as a magnetic return path, is designed to keep the external magnetic field to a minimum.

3.9 *BO Modulator*

The 6300-mc signal used as a receiver local oscillator is generated in the BO modulator shown in Fig. 17. It is a balanced upper-sideband up

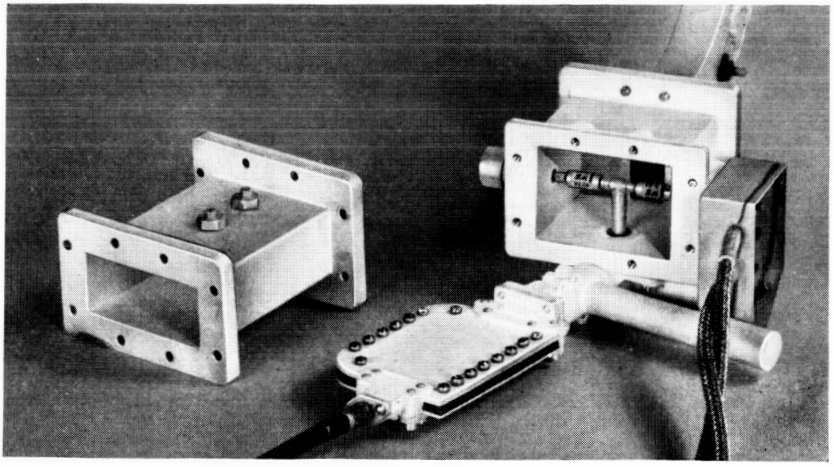

Fig. 17 — The BO modulator.

converter using gold-bonded varactor diodes which are mounted in line across a waveguide cavity. The 2220-mc input is connected to the center of the two diodes. Thus the diodes together with the center conductor of the 2220-mc coaxial input form a "T" inside and across the waveguide cavity. A two-section strip-line filter in the coaxial input provides decoupling to the higher frequencies present; the balanced structure is chosen to avoid generation of the 6300-mc signal across the 4080-mc input port, and all other necessary decoupling is provided by the natural cutoff frequencies of the waveguides used. No attempt was made to broadband the modulator since this was not necessary; the simplest possible matching device was provided in each transmission line external to the cavity. Adjustable tuning screws were used in the waveguide connections, while coaxial stub tuners were used at the 2220-mc input.

To ensure maximum stability, the modulator was operated somewhat conservatively, and the efficiency of the device was low. Due to filter losses there is a loss between the lower frequency input and the 6300-mc output of approximately 1.0 db.

3.10 *The Microwave Carrier Supply*

The local oscillator signals for the up and down converters are obtained by frequency multiplication following crystal-controlled oscillators, as shown in Fig. 18. These oscillators and the accompanying multipliers constitute the microwave carrier supply. The exact crystal frequencies are 17.342600 and 15.936440 mc. These frequencies are multiplied to provide nominal frequencies of 2220 and 4080 mc. As noted previously, the 4080-mc signal is further amplified by the TWT and used for the microwave beacon; it is also used as the pump for the up converter and mixed with the 2220-mc signal to provide the 6300-mc supply for the down converter.

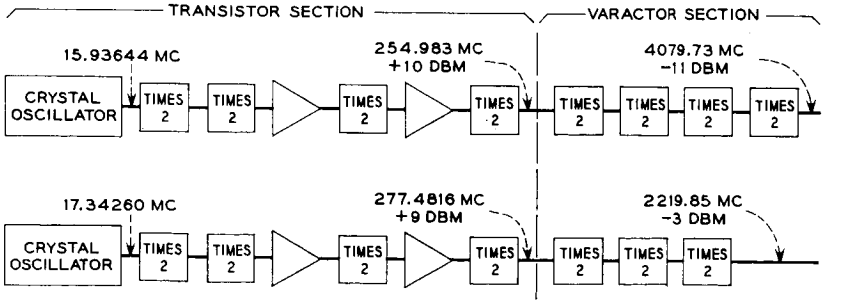

Fig. 18 — The microwave carrier supply.

A more detailed description of the components of the microwave carrier supply follows.

3.10.1 *Transistor Section*

The third overtone AT-cut crystals selected for use in the satellite had a frequency variation of only ±2 parts per million over a 0 to 50°C temperature range, so neither temperature stabilization nor temperature compensation was necessary. Good short-term stability was obtained by maintaining an RF crystal current of 6 milliamperes.

Since frequency multiplication decreases the ratio of signal power to noise power, it is necessary to start the multiplication process with an extremely pure signal. To obtain the spectral purity, extensive shielding, decoupling, and filtering were necessary to isolate the two transistor sections from each other, from the power supply, and from other oscillators in the satellite.

The transistor frequency doublers are class C amplifiers with a collector tank tuned to the second harmonic. The first and second multipliers are operated common-emitter, the third and fourth common-base. The efficiency of the third and fourth multipliers is improved by the inclusion of a full-wave rectifier in the input circuit.

3.10.2 *Varactor Octuplers*

Design of the varactor octuplers (250–2000 mc) is common for the two strings, only the tuning being different. The octupler consists of three doubler stages, each using lumped elements; early experimental work showed frequency doubling to be the most efficient means of multiplication.

The basic doubler circuit is shown in Fig. 19. The series resonant circuit in the output is resonant at frequency f, while the input trap is resonant at $2f$. The shunt input inductor is chosen to match the diode

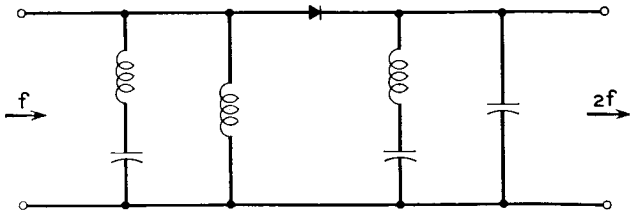

Fig. 19 — Basic varactor frequency doubler circuit.

impedance: the output capacitor is tuned for maximum output. Cascading of these stages requires additional tuning elements.

The first two stages are placed at zero bias by RF chokes connected to ground; the third stage is self-biased. Varactor diodes are Western Electric Co. units chosen for stability and high Q.

Shunt resistors were added around the diode in each stage to improve stability with changing input power level. The addition of these resistors also made tuning less critical and eliminated a problem of parametric oscillation. Critical cable lengths at both the input and output of each octupler were experimentally determined.

The octupler, before encapsulation, is shown in Fig. 20. Connections are made to the diodes through a cup welded to the small end of the diode and a shell screwed to the other. Tuning is accomplished with variable quartz capacitors and air inductors of 14-gauge tinned copper wire.

3.10.3 *The 2040- to 4080-mc Doubler*

This doubler, shown in exploded form in Fig. 21, uses the same principle as the varactor doubler described above. The diode is placed in a coaxial cable which terminates in a 4-gc waveguide. This waveguide effectively reflects the 2-gc energy. The input trap is provided by a quarter-wave sliding transformer.

A short length of rigid coaxial line matches the loop and waveguide to the diode. Output power at 4080 mc is set by rotating the output loop

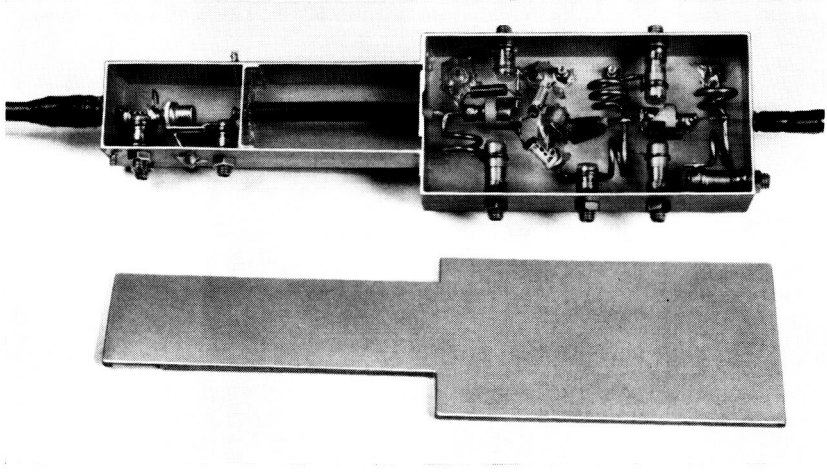

Fig. 20 — The varactor octupler.

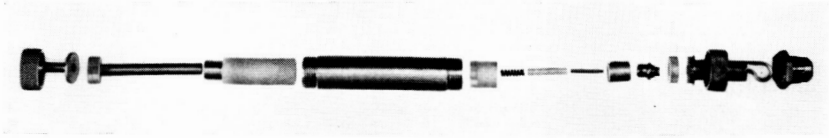

Fig. 21 — The 2- to 4-gc doubler.

in the waveguide. The spring shown in the photograph presses the chuck and diodes against the center conductor of the rigid coaxial cable. The capacitor wire which slides inside the insulating sleeve is selected to tune the circuit. The decoupling afforded by this capacitor results in self-biasing of the diode.

3.10.4 *Over-All Design Considerations*

The microwave carrier supply must be self-starting, must be free of spurious oscillation and must maintain proper output level over the temperature range. The above conditions require special attention to tuning procedures, especially for the varactor multipliers.

As mentioned above, relative amplification of noise and spurious sidebands in each multiplier stage required close attention to suppression of these unwanted signals in the early transistor stages. All inherent noise sidebands at 2000 and 4000 mc are at least 40 db below the desired signal.

The crystal-oscillator frequency is initially adjusted to within ± 1 part per million of the desired frequency, and aging in two years is expected to be less than one part per million.

3.11 *Microwave Filters*

Because space in the electronics canister is so limited, all the waveguide filters utilize direct-coupled cavities. There are four single waveguide filters, two dual waveguide filters, one coaxial low-pass filter, one strip-line filter, and a YIG limiter which is also a filter. All data given in this section are for room temperature.

Filter 1 is a two-section filter which is designed to give a 20-db insertion loss at the image frequency, 6210 mc, of the receiver. This filter has a half-power bandwidth of 100 mc and an insertion loss of 0.2 db at the center frequency of 6390 mc.

Filter 2 is also a two-section filter. It is built in a gradual 90° H-plane bend. The insertion loss at the center frequency of 6300 mc is 1.2 db, and the half-power bandwidth is 16 mc. The filter was made narrow band

to give high insertion losses except at 6300 mc. The need for the high insertion losses is discussed in the stability section of this paper.

Filter 3 is a three-section filter connected between the up converter and the monitor; its purpose is to pass the signal at (4080 + 90) mc and reject the signal at (4080 − 90) mc. It also must provide about 20 db insertion loss at 4080 mc so leakage of the pump signal through the up converter will not contribute to the output of the microwave monitor. This filter has a 90-mc bandwidth and an insertion loss of 0.15 db at the 4170-mc center frequency.

Filter 4 is the YIG limiter. The YIG crystal is placed in a resonant cavity, which below the threshold has loaded Q of about 200.

Filter 5 is a five-section direct-coupled filter having a center frequency of 4080 mc and a half-power bandwidth of 20 mc; the insertion loss at 4080 mc is less than 1 db. This filter was made as narrow band as space allowed to give high insertion losses except at 4080 mc. The high insertion loss is needed to ensure stability in some of the closed circuits in Fig. 1, which are discussed in the stability section of this paper. In order to position the large filter (15-inch length) in a canister of reasonable size, it was necessary to build the filter with a 90° E-plane bend in one of the cavities. It was found that by measuring the electrical length of the well-matched 90° mitered bend, the distance between the inductive posts separated by the bend could be calculated, and the resulting filter had no measurable difference from the "same" filter made in straight waveguide. The 90° mitered bend was placed as near the center of one of the five cavities as possible.

Filter 6 is a two-section strip-line filter that has a half-power bandwidth of 100 mc centered at 2220 mc. The purpose of this filter is to prevent the pump signal and harmonics and beat frequencies of the two input signals to the BO modulator from going back into the microwave carrier supply. The filter has excellent temperature stability and has an insertion loss of 0.7 db at 2220 mc.

The dual filters used in the combining and separating networks are described in previous sections of this paper.

IV. CIRCUIT STABILITY

As stated previously, the circuit stability problem is complicated by the feedback paths which are inseparably connected with the reflex circuit of Fig. 1. Three feedback paths created by the reflex circuit, the coupling between the satellite output and input, and miscellaneous couplings are described in this section. The loops are shown in Fig. 22.

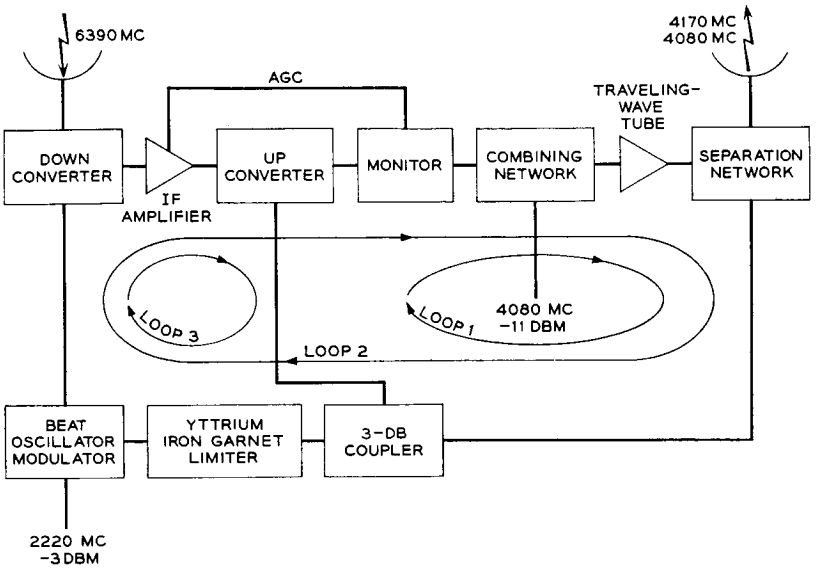

Fig. 22 — Simplified block diagram showing the feedback paths.

4.1 *Feedback Path One*

The circuit loop created by this feedback path from the separation network to the up converter includes the monitor, TWT and combining network. Two types of oscillation are possible in this loop.

The first is a straightforward RF oscillation. The TWT will act as an amplifier over a very wide frequency range; therefore the filters in this circuit were designed so at all frequencies there is margin against oscillation of at least 40 db at room temperature. This margin is made high because at least 30 db of this margin is due to the isolation between the pump input and signal output ports of the up converter, measured when it is new and the two diodes are balanced, and the isolation will be greatly reduced if one diode degrades. Also, the relatively narrow-band filters can change the margin by 5 db at the temperature extremes of 0 and 50°C. At frequencies high enough to allow higher-order modes to propagate in the waveguide, the waveguide filters give small insertion losses, so the low-pass coaxial filter was put in the circuit to provide the proper margin against oscillation at the higher frequencies. The coaxial filter has another use explained later in this article.

A second possible oscillation in this loop manifests itself in the form of amplitude modulation (AM) of existing signals. This is explained by showing that an AM signal applied to the input of the open loop causes

a similar AM signal at the output of the loop. If the amplitude and phase of the modulation envelope are proper, this circuit can oscillate in the AM mode; the phase of the carrier signal is not critical. Assume that the loop is opened at the input to the TWT and that an AM wave at 4170 mc is applied to the input. The data in Fig. 2 show that an increase in amplitude of the signal at 4170 mc results in a decrease in the output at 4080 mc. Thus, the envelope of the AM output at 4080 mc is 180° out-of-phase with the envelope of the input AM wave at 4170 mc. The amplitude-modulated wave from the output of the TWT goes through the separation network and filter 5 into the up converter. Unless the sidebands of the AM wave are attenuated more than the carrier, the output of the filter has the same general shape as the input to the filter. The curves in Fig. 12 show that if the pump signal to the up converter is amplitude modulated, the output signal at 4170 mc is also amplitude modulated, even though the modulation index of the output is much less than that of the input. If there is a phase delay in this loop corresponding to 180° at the modulation frequency, the AM feedback is positive; and if the modulation index of the signal at the output of the open loop is the same as or greater than the modulation index of the signal at the input to the loop, the circuit will oscillate in the AM mode when the loop is closed. It should be emphasized that the AM oscillation occurs only when there is a communications signal going through the TWT. The AM response of the various subassemblies in loop 1 are discussed in the next few paragraphs.

When the 4170-mc signal going into the TWT is amplitude modulated, both 4170- and 4080-mc signals from the tube are amplitude modulated. The degree of modulation of the beacon depends on the degree of modulation of the input signal and the operating point of the tube. The AM conversion gain (G_{cam}) of the TWT is defined at the ratio of the modulation index (m_{out}) of the beacon output to the modulation index (m_{in}) of of the input signal frequency. In decibels this is expressed as

$$G_{\text{cam}} = 20 \log_{10} \frac{m_{\text{out}}}{m_{\text{in}}}.$$

Since the ordinate and abscissa of Fig. 2 use the same scale, the TWT will have G_{cam} greater than 0 db when the magnitude of the slope of the beacon-output signal-input curve is greater than 45°. The operating point of the TWT is chosen so that the AM gain of the tube is less than 0 db and the power output at the signal frequency is near 35 dbm. Having the operating point below saturation is desirable, from the standpoints of AM gain and intermodulation of signals, but it is undesirable from a standpoint of obtaining maximum power output.

By selecting the proper biasing resistors for the diodes in the up converter, the output of the up converter can be made relatively independent of the 4080-mc pump signal (see Fig. 12), so this unit can be made to have very small (−18 db) AM conversion gain and thus provide good margin against AM instability for this loop.

At very low modulating frequencies, the feedback in this loop is negative because there is a 180° phase shift in the TWT and no phase shift in the up converter. However, at higher modulating frequencies, the phase delay in the various elements in this loop causes phase shifts of several hundred degrees, so the feedback at some frequencies is positive. The calculated delay for all the networks in the loop is approximately 75 ns; about 36 ns of this is due to the narrow-band filter 5.

If an AM signal with a modulating frequency f_b in loop 1 is delayed by T seconds, the envelope of the wave is shifted by

$$\varphi = 2\pi f_b T \text{ radians.}$$

When this phase angle φ is some odd multiple of 180°, the feedback will be positive because there is a constant 180° phase shift of the modulation envelope introduced in the TWT. Using these relationships and a 75-ns circuit delay, the lowest frequency f_b calculated to give positive feedback is 6.7 mc. When the circuit gain was adjusted to have more than 0 db (by changing the drive to the TWT), the output wave was amplitude modulated at 6.1 mc.

If the input wave to filter 5, which has a half-power bandwidth of 20 mc, is amplitude modulated at 6.1 mc, the sidebands and carrier all experience about the same insertion loss; so the AM gain of the filter is about 0 db. If, however, the modulating frequency is 20 mc, the next modulating frequency that gives positive feedback, the sidebands are attenuated 11 db more than the carrier; so the filter gives an AM gain of −11 db. Even if space were available to reduce the bandwidth of this filter, it would do no good because the filter delay, which contributes an appreciable part of the circuit delay, would increase and the frequency of oscillation would decrease, so the filter would have little effect on AM gain at the lower frequency. The remaining filters in this loop are quite broadband, so they have essentially 0-db AM gain.

The monitor circuit consists of two diodes inserted in the waveguide. The insertion loss caused by these diodes depends upon the resistors used in the self-biasing circuit; the smaller these biasing resistors, the higher the insertion loss. By putting selected capacitors across the biasing resistors, the monitor can be made to partially clip the peaks of the AM wave and have little effect on the troughs. By this means, the AM gain of the monitor is reduced to −3 db at f_b = 6 mc.

The final open-loop AM gain of the circuit was made as low as −18 db when the TWT voltages were normal. A decrease in tube supply voltages of 3 per cent causes the tube characteristics to change, and this can reduce this margin to −13 db.

If the 6390-mc received signal power is large enough to extend above the upper limit of the AGC circuit, the 4170-mc signal drive to the TWT is increased an amount depending on the input signal, and the AM conversion gain of the tube will be increased; see Fig. 2. This increase in signal drive to the TWT decreases the beacon output and the 4080-mc pump to the up converter and thus increases its AM conversion gain. An experiment on the ground has shown that if the 6390-mc input is increased to about −35 dbm, the AM oscillation will start, but does not damage the circuit. This high input level is not possible under normal orbital operating conditions.

4.2 *Feedback Path Two*

The local oscillator signal for the down converter is obtained by combining in the BO modulator the 4080-mc signal from the TWT with a 2220-mc signal from the microwave carrier supply. This method of obtaining the local oscillator signal creates feedback path two, which consists of the down converter, the IF amplifier, the up converter, the monitor, the TWT, the YIG limiter, the BO modulator, and several passive filters. Here, as in loop 1, two types of oscillation can exist, straight RF oscillation and AM oscillation.

In loop 2 a signal at frequency f, expressed in mc, in the IF amplifier will cause a frequency of $(4080 + f)$* mc in the output of the up converter. This signal is amplified by the TWT and is fed back through the separation network to the BO modulator through the YIG limiter. Even if the nonlinearities of the TWT and YIG limiter are neglected, this signal at $(4080 + f)$ mc plus the normal 4080-mc signal is combined in the BO modulator with the 2220-mc signal from the microwave carrier supply to give a frequency of $(6300 + f)$ mc. Going into the down converter is the "weak" signal at $(6300 + f)$ mc in addition to the strong local oscillator signal at 6300 mc. These signals are combined in the down converter to give an output frequency f. Since this frequency is the same as the assumed input frequency in the IF amplifier, this feedback loop can oscillate if the gain is large enough, even though the signal changes frequency three times in the loop. When no 6390-mc signal

* A frequency of $(4080 - f)$ mc is also present, but it is attenuated more than the higher frequency.

is applied to the down converter, the gain of the IF amplifier is about 87 db over a wide frequency range, and the gain of the TWT is greater than 42 db, so the total gain of the amplifiers in this loop is very high. As was the case in loop 1, the margin against oscillation was made 40 db or more because high insertion losses were obtained with two balanced modulators, the BO modulator and the down converter, and an unbalance in any one could change the insertion loss appreciably. In order to get the required margin for this loop, in which the combined gain of the amplifiers is at least 129 db, and still keep the microwave package small, two filters in this loop were built in waveguide bends: filter 5 has a 90° mitered E-plane bend, and filter 2 has a gradual 90° H-plane bend. Also to improve the margin, a high-pass filter was put at the input to the up converter.

The above discussion of loop 2 did not discuss the possibility of nonlinearity of the TWT. When the nonlinearity of the tube is considered and a frequency f occurs in the IF amplifier, there are output frequencies from the TWT of $m(4080 + f) \pm n(4080)$ mc, where m and n are integers. Many of these frequency components pass through the 4-gc filters because the frequencies are such that the waveguide can propagate higher-order modes. These frequencies can combine in the nonlinear limiter to produce frequencies of $4080 \pm f$, going into the BO modulator. For example, the 3×4080 component can combine in the limiter with the $4080 + (4080 + f)$ components to give a frequency of $(4080 - f)$ mc. This signal at $(4080 - f)$ mc combines with 2220-mc component to give a signal at $(6300 - f)$ mc which is fed into the down converter along with the normal 6300-mc signal. These two signals in the down converter give the original f frequency in the IF amplifier, so oscillation occurs if there is sufficient gain. There are many combinations of high frequencies which create this problem; only one example has been given. A three-section low-pass coaxial filter having an upper usable frequency of 4500 mc preceding the YIG limiter provides an insertion loss greater than 60 db above 6000 mc, and this is enough to eliminate oscillation of the type due to nonlinearities in the TWT and other elements.

The same AM problem exists in loop 2 as exists in loop 1, since the TWT is common to both loops. The YIG limiter does not eliminate the AM oscillation in either loop. Positive feedback occurs in loop 2 when the modulating frequency is about 2.5 mc, because the delay in this loop is approximately 200 ns. Four circuits are involved in loop 2 which were not in loop 1: (a) the BO modulator, (b) the YIG limiter, (c) the IF amplifier, and (d) the down converter.

The BO modulator was found to have an AM conversion gain of

approximately 0 db when the average pump input is +14 dbm (normal level) and the modulating frequency is below 2 mc. The AM gain decreases to about −3 db when the pump is increased to +16 dbm and increases to +2 db when the pump is decreased to +12 dbm. Decrease in AM gain with increase in modulating frequency is very small in the trouble region below 5 mc.

Characteristics of the YIG limiter show it has excellent limiting characteristics for slow variation in signal level; but unfortunately, when the envelope of the input is amplitude modulated at rates higher than 100 kc, the limiter has little effect on the peak-to-peak variations. Since the average value of the signal is limited, the limiter actually has AM gain. Under normal conditions the limiter has an AM gain of 3 db.

For purposes of AM analysis, the IF amplifier can be considered linear and thus has an AM gain of 0 db. At frequencies below a few thousand cycles, the AGC circuit reduces amplitude modulation, but at 20 kc and above it has virtually no effect; see Fig. 10.

The down converter alone has an AM conversion gain of about −15 db when the modulating frequency is less than 10 mc, and even less when the frequency is higher. However, in early tests on the down converter and IF amplifier together, the AM conversion gain was found to be greater than 0 db. The reason for the increase in gain is as follows. When an AM signal is used as the local oscillator for the down converter, the output will contain, among other signals, a signal at the modulation frequency. If the low-frequency circuitry preceding the first IF amplifier does not give sufficient attenuation to this modulating frequency, it can overload the first two stages and cause the output IF frequency to be amplitude modulated. When the front end of the IF amplifier was modified to properly attenuate the frequencies below 15 mc, the AM conversion gain of the down converter and IF amplifier was consistent with the value predicted from the gains of the units measured separately.

4.3 *Feedback Path Three*

As shown in Fig. 22, feedback path or loop 3 consists of the down converter, the IF amplifier, the up converter, the 3-db coupler and YIG limiter, and the BO modulator.

RF oscillation in this loop is very similar to the RF oscillation described in loop 2. Consider this loop opened at the IF amplifier, where an input signal at a frequency f in mc is applied. The sum and difference frequencies $(4080 + f)$ and $(4080 - f)$ mc, originating in the up converter, leak down the pump arm through the directional coupler and

into the BO modulator via the YIG limiter. In this modulator, the two frequencies combine with the 2220 mc to give $(6300 + f)$ and $(6300 - f)$ mc signals into the down converter. These signals combine with the normal 6300-mc signal in the down converter to give a signal f in the IF amplifier. Since this frequency is the same as the assumed input, the circuit can theoretically oscillate. Loop 3 has less gain than loop 2, and the conversion insertion loss from the IF arm to the pump input arm is very large (30 db). Conversion insertion loss is calculated using the ratio of the magnitude of the $(4080 \pm f)$ mc signal in the pump arm to the magnitude of the input signal at f mc. Loop 3 was analyzed after loop 2, and when the margin against RF oscillation in loop 2 was made 40 db, the resulting margin in loop 3 was greater than 50 db.

The AM problem of loops 1 and 2 is no problem in loop 3 because the AM conversion gain between the IF input and pump ports of the up converter is extremely low, and the YIG limiter and BO modulator give a combined AM gain of only a few db.

4.4 *Output-Input Coupling*

The TWT produces noise power over a wide range of frequencies including the satellite input and image frequency bands of 6390 and 6210 mc. Since the cutoff frequency for the TE_{20} mode in the waveguide used to make the filters in the separation network is 6300 mc, their insertion loss at 6390 mc is small. When the output of the repeater, less antennas, is connected to the input through an attenuator, the noise output from the repeater is 3 db higher when the attenuator setting is 27 db than when the attenuator is "infinite." The measured isolation between the transmitting and receiving antennas over the frequency range 6150 to 6450 mc is greater than 75 db in the temperature range -100 to $+100°$F, so the noise output of the TWT that is coupled into the down converter is negligible.

The coupling between the antennas at 4170 mc is not a problem because the input waveguide is below cutoff at this frequency and provides enough insertion loss to prevent the high power from the TWT from having any effect on the down-converter crystals.

4.5 *Miscellaneous Couplings*

Fig. 23 shows an end view of the cylindrical part of the electronics canister after all the electronics subassemblies have been mounted in the canister, but before it has been foamed and the metal domes have

been welded in place. After the domes are in place, the canister becomes a big echo box, and reducing the couplings between units to acceptable levels becomes very difficult. The power supply contains one flip-flop circuit operating at a fundamental frequency of 2.5 kc and another operating between 25 and 50 kc. Also, there are four crystal oscillators that are used to obtain the microwave carrier supply signals at 2220 and 4080 mc, the VHF beacon signal at 136 mc, and the local oscillator signal at 128 mc for the command receiver. The frequencies of the crystal oscillators (15.93644, 17.34260, 17.00625, and 31.9750 mc) and their harmonics, plus all harmonics from the flip-flop circuits, create a noise spectrum that can cause trouble in the IF amplifier and the converters. The problems associated with the myriad couplings in the canister were solved with extensive shielding, filtering, and patience.

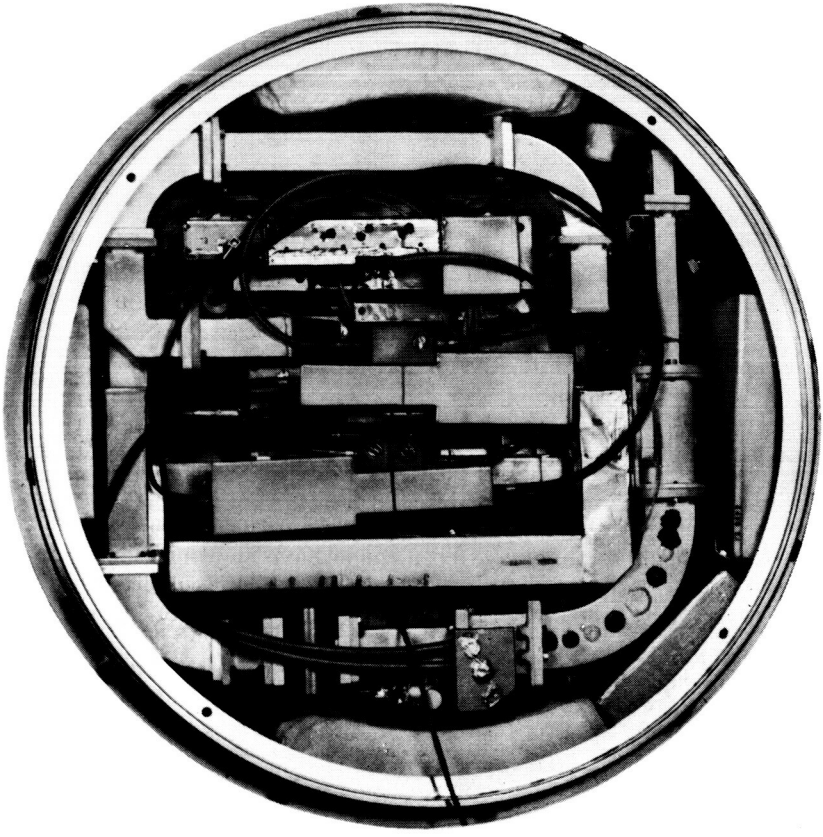

Fig. 23 — Electronic parts in the canister.

4.6 *Over-All Noise Performance*

The frequency modulation noise due to the satellite repeater is an important factor in the operation of the system as a whole. Consideration of this noise contribution is complicated by the complex nature of the repeater circuit because of the dual use of the traveling-wave tube. The predominant noise source is at the input to the IF amplifier. Operated as it is with a low level 6300-mc signal, the down converter does not add significantly to the noise, but there is considerable loss of signal power through the device, and the noise figure of the down converter and the IF amplifier together is as much as 12.5 db. Noise contributions due to other parts of the repeater, including the microwave carrier supply, increase this figure.

The noise figure of the satellite as measured before launch by a noise lamp is 13.5 db ±1 db.* However, the noise does not have a flat spectrum over the band of interest and this number applies in the region where the noise is flat.

V. CONCLUSIONS

The Telstar communications circuit is a broadband nondemodulating repeater. To obtain a high power efficiency the traveling-wave tube is caused to amplify two signals, a fact that somewhat complicates the circuit. Consequently, several stability problems exist which are overcome by the provision of frequency filters and by careful control of the nonlinearity of the circuits. Every portion of the circuit had to be specially designed for satellite use. Even where components were available with the required electrical performance, it proved necessary to seek reduced power consumption and to meet unusually stringent size and weight restrictions.

The circuit has given an exceptionally good performance. None of the complete assemblies that have been made have shown any significant variations of operating levels over the course of six months. Although no failure in this part of the satellite is expected, in many parts of the circuit sufficient margin has been built into the circuit that in the event of such a failure the circuit will continue to operate with reduced performance.

---

* Measurements made of the system noise spectrum using narrow-band analyzers indicate a satellite noise figure in the flat region of 15 db ±2 db. If the noise spectrum around the carrier is integrated over a 20-mc band, then an equivalent noise figure of 16.5 ±2 db is obtained.

VI. ACKNOWLEDGMENTS

The circuits described in this paper represents the combined efforts of so many key personnel that a complete listing is not practical. The work was done under the direction of R. H. Shennum, who suggested the use of the reflex circuit and most of the circuit arrangement.

REFERENCES

1. Bangert, J. T., Englebrecht, R. S., Harkless, E. T., and Sperry, R. V., The Spacecraft Antennas, B.S.T.J., this issue, p. 869.
2. Langford, F., Editor, *Radiotron Designer's Handbook*, Wireless Press, Sidney, Australia, pp. 1140–1146.
3. Hutchison, P. T., and Swift, R. A., Results of *Telstar* Satellite Space Experiments, B.S.T.J., this issue, Part 2.
4. Ballentine, W. E., Saari, V. R., and Witt, F. J., The Solid-State Receiver in the TL Radio System, B.S.T.J., **41**, November, 1962, pp. 1831–1863.
5. Ballentine, W. E., and Blecher, F. H., Broadband Transistor Video Amplifiers, Solid-State Circuits Conf., February, 1959, Digest, pp. 42–43.
6. Saari, W. R., Kirkpatrick, R. J., Bittmann, C. A., and Davis, R. E., Circuit Applications of a Coaxially Encapsulated Microwave Transistor, Solid-State Circuits Conf., February 1960, Digest, pp. 64–65.
7. Riblet, H., The Short-Slot Hybrid Junction, Proc. I.R.E., **40**, February, 1952, pp. 180–84.
8. Bodmer, M. G., Laico, J. P., Olsen, E. G., and Ross, A. T., The Spacecraft Traveling-Wave Tube, B.S.T.J., this issue, Part 3.
9. Anders, J. V., Higgins, E. F., Murray, J. L., and Schaefer, F. J., Jr., The Precision Tracker, B.S.T.J., this issue, Part 2.
10. Varnerin, L. J., Jr., Comstock, R. L., Dean, W. A., and Kordos, R. W., The Satellite Ferrimagnetic Power Limiter, B.S.T.J., this issue, Part 3.

Page intentionally left blank

The Spacecraft Antennas

By J. T. BANGERT, R. S. ENGELBRECHT, E. T. HARKLESS, R. V. SPERRY and E. J. WALSH

(Manuscript received February 13, 1963)

The spacecraft employs two microwave antennas for communications and a single VHF antenna for telemetry, beacon, and command functions. One microwave antenna centered at 6 gc is used to receive broadband signals from a ground transmitter while the other microwave antenna centered at 4 gc is used to transmit signals to a ground receiver. Each microwave antenna is composed of a large number of circularly polarized radiating elements equally spaced around the equator of the spacecraft and connected to the electronic receiver and transmitter by a complex precision feed system. The VHF antenna is a small multi-element helix mounted at the pole of the spacecraft and radiates a linearly polarized signal. All antennas provide nearly isotropic antenna patterns with the axis of symmetry corresponding to the spin axis of the spacecraft. The antenna systems were constructed of light, but rugged, materials and passed extensive electrical, mechanical, and thermal tests.

I. INTRODUCTION

The function of the spacecraft antennas is to receive and transmit two distinct classes of signals: broadband microwave frequencies for communication service, such as television; and narrow-band VHF for beacon, command, and telemetry.

The requirements on these antennas resulted from a thorough systems analysis which led to an intricate balance of many factors involving not only the spacecraft, but the ground station as well.

These factors include such vital questions as: the modulation method, the location of frequencies, the choice of polarizations, the degree of attitude stabilization, etc., and are discussed in companion papers.[1,2,3]

1.1 *Requirements*

One of the most important and difficult objectives was to make the patterns provided by both the microwave and VHF antennas as nearly

isotropic as possible. This is necessary because the spacecraft is spin stabilized; consequently the received and transmitted signal amplitudes will fluctuate by an amount depending on the anisotropy of the antenna pattern. In addition, the microwave antenna must receive right circularly polarized FM signals centered at 6390 mc and transmit left circularly polarized FM signals centered at 4170 plus a beacon signal at 4080 mc. The wide frequency separation and the opposite sense of circular polarization for the 4- and 6-gc signals suggests two microwave antennas. A single VHF antenna is used to receive command signals at 123 mc and to transmit a 136-mc beacon which can be amplitude modulated with telemetry information.

In a realistic allocation of the extremely valuable space in the spacecraft, the microwave antennas were assigned a band around the equator. This band had an outside diameter of 34.5 inches, a height of 6 inches, and a depth of 3 inches. In addition, a few extra cubic inches were available in the interior for the needed feed system. It was decided to mount the VHF antenna projecting outward from the top of the spin axis. All three antennas are shown in Fig. 1. The satellite maximum mass was

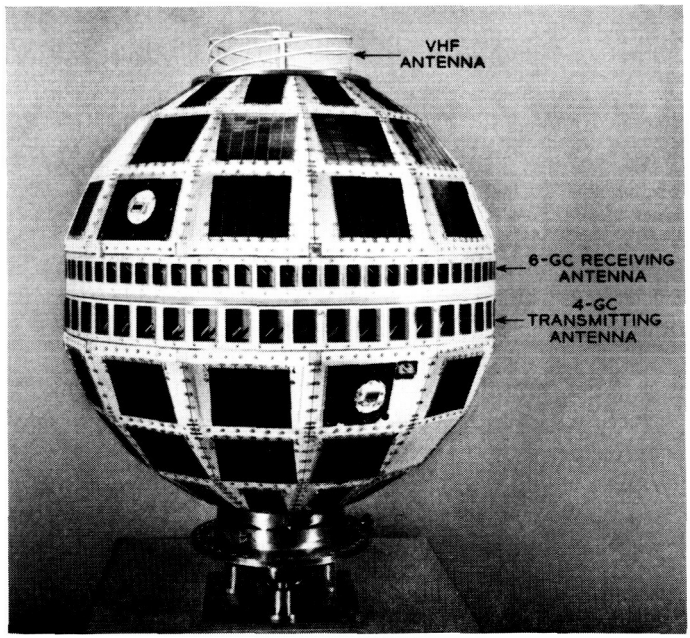

Fig. 1 — Spacecraft, showing microwave antennas and VHF antenna.

determined by the launch vehicle capabilities. The guiding design rule was that every item in the satellite was to be as light as possible. About 7 pounds was allotted to the complete antenna system. The completed satellite also had to be balanced and have a moment of inertia with respect to its spin axis such that there would be no tumbling effect while in orbit.

In addition to fulfilling the system's electrical performance requirements, the construction of the antennas had to be such that they would withstand the induced vibrational stresses of the launching and then continue at the desired level of performance in the high vacuum and extreme temperature variations of outer space. Furthermore, the antennas had to be able to withstand the high-energy nuclear particles as well as the low-energy microscopic particles found in space.

One of the most serious constraints affecting the antenna design was the necessity of building a full-scale electrical model in a total of twenty working days. It is clear that under such time pressure there was no opportunity to explore elegant proposals or to debate several alternatives. Only the most straightforward approach offering the highest probability of success could be pursued. An essential factor in the development was reliability. When reliability and urgency are both needed, new and unproven methods and materials are used only as a last resort. All materials and techniques, where possible, were proven ones. Those which were new were life tested within the limits allowed by the program's rapid pace.

A minor complication was the added requirement that the top and bottom hemispheres of Telstar be dc isolated from each other in order to reduce the eddy current damping of the spin energy. A continuous strip of insulated conductor was provided on the edge of the 4-gc radiator band to provide a bypass capacitor. Spring fingers on the 6-gc band provided continuous contact to one terminal of this RF bypass capacitor. A further complication was the need for the VHF antenna to operate during the launching operations.

Since the microwave antennas and the VHF antenna are distinct and independent systems, each will be described in separate sections of this paper.

II. MICROWAVE ANTENNA SYSTEM

The two microwave antenna systems shown schematically in Fig. 2 are each composed of an array of discrete radiating elements and a complex power distribution system to supply each element. The power distribution system consists of both resistive and reactive power dividers

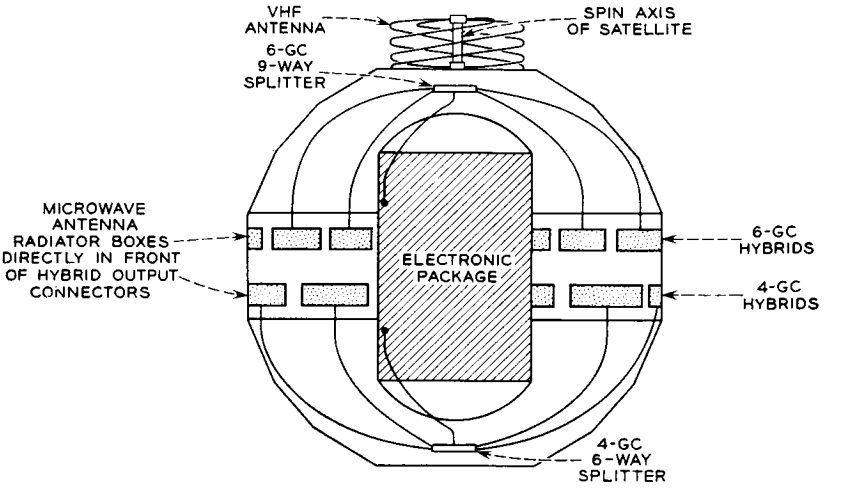

Fig. 2 — Schematic and physical arrangement of antennas in spacecraft.

and semiflexible coaxial cables. The various components of the microwave antenna systems will be described after a brief review of the basic theory underlying this approach.

2.1 *Basic Approach*

D. S. Bugnolo[4] has calculated the surface currents and radiation pattern for a large sphere excited by a great-circle slit. His analysis showed that good axial ratio and nearly isotropic radiation could be maintained to within about 20 degrees of the poles for both the 4-gc and 6-gc frequency bands on a 34.5-inch sphere. A straightforward method for exciting such a slit is by means of a radial disk line fed at the center of the sphere. Unfortunately this feed is impractical for a number of reasons. Bisecting the structures raises severe problems in maintaining structural rigidity between the two halves of the satellite and also impedes the heat flow necessary to minimize thermal gradients within the satellite. Furthermore, the electronic package occupies most of the volume at the center of the spacecraft. Elimination of the continuous radial disk line then suggests the use of some form of discrete approximation such as a belt of individually fed apertures to excite the two halves of the sphere. A further study of the problem revealed that less than one-half db of ripple would be produced in the far field pattern if discrete sources on the great circle were spaced closer than 0.8 wave-

length. For short intervals of time the path between satellite and ground station will intercept a constant latitude on the satellite. In order to avoid amplitude fluctuations of the received signal, the constant latitude of viewing should result in a constant amplitude signal, or the spin axis of the satellite must coincide with the symmetry axis of the radiation patterns. This coincidence can be provided by placing the radiating elements in two closely spaced bands near the equator of the spacecraft, one for the 4-gc transmitter and one for the 6-gc receiver. The use of two bands considerably reduces the individual bandwidth requirements for each set of radiating elements and the associated feed systems.

The variation in field pattern produced by discrete radiating elements near the equator of a sphere is a function of the sphere diameter and the number of elements. After calculating the minimum number of elements needed and allowing some margin, it was decided to employ 72 elements for the 6-gc antenna and 48 for the 4-gc antenna.

Several reservations about the performance of this system using the entire surface of the spacecraft as the radiator remained with the designers until near the end of the development. In particular, no theory was available to predict the interaction between the closely spaced sets of radiating elements at 4 gc and 6 gc and the modification of the radiation pattern by the facets and the solar cells which covered much of the surface area.

2.2 *Radiating Elements*

2.2.1 *Requirements*

Each radiating element must launch a circularly polarized wave over the frequency band of interest and at the same time provide a good impedance match for the feed system.

In view of the great importance of the individual radiating elements to the over-all performance, three alternate designs were considered before concentrating on the most promising one. Only a brief mention will be made of the first two as possibilities for future study.

2.2.2 *Two Early Realizations*

One early design of radiating element consisted of a circular opening on the satellite surface with a circular waveguide recessed into the satellite and fed by a probe from a coaxial line. Between the probe and aperture were two screws forming a quarter-wave plate. This structure worked very well over a wide band so long as sufficient space was pro-

vided between the coaxial probe and the screws forming the quarter-wave plate. Unfortunately, there was not sufficient room in the satellite to allow the circular waveguide to project into the satellite sphere as far as was necessary. When the structure was shortened, the coaxial probe and the quarter-wave plate coupled directly to each other's local fields and strongly interacted with each other. The network could still be tuned to produce circular polarization, but the bandwidth was very small (about 5 mc for a return loss exceeding 20 db).

Another early design proposed the use of a square aperture and waveguide which was excited by two probes, each fed by a coaxial line. By placing an extra 90° phase shift in one of the coaxial lines, circular polarization would be achieved. A serious disadvantage of this structure was the need for twice as many output ports on the power divider and twice as many coaxial connectors as well as provision for the additional 90° phase shift.

2.2.3 *Final Realization*

The final design shown in Fig. 3 employed a rectangular waveguide and aperture with dimensions large enough to propagate two cross-polarized modes (TE_{10} and TE_{01}). Since the two modes have different phase velocities, the length of rectangular waveguide could be adjusted to produce a 90° phase differential between the two polarizations, resulting in circularly polarized fields at the radiating aperture. A single probe was used to feed this structure, and because of space limitations it was decided to introduce the probe from the back wall of the radiating

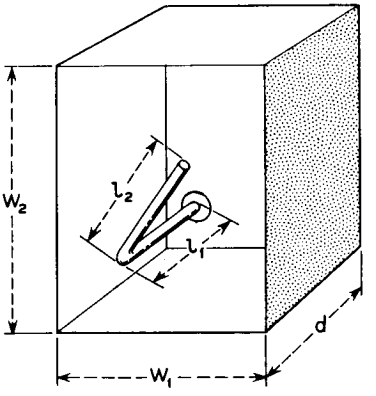

Fig. 3 — Radiating element for microwave antenna.

box. In order to obtain the 90° differential phase shift in as short a length as possible, one cross-sectional dimension of the box was chosen close to cutoff. The lowest frequency utilized in the 4-gc band is 4080 mc. The minimum dimension for propagation of this frequency in empty guide is 1.446 inches, so the narrow dimension was chosen to be 1.500 inches. The other cross-sectional dimension must be somewhat larger to provide a larger propagation constant, but not so large that the radiation patterns for the two polarizations are markedly different. A dimension of 2.100 inches was somewhat arbitrarily selected here. At band center of 4137 mc the two propagation constants are 0.658 radian per inch and 1.613 radians per inch. Therefore, in order to obtain a differential phase shift of $\pi/2$ radians, a path length of 1.65 inches is needed. Since the probe radiates in both directions in the box, some energy goes directly to the apertures and the rest is reflected from the back wall before reaching the aperture. Since there are also reflections from the radiating aperture, the effective path length is rather complex. The depth of the box was experimentally adjusted to 1.490 inches, which gave the best circular polarization for the radiated energy. The optimum axial ratio of the radiated energy is also dependent on the angle of the probe, which is close to 45 degrees.

After obtaining circularly polarized radiation, the remaining problem is to obtain a matched input impedance for the coaxial line. A 50-ohm dielectric bead support for the probe was designed and the two length dimensions of the probe, l_1 and l_2 in Fig. 3, were varied to obtain 50 ohms looking into the coaxial connector at the back of the box. The various adjustments for circularly polarized radiation and good impedance match interact with each other, so that considerable experimentation was found necessary to settle on dimensions which provided the necessary broadband performance. The 4-gc and 6-gc box dimensions are simply scaled in inverse frequency ratio.

Despite early recognition that the radiators would ultimately be magnesium extrusions for high strength-to-weight ratio and precision fabrication, the need for early demonstration of feasibility suggested the use of sheet metal techniques. The first radiating elements were made by cutting 15-mil brass sheet to the right size and shape and bending into the form of a rectangular box having four sides and a bottom, but no top. The adjoining edges were soldered to provide good electrical conductivity. The top edges were bent over at right angles to form lips which could be soldered to the cylindrical supporting midsection in which rectangular holes were punched. The first midsections were made in four parts to permit some tolerance in the associated

hemispheres. A hole was drilled in one corner of the bottom of the box to permit the insertion of a feed probe. The probe was supported by a coaxial connector soldered to the outside of the box bottom. The four quadrant radiator assemblies were fastened between a pair of smooth aluminum hemispheres to form a crude breadboard model. Although the tolerances which had been achieved in the dimensions of the radiators exceeded by several times the estimated allowable tolerances, the first radiation patterns were very encouraging in that they indicated the basic approach was sound, provided the physical structure could be fabricated to the necessary tolerances.

When final models were skillfully fabricated by Dow Metal Products of Bay City, Michigan, the radiating elements were formed as magnesium impact extrusions with a boss on the bottom which was drilled and threaded to serve as the shell of a coaxial connector. Despite the elaborate precautions taken during fabrication to hold the critical dimensions of the radiating elements, small departures from design center values combined in a complicated fashion to cause nonuniform electrical behavior. This problem was solved by shipping test equipment to the factory and selecting satisfactory boxes by measuring return loss over the frequency band of interest. The boxes were then magnesium welded into a wheel-like frame as shown in Fig. 4. During the welding process the frame and boxes were held rigidly in alignment by an elaborate

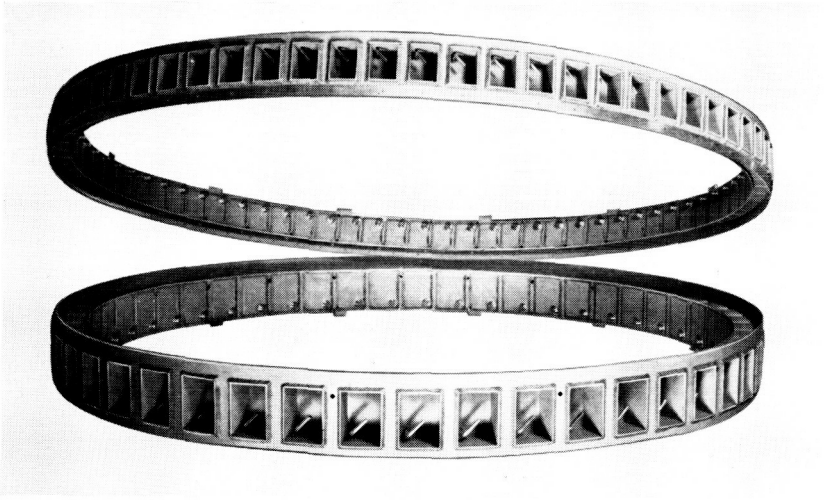

Fig. 4 — Microwave antenna radiating elements assembled into their frames before attachment to the spacecraft.

set of heavy steel jigs. The fixturing is such that when completed, the center of each connector lies within a few thousandths of an inch of a datum plane. The radiating probes were also accurately positioned by means of suitable fixtures before being clamped in place.

2.3 *Feed System of Microwave Antenna*

2.3.1 *Requirements*

Calculations showed that precise microwave distribution systems were required for funneling the 6-gc signals from the 72 receiving radiators to the single receiver within the satellite's electronics package, and similarly for fanning out the amplified 4-gc signals from the satellite's traveling-wave tube to the 48 transmitting apertures. The tolerable variations accumulated within the distributions systems must be restricted to about 15° peak-to-peak and 1 db peak-to-peak, of which no more than 5° and 0.5 db should be systematic.

2.3.2 *Single-Stage Reactive Distribution*

Initially, purely reactive single-stage distribution systems were investigated. These consisted simply of a 48-way power divider for the 4-gc band and a 72-way power divider for the 6-gc band. Each divider was arranged on a circular printed circuit board with a central input connector and the required number of output connectors around the periphery. Early measurements indicated that prohibitive manufacturing tolerances were required, not only for the power dividers themselves, but also for the connecting cables and radiators to keep the phase and amplitude variations within acceptable limits.

2.3.3 *Multistage Reactive and Resistive Distribution*

For the above reason, attention was directed toward multistage distribution systems using suitable resistive type power dividers which would provide isolation between output ports. The so-called resistive dividers are tree-like arrays of lossless hybrids, each with an internal terminating resistance. Furthermore, with this approach more flexibility was possible in the location and weight distribution of the various feed system components within the satellite.

Considering electrical performance alone, the arrangement chosen is one of many alternatives, some of which are undoubtedly better suited for precise microwave power distribution. The choice made resulted from consideration of available space between the radiating elements

and frame structure of the satellite, as well as from such constraints as minimum weight, minimum cross-section (to facilitate free internal heat exchange by radiation between the satellite hemispheres), maximum moment of inertia about the satellite's spin axis (in order to avoid tumbling), etc. The final 4-gc and 6-gc distribution systems chosen are illustrated schematically in Fig. 5. An assembled 72-way power divider for the 6-gc band is shown in Fig. 6. The reactive divider shown at the center is connected by coaxial cables to the nine resistive dividers mounted behind the radiating apertures.

2.3.4 *Reactive Power Dividers*

Centrally located in the 4-gc and 6-gc systems are a 6-way and 9-way reactive power splitter, respectively, connected to 50-ohm input and output cables. These dividers were produced on small circular printed circuit boards, with the input connector centrally located and the 6 or 9 outputs evenly spaced around the periphery as shown by Fig. 7. To maintain 50-ohm impedance levels on both the input and output cables, appropriate $\lambda/4$ transforming sections are incorporated in each of the 6 or 9 output lines near their common junction point. In addition, matching sections are built into the input connector of both the 4-gc

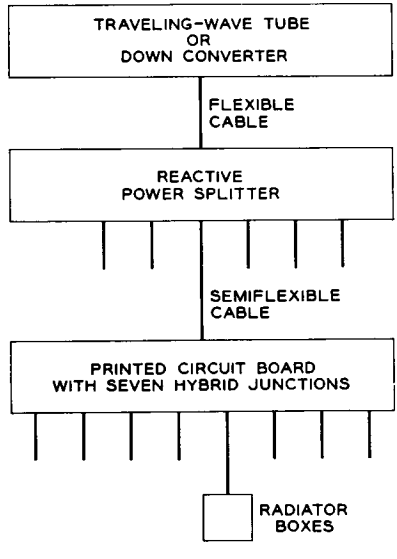

Fig. 5 — Block diagram of microwave antenna feed system.

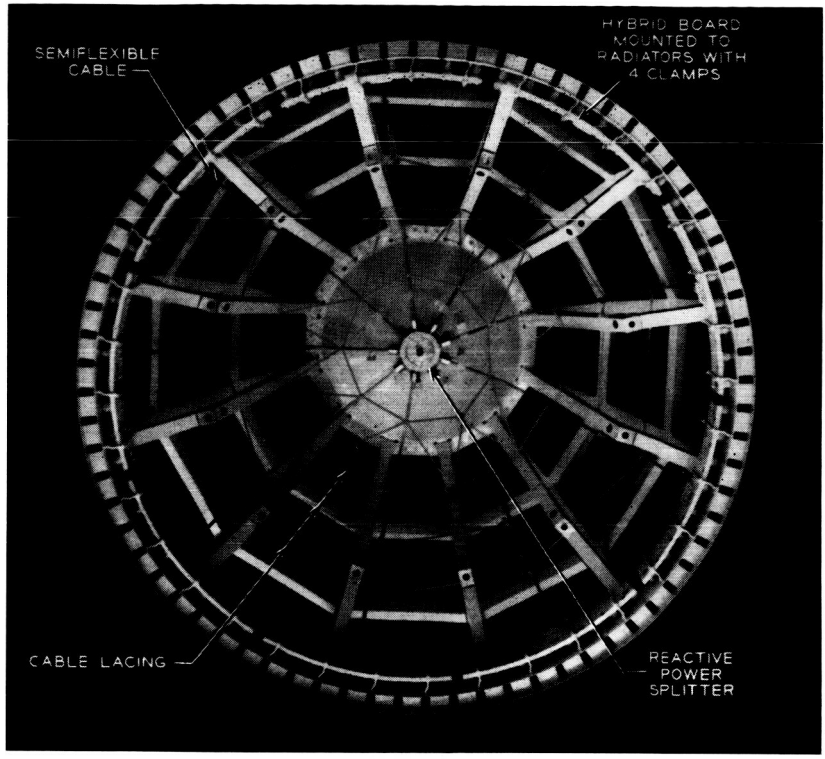

Fig. 6 — View of 6-gc antenna and feed system installed in spacecraft frame.

and 6-gc splitters to provide final over-all tuning of the complete antenna system.

2.3.5 *Resistive Power Dividers (Hybrids)*

Each hybrid board constitutes a resistive 8-way power divider. These hybrid boards are located around the satellite's equator and are curved so as to attach directly to the radiating apertures through special coaxial connectors. In this manner, each hybrid board is rigidly fastened to 8 transmitting or receiving apertures.

The configuration shown in Fig. 8 was chosen for the hybrids, which provides equal power split between ports 2 and 3 independent of frequency. Port 4 is terminated internally by a series resistance of $2Z_0$ (in this case 100 ohms) to maintain isolation between ports 2 and 3.

Fig. 9 shows the center conductor layout for the 4-gc hybrid board,

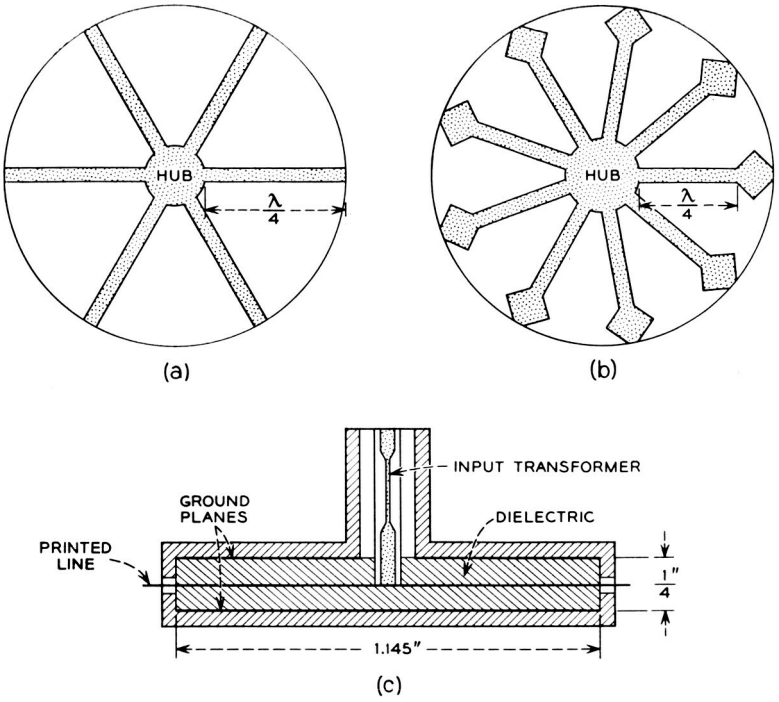

Fig. 7 — Reactive power splitter configuration: (a) 4-gc printed line; (b) 6-gc printed line; (c) cross-section showing input transformer.

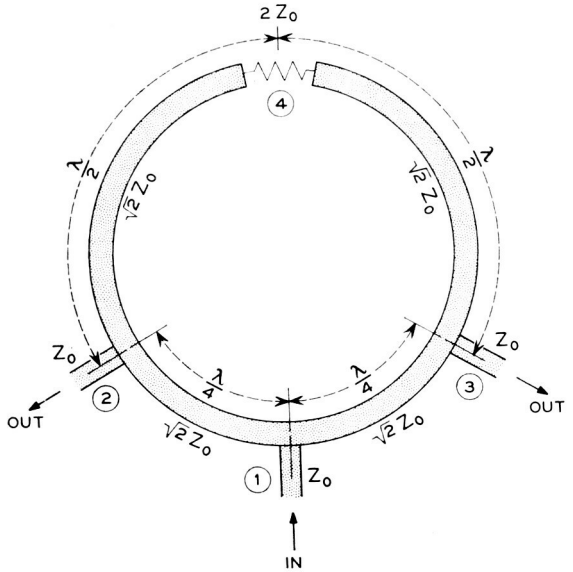

Fig. 8 — Transformed ring hybrid for frequency-independent symmetry.

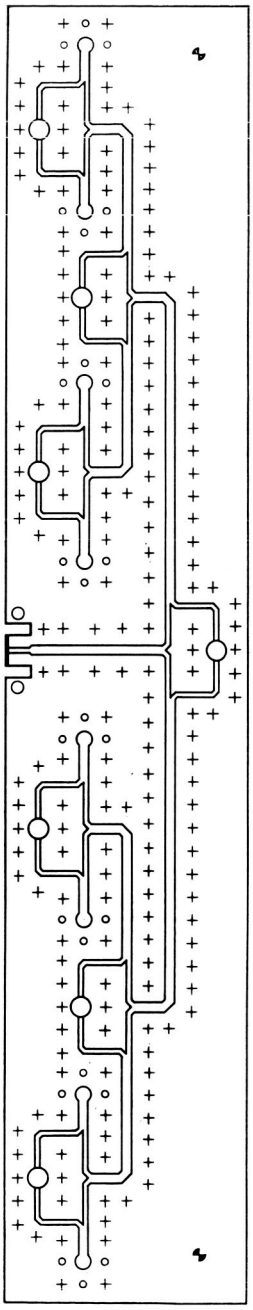

Fig. 9 — 4-ge hybrid printed circuit board.

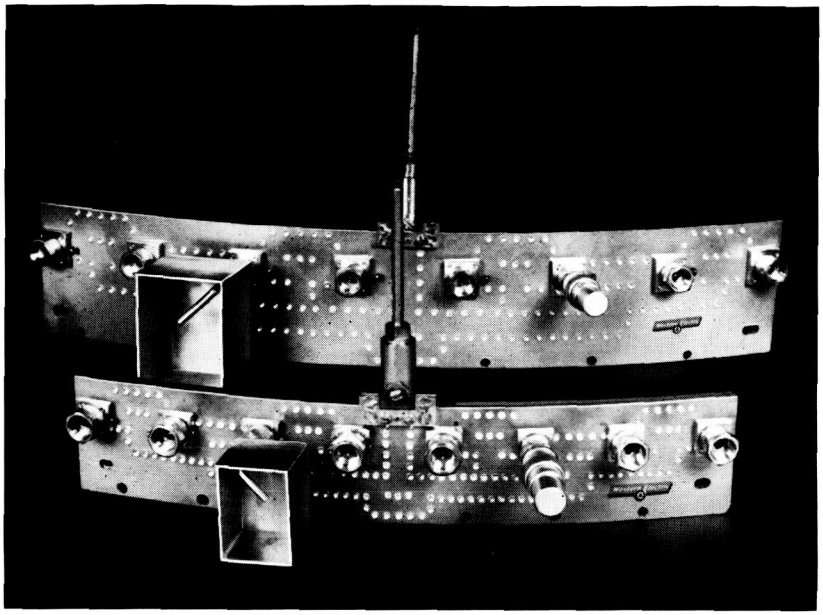

Fig. 10 — 4-gc and 6-gc resistive power dividers.

providing an 8-fold power division by cascading three hybrid stages from input to each output port. The dielectric material used is two sheets of 0.062-inch thick irradiated polyethylene ($\epsilon \approx 2.30$, $\tan \delta \approx 0.00005$). A 100-ohm miniature metal film resistor with flat ribbon leads fits into a circular recess in the dielectric boards and is soft-soldered to the adjoining center conductor to form port 4. Calculations show the absorption loss of the resistors to be $\approx$0.015 db per hybrid at 4 gc and $\approx$0.03 db at 6 gc. Thus, with the three cascaded hybrid stages in each board, the loss due to the 100-ohm resistors is approximately 0.05 db in the 4-gc boards and 0.1 db in the 6-gc boards.

Fig. 10 is a photograph of two assembled hybrid boards — one used at 4 gc and the other at 6 gc. A radiating box is attached to one output port of each hybrid and a short length of 0.160-inch coax is connected to the input ports.

Also noticeable on Fig. 10 are rows of rivets, each 0.090 inch in diameter, which serve both as mechanical fasteners and as electrical shorts around the center conductor, thus ensuring TEM wave propagation without measurable mode conversion. As a rule of thumb, these rivets must be spaced closer than $\lambda/4$ to provide effective shielding and must

be kept away from the center conductor edge by at least one dielectric thickness to prevent changes in characteristic impedance.

These hybrid distribution boards are an interesting use of extremely precise etched circuitry. Stability of performance and distribution of mass were two of the several factors that qualified them for use. The boards are curved riveted "sandwiches" consisting of four layers. The inner two are the dielectric with the etched circuit between them and with copper-clad surfaces adjacent to the outer two magnesium backing plates. All four are riveted together after the boards have been curved to approximately a 16-inch radius. Approximately 200 rivets are used in each board. The large number of rivets, dictated by electrical considerations, results in an extremely rugged and compact circuit board. The boards, 6 for the 4-gc and 9 for the 6-gc antennas, are immediately in back of, and are connected to, the radiating boxes by means of one coaxial connector per antenna box. Fig. 6 shows the hybrid boards as assembled behind the radiating elements. The control of both curvature and the position of the connectors was critical in order to insure proper mating with the radiator box stubs.

2.3.6 *Coaxial Cables*

A total of fifteen semiflexible 50-ohm coaxial cables connect the two central reactive power splitters located near the poles of the satellite to the associated resistive power splitters mounted behind the equatorial arrays of radiating elements. The coaxial is composed of a 43-mil copper wire encased in an irradiated polyethylene dielectric in the form of a helical winding with essentially zero space between turns. The sheath is a copper tube having a diameter of 160 mils and a wall thickness of 5 mils. These cables are sufficiently flexible to be bent so as to follow the contours of the satellite.

2.3.7 *Assembly of Radiating Elements and Feed*

The antenna bands and antenna feed were assembled to the satellite frame in such a manner as to prevent relative motion of the parts at their points of connection. The hybrid boards are rigidly clamped to the antenna bands through the use of four clamps per board, as shown in Fig. 6. The splitters are bolted directly to the frame at its poles and thus are rigidly held. Thus the relative motion that occurs between the hybrids and the splitters during the vibration of launch is accommodated by the bending of the semiflexible cables.

2.4 *Testing and Performance*

2.4.1 *Objectives*

In order to insure the best possible radiation pattern it was necessary to carry out an extensive program of electrical and mechanical tests on the individual components, various subassemblies, and the over-all system. The vital electrical objective is a good pattern, which is insured if microwave power generated or received in the electronics package is transmitted to or from each of the radiating elements with exactly the same phase and amplitude. These tests used a microwave bridge circuit incorporating a calibrated attenuator and phase shifter to measure the relative phase and amplitude between the output ports of the various components of the antennas as well as the over-all antenna assemblies. Phase and amplitude measurement accuracies of the bridge were approximately $\pm 2°$ and ± 0.1 db.

2.4.2 *Radiating Elements*

The radiating elements were checked for axial ratio and return loss over their operating bands. After brief experience with the fabrication of the radiating elements, it was apparent that realistic mechanical tolerances did not insure the necessary uniformity in electrical performance. A sensitive measure of the electrical performance of the individual boxes is the return loss. Return loss measuring equipment (a reflectometer setup) was moved to the fabrication plant, and the boxes were individually tested after they had been welded into the support bands. By electrical tests at the factory it was possible to use boxes in which the mechanical variations combined in a favorable manner and to replace subpar boxes before the whole assembly was removed from the welding fixtures. Although the factory tests indicated the acceptability of the radiators in a qualitative way, it was necessary to make more precise quantitative measurements in the laboratory. Uniformity of transmission through the boxes was checked by exciting them one at a time and terminating the open end of the radiator in a special test fixture. This fixture consisted of a short open-ended rectangular tube of lossy plastic with lips to fit into the mouth of the radiating box and a receiving box mounted on the other end of the tube. With this arrangement, the relative loss and phase of the individual radiators could be compared. These measurements showed a peak-to-peak loss variation of about 0.5 db and a peak-to-peak phase variation of about 8 degrees.

2.4.3 *Reactive Power Dividers*

All the printed circuit reactive power splitters were checked for equality of power division over their operating band. The matching section incorporated at the input to the power splitter was custom designed to allow for individual variations among the reactive and resistive dividers, cables, and radiating elements. The peak-to-peak variation of insertion loss and phase shift taken over the output ports of each splitter is given in Table I.

2.4.4 *Resistive Power Dividers (Hybrids)*

All hybrids boards were given complete electrical testing. Fig. 11 shows the phase and amplitude distribution of all the ports provided by the 4-gc boards; similar results were obtained for the 6-gc boards. Briefly, the peak-to-peak deviations on phase are approximately 8° at 4 gc and 10° at 6 gc, and on amplitude 0.3 db at 4 gc and 0.4 db at 6 gc. In addition, a variation from board to board existed in phase and to a smaller extent in amplitude, which is attributable to lack of precision in the attachment of the input connectors. This phase variation between boards amounted to 10° to 20° and was compensated by corresponding changes in length of the connecting coaxial cable. Input and output VSWR's were measured on all hybrid boards by means of microwave reflectometers and — for more accuracy — on a slotted line. Fig. 12 shows the input and output VSWR's on representative boards. The input match is shown for: (a) radiating elements attached to the output ports and (b) TNC terminations on the output ports. With the TNC terminations, the input VSWR is seen to be less than 1.4 to 1 for about 10 per cent bandwidth. Over the same bandwidths, the output VSWR's are under 1.4 to 1 for the 6-gc boards and under 1.1 to 1 for the 4-gc boards.

2.4.5 *Combined Radiating Elements and Feed*

After individual components, including connecting cables had been measured, the antennas were assembled on the spacecraft framework.

TABLE I—REACTIVE POWER DIVIDERS

Model	Peak-to-Peak Insertion Loss, db	Peak-to-Peak Phase Shift, degrees
Best 4-gc	0.2	1.4
Worst 4-gc	0.4	3.6
Best 6-gc	0.2	4.4
Worst 6-gc	0.55	5.3

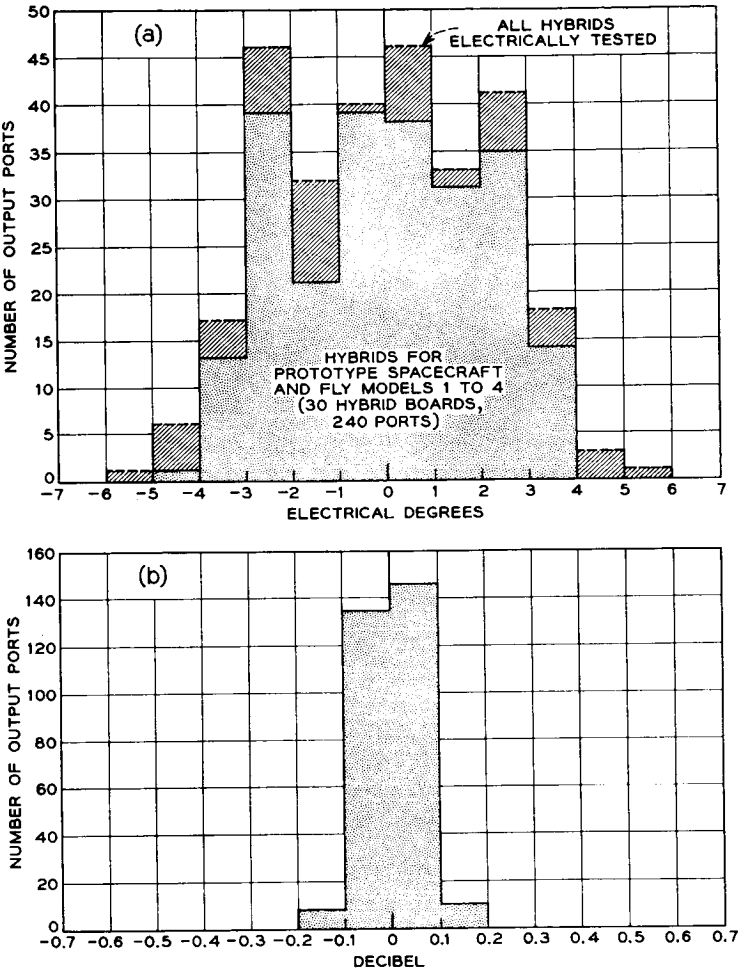

Fig. 11 — Distributions of measurements on the 4-gc hybrid boards: (a) phase distribution; (b) amplitude distribution.

A final check for uniformity of excitation was made of the complete assembly by comparing the phase and amplitude of the individual radiating elements. The test fixture for this purpose consisted of a band of absorbent material to fit around the satellite equator in which was embedded one of the previously described test fixtures for checking the individual radiators. By carefully selecting cable lengths, the average phase to each hybrid group could be accurately matched. This careful selection resulted in peak-to-peak variations as shown in Table II.

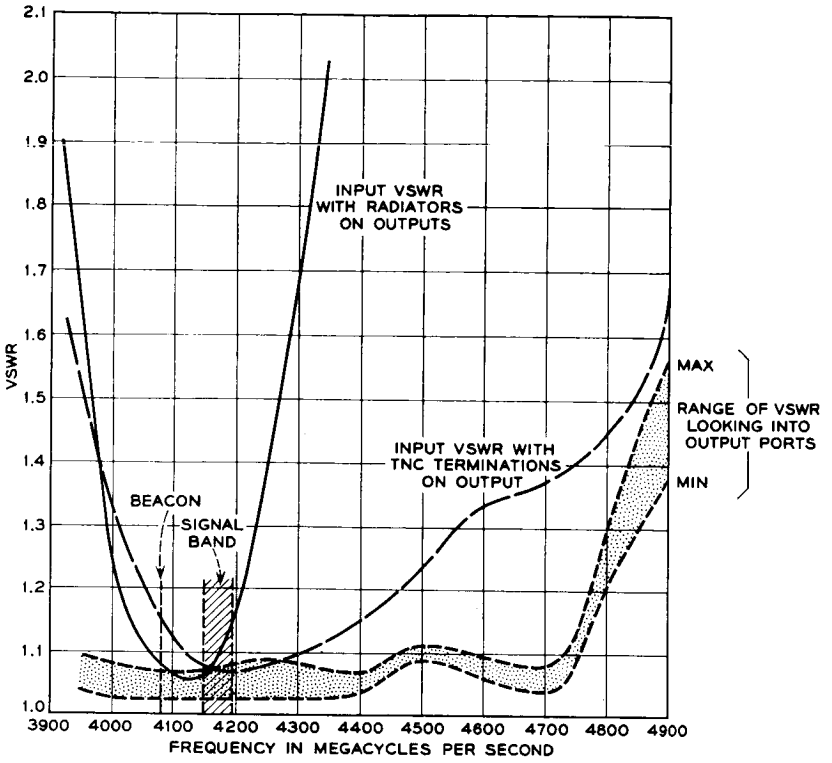

Fig. 12 — VSWR measurements on 4-gc hybrids.

2.4.6 *Over-all Patterns*

Most of the radiation patterns were obtained with an indoor anechoic chamber. These were checked later on an outdoor range with substantial agreement between results. Fig. 13 shows the results for the 6-gc receiving antenna system both for the equatorial and polar aspects. These patterns show the power relative to an isotropic circularly polarized antenna. The all-important equatorial pattern was especially gratifying, because it exhibited a peak-to-peak ripple of less than two db. The

TABLE II — RADIATING ELEMENTS AND FEED

Frequency, mc	Peak-to-Peak Insertion Loss, db	Peak-to-Peak Phase Shift, degrees
4170	1.1 db	10°
6390	1.4 db	14°

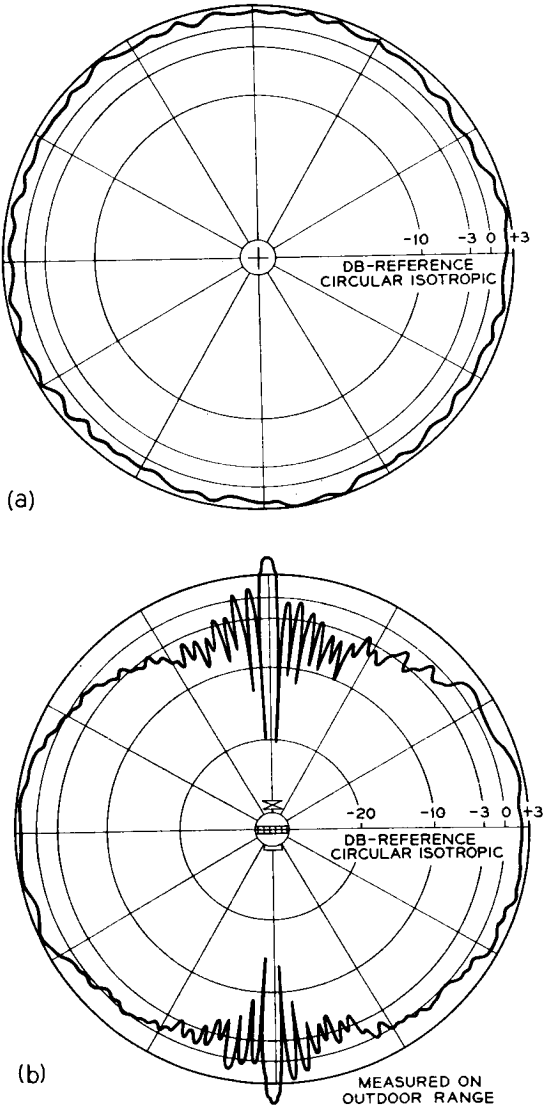

Fig. 13 — Antenna patterns at 6390 mc: (a) equatorial aspect; (b) polar aspect.

polar pattern is reasonably smooth except for the expected nulls near the poles. These patterns show the remarkably large solid angle of coverage provided by these antennas.

Fig. 14 presents the equatorial and polar aspects of the 4-gc transmitting antenna.

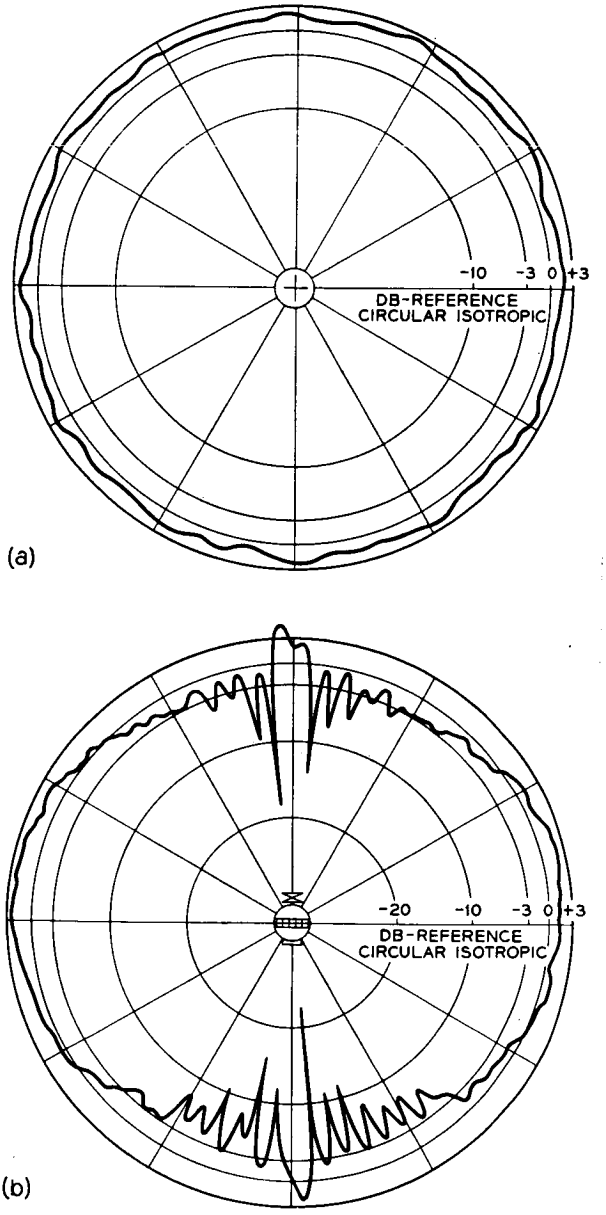

Fig. 14 — Antenna patterns at 4170 mc: (a) equatorial aspect; (b) polar aspect.

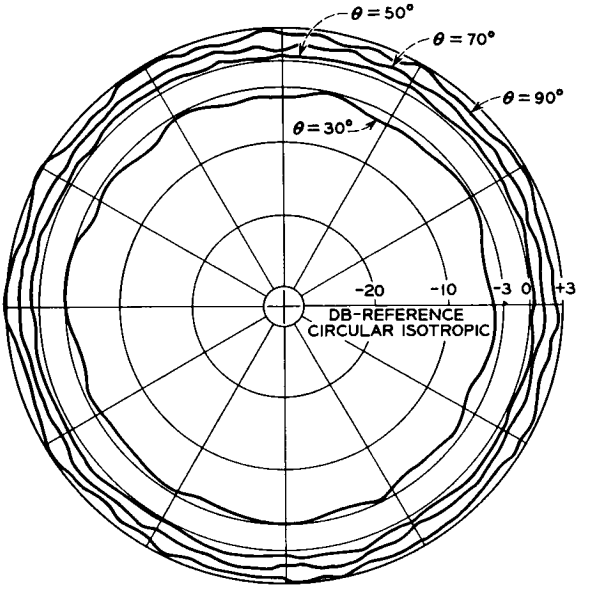

Fig. 15 — Constant-latitude antenna patterns at 4080 mc.

Fig. 15 shows measurements taken at different constant latitudes when measured in an indoor anechoic chamber. The satellite spin produces fluctuations in the received signal level corresponding to the ripples in these patterns. The curve marked $\theta = 90°$ corresponds to the equatorial aspect.

2.4.7 *Thermal and Vibration Considerations*

As pointed out in accompanying papers,[3,5] the spacecraft's spin-axis orientation should be perpendicular to the sun's rays for thermal reasons. The temperature of the antenna components is determined by the actual spin-axis orientation and the duration and frequency of eclipses of the satellite. Extrapolating the predicted skin temperature data in an accompanying article,[5] the temperatures noted in Table III are the ex-

TABLE III — PREDICTED TEMPERATURE EXTREMES

Component	Max. Possible Temp. Range (1 to 2 cycles)	Expected Temperature Range (2000 cycles)
Splitter	+34°C to −50°C	+20°C to −20°C
Hybrid	+10°C to −20°C	+10°C to −5°C
Cables	+40°C to −50°C	+20°C to −10°C

TABLE IV — TEMPERATURE CYCLING CAPABILITIES OF COMPONENTS

Splitter	+40°C to −100°C
Hybrid	+40°C to −100°C
Cables	+65°C to −100°C

tremes predicted, which could only occur once or twice during the satellite's two-year lifetime. In the same table, the temperature extremes are shown for the satellite when the spin axis is within ±30° of being normal to the sun. The range of temperature shown in both extremes includes the effects of full sunlit orbits and maximum eclipse conditions.

Extensive thermal tests were conducted on the hybrids, splitters and antenna cables to ensure that they were capable of withstanding the maximum possible temperature ranges listed above. Table IV is a summary of the temperature cycling capability of the components used in the spacecraft.

Because of the limited development time, extensive tests were not conducted at the more modest "expected temperature range." Based upon an analysis of the stresses which are built up under the extreme temperature cycling conditions and the number of cycles achieved in these tests, it can be confidently predicted that the antenna feed components are capable of withstanding the expected temperature limits for many thousands of cycles.

The thermal tests did disclose a number of weaknesses in the initial designs of the splitters and cables. Mechanical design changes based on these data eliminated the thermal cycling difficulties with the splitters. However, the cable difficulty was more fundamental. In the cable, relative motion occurred between the dielectric and both the inner and outer conductors as a result of temperature cycling. This resulted in a relative displacement of the three items after a few temperature cycles. Different materials and types of cables from a number of suppliers were tested, but all behaved in a similar manner. Through the cooperation of the Tellite Corporation of Orange, N. J., this serious problem was solved by incorporating a helical cut in the dielectric. The depth of the cut extended from the inner conductor to the outer conductor, so that the resulting configuration has a helical winding of dielectric with a small spacing between turns. This design accommodated the difference in expansion between the copper inner and outer conductors and dielectric material.

As a complete assembly the antenna structure was tested thermally in several ways. It was assembled into one of the thermal tester satellites and subjected to temperature cycling as encountered in the environ-

mental test chamber which included solar simulation. The temperature ranges under these conditions were equivalent to the expected temperature range for the high-temperature end, and equivalent to the extremes expected to be encountered for the low-temperature end. In addition, a laboratory test was conducted in which the antenna performance was checked while the poles of the satellite were being cooled down to the extreme low temperature with the antenna radiator section being kept at room temperature. This condition is more severe than that which could be encountered. The antenna satisfactorily passed all these tests.

Section 2.3.7 describes the attachment of the feed to the satellite. In view of the high acceleration levels to which the feed components are subjected and the complex nature of acceleration levels versus the frequency, the most realistic test for mechanical prove-in of the antenna feed structure is on an actual satellite. Hence, the antenna feed system as a whole was vibration tested only after it was assembled into a satellite frame. Accelerometers attached to various portions of the feed system showed a maximum reading at resonance of 260 g on one of the hybrids. Although subsequent electrical tests showed that the antenna systems were still usable, several mechanical weaknesses were uncovered. Further mechanical engineering changes in the mounting of the components eliminated the difficulties.

III. VHF ANTENNA SYSTEM

3.1 *Requirements*

The VHF antenna is used for beacon, telemetry, and command signals. This antenna should be nearly isotropic, have low dissipation loss and radiate circularly polarized waves. The size and position of the antenna is restricted in that it must not shade the solar cells. The VHF antenna is required to operate during the launching of the satellite as well as during orbit. This means that the antenna must radiate with substantially no change in pattern while the satellite is enclosed in the protective fairing and while mounted to the third stage of the rocket during the early phases of the launch. The dimensions of the fiber glass fairing placed upper limits on the height and diameter of the antenna in order to avoid interference during the severe vibration encountered during launch. The final dimensions of the antenna were chosen to make the antenna as large as possible within these restrictions.

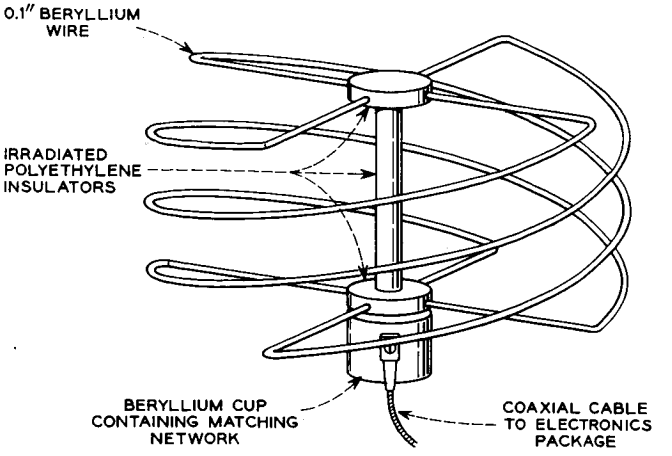

Fig. 16 — Sketch of VHF antenna.

3.2 *Initial Approach*

The decision to mount the communication antennas around the equator of the spacecraft eliminated that position for the VHF antenna. The requirement of nonshading of the solar cells eliminated the use of several sets of crossed dipoles located symmetrically about the satellite. It was therefore originally decided to use a small, multi-element, broadside helix mounted on an erectable mast. A sketch of this helix is given in Fig. 16. The antenna and mast would be collapsed during the launch, since the fairing dimensions would not allow the antenna to be extended, and upon injection into orbit an explosive charge would erect the mast and helix. During the launch a pair of auxiliary dipoles or whips mounted near the south pole of the satellite and fed by means of a directional coupler would maintain telemetry and command capability for the satellite. With this system, which was suggested by Wheeler Laboratories, Smithtown, N. Y., under Bell Laboratories contract, the helix radiated a circularly polarized wave with a pattern similar to that of a short dipole. This gives quite good coverage except near the poles of the satellite.

The helix may be thought of as an end-fed half-wave radiator coiled so as to look like a small loop antenna combined with a short dipole radiator. The loop field is in time quadrature and is at right angles to the dipole field. Circular polarization is obtained by adjusting the dimensions so that the magnitudes of the two field components are equal. The helix was designed by Wheeler Laboratories.[6] The antenna is a

small end-fed radiator with a high input impedance and its bandwidth is relatively small, in fact, considerably smaller than the 13-mc spread between the command and telemetry frequencies. Therefore, a matching network to avoid high standing wave loss was necessary. The dimensions were chosen such that the antenna was resonant at 129 mc, and the matching network provided a conjugate match as well as a transformation of impedance level at both frequencies. A circuit diagram of the matching network is given by Fig. 17.

Beryllium wire 0.1 inch in diameter was chosen to wind the helix because of its light weight and rigidity. A thin layer of gold was plated over the beryllium to reduce its dissipative loss. In order to provide the proper coefficient of emissivity to aid in the thermal balance of the spacecraft, the exterior portion of the antenna system was sprayed with an aluminum oxide coating by a plasma gun.

During the development a number of uncertainties arose to make an antenna on an erectable mast seem less and less desirable. The adverse effect on the moment of inertia was compounded, since the stringent requirements on the helix dimensions dictated elaborate jigs to insure these dimensions after the stress of launch and upon erection. The collapsed helix, while not a good radiator, did radiate enough to affect the patterns of the dipoles to an unpredictable extent if the vibration during launch caused the helix elements to intermittently touch one another. Also, the dipoles themselves affected the in-orbit pattern, not so much near the equator, but noticeably in the vicinity of both poles.

3.3 *Final Approach*

Because of these uncertainties it was decided to use the helix as a short vertically polarized dipole permanently mounted to the north pole of the satellite. Since the ground antenna used for the command and telemetry signals is circularly polarized, the problem of polarization

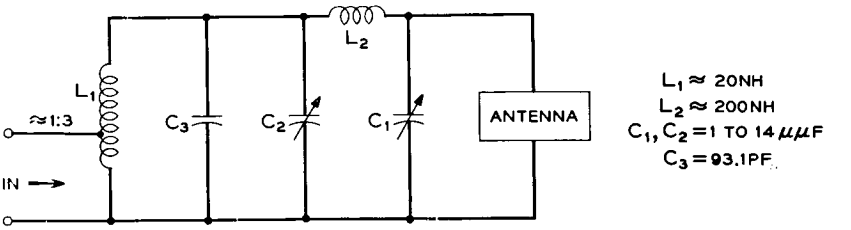

Fig. 17 — Schematic diagram of VHF antenna matching network.

tracking does not arise if the system can tolerate the additional 3-db loss. A careful study of the signal levels and path losses showed essentially no penalty for commandability and a small penalty for telemetry. Mounting the helix directly on top of the satellite resulted in the following advantages:

(a) Since the helix is not collapsed during launch, the whips and associated directional coupler can be eliminated.

(b) Since the helix is directly on the sphere, the additional cable length required for the erectable mast is eliminated. This results in a 0.5 db decrease in loss.

(c) The elimination of the mast erecting package results in an increase in reliability since the antenna would have been useless had the firing mechanism failed.

Since mounting the helix directly on top of the satellite destroys the balance between the loop and dipole radiation components, the dimensions were altered to insure that it would fit into the launch fairing, yet retain the same impedances. This alteration did not change the matching network and left the dipole component unaffected.

The matching network was adjusted while mounted on a model of the satellite. The model was mounted on the roof of the Hillside, N. J., laboratory, and final adjustments were made with the base of the helix and the network cup surrounded by dry ice; a thermocouple attached to the network cup indicated −75°C. Fig. 18 shows that the match at both frequencies is degraded as the temperature increases, but the

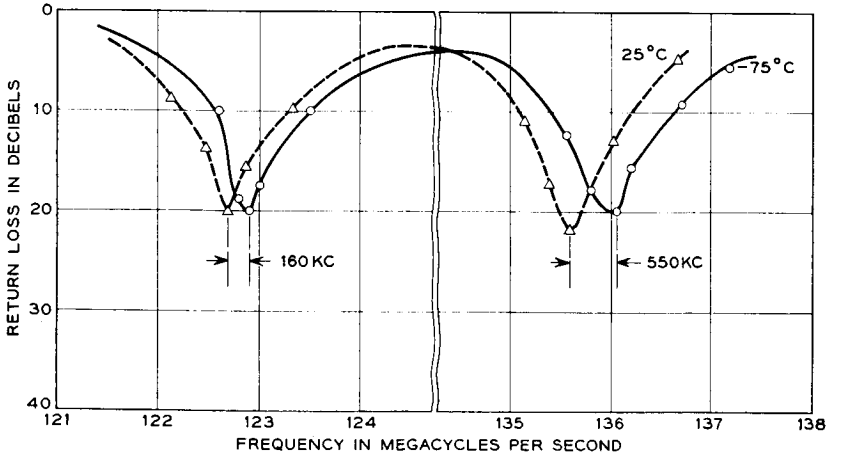

Fig. 18 — Return loss measurements of VHF antenna.

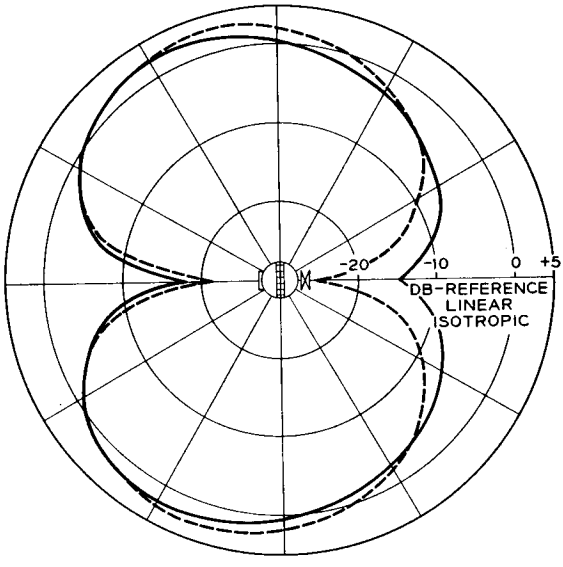

Fig. 19 — Polar aspect VHF antenna pattern at 123 mc: solid curve—measured pattern; dotted curve—calculated pattern.

antenna is still quite usable at +25°C, although, except at launch, it is never expected to be warmer than −50°C.

3.4 *Testing and Performance*

The radiation patterns of the antenna are perfectly uniform when viewed at a constant latitude and when the satellite is rotated about its spin axis. The pattern does vary as the satellite is rotated at right angles to the spin axis, as is shown by Fig. 19. This figure shows the radiation pattern at approximately 123 mc as well as a theoretical pattern assuming a lossless antenna. The differences in maximum gain points indicate a loss in the matching network and dissipation loss in the helix of 1.5 db at approximately 123 mc. The corresponding comparison at approximately 136 mc shows a loss of 2.5 db.

IV. CONCLUSION

Two high-performance, isotropic, circularly polarized, microwave antenna systems have been designed, constructed, and operated successfully in the environment of outer space. The radiation patterns demonstrate that by use of extremely precise techniques of magnesium

fabrication and printed wiring a spherical surface can be uniformly excited by as many as seventy-two discrete radiating elements.

In addition, reliable and efficient narrow-band radiation of VHF signals has been achieved by employing a multi-element helix with a matching network.

V. ACKNOWLEDGMENT

The authors wish to pay tribute to their many colleagues in Bell Telephone Laboratories and Western Electric who devoted their skill and energies far beyond the call of duty in making this development possible. Special mention should also be made of the wholehearted cooperation of many companies outside the Bell System.

REFERENCES

1. Dickieson, A. C., The *Telstar* Experiment, B.S.T.J., this issue, p. 739.
2. Hoth, D. F., O'Neill, E. F., and Welber, I., The *Telstar* Satellite System, B.S.T.J., this issue, p. 765.
3. Shennum, R. H., and Haury, P. T., A General Description of the *Telstar* Spacecraft, B.S.T.J., this issue, p. 801.
4. Bugnolo, D. S., A Quasi-Isotropic Antenna in the Microwave Spectrum, I.R.E. Trans. on Ant. and Prop., **AP-10,** No. 4, July, 1962.
5. Hrycak, P., Koontz, D. E., Maggs, C., Unger, B. A., Stafford, J. W., and Wittenberg, A. M., The Spacecraft Structure and Thermal Design Considerations, B.S.T.J., this issue, p. 973.
6. Wheeler, H. A., A Helical Antenna for Circular Polarization, Proc. I.R.E., **35,** December, 1947, p. 1484.

Page intentionally left blank

(Brookhaven Nat. Lab.)

The Spacecraft Radiation Experiments

By W. L. BROWN, T. M. BUCK, L. V. MEDFORD, E. W. THOMAS, H. K. GUMMEL, G. L MILLER† and F. M. SMITS† (Sandia Corp.)

(Manuscript received March 22, 1963)

10875

The radiation experiments on the Telstar spacecraft were designed to measure the electron and proton particle distributions in the region of space explored by the satellite orbit and to give information on the integral semiconductor radiation damage produced by these particles. A solar aspect experiment is included with the radiation experiments because of its direct importance to solar cell damage results. The design and the hardware for these experiments are described in the present paper. Results of the experiments are included in a companion paper in this issue.

AUTHOR

I. INTRODUCTION

The radiation experiments on the Telstar spacecraft were designed to measure the distribution in energy, position, and time of electrons and protons trapped in the earth's magnetic field in the Van Allen belts. Such particle distributions characterize the radiation environment of the satellite, and in addition help provide an understanding of the mechanisms that are responsible for injection of particles into the Van Allen belts and for loss of particles from the belts. The radiation experiments also measure directly the integral radiation damage effects on semiconductors. Only magnetically trapped particles are important for damage considerations on the satellite, and only they are being examined in the particle experiments. The direct effects of primary cosmic rays are negligible, as are also the effects of solar protons which stream into the earth's polar regions but do not reach the Telstar satellite's extremes in latitude. However, these two classes of particles are important because of the secondary neutrons they produce in the earth's atmosphere, which subsequently decay in the trapped particle region and contribute both protons and electrons to the Van Allen belts.

Although the radiation belts have been examined in a large number of

* Brookhaven National Laboratory, Upton, Long Island, N.Y.
† Sandia Corporation, Sandia Base, Albuquerque, New Mexico.

In its Telstar I, Vol. I June 1963
P 899-941 refs (See N64-10868 02-01)

experiments, the region of space traversed by the Telstar satellite has not previously been studied extensively. The satellite provides an unusually fine opportunity for quantitative observation of a large region that includes essentially the whole of the inner Van Allen belt as well as part of the high latitude "horns" of the outer belt. As it turned out, the satellite was to examine not only the natural particles in the radiation belts, as had been originally intended, but also particles artifically introduced into the belts by U. S. and Russian high-altitude nuclear explosions. These new particles were destined to play a major role in the radiation effects sustained by the satellite's electronic equipment.

The radiation experiments on the satellite are divided into those measuring radiation damage and those studying energetic particles. These will be discussed in detail in Sections III and IV, respectively. A solar aspect experiment which measures the orientation of the satellite with respect to the sun is also included as a part of the present paper, because it is essential to the radiation damage experiment on solar cells. It will be discussed in Section II.

II. SOLAR ASPECT

The attitude that the satellite presents to the sun is important for the performance of the solar cell power supply and for the temperature distribution of the satellite. The knowledge of this is also important for evaluation of the degradation of solar cells as a result of radiation damage, since changes in solar aspect affect the illumination of the cells whose output is being monitored. The satellite is spinning and, as a result, the satellite temperature and the average power from the solar power plant depend only on the angle α between the spin axis and the satellite-sun line, essentially the colatitude of the satellite-sun line with respect to the satellite. However, for a single solar cell or a group of cells which are parallel, the instantaneous output depends both on the colatitude of the satellite-sun line and its longitude φ with respect to the satellite. These two angles are determined in the solar aspect experiment.

The angles α and φ are determined by simultaneous measurement of the outputs of a group of six solar cells arranged as in Fig. 1. These cells have mutually perpendicular normals. In essence their directions are those of the faces of a cube. The three perpendicular axes defining the normals of the group could be located in any direction with respect to the spin axis of the satellite and still uniquely define the sun's position. For example, four cells could look out perpendicular to the spin axis and

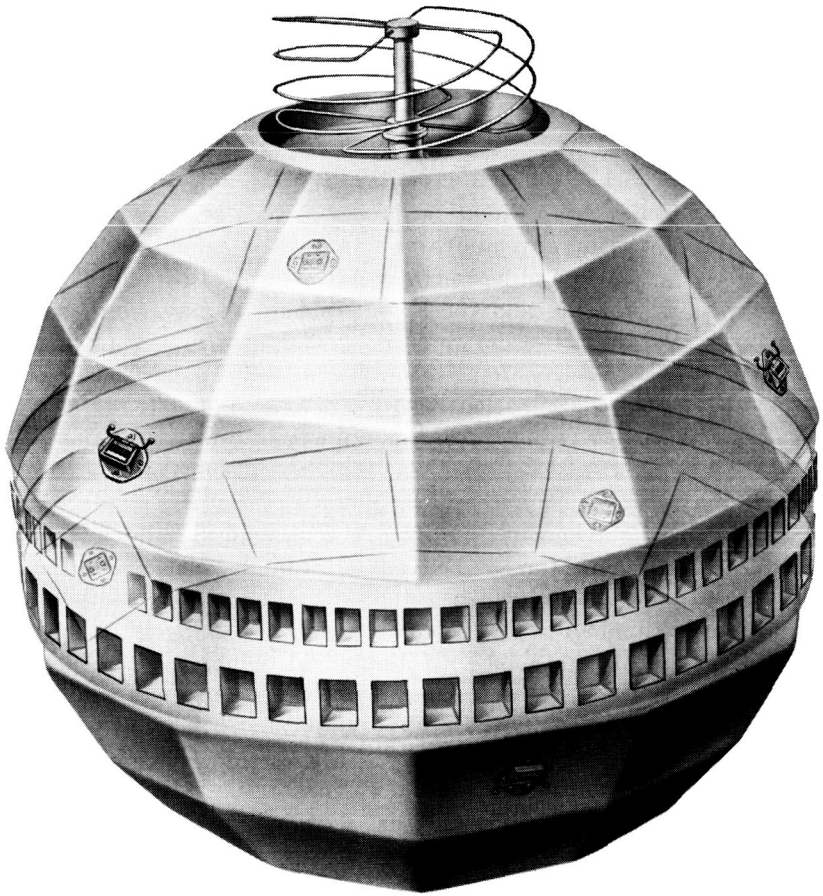

Fig. 1 — Placement of the solar aspect cells.

two in opposite directions along that axis. However, the arrangement of Fig. 1 has several advantages. The angle α is expected to be near 90 degrees, and reliable measurements near this angle are desired. With the cell positions of Fig. 1, one per cent measurements of the cell outputs define α and φ to one degree or better. Furthermore, as the instant of simultaneous measurement (determined by the telemetry frame rate) is not in general synchronous with the rotation rate of the satellite, the measurement of α depends in successive telemetry frames on different combinations of the six cells, so that failure or degradation of one is not disastrous.

The cells are mounted on the satellite facets nearest the antenna band to minimize the temperature extremes encountered as α departs from 90 degrees. The individual cells are of the same type (n-on-p) and are mounted with the same techniques used on the main solar power supply:[1] a ceramic base, platinum side strips and 30-mil sapphire covers. The cover width is much wider than a single cell, for uniformity in illumination and protection from radiation damage. Angle brackets orient the cell normals to 35 degrees above and below the satellite equator as required. With this mounting on the nearly spherical satellite surface, there are no shadowing and reflection problems of any consequence.

The six solar aspect cells were preirradiated with approximately 2×10^{16} 1-Mev electrons/cm^2 before mounting. This reduced their output under solar illumination by a factor of 2, but it reduced their sensitivity to further reduction in this number by radiation damage in space by a factor of at least 100.[1] The short-circuit current of each cell is measured as a voltage across a 2.75-ohm shunting resistor actually positioned in the telemetry interface circuitry inside the electronic canister. The currents for the six cells are sampled in a total of 600 microseconds, a time in which the satellite at its maximum rotation rate turns only by about one half of a degree. The timing is accurately known, so that an additional correction could be applied, but for this experiment the sampling is essentially instantaneous.

The telemetry examining the cell outputs has 100-millivolt full-scale sensitivity.[2] Changes in its gain are of relatively minor significance because the solar aspect angle really depends on ratios of the outputs of different cells. However, drifts in the amplifier zero would be quite serious. To provide a check on the zero, a seventh cell is placed inside the satellite skin and is covered with an opaque aluminum coating. To permit detection of zero drifts of either sign, a one-milliampere current is bled into the shunting resistor of this dark cell to offset its reading above zero by two telemetry bits.

The short-circuit current of an individual cell as a function of the angle of illumination with respect to its normal has been experimentally determined and is shown in Fig. 2. The shape does not depart substantially from a cosine law at small angles, but drops much more rapidly because of reflection losses toward grazing incidence. In addition to this calibration, interpretation of the telemetry readings to deduce the angle of illumination of a single cell involves temperature correction as illustrated by line A of Fig. 3. This is much larger than the temperature correction to the short-circuit current of nonirradiated cells, line B of the figure, because the recombination centers introduced by radia-

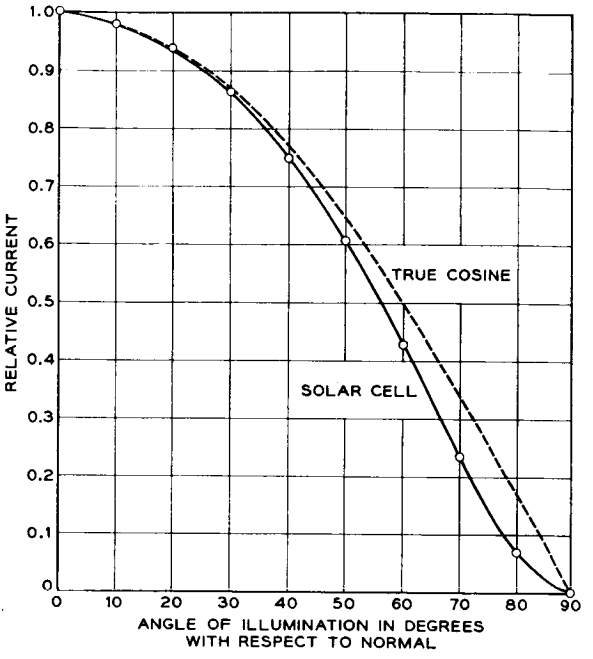

Fig. 2 — Solar cell short-circuit current vs angle of illumination.

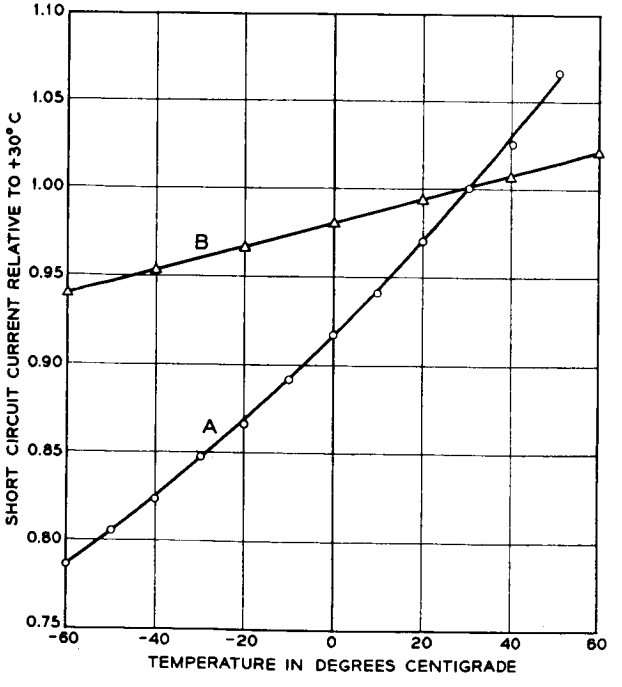

Fig. 3 — Temperature dependence of solar cell short-circuit current: (a) cell preirradiated with 2×10^{16} 1-Mev electrons/cm^2; (b) nonirradiated cell.

tion are quite different than those normally present. The operating temperatures in orbit range[3] from −30°C to +14°C, but measurements have usually been made between −10°C and +5°C.

Fig. 4 shows the anticipated output from the cells as a function of φ and for two values of α at 80 degrees and 90 degrees. In general, three cells are involved in the measurement, except at specific symmetry points where only two are illuminated, such as point A. The most critical measurement positions, those giving best definition to α and φ, are of type B, where three cells have substantial outputs and two are nearly alike. Such positions correspond to the sun being on the meridian of a cell in one hemisphere, and hence midway between the meridians of two cells on the other hemisphere. The ratio of the two nearly equal outputs to the one larger output is quite sensitive to α, and the ratio of the two nearly equal outputs to one another is very sensitive to φ. Because of the satellite rotation rate and its change with time, the sequence of one-minute measurements of the cell outputs will display a variety of patterns on different orbits of the satellite. Examples will be discussed

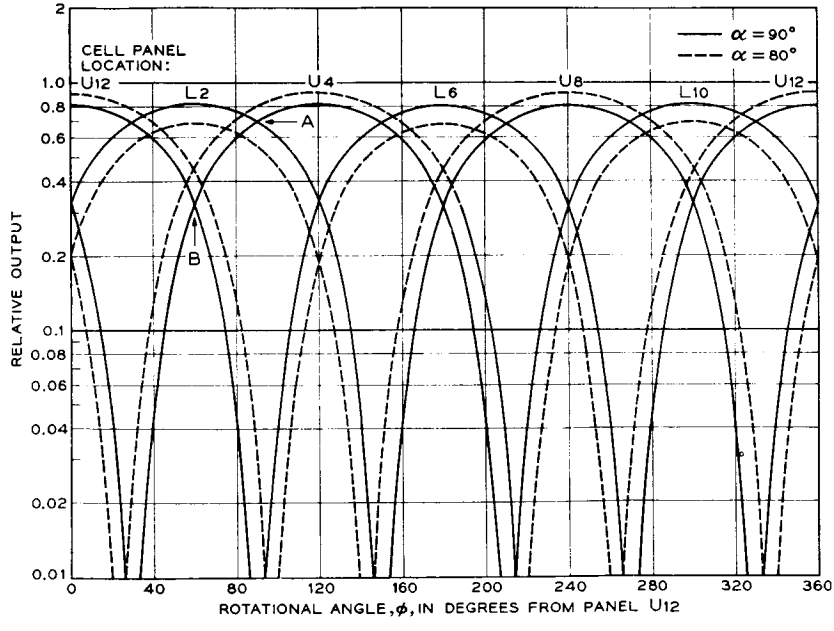

Fig. 4 — Anticipated dependence of the output of the solar aspect cells on the rotational angle of the sun with respect to the satellite for two different angles of the satellite spin axis with respect to the satellite-sun line.

in connection with the results of the radiation experiments in a separate paper.[4] The angle α can in general be determined from a single set of readings of the telemetry, but in practice many more points are used to avoid the possibility of error and to check on the reproducibility of the result obtained as different cells dominate in its determination.

III. RADIATION DAMAGE

3.1 *Solar Cells*

A solar cell damage experiment provides a direct measure of the degradation in short-circuit current due to radiation damage in three cells shielded by different thicknesses of sapphire. The cells are of the same type as the main solar power supply cells and the mounting is the same as for the solar aspect cells. It was not possible, using this mounting technique, to provide reliable attachment of thin covers, and hence the range in shielding thickness is narrower than would have been desirable. The cells are protected with 20, 25, and 30 mils of sapphire.

The group of three damage cells is mounted on the same facet of the satellite skin as one of the preirradiated solar aspect cells. This panel is shown in Fig. 5. The outputs of the damage cells are handled in the telemetry in the same way as those from the aspect cells, except that a 1.5-ohm resistor is used for a shunt because of the higher anticipated short-circuit current. The sampling time for the total of ten cells (six aspect, one zero-drift, three damage) is approximately 1100 microseconds.[2] The damage cells thus have the same illumination at the time of measurement as the solar aspect cell with the same orientation. With this arrangement, determination of changes in the unirradiated cells due to radiation damage can be made directly by comparison with that preirradiated aspect cell. The accuracy of the measurement depends markedly on the magnitude of all the outputs, but no correction for sun position is necessary in evaluating solar cell degradation. Furthermore, changes in illumination such as might arise from roughening of the sapphire surface by micrometeorites are not involved. Observation of the absolute current from the aspect cells measures this type of variation if it exists, although not distinct from changes in amplifier gain in the telemetry. Even if the aspect cell on the panel with the damage cell should fail, the redundancy of the determination of the solar aspect between remaining cells would make a continuing measure of damage possible without reliance on the absolute current. All of the cells in the aspect and damage parts of the experiment were measured with a spectral

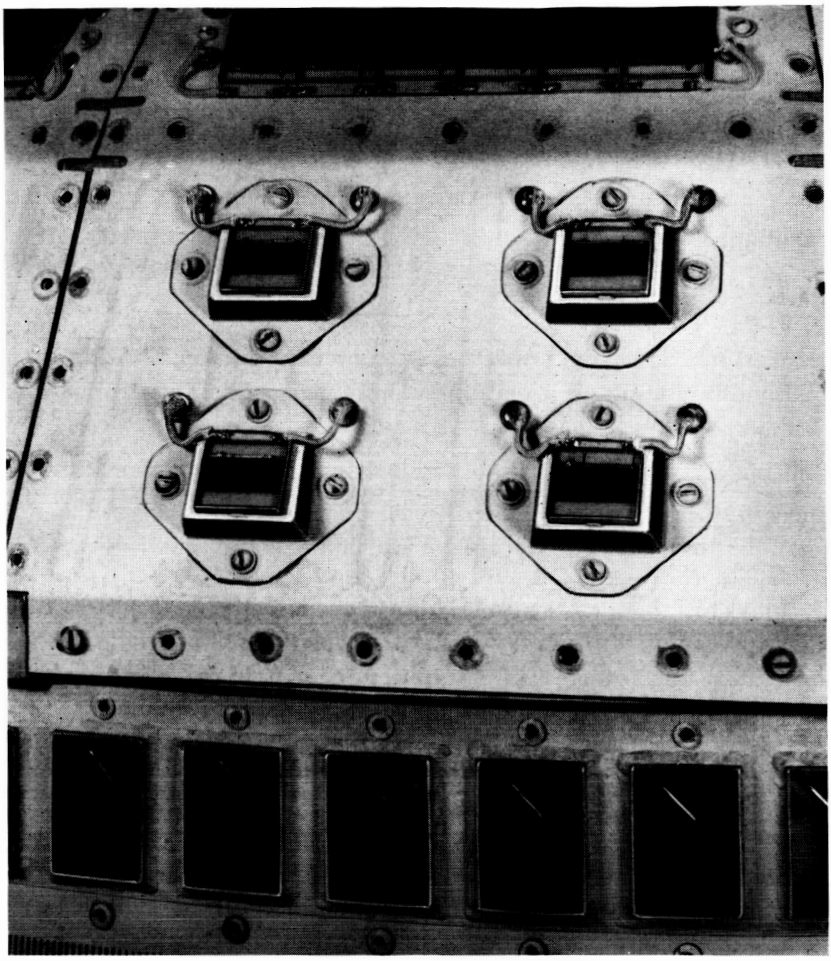

Fig. 5 — Radiation damage solar cell array. The lower right-hand cell is one of the six solar aspect cells.

analyzer developed by H. K. Gummel,[5] and predictions of their output under outer-space illumination were made. The shunt resistance choice was conservatively based on these measurements. For the damage cells the anticipated output was 52.5 milliamperes, the cells being similar within ±2 per cent. For the aspect cells, the predicted current was 23.5 milliamperes, with individual variations of less than ±3 per cent.

3.2 *Transistors*

To provide a direct measure of radiation damage in silicon independent of light, a group of npn diffused silicon transistors was specially fabricated. These devices provide a check on the solar cell results and permit extension of the study of shielding effectiveness to thinner shields. The degradation of solar cell performance under radiation results from a decrease in the lifetime of electrons (for n-on-p solar cells) in the p-type base material of the cell. This same property controls the α of transistors through the transport factor: the fraction of minority carriers introduced into the transistor base at the emitter which arrive at the collector junction. If lifetime is decreased by radiation damage, the light-created electrons (in the solar cell) and emitter-injected electrons (in the transistor) have increasing probability of recombination before they reach the solar cell junction or the transistor collector junction. Thus a direct comparison can be made between the results of one experiment and the other. As an experiment, the transistor has the advantage not only that the α measurement is independent of the sun, but also that the sensitivity to radiation damage can be made considerably greater by the use of a very wide base region.

The construction of the damage transistors is shown in Fig. 6. The device is made of the same kind of silicon used in solar cells (approximately one ohm-cm p-type) and the two junctions are made by solar cell junction diffusion techniques. These steps make a comparison of the results most direct. The transistor wafer is mounted on a pedestal close beneath the lid of the encapsulating Kovar can. For minimum shielding, the lid has been ground down to 3 mils from its normal 10-mil thickness. Through this thin lid the device sees particles over a 3.5-steradian solid angle.

The maximum sensitivity for damage measurement in transistors is limited by the maximum initial lifetime that can be maintained in the base region through device fabrication. The common-base current gain, α_{DC}, is related to the transport factor β across the base region as $\alpha_{DC} = \gamma\beta = I_c/I_e$, where γ is emitter efficiency, which we will assume to be independent of radiation damage. The lifetime τ of minority carriers in the base determines β in a device with base width W as

$$\beta = \operatorname{sech}\left(W/\sqrt{D\tau}\right) = \operatorname{sech}\left(W/L\right)$$

where D is a diffusion coefficient and L is the diffusion length for electrons in the p-type base. Radiation damage changes the lifetime[6] as

Fig. 6 — Construction of the radiation damage transistors.

$$1/\tau = 1/\tau_0 + K\Phi$$

where Φ is the integral flux of damaging particles and K depends on particle type and energy.

$$d\alpha/d\Phi = \gamma d\beta/d\Phi = -\frac{LK}{2D}\frac{W \sinh W/L}{\cosh^2 W/L}.$$

For small values of W/L, $d\alpha/d\Phi$ increases as W^2 for fixed L, the sensitivity to damage increasing with base width simply because the minority-carrier diffusion time increases and recombination processes become more evident. However, the expression has a maximum at $W \approx 1.5L$, corresponding to an α of about 0.43. Since τ_0 is limited by device processing, there is no advantage in increasing W beyond this point. In the damage transistors of the Telstar satellite, α is between 0.3 and 0.5 and the base width is on the order of 4 mils. As a result, the

devices have a low α cutoff frequency, about 100 kc. (Low-frequency cutoff and high damage sensitivity in transistors are almost invariably found together.[7] In examining components for potential susceptibility to damage, it is the low-frequency power devices that are of primary concern.)

The α_{DC} of the damage transistors is measured in the Telstar satellite in the circuit shown in Fig. 7. An approximately constant 0.5-milliampere dc emitter current is determined by the 8-volt zener diode and the 16.2-kilohm resistor in the emitter circuit. The extra diode in series with the zener partially compensates for change in the emitter current that would arise from the temperature dependence in the emitter junction. The collector current is read by the telemetry[2] as the voltage across the 16.2-kilohm collector resistor. With an α of 0.5, the output voltage has a maximum of approximately 4 volts. The output drops in proportion to α until it reaches the collector saturation current, specified in these devices to be less than 5 microamperes. This collector saturation current ultimately limits the minimum measurable α at two per cent of its initial value or less.

The relative change in α_{DC} in the transistors with radiation compared with the change in I_{SC} in solar cells is shown in Fig. 8. The initial rate of change of the transistor is somewhat greater, but even more striking is its continued high rate of change as the radiation proceeds. From the standpoint of a solar cell power supply, the decrease in the sensitivity to radiation with increasing damage is very helpful in providing extended life; but from an experimental standpoint, it makes evaluation of the damaging environment increasingly difficult.

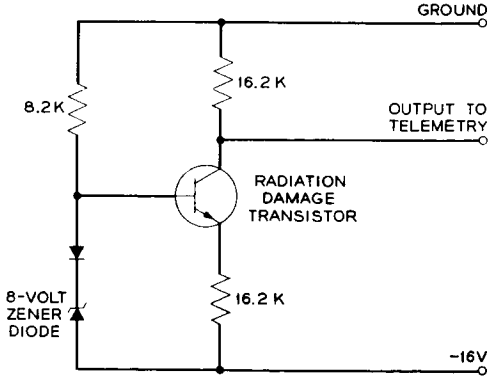

Fig. 7 — Radiation damage transistor circuit.

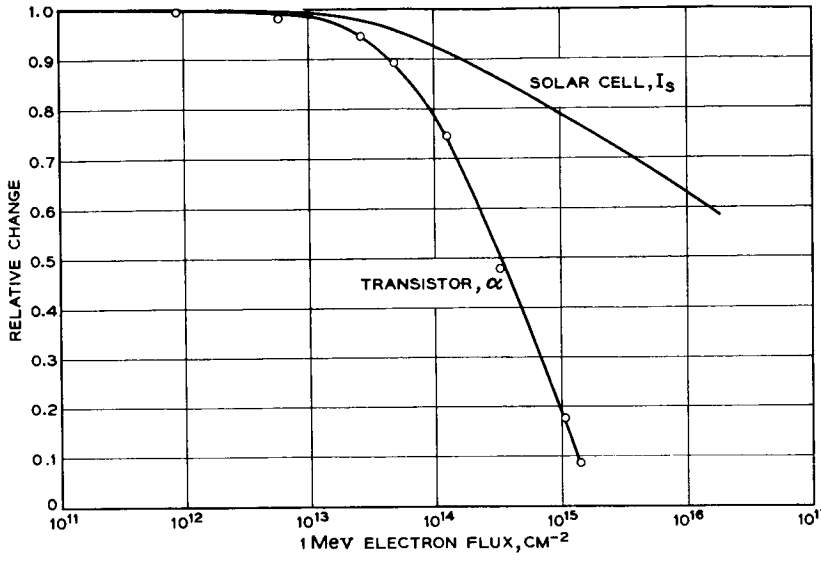

Fig. 8 — Comparison of radiation damage in solar cells and damage transistor.

Seven damage transistors are included in the transistor experiment, two each with three different shield thicknesses and a seventh which is heavily shielded and preirradiated to serve as a general check on the stability of the measurements. The devices and their associated circuits are assembled in a single package, shown in Fig. 9. This package (foamed and in a complete can) is mounted at a hole in the satellite skin, with its face almost flush with the surface of the satellite. The shield thickness of one of the pairs of devices, 35 mils of aluminum in addition to the 3-mil Kovar can, is comparable to the shielding of the main solar cell power supply, 30 mils of sapphire, and of one of the damage solar cells discussed in Section 3.1. The other two pairs have less shielding: 3-mil Kovar only and 3-mil Kovar plus 15 mils of aluminum.

IV. ENERGETIC PARTICLES

The Telstar satellite carries a group of four detectors designed to measure the spatial distribution and time variation of electrons and protons trapped in the earth's magnetic field and crude properties of their energy distribution. The satellite's orbit takes it through the most intense part of the inner Van Allen belt where protons of up to at least 500 Mev are known to exist[8] and where the proton flux increases with

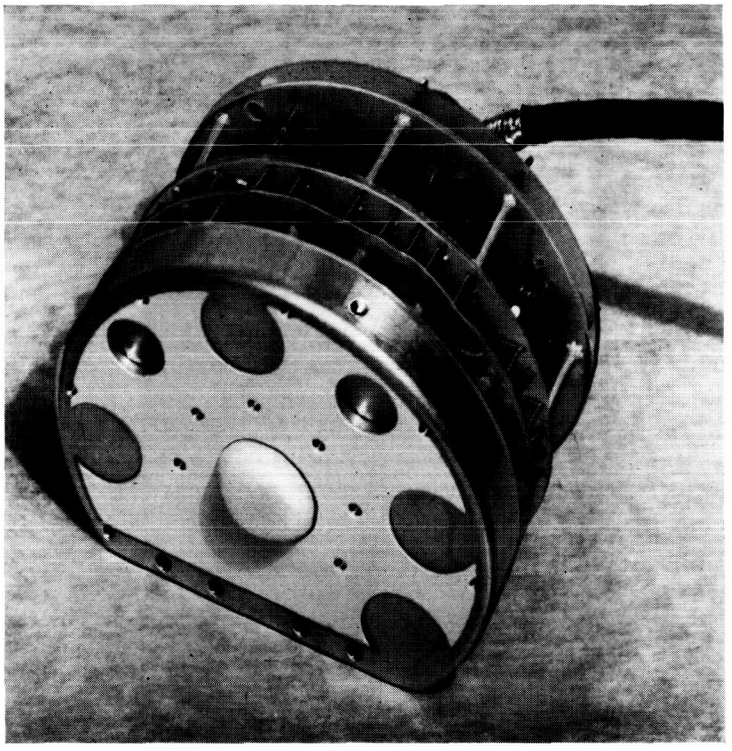

Fig. 9 — The radiation damage transistor assembly.

decreasing energy. The region also contains high fluxes of electrons whose intensity and energy distribution were poorly known. The orbit at high latitudes touches the horns of the outer Van Allen belt, which contains electrons and very low energy protons in concentrations that are highly variable as a result of solar activity.[9] One objective of the particle experiment is to establish a correspondence between the radiation damage in the solar cell power supply, the solar cells and transistors of the radiation experiment, and the distribution of particles responsible for the damage. Of even greater importance is the acquisition of data that will help provide a detailed understanding of the geophysical processes that produce and limit the radiation belts. Such an understanding is ultimately essential for assessing the radiation environment, not only in the Telstar satellite orbit but in other orbits of interest for communications satellite systems. In conceiving the experiments, no consideration was given to the possibility that effects of high-altitude

nuclear explosions might alter the belts in very significant ways,[10] although these artificial perturbations turned out to be of great importance. The next sections will describe the particle experiments, some details of the particle detectors, and some of the unique circuit features in the particle measuring experiments.

4.1 *The Particle Experiments*

The high particle intensity anticipated in the heart of the inner Van Allen belt requires the use of detectors which are fast and which have rather small geometrical factors (the product of the solid angle of particle acceptance and effective detector area). To avoid severe background problems that would arise if the solid angle of interest were made very small, the detector itself must be small. To permit discrimination of electrons from protons, some energy-proportional measurement is almost essential. To withstand the rigorous vibration of launch, a rugged device is required, and to provide for satisfactory operation in the vacuum of space, under the temperature variations of the satellite in orbit and in the presence of high levels of radiation, a device of great reliability is a necessity. Semiconductor particle detectors were selected as being nearly ideal. These are p-n junction devices which in effect are small solid-state ionization chambers.[11] They give output charge pulses proportional to the energy deposited by an incident charged particle in a disk-shaped active volume a few millimeters in diameter and a few tenths of a millimeter thick. They can be made with high reliability, as will be described in detail in Section 4.2. This kind of device has been extensively used in low-energy nuclear physics experiments in the last several years and provides high energy resolution[12] and relatively high speed.[13] In the Telstar experiment, the detectors are not being used as high-resolution devices or at their maximum capabilities of speed. Nevertheless, the nuclear physics experience with them has been invaluable in the satellite experiment design. Semiconductor detectors have been flown in the Injun and TRAAC satellites and in several Air Force satellites in the past two years, but very little of this information is yet available.

Three of the four detectors in the Telstar particle experiment measure protons, and the fourth measures electrons. Their energy ranges are:

low-energy protons	2.4–25 Mev
medium-energy protons	26–34 Mev
high-energy protons	>50 Mev
electrons	200 Kev–1 Mev (the detector response continuing to higher energies).

The outputs from the detectors time-share a single 14-bit register in the

telemetry, accumulating counts over periods between 3 and 15 seconds and reading out the register in all cases in two consecutive 7-bit telemetry words. The detectors are described individually in Sections 4.1.1 through 4.1.4.

4.1.1 *Low-Energy Protons (2.4 to 25 Mev)*

A cutaway view of the low-energy proton detector mount is shown in Fig. 10. The active p-n junction device is inside a transistor-like

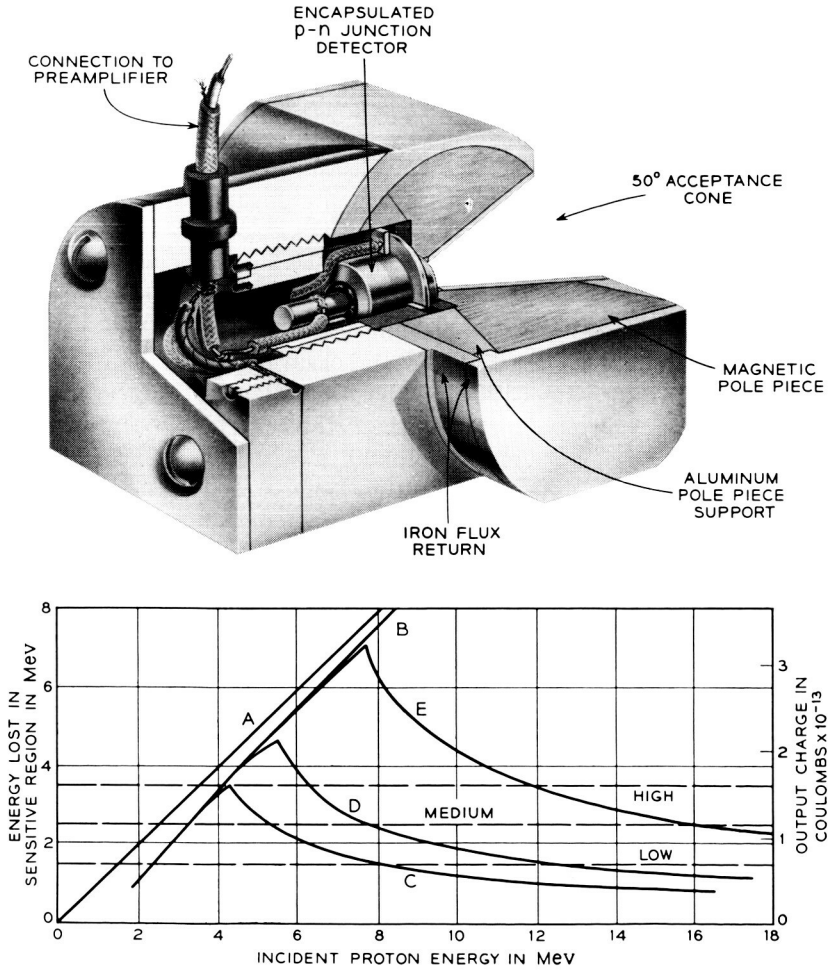

Fig. 10 — Cutaway view of the low-energy proton detector mount and the response of the detector to protons.

can (see Fig. 14, Section 4.2.1) surrounded by a relatively massive housing. The particles of interest enter through a cone with an acceptance angle of 50 degrees, truncated near its apex in an aperture 82 mils in diameter. Immediately behind this aperture is a Kovar window 80 mils in diameter and 0.3 mil thick which admits particles through the vacuum-tight enclosure of the detector encapsulation to the p-n junction device itself. Construction of this device is described in Section 4.2. The Kovar window excludes light, which would generate current in the device with high efficiency, and also removes protons with energies below 1.1 Mev and electrons below 15 Kev. A permanent magnet with tapered pole-pieces and a surrounding cylindrical soft steel magnetic flux return path provides a field in the acceptance cone that increases toward the apex and has a value of approximately 1500 gauss a quarter-inch from the detector. This magnet excludes electrons with energies below 300 Kev with increasing efficiency toward lower energies. It does so by deflecting them into the side walls of the cone, which is lined with aluminum to reduce electron back scattering. For electrons of 500 Kev or higher the magnetic exclusion efficiency becomes very low, and for all protons above a few Kev the magnetic field is insignificant in its effect. In directions outside the acceptance cone, the shielding of the detector is heavy enough to exclude protons of less than 80 Mev and electrons of less than 10 Mev. The detector mount extends behind the tubulation of the detector encapsulation to permit attachment of the detector to a coaxial preamplifier lead, still retaining the effective shielding.

The response of the detector to protons is illustrated in the lower half of Fig. 10. The electrical pulse developed by the detector is expressed in terms of the energy that an incident particle must leave in the detector to produce that pulse. One electron is available to the external detector circuit for each 3.5 ev of energy deposited by an energetic particle in the sensitive volume of the detector. This equivalence is independent of the particle type. The charge associated with an energy deposition is shown in the second vertical scale of the figure. The straight line A in the figure is a theoretical response just equal to the incident proton energy. The line B takes account of the effects of the 0.3-mil Kovar window and the diffused layer on the silicon detector, which together exclude protons of less than approximately 1.3 Mev and remove a smaller and smaller energy increment from protons of higher energy. The measured curves C, D and E correspond to three different effective detector thicknesses. This thickness is a little larger than the thickness of the p-n junction space-charge region — the region containing a high electric field. It is

variable with the bias on the detector. When the range of a proton just equals this thickness, the maximum energy loss and corresponding electrical pulse are obtained. For higher-energy protons less and less energy is left in the space-charge thickness. Curve C corresponds to a detector biased at 4.2 volts; D, 15 volts; E, 95 volts. The double-valued nature of each of these curves provides an energy band within which a pulse of a given size or larger can be observed. To change this band, either the sensitive thickness can be varied or the electrical pulse height discrimination level can be changed. In the low-energy proton detector, both of these variations are used. Nine distinct outputs can be obtained by measuring at each of three detector biases corresponding to curves C, D and E and by examining pulses within three different pulse height ranges marked by the horizontal lines on the figure: low, medium and high discrimination level.

The total span of energies covered by the detector is 2.4 to 25 Mev. However, it is not possible to measure a segment in energy close to the 25 Mev without including pulses from lower-energy particles as well. In a particle energy spectrum which falls rapidly with increasing energy, only an upper limit can be set on the number of the highest energy particles the detector is observing. The highest segment of energy which the present arrangement provides without a separate lower-energy component is that between 4.2 and 12 Mev, observed in the highest discrimination channel at the highest detector bias.

The probability that a single electron can produce a pulse as large as the 1.4 Mev of the lowest discrimination level is very small, less than one in 10^3. This is a result of the low rate of energy loss by electrons of this or higher energy. Pulse pile-up can occur from an anticipated high flux of low-energy electrons. The magnetic rejection reduces this problem for electrons of less than 300 Kev. Electrons of between 300 Kev and 600 Kev are of most serious concern. They are not well removed magnetically. They produce pulses comparable to their energy in many cases and pulse pile-up can reach the lowest discrimination level of the detector with only a three to fivefold multiplicity. A very high electron flux is needed to produce this pile-up, but a very high electron flux was measured in space during July, and the results of the low-energy proton detector consequently require careful examination.

The low-energy proton detector looks out perpendicular to the spin axis of the satellite through a hole in the satellite skin. It utilizes the single 14-bit register[2] in the telemetry for three seven-second periods during a one-minute telemetry frame, one period for the output of each

of the three discrimination levels. The detector bias is changed each frame, so that a complete sequence of nine readings requires three minutes.

4.1.2 *Medium-Energy Protons (26–34 Mev)*

The medium-energy proton detector mount is illustrated in Fig. 11. In this case the p-n junction detector is being used essentially on edge, particles of interest entering within a few degrees of perpendicular to the axis of the cylindrical detector disk and not nearly parallel to it as in the low-energy proton case. The acceptance aperture is a pair of 20-degree wedges like orange slices that have a common apex line through the junction device perpendicular to its cylindrical axis. This common apex line is parallel to the spin axis of the satellite. As the satellite makes half a rotation these wedges together sweep out a 4π solid angle. The detector is thus omnidirectional, sensing equally particles in all directions if its output is averaged over a time long compared to half a rotation of the satellite. As it is used, output pulses from the detector are summed for a 15-second period, corresponding to 45 complete rotations at the initial satellite spin rate. The detector protrudes through the skin of the satellite to permit essentially unobstructed access of particles to the wedges.

Protons penetrate this detector more or less along its diameter, and consequently can leave much larger amounts of energy in the space-charge region than was the case in the low-energy proton detector. The maximum path length is approximately 2.5 mm instead of about 0.4 mm as in the previous case. This makes it possible to set a high pulse height discrimination level, 11.4 Mev. No proton entering along the axis of the detector, or even at angles of up to 60° from the axis, can deposit enough energy to trigger this level. No electron is capable of triggering this level with any significant probability, no matter what its incident direction. Moderate shielding along the axis in the forward and back directions is used to remove problems of pulse pile-up, and very heavy shielding is used between 60° to the axis and the acceptance wedges to reject any protons of lower than 100 Mev. The detector should be extremely free from response to unwanted particles.

If the junction device were not surrounded by any material in the acceptance wedges, it would detect protons starting at an energy of 11.4 Mev. However, the thickness of the Kovar detector can wall (5 mils from the side) and an additional absorber placed within the acceptance wedges pushes this minimum energy up to approximately 26 Mev. The calculated detector response is shown in the lower part of Fig. 11. The curve represents the average response for protons incident over the ac-

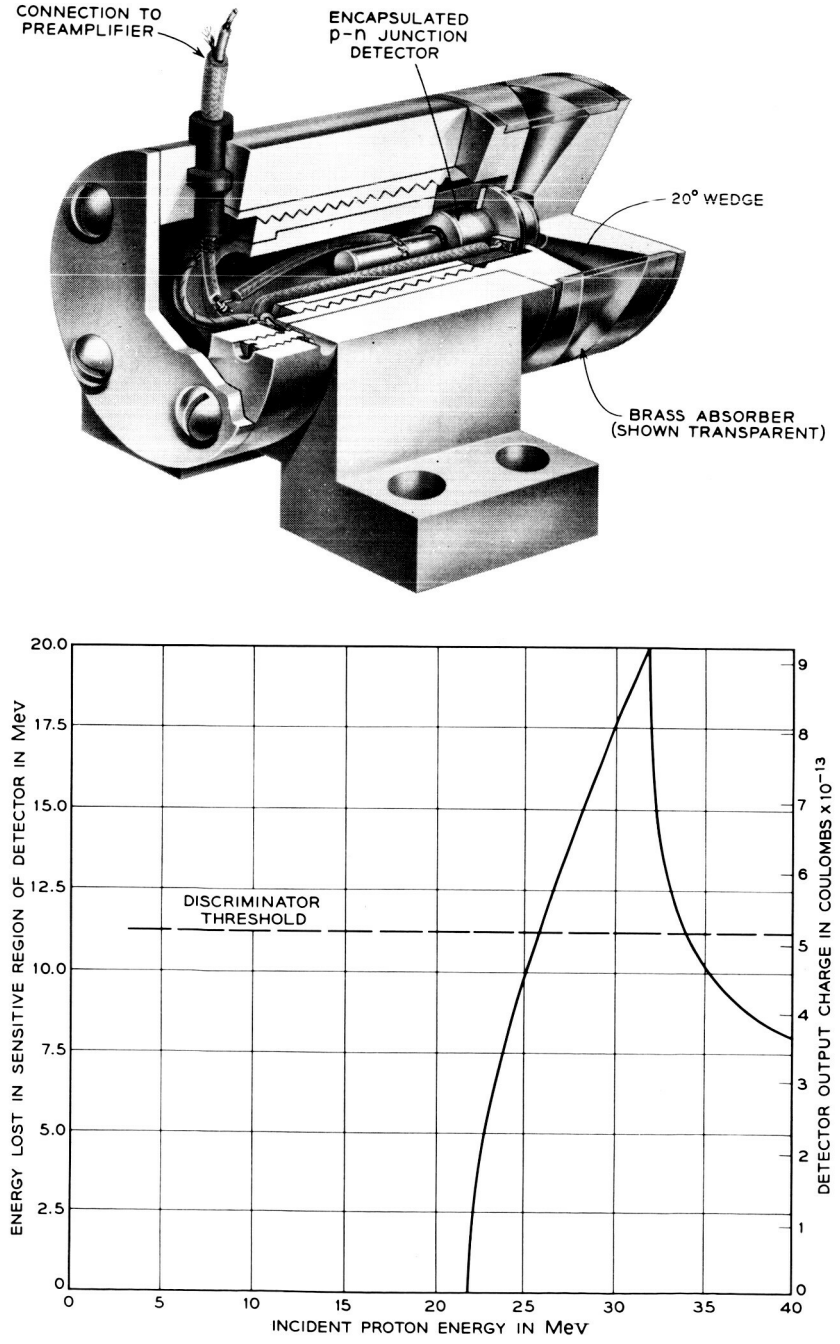

Fig. 11 — Cutaway view of the medium-energy proton detector mount and the calculated response of the detector to protons.

ceptance aperture. The shape for a particular angle of incidence and position of the particle path with respect to the disk diameter will vary because of the different path lengths the particles take. This detector supplies pulses from its single discrimination channel to the 14-bit register of the telemetry for a period of 15 seconds each telemetry frame.

4.1.3 *High-Energy Protons (>50 Mev)*

Energy discrimination in this detector is obtained by use of an absorber. The detector mount is shown in Fig. 12. The junction device is placed in the center of a hemispherical aluminum shell to provide an approximately uniform absorber over a 2π solid angle. The detector mount is inside the satellite skin, and taking into account the satellite structure near the detector, the effective threshold energy of the device is calculated to be approximately 50 Mev. The detector is not truly omnidirectional because of nonuniformity in the absorber thickness in different directions. However, because of the rotation of the satellite this lack of directional uniformity is largely averaged out. All pulses in the detector greater than 2.1 Mev are accepted. The calculated detector response for particles entering in a representative direction is shown in the lower part of Fig. 12.

The single discrimination channel of the high-energy detector makes use of the 14-bit telemetry register for 11 seconds of the one-minute telemetry frame.

4.1.4 *Electrons*

The electron detector mount is illustrated in Fig. 13. This mount protrudes through the satellite skin and looks out perpendicular to the spin axis. Particles are accepted in a cone having an angle of 20 degrees with an 82-mil diameter aperture immediately in front of the junction detector can. The deposition of energy by electrons in the sensitive volume of the detector is much less clearly related to the actual particle energy than is the case for protons. A 600-Kev electron may leave all its energy in a sensitive volume 0.43 mm thick (the thickness of the electron detector on the Telstar satellite); it may back scatter in the first fraction of this thickness and leave only a small part of its total energy; or it may penetrate entirely and leave less than all its energy to be detected. By examining the distribution of pulse heights produced in the detector, only a rough evaluation of the spectrum of incident electrons can be obtained, since the spectrum must be unfolded from the distribution of pulse heights produced by monoenergetic particle groups. (See Fig. 15, Section 4.2.3.1.) The probability that an electron of more

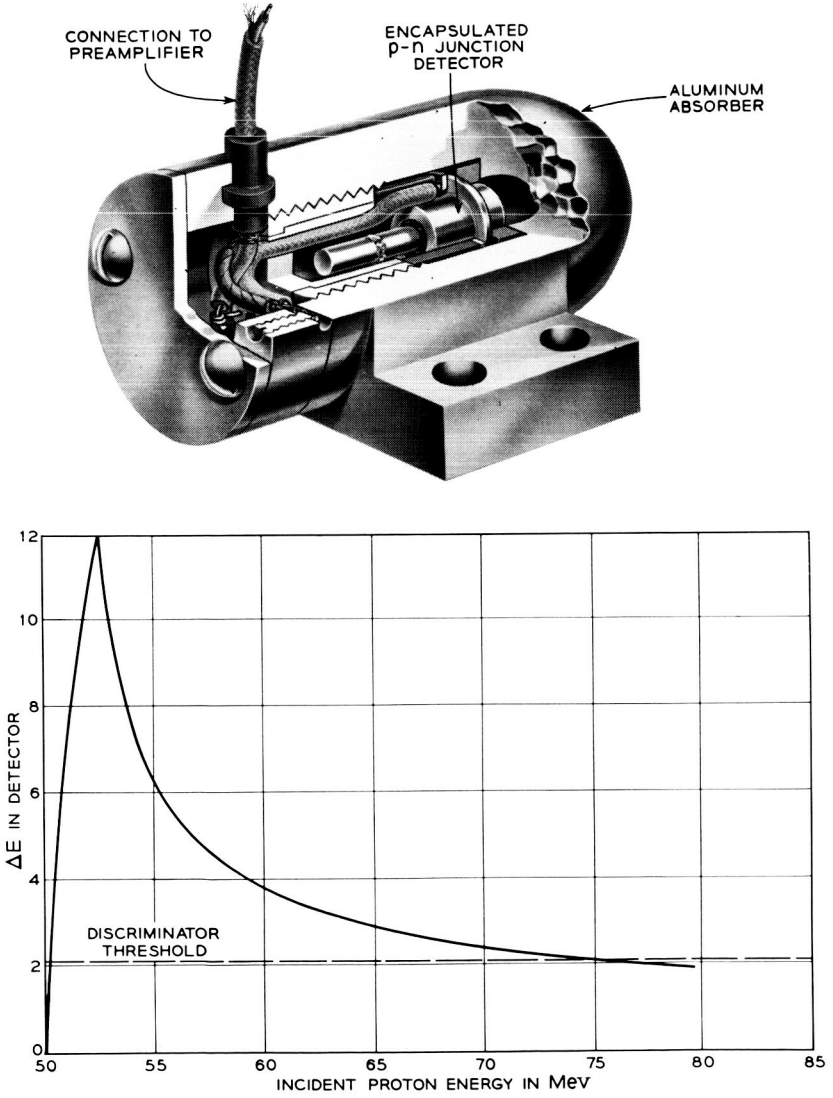

Fig. 12 — Cutaway view of the high-energy proton detector mount and the calculated response of the detector to protons.

than 1 Mev will leave all its energy in the sensitive detector thickness is very small. Such electrons can be detected by the lower energy pulses they produce, but their energy cannot be directly deduced.

In the Telstar electron detector, particle pulses are sorted into four pulse height channels: 180–280, 285–440, 390–615 and 635–990 Kev.

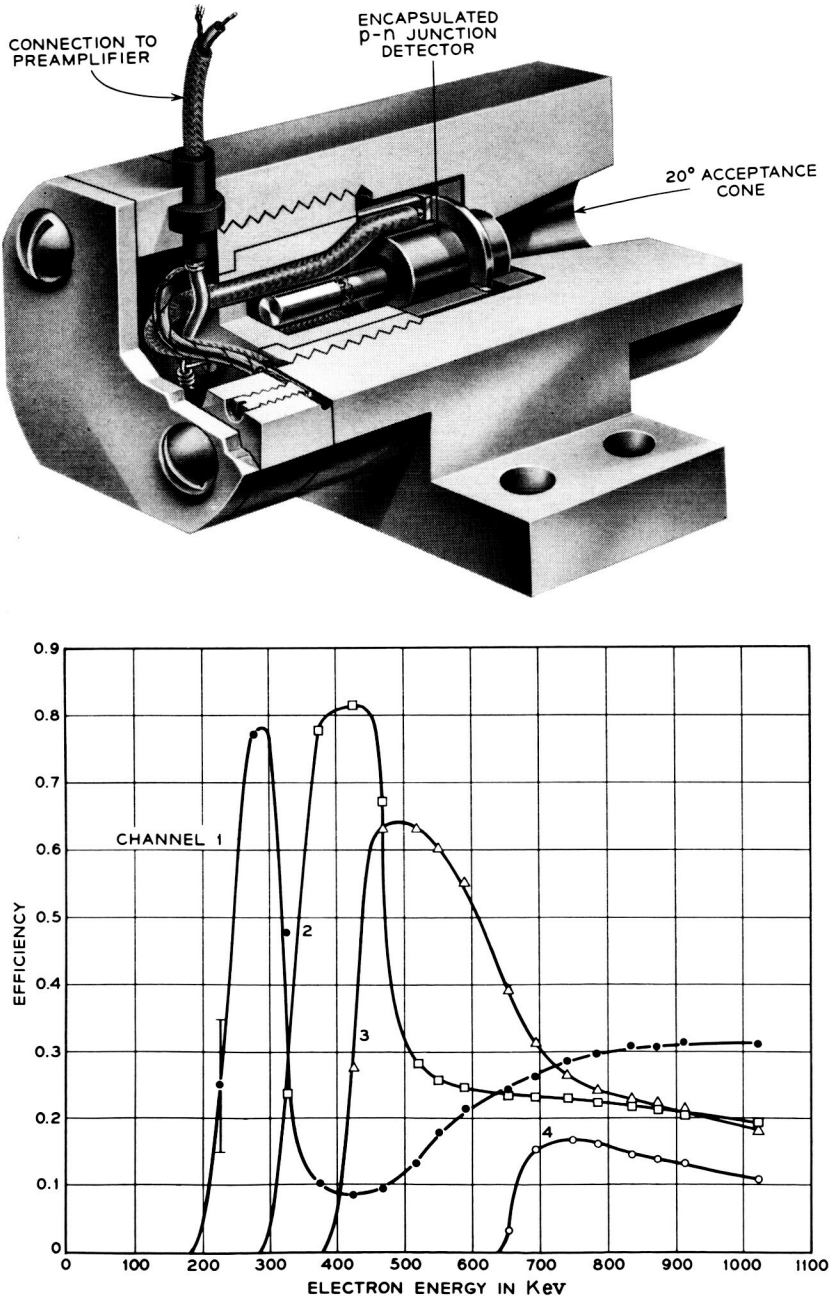

Fig. 13 — Cutaway view of the electron detector mount and the response of the detector to electrons.

The bottom edges of these channels correspond to 215, 315, 420 and 660 Kev, taking into account the energy lost by electrons in penetrating the 0.3-mil detector can window and an additional 1.6-mil aluminum absorber used to remove protons of less than 2.3 Mev. Pulses from two of the four channels are fed to the 14-bit telemetry register for three seconds each in every other telemetry frame. The second pair of channels, produced by a change in amplifier gain, is measured in the alternate frames.

The efficiency of each of the four channels for counting electrons up to approximately 1 Mev is illustrated in the lower part of Fig. 13. Each channel starts abruptly as the energy requirement of the channel is met, but retains a substantial efficiency at electron energies above the upper pulse height limit of the channel.

The electron detector is potentially susceptible to background problems from protons. The addition of the 1.6-mil aluminum absorber eliminates the problem for very low energy protons. In addition, the top pulse height channel is closed. Pulses in excess of 990 Kev will not be counted. To be recorded, protons must have energies greater than 2.4 Mev to penetrate the entrance window and leave at least 180 Kev in the detector, but energy less than 2.7 Mev, so they do not leave more than 990 Kev (a shield that just stops 2.3-Mev protons will extract less than 2.3 Mev from 2.7-Mev protons). This very narrow energy range for proton acceptance makes the proton contribution to the counting rate small except when the electron flux nears the minimum values that it has in the Telstar satellite's portion of space.

4.2 *Silicon p-n Junction Detectors*

Silicon p-n junction detectors were used in all the particle experiments, as described in Section 4.1. They satisfy the requirements of small size and rugged construction, high sensitivity, high speed, low noise, and in addition provide high reliability in the space environment where temperature and radiation intensity vary continuously. The construction and testing of these detectors will be discussed in the following sections.

4.2.1 *Mechanical Construction*

Surface reliability was recognized as a problem of major proportions in designing the Telstar satellite detectors. Surface control was achieved by adopting a hermetically sealed transistor-type encapsulation with a thin window. Such a window was permissible in this experiment, although it would not be for many nuclear physics experiments. The design which evolved is shown in a schematic cross-sectional view in Fig. 14. The

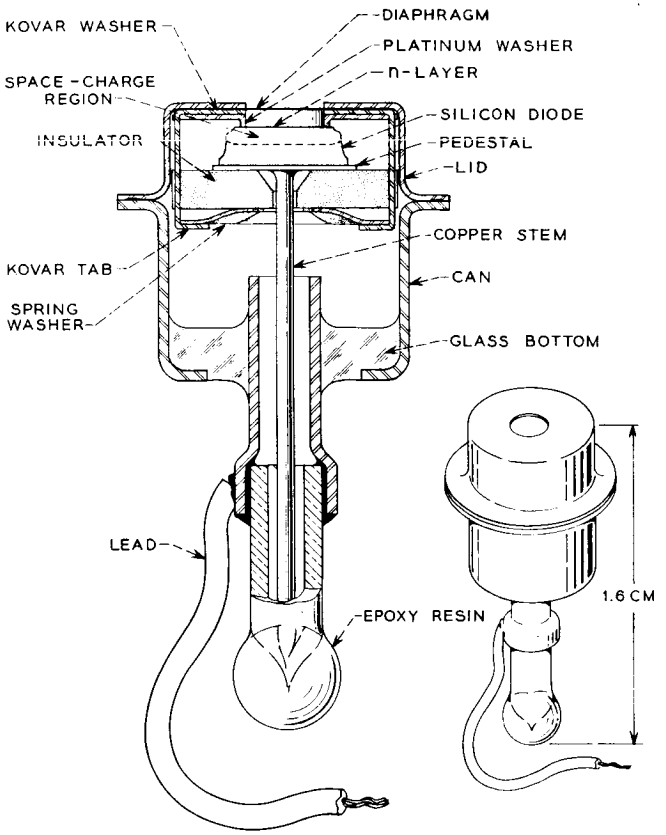

Fig. 14 — Cross-section view of encapsulated detector.

encapsulation consists of a Kovar can with a glass bottom and a metal tubulation, and a Kovar lid which is welded onto the can in final assembly. All Kovar parts are gold plated. The diode with the diffused n-layer looks out through the hole in the lid, which is covered by a Kovar diaphragm which may be as thin as 0.3 mil. The diaphragm is welded between the lid and a Kovar washer to make a good vacuum seal. The diode is pressed against a platinum washer which has a raised rim around the hole and thus provides contact to the n-layer. Contact to the back or p-region of the diode is made through the gold-plated Kovar pedestal alloyed to it. A good low-resistance contact is needed here to provide a pulse rise time of less than 0.2 μsec. A copper stem completes the connection to the tubulation and a stranded lead makes contact to it.

The p-region of the diode is insulated from the main body of the encapsulation by a ceramic insulator. A spring washer is compressed against the insulator by tabs which extend from the Kovar washer welded to the lid. After assembly the device is evacuated, baked at 200°C for an hour or more, cooled to room temperature, back filled with a suitable atmosphere and the tubulation pinched off. A drop of epoxy resin is used to protect the delicate feather edge of the pinch off.

4.2.2 *Materials and Processing*

The detector diodes are of the n-on-p type,[14] made by diffusing phosphorus into silicon of the highest available resistivity, i.e., about 10,000 ohm-cm to 20,000 ohm-cm. At 100 v the space-charge depth in this material is 0.30–0.45 mm. Deeper sensitive regions could have been obtained by using the lithium-drift technique[15] which produces a p-i-n structure with very close compensation in the middle, drifted region. However, preliminary tests showed that Li-drifted diodes are much more rapidly degraded by radiation damage than are the n-on-p diffused diodes and would have too short a life in the radiation environment the Telstar satellite was expected to encounter. They also exhibit a more complicated surface behavior.[16] The phosphorus diffusion is carried out at 1050°C, using P_2O_5 in an open tube system. A diffusion time of three hours gives a junction depth of about 4 microns. This "dead layer" or "window" is negligible compared to the thickness of the Kovar diaphragm. After diffusion, the slices are wafered and the small diodes then alloyed to pedestals, etched and encapsulated.

4.2.3 *Performance and Testing*

4.2.3.1 *Calibration and Counting Behavior.* Direct calibration of the particle detectors was carried out with electrons from a 1-Mev Van de Graaff generator and also with 17-Mev protons from the Princeton cyclotron.* Fig. 15 shows pulse height spectra for electrons of 5 different energies, taken on a detector with 100-v bias. These results differ only slightly from those corresponding to the 95-v detector bias in the satellite. It may be seen that the total absorption peak is quite high for 220 and 425-Kev electrons and then becomes progressively smaller until it has almost disappeared at 990 Kev. At the same time, a broader peak due to electrons which lose only part of their energy in the space-charge

* These calibrations were carried out with the kind cooperation of Professor R. Scheer of the Princeton University Physics Department.

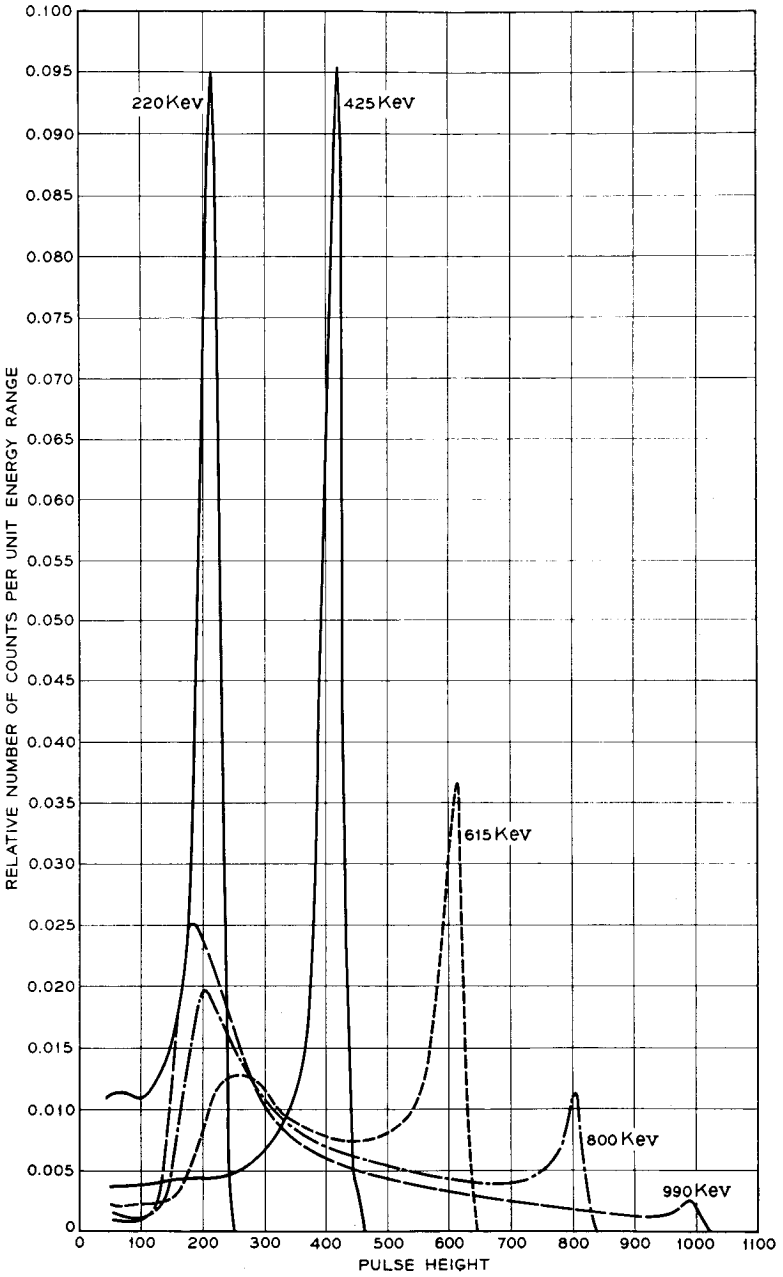

Fig. 15 — Pulse height spectra for electrons of five different incident energies. Pulse heights are indicated in terms of energy deposited by an electron in the sensitive region of the detector.

region is increasing in size.* By calibration with protons which, unlike electrons, have a precisely defined range at a given energy, the depth of this detector was found to be approximately 0.43 mm at 100 v.

Detector noise is an extremely important characteristic of the junction detector, particularly in the case of the electron detector, where pulses corresponding to particle energy losses in the detector of less than 200 Kev are to be measured. Spurious noise pulses which even approach this threshold level are serious because of the distortion they produce in the pulse height distribution. The noise in low-noise devices can be examined most easily, not in terms of the probability of finding a spurious pulse equivalent to 200 Kev, but as a broadening in the distribution of pulse heights produced in response to a series of uniform electrical pulses artificially introduced in the detector. The full width at half height of this pulse height distribution is measured and expressed in terms of an equivalent particle energy. Such noise linewidth measurements were obtained in all detectors under standard conditions, and in a number of cases whole sequences of noise measurements were made through a series of environmental tests.

4.2.3.2 *Reliability*

i. Surface Reliability. The essence of the surface reliability problem on the detectors is illustrated in Fig. 16, in which reverse current is plotted against bias for three representative cases. These curves were measured on different encapsulated units which were all good initially but which aged in different ways to arrive at the conditions shown. Curve A is a typical good, low-noise characteristic which is obtained with the surface (of the high resistivity p-side) nearly intrinsic or perhaps slightly n-type.[18] The current is 0.14 μa at 100 v and noise linewidth was 10 Kev. (Note that the current scale for A differs by a factor of 100 from that for B and C.) Curve B results from a strong n-type inversion layer over the p-region. The current is 48 μa at 100 v and the noise linewidth 85 Kev. The behavior depicted by curve C is due to an accumulation layer at the surface; i.e., the surface is more strongly p-type than the bulk. The charge in surface states is negative, and the resulting high field at the edge of the junction causes surface breakdown at many little spots around the junction. Even at 1 v, where the current is only 0.04 μa, the noise linewidth is 90 Kev, and at 5 v bias the noise is greater than 450 Kev. The diode represented by this type of characteristic is the noisiest of all for a given current. There is very good correlation between

* These results are similar to those of Ref. 17.

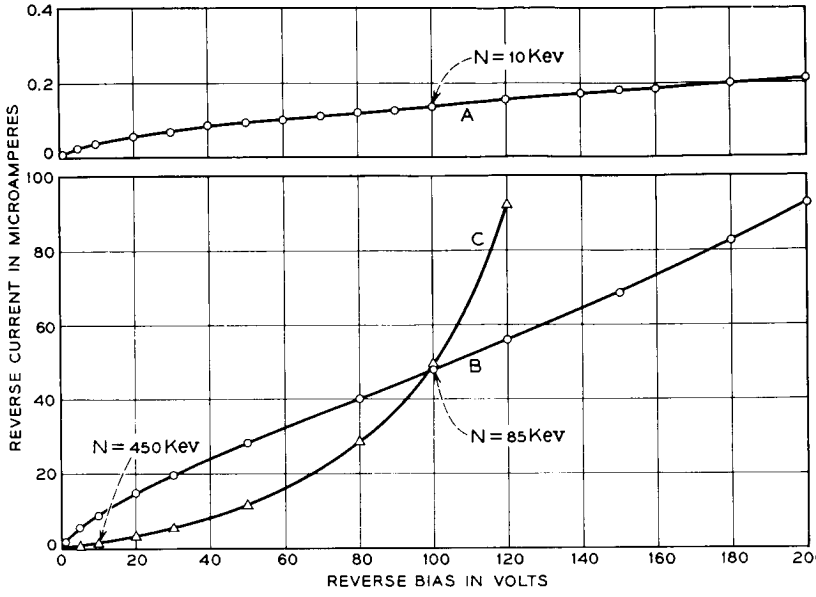

Fig. 16 — Typical reverse current-voltage characteristics for detector diodes with: (a) normal low-noise characteristic; (b) strong n-type inversion layer; (c) p-type surface accumulation layer. Note smaller scale for A. Noise linewidth values N are indicated at particular points on the curves.

noise and I–V characteristics* that has made it possible to predict noise by inspection of an I–V curve. Even a small departure from curve A toward the B or C conditions shows up as an increase in noise.

The maximum permissible noise linewidth was about 50 Kev for the electron detector, and several hundred Kev for the proton detectors. Newly fabricated detectors were all well below this, at about 10–15 Kev, but many of the early models developed poor I–V characteristics and high noise within a few weeks on shelf aging. Of the first 100 produced, only 44 survived after a few weeks. Transistions between characteristics of the type illustrated in Fig. 16 may be brought about very quickly by atmosphere changes or wet chemical treatments which shift the surface potential in known ways,[19] but the causes of long-term shifts on shelf aging, bias aging and temperature cycling are harder to detect and control. Nevertheless, by careful adjustment of surface potential by initial chemical treatments and by control of the ambient atmosphere

* Early studies of noise in the detectors were made in collaboration with H. C. Montgomery and L. K. Monteith. See also Ref. 16.

in the encapsulations it was possible to improve the yields to about 90–95 per cent by the end of the project. The processing will be described more fully in another paper.[20]

Indirect effects of radiation on the detector surfaces as a result of ionization of the ambient gas within the encapsulating can were considered, since such effects had recently been observed on transistors.[21] Selected groups of detectors were tested under intermittent bias and continuous bias in γ radiation of 50 rads/hr, approximately the average encountered in space. In general the effects have been rather small, although complicated. Changes do occur when the conditions are changed; as the bias or radiation is turned on or off the currents may increase or decrease, but after a few days in a new condition the current levels off at a new steady-state value. Detectors vary in their sensitivity to radiation for reasons not yet understood, but not many are severely affected by radiation at this dose rate level.

ii. Bulk Radiation Damage Effects. The effects of particle radiation on bulk properties of the detectors are not yet well understood, although it can be said that really serious effects are not expected in less than about a year. After a bombardment with about 10^{14} electrons/cm^2 of 1-Mev energy, a loss in pulse height begins to appear. The electron detector in the Telstar satellite has received damaging particles equivalent to about 5×10^{11} 1-Mev electrons/cm^2 day. On this basis one may expect that the electron data will begin to be affected by bulk damage after about six months in orbit, and that thereafter it may be necessary to estimate corrections by using damage measurements obtained on the ground. The low-energy proton detector, with the largest solid angle and the thinnest diaphragm, may be affected somewhat sooner. The medium and high-energy proton detectors with their thick shielding will not be affected until much later.

iii. Life Testing Program. Finished detectors were put through a life testing program which included:

(a) Vibration at frequencies from 50 to 2000 cycles/sec and accelerations of either 40 or 80 g's in both the longitudinal and transverse directions. Two typical detectors were subjected to 12 shock tests with successively higher accelerations, up to 1100 g, without any apparent damage.

(b) High humidity soaks at 95 per cent RH for 16 to 24 hrs, followed by vacuum pumping and exposure to oxygen. The surface sensitivity of the diodes is such that any leak would be easily detected by this test.

(c) Temperature and bias cycling in a vacuum chamber for at least one month. Temperature was cycled continuously from $-50°$C to

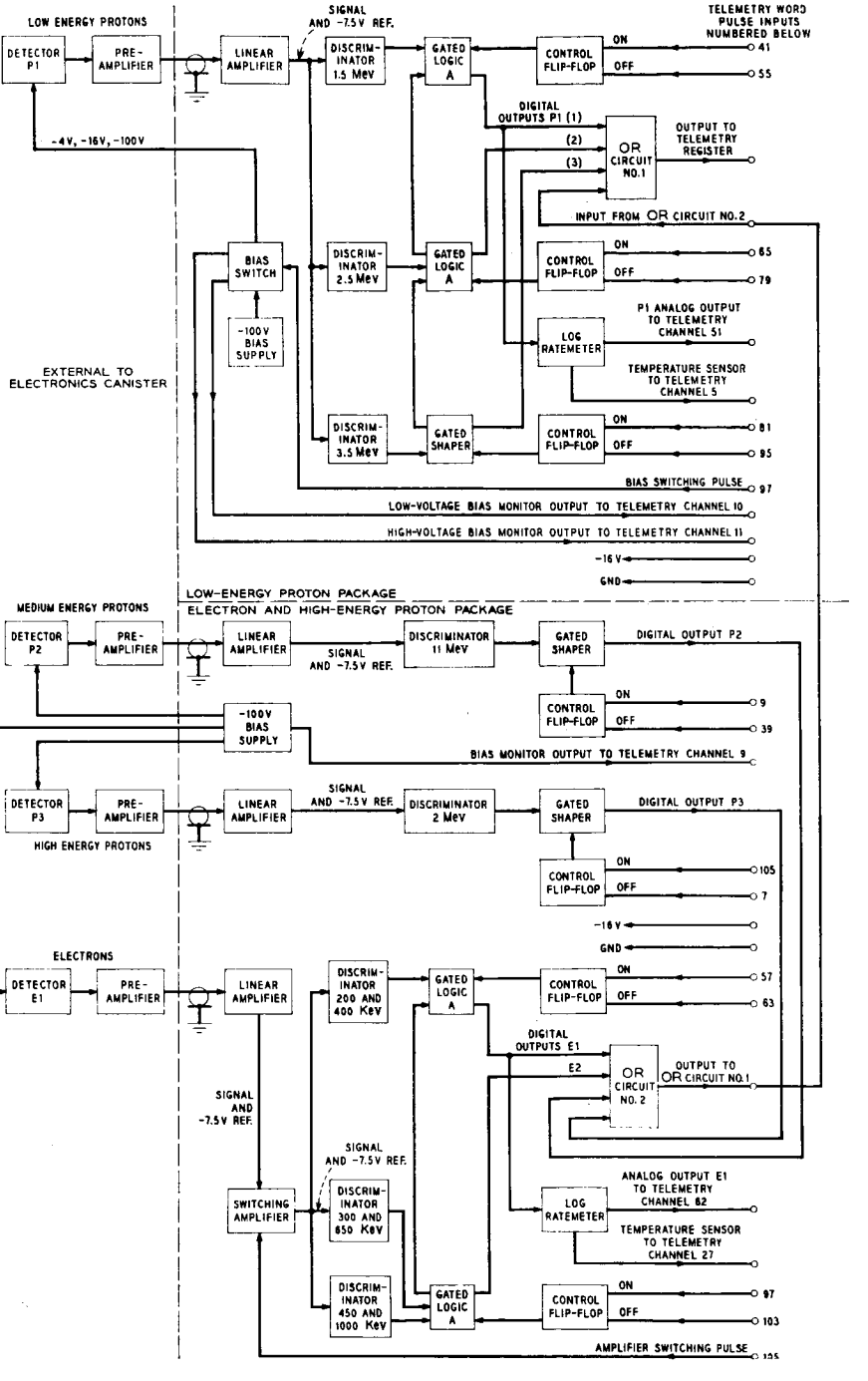

Fig. 17 — Radiation particle experiment block diagram.

+50°C with a period of 3 hours, while reverse bias of 120 v was cycling 20 minutes on and 1 hour off.

(d) Exposure to γ radiation at 50 rads/hr during bias cycling.

During all this testing and also during shelf-aging, accurate measurements of the reverse current-voltage characteristics were made frequently, as a very sensitive indication of surface stability. Only stable devices were selected for use.

4.3 *Electronic Circuits*

4.3.1 *Block Diagrams*

The electronic circuits of the radiation particle experiments are shown in block diagram form in Fig. 17. Each block represents the smallest part of a circuit that has an essentially independent function. The four detectors are at the left of the diagram. The function of the preamplifiers, which are to the right of the detectors, is to produce an output current pulse whose maximum is proportional to the charge produced in the detector by an incident particle. The linear amplifiers amplify this current pulse and present a proportionate output voltage pulse to one or more pulse amplitude discriminators. The discriminators produce an output current pulse of fixed shape for each input pulse above a threshold amplitude at the discriminator input. The gated logic and shaper circuits decide, for any input pulse, the highest discriminator threshold exceeded and produce an output pulse corresponding to that decision. The control flip-flops control the digital outputs and are turned "on" and "off" by signals from the telemetry timing circuits. Only one gated logic or shaper circuit is operative at any one time. All others are held off by their respective control flip-flop. The OR circuits combine all logic and shaper outputs on one output line to a register in the telemetry section. The log ratemeters take the average of the logarithm of the counting rate and present this average as a dc voltage to analog telemetry channels. A tristable multivibrator, bias switch and −100-volt bias supply provide three levels of bias to the low-energy proton detector.

Many of the problems encountered in the design of a satellite radiation measuring instrument are due to the random arrival of the particles and to their wide variation in energy. Problems of this nature are encountered in the analysis of the radiation from atomic nuclei and have been extensively treated in the literature.[22,23] In addition, electronic circuits for this application must be designed with adequate stability against changes in ambient temperature, supply voltage, and transistor parameters. Stability requirements are most severe in the linear amplify-

ing system and in the discriminators, where changes would shift the energy calibration of the experiment. In the amplifiers these requirements are met by the use of negative feedback through passive low-temperature coefficient elements in loops having large reserve gain.

Shifts in baseline with pulse rate are eliminated by using double RC differentiation to produce a bipolar pulse. The maximum counting rate of each experiment is limited to 100,000 pulses per second by the linear system shaping network and digital circuit recovery times.

Overload of the amplifying system by large input pulses is handled by arranging gains and bias so that overloads occur outside the feedback loops at the output of the preamplifier. The system quickly recovers from the overload with negligible baseline shift.

Electronic noise in the preamplifier is a limiting factor in the lowest energy of electrons that can be measured. A 25-Kev equivalent noise linewidth has been attained, a value well below the threshold of the lowest electron channel.

4.3.2 *Circuit Reliability*

With extended operation in space as a design goal, special attention was given to circuit reliability. Reliability has been enhanced through design simplicity, outstanding cases of which are the log ratemeters, bias supplies, and gated logic and shaper circuits which require only a single transistor to perform their function. Another method used to improve reliability was to design the system so that failure of a circuit would not terminate the entire experiment. The three proton experiments have been divided into independent parts so that the loss of one does not affect the operation of the others. In the low-energy proton and electron experiments, several independent discriminators enable collection of meaningful data even if a single discriminator fails. A -100-v bias supply common to three detectors is equipped with a diode OR circuit which, in the event of failure, would automatically switch in the -16-v satellite supply. Although performance would be limited at this reduced bias, useful data would still be received. Care was taken to avoid series failure mechanisms such as single power line filters and fuses. All circuits are separately decoupled and load limited.

4.3.3 *Linear System*

4.3.3.1 *Preamplifier.* The total detector output charge q_s produced by an incident particle is amplified in a linear system whose peak output voltage is proportional to q_s. A conventional method of doing this is

to amplify the voltage appearing across the total capacitance from input to ground. This voltage is

$$e_s = q_s/C_T$$

where e_s is the input signal voltage, and C_T is the total capacitance from the input to ground including the junction capacitance. In the solid-state detector, however, the junction capacitance changes with bias and ambient conditions, and consequently the voltage signal, e_s, would not always maintain the same relationship to the input charge.

An integrating preamplifier whose output is relatively unaffected by changes in detector capacitance is shown in Fig. 18.[24] The output voltage, e_o, is nearly equal to the input charge, q_s, divided by the feedback capacitance, C_F, if the open loop voltage gain is large. Thus the output signal is relatively insensitive to changes in detector capacitance. The preamplifiers in the Telstar satellite are of this type.

4.3.3.2 *Linear Amplifier.* After the preamplifier, the signal is amplified further in a linear current amplifier, which uses a two-transistor configuration described by Goulding.[25]

4.3.3.3 *Linear Signal Shaping.* The signal from the detectors is differentiated twice in the linear system with equal one-microsecond RC clipping networks, which are shown in Fig. 18. A resistor, R_C, of resistance such that R_CC_F equals one microsecond, is placed across the preamplifier feedback capacitor, C_F, to provide the first clip. A second clip is made by the combination of the output impedance of the preamplifier and a capacitor, C_C, between the preamplifier and the linear amplifier. The output resistance of the preamplifier is conveniently fixed

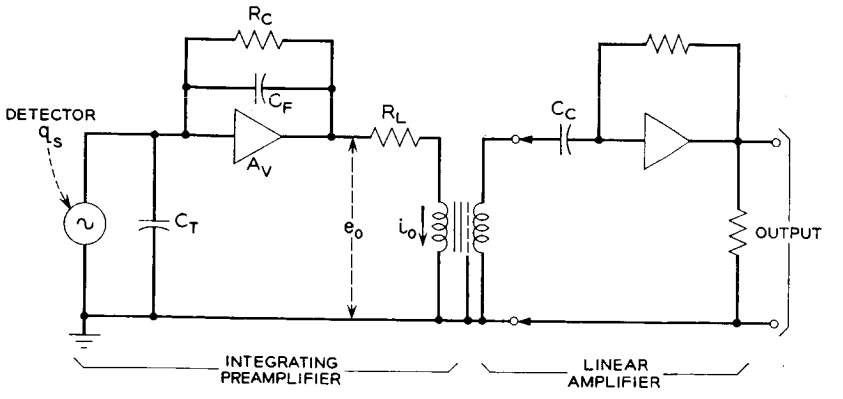

Fig. 18 — The linear system.

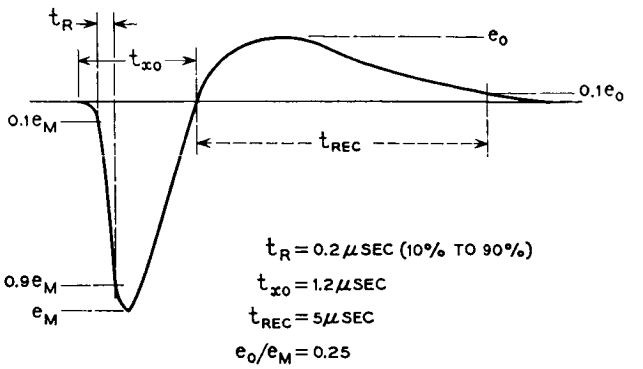

Fig. 19 — Linear amplifier output waveform.

by resistor R_L. The impedance looking into the input of the linear amplifier is very small (about 40 ohms), so it does not significantly affect the second clip time constant. The double-clipped signal as it appears at the linear amplifier output is shown in Fig. 19. The transformer at the output of the preamplifier contains an electrostatic shield to prevent coupling of common mode interference into the amplifier.

4.3.3.4 *Switching Amplifier.* The electron experiment, which is at the bottom of the block diagram, Fig. 17, has four levels of data but uses only two telemetry channels. This is accomplished by changing the gain of the linear amplifier system between successive telemetry frames. A plot of the electron channels for the electron analyzer is shown in Fig. 20. Three discriminators set the two channels shown by the solid lines.

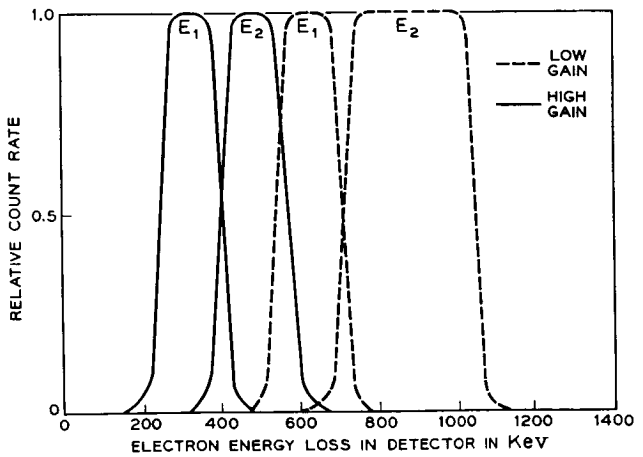

Fig. 20 — Response of electron channels as a function of input pulse height.

Decreasing the gain of the linear system shifts the energy thresholds up to those indicated by the dashed lines. In the satellite, the electron detectors count at one gain during a given telemetry frame and at another gain during the next frame.

The switching amplifier is shown in Fig. 21. The amplifier loop is similar to that of the ordinary linear amplifier. The gain of the amplifier is proportional to $1/R_4$ when transistor Q_3 is on, and $1/(R_4 + R_5)$ when Q_3 is off.

The switching transistor, Q_3, is driven by the bistable switch. The switching signal input is a timing signal from the telemetry package that occurs once each frame. An indication of the position of the bistable is telemetered.

4.3.4 *Digital System*

4.3.4.1 *Pulse Height Analyzers.* Two methods of pulse height analysis are conventionally used in random pulse height measurements: the stacked-discriminator method[22] and the pulse-height-to-time-converter method.[26] The relative simplicity of the stacked-discriminator analyzer was felt to be of commanding importance in this application.

In the stacked-discriminator analyzer each discriminator is biased at a different level or threshold. Any input pulse causes each discriminator whose threshold it exceeds to trigger and produce an output pulse. Since only the highest discriminator threshold exceeded is of interest,

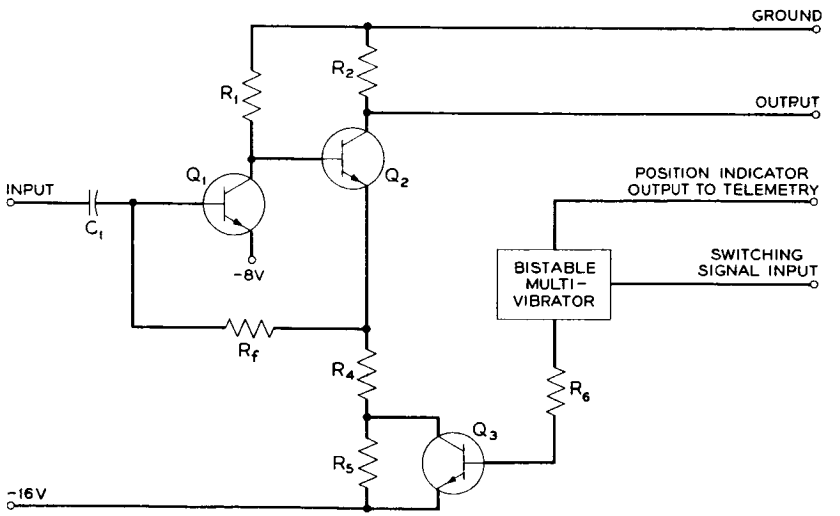

Fig. 21 — Switching amplifier (simplified).

logic circuits following the discriminators determine the one with the highest threshold that was triggered.

4.3.4.2 *Discriminator.* The characteristic most difficult to achieve in the design of a threshold discriminator for satellite use is thermal stability. The circuit used in the Telstar satellite (Fig. 22) is based on the emitter-coupled monostable multivibrator to take advantage of the inherent compensation of base-emitter voltage change with temperature. All other voltage drops that would affect threshold sensitivity are eliminated except an adjustable potential, V_t, that is derived from a zero temperature-coefficient reference element. An inductor, L_1, used instead of a base return resistor on the normally conducting transistor of the emitter-coupled pair, eliminates a temperature-sensitive voltage drop at that point.

A second-order effect on the threshold thermal stability is the variation of transistor beta with temperature. To trigger the multivibrator, the input signal must raise the base of Q_3, the normally "off" transistor, until its beta is large enough to produce a gain around the feedback loop of greater than one. At low temperatures the beta of Q_3 is reduced, so the input signal must be slightly larger than at higher temperatures. Nevertheless the discriminator threshold is quite stable. From $-50°C$ to $+50°C$ the threshold does not vary more than ± 1 per cent. The discriminator output, taken from the collector of Q_3, is a current pulse of about 600 μa, with a duration determined mainly by the shape of the input pulse.

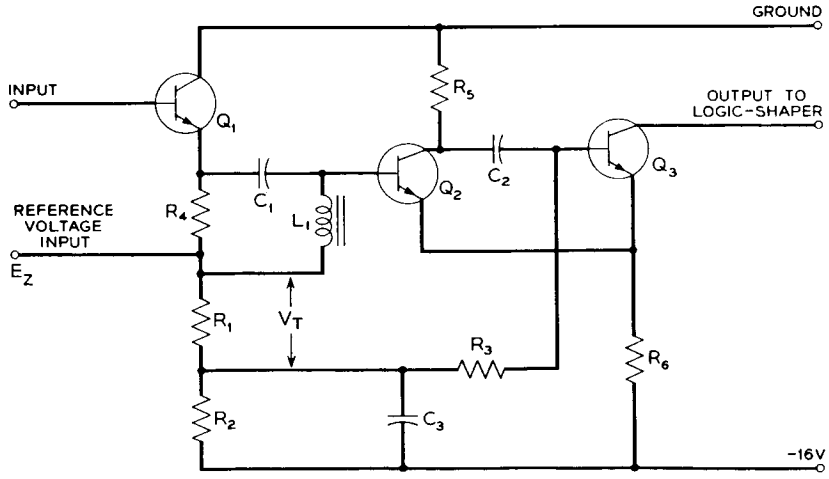

Fig. 22 — Discriminator circuit.

4.3.4.3 *Gated Logic Circuit.* The gated logic circuits have two functions: first, to determine the discriminator with the highest threshold that was triggered by a signal from the linear system; second, to produce an output pulse suitable for driving a coaxial cable and a register. Each discriminator's output is trying to turn a gated logic circuit on while at the same time keeping the one below it from turning on. A discriminator turns on a logic circuit only if the next higher discriminator does not produce an output during the rise of the pulse from the linear amplifier driving them. Since the input pulse has a finite rise time, a discriminator with a higher threshold will trigger later than one with a lower threshold. The logic circuit must delay its decision until the higher discriminators have had time to fire.

These operations are performed in an unusual manner in a modified blocking oscillator, shown in Fig. 23. Two input windings of a pulse transformer connect to the discriminator outputs, and a third winding that has the same number of turns as the input windings connects to the transistor base. The current in the base winding is the algebraic sum of the current in the input windings as long as the transistor is turned off. Winding 1 is connected to the upper discriminator in the direction that produces a base winding current that drives the base of Q_1 negative. Winding 2 is connected to the lower discriminator in the opposite phase; when this discriminator fires, the base of Q_1 goes positive.

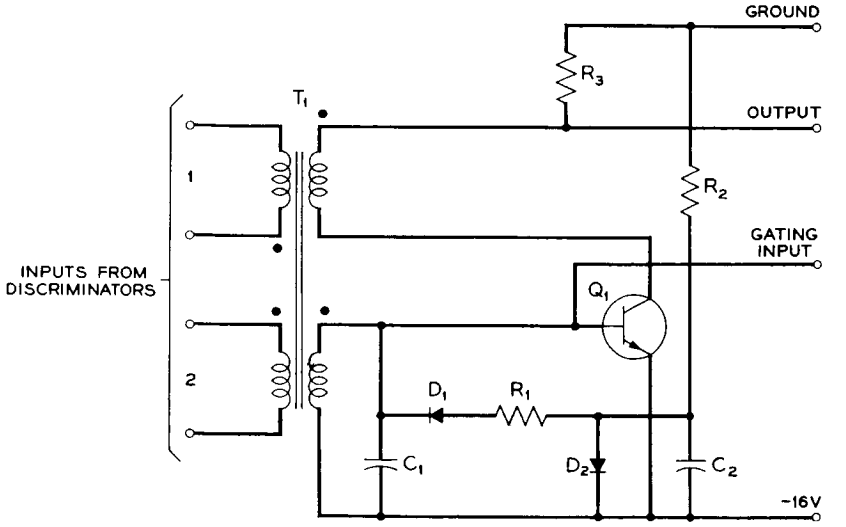

Fig. 23 — Logic-shaper circuit.

When the input pulse is large enough to trigger the lower but not the upper of two discriminators connected to a gated logic unit, the current pulse pours into C_1 and charges it linearly with time. Transistor Q_1 is normally biased off by holding the base at the emitter voltage. The capacitor C_1 must then charge to about 0.7 v before the transistor turns on. In the circuit shown, the input current from a discriminator is about 600 μa. The time required to charge the capacitor to 0.7 v is about 0.5 μsec, allowing the input pulse to rise to the next discriminator threshold if it will. If the next higher discriminator were to trigger during this 0.5-μsec period, its output current, pouring in the other input winding, would prevent the capacitor from charging enough to turn on Q_1.

When Q_1 does turn on, it operates as a blocking oscillator. Current in the collector circuit is fed back to the base and the transistor rapidly saturates. The saturation current is limited to about 2 ma by R_3. The inductance of the collector winding is such that the transistor is held on in saturation for about 4 μsec. Then Q_1 turns off and the energy stored in the transformer inductance is dissipated in resistor R_1, which is chosen to slightly underdamp the overshoot. With this damping the blocking oscillator is completely recovered in about 10 μsec. Diode D_1 prevents R_1 from taking any of the 600 μa charging current; diode D_2 biases diode D_1 so that R_1 is effective for the entire negative swing in the base circuit. Fig. 24(a) shows the base waveform for both conditions of operation: when just one discriminator fires (solid line), the capacitor charges linearly until the blocking oscillator fires; when both

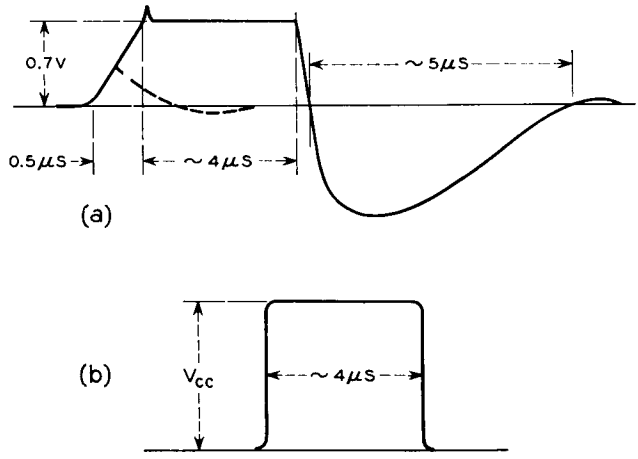

Fig. 24 — Logic shaper waveforms: (a) base waveform (b) output waveform.

discriminators fire (dashed line), the charge of the capacitor is stopped before the blocking oscillator fires. The shaper circuits are similar to the logic circuits, the chief difference being that only one input is provided. Fig. 24(b) shows the output waveform.

A 14-bit register[2] is provided in the telemetry package to accumulate the pulses from the radiation circuits. Time sharing of the outputs of the logic and shaper circuits into this register is accomplished by holding off all except one with saturating transistor gates connected between the gating inputs and −16 v. The gates are controlled by flip-flops shown in the block diagram. The flip-flops are switched by signals from the telemetry timing circuit. The timing is indicated by the telemetry word number given on the block diagram. Two word times are allowed between each counting period for read-out of the telemetry register. The OR circuits which combine all outputs onto one line are simply diode OR's and an emitter follower.

4.3.4.4 *System Response to Closely Spaced Pulses.* The handling of closely spaced pulses by the analyzer and linear system is somewhat complicated. Pulses further apart than about 7 μsec are essentially independent, since the system will have had time to recover sufficiently between them. (The 7 μsec limitation occurs in the logic circuit.) A pulse that occurs between 7 μsec and about 2 μsec after another is reduced in amplitude by the "undershoot" of the first pulse in the linear system as shown in Fig. 19. (The 2-μsec time is the recovery time of the discriminator.) If the reduced second pulse falls in a different channel than the first pulse it will be counted, but if it falls in the same channel as the first pulse it will not count, since the logic unit has not recovered from counting the first pulse. Signals that occur from 2 μsec to 0.6 μsec after a first pulse are distorted by the first pulse and are counted if their amplitude is sufficiently higher than the first pulse to trigger a discriminator that was not triggered by the first pulse. These signals (2.0 μsec to 0.6 μscc) cannot trigger discriminators that were triggered by the first pulse, since they have not sufficiently recovered. Signals occurring closer together than 0.6 μsec are indistinguishable and are counted as a single pulse that is larger than either of them. These effects are not considered as serious limitations on the system's performance in its intended application.

4.3.5 *Log Ratemeter*

The radiation experiment telemetry register has a capacity of 14 bits (16,383 counts). Whenever the register has filled and input pulses are still entering, it returns to zero and continues to count. In a region of

high activity the register may "overflow" several times, leaving an uncertainty in the total count. A log ratemeter[27] is used on the most sensitive levels to determine how many times the register has filled; during normal periods it provides redundancy. This circuit, which produces an output voltage that increases approximately as the log of the input pulse rate from 1 to 100,000 pps, contains a blocking oscillator which is triggered by the output of the logic circuit. The oscillator completely discharges a bank of five capacitors, differing by factors of 20, each time it fires. Isolating diodes enable the capacitors to discharge simultaneously but charge individually through large identical series resistors. Charging currents for the capacitors are added and integrated to produce an analog output voltage. This voltage is coupled to an analog telemetry channel, which is read out just before the digital information from the level to which the ratemeter is connected. The output is the average of the logarithm of the counting rate, an important consideration in the case of rapidly varying random pulse rates. A typical plot of output voltage vs input rate is shown in Fig. 25.

4.3.6 *Detector Bias*

4.3.6.1 *100-volt Bias Supply.* The −100-v bias supply is basically a free-running blocking oscillator driving a transformer with a 10:1 tertiary winding. The resulting high voltage is rectified and RC-filtered

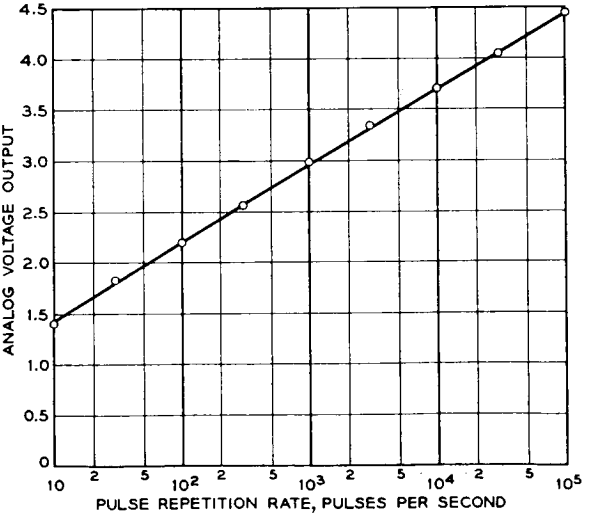

Fig. 25 — Ratemeter response.

in a conventional manner. However, the method by which load regulation is obtained is rather unique. DC feedback from a high-resistance divider on the output controls the oscillator repetition rate in proportion to the load by determining the charging time of a capacitor in the oscillator base circuit.

The detector load is nominally less than one microampere; load regulation is 0.1 per cent per microampere for loads up to 100 microamperes. Temperature stability is 0.05 per cent per degree centigrade.

4.3.6.2 *Tristable Multivibrator and Bias Switch.* The low-energy proton detector operates sequentially at three levels of bias. The tristable multivibrator circuit controls the position of the bias switch. A timing signal from the telemetry package switches the state of the tristable once each frame. The bias switch consists of transistor gates which turn off the −100-v bias supply and set the other levels of bias.

All three bias levels are monitored by an analog telemetry channel.

4.3.7 *Construction*

The detectors and their preamplifiers are mounted on the outer framework, with three of the four detectors protruding into space through holes in the satellite skin. The remainder of the radiation circuitry is located within the temperature-controlled electronics canister.

With the exception of the preamplifiers, the radiation electronics in the Telstar satellite are constructed in modules,[28] each represented by a square in the block diagram, Fig. 17. These modules consist of fiber glass epoxy circuit board wafers forming the top and bottom of a sandwich with components stacked like cordwood between them. Leads extend through a "mother board" on which all modules are mounted and interconnected. The entire subassembly is encapsulated in polyurethane foam, giving it good rigidity with little added weight. The radiation circuit is divided into two subassemblies to facilitate placement among the communications equipment complex within the canister.

V. PERFORMANCE IN SPACE

All parts of the radiation experiment have performed in space as expected and have provided a wealth of data, part of which will be described in a separate paper in this issue. The particle detectors, which are potentially susceptible to changes in their characteristics due to radiation surface effects,[21] have shown an internal consistency which indicates their continuing satisfactory operation after several months in space. This is true in spite of the higher radiation intensity encountered than

had been anticipated, and in spite of the often extensive periods of continuous bias under which the devices have been in operation, a condition which aggravates the radiation surface effects.

VI. ACKNOWLEDGMENTS

A large number of people have participated in an important way in this work. We wish in particular to acknowledge the contributions of: G. H. Wheatley, J. W. Rodgers, J. J. Darold and P. V. Chase in the development, production and testing of the particle detectors; W. M. Augustyniak in calibration of the detectors; B. H. McGahey in the development of the aspect and radiation damage solar cells; and D. J. D'Stefan, T. E. Davis, M. F. Slana, R. R. Blair and D. G. DeNure in the development and testing of the radiation damage transistors.

REFERENCES

1. Smith, K. D., Gummel, H. K., Bode, J. D., Cuttriss, D. B., Nielsen, R. J., and Rosenzweig, W., The Solar Cells and Their Mounting, B.S.T.J., this issue, Part 3.
2. Chapman, R. C., Jr., Critchlow, G. F., and Mann, H., The Telemetry and Command Systems, B.S.T.J., this issue, p. 1027.
3. Hutchison, P. T., and Swift, R. A., Results of *Telstar* Satellite Space Experiments, B.S.T.J., this issue, Part 2.
4. Brown, W. L., Gabbe, J. D., and Rosenzweig, W., Results of the *Telstar* Radiation Experiment, B.S.T.J., this issue, Part 2.
5. Gummel, H. K., and Smits, F. M., Testing of Solar Cells by Means of Spectral Analysis, Proc. of the Solar Working Group Conference, **2,** February 27, 28, 1962, pp. 3–17.
6. Loferski, J. J., and Rappaport, P., Radiation Damage in Ge and Si Detected by Carrier Lifetime Changes: Damage Thresholds, Phys. Rev., **111,** March, 1958, p. 432.
7. Easley, J. W., and Dooley, J. A., Fast Neutron Bombardment Reduction of Transistor Current Gain, J. Appl. Phys., **31,** June, 1960, p. 1024.
8. Freden, S. C., and White, R. S., Protons in the Earth's Magnetic Field, Phys. Rev. Letters, **3,** July 1, 1959, p. 9.
9. Van Allen, J. A., *Space Research,* Ed. H. K. Kallman Bijl, North Holland Publishing Co., Amsterdam, 1960, pp. 749–750.
10. Singer, S. F., Nuclear Explosions in Space, Nature, October 27, 1962, p. 301.
11. Brown, W. L., Introduction to Semiconductor Particle Detectors, I.R.E. Trans. Nuc. Sci., **NS-8,** 1961, pp. 2–10.
12. Blankenship, J. L., and Borkowski, C. J., Performance of Silicon Surface Barrier Detectors with Charge Sensitive Preamplifiers, I.R.E. Trans. Nuc. Sci., **NS-7,** 1960, p. 185.
13. Miller, G. L., Brown, W. L., Donovan, P. F., and MacIntosh, I. M., Silicon p-n Junction Particle Detectors, I.R.E. Trans. Nuc. Sci., **NS-7,** 1960, p. 185.
14. See I.R.E. Trans. Nuc. Sci., **NS-8,** January 1, 1961, and **NS-9,** June 1, 1962.
15. Pell, E. M., Ion Drift in an n-p Junction, J. Appl. Phys., **31,** February, 1960, pp. 291–302.
16. Monteith, L. K., M.S. thesis, Duke University, 1962.
17. McKenzie, J. M., and Ewan, G. T., Semiconductor Electron Detectors, I.R.E. Trans. Nuc. Sci. **NS-8,** 1961, pp. 50–53.
18. Buck, T. M., Proceedings of the Asheville Conference on Semiconductor Nuclear Particle Detectors, Dabbs, J. W. T., and Walter, F. J., Editors, NAS-NRC Pub. 871, 1961, p. 111.

19. Buck, T. M., and McKim, F. S., Effects of Certain Chemical Treatments and Ambient Atmospheres on Surface Properties of Silicon, J. Electrochem. Soc., **105,** December, 1958, pp. 709–714.
20. Buck, T. M., Wheatley, G. H., and Rodgers, J. W., to be published.
21. Peck, D. S., Blair, R. R., Brown, W. L., and Smits, F. M., Surface Effects of Radiation on Transistors, B.S.T.J., **42,** January, 1963, p. 95.
22. Elmore, W. C., and Sands, M., *Electronics*, McGraw-Hill, New York, 1949, pp. 241–249.
23. Chase, R. L., *Nuclear Pulse Spectrometry*, McGraw-Hill, New York, 1961, 22 pages.
24. Kelly, G. A., I.R.E. National Convention Record, Part 9, 1957, p. 63.
25. Goulding, F. S., Transistorized Radiation Monitors, I.R.E. Trans. Nuc. Sci., **NS-5,** 1958, pp. 38–43.
26. Wilkinson, D. H., Stable Ninety-Nine Channel Pulse Amplitude Analyzer for Slow Counting, Proc. Cambridge Phil. Soc., **46,** Part 3, 1950, p. 508.
27. Cooke-Yarborough, E. H., Counting-Rate Meter of High Accuracy, Proc. Inst. Elec. Engrs., London, 1951, p. 196.
28. Shennum, R. H., and Haury, P. T., A General Description of the *Telstar* Spacecraft, B.S.T.J., this issue, p. 801.

Page intentionally left blank

The Spacecraft Power Supply System

By D. C. BOMBERGER, D. FELDMAN, D. E. TRUCKSESS, S. J. BROLIN, and P. W. USSERY

(Manuscript received February 11, 1963)

The power supply system in the Telstar spacecraft consists of a solar cell plant to convert solar radiation to electrical energy when the satellite is illuminated by the sun, a 19-cell nickel-cadmium battery to store energy, and a regulation circuit to supply constant output voltages over a wide variation in input voltages. Additionally, the power supply system provides switching to conserve power and allow battery recharging during periods between communications experiments.

I. INTRODUCTION

The power supply system used in the Telstar spacecraft employs a solar cell plant which converts solar radiation to electrical energy when the satellite is illuminated by the sun. During periods of eclipse and/or peak power drain of transmission, reserve power is provided by a 19-cell, nickel-cadmium battery. To conserve power and allow battery recharging, continuous power is supplied only to those circuits in the satellite necessary for ground tracking and command. All others are turned off when not required.

1.1 *Characterization of Loads*

The electrical systems in the spacecraft are divided into three major parts:

(a) the communications repeater, which contains the microwave transmitter, microwave receiver and microwave beacon;

(b) the radiation damage and particle distribution experiment;

(c) the command receivers, telemetry system, and VHF beacon transmitter.

The microwave transmitter contains a traveling-wave tube, the only electron tube in the satellite. The power requirements for the traveling-wave tube total 15.8 watts.

A transistorized dc-to-dc high-voltage converter was designed to achieve the desired voltages. The single converter provides all the required TWT power. All subsystems employ solid-state devices as active circuit elements and operate at 16 volts.

The power requirements for the microwave receiver and beacon total 3.2 watts. Together with the microwave transmitter, the power requirements for the communications experiment amount to 19.0 watts.

The instrumentation for the radiation damage and particle distribution experiment requires approximately 0.3 watt. For reliability, two command receivers are employed, each requiring 1.0 watt; the 136-mc VHF beacon transmitter requires 1.8 watts. The VHF beacon transmitter and the command receivers are continuously powered and require a total of 3.8 watts. The telemetry system requires approximately 0.9 watt.

The programming of the systems by ground command results in a power drain profile having three major levels. The first is the continuous drain of the VHF beacon transmitter and command system. This totals 3.8 watts. A second level adds the telemetry and radiation experiments which may be commanded "on"; the second level brings the total to 5.0 watts. The third level adds the power requirements of the communication repeater, resulting in a maximum power demand of 24 watts distributed among the several subsystems. An experiment considered typical for any 24-hour period is shown in the power profile of Fig. 1. The power level shown includes the losses of the high-voltage converter for the TWT and of the main 16-volt regulator. The details of these circuits are covered in later sections of this paper.

1.2 *Power System Design Considerations*

In addition to the specific power requirements of the electronic loads described in the preceding section, there are several general requirements which must be met by the power system.

(*i*) *Temperature Range* — An objective of the spacecraft thermal design was to attain an electronic canister temperature as close to 70°F as possible, regardless of the satellite spin-axis orientation with regard to the sun, during full sunlight, during maximum eclipse and with an estimated decrease in solar plant power from an initial 14 watts to 7 watts after a two-year life. Normal temperature range for these conditions over a two-year period was calculated to be 32°F to 70°F. Operational design limits of 15°F to 90°F were established for compo-

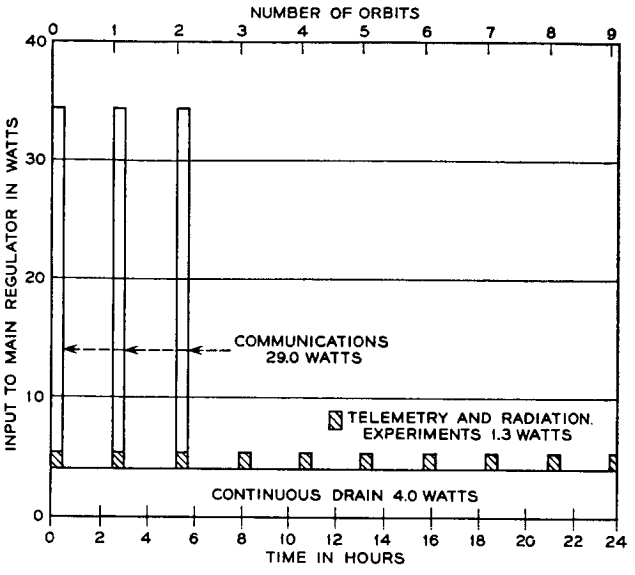

Fig. 1 — Power duty cycle referred to the input of the main regulator.

nents of the power system, and qualification tests include temperature checks at 0°F and 140°F.

(*ii*) *Efficiency and Weight* — Every effort was made to minimize the weight of the Telstar power system consistent with maintaining high power conversion efficiency, high reliability, and repeated operation in the radiation environment of the Van Allen belt. The battery and mounting weigh 11 pounds; the regulator and converter combined, including auxiliary control apparatus and wiring, weigh 7 pounds.

(*iii*) *Telemetry* — There are 30 channels of telemetry associated with the power system to provide information on its behavior. Battery voltage and temperature are monitored. The performance of the main regulator is assessed by monitoring various voltages and transistor case temperatures. The dc-to-dc converter is monitored by telemetering the heater voltage and collector current along with the helix and accelerator currents; in addition, the case temperature of switching transistors is monitored. Three channels are used to monitor the status of the relays associated with control sequence for commanding the TWT on. In addition, the current available from the solar cell plant is telemetered; this information, together with voltage measurements for the entire

nickel-cadmium storage battery, permits calculations of the available solar power to be readily made.

II. DESCRIPTION OF POWER SYSTEM

The Telstar power system employs silicon solar cells as the primary power source and a sealed nickel-cadmium storage battery which provides power for peak loads and for eclipse periods. An over-all block diagram is shown in Fig. 2. The number and arrangement of solar cells were designed to provide nearly constant power regardless of satellite attitude, at the value required to provide for the average power requirements of an orbit, including battery losses. The solar cell portion of the power system was designed to provide an initial power output of approximately 14 watts, which is sufficient to permit a flexible experimental program.

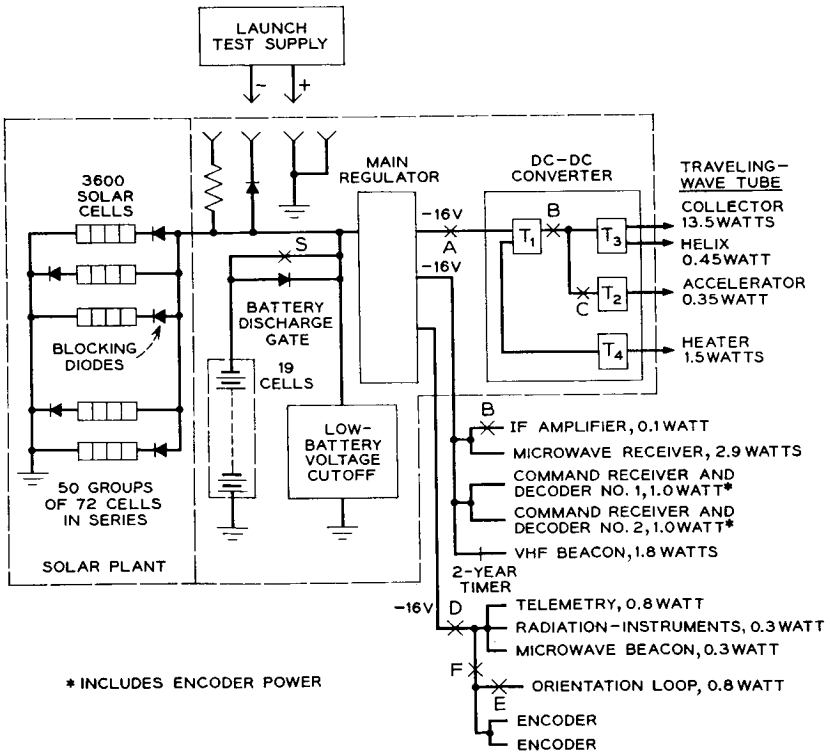

Fig. 2 — Block diagram of spacecraft power system.

The early objectives for the spacecraft included a minimum capability of 30 minutes per orbit for monitoring the telemetry and radiation experiments, with continuous use representing a desirable upper limit. An objective of at least 90 minutes per day was established for the communications experiments requiring operation of the TWT. The maximum duration of any single pass for which the spacecraft is usable to the Andover, Maine, station is approximately 60 minutes.

The objective of 90 minutes per day for communications experiments may be distributed among the visible orbits with the possibility of equal distribution in three consecutive orbits.

2.1 *Solar Power Requirements*

The solar power plant requirements were calculated by considering the continuous and peak power requirements of the electrical systems, the efficiency of the regulator and converter, the battery efficiency, the eclipse time per orbit, the duty cycle of the various intermittent loads, the orbital period, and total light time per day.

The following formula was developed to determine the required power from the solar cell plant:

$$P_S = (W_S/T_L) = [(W_L + kW_D)/T_L] \tag{1}$$

where W_S = energy supplied by the solar source in one periodic interval,
W_L = energy consumed in the load during the light periods,
W_D = energy consumed in the load during the eclipse periods,
k = ratio of the energy put into the battery during charging to the energy available from the charged battery, and
T_L = light period.

The energy efficiency factor, k, is a complicated function which depends on battery temperature, charge rate, depth of discharge, discharge rate, charge time, and cycle behavior. Laboratory data on commercial nickel-cadmium storage cells evaluated during the early stages of Telstar system development indicated that a typical charging efficiency for sealed nickel-cadmium cells, based on deep discharges and charge rates of $C/50$* to $C/20$ for complete recharge, was approximately 55 per cent. The value of k for a charging efficiency of 55 per cent was calculated to be 2.23. This value of k was employed in determining the required solar cell power output. During the short development period there

* C is the current which would flow out of the battery during discharge if the nominal capacity of the battery could be removed in one hour at constant current.

were a number of revisions in the power requirements of the several electrical systems, and a considerable amount of necessary interaction among the various development activities. The maximum required solar power was calculated to be 14 watts using (1) and maximum load and eclipse requirements. Current data on the specially developed nickel-cadmium cell indicate that an energy ratio factor k of approximately 1.5 can be achieved in the required temperature range, with charge rates of $C/40$ to $C/10$.

Telstar employs 3600 n-p silicon solar cells, made up into 50 groups of cells in parallel, each group containing 72 cells in series. A silicon diode is placed in series with each parallel string to prevent cells which are not illuminated by the sun from loading the illuminated cells and also to prevent the battery from discharging into the solar cell plant. The solar cell arrangement occupies approximately 35 per cent of the exterior surface of the spacecraft.

2.2 *The Storage Battery*

The storage battery contains 19 specially prepared sealed nickel-cadmium cells with a nominal capacity of 6 ampere-hours. Fig. 3 is a photograph of the cell, which is discussed in detail in a companion paper.[1] The 19-cell battery is mounted in the canister in 3 groups of 5 cells each and 1 group of 4 cells. Each cell is individually insulated from the canister with a thin polyethelene sleeve.

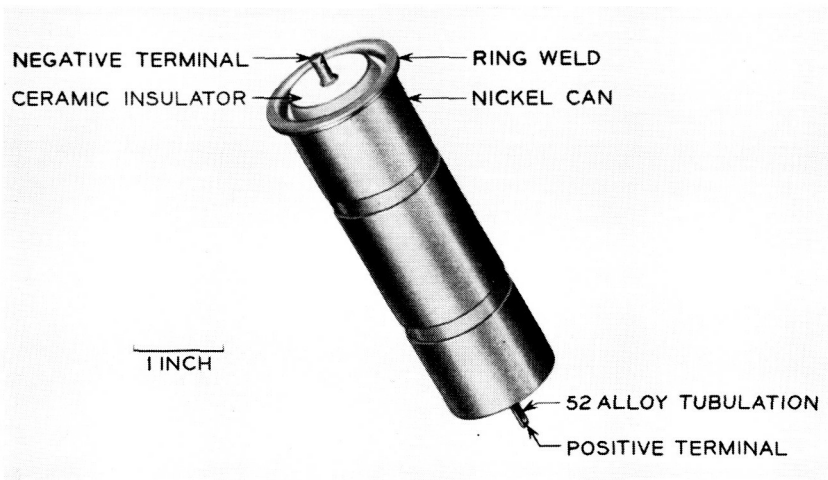

Fig. 3 — Nickel-cadmium cell for the spacecraft.

The battery is connected directly across the output of the solar cell plant through a diode normally bypassed by relay contacts. This diode circuit, called the "battery discharge gate," is described elsewhere in this paper. In this arrangement the maximum voltage of the solar power plant is 29.5 volts, which is the end-of-charge voltage of the 19-cell battery at the lowest expected temperature. The minimum voltage at the input to the main regulator is determined by the discharge voltage of the battery. The power system was designed to operate with a minimum voltage of 19.8 volts, based on 18 cells in the event of a short circuit of one cell.

2.3 *Main Regulator and dc-to-dc Converter*

The main regulator, shown in Fig. 2, provides a regulated voltage for the different loads from the varying battery voltage. A switching type series voltage regulator design was selected rather than quasi-linear series or shunt type regulators because of the higher efficiency that can be obtained with wide variations in battery voltage and load current. The main regulator provides three separate filtered outputs at nominally minus 16 volts. Separate filters are employed to reduce crosstalk between the command receivers, the radiation experiment and the switching transistor dc-to-dc converter. The efficiency of the regulator at maximum load is approximately 92 per cent.

The dc-to-dc high-voltage converter furnishes heater, anode, helix and collector voltages for the TWT, derived from the minus 16-volt supply. The converter is unregulated and its output regulation is governed by the changes in the minus 16-volt output of the main regulator and the load variations in the TWT. The over-all efficiency of the converter is approximately 70 per cent, including losses in the low-voltage command switching circuits. To conserve power, the converter is energized only during the communications experiment by sequential application of the TWT voltages by ground command.

The major items of the satellite power system are described in greater detail in the following sections, along with several auxiliary features.

III. NICKEL-CADMIUM STORAGE BATTERY

A sealed nickel-cadmium battery was selected for the spacecraft because this storage system is considered to be capable of

(a) accepting continuous overcharge during long periods of constant sunlight,

(b) displaying long cycle life under shallow depths of discharge and moderate life under deep discharges,

(c) being hermetically sealed, permitting long life in a space environment,

(d) operating in the temperature range of 15°F to 90°F, and

(e) providing nearly constant voltage during discharge.

3.1 *Battery Capacity*

Thermal calculations of the satellite chassis temperature indicated that the nominal battery temperature would be 70°F under conditions of initial available solar power of 14 watts and continuous sunlight. Data obtained with nickel-cadmium cells having a construction similar to those chosen for the power supply indicated that for a temperature of 70°F and a maximum cell voltage of 1.48 volts the overcharge current should not exceed $C/15$. Orbital predictions for the Telstar satellite indicated that early in life the satellite would be in continuous sunlight, under conditions of maximum available solar power, and would for long periods be operated with only the continuous power drain of the VHF beacon transmitter and command system. Under these conditions the charging power available to the battery would be approximately 10 watts, leading to a continuous charging current of approximately 0.36 ampere. To insure a safe continuous overcharge at this rate and a cell temperature of 70°F requires a cell having a nominal capacity of at least 5.4 ampere-hours. A smaller-capacity storage cell would require the addition of a battery charging current limiter.

In addition to the overcharge characteristics desired in the spacecraft battery because of long periods of continuous sunlight, consideration was necessarily given to the discharge capacity. Since the peak power required for a communications experiment exceeds the power available from the solar cells, the storage battery is subjected to many charge-discharge cycles during the satellite life. The battery is designed so that the peak load requirements can be met during at least three consecutive periods of longest eclipse. It is not feasible to completely recharge the battery during interim sunlight periods. Initially, 20 per cent was considered to be a safe maximum depth of discharge at the end of three peak eclipse time discharges. Each peak power drain represents a discharge of about 0.75 ampere-hour. Interim recharge is a function of the charge rate, cell temperature, and ampere-hour charge efficiency. For spacecraft nickel-cadmium cells the charge efficiency of partially discharged cells may range from 75 to 97 per cent. For the purpose of establishing a required cell capacity, the minimum recharge efficiency was used. Each charge interval between communications experiments returns approximately 0.5 ampere-hour; therefore at the end of the third consecu-

tive peak power drain, the capacity discharged from the battery is approximately 1.25 ampere-hours. Allowing this peak discharge to represent 20 per cent of the battery total capacity indicates that a 6.2-ampere-hour nominal capacity is required.

Consideration of the required continuous overcharge characteristics, along with the required discharge capacity, suggests that a battery having a nominal capacity of 6 ampere-hours is adequate for the spacecraft power system. Laboratory data on the power system performance obtained during the development program revealed satisfactory battery system behavior with maximum depths of discharge as high as 40 per cent when providing for frequent communication experiment usage during periods of greatest satellite visibility and maximum eclipse periods. Under these conditions, the battery may be discharged from a fully charged state during four consecutive orbits, with each discharge period equal to or greater than the maximum eclipse period. Fig. 4 illustrates the capacity removed from a fully charged storage battery as a result of the four consecutive peak power drains, three of which are

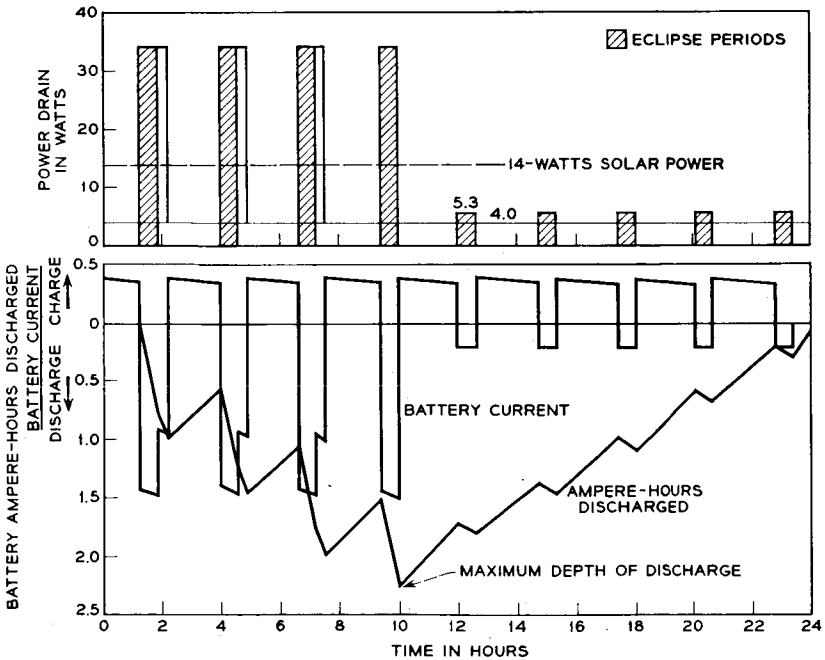

Fig. 4 — Battery charging and discharging, along with capacity removed from battery, during a typical 24-hour period.

for periods exceeding the maximum eclipse time. The maximum capacity removed is approximately 2.3 ampere-hours or 40 per cent of the available capacity of the battery, calculated on the basis of a charge efficiency of 75 per cent, a solar cell plant output of 14 watts, and illumination intervals and loads as shown in Fig. 4. This usage represents a large short-term discharge of the nickel-cadmium battery and requires that the sunlight periods during the balance of the day, approximately 11.5 hours in this illustration, be available for charging the battery to insure restoral of full battery capacity.

3.2 *Battery Energy Balance*

Analyzing the energy flow equations for the battery permits a flexible program involving communication experiments of varying duration. This analysis correlates the charging energy available from the solar cell plant, over any 24-hour period, with the energy requirements of the load. Thus, the power system designer can take into account different battery depths of discharge, reduced available solar cell power and different eclipse periods. Figs. 5 and 6 show the time allowable for com-

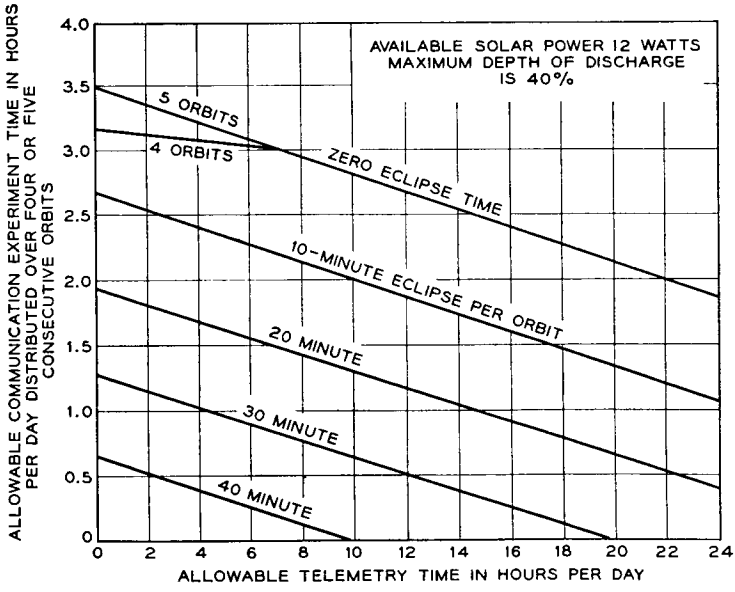

Fig. 5 — Allowable satellite utilization with communications experiments distributed over 4 or 5 consecutive orbits (solar power 12 watts).

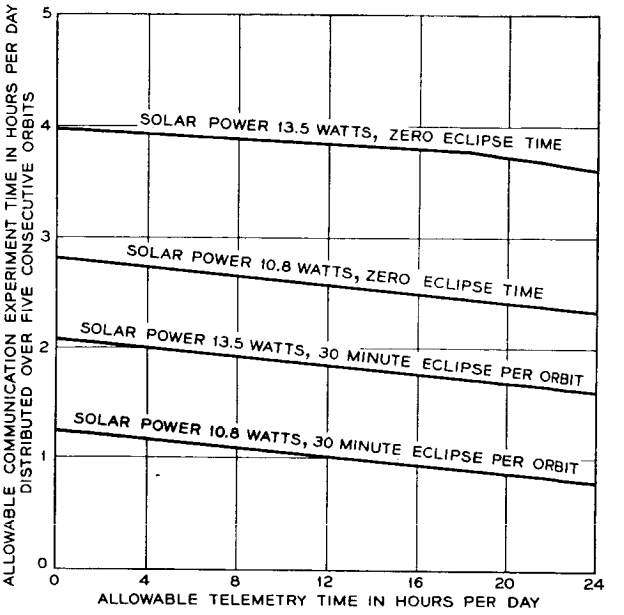

Fig. 6 — Allowable satellite utilization with communications experiments distributed over 5 consecutive orbits (variable solar power).

munication experiments as a function of the total time spent telemetering data to various ground stations. Families of such curves were developed for different values of available solar power, orbit eclipse time and battery depth of discharge, and for communication experiments distributed among 3, 4 and 5 consecutive orbits.

IV. MAIN REGULATOR

The principal function of the main regulator is to provide a regulated voltage with low ripple from the nickel-cadmium battery, whose voltage varies during the charge and discharge cycle. Fig. 7 is a photograph of the main regulator, packaged with a portion of the dc-to-dc converter. The main regulator is on the middle and bottom mounting boards of this package.

4.1 *Performance*

The main regulator supplies 16 volts ±0.17 per cent output, for loads varying between 0.2 and 2.0 amperes and an input voltage between 19.8

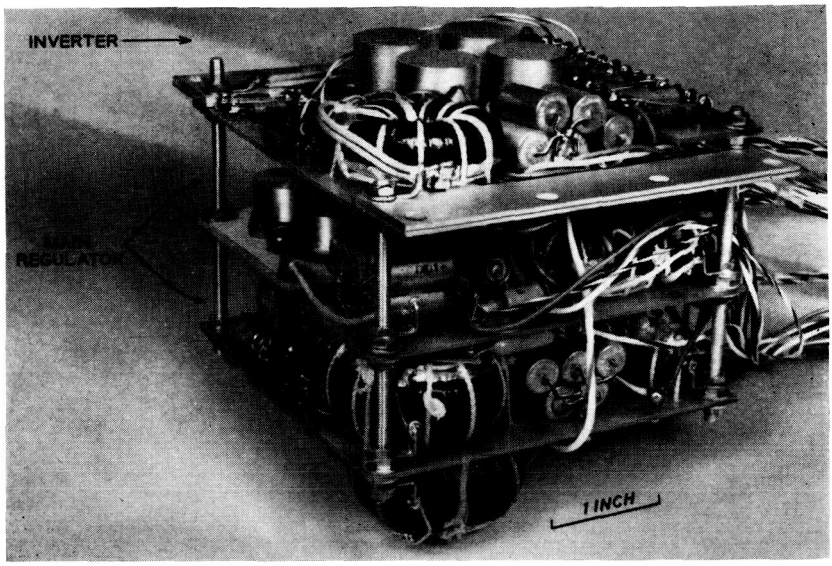

Fig. 7 — Main regulator assembly (unfoamed).

and 29.5 volts. The efficiency is approximately 92 per cent at maximum load and 85 per cent at minimum load.

Fig. 8 shows the basic performance characteristics of the regulator. Curves are drawn for conditions of minimum and maximum loading. The upper graph shows the output voltage vs input voltage; the flat portion is the region of regulation. The lower graph shows input current vs input voltage. The input current increases with input voltage until the minimum regulating voltage is reached. Then the input current falls off with increasing input voltage, since the regulator draws essentially constant power while regulating. Above the regulating range both the input current and output voltage increase with input voltage.

4.2 *Block Diagram of Main Regulator*

The block diagram of the main regulator is shown in Fig. 9. The dc input is "chopped" into a series of rectangular waves by means of a transistor switch. This switch is alternately a short circuit and an open circuit, dissipating relatively little power in either state.

The rectangular wave is imposed upon the main filter, a low-pass LC filter. The rectangular wave consists of alternate intervals of dc input voltage and ground; the main filter extracts the average of this

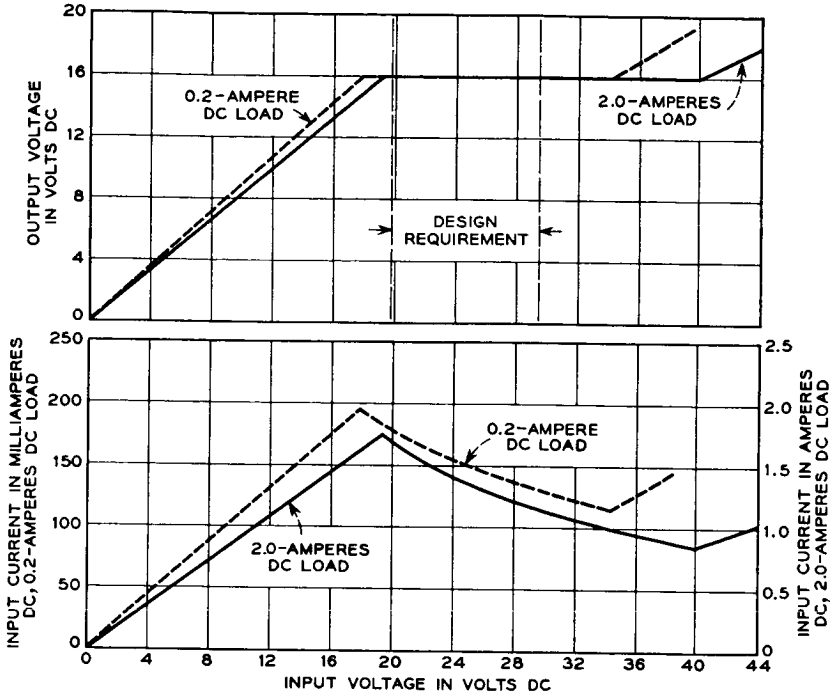

Fig. 8 — Main regulator nput-output characteristics.

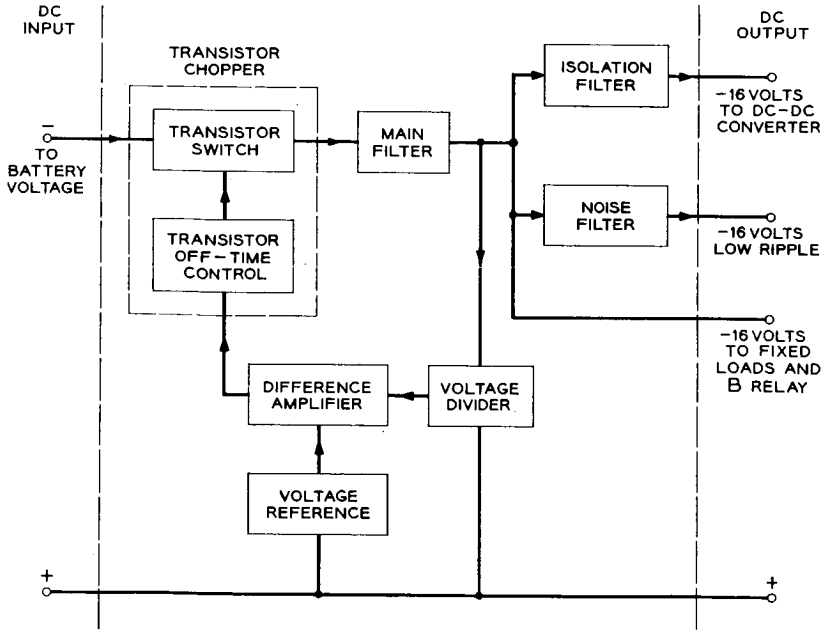

Fig. 9 — Block diagram of main regulator.

wave, which becomes the −16-volt output. Further filtering is provided by an isolation filter, which prevents interaction between the main regulator and the dc-to-dc converter. The noise filter provides an output whose fundamental component (at the main regulator frequency) is approximately 1 millivolt peak-to-peak.

The difference amplifier compares the output of the voltage divider, a fixed fraction of the output voltage (approximately 8.0 volts), with that of the voltage reference, a voltage regulator diode. If the output voltage goes above or below its correct value, an error signal is sent to transistor off-time control, which adjusts the off time, or time during which the transistor switch is an open circuit. This in turn controls the −16-volt dc output. The output voltage is thereby regulated by a closed feedback loop. The transistor switch and transistor off-time control can be considered as a single block, labeled "transistor chopper" in Fig. 9.

4.3 *Qualitative Discussion of Main Regulator*

4.3.1 *Design Approach*

Fig. 10 displays a simplified schematic of the transistor chopper. Transistor Q_1 is the switching power transistor, which alternates between cutoff and saturation to create rectangular waves. Since Q_1 regulates by

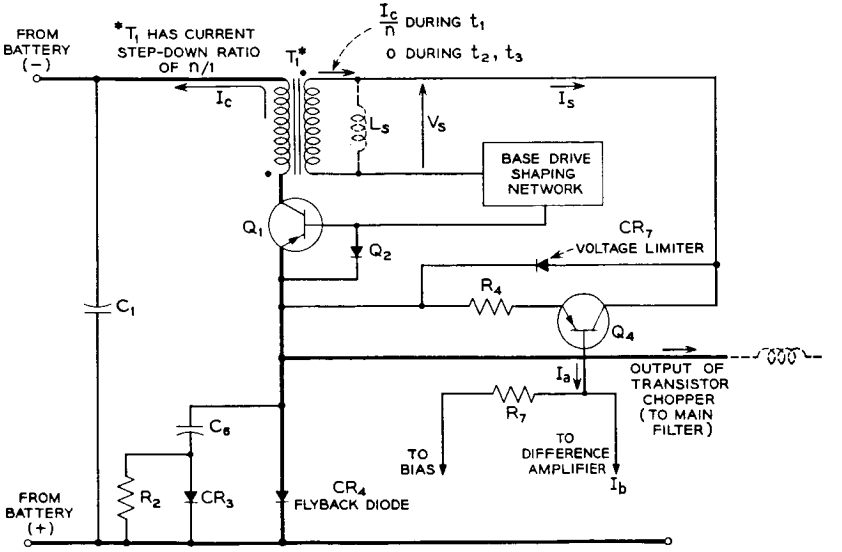

Fig. 10 — Simplified schematic main regulator of transistor chopper.

means of a switching mode, highly efficient regulation is possible. Given ideal components, a switching regulator can approach lossless regulation. This contrasts with the more familiar series or shunt type regulators where regulation is accomplished through a controlled dissipation of power.

While a switching regulator has the advantage of achieving high efficiency, it has the disadvantage of creating rectangular waves which must be filtered before application to the various loads. This filtering, to be efficient, is of the LC low-pass type and accounts for more than half the weight of the regulator. To minimize this weight it is desirable to switch at a relatively high frequency, where LC filtering is increasingly effective.

There are several practical limitations as to how high a frequency one can switch. First, there are the inevitable switching losses in transistor Q_1. While Q_1 dissipates little power in cutoff and saturation, the instantaneous power dissipated while switching from cutoff to saturation is high (roughly equal to one-half the input voltage multiplied by the load current, or 25 watts at 25 volts input and 2 amperes load), but the average loss is small because the switching times are very short compared to the over-all period. The power loss in Q_1 due to switching is approximately 0.5 watt. The switching frequency is approximately 20 kc at a 2-ampere load and 35 kc at a 0.2-ampere load.

The requirements for Q_1 were for a power transistor with fast rise and fall times and low saturation resistance (0.1 ohm). These requirements were met by an alloy-diffused germanium power transistor, a relatively recent semiconductor development. This type of transistor also proved to be less sensitive to proton bombardment than conventional germanium alloy power transistors.

The output of the transistor chopper feeds the inductor input filter (main filter). Diode CR_4, a flyback diode, maintains continuity of current in this inductor when Q_1 switches off. The network consisting of capacitor C_6, resistor R_2 and diode CR_3 improves the turn-off switching locus of transistor Q_1. Without this network, it would be necessary, on turn off, for Q_1 to block the entire input voltage, before CR_4 could start to conduct. However, with the network, C_6 charges up during the on time of Q_1 and can absorb current through C_6 and CR_3 as Q_1 starts to turn-off, without first requiring Q_1 to absorb the complete input voltage. Since C_6 charges and discharges every cycle, with power dissipated in R_2, it is obvious that losses in this network also increase with frequency.

Another source of frequency-dependent losses is the input inductor of the main filter. Here eddy current and hysteresis losses were minimized by the use of a powdered iron toroid.

Another frequency limitation besides losses is the storage time of transistor Q_1. While Q_1 has rise and fall times at least an order of magnitude shorter than those of a conventional germanium alloy transistor, its storage time is roughly equivalent (about 5 microseconds in a typical application). While the storage time does not appreciably affect efficiency, since Q_1 is saturated during this interval, it does affect frequency and the length of Q_1 on time, if it is allowed to become an appreciable percentage of the period. Since storage time is highly variable between transistors of the same code and also is reduced with time by proton radiation, it is desirable to have the circuit, rather than the storage time, predominate in controlling frequency.

Two other frequency limitations are the response times of transistor Q_4 and diode CR_4.

4.3.2 *Principle of Self-Excited Oscillations*

Transistor Q_1 in conjunction with current transformer T_1 forms a self-excited blocking oscillator. When Q_1 starts to turn on, the positive feedback polarity of T_1 causes current, I_s, to flow through CR_7 (forward biased), the emitter to base of Q_1 and the base drive shaping network, driving Q_1 further into saturation.

Inductor L_s represents the finite magnetizing inductance of the T_1 secondary. An ideal current transformer, of course, has infinite magnetizing inductance. The finite inductance of T_1 is deliberately controlled as a means of controlling the regulator switching frequency.

The waveforms of Fig. 11 relate the T_1 secondary voltage and current as a function of time and are idealized for simplicity. Assume Q_1 has just turned on. Then the current flowing out of the secondary of the "ideal" transformer is I_c/n, where I_c is the primary and transistor Q_1 collector current and n is the current stepdown turns ratio of T_1. Initially, L_s accepts no current and I_s, the "actual" transformer secondary current, is also I_c/n. This is displayed on the I_s waveform at $t = 0$. Since the idealized waveforms show a constant voltage, V_1, across T_1 secondary during the on time (t_1) of Q_1, then the current through L_s increases linearly with time, causing I_s to fall linearly with time. The total current out of the "ideal" secondary remains constant during t_1.

Since Q_1 has a large dc current gain (typically 150) over the load currents considered, it is reasonable to assume that I_s, which is also the base drive of Q_1, falls to zero before Q_1 switches off. At this time, the current through L_s is I_c/n, the entire "ideal" secondary current.

When Q_1 switches off, the "ideal" secondary current drops immediately from I_c/n to zero. At the same time, I_s reverses and initially becomes

$-I_c/n$ due to the demands of L_s. This current reverse biases Q_1 to maintain Q_1 in cutoff throughout the interval $t_2 + t_3$. Diode Q_2 bypasses the excess reverse current not needed to supply Q_1 reverse leakage currents.

Reverse current I_s passes through the parallel combination of CR_7 (reverse breakdown) direction and transistor Q_4. Resistor R_4 provides local negative feedback. At this point it is assumed that Q_4 acts as a current device, where collector current is independent of emitter-collector voltage. For a given value of I_s it is thus understood that either the base current to Q_4 is sufficient to saturate (zero voltage across Q_4) or the voltage across Q_4 is the breakdown voltage of limiter diode CR_7.

Referring once again to the waveforms of Fig. 11, t_2 is the interval during which limiter diode CR_7 conducts and t_3 is the interval during which Q_4 is saturated. The sum of t_2 and t_3 is the off time of Q_1. It will be noticed that T_1 secondary voltage, V_s, is much larger during t_2 (equal to $-V_2$) than during t_3 (equal to $-V_3$). As a consequence of this, I_s falls much more rapidly during t_2 than during t_3.

I_s is seen to fall rapidly till it reaches the value $-\beta I_a$, at which Q_4 saturates. β is the common-emitter current gain and I_a the base drive of transistor Q_4.

The off time of Q_1, and thus the dc output voltage, can be controlled

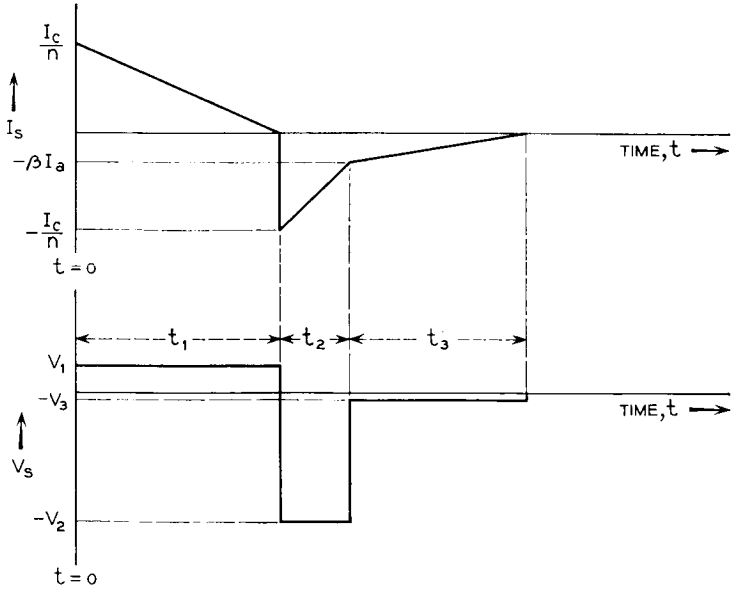

Fig. 11 — Waveforms of main regulator current transformer T_1.

by varying I_a . If I_a is zero, the reverse I_s will fall in the shortest possible time, minimizing the transistor Q_1 off time. If I_a equals $I_c/n\beta$, Q_4 will saturate as soon as Q_1 turns off, resulting in the longest possible off time. Regulation occurs only during the off time of Q_1 .

V. DC-TO-DC CONVERTER

The dc-to-dc converter furnishes high and low dc voltages for the TWT and a low dc voltage for the bias for the down converter. Important in the derivation of these voltages is the dc-to-ac inverter shown on Fig. 12; this inverter changes the −16-volt dc input voltage to an ac voltage which is applied to transformers. The secondaries of the transformers are applied to rectifiers and filters to obtain dc voltages. The converter is unregulated, and its output regulation is the sum of changes due to temperature and to load variations in the TWT. The over-all converter efficiency is approximately 71 per cent. A simplified diagram of the dc-to-dc converter is shown in Fig. 13.

To conserve power, the converter is energized only during the communications experiment. Command signals to the satellite to operate the traveling-wave tube and bias the down converter of the transmission equipment are accomplished by use of three magnetic-latching relays mounted in the power supply.[3] Relay A responds to the A command to the satellite, which causes the heater voltage to the TWT and the positive bias voltage for the down converter to be applied.[4] The B relay responds to the B command and causes the helix and collector voltages to be applied but no beam current to flow in the TWT when B relay is

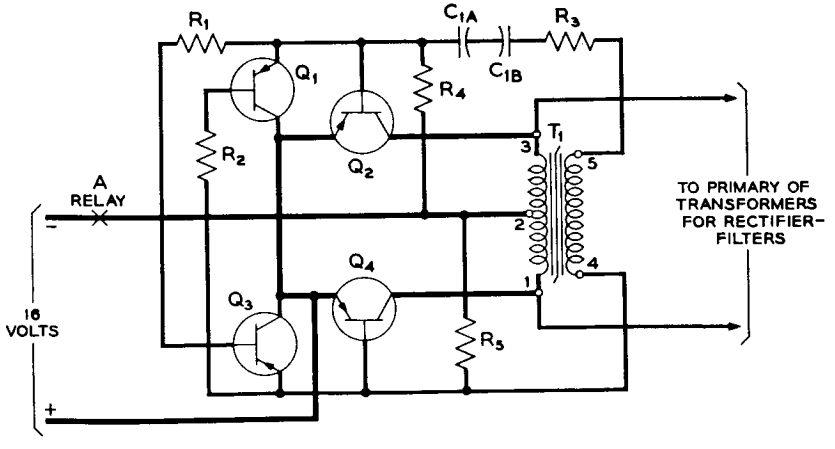

Fig. 12 — Schematic diagram of dc-to-ac inverter.

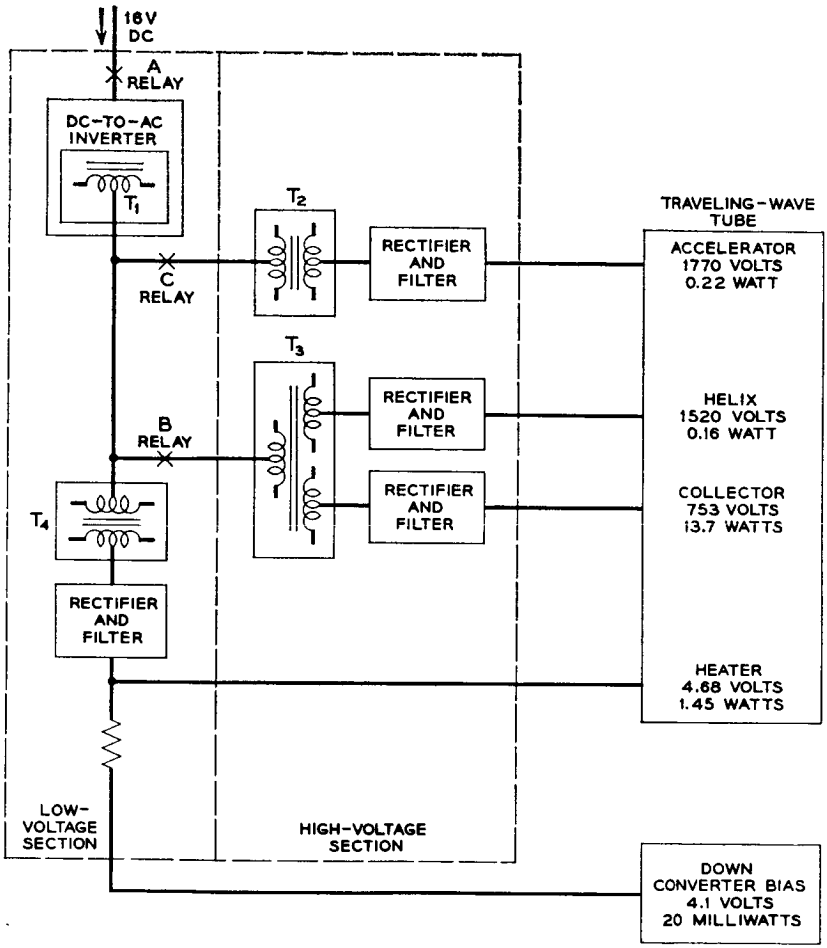

Fig. 13 — Block diagram of dc-to-dc converter.

closed. Beam current flows when the A, B and C relays are commanded on. This eliminates the possibility of other voltages being applied to the TWT prior to the heater voltage. After a minimum of three minutes warm-up time for the heater of the TWT, the C command to the satellite causes the accelerator voltage to be applied to the TWT. The CC command causes the accelerator voltage to be removed. The A and B relays respond to the AA command on turn-off. Switching in the low-voltage ac circuits provides a satisfactory means of effectively switching the high voltage to the TWT through the use of separate transformers for the helix-collector and accelerator rectifiers. The primaries of the transform-

ers are connected as required by the B and C relays to the dc-to-ac inverter. The inverter is operated from the −16-volt dc source by the A relay being commanded on.

5.1 *DC-to-AC Inverter*

A schematic diagram of the inverter is shown in Fig. 12. The inverter produces a square-wave ac voltage with a nominal frequency of 2.5 kc at full load. This frequency is selected to provide minimum transistor switching and transformer losses. Also, it is desirable that the switching frequency of the dc-to-ac inverter be separated from the switching frequency range of the −16-volt regulator. The dc-to-ac inverter, along with relays D, E and F, is mounted in the main regulator package. The D relay causes −16 volts to be applied to the converter for the TWT heater telemetry network in addition to applying −16 volts to other circuits in the satellite. Relay E is used to apply voltage to the orientation loop and relay F is used to switch operation of encoders 1 or 2.

A feedback winding on transformer T_1 (shown in Fig. 12) is provided to furnish the source voltage for the drive circuit of the "on" power transistor, Q_2 or Q_4. The simplified drive circuit shown in the schematic of Fig. 14 may be used to describe operation during the half-cycle that transistors Q_3 and Q_2 are conducting and transistors Q_1 and Q_4 are cut off.

The inverter-transformer saturates each half-cycle and transformer action ceases, so that the feedback voltage on the secondary winding collapses. This causes the "on" power transistor to fall out of saturation because of lack of base drive current necessary to maintain low emitter-to-collector voltage. Consequently, the voltage applied to the primary

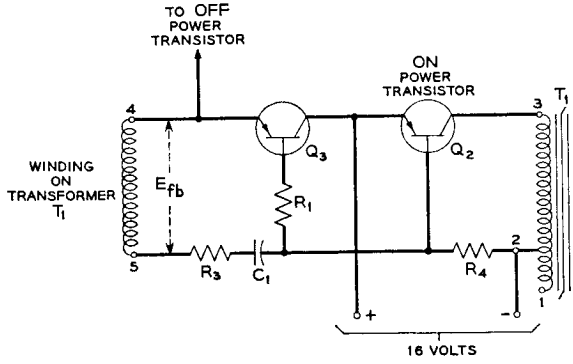

Fig. 14 — Simplified schematic of inverter drive circuit.

winding of transformer T_1 is reduced, causing a further reduction of feedback voltage. This action results in turning off the conducting transistor and turning on the transistor that has been cut off.

Since the power transistors require a finite time to turn off because of the storage time of the transistor, it is necessary to provide switching of the transistors so that at no time are transistors Q_2 or Q_4 conducting simultaneously. The collector current of the conducting transistor, Q_2 or Q_4, increases when transformer T_1 saturates because of the effective low impedance in the collector circuit. This increased current causes an increase of the power dissipation during switching of each half-cycle. To limit these losses and improve reliability, the base current of the power transistors is just sufficient to cause saturation at the time prior to turn-off but not large enough to cause excessive storage time. This is a value of base current determined for an expected degradation of gain due to aging and radiation damage. The base current is made large enough at the turn-on portion of the cycle to provide fast switching at each half-cycle, and the feedback is sufficient to initiate and maintain oscillation when the A, B, or C relays operate. The power transistor losses can be divided into three classifications: conduction, switching, and cutoff. The conduction losses are minimized by operating the power transistors in a saturated mode. The loss during switching is reduced by limiting the rise of collector current when the inverter-transformer saturates at the end of each conduction cycle. The drive circuit also provides negative base current to sweep out the minority carriers of the conducting transistor and reduce the transistor storage time. This helps prevent both power transistors from being on simultaneously, a condition which could result in catastrophic failure. Resistor R_4 provides initial base current to power transistor Q_2 when the A relay is commanded on. The magnitude of the base current is large enough to insure reliable starting of the inverter.

The base current for transister Q_2 (shown in Fig. 14) prior to switching is

$$i_{fb} = \frac{E_{fb} + (q_0/C_1)}{R_T} \exp - \frac{t_1}{R_T C_1}$$

where

E_{fb} = voltage of secondary winding on T_1

q_0 = charge on C_1 at time of switching

$t_1 = 1/2f$, where f is the switching frequency, and

R_T = effective resistance of driver circuit for "on" transistor Q_2.

Also

$$R_T \approx R_3 + \frac{R_1}{h_{FE} \text{ of } Q_3}.$$

The waveform of the drive current is shown in Fig. 15.

When the A command is sent to the satellite, the −16 volts is applied to the inverter input. Oscillation is initiated and the output of the rectifier-filter provides power for the heater of the TWT. At the instant

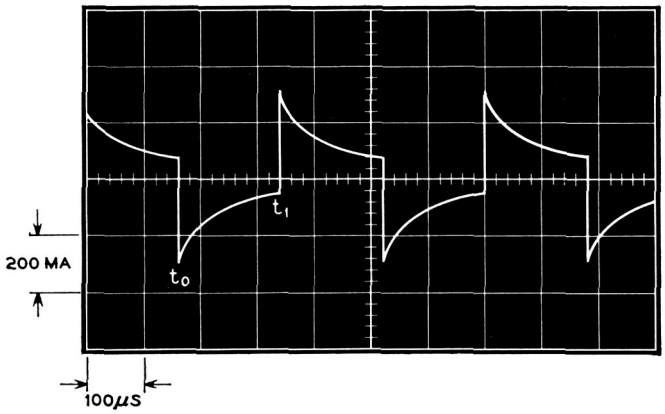

Fig. 15 — Waveform of inverter feedback current.

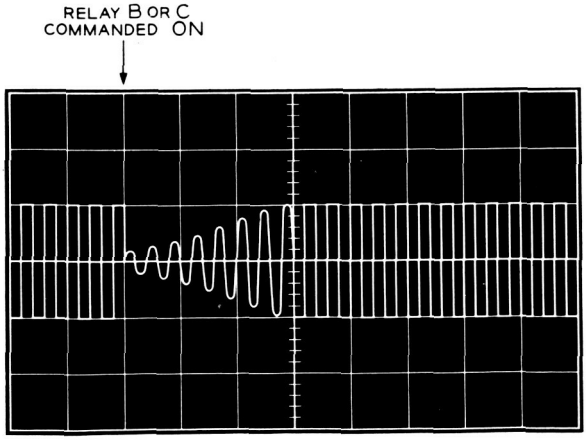

Fig. 16 — Inverter output voltage when relays B or C are commanded on.

the B and C relays operate, an effective short is placed on the output of the inverter due to the inrush current of the transformers connected when each relay operates. Also, the high-voltage capacitors in the rectifier-filter tend to draw large initial surge currents. To prevent excessive transistor collector power dissipation due to these transients, the drive circuit is designed to cause a gradual buildup to steady-state operation. Fig. 16 indicates the waveform produced on the output of the inverter when relay B or C is commanded on.

5.2 *Rectifier-Filter*

A photograph of the rectifier-filter section of the TWT power supply is shown in Fig. 17. Included in this unit are the telemetry networks for the heater voltage, collector, helix and accelerator currents.

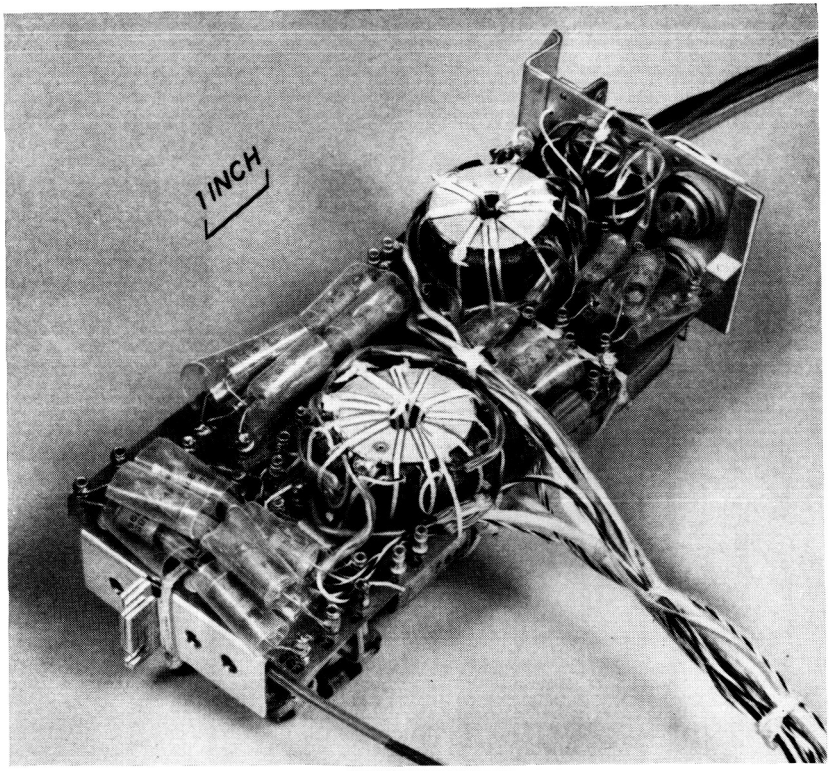

Fig. 17 — Traveling-wave tube power supply.

5.2.1 *Heater*

The square-wave ac voltage across the full primary of the inverter-transformer T_1 of Fig. 12 is applied to the primary of the heater-transformer, T_4, which provides bias and collector voltages for the transistorized synchronous rectifier Q_1 and Q_2 as shown in Fig. 18. The low voltage drop between the emitter and collector of the conducting transistor and

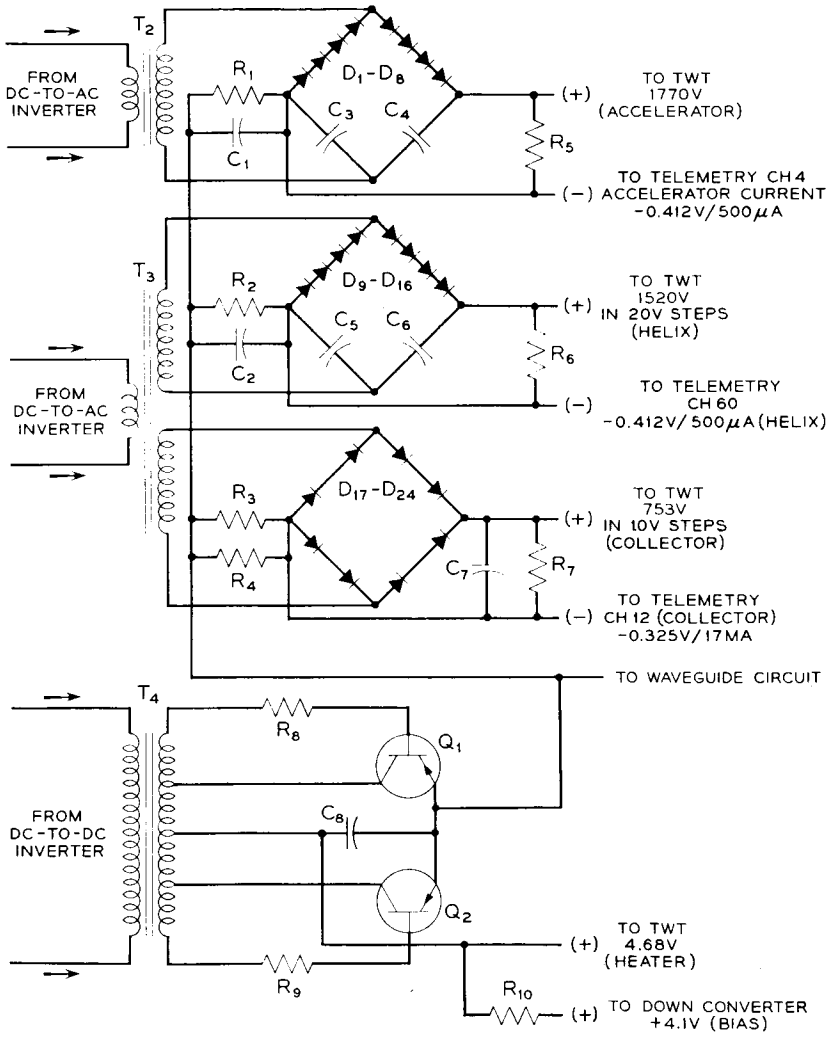

Fig. 18 — Schematic of traveling-wave tube power supply.

the small power necessary to maintain saturation affords an efficient means of obtaining dc for the heater of the TWT. Since the output is a rectified square-wave voltage, sufficient filtering is accomplished with only a capacitor filter.

5.2.2 *Helix-Collector*

Two separate secondary windings on transformer T_3 (shown in Fig. 18) provide helix and collector voltages for the TWT. One secondary winding is connected to a full-wave bridge rectifier and capacitor filter to obtain the dc voltage for the collector, and the other is connected to a voltage doubler rectifier-filter to obtain the dc voltage for the helix. A bleeder resistance across the collector output is provided to discharge the capacitor. Also, the bleeder in the helix rectifier prevents a rise of voltage at very low helix currents of 20 to 40 microamperes.

5.2.3 *Accelerator*

A separate transformer with one secondary is used to furnish high voltage for the voltage doubler rectifier-filter to obtain the dc voltage for the accelerator of the TWT. It is necessary to use a bleeder resistor to discharge the capacitors of the voltage doubler to prevent damage to the TWT.

5.3 *Performance*

5.3.1 *Heater* (A *Command On*)

Since the TWT heater resistance, when cold, is estimated to be approximately one-sixth the hot or steady-state resistance, there is a tendency for the heater to draw large initial current. Operational tests indicate that several cycles of the dc-to-ac inverter are required for the heater voltage to build up to full output. Steady-state operating temperature of the TWT heater is reached in approximately three minutes. The heater voltage is approximately 4.5 per cent higher with only the heater on than when the A, B, and C relays are on. This is due to the light load on the converter until there is TWT beam current. The slight over-voltage helps the TWT tube heater to stabilize in the three-minute warmup period.

5.3.2 *Heater, Collector and Helix* (A *and* B *Commands On*)

Since no beam current exists until the accelerator voltage is applied, there is a tendency for high voltage to be produced on the collector and

helix outputs during the time before the accelerator voltage is applied to the tube. A fixed minimum resistance load in the power supply reduces the rise of voltage on the collector of the TWT to less than 1150 volts, which is the maximum safe voltage for the filter-capacitor, transformer and TWT.

5.3.3 *Heater, Collector, Helix and Accelerator* (A, B, *and* C *Commands On*)

With the C relay on, there exists collector current of approximately 18 milliamperes, helix current between 20 and 50 microamperes with no RF drive to the TWT and 100 to 300 microamperes with RF drive, and an accelerator current between 100 and 150 microamperes. This current may build up to 500 microamperes after a year of operation in space. The most critical voltage on the TWT is the helix voltage. The regulation of this voltage is improved by designing the collector-helix transformer to have minimum leakage reactance on the helix winding of the transformer.

The power supply and TWT of each satellite are tested together prior to installation in the canister of the satellite. The final voltage and currents for optimum performance of the TWT are determined by observing the variation of RF output of the TWT when different voltage taps are selected on the transformers of the converter. The 16-volt dc input to the inverter is varied ±3 per cent, and taps are selected which give the smallest variation of RF output with the change of voltage to the TWT.

Measurements on the power supply and TWT of the spacecraft are given in Table I.

The total output power of the converter when the TWT is on is 15.48 watts. The input power is 21.8 watts. The efficiency is 71 per cent. The input current to the dc-to-ac inverter is 1.36 amperes. The bias voltage

TABLE I—MEASUREMENTS OF POWER SUPPLY AND TWT OF SPACECRAFT

Command	Item Measured	Volts	Current	Ripple
A only	heater	4.89	322 ma	
A + B	heater	4.850	320 ma	
	collector	1035	0	
	helix	1710	0	
A + B + C	heater	4.68	310 ma	135 mv
	collector	753	18.1 ma	310 mv
	helix	1520	110 μa	800 mv
	accelerator	1770	125 μa	600 mv
	down-converter bias	4.1	4.8 ma	

for the down converter is derived from the same rectifier-filter used to supply the heater voltage.

5.4 *Operational Tests*

The dc-to-ac inverter is combined with the −16-volt regulator to form a subassembly, and tests are made with the rectifier-filter section of the converter. The two units are foamed and then temperature cycled. The two subassemblies are soaked at −22°F and +140°F for six hours at each temperature. An operational temperature run is performed between +15°F and +105°F.

The −16 volts is operated continuously during the vibration test, and the states of relays A, B, C, and D are monitored. A change of state of the relays would have indicated that the TWT could have come on during launch.

Temperature cycling of the power supply in the canister includes soaking at 0°F and +125°F, and operation between +25°F and +90°F. During shake and environmental tests at Whippany[5] and extended transmission tests at the Murray Hill Laboratories, data from the power supply telemetry channels are evaluated to confirm that the power supply is performing satisfactorily.

VI. CONSTRUCTION FEATURES

Design and construction changes during the development period included the placement of aluminum caps on the transistors of the main regulator and inverter to reduce the effect of radiation damage. Separation of the high and low potential terminal posts gave greater assurance that corona would not occur.

VII. AUXILIARY FEATURES

7.1 *Two-Year Timer*

It was required that two years after spacecraft launching the VHF beacon of the satellite be irrevocably turned off to clear the radio channel; this is to be done by a timer which operates from an independent source of power. The timer consists of a tuning fork mechanically coupled to a gear train and switch to disconnect power to the VHF beacon transmitter. The oscillation of the tuning fork is maintained by means of a 360-cycle transistor oscillator driven by a battery. The power source is a single primary mercury cell with sufficient ampere-hour capacity to supply the current for 18,000 hours.

7.2 *Battery Discharge Gate*

There was need for a means to control remotely the discharge of the Ni-Cd battery by removing the loads after sealing the canister prior to launching. This switch must not prevent the charging of the battery by the solar cell plant. To perform this switching function a silicon diode, used as a gate, was connected in series with the battery. The diode was connected, as shown in Fig. 2, with its polarity in a direction to allow the solar cell plant to charge the battery, with the loss of its forward drop of approximately one volt. When load is to be supplied from the battery, the contacts of the S relay short out the diode. The S relay is operated under control of the command receiver in the satellite or by means of the low-voltage cutoff circuit.[3]

Before launching, the S relay is open and the diode gate prevents discharge of the battery between tests and during shipment. After launching, if it is determined from telemetered data that the battery is excessively discharged due to long periods of transmission, or due to low solar cell output voltage which could occur during extended periods of polar illumination of the satellite, the S relay can be opened to disconnect the load from the battery. The command receiver will operate with power from the solar cell plant, through the main regulator, making it possible to command the S relay to close, shorting the diode gate.

7.3 *Pre-Launch Test and Auxiliary Power Supply*

During the testing period of the satellite on the ground and during the launching period, the solar cells are not illuminated, so that an auxiliary source of power is required. A passive ferroresonant regulating circuit was used to eliminate the effects of input ac line voltage variations and limit the charging current to the maximum safe value for the nickel-cadmium battery.

VIII. PERFORMANCE

The performance of the Telstar power system has agreed very closely with the design objectives. Voltage requirements of all active elements of the satellite have been met, as evidenced both by the results of measurements before launch and by telemetry data after launch. The main regulator has successfully adjusted for a wide range of input voltage, as shown in Fig. 19. This figure presents the battery voltage time history for three different satellite passes within range of the Andover ground station.

The voltage behavior for orbit 414 is typical of an orbit in full sun-

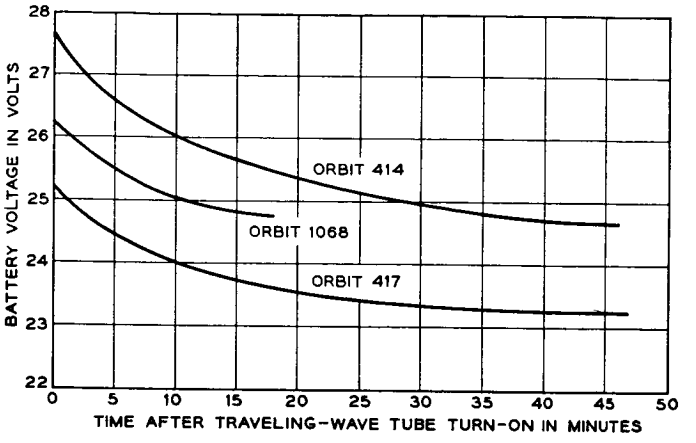

Fig. 19 — Input voltage to main regulator.

light with the battery fully charged at the beginning of the orbit; the communications experiment was in operation for nearly 50 minutes. A similar communications experiment was performed during orbits 415, 416 and 417. The voltage record for orbit 417, shown in Fig. 19, shows a substantially lower initial value as a result of battery discharge; at the end of orbit 417 the battery had been discharged to 60 per cent of its capacity.

The voltage data for orbit 1068 show a low initial voltage despite the fact that the battery was fully charged initially, for the reason that the satellite was in eclipse for the first 10 minutes of the orbit.

The state of charge of the battery has been monitored carefully through detailed histories of charge and discharge currents. These histories take into account actual solar plant current and actual load currents as reflected in telemetry data. Satellite use has been programmed so that at no time has the battery been discharged below 60 per cent of capacity.

IX. ACKNOWLEDGMENTS

Acknowledgment is hereby made of the contributions of many members of the Power Systems Laboratory, too numerous to mention by name.

REFERENCES

1. Bomberger, D. C., and Moose, L. F., Nickel-Cadmium Cells for the Spacecraft Battery, B.S.T.J., this issue, Part 3.

2. Feldman, D., and Thomas, U. B., Current Status of Sealed Nickel-Cadmium Storage Cells, Proc. of 1962 A.I.E.E. Pacific Energy Conversion Conference.
3. Chapman, R. C., Jr., Critchlow, G. F., and Mann, H., Command and Telemetry Systems, B.S.T.J., this issue, p. 1027.
4. Davis, C. G., Hutchison, P. T., Witt, F. J., and Maunsell, H. I., The Spacecraft Communications Repeater, B.S.T.J., this issue, p. 831.
5. Delchamps, T. B., Jonasson, G. C., and Swift, R. A., The Spacecraft Test and Evaluation Program, B.S.T.J., this issue, p. 1007.

The Spacecraft Structure and Thermal Design Considerations

By P. HRYCAK, D. E. KOONTZ, C. MACCS, I. W. STAFFORD, B. A. UNGER, and A. M. WITTENBERG

(Manuscript received March 22, 1963)

This paper covers the general structural and thermal design considerations of the Telstar satellite. The basic objectives were to maintain the electronic components in a near room temperature environment and to protect the electronics package from high-frequency vibration excitation. These objectives were realized by dividing the satellite into two lumped masses, the shell and the centrally located electronics package, and by utilizing nylon lacing for support of the electronics package. The package was provided with an active temperature control, regulating radiative heat flow between the skin and the package. Results of on-the-ground experimental evaluation and of telemetry data are given.

I. INTRODUCTION

The general size and shape constraints for the Telstar satellite have been reviewed in a previous paper.[1] The present paper discusses the important features of the spacecraft structural and thermal design.

The function of the spacecraft structure is to support and isolate the electronic components from the shock and vibration loads due to launch, and to provide a geometry compatible with an isotropic solar cell power plant.[2]

Since a majority of the critical components used in the electronics package were designed to operate in a room temperature environment, a major objective of the thermal design was to provide a package temperature as close to room temperature as possible. This objective was to be maintained during a two-year life in orbit. Therefore, all orbital effects on the satellite temperature had to be considered: full sunlight, maximum eclipse orbit, seasonal variation of the solar constant, satellite orientation, and long-term effects on surface coatings exposed to ultraviolet light and other radiation effects. Another thermal objective

was that the solar cell power plant operate at as low a temperature as practicable, for maximum efficiency in the conversion of solar energy to electrical power.

These apparently contradictory objectives — warm package and cold skin — were met by compacting the electronics components in a central container referred to as the "electronics package," isolating them from conductive heat transfer to the skin, and providing an active temperature control which regulates the radiant heat transfer from the electronics package to the colder skin. The power from the solar plant, which is dissipated in the electronics package, provides the heat to keep the electronics near room temperature.

The over-all design concept of the Telstar spacecraft structure is depicted in Fig. 1. A "ball-within-a-ball" configuration is employed. Those portions of the outer shell not used for supporting the solar cell power plant are coated with plasma-sprayed aluminum oxide, to keep the satellite skin temperature at about 30°F for best efficiency of the solar cell power plant. The inner "ball" contains the electronics circuitry, which is hermetically sealed from the high vacuum of space. The nylon lacing minimizes thermal conduction from the warm package to the colder skin. To minimize temperature effects on the chassis when

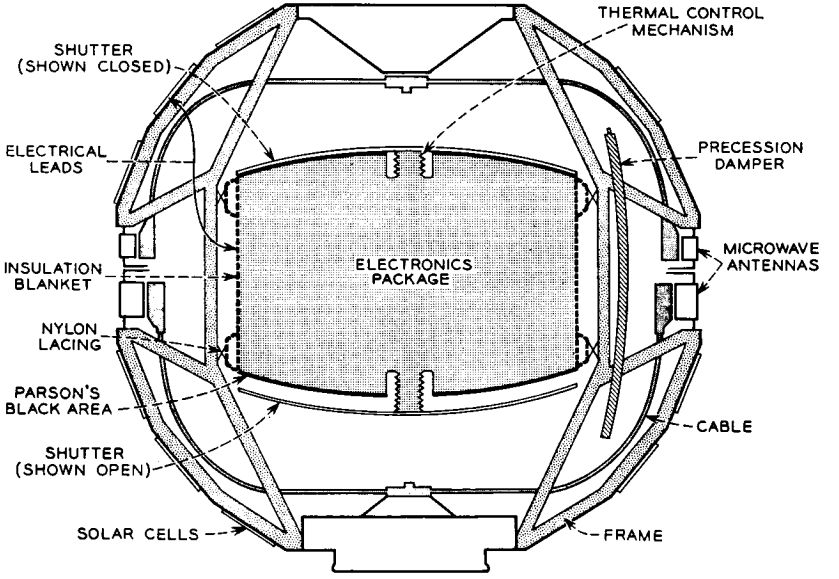

Fig. 1 — Sectional schematic of spacecraft.

the satellite is in either a fully sunlit orbital period or a maximum eclipse period, the radiative heat transfer between the insulated package and the satellite skin is varied by means of thermally actuated shutters. Fig. 2 shows the internal arrangement of the spacecraft parts.

The significant feature of the compact electronics package is that the critical components can be housed in a separate container and through suitable suspension be protected from the high-frequency vibration excitation due to launch. It seemed prudent to protect the electronics from high-frequency vibration excitation, since vibrational failure of electronic devices is most likely to occur in this frequency range. Nylon lacing which supports the electronics package provides both the high-frequency vibration and thermal conductive isolation. This arrangement required that the spacecraft structure support a lumped mass of about 85 pounds subjected to combined vibration and rocket thrust loading. During resonance of the electronics package in its nylon lacing support, the frame must support a combined loading of about 6000 pounds in the thrust direction.

The Telstar satellite is spin stabilized. In a geomagnetic field, its spin rate will be slowed down by induced eddy currents. For this reason, the

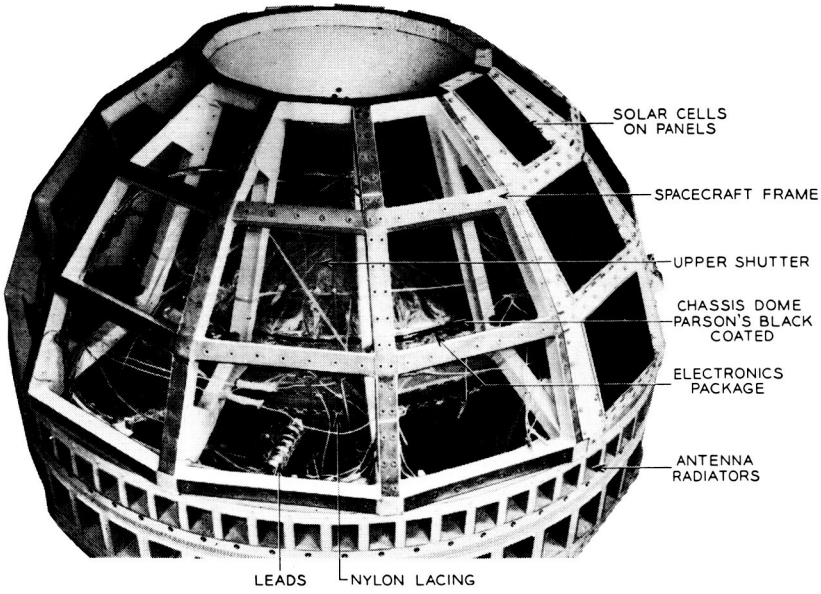

Fig. 2 — Side view of electronics package in spacecraft, showing upper shutter open.

shell is divided into two hemispheres, which are electrically insulated from each other.

Precession dampers are required to keep the satellite spinning about its principal axis of maximum moment of inertia, which is also the symmetry axis of the antenna. Disturbances which could cause a spinning satellite to have short-time precession (wobble) are electromagnetic torques, the uneven forces imparted by the spring during separation from the rocket, and collisions with meteoroids. Precession dampers quickly remove this wobble.[3]

II. SPACECRAFT CONSTRUCTION AND DESIGN

2.1 *Frame Construction and Design*

The frame of the Telstar satellite is the basic load carrying structure. It must support all other components, and it comprises 13 per cent of the total spacecraft weight of about 170 pounds. The frame provides support for the skin, which is roughly spherical in shape and has a nominal diameter of 34.5 inches. The frame is of an all-welded construction, fabricated from $\frac{3}{4}$-inch square ZK-21-A magnesium alloy tubing with a wall thickness of 0.025 inch. The frame is constructed in two parts, as shown in Fig. 3.

The sections of the frame are made of 12 truss assemblies, 30 degrees apart; the assemblies are joined by chordal members at their exterior

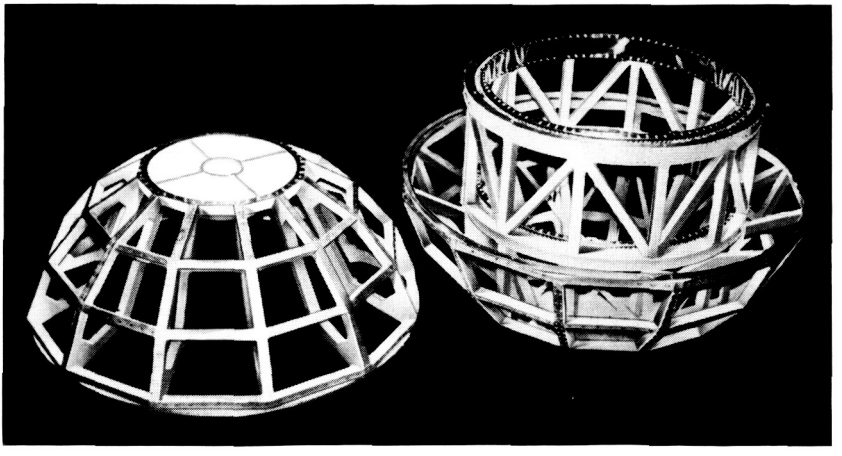

Fig. 3 — Spacecraft frame: upper half at left, lower half at right.

joints. The size of the facets, which is determined by the spacing of the truss assemblies, was selected to provide mounting surfaces of sufficient size for the solar cell modules.[2] One-half of the framework contains additional structural members, which form a cylindrical cage to support the 85-pound electronics package. The end rings of this cage are made from AZ-31-B-H24 magnesium alloy and contain radial holes with eyelet inserts for lacing the electronics package mounting rings to the frame. A machined AZ-31-B-H24 magnesium alloy plate, which is used to attach the spacecraft to the launch vehicle, is welded to this portion of the frame. In addition, several diagonal members are incorporated into this part of the framework to provide torsional and lateral rigidity.

Because of the mass of the electronics package, the combined sustained acceleration loading due to the thrust of the launch vehicle and the vibrational loading due to the first resonance of the electronics package had to be given special consideration in the frame design. The average (mean) stress in the frame members was limited to a value below the minimum guaranteed compressive yield stress of the ZK-21-A magnesium alloy tubing. The mean stress figure included an appropriate weld efficiency factor, which was determined experimentally. Sufficient rigidity was provided in the construction to minimize secondary bending stresses in the frame members. Limiting the average stresses in the frame members to values below the compressive yield stress of the ZK-21-A tubing and minimizing secondary bending stresses precluded any possibility of a frame collapse due to the combined loading. For the spacecraft, the allowable buckling stress for the frame members exceeded the compressive yield stress for the ZK-21-A tubing.

The hemispherical portions of the frame are electrically insulated from each other to limit the eddy current paths of the satellite. The frame halves are connected by insulated steel bolts, the only structural connection between the two portions of the frame. The 6-kilomegacycle antenna is supported by the upper half of the framework, and the 4-kilomegacycle antenna by the lower half of the framework. Except for internal wiring, these two antennas are dc-insulated from each other.[4]

The faceted surfaces formed by the truss and chordal members support the panels which form the skin on which the solar cell modules are mounted. The solar cell modules which compose the solar power plant are attached to these panels by beryllium copper tabs pulled through mounting slots in the panels and twisted to provide intimate contact of the modules to the panels.[2] The solar cell panels are attached to the frame by screws held in place by lockwashers.

2.2 *Solar Cell Panel Construction and Design*

Design objectives for the panels which support the solar cell modules were: (a) minimum weight consistent with structural rigidity requirements, (b) flat exterior panel surface to provide good contact with solar cell modules, and (c) thermal behavior of panels equivalent to that of thin, uniform sheets.

The panels, shown in Figs. 4 and 5, are of an integrally stiffened design. They are of brazed construction, fabricated from 6061-T6 aluminum alloy. Total weight of the panels, excluding modules, is 4 per cent of the satellite weight. The panels essentially consist of a cover sheet with so-called "hat" sections brazed on the inside face (i.e., face interior to the spacecraft) of the cover sheet. The hat sections have large holes which provide for radiant heat transfer by eliminating the effect of the additional reflective surface of the hat section. The brazed construction provides good thermal conduction throughout the panel.

The fundamental frequency of the solar cell panels with modules attached occurs at approximately 200 cps when the panels are screwed to the spacecraft frame. The panel design was a compromise between weight and fundamental frequency. From a structural standpoint, it would have been desirable to design for a resonant frequency above 2000 cps; however, the weight penalty would have been enormous even

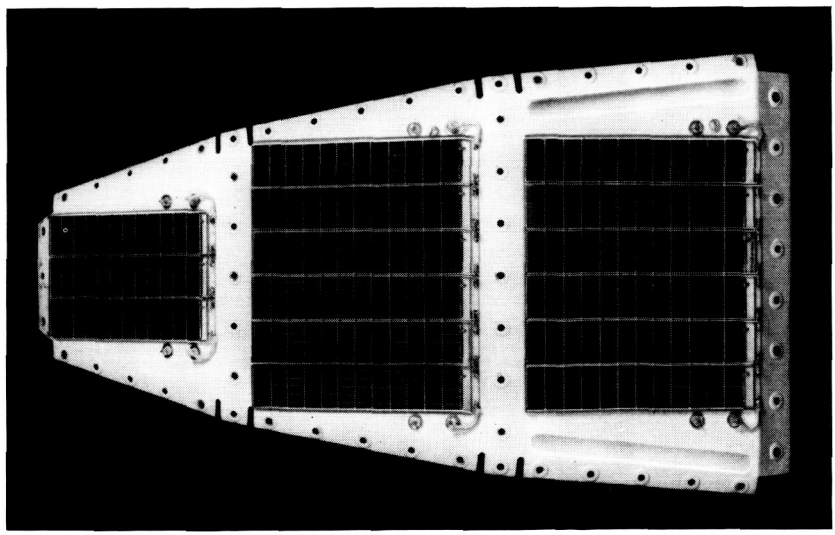

Fig. 4 — Front view of complete solar cell panel.

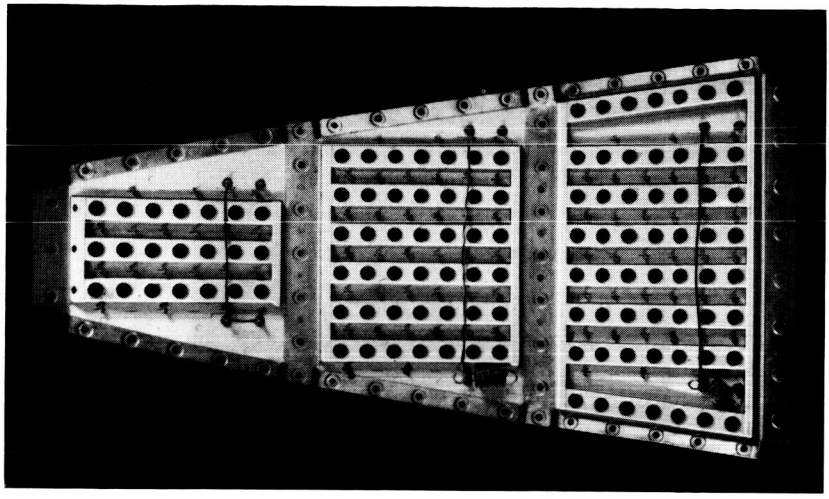

Fig. 5 — Rear view of solar cell panels, showing hat sections.

if such a design could have been achieved. The 200-cps resonance was selected to provide a minimum-weight design which also minimizes deflections of the panel during vibration to avoid damaging the solar cell modules.

Magnesium had been considered for the solar cell supporting panels, with the objective of achieving minimum weight. However, satisfactory brazing techniques were not available for magnesium, and welded construction would have been required. This in turn would have required thicker sections, and the magnesium panel would have weighed about 50 per cent more than the aluminum panel adopted.

2.3 *Insulation Support for the Electronics Package*

As mentioned previously, the electronics package is supported by nylon lacing to isolate the package from the high-frequency vibrations of launch and, for thermal reasons, to minimize conductive heat transfer to the skin. The spacecraft qualification test specification[5] suggests the desirability of placing the fundamental resonance of the electronics package below 50 cps; below this frequency, the g level applied to the base of the satellite is minimum (i.e., 0-to-2.3 g peak).

Braided nylon cord was selected for the electronics package lacing because its spring constant would place the fundamental frequency of the electronics package at approximately 42 cps, and yet would have

sufficient strength to support the package under combined loading due to sustained acceleration plus first resonance of the electronics package. Fig. 6 shows that the first resonance of the electronics package occurs at 40 cps; above 40 cps the package is essentially vibrationally isolated from the frame. A similar situation exists for the lateral direction, where the first resonance occurs at 15 cps. Techniques utilizing small spring balances were developed to control the pretensioning of the lacing; as a result, the fundamental frequency of the package was found to be reproducible within a few cps.

In addition to isolating the electronics package from high-frequency vibration, the lacing also supports the package under combined loading and behaves approximately as though it were a linear spring. In the direction of the thrust axis under combined loading, the nylon lacing must withstand a 4050-pound load. Individual braided nylon cord strands are subjected to a load of 32 pounds, which is well below the knot breaking strength of 60 pounds.

Extensive testing of nylon, Dacron, and fiber glass cords was performed to determine their structural characteristics in order to select the appropriate fiber cord with which to lace the electronics package. Load-deflection curves, ultimate strength (unknotted), knot breaking strength, and creep data were obtained for all fibers. The fiber glass cord was rejected for use because of its poor dynamic strength properties. In addition to other tests, the Dacron and nylon cords were subjected to temperature, humidity, high vacuum, and proton and electron radiation

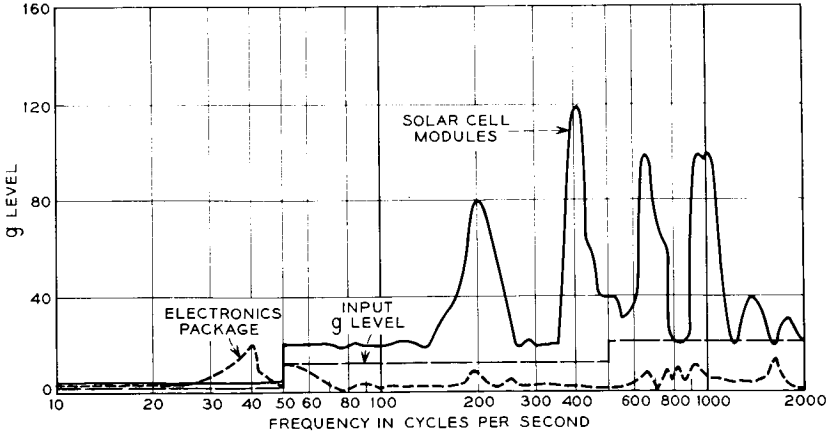

Fig. 6 — Response of electronics package and solar cell modules to sinusoidal vibration excitation in the thrust direction.

tests equivalent to two years in space. Although these tests indicated that there should be no problem with the nylon cord in high vacuum for the desired life of two years, reliability considerations dictated that several pieces of Dacron cord, which is a good deal more space stable than nylon, should also be used to completely insure support of the electronics package.

2.4 *Structural Design Testing*

The objective of the structural design testing program is to ensure that the complete spacecraft will meet the requirements of the qualification level tests.[5] It should be noted that the qualification level testing does not include the combined effects of sustained acceleration loading due to the thrust of the launch vehicle and vibrational loading due to the first resonance of the electronics package. Nevertheless, combined loading effects were simulated on an early test model. To meet these objectives, an extensive mechanical test program was instituted in August, 1961, to ensure that (a) the frame structure was capable of withstanding qualification level tests and combined loading, (b) the electronics package was protected from high level vibration excitation during launch, and (c) the spacecraft structure responses during vibration testing were known. The last item determines the appropriate testing levels which should be assigned to the parts connected directly to the satellite frame. Some of these parts are (a) solar cell modules, (b) precession dampers, (c) antenna feed structure, and (d) radiation experiments.

During this extensive structural evaluation program, two vibration test model spacecraft, a structural frame model and a mechanical development model, were used. In October, 1961, the first full-size test model was subjected to shock, centrifuge, and vibration qualification level tests. This model successfully passed the tests and provided the vibration spectrum that the spacecraft components associated with the shell would have to sustain. It also demonstrated that the nylon lacing performed its function of substantially isolating the electronics package from high-frequency vibration excitation. It should be observed that this frame withstood many hours of vibration testing at qualification level, in contrast to the few minutes encountered during launch.

Fig. 6 shows the vibration response of the electronics package and solar cell modules. The required input level to the spacecraft is shown by the heavy dashed line. The design objective of protecting the electronics components from high frequency levels has been substantially achieved. The 20-g level at one discrete frequency at approximately 40 cps is not

undesirable, because electronic components do not have resonances at such a low value. The solar cell modules are subjected to levels as high as 80 to 120 g at several narrow-frequency bands. Amplification factors of 5:1 to 10:1 result from frame resonances, and are to be expected in a structure which is as large as 3 feet in diameter. During resonance dwell tests, which are conducted at the third-stage rocket resonances of 550 to 650 cps, the solar cell modules reached levels as high as 200 g with a 42-g input to the base of the spacecraft.

Another series of vibration tests was performed, using a second vibration test model as a vehicle for the design testing of components which are attached to the frame. Many tests were conducted on the antenna feed structure and techniques were developed for securing their cables.[4] Tests were also performed to develop the best techniques for securing the many leads and cables connected between the electronics package and frame components. The leads are about 9 inches long, to minimize thermal conduction from the package to the skin.

As mentioned previously, qualification level tests in themselves do not supply absolute proof of the adequacy of the frame and lacing under possible combinations of sustained acceleration and vibration loading due to the first resonance of the electronics package. Static simulation of the possible modes of combined loading were performed on one of the first frames at Lehigh University, Bethlehem, Pennsylvania. The test setup is shown in Fig. 7. All loads were applied to a canister whose outline was similar to that of the electronics package. The canister was specially designed so that the vertical, lateral and torsional loads could be applied to the frame. The method of load application was a conservative approximation to the actual case. The three basic loading conditions, which were applied individually and in suitable combinations, are given in the Table I.

The deflection of the dummy electronics package was measured and strain gauge readings of the various frame members taken. The recorded strains and the stresses calculated therefrom show that the basic spacecraft frame has a margin of safety of 46 per cent for the static loads applied, where due consideration of weld efficiency has been taken into account. The actual margin of safety is somewhat less than 46 per cent, because the static test performed does not completely simulate the fatigue effects of combined vibration and thrust loading. With the present state of the art, this type of test is not possible. Nevertheless, the extensive vibration tests which were conducted on the other models, coupled with the static test, left little room for doubt that the frame is capable of withstanding the actual launch conditions.

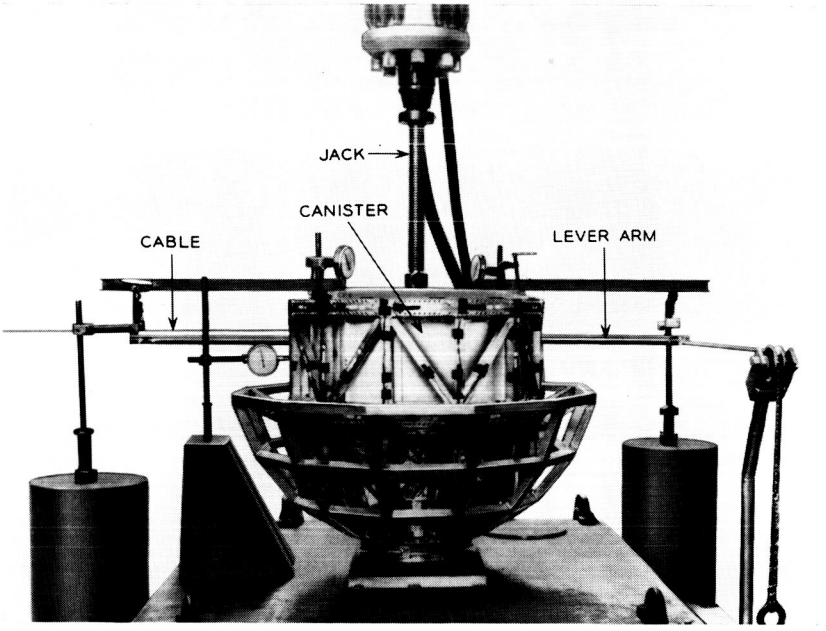

Fig. 7 — Spacecraft static test setup.

TABLE I

Direction of Loading	Due to Sustained Acceleration of 170-lb Satellite	Due to First Resonance of 90-lb Electronics Package	Total Maximum Load
Thrust axis	(25 g) (170 lb) = 4250 lb	(20 g) (90 lb) = 1800 lb	(4250 lb + 1800 lb) = 6050 lb
Transverse (lateral) axis	(2.25 g) (170 lb) = 382 lb	(6 g) (90 lb) = 540 lb	(382 lb + 540 lb) = 922 lb

Direction of Loading	Maximum Torque due to Spin-Up	Residual Torque at End of Spin-Up
Torsional moment about spin axis due to flexibility of electronics package mounting	3000 in-lbs	1500 in-lbs

Note: In the thrust direction, the 25-g sustained acceleration is from the rocket thrust and the 20-g vibration acceleration is the level imparted to the package during its resonance. In the transverse direction, the accelerations were determined on a similar basis.

The apparent weight of the satellite along the thrust axis in the 550 to 650-cps frequency range was determined so as to establish the necessary vibration level to be applied in the simulation of the combustion resonance dwell test.[5] Since the apparent spacecraft weight was of the order of 7 pounds, the combustion test should have been conducted at an 86-g input level over the 550- to 650-cps band. However, vibration equipment was not available to conduct the tests at this high level. Development model spacecraft were tested at a 75-g input level over the required frequency band. As a result of these high-level tests, minor modifications were made to the method of attaching the solar cell modules to the panels and to the interconnections between them. These tests also reconfirmed the adequacy of the spacecraft frame and were useful in proving in many of the components attached to the spacecraft shell structure. Details on qualification tests on the final model are given in Ref. 5.

In December, 1961, a mechanical development model spacecraft, complete except for the electronics package, was subjected to all mechanical tests at qualification level. A dummy weighted canister was used instead of the actual electronics package. This model successfully passed all development tests without failure. In subsequent testing, this model was subjected to the equivalent of four complete qualification-level vibration tests without any failure of any component part.

III. THERMAL DESIGN OF THE SPACECRAFT*

3.1 *Requirements and Design Approach*

The introductory section of this paper outlined the two major thermal design objectives for the Telstar satellite: to provide an environment for the electronics components as close to 70°F as possible, and to maintain the solar cell power plant at as low a temperature as practical. This section of the paper covers the spacecraft thermal design in greater detail.

The temperature of the electronics package shell is used as a reference point to describe the environment for the electronic components. This reference point, of course, is not at the actual temperature of the components themselves. In the design of the electronics package, high-conduction paths were provided to minimize temperature differentials between the components and the package wall. Detailed studies of operating tem-

* Two comprehensive reports on the Telstar satellite thermal design and analysis, including the results of space simulation tests, were submitted to NASA in March and May, 1962. Substantially all of the thermal information reported upon in this paper was included in the foregoing reports.

peratures of internal components provided temperature limits of 15°F to 90°F on the package wall to assure satisfactory operation of the electronics circuitry.[1] Nevertheless, a 70°F objective for the package wall temperature was established, since practically all component life test data were obtained at room temperature.

A knowledge of the temperature distribution over the surface of the satellite was required to determine the power available from the solar cell plant and to establish temperature extremes to which the components attached to the skin would be subjected. These temperature ranges had to be determined in relation to the extremes of the satellite thermal environment.

The thermal and long-life requirements made a good portion of the practical experience gained with other artificial satellites not directly applicable to the Telstar satellite,[6] and new concepts in the over-all thermal design had to be explored. In particular, thermal analysis disclosed that an active temperature control system was required to minimize temperature variations in the electronics package during a long lifetime in orbit. The control system chosen was unique in that it regulated only the radiative coupling between the package and the skin, while the temperature of the skin itself was to be controlled by passive means. In the early development stages, very little was known of this type of temperature control. Instead, detailed information on an active skin-temperature control, as originally proposed by Hanel[7] or by Acker,[8] was available.

3.2 *Thermal Radiation Environment of the Telstar Satellite*

There are two kinds of thermal radiation which affect Telstar's thermal design: the primary radiation coming directly from the sun and the secondary radiation. Secondary radiation intercepted by the satellite consists of albedo radiation and the earth's infrared radiation. Albedo is solar radiation reflected by the earth. Since energy can be gained or lost in the space environment only by radiation, the extremes of the total radiative heat input had to be determined as the starting point of the entire thermal design.

Direct solar radiation is the major contributor of incident energy, amounting to about 84 per cent of the energy received by the satellite when it is in a fully sunlit orbit. However, this energy may be reduced significantly when the satellite is in an eclipsed orbit. During a maximum 45-minute eclipse in the satellite orbit, the orbital average primary energy will be reduced to 70 per cent of its full sunlit value. In addition,

the direct solar radiation, which may be expressed in terms of the solar constant S, varies ± 3.3 per cent in the course of one year.

The significance of the reflected radiation would, in general, depend on the orientation of the satellite; only in the case of a spherical satellite with an isotropic surface are the effects of the orientation eliminated. Geometrically, the spacecraft was considered to be a sufficiently close approximation to a sphere with an isotropic surface. In addition, the reflected radiation would depend on the altitude of the satellite and its phase angle, defined as the angle between the line joining the sun and the center of the earth and that between the satellite and the earth's center. For a general elliptical orbit, both the altitude and the phase angle will vary with time. The situation is somewhat simpler with regard to the infrared radiation of the earth, which is to a first approximation dependent on the altitude only. The further details of the secondary radiation problem in its relation to spherical satellites have been outlined in a special study.[9]

3.3 *Thermal Model of Telstar Spacecraft and Its Environment*

In the following, as a thermal model, the satellite will be considered to consist of two lumped masses: M_S, with thermal capacitance C_S, corresponding to the skin; and M_P, with thermal capacitance C_P, corresponding to the electronics package of the satellite. Since the package is thermally insulated from the skin by means of a high conductive resistance, all heat transfer between M_S and M_P will have to take place by radiation. Then the package will be, in the steady state, essentially in radiative equilibrium with the skin. In particular, if the time constant of the package is long with respect to the orbital period, a sufficiently close approximation to the steady-state heat transfer will be realized at all times. In other words, the package will then be only very little thermally disturbed by short-term temperature fluctuations of the skin caused by an individual eclipse of the satellite, but will have to adapt itself to long-term orbital changes, i.e., drastic variations of the eclipse periods and seasonal variation in the solar constant.

The long time constant of the package is realized by its high heat capacity and by the application of a low-emissivity material over its surface. The use of the linear concept of a time constant with respect to the relations involving the fourth-power law of radiation is only a convenient approximation.

For a sufficiently uniform temperature prevailing within the package, the temperature extremes of the package will be based on the extremes of the heat radiation intercepted by the skin. This dependence may be

expressed in terms of a reference skin temperature, as discussed in Section 3.4. An expression for such a reference skin temperature, $\bar{T}_s$, is given by

$$\bar{T}_S = \left(\frac{S}{4\sigma}\right)^{\frac{1}{4}} \left[\frac{\bar{\alpha}}{\bar{\epsilon}}\left(1 - \frac{t_e}{t_o} + \bar{a}\bar{f}\right) + \tfrac{1}{4}\,(1 - \bar{a})\bar{g}\right]^{\frac{1}{4}} \tag{1}$$

where S is the solar constant, σ the Stefan-Boltzmann constant, $\bar{\alpha}$ the over-all value of solar absorptivity of the skin of the satellite, $\bar{\epsilon}$ the over-all value of the infrared emissivity of the satellite, t_e the eclipse time, t_o the orbital period, $\bar{a}$ the mean value of the earth's albedo, $\bar{f}$ the mean integral value of the albedo, and $\bar{g}$ the mean integral value of the earth's infrared radiation. Equation (1) is derived from the consideration that the orbital mean average temperature of the skin of the satellite, $\bar{T}_S$, can be determined from a balance between the total heat energy absorbed over one orbit and the energy emitted by the satellite during the same orbit, according to the Stefan-Boltzmann law. This equation applies for an isotropic sphere and represents the effective radiation temperature of the skin; for the important special case of two lumped masses, M_S and M_P, it may be used to obtain a convenient reference temperature for the instrument package, as will be shown below.

For an elliptical orbit, the speed of the satellite varies according to Kepler's law, which states that equal areas are swept out in equal times by the radius vector. Therefore, in getting the values of $\bar{f}$ and $\bar{g}$, time must be taken as the weighting factor. The integration itself is best carried out numerically.

To get the upper limit for $\bar{T}_S$, one has to consider that, in general, the contribution due to the eclipse time t_e is relatively more important than that due to $\bar{f}$ and $\bar{g}$. Therefore, it is sufficiently accurate to calculate $\bar{f}$ and $\bar{g}$ for the case where $t_e = 0$ is combined with the largest possible albedo effect. This is the case when the satellite just grazes the earth's shadow at apogee.

Similarly, one can set the lower limit on $\bar{T}_S$ by considering in (1) the longest eclipse time t_e compatible with the given orbital configuration. These two temperature extremes $\bar{T}_{\max,S}$ and $\bar{T}_{\min,S}$ can, for a given orbit and $\bar{\alpha}/\bar{\epsilon}$, be conveniently expressed in terms of an equivalent solar constant S_{eq}

$$\bar{T}_S = \left(\frac{S_{\text{eq}}}{4\sigma}\,\frac{\bar{\alpha}}{\bar{\epsilon}}\right)^{\frac{1}{4}}. \tag{2}$$

For an orbit of 500 nm perigee and 3000 nm apogee, $\bar{T}_{\max,S}$ corresponds to $S_{\text{eq}} = 1.19\ S$, and $\bar{T}_{\min,S}$ to $S_{\text{eq}} = 0.917\ S$. A value of $\bar{\alpha}/\bar{\epsilon}$ of 0.65

was obtained from calculations based upon the individual surface properties of the skin exterior and was subsequently confirmed by space chamber measurements on several spacecraft models, as will be described later.

For a given S_{eq} and $\bar{\alpha}/\bar{\epsilon}$, the temperature $\bar{T}_S$ can be easily calculated from (2). If this temperature is reached (for example, in the space chamber), it means that the satellite has been exposed to the equivalent "full sunlight" or "maximum eclipse" corresponding to the maximum and the minimum values of S_{eq}, respectively. Thus experimental determination of temperature extremes of all internal components becomes a possibility.

3.4 *Thermal Design Considerations for Electronics Package*

The information on S_{eq} and the extremes of $\bar{T}_S$ may be used in the design of the electronics package in the following way: in the steady state, and in the absence of heat conduction to the skin, the package will assume the temperature $\bar{T}_P$ defined by the equation

$$Q_P = A_p h\sigma[\bar{T}_P^4 - \bar{T}_S^4] \tag{3}$$

where Q_P is the heat power developed in the package due to the operation of its electronic components and battery charging and h is the overall effective emissivity of the package-skin system. A_p is the surface area of the package.

For a package with a high internal thermal conductivity as a feature of its design, $\bar{T}_P$ will not differ significantly from the operating temperatures of its internal components. The extremes on $\bar{T}_P$ will be obtained from (3). The extreme values of Q_P depend, for a given design of the solar-cell power plant, upon the orientation of the spin axis of the satellite with respect to the sun (a major factor in the output of the solar cells) and upon radiation damage to the solar power plant in space.

The solar plant output has been calculated to be $Q_{P,\min} = 7$ watts if the spin axis stays parallel to sun rays for an extended period of time, and $Q_{P,\max} = 14$ watts for the initial power with the spin axis perpendicular to the sun's rays.[2] The minimum power figure took into account a 30 per cent deterioration factor due to the space environment during a two-year period, and also included the effects of shading during the eclipse time. The minimum power figure also considered the elevated temperatures of the active areas of the solar cell plant that result from the parallel orientation of the spin axis with respect to the sun's rays. The higher power figure reflects the fact that, for a spin-stabilized

satellite with the proper orientation of the spin axis, spinning is effective in reducing the solar cell temperatures, with improved conversion efficiency. For thermal tests, a conservative value of 16 watts was used for the maximum power, a value based upon very early estimates of the maximum possible power from the plant.

For a given h, the extremes of the calculated values of Q_P and $\bar{T}_S$ will determine the extremes of $\bar{T}_P$ from (3). The calculated extremes of $\bar{T}_P$ must then fall into the range of temperatures compatible with efficient and reliable operation of all temperature-sensitive package components. The design objectives of maintaining a temperature range of 15°F–90°F on the periphery of the electronics package were the result of an assessment of the reasonable minimum and maximum operating temperatures of the vital components of the package.[1] Initial calculations indicated that these temperature requirements for $\bar{T}_P$ could not be maintained for a fixed h because of the rather drastic changes in S_{eq} and Q_P discussed above. In addition, with respect to $\bar{T}_P$ certain safety margins had to be taken into consideration to account for changes in surface properties of the skin due to the space environment, and to include unavoidable differences between individual satellite models due to processing and assembly. One way of doing this would have been to include the expected variation of $\bar{\alpha}/\bar{\epsilon}$ in the calculation of S_{eq}, with the alternative of simply adding reasonable safety margins to the skin temperature directly.

It was determined that $\bar{\alpha}/\bar{\epsilon} \pm \Delta(\bar{\alpha}/\bar{\epsilon}) = 0.65 \pm 0.1$ was a realistic figure, based on possible variation of the properties of the skin, both initially and after the satellite was subjected for a long time to the space environment. Using the figure of 0.65 for $\bar{\alpha}/\bar{\epsilon}$, $\bar{T}_S$ for a fully sunlit condition is 12°F, and for the maximum eclipse time of 45 minutes, $\bar{T}_S$ is −18°F. In practice, the effect of this variation in $\bar{\alpha}/\bar{\epsilon}$ could be reflected in its influence on package temperatures by applying a safety margin of ±18°F directly to the skin. The ±18°F safety margin is also the figure recommended by NASA from their experience. As will be pointed out later, the calculated values plus 18°F margins were used for space chamber simulation.

3.5 *Active Temperature Control System*

In the foregoing discussion it was pointed out that the effective emissivity parameter h in (2) would have to be made variable in a suitable way to maintain a range of 15°F–90°F for the electronics package shell. The variable emissivity would also assist in maintaining the shell close to the room temperature objective previously mentioned.

This was accomplished by providing thermostatically controlled "black areas" on surfaces that had to be otherwise insulated to keep the general temperature level of the package higher than the skin reference temperature. The black areas on the surface of the package were obtained by coating with Parson's black lacquer.* Because of the relatively large surface area of the package and the small amount of power available for heating it internally, the whole package exterior was insulated with up to 30 layers of aluminized Mylar, with fiber glass separators.

The amount of exposed black area was controlled by two independently operated, umbrella-type shutters (Fig. 1) that could close very tightly for situations where maximum eclipse and low power input would require a relatively low value of the effective emissivity h. The control element was a bellows filled with n-pentane, designed to be completely open at 75°F and fully closed at 55°F. Because the bellows had to operate in the vacuum environment, a spring arrangement was used to keep the operating fluid at nearly constant pressure. Experimentally, it was verified that the required h range of $0.05 \leqq h \leqq 0.1$ had been achieved. It must be stated here, however, that the active thermal system designed for the Telstar satellite had to respond primarily to the long-term changes in orbital parameters for purposes of temperature stabilization. For short-term temperature changes (such as those due to a single eclipse), the particular radiative coupling chosen, together with the long time constant of the package with the shutters nearly closed, provided for a temperature response of the package of less than 3°F, as telemetered from the satellite in orbit. It was found experimentally that, should one of the shutters fail, the temperature of the package wall would only slightly exceed the 15°F–90°F range.

3.6 *Thermal Design of Satellite Skin*

The energy conversion efficiency of solar cells is temperature dependent; the operating efficiency increases as the temperature is reduced. A design objective of approximately 30°F was determined to be a practical average temperature for solar cell operation. This value was based on a compromise between the power required from the solar cell plant, the area on the skin used as cooling areas, and the influence of shell temperature on the package temperature (3). Therefore, the overall temperature level of the skin has to be low. Since the $\bar{\alpha}/\bar{\epsilon}$ of the

* Parson's black lacquer, distributed by Eppley Laboratories, Newport, R. I.

sapphire-covered solar cell module was about 1.5, additional cooling areas of low absorptivity and high emissivity were dispersed between banks of solar cells.* For the cooling areas, surfaces covered with plasma-jet deposited aluminum oxide with $\alpha/\epsilon = 0.26$ were used. This arrangement resulted in the characteristic checkered appearance of the spacecraft shell, which has an over-all value of $\bar{\alpha}/\bar{\epsilon} = 0.65$ for the entire skin.

In addition to having low absorptivity, the external surface finish must be adherent and stable in space to assure that the cooling effect will be maintained. The surface properties of the 5-mil layer of rough aluminum oxide should be insensitive to change because of abrasion by micrometeoroids in space. The stability of plasma-sprayed aluminum oxide coatings was evaluated in the laboratory, prior to their final selection, by examining their absorptivity and emissivity and by measuring changes in these values with exposure to high vacuum, ultraviolet radiation and electron bombardment. Because the material is a fused inorganic compound, it exhibits high-vacuum stability. Also, its optical properties are more stable than the optical properties of other materials which might have been used for this purpose. The absorptivity of the aluminum oxide surface increased from 0.21 to 0.24 when exposed to ultraviolet radiation equivalent to 8 months in orbit. Thereafter, the absorptivity did not change with further irradiation equivalent to 18 months in orbit. Other tests showed that absorptivity increases from 0.21 to 0.25 after radiation with 100-Kev electrons equivalent to three months in orbit. Additional electron radiation did not cause further change in the absorptivity. The emissivity of the aluminum oxide coating does not change with any of the environmental stresses described above. Therefore, the skin temperature of the satellite should increase slowly with its time in orbit; this will be discussed later in more detail.

A separate investigation[10] was conducted to establish the minimum spin rates for which satellite surface temperatures are radially uniform, so that local surface temperatures are symmetrical with respect to the spin axis. This investigation showed that a spin rate of 3 to 4 rpm is adequate to achieve a radially symmetric temperature distribution. Spinning the satellite, with proper alignment of the spin axis with respect to the sun, reduces the temperatures of the areas in sunlight below those of comparable areas on a nonspinning satellite.

In the above temperature calculations, thin-shell techniques for temperature distribution in the skin have been used. This was again

* The solar cells were covered with sapphire windows to protect them against space hazards. The module was designed to minimize the greenhouse effect due to the presence of the sapphire windows, and to conduct heat efficiently to the skin structure of the satellite.

mainly possible because of the effective separation of the satellite into two lumped masses, that of the skin and that of the package, and through careful elimination of conduction between them. In order to reduce the temperature of areas directly exposed to the solar light, a provision was made for internal radiative heat exchange between hot and cold portions of the skin. Internal radiation has also been found to be very effective in reducing the undesirable temperature differences between the aluminum oxide covered areas of the skin and the areas occupied by the solar cell modules.

The internal surface of the satellite shell and the frame were coated with a white polyurethane paint. Since the finish for the inside of the satellite is not subject to ultraviolet radiation and is less susceptible to electron damage than the external finish, the principal factors to be considered in its selection are high emissivity, vacuum stability and ease of application. The organic finish was chosen in preference to aluminum oxide primarily because it could be applied without the danger of thermally stressing the panels and the satellite frame. The white polyurethane finish has an emissivity of 0.85 and does not change with exposure to vacuum at the temperatures of the satellite shell in orbit.

Methods for calculating local surface temperatures for several orientations of a spinning satellite have been derived.[11] In the design stage of the spacecraft, surface temperature distribution was calculated using the above techniques, which take into account the local variation of the $\bar{\alpha}/\bar{\epsilon}$ due to inhomogeneous composition of the individual satellite facet surfaces, internal radiation and orientation of the spin axis with respect to the sun rays.

If can be shown that the appropriate formulas are, for the jth facet, whose normal makes the angle θ_j with the sun rays

$$T_j = T_j \frac{\sqrt{2}}{(1 + \beta_j')^{\frac{1}{4}}} (\cos \theta_j + \beta_j/4)^{\frac{1}{4}} \tag{4}$$

for the case of spin axis being parallel to sun rays, and

$$T_j = T_j \frac{\sqrt{2}}{\pi^{\frac{1}{4}}(1 + \beta)^{\frac{1}{4}}} \left[\cos (90° - \theta_j) + \frac{\pi}{4} \beta_j\right]^{\frac{1}{4}} \tag{5}$$

for spin axis perpendicular to sun rays.

For the intermediate orientations, similar formulas have been developed. In (4) and (5), T_j refers to T as a function of the local values of α_j and ϵ_j. The term β stands for the contribution due to the internal radiation (which depends on the internal emissivity, ϵ_i) and is defined as $\beta_j = \epsilon_i/\bar{\epsilon}_j$. Since for the case of the spin axis being aligned with the

sun rays (4) the effect of the instrument package is to reduce the internal heat transfer the "effective value" of β, β', is used instead of the full value of β. As a first approximation, β' is proportional to the amount of free area at the equator of the satellite and to β. The results of temperature calculations using (4) and (5) are shown in Table II; the temperatures for 30° and 60° orientations calculated by other equations are also included. For comparison, some telemetered data from orbits 9 and 17 are shown.

The temperatures listed in Table II were intended to be limiting values, so that the power output calculated from the solar cell plant would not be over-optimistic. For the indicated temperatures, a safety margin of 18°F was included to take care of changes in coating characteristics in space, solar cell module thermal impedance and variations in the secondary radiation from the earth. The calculated temperature extremes for the solar cell modules when the satellite spin axis is parallel to the sun are 150°F for the pole nearest the sun and −150°F for the pole away from the sun after a 45-minute eclipse. These limits were used for the design of the solar cell modules and antenna feed components.[2,4]

In the temperature calculations, the secondary radiation effects were included as average values regardless of satellite altitude and spin axis orientation in relation to the earth, whereas telemetered temperatures include secondary radiation effects for the particular altitude and orien-

TABLE II—LOCAL TEMPERATURE DISTRIBUTION OF SOLAR CELL BANDS* (°F)

Band	Calculated				Telemetry Data from Space	
					Orbit 9	Orbit 17
	Angle Between Spin Axis and Sun Rays					
	0°	30°	60°	90°	90°	90°
1	156	120	59	27	26	19
2	145	111	77	46	38	32
3	55	46	46	34	36	35
4	†	−94	−29	34	43	45
5			−41	46	30	32
6			−92	27	26	29

* A band is a faceted zone of the skin contained between two planes which are perpendicular to the spin axis of the satellite. The bands are numbered in the table starting at one pole. Bands 1 and 6 are at the poles; bands 3 and 4 are adjacent to the communications antennas.

† Temperatures for bands that do not see the sun directly have not been included in the table.

tation of the satellite at the time the data were taken. In view of these factors, results compare very favorably with predictions.

IV. SATELLITE TESTS IN THE SPACE SIMULATOR

Experimental evaluation of the thermal design of the spacecraft was conducted in a space simulation chamber, with solar radiation provided by carbon arc lamps. The thermal test program had a twofold objective. The first objective was determination of the over-all ratio of solar absorptivity to infrared emissivity of the complete satellite, to verify calculations based upon individual measurements of the satelite's exterior surfaces. Such tests were performed on several satellites with various orientations of the spin axis to the light beam from the solar simulator. With the $\bar{\alpha}/\bar{\epsilon}$ ratio known, the thermal environment for the electronics package can be determined from (2) and (3). The other objective was to simulate extreme orbital conditions, such as full sunlight and maximum eclipse periods, so that the anticipated thermal performance in space could be verified by on-the-ground tests.

4.1 *Determination of $\bar{\alpha}/\bar{\epsilon}$ from Simulator Tests*

The appendix describes the space simulation facility and presents the method used to calibrate the chamber. The black- and Al_2O_3-coated satellite experiments determined the average values of solar flux and infrared flux for the case when a real spacecraft was tested in the chamber.

Using these values, four satellite shells were tested in the space chamber under various conditions of illumination to determine the average value of $\bar{\alpha}/\bar{\epsilon}$. These tests were conducted with illumination normal to the spin axis; see Table III. The average $\bar{\alpha}/\bar{\epsilon}$ of the four satellites for illumination normal to the spin axis is 0.702. An experiment was also conducted to determine the variation in $\bar{T}_s$ for spin-axis orientations to the arc lamps of 0°, 30°, 60° and 90°, and showed that $\bar{T}_s$ varied by less than 1.5 per cent for these four orientations.

TABLE III

Satellite Shell	Average $\bar{\alpha}/\bar{\epsilon}$
Mechanical model	0.700
Prototype	0.699
Flyable model no. 1	0.695
Flyable model no. 2	0.716

The $\bar{\alpha}/\bar{\epsilon}$ ratio determined in the space chamber experiments is well within the design tolerance for $\bar{\alpha}/\bar{\epsilon}$ of 0.65 $\pm$ 0.1. Using this median value for $\bar{\alpha}/\bar{\epsilon}$ of 0.65 with the S_{eq} from Section 3.3 ranging from 0.917 to 1.19, the temperature extremes that the satellite skin will experience in its intended orbit will be $\bar{T}_{s,\text{low}} = -18°\text{F}$ and $\bar{T}_{s,\text{high}} = 12°\text{F}$. With an 18°F safety margin, limiting mean skin temperatures are $\bar{T}_{s,\text{low}} = -36°\text{F}$ and $\bar{T}_{s,\text{high}} = 30°\text{F}$. These limiting temperatures were simulated in the chamber with an arc lamp schedule of 2.93 lamps and 1.57 lamps respectively. The lamp schedule refers to the average number of lamps in operation during a test, where a fractional lamp represents the ratio of its "on" time to total test time. Fig. 8 is a plot of mean spacecraft shell temperatures as a function of the arc lamp schedule for four shells tested in the space chamber.

4.2 *Space Simulation Tests*

During development, many thermal tests were performed on two thermal models and on the mechanical development model. These models were essentially complete, except that a dummy electronics package with heat dissipation means was used in lieu of actual components in the package. Except for thermal conductivity effects internal

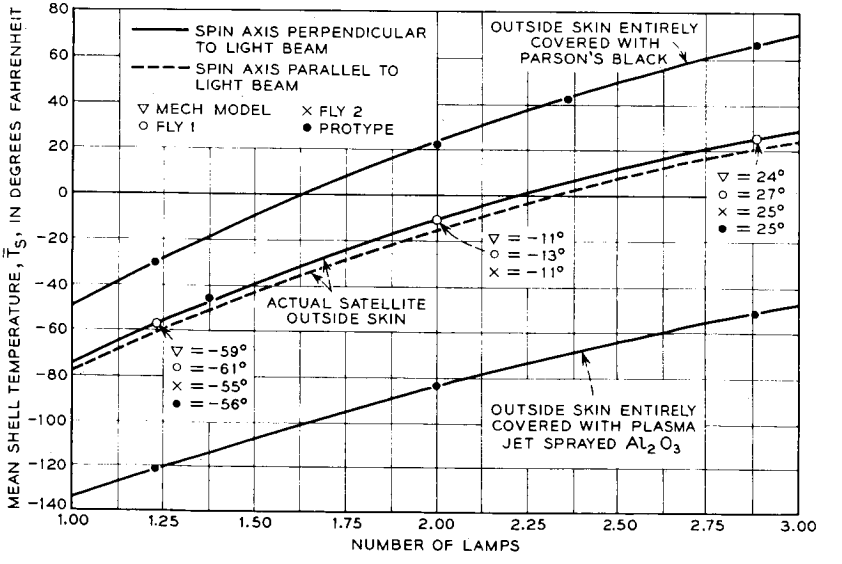

Fig. 8 — Mean shell temperature test results.

to the electronics package, these thermal models duplicated in every respect the thermal behavior of the complete spacecraft in the chamber. These tests were performed to determine the $\bar{T}_S$ of several spacecraft shells, to develop the required degree of emissivity control for the electronics package, to develop support techniques to minimize thermal conduction along the leads from the package to the skin, and to evaluate the operation of the thermal control mechanisms.

In addition, thermal tests were performed on the mechanical development model to evaluate the electronics package temperatures under extreme conditions. The tests listed below were of particular interest in comparing on-the-ground predictions with space performance. The test conditions were:

(a) initial conditions in orbit — maximum power in electronics package (16 watts), full sunlight, +18°F margin on satellite skin, spin axis perpendicular to solar simulator beam, and

(b) end-of-life conditions (two years) — minimum power in electronics package (7 watts), maximum eclipse, −18°F margin on satellite skin, spin axis perpendicular to solar simulator beam.

These test conditions were more stringent than those predicted for the spacecraft in orbit, for the following reasons:

(a) With the initial highest power from the solar plant dissipated in the electronics package, the satellite skin temperature included the +18°F safety margin for a full sunlit orbit. Part of this safety margin was for space deterioration effects on the surface coatings, which tend to warm the skin. Based upon measurements of the surface coating deterioration, this condition would not occur until after several months in orbit, at which time the power from the solar plant would be lower.

(b) With the minimum power at the end of two years in space dissipated in the electronics package, the satellite skin temperature was operated with a −18°F safety margin for a fully eclipsed orbit. After two years in orbit, the skin temperature would have been higher than its initial value because of deterioration of the surface coatings.

Nevertheless, these tests were conducted in this manner to be sure that the 15°F to 90°F limits could be met under extreme theoretical conditions. The results of these two extreme tests are given in Table IV along with the anticipated temperatures.

It is interesting to compare the actual package wall temperatures encountered in space with those predicted by the foregoing tests. Fig. 9 is a graph of the package wall temperatures versus time for the satellite's first seven months in orbit. Also included are the eclipse times, which significantly affect package temperatures as well as the power dissipated

TABLE IV

(a) Initial Conditions (Full Sunlight — 16 Watts Maximum Power)

Measured Package Wall Temperature with +18°F Margin on Skin	Anticipated Package Wall Temperature in Space
87°F	73°F*

(b) End of Life (Maximum Eclipse — 7 Watts Minimum Power)

Measured Package Wall Temperature with −18° F Margin on Skin	Anticipated Package Wall Temperature in Space
34°F	55°F

* The 18°F margin on the mean skin temperature in (a) is reflected as a 14°F difference in the package wall temperature. In (b), the 21°F temperature difference is a result of the 14°F margin plus a 7°F addition to account for increased absorptivity due to deterioration of surface coatings.

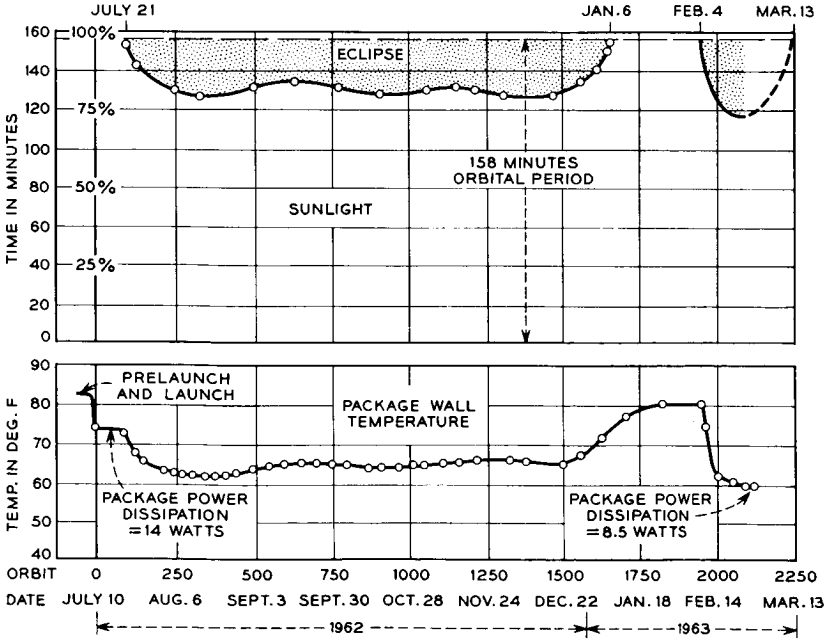

Fig. 9 — Package wall temperature as related to eclipse time.

in the package. The initial temperature in a fully sunlit orbit was 74°F, in comparison to the anticipated 73°F which, of course, had an uncertainty margin of several degrees. At the end of seven and one-half months, the satellite was in the maximum eclipse period of 45 minutes, and the package wall temperature was 60°F with 8.5 watts average orbital power dissipated in the package. At this time the spin axis was nearly normal to the sun. Hence the 60°F temperature encountered in space with 8.5 watts dissipated in the package can be compared to the on-the-ground test figure of 55°F with 7 watts dissipated in the package. The 1.5 watt higher power in space easily accounts for the 5°F higher temperature on the package. It must be emphasized again that these package wall temperatures provide the environment for the electronic components and are not the actual temperatures of the components themselves, which run slightly warmer.[1]

A few over-all observations should be made regarding the package wall temperature in space, shown in Fig. 9. Just prior to launch, the package temperature was 83°F; within nine orbits it dropped to 74°F, where it remained stable for two weeks while the satellite was in a fully sunlit orbit. It will be noted that the variation in package temperature followed very closely the percentage of time that the satellite was in the sun. In January, 1963, the satellite was again in a fully sunlit orbit and the package temperature was about 6°F warmer than in July, 1962. This 6°F change in electronics package temperature can be accounted for by the cumulative effects of the three factors outlined below; figures in parentheses are estimated effects of change on package temperature:

(a) In January the solar constant is 7 per cent higher than it is in July (+6°F),

(b) The absorptivity of the aluminum oxide coating on the satellite skin is presumed to have increased because of ultraviolet and particle radiation effects (+5°F), and

(c) The power dissipated in the electronics package was decreased from 14 watts in July to 11 watts in January (−5°F).

Had the satellite's spin axis precessed from being reasonably perpendicular to the sun rays, there would have been a minimum electronics package wall temperature. Based upon solar simulator tests, the lowest package temperature would be reached with the spin axis parallel to the sun at the end of a two-year life in orbit. In the simulated test, the measured package wall temperature was 14°F with the −18°F safety margin on the skin and the 7 watts expected minimum power in the package. For the reasons outlined previously, the estimated 14°F seems to be unrealistically low: the expected temperature would be 21°F higher, or 35°F.

During the seven months the satellite has been in orbit, the spin axis has remained within 10° of being normal to the sun rays.[12] Hence, no space confirmation of this minimum figure has been possible.

V. CONCLUSIONS

The important features of the Telstar spacecraft structural and thermal design have been presented. In addition, the details of the comprehensive development and environmental test programs have been reviewed.

All mechanical and thermal objectives were achieved, as confirmed by several spacecraft having passed the rigorous environmental tests and the satellite's seven-month performance in space at the time of writing.

The over-all structure and method of support for the electronics package have isolated the vital electronics components from the rigors of launch. Other components, associated with the shell structure, have been designed and proven to withstand qualification level testing.

The active temperature control system has provided a near room temperature environment for the electronic components. Telemetered data from the Telstar satellite have shown that the electronics package wall temperature (component environment) has been maintained between 60°F and 80°F during seven months in orbit. Conditions during this period included fully sunlit orbits, maximum 45-minute eclipse orbits, variation of 7 per cent in the solar constant, and a variable package power of 14 watts to 8.5 watts. When the satellite's spin axis has been normal to the sun, the solar cell temperatures have been maintained close to the 30°F objective.

VI. ACKNOWLEDGMENTS

The writers are indebted to L. Rongved and J. W. West, whose advice, valuable ideas, and over-all guidance contributed so much to the success of the spacecraft structural and thermal design.

APPENDIX

Description and Calibration of Space Simulator

A.1 *Description*

The space simulation facility shown in Figs. 10 and 11 consists of a vacuum chamber with an operating pressure in the low 10^{-6} torr range;

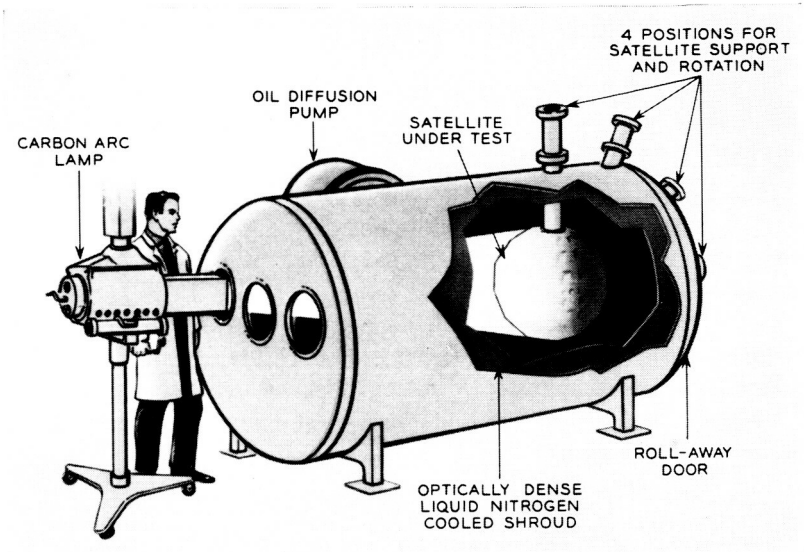

Fig. 10 — Space simulation test facility.

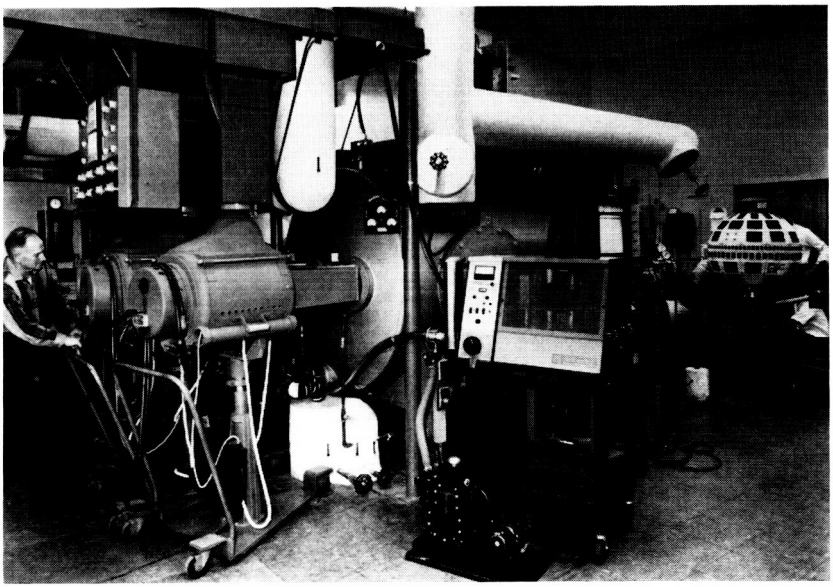

Fig. 11 — Space simulation test facility, showing three carbon arc lamps in place and spacecraft being prepared for test.

a high-absorptivity, liquid nitrogen cooled shroud surrounding the work space; and carbon arc lamps to provide simulated solar energy. The useful working volume in the interior of the chamber is approximately 4.5 feet in diameter by 7 feet long. The solar simulator arc lamps illuminate the spacecraft through three glass ports at the rear of the chamber. Four support positions are provided on the chamber, to permit testing of the satellite with the spin axis at angles of 0°, 30°, 60° and 90°, with respect to the symmetry axis of the chamber.

During the tests, the spacecraft was suspended on a hollow rotating shaft extending into the chamber through a vacuum-tight seal. All electrical leads and instrument connections were brought through the shaft to vacuum-tight feedthroughs at the shaft end. During a test, the spacecraft was rotated about its spin axis; the direction of rotation was reversed about every six revolutions. All external wire connections were installed with enough slack to allow the wires to twist around themselves during rotation, thereby eliminating the need for slip-rings. The rate of rotation was sufficient to avoid any noticeable temperature fluctuations on the skin as a particular portion of the surface rotated in and out of the beam. The point of reversal was staggered during each cycle to eliminate nonuniform illumination of the surface. The test vehicle was insulated from the shaft to minimize conductive heat loss through the shaft.

The radiation from each arc lamp was collected and focused by four glass lenses, and the intensity of each beam was roughly fixed by adjusting the relative positions of these lenses. Each arc emits over 1300 BTU/hr of simulated solar radiation. No attempt was made to collimate the radiation from the lamps, since lack of collimation has a negligible effect on the determination of the $\bar{\alpha}/\bar{\epsilon}$ ratio for an isotropic spherical spacecraft.

For test purposes, the beam cones of the three arcs were adjusted to extend about two inches past the spacecraft cross section, so that the nonuniform beam edge did not influence the tests. The intensity was found to change with time because of variations in supply voltage, differences in electrodes, etc. However, it was possible to compensate for these intensity changes, without appreciably affecting other characteristics of the radiation, by making small adjustments in the spacing between the positive and negative carbons. This was found to be sufficient to control the intensity variations encountered during any run. Solar cells, which are described below, were suspended in the beam inside the chamber to act as intensity monitors for the arc lamp radiation. The electrode spacing was manually trimmed to maintain predetermined short-circuit current outputs on the solar cell monitors.

In all the tests, the intensity of the individual arc lamps was kept constant, and changes in the time-averaged intensity were accomplished by turning the lamps on and off in a suitably scheduled manner. Each arc lamp could be operated for over an hour before its electrodes were consumed. It was a relatively simple matter at this point to remove the spent lamp and replace it with a freshly carboned one.

Three 1 × 2 cm solar cells were suspended in the chamber in front of the spacecraft and were used as arc intensity monitors. The short-circuit current from these cells was calibrated against the intensity of the arc lamps and provided a reference for carbon electrode adjustments. During a test, the short-circuit current from banks of solar cells on the spacecraft surface was also recorded. This provided an additional check on the control of the over-all intensity of arc radiation, although these cells were not specifically calibrated for that purpose. While the short-circuit current from the spacecraft solar plant was not used as a standard for adjusting the arc lamp intensity, it was useful in observing changes in the characteristics of the individual solar cell strings.

The spectral characteristics of the radiation from the carbon arc lamp match quite closely the spectrum of the sun's radiation outside the earth's atmosphere (Johnson curve).[12] The glass lenses in the facility prevent all radiation below 0.35 micron from entering the chamber; however, this small loss in the ultraviolet region does not have a significant effect on the thermal measurements discussed here.

A.2 Arc Lamp Calibration

The arc lamps were positioned to face the center of the test region and were equidistant from it. The centers of the arc beams were all projected along the same horizontal plane, and the areas illuminated by each arc were equal.

The radiation from the arc lamps in the region near the specimen acts as if it were emitted by a point source: i.e., the relationship between intensity and distance is closely represented by an inverse square function. When the power density at the location of the center of the satellite is set equal to some value, I, the average power density on the surface of the spherical satellite from a collimated source also has an intensity I.[15]

Each arc lamp was adjusted to give approximately $\frac{1}{3}$ S at the center of the satellite, where S is the solar constant. This was found to provide sufficient radiative input to the test vehicle to produce the maximum energy condition — i.e., a fully sunlit orbit plus appropriate margins. The lamps were then placed in position, and, with the chamber at am-

bient conditions, the three monitoring solar cells were illuminated by the lamps and their output was compared to a calibrated Eppley pyrheliometer at the point corresponding to the center of the test specimen.

A.3 *Calibration of Space Simulator*

A.3.1 *Thermal Balance Equation*

The total net power stored in a test specimen in the space simulation chamber can be described by a thermal balance equation of the form

$$Q_T = Q_S + Q_R + Q_{IR} - Q_E \tag{6}$$

where the first three terms on the right represent power absorbed by the specimen from, respectively, the simulated solar source, simulated solar power reflected from the surroundings, and infrared power from the surroundings. The last term in (6) describes the power radiated by the test specimen. Here, we have assumed that all thermal energy exchange is by radiation, and that there is no heat dissipation within the specimen.

At thermal equilibrium, (6) can be set equal to zero and rewritten as:

$$\bar{\alpha}A_1 I + \bar{\rho}\bar{\alpha}A_2 I + \bar{\alpha}'A_1 I_w - \bar{\epsilon}\sigma A_2 \bar{T}_S^4 = 0 \tag{7}$$

where

$\bar{\alpha}$ = average absorptivity of specimen to carbon arc radiation
A_1 = cross-sectional area of specimen
I = time-averaged intensity of carbon arc radiation
$\bar{\rho}$ = fraction of I received by the specimen by reflection from the surroundings, averaged over the surface of the specimen
A_2 = surface area of specimen; for a spherical specimen, $A_2 = 4A_1$
$\bar{\alpha}'$ = average absorptivity of specimen for radiation emitted and reflected by the surroundings in the infrared region
σ = Stefan-Boltzmann constant
I_w = intensity of total equivalent collimated infrared flux emitted and reflected by the surroundings
$\bar{\epsilon}$ = average emissivity of the specimen, and
$\bar{T}_S$ = average temperature of the specimen.

Now, making the simplifying assumption that $\bar{\alpha}' = \bar{\epsilon}$ and substituting the appropriate area factors for a spherical specimen, (7), after a slight rearrangement, becomes

$$\frac{\bar{\alpha}}{\bar{\epsilon}} = \frac{4\sigma \bar{T}_S^4 - I_w}{I(1 + 4\bar{\rho})} \tag{8}$$

A.3.2 *Determination of Total Energy Flux in Chamber*

The total energy that a satellite receives in the chamber at a particular lamp intensity has been determined in a test on a "black satellite." The black satellite is a dummy satellite shell of the same dimensions as the Telstar satellite, but covered on the entire exterior with Parson's black lacquer. This paint has an absorptivity and emissivity both approximately equal to 0.98. In the center of the hollow black satellite, a small ball was suspended with nonconducting supports and instrumented with thermocouples. The ball and the interior of the black satellite were also painted black. The steady-state temperature that this ball assumes may be shown mathematically to be the mean shell temperature of the black satellite.

The arc lamp energy reflected from the walls with the black and other satellites in the chamber was measured with a calibrated solar cell. The average reflected flux $\bar{\rho}$ with the black satellite was 0.003. Similar measurements were carried out with an actual satellite installed in the chamber, and $\bar{\rho}$ was determined to be 0.007.

The black satellite was installed in the chamber and the test conducted with the walls at liquid nitrogen temperature and the pressure in the 10^{-6} torr range. The arc lamps were turned on, and the equilibrium temperature of the black satellite was recorded at three different lamp intensities, I. Table V gives the results of these tests. The quantity q_c, which represents the total collimated intensity of radiation incident

TABLE V—CALIBRATION OF ENVIRONMENTAL CHAMBER USING PARSON'S BLACK COATED SPHERE

I BTU/hr-ft²	$\bar{T}_S$ °R	$\bar{\alpha}/\bar{\epsilon}$	I_w BTU/hr-ft²	q_c BTU/hr-ft²
443	526	1	83	530
307	482	1	64	374
189	429	1	44	235
0	215	1	15	15

TABLE VI—DETERMINATION OF $\bar{\alpha}/\bar{\epsilon}$ FOR A *Telstar* SATELLITE SKIN

I BTU/hr-ft²	q_c BTU/hr-ft²	I_w BTU/hr-ft²	$\bar{T}_S$ °R	$\bar{\alpha}/\bar{\epsilon}$
443	529	73	486	0.68
307	372	56	448	0.70
189	234	39	399	0.70

on the surface of the test specimen, has been computed from the relationship

$$q_c = I(1 + 4\bar{\rho}) + I_w \tag{9}$$

where the first term on the right is the radiation from the arc lamps (direct plus reflected), and the second term is the thermal infrared radiation.

The quantity q_c was also determined in a similar manner in a test on a jet-sprayed aluminum oxide (Al_2O_3) covered satellite with known α/ϵ ratio. The values of q_c for both tests showed good agreement.

Table VI gives an example of the calculation of $\bar{\alpha}/\bar{\epsilon}$ for one of the actual spacecraft shells measured in the environmental chamber. The temperature $\bar{T}_S$ was determined with a black ball centrally located in the interior of the spacecraft, as in the previous cases. The interior surface of the skin had a high-emissivity finish and no electronics package was used. The $\bar{\alpha}/\bar{\epsilon}$ ratio in the table was determined from (8). With this ratio known, it is now possible to simulate the extreme orbital conditions by adjusting the time-averaged lamp intensity to produce the calculated mean shell temperature from (2).

REFERENCES

1. Shennum, R. H., and Haury, P. T., A General Description of the *Telstar* Satellite, B.S.T.J., this issue, p. 801.
2. Smith, K. D., Gummel, H. K., Bode, J. D., Cuttriss, D. B., Nielsen, R. J., and Rosenzweig, W., The Solar Cells and Their Mounting, B.S.T.J., this issue, Part 3.
3. Yu, E. Y., Spin Decay, Spin Precession Damping, and Spin-Axis Drift of the *Telstar* Satellite, to be published.
4. Bangert, J. T., Engelbrecht, R. S., Harkless, E. T., Sperry, R. V., and Walsh, E. J., The Spacecraft Antennas, B.S.T.J., this issue, p. 869.
5. Delchamps, T. B., Jonasson, G. C., and Swift, R. A., The Spacecraft Test and Evaluation Program, B.S.T.J., this issue, p. 1007.
6. Heller, G., Thermal Control of the Explorer Satellites, ARS Journal, **30,** Apr., 1960, pp. 344–352.
7. Hanel, R. A., Thermostatic Temperature Control of Satellites and Space Vehicles, ARS Journal, **29,** May, 1959, pp. 358–361.
8. Acker, R. M., Lipkis, R. P., and Vehrencamp, J. E., Temperature Control System for the Atlas Able-4 Lunar Satellite, ASME Paper No. 60-AV-46, June, 1960.
9. Hrycak, P., Effects of Secondary Radiation on an Orbiting Satellite, ARS Journal, **32,** Aug., 1962, pp. 1294–1295.
10. Hrycak, P., Temperature Distribution in a Spinning Space Vehicle, AIAA Journal, **1,** Jan., 1963, pp. 96–99.
11. Hrycak, P., Calculation of Satellite Surface Temperature Distribution, to be published.
12. Hutchison, P. T., and Swift, R. A., Results of the *Telstar* Satellite Space Experiments, B.S.T.J., this issue, Part 2.
13. Hrycak, P., Unger, B. A., and Wittenberg, A. M., Thermal Testing of the *Telstar* Satellite, Proc. Inst. Environmental Sci., 1963, pp. 477–484.

Page intentionally left blank

The Spacecraft Test and Evaluation Program

By T. B. DELCHAMPS, G. C. JONASSON, and R. A. SWIFT

(Manuscript received January 21, 1963)

Considerations guiding the planning and execution of environmental tests in the development, design qualification and flight acceptance phases of the Telstar satellite program are discussed. Specific test procedures are covered and highlights of test results involving mechanical, thermal and magnetic properties of the spacecraft are reviewed.

I. INTRODUCTION

Essential to the success of any development program are: (a) sound basic design; (b) discriminate selection of materials and components; and (c) careful fabrication. The function of test evaluation, as a fourth phase in the development plan, is to determine the degree to which the three basic requirements listed have been satisfied. It might be suggested that a unique feature of the Telstar satellite program has been the joint achievement of *depth* and *concurrency* in all four development phases. Such an approach has been dictated both by program urgency and the extraordinary cost of failure in an undertaking of this nature. In the process, each phase of the spacecraft development effort has served to reinforce collaterally every other phase, to a degree not normally realized in a sequentially structured program.

The spacecraft design is largely derived from existing systems of proven reliability. Maximum safety margins permitted by size and weight limitations have been utilized. Components and materials have been selected wherever possible on the basis of successful prior use in related applications. Manufacture and assembly operations have been carried out under carefully controlled conditions. The spacecraft test evaluation has served to demonstrate the effectiveness of these measures in providing a design which would survive the launch and operate satisfactorily in the orbital environment. This article will cover both general and detailed aspects of the spacecraft test evaluation, as the

program progressed through the basic-development, design-qualification and flight-acceptance phases.

In the development phase, testing effort was directed toward the evaluation and qualification of spacecraft components and subassemblies, and the study of full-scale models. These tests were conducted under the mechanical and thermal conditions associated with launch and operation in orbit. It was during this phase, through a process of selection and elimination involving available alternatives, that the final design was crystallized. This was followed by design-qualification tests on the prototype spacecraft. In this phase, the controlling philosophy was to achieve maximum assurance, in the limited time available, that the design was capable of surviving launch and performing the intended function under conditions anticipated in orbit. To fulfil this objective, test conditions were selected in a manner which introduced a margin of severity beyond the specific environments predicted for the operational satellite. Finally, flight-acceptance tests performed on operational models were designed to reveal defects which may have been introduced in the manufacturing process. In this phase, the selected test conditions reflected the best estimate of the actual launch environment, but retained, in the thermal-vacuum portion, the added margin previously included in the prototype evaluation. This latter consideration recognized an element of uncertainty in predicting long-term thermal response of the satellite in space.

II. PRELIMINARY MODEL AND SUBASSEMBLY TESTING

The purpose of the preliminary test program was to evaluate the mechanical and electrical design of parts and subassemblies prior to their installation into an actual spacecraft. The tests on structural models with dummy electronics packages provided the necessary data to formulate the subassembly vibration test levels and durations. The levels for temperature tests were based on design objectives and calculated values expected in the space environment.[1] Once a subassembly design had been successfully qualified, there was reasonable assurance that it would survive the dynamic environment of powered flight on the launch vehicle and that it would operate properly in the temperature range predicted for orbital flight.

2.1 *Tests Performed on Development Models*

To conserve time and allow parallel testing, five satellite development models were assembled and used to provide data on system responses to

environmental conditions. The use of models provided information required for subassembly design and pinpointed the possible trouble areas prior to the prototype phase of the project. This allowed any necessary changes to be made before assembly of the prototype. The models used were two structural models (referred to as the vibration and mechanical models), two thermal models, and one electrical development model. The latter, as the name implies, was assembled primarily to evaluate the spacecraft electronics as a complete system, but it also served to provide data on electrical performance under certain environmental conditions. A tabulation of the test models appears in Table I.

2.1.1 *Vibration and Shock Tests*

Vibration tests were performed on the two structural models to evaluate the mechanical design. Vibration levels were determined at various points in the structure when the entire system was subjected to sinusoidal and random vibration over a wide band of frequencies. The areas to which the most attention was directed were the nylon lacing supporting the electronics canister, the solar cells and their method of attachment, and the structure itself. Results of these early tests proved that from the standpoint of vibration: (a) the mechanical design was basically sound, (b) the solar cells would survive a vibration environment more severe than that expected during launch, and (c) that the nylon lacing provided sufficient isolation of the electronics canister for the anticipated environment. On the basis of these results, it was possible to predict the vibration levels which would be experienced by any of the various subassemblies located either inside the electronics canister or on the outer structure of the spacecraft. The vibration response of the electronics canister is shown in Fig. 1. It is evident that

TABLE I — SPACECRAFT TEST MODELS

Model	Panels	Antennas	Electronic Chassis
Vibration	Brass modules to simulate solar cells	No VHF antenna. Brass dummy for microwave	Dummy-weighted to simulate actual chassis
Mechanical	Full complement of actual solar cells	All antennas installed	Dummy-weighted to simulate actual chassis
Thermal model 1	Full complement of actual solar cells	All antennas installed	Dummy—not weighted
Thermal model 2	No solar cells	Microwave only	Dummy—not weighted
Electrical development	Full complement of actual solar cells	All antennas installed	Actual chassis, but not foamed

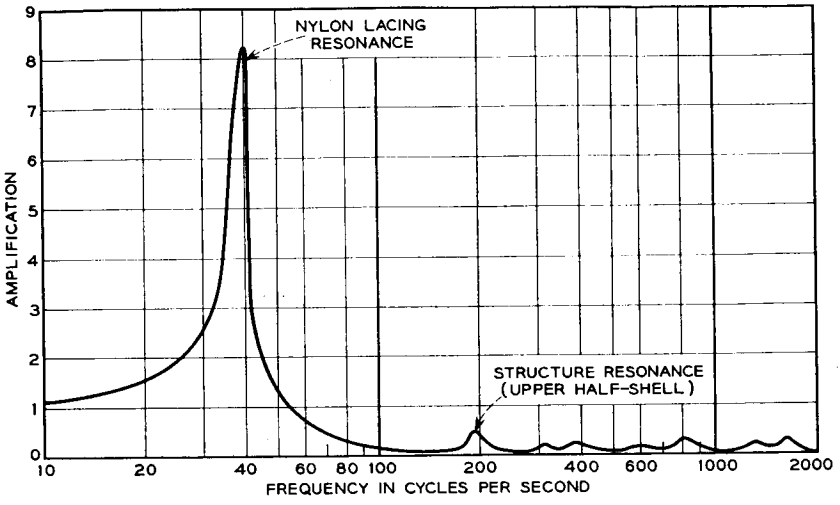

Fig. 1 — Amplification vs frequency, electronics chassis.

at frequencies between 54 and 2000 cycles per second the isolation provided by the lacing is very good.

Figs. 2 and 3 illustrate typical responses at two points on the outer structure. The peaks on these curves represent the resonant frequencies of various parts of the spacecraft. The frequency and amplification factor

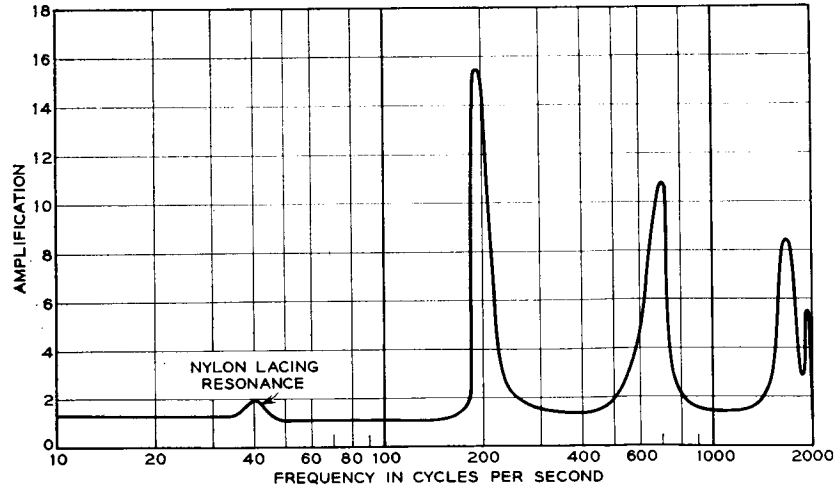

Fig. 2 — Amplification vs frequency, typical solar cell panel.

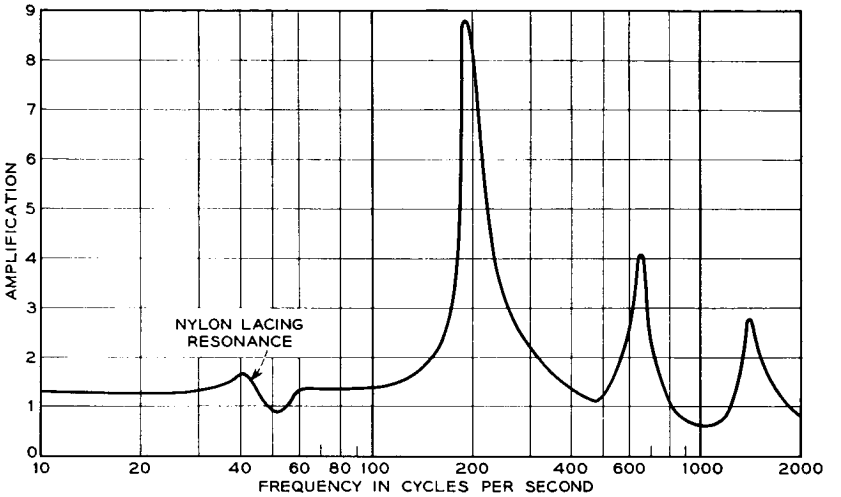

Fig. 3 — Amplication vs frequency, typical structural member (upper half-shell).

associated with each response provided the data necessary to determine the levels for qualification and acceptance vibration of subassemblies, prior to their installation in the spacecraft.

The vibration model was also subjected to several shock tests for the purpose of calibrating the shock test machine and determining the effect of shock on the satellite structure. These tests are summarized in Table II. Pulse shapes from four tests are presented in Fig. 4. The pulse shown in Fig. 4(a) was chosen for the subsequent prototype shock test. No deterioration of the structure occurred as a result of this test.

TABLE II — PRELIMINARY SHOCK TESTS

Drop Number	Drop Height (Inches)	Pulse Time (Milliseconds)	Maximum Acceleration (g's)
1	6.5	—	—
2	6.5	20	21
3	7.5	20	22.7
4	8.25	20	27
5	8.5	19.2	29.4
6	8.0	16.8	33.6
7	7.5	14.4	34.2
8	7.0	15.2	34.5
9	6.0	15.2	31.5

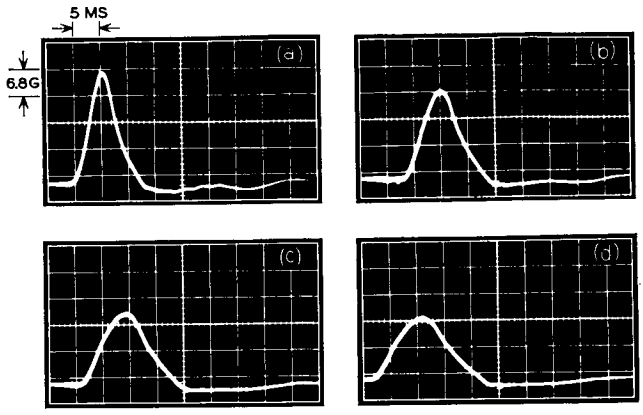

Fig. 4 — Pulse shapes formed using various arrestor rubber thicknesses with Barry 15000 vertical-drop machine: (a) 30-g peak — 13-millisecond pulse obtained with 1-inch rubber arrestor; (b) 24-g peak — 14-millisecond pulse obtained with 1.5-inch rubber arrestor; (c) 20-g peak — 18-millisecond pulse obtained with 2-inch rubber arrestor; (d) 17-g peak — 19-millisecond pulse obtained with 2.5-inch rubber arrestor.

2.1.2 *Preliminary Thermal-Vacuum Tests*

Several tests were performed with the two thermal models in the space simulator for calibration purposes and for verification of the predicted satellite temperatures under extreme orbital conditions. The results of these tests are summarized in Table III. The data obtained from the thermal models show that the chassis temperatures were between 15°F and 90°F. Further tests were performed to observe the thermal-shutter operation and the consequence of a failure of one or both shutter mechanisms. The results of these tests indicated that with the shutters closed in a fully sunlit orbit or open in a maximum eclipse orbit, canister temperatures of 92°F and −20°F, respectively, would prevail. The latter type of failure is the most critical with respect to the operation of the electronic circuits, but, by virtue of the fail-safe nature of the shutter mechanism design, this failure is also the least likely to occur. The shutters have been designed to avoid bearing surfaces which might seize. This leaves loss of fluid in the bellows assembly as the most likely mode of failure. Should this occur, spring loading will force the shutter to return to the closed position.

2.2 *Subassembly Qualification and Acceptance*

Each spacecraft subassembly was subjected to several vibration and temperature cycles prior to installation in the spacecraft. These tests

TABLE III — THERMAL-VACUUM TEST RESULTS

Spin Axis Parallel to Arc Lamps		
Chassis Power	Simulated Orbital Condition	Canister Wall Temperature
16.0 watts	Fully sunlit (plus 18°F margin on skin)	74°F
7.0 watts	Maximum eclipse (minus 18°F margin on skin)	14°F
Spin Axis Perpendicular to Arc Lamps		
Chassis Power	Simulated Orbital Condition	Canister Wall Temperature
16.0 watts	Fully sunlit (plus 18°F margin on skin)	87°F
7.0 watts	Maximum eclipse (minus 18°F margin on skin)	32°F

were performed to detect marginal components which may have slipped by quality control and to pinpoint manufacturing defects. A prototype of each subassembly was vibrated at qualification levels, determined from the results of the vibration tests performed on the structural models. Once a particular design was so qualified, the subsequent flyable units were subjected to acceptance level tests which were somewhat less stringent than those required for initial qualification. The vibration test levels and durations for qualification and acceptance of subassemblies located either inside the electronics canister or on the outer structure, are given in Table IV.

Most flyable subassemblies were temperature cycled over the range of 0°F to 125°F, stabilized at each extreme for a period of six hours and electrically tested at the maximum and minimum conditions. This test represented an extension of 15°F below and 35°F above the temperature range expected during the satellite lifetime.

III. PROTOTYPE QUALIFICATION TESTS

The design qualification program included a complete sequence of tests intended to subject the prototype model to environmental rigors more stringent than those expected from transportation, handling, test, pre-launch, launch, injection, and orbit. The prototype was deliberately over-tested to assure that the basic design possessed a margin of safety which would allow for variations in subsequent systems. The purpose of the design qualification tests was to demonstrate the ability of the design to meet all performance requirements without degradation due

TABLE IV

(a) Vibration Inputs for Inside-the-Canister Assemblies: Qualification Levels

Vibration Axis	Frequency Range (cps)	Sweep Duration (Minutes)	Acceleration (g's Vector)
Thrust	10–30	1.00	2.3*
	30–60	1.00	21.0
	60–2000	2.7	14.0
	550–650	0.5	21.0
Lateral	5–30	1.25	0.9*
	30–60	1.00	4.8
	60–2000	2.7	2.8
	550–650	0.5	4.8

(b) Vibration Inputs for Inside-the-Canister Assemblies: Acceptance Levels

Vibration Axis	Frequency Range (cps)	Sweep Duration (Minutes)	Acceleration (g's Vector)
Thrust	5–30	1.2	1.5*
	30–60	0.5	14.0
	60–2000	1.1	7.1
	550–650	0.5	14.0
Lateral	5–30	1.2	0.6*
	30–60	0.5	4.2
	60–2000	1.1	1.5
	550–650	0.5	4.2

(c) Vibration Inputs for On-the-Frame Assemblies: Qualification Levels (Typical)

Vibration Axis	Frequency Range (cps)	Sweep Duration (Minutes)	Acceleration (g's Vector)
Thrust	10–2000	1.7	2.3†
	150–300	0.5	46.0
	300–2000	1.5	20.0
	550–650	0.5	27.0

(d) Vibration Inputs for On-the-Frame Assemblies Acceptance Levels (Typical)

Vibration Axis	Frequency Range (cps)	Sweep Duration (Minutes)	Acceleration (g's Vector)
Thrust	10–2000	1.7	2.3
	150–300	0.5	28.0
	300–2000	1.5	14.0
	550–650	0.5	21.0

* Maximum table excursion — 0.5 inch double amplitude.
† This run was to observe possible fixture resonances.

to exposure to these more stringent environments. The spacecraft test sequence is tabulated in Table V, and the levels required for design qualification in Table VI. The specific test requirements were jointly agreed upon by Bell Telephone Laboratories, Incorporated, and the National Aeronautics and Space Administration.

3.1 *Balance, Moments of Inertia and Center of Gravity Determination*

To insure correct performance during launch and orbit, the mechanical parameters of weight, center of gravity location, moments of inertia, and degree of unbalance must be accurately measured, and corrected if out of established limits. Briefly, the part each parameter plays in the over-all performance of the satellite is as follows: The permissible weight is determined by the desired orbit and the type of launch vehicle used; for the Telstar satellite, the chosen orbit and Thor-Delta vehicle limited the final weight to a maximum of 175 pounds. The center of gravity location and moments of inertia affect the satellite attitude stabilization in orbit, and also influence corrections required during the guided portion of powered flight. The moments of inertia also determine the size of the rocket motors to provide spin for stabilization of the third stage. The static and dynamic balance of the satellite determine the degree of stability during third-stage flight and orbit.

Since the Telstar satellite is spin-stabilized, it is necessary that the major moment of inertia: (a) be greater than the remaining principal moments of inertia, and (b) have its axis coincident with the desired spin axis. The first requirement may be met by designing for correct

TABLE V — SPACECRAFT TEST SEQUENCE

Qualification Tests	Acceptance Tests
Leak	Leak
Electrical Acceptance	Electrical Acceptance
Static Balance	Static Balance
Spin	
Dynamic Balance	Dynamic Balance
Weight	Weight
Moments of Inertia	Moments of Inertia
Temperature	
Humidity	
Sustained Acceleration	
Shock	
Vibration	Vibration
Dynamic Balance	Dynamic Balance
Thermal Vacuum	Thermal Vacuum
Leak	Leak
System Check	System Check
Electrical Acceptance	Electrical Acceptance

TABLE VI — SPACECRAFT QUALIFICATION TEST LEVELS

Test	Levels		Total Time
	Thrust	Transverse	
Vibration			
5–50 cps	2.3 g peak	0.9 g peak	3.3 min.
50–500 cps	10.7 g peak	2.1 g peak	3.3 min.
500–2000 cps	21.0 g peak	4.2 g peak	2.0 min.
550–650 cps	40.0 g peak	14.0 g peak	1.0 min.
Random (20–2000 cps)	11.5 g rms	11.5 g rms	8.0 min.
Temperature			
Low temperature soak	0°F		6 hours
High temperature soak	140°F		6 hours
Low temperature operate	15°F		6 hours
High temperature operate	90°F		6 hours
Humidity	86°F-95%		24 hours
Thermal vacuum	pressure $<10^{-5}$ mm Hg		
High temperature	max. predicted MRT +18°F		6 days
Low temperature	min. predicted MRT −18°F		3 days
Sustained acceleration			
Thrust	+25 g		3 min.
Transverse (4 orientations)	±3 g		4 min.
Shock			
Thrust (3 drops)	30-g 10–15 millisec half-sine pulse		—
Spin	225 rpm		3 hours

mass distribution and the second by fine adjustment of the static and dynamic balance of the satellite. The design objective for the ratio of maximum transverse moment to the major moment of inertia was a ratio of less than 0.95.

The balance requirements imposed on the satellite by the launch vehicle were a center of gravity offset of less than 0.005 inch and a principal axis shift of less than 0.008 radian.

The prototype spacecraft was balanced to achieve a center of gravity offset of less than 0.003 inch and a principal axis shift of less than 0.002 radian. The moment of inertia ratio was found to be 0.956, which was slightly above the design objective; however, it was known at the time that the flyable satellites would have lower ratios, so no effort was made to optimize the prototype.

3.2 *Temperature and Humidity Tests*

The purpose of the temperature and humidity tests was to show that the spacecraft would survive temperature and humidity extremes that

might be encountered during storage or operation in an uncontrolled environment for short periods. The levels employed for these tests were those which might result from a failure of either heating or air-conditioning equipment in the satellite storage and testing areas.

The tests were performed as follows: storage for a period of six hours at an ambient temperature of 140°F; storage for six hours at a temperature of 0°F; operation at a chassis temperature of 15°F; and operation at a chassis temperature of 90°F. The humidity test consisted of a 24-hour storage period at a temperature of 86°F and a relative humidity of 95 per cent.

During the temperature test, it was found that the telemetry failed to operate below 60°F. The failure was isolated to a switching transistor in the voltage-controlled oscillator and the circuit was redesigned for later spacecraft.

Following the temperature and humidity tests, physical examination of the spacecraft revealed that the oxide coating had flaked off in some areas, and it was noted that several gray stains, which were later found to be caused by oil, had appeared during the test. As a result of these findings, steps were taken to prevent exposure of subsequent satellites to an oil-contaminated atmosphere.

3.3 *Vibration Tests*

The prototype model was subjected to the series of vibration tests outlined in Table VI. The following failures were noted during the vibration tests: (a) radiation detectors P1, P2, E1 became inoperative, (b) one of the static balance weights was torn loose from the framework and damaged a solar cell panel, (c) two helix wires on the VHF antenna were broken, and (d) several short circuits developed in the solar power plant.

It was found that two of the radiation detector failures had been caused by broken wiring at the canister header and the third by a defective diode. In order to prevent failures of the same type, the wiring harness was modified and a more severe diode screening process was instituted. The improved wiring harness and more reliable diodes were installed in all subsequent spacecraft.

The loss of the static balance weight was attributed to local stress concentrations in the satellite frame at the point of attachment. The stress was relieved by distributing the weight over a larger area, allowing more space between the screws used to attach each weight, and by providing some degree of mechanical damping through the use of epoxy between the frame member and the balance weight. As a result of these

modifications, no further difficulty has been encountered with the balance weight mounting.

Close inspection of the breaks in the helix antenna revealed that in both cases the fracture had been started during fabrication. In subsequent units the possibility of breakage was minimized by increasing the radii of the various bends, inspecting the wire more closely before forming, and inspecting the completed antenna assembly for cracks by means of a dye penetrant.

Inspection of the solar power plant wiring revealed that the insulation had ruptured at points where it crossed sharp corners of the spacecraft framework and at cable tie points, resulting in short circuits. The wire was replaced with a wire having a higher density insulation and wrapped with Mylar tape at tie points and areas where the cabling crossed the framework.

3.4 *Shock Test*

The shock test consisted of four half-sine pulses, 30 g's in amplitude and 13 milliseconds in duration, applied along the thrust axis of the spacecraft. Performance of the satellite following the test was satisfactory and gave no evidence of deterioration as a result of the test. During impacts, however, the telemetry dropped out of synchronization on the second, third and fourth shocks. Investigation failed to indicate any reason for the loss of synchronization, and it did not recur during any of the later environmental tests.

3.5 *Thermal-Vacuum Tests*[1]

The thermal-vacuum tests were a simulation of the extreme thermal conditions expected in orbit.[1] For the qualification test, it was required that the satellite be exposed to simulated solar illumination at a pressure of less than 1.0×10^{-5} mm Hg, with a chamber-wall temperature of less than $-280°$F, for a period of nine days. A fully sunlit orbit was simulated for six days with power dissipation within the electronics canister corresponding to maximum efficiency of the solar power plant. This was immediately followed by simulation of the maximum eclipse orbit for three days with a dissipation within the canister corresponding to a solar plant efficiency of 68 per cent of its initial value, the condition expected near the end of Telstar's two-year life. During the six-day test, the simulated solar input was controlled to give a mean radiant temperature[1] 18°F above the value predicted for the fully sunlit orbit, and the power input to the electronics chassis was maintained at 16 watts. The mean radiant temperature during the three-day test was

maintained 18°F below that expected in the maximum eclipse orbit and the power input was limited to 7 watts.

Electrical operation represented maximum use of the satellite in the two extreme conditions and was conducted on the following schedule: the communications experiment and telemetry was turned on for three half-hour periods each day, beginning at approximately 0900, 1200 and 1500 hours, and the telemetry was operated for the first five minutes of each remaining half-hour period.

Shortly after the start of the prototype test, telemetry data showed that the canister pressure had decreased, indicating that a leak had developed. An electrical check indicated that a failure had occurred in the microwave circuitry. The test was terminated at that time and the satellite returned to the Hillside laboratory for disassembly and inspection.

It was discovered that the material around the top shutter mounting stud had failed, causing a leak in the dome of the canister. Since the failure had apparently occurred during either the vibration or shock tests, it served to emphasize the importance of performing the thermal-vacuum test after completion of the mechanical tests. Further investigation revealed the cause of the microwave failure to be destruction of the output transistors in the 255 and 277-mc transistor multipliers caused by voltage breakdown in the power supply resulting from loss of canister pressure. Laboratory experiment confirmed that the failure was a direct result of the corona effect present in the power supply when operated at reduced pressures.

The prototype unit was repaired and returned to the Whippany environmental test laboratory for completion of the qualification tests. The thermal-vacuum test was completed without further incident. The test results are shown in Table VII.

3.6 *Leak Tests*

Since the spacecraft electronics are contained within a hermetically-sealed canister and are designed to operate at a pressure of approximately 10 psia, it was necessary that the canister leak rate be evaluated. The

TABLE VII — THERMAL-VACUUM QUALIFICATION TEST RESULTS

Test	Canister Temperature		Mean Skin Temperature
	Predicted	Actual	
Full sunlight	73°F	73.3°F	21°F
Maximum eclipse	14°F	17.3°F	−47°F

leak test also served as a means of determining if the canister had ruptured or if a weld had failed since sealing. The canister was backfilled with argon gas and the leak rate determined in an evacuated chamber, using a mass spectrometer. Leak tests were performed in this manner prior to and after the environmental test series.

Before testing, the prototype leak rate was less than the measurement capability of the detector. Following the test program, a leak rate of 5×10^{-4} std cc/sec of argon was indicated. Investigation revealed that the chamber, the Mylar insulating blankets around the canister, and the satellite itself, had become contaminated with argon at the time canister pressure was lost during the initial thermal-vacuum test. These findings raised serious doubt as to the significance of this final leak reading. Subsequent tests on flyable spacecraft have revealed that the leak rates are well below the specified 8×10^{-5} std cc/sec of argon.

3.7 *Spin Test*

The prototype was subjected to a spin rate of 225 rpm for a period of three hours, the last hour of which was under electrical load simulating operation in orbit. The 225 rpm spin rate was a 25 per cent increase over that expected in actual flight (the satellite was injected into orbit with an initial spin rate of 177.7 rpm). There were no spacecraft malfunctions during this test.

3.8 *Sustained Acceleration*

The prototype was mounted on a horizontal centrifuge and sustained acceleration, measured at the spacecraft center of gravity, was applied along each of its three coordinate axes. The first test consisted of one run with 25 g's applied in the thrust direction for a period of three minutes. The second test consisted of four runs in the lateral plane, with the prototype spacecraft being rotated 90 degrees after each run. The levels during the latter runs were 3 g's, maintained for a period of one minute in each position. The electrical performance of the spacecraft was monitored during the periods of constant acceleration, and electrical checks were performed following each run. There was no evidence that satellite performance was in any way degraded either during or as a result of the applied accelerations.

3.9 *Magnetic Drag and Moment Measurements*

Since the Telstar satellite is spin-stabilized and orbits within the magnetic field of the earth, it was necessary that the effect of that field

on the spin rate and precession of the satellite be determined. For this reason, the torque due to eddy currents, and the residual magnetic moment along the spin axis of the spacecraft were measured. The former effect is the cause of spin decay and the latter causes precession.

The magnetic drag constant was found to be 1355 ± 15 per cent meters[4] per ohm. The drag torque due to a given field strength was calculated from the relationship $T_0 = p\omega B^2$, where p is the magnetic drag constant, ω the angular velocity of the satellite and B the field strength normal to the satellite spin axis. The flyable spacecraft were essentially the same as the prototype with respect to eddy current generation, and subsequent models were not drag tested.

The magnetic moment of the prototype was measured, and a coarse correction was made to investigate the feasibility of compensating for the effect of the traveling-wave-tube field.

IV. SPACECRAFT ACCEPTANCE TESTS

The spacecraft acceptance test program, illustrated in Table VIII, was similar to the qualification program but consisted of only vibration, thermal-vacuum, balancing, and measurement of weight, center of gravity and the principle moments of inertia. The vibration levels and durations closely approximated those expected during launch. The thermal-vacuum test was shortened to three days maximum sunlight and two days maximum eclipse, at the same levels required for qualification. The same requirements and objectives were met for balance, weight, center of gravity and moments of inertia as for the prototype. The remaining tests (spin, temperature, humidity, sustained acceleration and shock) which had been performed on the prototype model were for

TABLE VIII — SPACECRAFT ACCEPTANCE TESTS

Test	Levels		Total Time
Vibration	Thrust	Transverse	
5–50 cps	1.5 g peak	0.6 g peak	1.7 min.
50–500 cps	7.1 g peak	1.4 g peak	1.7 min.
500–2000 cps	14.0 g peak	2.8 g peak	1.0 min.
550–650 cps	40.0 g peak	9.4 g peak	0.5 min.
Random (20–2000 cps)	7.7 g rms	7.7 g rms	4.0 min.
Thermal Vacuum	Pressure 10^{-5} mm Hg		
High Temperature	max. predicted MRT + 18°F		3 days
Low Temperature	min. predicted MRT − 18°F		2 days

the purpose of design qualification and were not required for flyable spacecraft.

4.1 *Balance, Moments of Inertia and Center of Gravity Determination*

The flyable model spacecraft were subject to the same requirements for static and dynamic balance, moments of inertia, and center of gravity as the prototype model. The results of these measurements are shown in Table IX. All five spacecraft were well within all specification requirements and design objectives.

4.2 *Vibration Tests*

The vibration levels for acceptance testing of flyable spacecraft are shown in Table VIII. The acceptance tests for five flyable spacecraft were completed with no failures of in-line systems or serious malfunction of secondary systems. The two malfunctions which did occur were: flyable 2 — the radiation damage data assigned to telemetry channel 49 gave faulty information following sinusoidal vibration in the thrust direction (the same data are carried on channel 47, so no effort

TABLE IX — BALANCE, WEIGHT, C.G. DETERMINATION, AND MOMENTS OF INERTIA MEASUREMENTS

Parameter	NASA Requirement	Design Objective	Fly 1	Fly 2	Fly 3	Fly 4	Fly 5
Weight (lbs)	None	175.0 max	172.00	170.94	172.30	173.81	174.28
Spin-axis moment of inertia, slug-ft²	None	Not specified	4.164	4.141	4.207	4.202	4.1961
Maximum transverse moments of inertia, slug-ft²	None	Not specified	3.822	3.825	3.872	3.888	3.9184
Moment of inertia ratio	None	0.95	0.918	0.924	0.920	0.925	0.934
C.G. location (inches)							
From separation plane	None	16.5	16.48	16.46	16.36	16.4	16.26
Spin-axis offset	Less than 0.005	—	Less than 0.003*	Less than 0.003*	Less than 0.003*	Less than 0.003*	Less than 0.003*
Principle axis shift (radius)	Less than 0.008	—	Less than 0.002*	Less than 0.002*	Less than 0.002*	Less than 0.002*	Less than 0.002*

* Lower limit of reliable measurement.

was made to isolate the trouble); flyable 5 — following sinusoidal vibration in the thrust direction, telemetry channels 63 and 64 had no output, indicating a failure in one of the radiation detectors located on the skin of the spacecraft. It was agreed that the remaining two channels provided adequate coverage for the radiation experiment. Since complete isolation or repair would have been impossible without opening the canister, no corrective action was taken.

4.3 *Thermal-Vacuum Tests*

The flyable model spacecraft were exposed to the same thermal-vacuum conditions as the prototype, but for a shorter duration. The acceptance tests ran for five days (three days under maximum sunlight conditions and two days under maximum eclipse conditions). The flyable satellites were operated on the same duty cycle as outlined for the prototype.

Performance of the flyable spacecraft during thermal-vacuum tests was satisfactory in all respects. A tabulation of temperatures attained and chamber pressures for each test is presented in Table X. A graph illustrating the range of electronics chassis temperatures for five flyable satellites is shown on Fig. 5. Results from flyable model 2, which is the Telstar satellite, have been plotted for reference.

4.4 *Leak Tests*

The sealed electronics canister of each flyable model spacecraft was leak tested in the same manner as the prototype, before and after the acceptance test program. The results of these tests are shown in Table XI.

TABLE X — THERMAL-VACUUM ACCEPTANCE TEST RESULTS

Satellite	Canister Temperature*		Mean Skin Temperature†		Chamber Pressure	
	Maximum Eclipse	Full Sunlight	Maximum Eclipse	Full Sunlight	Minimum	Maximum
Fly 1	43°F	88.5°F	−34°F	35°F	1.4×10^{-6} mm Hg	2.5×10^{-6} mm Hg
Fly 2	34°F	80.5°F	−40°F	27°F	1.0×10^{-6} mm Hg	2.1×10^{-6} mm Hg
Fly 3	43°F	83°F	−40°F	32°F	1.4×10^{-6} mm Hg	2.7×10^{-6} mm Hg
Fly 4	35°F	83°F	−35°F	36°F	4.8×10^{-7} mm Hg	9.1×10^{-7} mm Hg
Fly 5	38°F	78°F	−41°F	28°F	7.7×10^{-7} mm Hg	1.2×10^{-6} mm Hg

* Average temperature of four battery groups.
† Average of six points on skin.

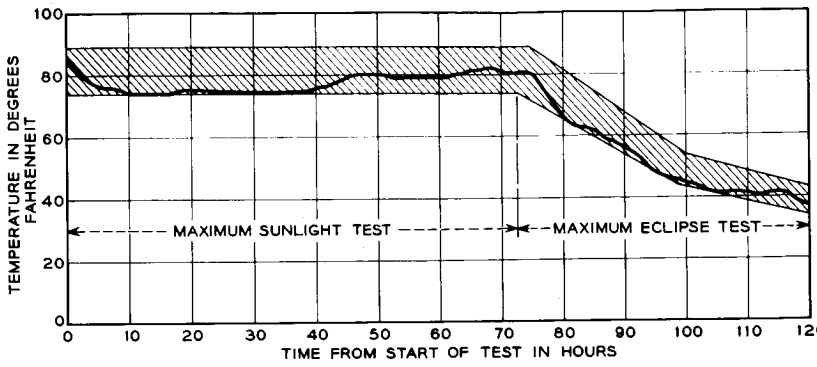

Fig. 5 — Electronic chassis temperature for five flyable satellites; flyable model 2 plotted for reference.

4.5 *Magnetic Moment Measurement*

The magnetic moment along the spin axis of the flyable spacecraft was measured and compensated to achieve the values indicated in Table XII. The plus and minus signs refer to the direction of the magnetic moment vector, the positive direction being toward the top of the satellite.

TABLE XI — LEAK TEST RESULTS

	Before Test	After Test
Fly 1	1×10^{-7} cc/sec argon	2×10^{-6} cc/sec argon
Fly 2	2×10^{-6} cc/sec argon	3×10^{-6} cc/sec argon
Fly 3	2.3×10^{-7} cc/sec argon	1.25×10^{-5} cc/sec argon
Fly 4	2.5×10^{-7} cc/sec argon	1.8×10^{-6} cc/sec argon
Fly 5	3×10^{-7} cc/sec argon	4×10^{-5} cc/sec argon

TABLE XII — MAGNETIC MOMENT MEASUREMENT (FLYABLE SPACECRAFT)

Satellite	Equivalent Torque in a 0.01-Oersted Field
Fly 1	1.9×10^{-6} ft-lbs
Fly 2	-3.3×10^{-6} ft-lbs
Fly 3	Less than measurement accuracy
Fly 4	-2.0×10^{-6} ft-lbs
Fly 5	Less than measurement accuracy

V. CONCLUSION

Components and materials selected for use in the Telstar satellite program were those which reflected a history of reliable usage in previous

successful programs. The system design included the maximum practical margin of safety, commensurate with weight and space limitations of satellite systems. In addition to designing with a maximum safety factor, all manufacturing was accomplished under the closest possible control. Extensive testing of subassemblies and satellite models, carried out in parallel with the design and assembly of actual spacecraft, enhanced reliability of the finished product, and permitted timely modifications where required.

The environmental test program was designed to provide the most comprehensive evaluation of the spacecraft design in the time available. The qualification tests performed on the prototype provided assurance that the Telstar satellite was compatible with the environments expected during powered and orbital flight. The acceptance tests served to uncover manufacturing defects which may have developed during assembly of the various subassemblies into a completed system. Five flyable spacecraft have successfully completed the acceptance test program with no major failures or malfunctions in the in-line systems.

REFERENCE

1. Hrycak, P,. Koontz, D., Maggs, C., Stafford, J. W., Unger, B., and Wittenburg, A. M., The Spacecraft Structure and Thermal Design Considerations, B.S.T.J., this issue, p. 973.

Page intentionally left blank

Command and Telemetry Systems

By R. C. CHAPMAN, JR., G. F. CRITCHLOW, and H. MANN

(Manuscript received March 22, 1963)

The command and telemetry portions of the Telstar system provide necessary support functions for the basic communications experiment and the radiation experiment. By means of the command system, the states of 9 magnetic latching relays in the satellite are controlled from the ground. Commands are sent to the satellite by coded signals modulated on a carrier in the VHF band. The telemetry system also uses a VHF carrier to transmit encoded information from the satellite. Data on 112 items are provided once each minute. This paper discusses the over-all command and telemetry systems and considers the general objectives, system aspects and detailed implementation.

I. INTRODUCTION

The Telstar satellite includes circuits designed to perform two basic experiments: (*i*) a communications experiment using a wideband, active repeater and (*ii*) a radiation experiment designed to provide information on the environment in outer space and the effects of this environment on devices used in communication circuits. The command and telemetry portions of the Telstar system provide a very necessary support function for these experiments. This paper discusses the over-all command and telemetry systems; it considers first the need and general objectives and then the systems aspects of the design. Finally it gives a detailed discussion of the implementation of each system.

The need for a command system for the Telstar project arises primarily because of power considerations associated with the satellite repeater: the communications circuits consume more power than the solar plant is capable of supplying.[1] To be able to operate under full load, batteries are provided which supply the additional power needed during operation of the communications circuits. During those intervals when the communications circuits are not on, the batteries are recharged by the solar plant. Hence a command system is necessary to turn the high-power communications circuits on and off. Having provided a

command system, it is then convenient to turn other circuits on and off and provide some other functions which can only be available with a command system. These functions include changing telemetry encoders, testing the two command receivers, and activating a torquing coil for attitude control, as well as turning on and off the traveling-wave tube, the IF amplifiers, the microwave carrier supply, telemetry and the radiation experiments. The command receiver circuits must always be energized so that commands may be acted upon to turn on other circuits. The VHF beacon, used for wide-angle acquisition and tracking, is also left on; however, it can be turned off under special conditions.

The telemetry carried aboard the Telstar satellite provides information on 112 different quantities at a rate of one full frame per minute. These quantities fall in four major categories. One type of data relayed from the satellite consists of status information: for example, the state of control relays, some critical temperatures, the solar plant output, and the battery voltage. These data must be decoded and displayed in real time so that the satellite can be operated with the least chance of damage. The second class of data includes those items which pertain to the general condition of the satellite. Such items include internal and external temperatures, pressure, and solar aspect angle. These data are normally monitored and recorded to be analyzed at a later time. They provide a continuous record of the condition of the satellite and some of the effects of its environment. The third main category of telemetry data is that which monitors parameters pertinent to the communications repeater. These data are monitored and recorded to provide correlation data for the communications experiments. Such items as satellite receiver AGC voltage, transmitted power levels, and certain temperatures are necessary for correlating test data. The fourth category of telemetry information is that which provides data from the radiation damage experiments and those channels which contain the radiation counter information. About one fourth of all the telemetry channels are used in the radiation experiment, one third are used to measure various temperatures, and the remaining channels are used to measure a variety of relay states, currents, voltages, biases and calibrations.

II. SYSTEMS DESCRIPTION

The command and telemetry systems are each one-link transmission systems. The command system has its transmitting terminal on the ground and the receiver in the satellite. The telemetry system, on the other hand, transmits from the satellite and the signals are received on the ground. Fig. 1 shows a block diagram of each system and those por-

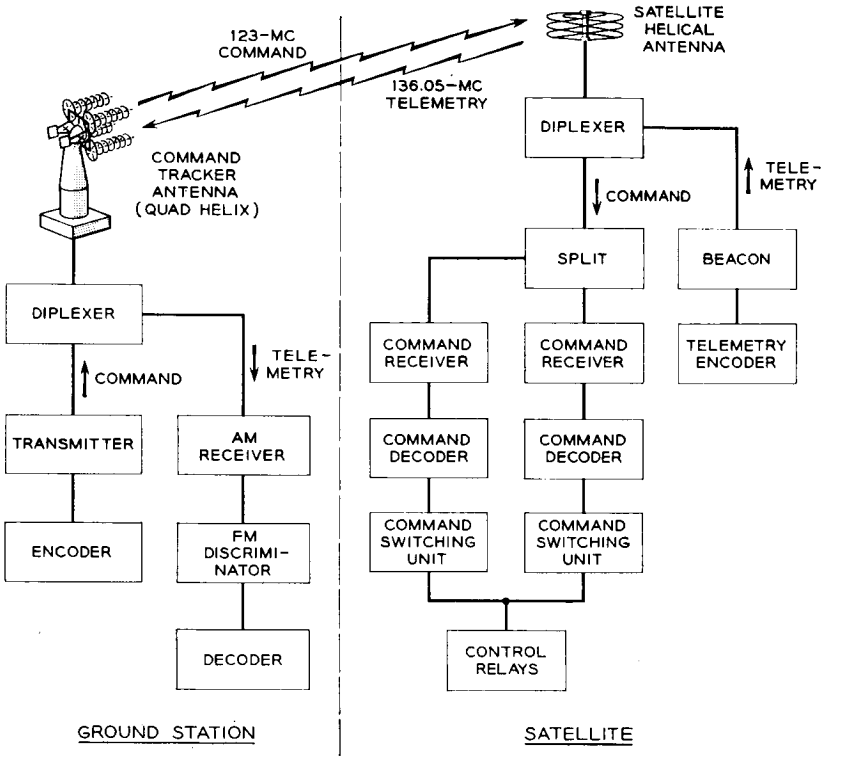

Fig. 1 — Block diagram of command and telemetry systems.

tions of the equipment which are common to the two systems, such as the diplexers and the antennas.

The command system transmits signals to the satellite at approximately 123 mc. The transmitting terminal consists of a command encoder which generates the specified code and a VHF command transmitter which is amplitude modulated by the command signal. The output of the command transmitter goes through the ground diplexer to the command tracker antenna and is radiated to the satellite. The signal picked up by the satellite helical antenna goes through the satellite diplexer and a splitting arrangement into two command receivers. The baseband pulses out of each receiver drive a decoder which activates the proper relay through the action of the switching unit.

The telemetry system transmits information from the satellite back to ground. The transmitting equipment in the satellite consists of a telemetry encoder whose output modulates the 136-mc beacon. The

signal then goes through the satellite diplexer to the helical antenna where it is radiated. The telemetry signal is picked up on the ground by the command tracker antenna and then goes through the ground diplexer to the telemetry receiver. The output of the telemetry receiver drives the decommutator, which presents the information in printouts and displays.

The details of each of these systems will be discussed separately in later portions of this paper. The nature of the signals and the over-all system design considerations will be covered in the following sections.

III. GENERAL DESCRIPTION OF TRANSMISSION SIGNALS

3.1 *Command Signals*

The commands are transmitted to the satellite in the VHF band. The 123-mc carrier is amplitude modulated with a keyed subcarrier. The subcarrier, a 5.451-kc signal, is keyed on and off to generate a code made up of bursts of subcarrier of different widths. A command word is composed of a guard space, a start pulse and six code bits, each occupying a time slot equal in length to 72 cycles of subcarrier. A guard space is no pulse (a blank time slot), and a start pulse is a burst of subcarrier for three fourths of the time slot. The six code bits are made up of three ones (50 per cent duty cycle, burst of subcarrier for half a time slot) and three zeros (25 per cent duty cycle, burst for one fourth of the time slot). This three-out-of-six code permits 20 unique commands, of which 15 are used in the Telstar system. The transmission of a command consists of sending the desired code word five times in succession. This repetition is strictly redundant since each word is decoded and acted upon independently in the satellite. Fig. 2 shows the baseband waveform of a typical word (110100), the keyed subcarrier, and the carrier modulated by this subcarrier. This particular code structure, the carrier, and the subcarrier frequencies were chosen to be compatible with existing command facilities at the NASA Minitrack stations. The command and telemetry signals were thus chosen to provide the greatest flexibility and compatibility with these existing facilities.

The code signal, as described above, is generated in the command encoder. This signal 100 per cent amplitude modulates the command transmitter. The command signal is transmitted from the command tracker antenna and is received at the satellite by the helical VHF antenna situated at one of the poles of the satellite. The command receiver in the satellite shifts the carrier to a 5-mc IF, amplifies it, and detects the code to produce a baseband pulse train which is decoded and which

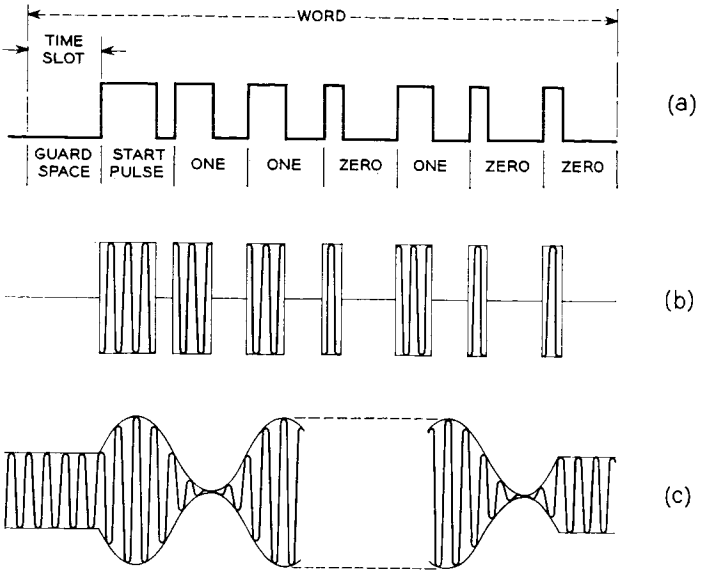

Fig. 2 — Command signal waveforms: (a) baseband code, (b) gated subcarrier (c) modulated carrier (expanded time scale).

causes the proper relay switching to accomplish the function designated by the command being sent.

3.2 *Telemetry Signal*

The telemetry signal is transmitted from the satellite to the ground telemetry receiver, also in the VHF band. The same antennas are used: the satellite helix transmits the 136-mc beacon signal and the command tracker antenna receives it. The telemetry encoder within the satellite generates a PCM signal made up of 120 eight-bit words. Each eight-bit word is made up of a seven-bit binary code with an eighth bit used for word synchronization. Of the 120 words there are 118 data words, and two words (119 and 120) are used for frame synchronization. The baseband PCM signal frequency modulates a 3-kc subcarrier with a deviation of ± 7.5 per cent (± 225 cps). The modulating signal is two-level, so the output of the FM modulator is a signal alternating between two frequencies, 2775 and 3225 cps. This signal in turn 50 per cent amplitude modulates the beacon. Fig. 3 shows a typical telemetry word (level 90, on a 7-bit binary scale from 0 to 127), the corresponding plot of frequency versus time of the subcarrier, and the modulated

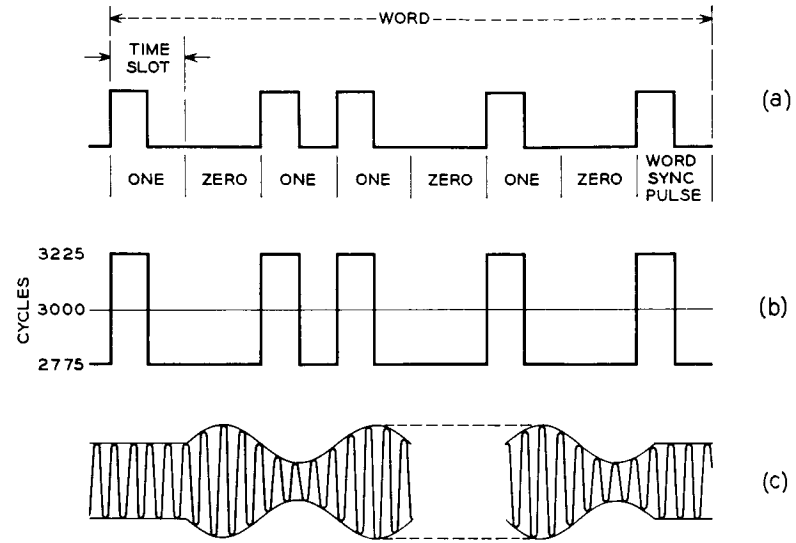

Fig. 3 — Telemetry signal waveforms: (a) baseband code (bit level 90); (b) subcarrier frequency deviation; (c) modulated carrier (expanded time scale).

carrier. This PCM/FM/AM signal is transmitted from the satellite helical antenna and is received by the command tracker antenna. After amplification, the carrier is shifted to a 10-mc IF, and an amplitude detector retrieves the frequency modulated 3-kc subcarrier. A frequency discriminator extracts the baseband PCM signal, which is then decoded to provide the corresponding output for each of the telemetry channels.

3.3 *Command and Telemetry Interaction*

The command and telemetry systems are essentially independent systems. Certain commands are interlocked in such a way that their use depends on what commands have been sent and upon the status indicated by the received telemetry. The telemetry circuits in the satellite can be turned on and off, and some of the telemetry channels monitor parameters in the command circuits. To this extent the two systems interact. Since the two directions of transmission use the same antennas, diplexers are used at each terminal, and there will be some leakage of each transmitter into the other receiver. The frequency separation is large enough so that the leakage problem is not severe. The details of this effect will be discussed under System Performance, Section V.

IV. SIGNAL LEVELS

4.1 *Command*

The command transmitter has an output capability of 200 watts of average unmodulated carrier power. At the Andover, Maine, ground station the cabling distance from the command transmitter to the command tracker antenna is about 150 feet. The signal then goes through the diplexer before being radiated from the antenna. Cabling and diplexer losses are 2.5 db, and the antenna provides a gain of 17.5 db at 123 mc, for a net gain of 15 db.

Loss from transmitting antenna on the ground to the receiving antenna on the satellite may be calculated from the theoretical free-space path loss. Since the range (distance from transmitting to receiving antenna) is constantly changing in a satellite system, the path loss is a variable. For the Telstar satellite launched July 10, 1962, the range may vary from as much as 6500 miles (looking at apogee on the horizon) to as little as 500 miles (perigee directly overhead). These variations in range will result in a path loss variation of 22 db (from 155 to 133 db).

The radiation pattern of the satellite helical antenna is described in detail elsewhere in this issue.[2] Ideally, the antenna would be isotropic. The antenna pattern is essentially a surface of revolution; that is, the gain at any angle does not change as the satellite spins on its axis. However, the gain is not constant as a function of the angle between the satellite spin axis and the direction from which the satellite is viewed. This angle, when measured from the end of the spin axis away from the helical antenna, is called the spin angle. Fig. 4(a) shows the antenna gain (including cabling and matching network losses) as a function of the spin angle. Near the poles the antenna has considerable loss and is difficult to measure; however, if we consider only those angles between 5 and 165 degrees, we see a range in antenna gain of 16 db. Combining this variation with the variation due to range as given by Fig. 4(b), the signal level at the command receiver may vary as much as 38 db over all combinations of range and spin angle. It is possible on a given pass to see a wide range of spin angles; however, to see the full variations in range requires that the apsides advance through half a cycle, which in this case takes about 3 months. The command receiver in the satellite is designed to handle a signal level range of 30 db. This AGC range, while not adequate to cover all cases, is adequate to cover the range of signal levels that result during any pass or group of passes.

In addition to the path loss and the loss in the satellite helical antenna.

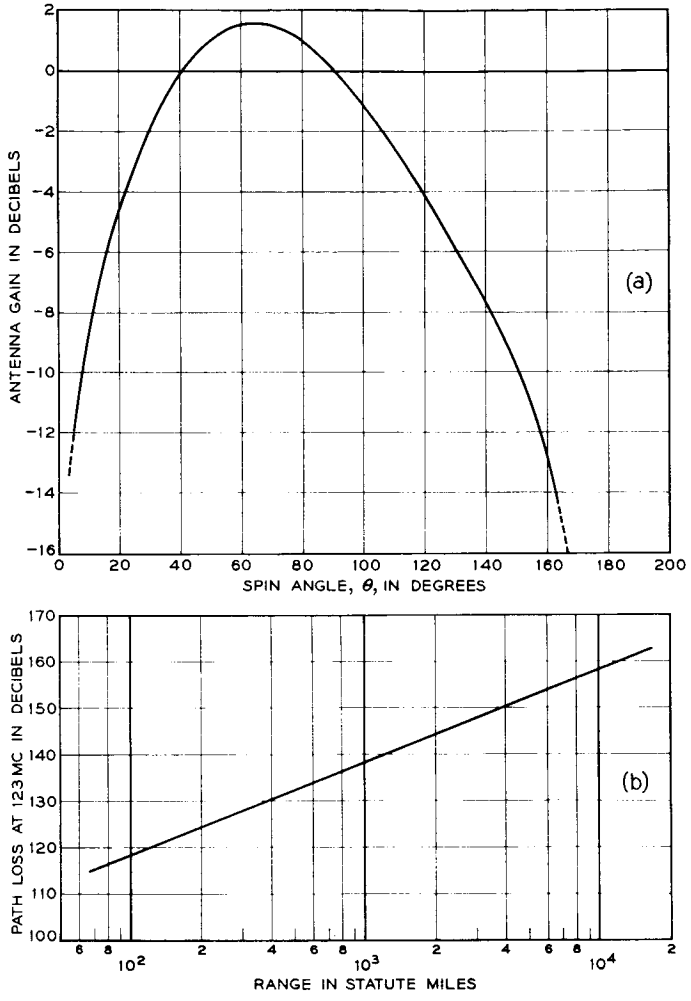

Fig. 4 — (a) Satellite antenna gain as a function of spin angle, (b) free-space path loss at 123 mc as a function of range.

there is a 3-db polarization loss. The helical antenna on the satellite has an essentially linear polarization, and the command tracker antenna quad-helix has a right-hand circular polarization. To get from the antenna to the command receiver, the signal loses 2.5 db in the diplexer and another 3 db in a splitting pad (two receivers operating in parallel for redundancy). The AGC range of each command receiver is such that it can handle signals at its input of -100 to -70 dbm.

4.2 *Telemetry*

The down link of the command and telemetry system consists primarily of the satellite beacon transmitter, the transmission medium, and the RF and telemetry receivers. The beacon puts out 200 milliwatts (+23 dbm) of average unmodulated carrier power. The satellite antenna pattern at 136 mc has approximately the same shape as at 123 mc, but the gain is down about 1 db due to cabling and matching network losses. Free-space path loss at 136 mc is about 0.8 db greater than at 123 mc, and the net gain associated with the command tracker antenna is about 18 db rather than the 15 db at 123 mc. The command tracker antenna is 3 db better at the telemetry frequency than at the command frequency for two reasons. First, the beam is narrower at 136 mc, giving a gain increase of about 1.5 db, and secondly, the 1.5 db of cabling loss is avoided by placing the RF preamplifier in the antenna pedestal instead of in the control room 150 feet away.

There is again a loss of 3 db due to polarization, and the range of received signal levels as before is 38 db. The limitation on the signal level received at the ground is that it be strong enough to produce a detectable signal. The next section will show that a detectable signal will be received if the command link is workable.

V. SYSTEM PERFORMANCE

5.1 *The Command System*

The performance of the command and telemetry systems can best be described by first considering the parameters of the command system. From noise considerations, the minimum allowable received signal level can be determined. Then, knowing the properties of the ground transmitter and of the satellite receiver, the worst combinations of spin angle and range can be determined. The performance of the telemetry system will then be determined, based on the poorest combination of range and spin angle allowed by the command system.

Contributors to the noise performance of the command receiver are (*i*) thermal noise, (*ii*) galactic or cosmic noise, and (*iii*) leakage of the beacon signal into the command system. The effective bandwidth of the command receiver is less than 60 kc. The thermal noise power available in a 60-kc band referred to the input of a 5-db noise figure amplifier is −122.8 dbm. Cosmic noise available in a 60-kc band at 123 mc is taken to be −121 dbm (1000°K)[3]. The leakage of the 136-mc beacon into the command receiver results in an interfering signal at the

output of the receiver. The off-frequency rejection in the receiver referred to −100 dbm at the input is 64 db; the diplexer has 80 db rejection against the +24-dbm, 136-mc signal getting into the command system; and taking the 3-db splitting pad loss, the leakage signal referred to the input of the command receiver is −123 dbm. Adding these three interferences on a power basis results in an interference level at the input to the command receiver of −117.5 dbm. With a −100-dbm input signal, the resulting signal-to-noise ratio of 17.5 db will provide essentially error-free performance in the command decoder.

The minimum signal level within the AGC range of the receiver, as stated earlier, is −100 dbm. Since this also results in a signal-to-noise ratio corresponding to error-free operation, it will be taken as the threshold of commandability. In practice it has been found that a received signal level of −100 dbm is 3 to 5 db above the point where commands will be recognized but with an occasional error.

The received power equation for the command system is

$$P_R = P_T + G_1 - PL + G_2 - 8.5 \text{ db} \tag{1}$$

where P_R = received signal level at the input to each command receiver in dbm

P_T = ground transmitter output power (+53 dbm)

G_1 = command tracker antenna gain at command frequency minus cable and diplexer loss (+15 dbm)

PL = path loss at command frequency (db)

G_2 = satellite helical antenna gain at command frequency (db).

The 8.5 db is made up of 3 db polarization loss, 2.5 db satellite diplexer loss, and 3 db splitting pad loss for driving the two command receivers in parallel. To keep the minimum signal at the command receiver input at −100 dbm requires that the path loss minus the satellite antenna gain shall not exceed 159 db. The path loss at the command frequency is given by

$$PL = 78.4 + 20 \log R \text{ (db)} \tag{2}$$

where R is the range from transmitter to satellite in statute miles. Fig. 4 shows path loss as a function of range and the satellite antenna gain as a function of spin angle. Fig. 5 shows the relationship between range and spin angle such that the minimum workable signal is assured. The contour plotted is for $P_R = -100$ dbm. The received signal level anywhere to the left of the curve will exceed −100 dbm; to the right of the curve the level will be less than −100 dbm and commanding should not be attempted. For an isotropic antenna (the actual antenna has unity

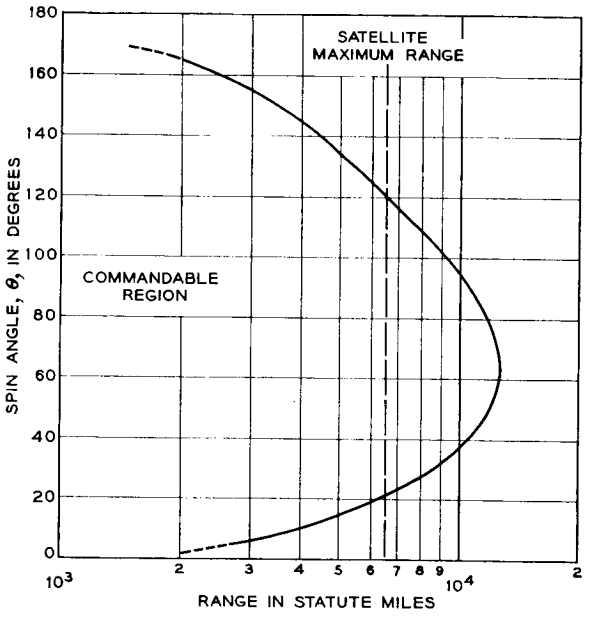

Fig. 5 — Commandability contour for received signal level of −100 dbm.

gain at 90 and 40 degrees) the maximum workable range is 10,700 miles. For the actual antenna, the maximum range which will be safe for any spin angle between 5 and 165 degrees is 2000 miles, and the maximum range for the best spin angle (65 degrees) is 12,900 miles. For the Telstar satellite orbit with its maximum slant range of 6500 miles, the command system will be workable as long as the spin angle stays within 20 to 120 degrees.

5.2 *The Telemetry System*

If the command system is within range, then the path loss minus satellite antenna gain is less than 159 db at the command frequency. Under the same conditions, the path loss minus satellite antenna gain at the telemetry frequency will be less than 161 db (the difference in path loss and antenna gains were pointed out previously) and the received signal level at the input to the telemetry receiver will be at least −120 dbm: satellite transmitted beacon power of +23 dbm, minus 161 db for path loss and antenna gain, plus 18 db for the ground antenna, results in a received signal level of −120 dbm. The noise level referred

to the input of a 3.5-db noise figure receiver with a 20-kc band is −130 dbm. The minimum carrier-to-noise ratio (C/N) for the AM detection is then 10 db. With a C/N ratio of 10 db, the AM detector will not enhance the noise appreciably and the signal-to-noise ratio (S/N) for the FM detector may be calculated directly. The signal power in each sideband for a 50 per cent amplitude modulated carrier is 12 db below the carrier level. With double-sideband detection and a 600-cps bandwidth, the S/N at the input to the FM detector is 16 db: power in each sideband is −132 dbm; noise in a 600-cps band is −145 dbm. Single-sideband detection would give S/N = 13 db, and double-sideband detection results in S/N = 16 db. This signal-to-noise ratio at the input to the FM detector will result in output performance which is essentially error free. To keep a S/N ratio of at least 10 db at the FM detector, the signal level might be allowed to drop another 4 db to −124 dbm. At this point the C/N ratio at the AM detector would be 6 db and the full 3-db advantage of double-sideband detection could not be realized. Hence, the S/N ratio at the input to the FM detector would be about 10 db, and this should be near the breaking point of the system. This has been borne out in practice since the telemetry system has been found to break at input levels of −122 to −124 dbm.

As seen from the above discussion, the command and telemetry systems are both workable under just about the same conditions. In the Telstar satellite orbit (maximum range 6500 miles) both systems are operable with 2- to 4-db margin for spin angles between 20 and 120 degrees. To date the spin angle from the Andover station has not been less than 20 degrees, but it has been as high as 165 degrees. At the command and telemetry station at Cape Canaveral the spin angle has been much greater; in fact spin angles very near 180 degrees have been encountered. Under these conditions both the command and telemetry systems were unworkable as expected. The times of these "spin outages" are predictable and can be avoided by appropriate scheduling.

VI. COMMAND SYSTEM

Previous sections stated the purpose of the command system, gave a brief over-all system description, and discussed signal levels and noise performance. We now proceed to a more detailed description of the command system. First the entire system will be given a general description to functionally relate the major portions. This will be followed by still more detailed descriptions of the major blocks.

6.1 *General Description*

The command system employs fifteen different commands as given in Table I. These are listed here as a matter of general interest and for convenience in understanding subsequent sections.

A functional block diagram of the command system is shown in Fig. 6. A command can be originated in the ground station at the telemetry and operating panel or remotely at the ground station control console. The command encoder translates the specific command to a preselected code and sends this code via the ground station command transmitter to the satellite.

Upon initiation of a command, a control signal is sent over one out of 20 lines to the encoding circuit. This signal is translated to an individual 6-bit parallel code consisting of three ones and three zeros.

A decoding circuit converts the code back to a signal suitable for lighting indicators to show that the proper command has been encoded. Thus, when the command button is pressed it lights up, and another group of six indicator lights shows the actual binary code.

The encoder output is also applied to the word assembly and to "parity and lockout" circuits. The word assembly unit transforms the 6-bit parallel word to an 8-bit serial word consisting of a start bit, the 6-bit code, and a guard space. The 8-bit word is applied to the "parity and lockout" circuit where the code is checked for an odd parity of three

TABLE I — COMMANDS

Command	Function
A	turns on TWT filament voltage
B	turns on TWT helix and collector voltages, energizes circuits associated with the communications experiment
C	turns on TWT anode voltage
CC	turns off TWT anode voltage
AA	turns off TWT helix, collector, and filament voltages; de-energizes circuits used in the communications experiment
D	turns on telemetry and radiation experiment circuits
DD	turns off telemetry and radiation experiment circuits
E	turns on current orientation loop
EE	turns off current orientation loop
F	connects telemetry encoder No. 1
FF	connects telemetry encoder No. 2; F and FF also control direction of current through the orientation loop
SS	initiates CC, AA, DD, and EE and disconnects battery and VHF beacon
S	connects battery back into circuit and turns on VHF beacon
T-1	turns off command decoder No. 2 for 15 seconds
T-2	turns off command decoder No. 1 for 15 seconds

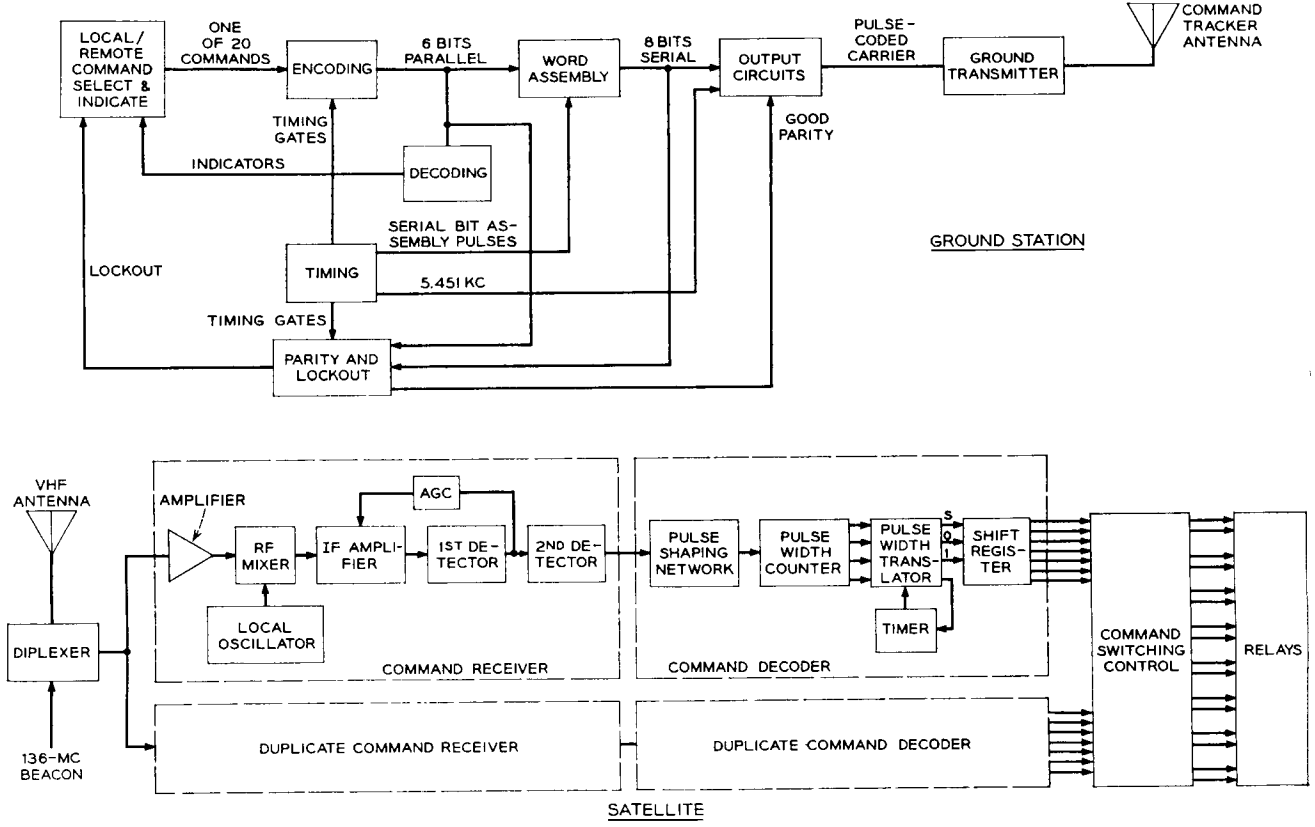

Fig. 6 — Command system block diagram.

ones. If an improper code is detected, a parity relay operates which in turn actuates the lockout circuit. The lockout circuit prevents transmission of the invalid code and selection of a new command until a reset button is depressed.

The word assembly output, if found to be proper, is applied to the output circuit five times in succession. In the output circuit the 8-bit word 100 per cent modulates a 5.451-kc carrier. This amplitude-modulated subcarrier signal is sent to the command transmitter where it 100 per cent amplitude modulates the 123-mc carrier and is then transmitted to the satellite via the quad-helix command tracker antenna.

For reliability, the command portion of the satellite (except for relays) is duplicated and is powered continuously. The two halves of the command system are nearly independent except for some interconnections made to insure proper operations under unusual circumstances. The signal from the diplexer is transformer-coupled to the two command receivers.

The command receiver is of the superheterodyne type and consists of an RF mixer, local oscillator, IF amplifier, AGC, and a two-stage detector. The receiver AGC obviates the need for a variable threshold in the command decoder.

The command receiver output is detected in the shaping network, which has a threshold level fixed at half the average signal amplitude.

The command decoder translates the baseband train of pulses which the receiver has recovered into a pulse on the appropriate one-out-of-fourteen output leads. The decoder consists of a pulse shaping network, pulse width counter, pulse width translator, timer, and shift register.

The one-out-of-fourteen outputs of the decoder are amplified and stretched in the switching units, and the resultant outputs trigger magnetic latching relays. Sensitive magnetic latching relays are employed to conserve power.

To prevent damage to the TWT and the battery of the satellite, a number of safety interlock features are incorporated in the command encoder on the ground and in the switching unit in the satellite.

The TWT anode turn-on (C command) cannot be sent unless three minutes have elapsed since the TWT filament was turned on (A command) and unless telemetry indicates that the filaments are actually on, except when an override push-button is depressed. The override feature is used to permit rapid turn-on of the tube when the 3-minute warm-up time is unnecessary (i.e., if the tube had just been turned off).

Whenever the A relay in the satellite transfers (TWT heater on or TWT off), the B relay (TWT helix and collector) is reset. This obviates the need for a BB command and prevents turning on the TWT helix and collector voltages prior to the TWT heater. The A and C relays are interlocked to assure that the TWT anode voltage (C relay) will be

turned off before the heater, helix and collector voltages are removed. These features prevent damage to the TWT.

A low-voltage trigger circuit removes all loads (except for the command system) and disconnects the battery by resetting the S relay. With the S relay reset, the 136-mc beacon is inoperative and no telemetry is available. The S relay reset state also inhibits the commands A, B, and C, thus preventing turn-on of the TWT with low battery voltage. If the S relay is reset by the low-voltage trigger, it cannot be set by a ground command (S) until the low-voltage condition subsides. This safety feature prevents damage to the battery and to the TWT due to a low-voltage condition which, for example, might be caused by leaving the TWT on for an excessive period.

6.2 *Ground Command System*

6.2.1 *Command Encoder*

A detailed diagram of the encoder is shown in Fig. 7. Operation of a command switch momentarily energizes a command select relay. The matrix input register stores this information temporarily until it is transferred (in the form of a parallel 6-bit code) to the matrix output registers. The use of two stores permits a new command to be selected without interfering with the transmission of the previous command.

The heart of the encoder is the crystal oscillator which furnishes the basic 5.451-kc subcarrier frequency to be used for code transmission. All of the encoder timing is generated from this frequency with countdown circuits. To insure proper timing accuracy in the frequency divider circuits, the oscillator output is applied to a Schmitt Trigger circuit

The N/3 countdown circuit of the cycle counter is of the relaxation divider type, whereas the N/2 countdown circuits consist of binary counter stages. The primary and secondary outputs from the final two binary counters, representing the zero and the one respectively of the ternary code, are applied to the logic I unit to obtain the start pulse and the bit duration. The one and zero are also applied to the parity counter gate. A parity count can be taken in AND gates since, as shown in Fig. 8, the coincidence of the eight code (excluding start) with ones and zeros can have three outputs if and only if the code contains only three ones and three zeros. (The parity enable eliminates the start pulse.) The start, zero, and one outputs control the duration of the outputs of the word timing gate.

A three-stage binary bit counter counts out the 8-bit code word, and feeds the logic II gate whose outputs are used for timing and for the

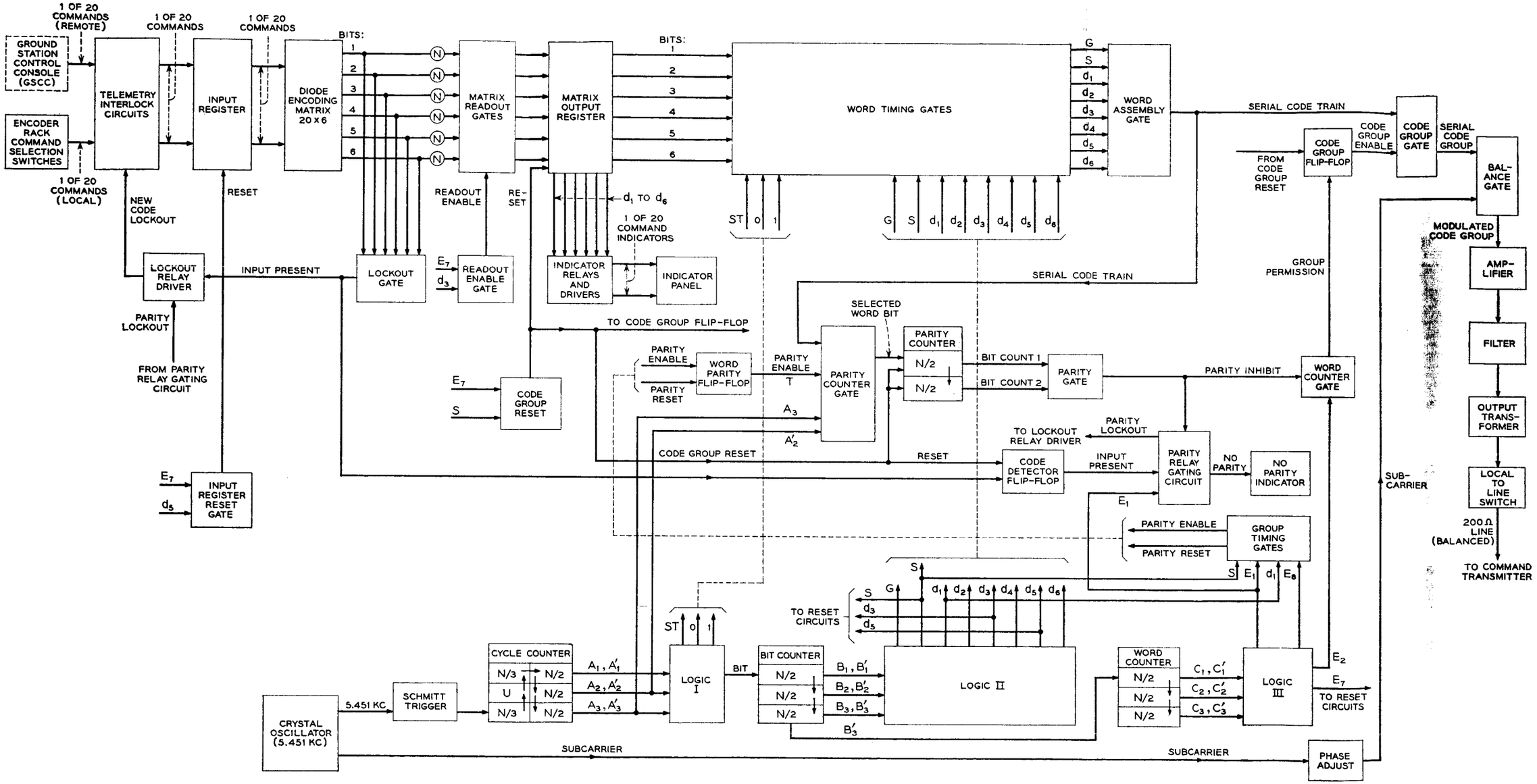

Fig. 7 — Command encoder.

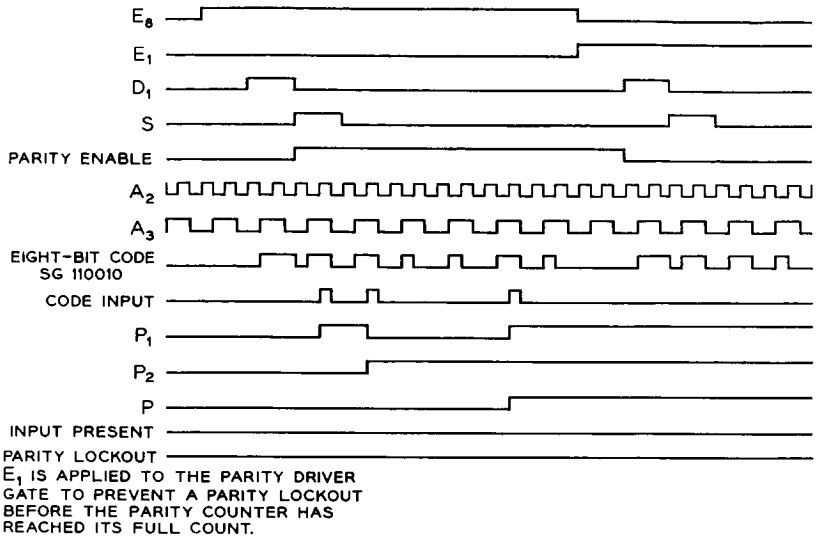

Fig. 8 — Parity count timing sequence.

parallel code to serial code conversion. The output of the third stage of the bit counter feeds the word counter, which in conjunction with logic III permits the code to be generated five times in succession. By the nature of the circuits, a gap of three word intervals follows the generation of the five code groups. Since the timing block of the encoder operates continuously, there can be a delay of about $\frac{1}{2}$ second in transmission of a command if a command is selected just after a word counter cycle has started. Partial code transmission is prevented by the parity and lockout, which can only operate once during a code group (five codes) and is initiated with the third code (dead interval).

6.2.2 *Command Transmitter*

The command transmitter consists of an RF exciter, intermediate power amplifier, modulator, RF power amplifier and an output section. The exciter generates the 123-mc crystal-controlled carrier which drives the intermediate power amplifier. The RF power amplifier then provides the power gain necessary to radiate 200 watts. The output stage is push-pull and is plate-modulated by the signal out of the modulator. The modulator is flat to ± 1 db from 200 cps to 10 kc and is capable of providing 100 per cent modulation of the 200-watt output. The output section provides coupling into the load, and matching trimmers and filters. The equipment is housed in two bays and was designed and man-

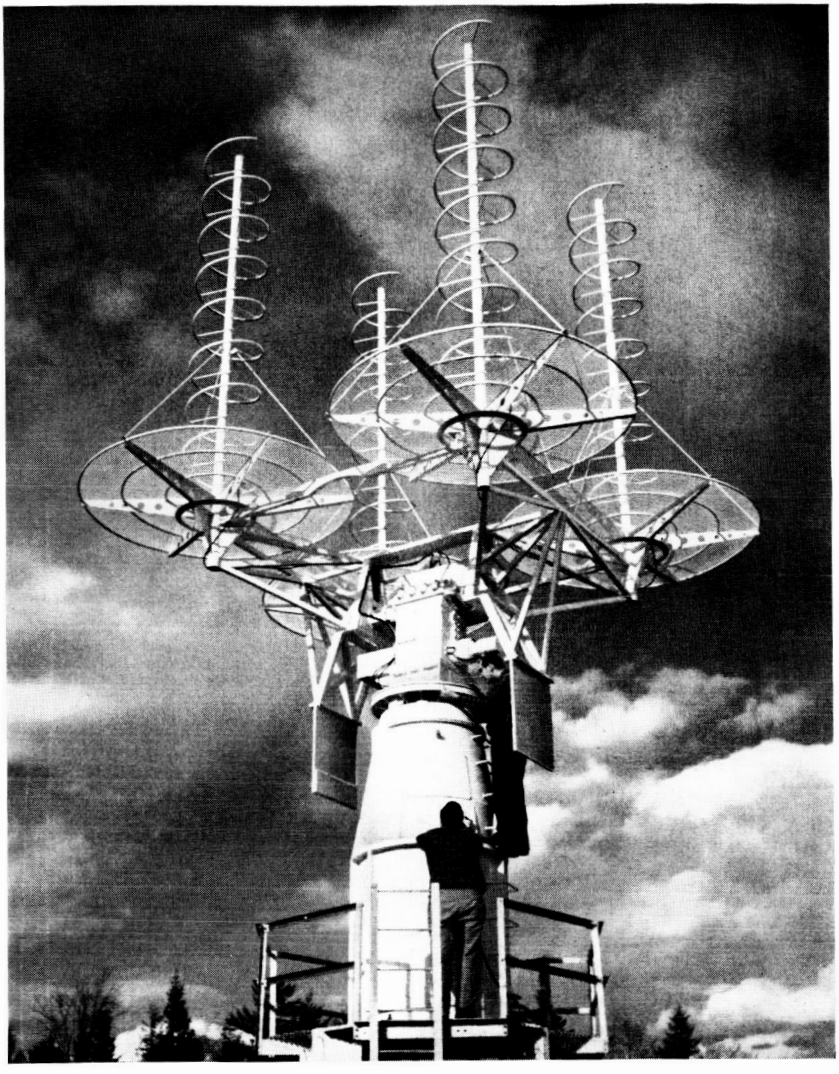

Fig. 9 — Command tracker antenna.

ufactured to Bell Telephone Laboratories specifications by Lockheed Electronics Company, a division of Lockheed Aircraft Corporation.

6.2.3 *Command Tracker Antenna*

The command tracker antenna shown in Fig. 9 is a quad-helix VHF antenna used to transmit the command signals, receive the telemetry

signals, and track the VHF beacon. The antenna has full autotrack capabilities, so the command and telemetry operation can be completely independent of other satellite operations. It can, however, serve as an acquisition aid by providing pointing information to other antennas, such as the precision tracker.[4] It uses phase-sensitive monopulse tracking employing a 4-element helix array and giving over-all pointing accuracy of approximately ± 1 degree.

As a transmitting antenna (123 mc) it has a gain of 17.5 db with right-hand circular polarization, and its side lobe levels do not exceed -11 db. For receiving at 136 mc, the gain is 19 db and the polarization and side lobe performance are the same as at 123 mc. The command tracker antenna was designed and built to Bell Telephone Laboratories specifications by Radiation, Incorporated, of Melbourne, Florida.

6.3 *Satellite Command System*

6.3.1 *Command Receiver*

Each of the two command receivers consists of an RF section, mixer, local oscillator, amplifier and detector. The two command receivers (See Fig. 10) are transformer coupled to the diplexer. The manner of making the connection places the loads in series, permits the use of ground for all returns, and provides the proper generator impedance for optimum noise figure.

The RF section provides 18 to 20 db of gain at 123 mc and has an over-all bandwidth of 3 mc (3 db points). This section consists of two stages separated by a low-Q parallel tuned circuit while the second stage has connected to its emitter a high-Q tuned series circuit. This combination provides a low over-all noise figure with at least 10 db image frequency rejection. The mixer is a single-stage amplifier employing emitter injection of the local oscillator while the RF signal is applied to the base. The conversion gain of the stage is approximately 4 db and the IF signal is at 5 mc. A temperature-stabilized crystal oscillator followed by two diode doubler circuits provides the local oscillator signal of 128 mc for the mixer.

A 4-stage IF amplifier provides 50-80 db of gain, depending upon the AGC control. AGC control is maintained on the first three IF stages and provides a constant detected output level over a 30 db range of receiver input signals. Primary-tuned interstage coupling transformers provide an IF bandwidth of approximately 50 kc (3 db points), which allows for Doppler shifts and transmitter and receiver frequency drifts.

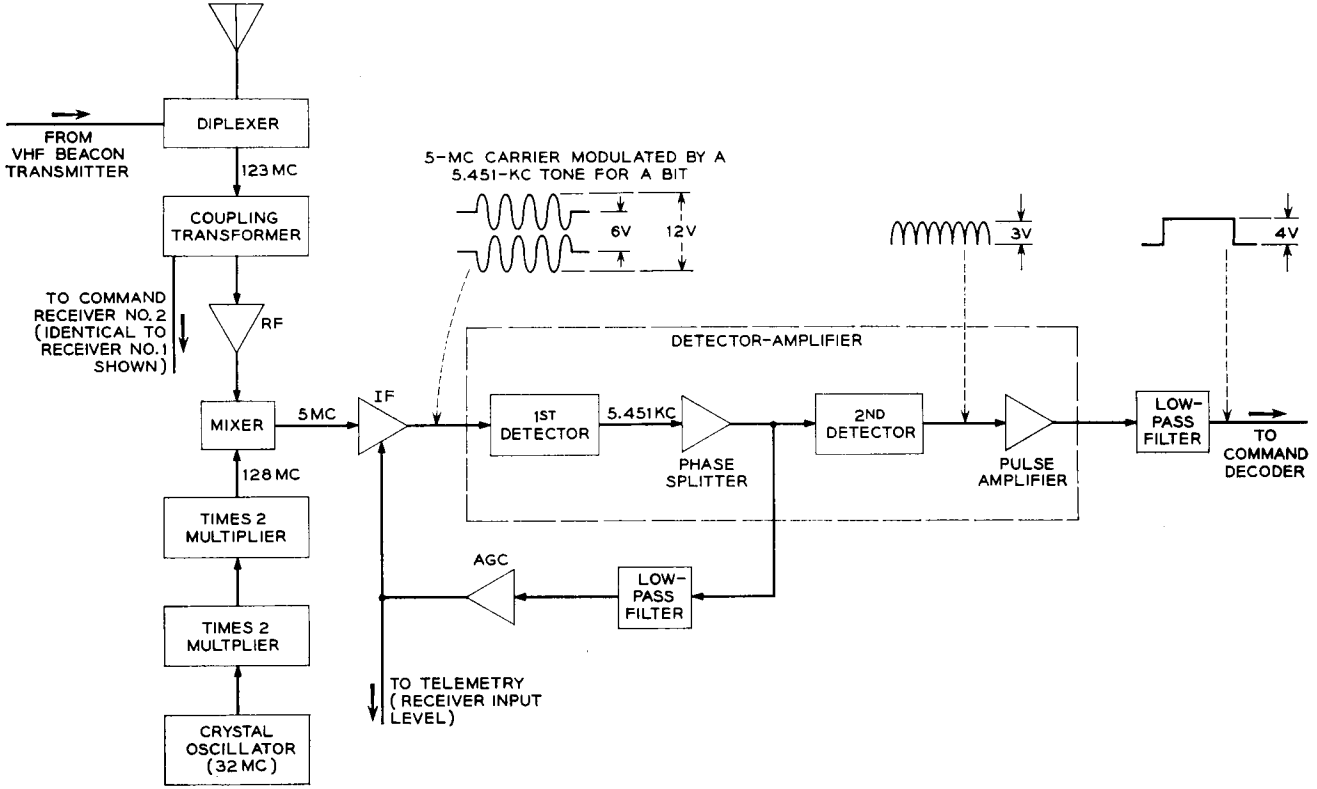

Fig. 10 — Command receiver.

Because of the use of a subcarrier, double detection is necessary. The first detector recovers the 5.451-kc subcarrier. An amplifier supplies a signal to the AGC loop and to the second detector, which consists of a full-wave rectifier followed by an amplifier and a low-pass filter, having a 500-cps cutoff with a 6 db per octave slope. The output signal is a train of pulses having an amplitude between 4 and 4.5 volts and containing less than 1 db of ripple.

6.3.2 *Command Decoder*

A simplified block diagram of the command decoder is shown in Fig. 11 and the timing relationships are shown in Fig. 12. The command receiver output signal is detected in the shaping network. Because the receiver has AGC, the shaping network threshold level is fixed at the average-signal, half-amplitude value. The detected signal permits the gated multivibrator pulse generator to free run for the length of time that the signal exceeds the threshold level. The pulse generator will generate three, two, or one pulse(s) for a start, one, and zero input respectively. The output of the shaping network is also used for readout and reset functions. The pulse width counter and digit gates (zero, one and reset) translate the ternary code to a pulse on one of three output leads. The counter and gates are "reset" by the detected signal. To prevent the inadvertent joining of two code fragments, a consecutive pulse timer controls the one and zero gate outputs. The loss of a word bit resets the timer, thus preventing further one and zero gate outputs. Because of the positive feedback aspects of this circuit, the timer inputs are controlled by the shaping network output.

A detected start pulse at the R gate output is used to reset the flip-flop stores and the digit counter. It also starts the consecutive pulse timer. The combined zero and one outputs drive the digit counter. The digit counter and the counting gates form a series-to-parallel converter for the detected ones. With the inclusion of the flip-flop stores, the combination forms a shift register. The output gates translate the stored binary code to an output pulse on one-of-fourteen leads. To restrict power consumption and to control the output gate readout time, a strobe unit applies power to these gates. The strobe, in turn, is controlled by the digit counter and will generate an output when the digit counter has counted to six. Since the strobe is internally ac coupled, the power to the gates is applied for only a few milliseconds.

To permit disabling of a decoder, the strobe ground can be removed by sending a ground command through its companion decoder. Each decoder can be disabled for approximately 15 seconds by sending the

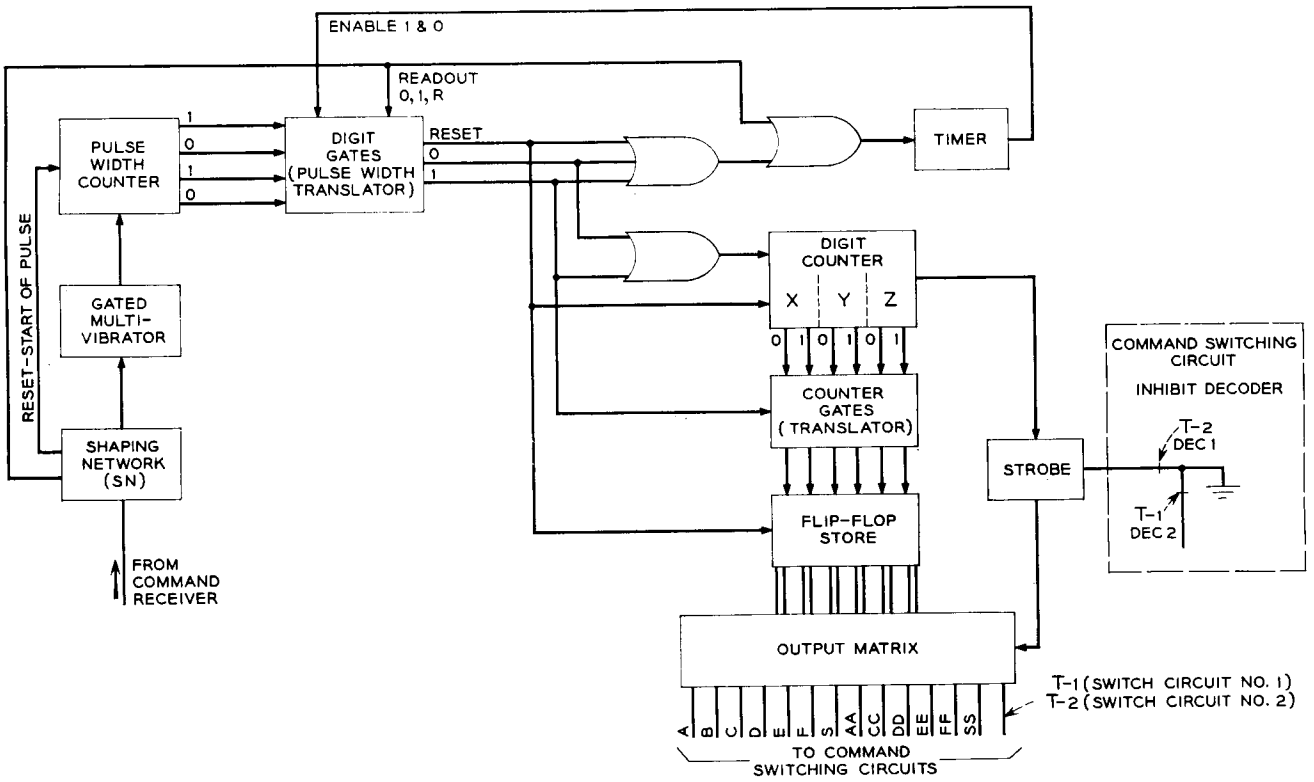

Fig. 11 — Command decoder.

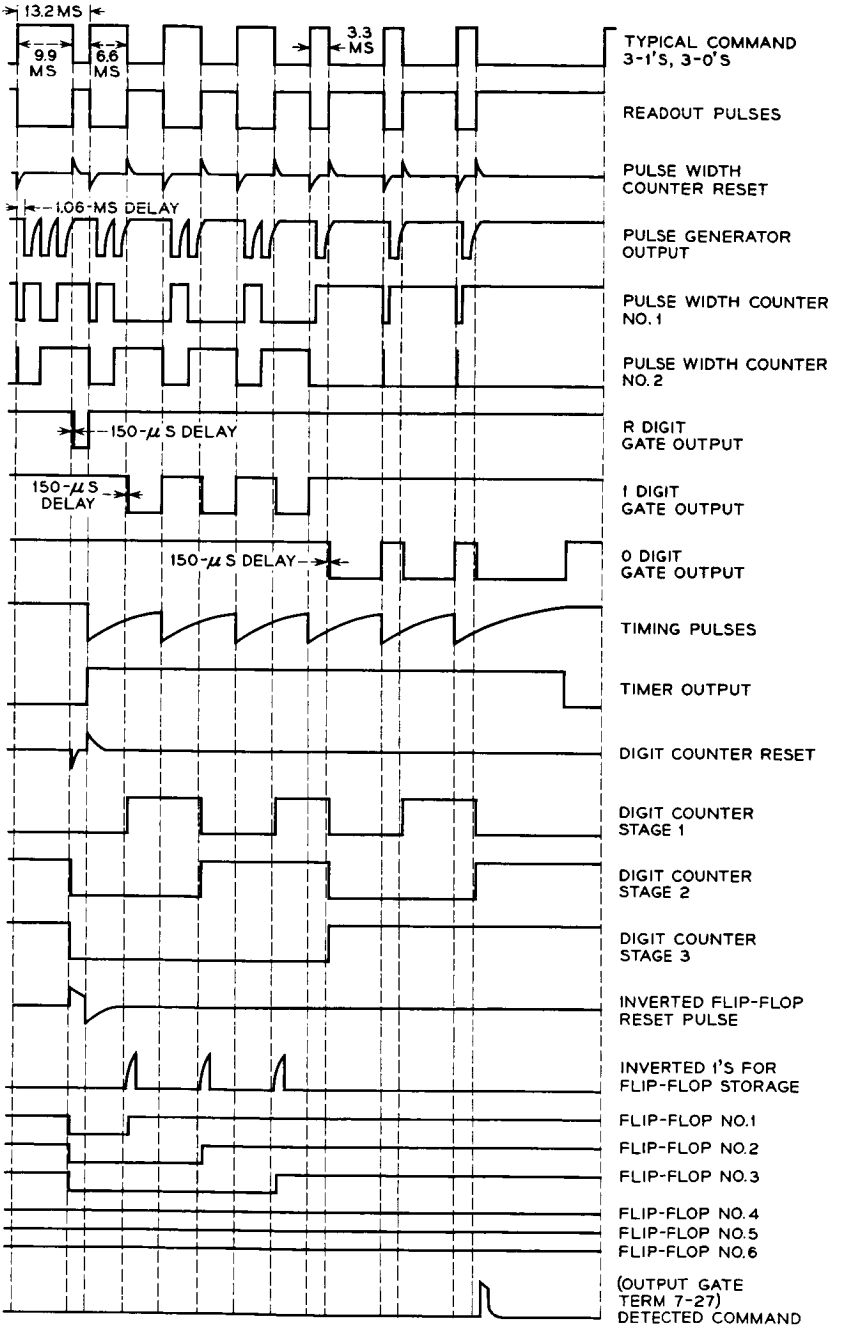

Fig. 12 — Command decoder waveforms.

appropriate (T) command to the other decoder. Thus, if a decoder is detecting a command falsely, it can temporarily be removed from service.

6.3.3 *Command Switching Unit*

The switching unit (Fig. 13) is subdivided into two parts. Each channel performs the same function, thereby providing two separate paths for command execution (except for the T-1 and T-2 commands). Monostable multivibrators provide the necessary amplification and pulse stretching. Driver outputs are combined in OR gates to activate each relay. Single letters designate "set" operations while double letters designate "reset" operations.

As mentioned previously, the S relay is a safety device. Although it can be set and reset by ground command, it can also be reset by the low-voltage trigger circuit. Whenever the battery supply reaches 19.6 volts $\pm$ 0.4 volt, the low-voltage trigger circuit responds, thereby triggering the SS driver. Resetting of the S relay resets all other relays except the F (choice of telemetry encoders) and removes ground command control from the A, B, and C relays. The S relay cannot be prematurely reset while the low-voltage condition persists. These features are incorporated to avoid damage to the battery and the TWT.

To avoid permanently disabling the satellite because of failure of a single low-voltage trigger circuit, an override feature is incorporated. The T-1 and T-2 relays inhibit the operation of the SS-2 and SS-1 drivers, respectively, thus permitting the S relay to be set by command during the 15 seconds deactivation of the faulty trigger circuit. Since T-1 and T-2 cannot be transmitted simultaneously, overriding of a legitimate low-voltage condition cannot occur.

VII. TELEMETRY SYSTEM

7.1 *Over-All Description of Telemetry System*

In the satellite, the signals to be telemetered are time multiplexed by sampling gates, encoded into PCM, frequency modulated on a 3-kc subcarrier, amplitude modulated on the 136-mc beacon, and radiated to the earth by the VHF antenna. On the ground, the signal is picked up by the VHF command-tracker antenna, amplified, and amplitude detected; then frequency discriminated to recover the PCM, decoded, and decommutated; and fed to a printout, punch-out, and various displays.

Figs. 14 and 15 show in block diagram form the principal functional

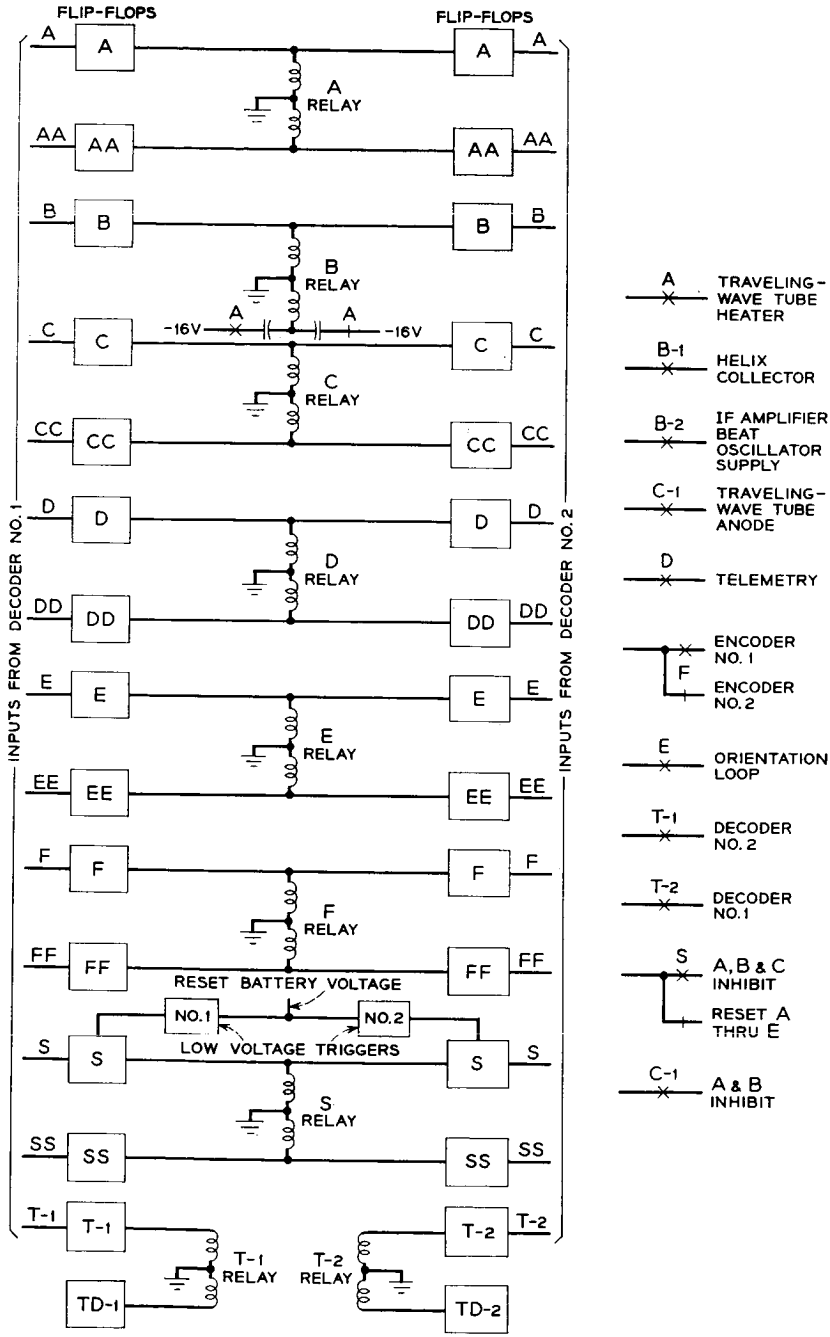

Fig. 13 — Command switching unit.

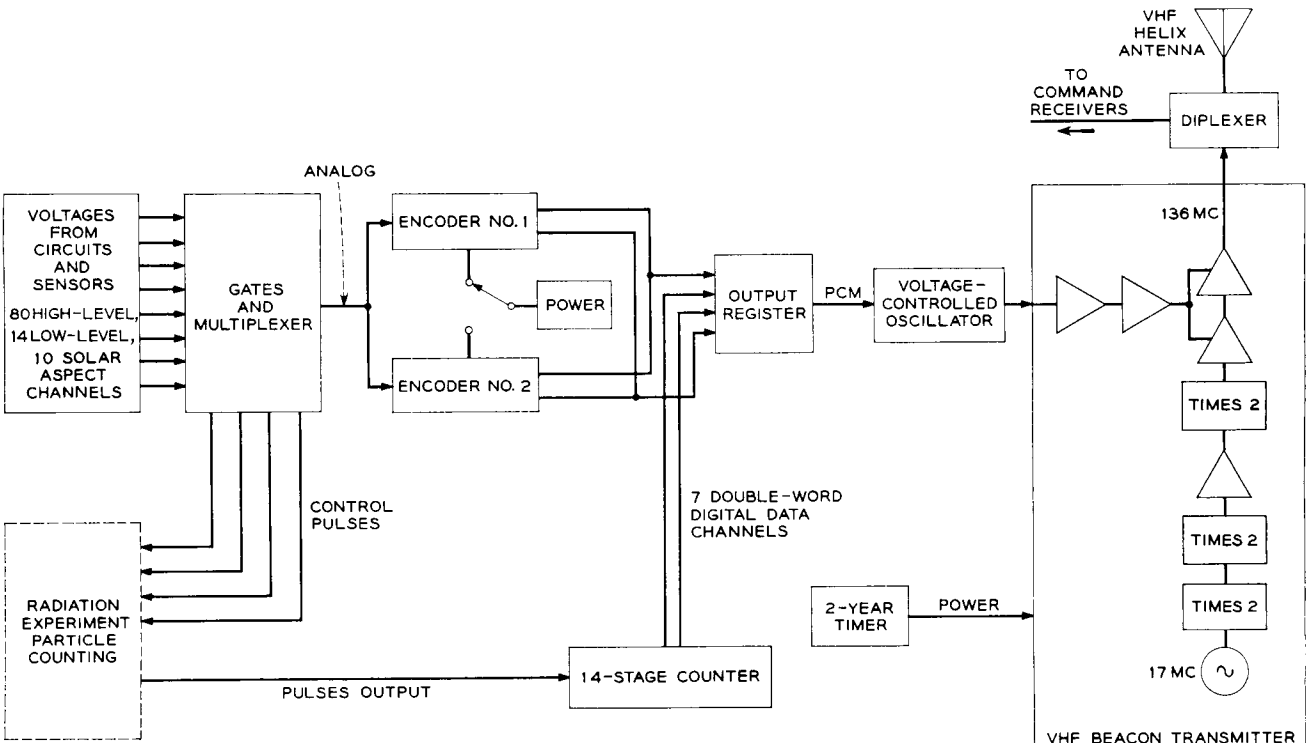

Fig. 14 — Satellite telemetry system.

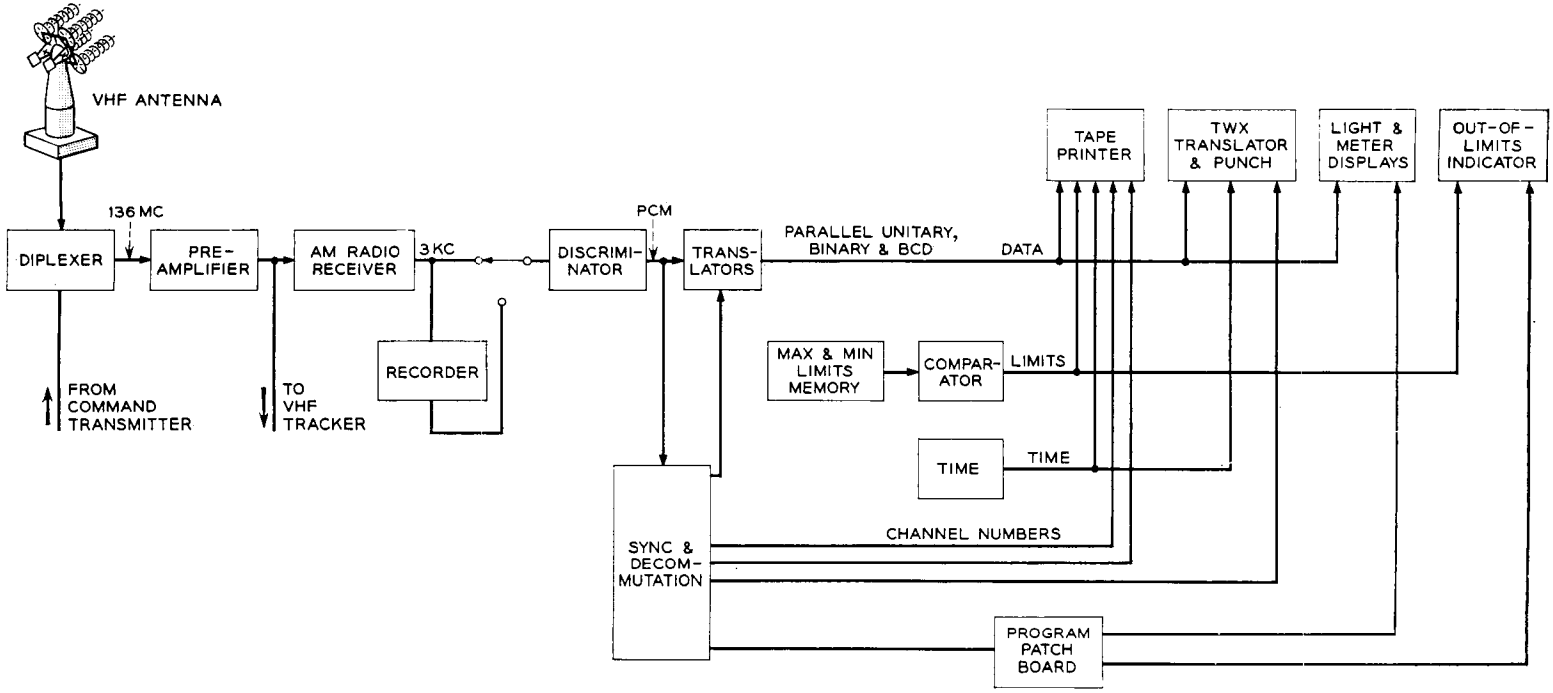

Fig. 15 — Ground telemetry system.

portions of the satellite and ground telemetry systems, respectively. For the satellite system, the portion of the circuit including multiplexer, redundant coders, registers, and voltage-controlled oscillator was developed and constructed for Bell Laboratories by Radiation, Incorporated, of Melbourne, Florida. The ground telemetry, except for the antenna and preamplifiers which are part of the VHF tracker, was supplied by Electro-Mechanical Research, Incorporated, of Sarasota, Florida.

7.2 *Types of Information Telemetered*

The information telemetered falls into several categories as listed in Table II.

The radiation experiment is discussed in detail in another article in this issue.[5] Of the telemetry channels, 16 are used for electron and proton energetic particle counts, 4 for bias of counting detectors, 7 for transistor damage, 4 for solar cell damage, and 6 for solar aspect. In addition to handling the count or measured values of the radiation experiment, the telemetry circuit also provides synchronized pulses for gating on and off the particle-counting circuits and for shifting their thresholds.

Internal temperatures are measured at a number of points in the electronics canister. These are distributed throughout the structure to give both a general temperature picture and to follow certain items of special interest such as battery and traveling-wave tube temperatures. External temperatures are measured at strategic points just under the outer skin and at points associated with the radiation experiment.

TABLE II — TELEMETERED INFORMATION

	Number of Channels
Radiation experiment	37
Internal temperatures	24
External temperatures	16
Microwave circuit	13
Power supply	9
Relay states	4
Command system	6
Canister pressure	2
Calibration	1
Frame synchronization	2
Unassigned	6
Total	120

Various items of the microwave circuit that are monitored via telemetry include the traveling-wave tube accelerator, collector and helix currents, the TWT heater voltage, converter biases, and the IF amplifier AGC. These are of special interest both for the operational control and for the monitoring of performance of the communications repeater. Of the power supply items monitored, perhaps the most important are the solar plant current and the battery voltages. Also monitored are key voltages of the regulator.

Command relay state monitoring is important from an operational standpoint in checking the turn-on and turn-off steps for the traveling-wave tube, the status of the torquing loop, and monitoring the responses to two special commands, T-1 and T-2. Both input and output signals of the command receiver pairs are monitored.

Canister pressure is checked to see whether it is above or below discrete levels of 5 and 1 psia.

7.3 *Types of Telemetry Channels*

To handle the various items to be telemetered, several ranges and types of channels have been employed as listed in Table III.

Where possible, high-level channels were employed. Low-level channels were employed for small signals and differential inputs. The solar aspect channels, in addition to being still more sensitive, are sampled quasi-simultaneously. The digital data channels are for the radiation experiment energetic particle count where the input consists of pulses to be counted. In all cases, the channels are sampled once every minute and converted to binary PCM for transmission.

7.4 *Satellite Telemetry Sending System*

7.4.1 *Sensors*

Except for the so-called digital data channels of the radiation experiment, all the items to be telemetered are first converted to voltages

TABLE III — TYPES OF CHANNELS

Number	Type of Channel	Input
80	High-level	0 to −5 volts analog
14	Low-level	0 to −0.5 volt analog
10	Solar aspect	0 to −0.1 volt analog
14	Digital data (7 pairs)	0 to 16,383 pulses
2	Frame synchronization	

which are subsequently converted to PCM by the encoder. In some cases the analog signal is simply an existing voltage, such as a bias, or a rectified wave, derived directly from the circuit to be monitored. In other cases, transducers or sensors such as thermistors or pressure switches and auxiliary circuits are used to convert the physical quantity to be measured, such as temperature or pressure, to a dc analog signal.

7.4.2 *Multiplexer*

Each analog signal to be telemetered is sampled through sampling gates once every minute and its value encoded into a seven-bit binary code. Channel gates are matched pairs of transistors that are pulsed on in proper channel sequence by transformers of the multiplexer matrix. The 8 × 14 matrix of square-loop magnetic core transformers is driven by horizontal and vertical shift registers and control counters which, in turn, are driven at the word rate. Basic timing at word and bit rate is obtained from a 32-cps oscillator and counters.

In addition to controlling the channel sampling gates, the multiplex matrix also provides timing pulses for the control of the radiation experiment, synchronized with particular word positions. Internal telemetry circuit commands tied to the channel format are also derived from the matrix.

Multiplexing of the solar aspect channels is accomplished by a separate multiplexer operating at high speed in order to effect quasi-simultaneous acquisition of the data. For this, a blocking oscillator, triggered by the main multiplexer, drives a counter and diode matrix which, in turn, drives the transformer-coupled transistor gates.

High-level channel output of the matrix is fed directly to the encoder. Low-level channel output is fed through a 10:1 amplifier and solar aspect channel output is fed through a 50:1 amplifier before going to the encoder. Thus, in all cases, the analog input signals leaving the multiplexer are adjusted to a common 0 to −5 volt range for the encoder to handle.

7.4.3 *Encoders*

To improve reliability, two encoders have been incorporated in the system. Either encoder can be put in operation by ground command (F or FF). The timing circuit oscillators, which are closely linked to the encoders, are also redundant.

For normal high- and low-level channels, each analog signal is sampled once per minute at a rate of one channel each half second. The encoding of each analog signal is accomplished in approximately 50 μsec.

Through consecutive half-amplitude comparisons, the signal is encoded into a 7-bit binary code representing the input signal to an accuracy of ± 1 per cent of full scale range for high-level channels and ± 2 per cent for low-level channels. Thus, each channel input signal is quantized into a code representing one of 127 levels. The binary-coded information is stored in the output register for readout. A word sync pulse is added at the end of the 7 information slots, resulting in an 8-bit word which is then read out at the normal transmitting rate of 16 bits per second.

To conserve power, the encoders are energized in a pulsed-power mode for approximately 170 μsec during each word time.

For solar aspect and solar cell damage measurement, however, essentially simultaneous sampling of ten channels is required. Practically, this has been accomplished by sampling and encoding all ten of these channels in 1100 μsec, during which time the satellite will have rotated approximately one degree. The ten encoded signals are stored in the output register matrix until they are read out at the uniform output rate of 16 bits per second, or one word per half second.

7.4.4 *Digital Data Channels for Radiation Experiment*

Another article[5] in this issue discusses the radiation experiment particle count circuitry. The telemetry system is linked with that circuitry by supplying to it timed control pulses for turning on and turning off various gates and biases at the appropriate times relative to the telemetry frame progression. The result of this is that the particle experiment pulse groups to be counted and telemetered are time multiplexed into seven different time intervals and are fed to a 14-stage counter. Seven times in the course of each frame, corresponding to the seven digital data channel pairs, the 14-bit digital data counter is read in parallel form into the output register, from which the data are read out sequentially as two adjacent channel words. Each pair of these digital data channels can handle pulse counts ranging from 0 to 16,383.

7.4.5 *Output Register*

The sampling, encoding or counting of channel data takes place at several different rates. In order to transmit it at a uniform rate, an output storage register is used. This register has 10 rows and 7 columns of square loop magnetic cores appropriately interconnected with read-in, set, shift and read-out windings. In all cases the final serial read-out for transmission is taken from the top row (row 10). High-level and low-level

data are read into the top row on the completion of encoding. The ten solar aspect channels are read into the bottom row (row 1) one word at a time and shifted upward, filling the register in approximately 1100 μsec. The data are then read out of the top row at the normal read-out rate, shifting the stored words up at word rate. Digital data counts from the 14-bit register are read into rows 8 and 9, which are subsequently shifted up for read-out.

Synchronization information is introduced into the format in the output register. A word sync pulse is added at the end of each group of seven information bit time slots, giving an 8-bit word length in which the most significant bit comes first. Frame synchronization is introduced by putting out an invariant train of pulses in the 16 time slots of the last two word slots of each frame. This pattern of frame sync pulses is read into rows 8 and 9 of the output register by energizing set windings on the appropriate cores. The frame sync words are then shifted up and read out in the normal fashion.

7.4.6 *Voltage-Controlled Oscillator*

The resulting output train of pulses from the output register is sent to the voltage-controlled oscillator (VCO) where it is converted into a frequency modulated signal. The voltage-controlled oscillator is a 3-kc oscillator in which frequency is changed by switching in and out an incremental capacitance in the tank circuit. For a zero bit the frequency stays at 2775 cps for the full one-sixteenth of a second. For a one bit, the frequency is shifted up to 3225 cps for one thirty-second of a second and returned to 2775 cps for the remaining half of the bit time slot.

7.4.7 *VHF Beacon*

The 136-mc beacon has the dual functions of providing a signal for tracking at VHF and serving as the RF carrier for the telemetry 3-kc subcarrier. The beacon can be turned off and on by ground command (S), but it is normally kept on at all times, regardless of the state of telemetry. The beacon will also be shut off automatically if the satellite battery voltage drops below a predetermined low-voltage danger point. Power for the beacon is drawn through contacts of a precision timer which will automatically and irrevocably shut off the VHF beacon at the end of two years. This latter feature is to keep the satellite from indefinitely occupying this spot in the radio frequency spectrum.

The 136-mc frequency is produced by starting with a crystal oscillator

at 17 mc and multiplying successively by factors of two. The crystal is a third-overtone AT-cut quartz unit having a ruggedized mount and is used in a Pierce oscillator circuit using the transistor in a common emitter configuration and operating the crystal as a positive reactance at a frequency slightly above series resonance. Initial frequency adjustment was within ± 1 part per million. Frequency variation with temperature over the anticipated range is less than $\pm \frac{1}{4}$ part per million, and aging is expected not to exceed 1 part per million.

The oscillator is followed immediately by two stages of doublers in which the transistors in common emitter mode are operated as class C amplifiers into collector tank circuits tuned to the second harmonics. Following this is a buffer amplifier and the last stage of multiplication, in which a transistor with common emitter is operated class C into a second harmonic tuned tank, thus producing the final desired frequency of 136 mc. Next, the power level is raised by a driver stage using a common base transistor. Final amplification is obtained in a power amplifier using a transistor in a common base configuration. All stages of the circuit are transformer coupled.

The frequency modulated 3-kc subcarrier from the telemetry VCO is fed to a driver stage and thence to a power amplifier using a pair of transistors in common emitter push-pull. This signal is fed to the collectors of the driver and power amplifier stages of the beacon, producing 50 per cent modulation of the carrier. The signal is then fed to the diplexer which connects the VHF helix antenna to both the beacon and the command receiver while providing isolation between them. The signal is radiated approximately isotropically and linearly polarized from the antenna at a level of 250 milliwatts.

7.5 *Ground Telemetry Receiving System*

7.5.1 *Antenna and Diplexer*

On the ground, the 136-mc signal is picked up by the command tracker antenna. This is a circularly polarized antenna; hence, effective signal strength is not dependent on the orientation of the linearly polarized wave from the satellite. From the antenna the signal goes to the diplexer which permits the use of the single antenna for simultaneous transmitting and receiving purposes without interference. From there, the incoming signal goes to a preamplifier with a noise figure of 3.5 db. The total effective gain of the ground system to this point, including antenna gain, diplexer, and cable losses, is 18 db.

7.5.2 *Preamplifier, Receiver, Discriminator, and Recorder*

After preamplification, the signal goes from the antenna pedestal to the telemetry radio receiver, which recovers the 3-kc subcarrier by AM detection. The 3-kc signal is then fed to a phaselock discriminator which recovers the original pulse train PCM signal. The subcarrier is also fed to a magnetic tape recorder which serves as a back-up to make possible the recovery of telemetry data at a later time in the event of a failure in the ground system beyond this point. The tape can be played back into the discriminator and processing continued in the normal fashion should this be necessary.

7.5.3 *Synchronizer, Translator, and Decommutator*

From the discriminator, the pulse train goes to the synchronizing, translating, and decommutation equipment. Bit rate, word sync, and frame sync are sought and recovered, synchronizing the rest of the equipment. This takes place automatically, progressing from a search mode to a tentative sync or check mode, to a full sync mode. In the event of loss of sync, the circuit automatically reverts to the next lower mode in order to effect recovery. Adjustable controls permit presetting of sync error rate limits at which this reversion takes place. Thus, if desired, the equipment can, in effect, be programmed to accept limited numbers of errors and tide synchronization over temporary fading or interference. After synchronization, the signal is decoded or translated into forms suitable for the several read-out options. Channel numbers are generated in step with the data, and strobing pulses are made available to decommutate the data into selected channel readouts.

7.5.4 *Print-out*

All channels are printed out sequentially with data and corresponding channel number by a Hewlett Packard tape printer. Time is also printed on this record at the spot where the frame sync words would appear (channels 119 and 120). The data read-out is virtually a real time read-out, being delayed by approximately one and one-half seconds. It serves as the primary source of information on all channels.

7.5.5 *Data Limits*

When a channel value is either above or below preset limit values, an out-of-limits mark is printed next to the data. Both maximum and mini-

mum limit values can be set up in a plug board memory for each of the 118 channels individually. The values are set in binary code with plug-in diodes.

7.5.6 *Teletypewriter Punch*

All channel values are also punched in teletypewriter tape, along with appropriate format information to give a page print-out. The teletypewriter tape can be read out and transmitted to other locations either immediately or at a later time.

7.5.7 *Light and Meter Displays*

In addition to the all-channels printed displays, there are also a limited number of binary light displays, analog meter displays, and decimal light displays which can be connected to any of the channels. The choice of channels to be displayed is set up on a program patch board. Out-of-limits relays for remote indicators and command interlock are also connected to the desired channels by means of this program board.

7.5.8 *Operational Considerations*

In the normal mode of operation, the numeric print-out tape is used by an operator to monitor all channels. Commands are marked on the tape at the channel times corresponding to their transmittal by the operator. Remote indicators at the ground station console display the states of the TWT (A, B and C commands) relays as deduced by telemetry. Operating decisions are made with the help of telemetry data thus supplied.

In addition to the VHF ground facilities at the Andover, Maine, station the command and telemetry ground equipment is duplicated at the Bell Laboratories station at Cape Canaveral. The Cape facilities were, of course, used for prelaunch and launch operations and are now used for monitoring of passes. A third telemetry bay, located in New Jersey, was used for satellite manufacturing testing. This bay has modifications which permit it to decommutate magnetic tape recordings at speeds four and eight times real time, and this facility is used to process telemetry subcarrier recordings made by Minitrack stations.

By means of audio tie-lines and teletypewriter lines, the telemetry facilities at these three locations may be interconnected in various ways to provide mutual back-up.

7.6 *Performance*

The telemetry system has been used in the satellites at all stages of its life: during manufacturing tests, launch operations, and in orbit. Thus far, it has been performing normally and is supplying the desired data.

VIII. ACKNOWLEDGMENTS

As is usual on a project of this magnitude, the work represents the combined efforts of a large number of people, with key roles played by so many as to make individual listings difficult. The authors of this article have been fortunate in being a part of the team and wish to thank all who have had any part in making this work successful.

REFERENCES

1. Bomberger, D. C., Feldman, D., Trucksess, D. E., Brolin, S. J., and Ussery, P. W., The Spacecraft Power Supply System, B.S.T.J., this issue, p. 943.
2. Bangert, J. T., Englebrecht, R. S., Harkless, E. T., Sperry, R. V., and Walsh, E. J., The Spacecraft Antennas, B.S.T.J., this issue, p. 869.
3. Hogg, D. C., and Mumford, W. W., The Effective Noise Temperature of the Sky, The Microwave Journal, **3,** Number 3, March, 1960, pp. 80–84.
4. Githens, J. A., Kelly, H. P., Lozier, J. C., and Lundstrom, A. A., Antenna-Pointing System: Organization and Performance, B.S.T.J., this issue, Part 2.
5. Brown, W. L., Buck, T. M., Medford, L. V., Thomas, E. W., Gummel, H. K., Miller, G. L., and Smits, F. M., The Spacecraft Radiation Experiment, B.S.T.J., this issue, p. 899.

The Ground Transmitter and Receiver

By A. J. GIGER, S. PARDEE, JR., and P. R. WICKLIFFE, JR.

(Manuscript received March 22, 1963)

Ground station equipment for the Telstar experiment includes a 6-kmc transmitter and a 4-kmc receiver used for television and telephone channels. This paper describes the over-all transmitting and receiving arrangements and presents detailed accounts of the RF and power-supply subsystems. Information is also presented on protection, control and equipment features, and on receiver noise performance.

I. TRANSMITTER

1.1 *General*

The Telstar ground transmitter is designed to produce a 2-kw frequency-modulated signal in the 6-kmc band, suitable for the transmission of television or multiplex telephony. Fig. 1 is a simplified block diagram which shows the basic features of the four sections of the transmitter: FM deviator, modulator-amplifier, transmitter carrier supply, and power amplifier. The Telstar transmission objectives[1,2] are similar in many respects to those established for domestic microwave radio relay systems. As a result, it has been possible to use in the Telstar transmitter many pieces of equipment designed for that service. The FM deviator, modulator-amplifier and transmitter carrier supply are direct adaptations of units currently being manufactured for the 6-kmc TH radio relay system.[3,4,5] The power amplifier is designed around a 2-kw traveling-wave tube[6] developed at Bell Telephone Laboratories.

1.2 *Design Considerations*

Table I summarizes the transmission objectives established for the ground transmitter. These are derived from system objectives based, primarily, on one-way transmission of monochrome television and 600-channel multiplex telephone. Simultaneous two-way transmission through the satellite, together with its restricted AGC range, deter-

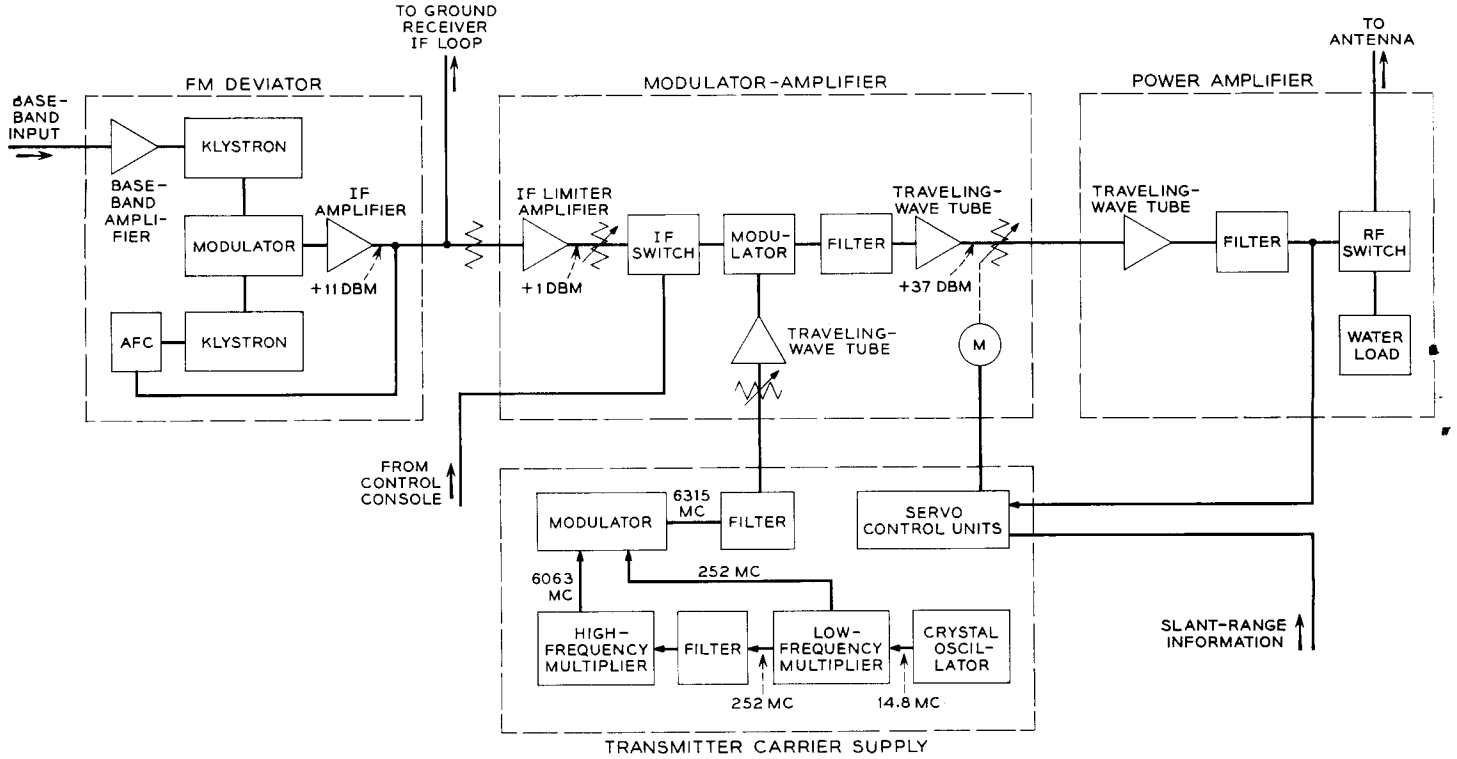

Fig. 1 — Block diagram of the ground transmitter.

TABLE I — TRANSMISSION OBJECTIVES, GROUND TRANSMITTER

Baseband response	2 cps to 5 mc
Peak frequency deviation	10 mc
RF and IF bandwidth	32 mc at 1-db points
Output power	2 kw, continuously variable from 2 kw to 0.02 kw
Center frequency:	
TV and 600-channel telephone	6389.58 mc
12-channel two-way telephone	6384.58 or 6394.58 mc
Frequency stability:	
FM deviator	
without modulation	±50 kc
with modulation	± [50 kc + 0.1 (rms frequency deviation)]
Transmitter carrier supply	±60 kc

mined the need to control the transmitter output. For 12-channel two-way telephony,* it is particularly desirable that the 6-kmc signals at the satellite be independent of slant range.

Operating practices are patterned after those established for domestic radio relay systems. Maintenance procedures, based on the use of standard Bell System test equipment,[7] enable all testing to be performed with the transmitter disconnected from the antenna. In addition, extensive alarm and control circuits have been incorporated in the transmitter to permit continuous, unattended operation.

1.3 *Description*

1.3.1 *General*

In this section the signal is traced through the transmitter; the following sections discuss the individual units of the transmitter in greater detail. Referring to Fig. 1, frequency modulation is generated by applying the television or multiplex telephone signal to the repeller of a reflex klystron. A 1-volt peak-to-peak signal at the 124-ohm balanced input to the baseband amplifier produces a peak deviation of 10 mc. The resulting frequency-modulated microwave signal is translated to the required intermediate frequency by combining it with the output of a second reflex klystron in a modulator. The output of the modulator, corresponding to the frequency difference of the two inputs, is the desired frequency-modulated IF signal. For television or 600-channel multiplex the center frequency is 74.13 mc; for 12-channel two-way multiplex it is 69.13 or 79.13 mc. Shifting the center frequency of the

* Twelve two-way channels is the number selected for this experiment and does not necessarily represent the capacity of the system.

FM deviator plus or minus 5 mc is a convenient means of obtaining either of the two transmitter frequencies required for two-way telephony. At the output of the wideband IF amplifier that follows the modulator, the signal power is +11 dbm. The automatic frequency control circuit samples the output and adjusts the repeller voltage of the second klystron to maintain a constant average output frequency.

In the modulator-amplifier the FM signal initially passes through an IF limiter, which removes any amplitude modulation, and then through an IF switch to the transmitter modulator. The controls of this high-speed switch are connected to the protective circuits in the power amplifier as well as to local and remote operating positions. In the modulator the IF signal is translated to the required RF frequency. The filter following the modulator permits only the signal corresponding to the sum of the frequencies of the IF signal and the 6315-mc output of the transmitter carrier supply to be amplified in the medium-power traveling-wave tube (TWT). At the output of this TWT the signal power is +37 dbm. The motor-driven waveguide attenuator at the output of the modulator-amplifier determines the input to the 2-kw traveling-wave tube in the power amplifier. The attenuator is part of the servo loop that varies the output of the ground transmitter to compensate for the changes in free-space path loss with satellite range. The filter following the 2-kw traveling-wave tube offers approximately 50 db suppression to second harmonic signals in the output. The waveguide switch and water load are part of the test facilities built into the power amplifier.

1.3.2 *FM Deviator*

The FM deviator is an adaptation of the FM terminal transmitter[5] designed for the TH radio relay system. The TH terminal transmitter is characterized by a 4-mc peak deviation capability, a 10-mc baseband response, excellent linearity, and an IF bandwidth of 32 mc. Increasing the gain of the original baseband amplifier was the only change required in the signal path to extend the peak deviation capability to 10 mc. Even at this increased deviation, the linearity of the Western Electric 450A reflex klystron, designed especially as a deviation oscillator for the TH FM terminal transmitter, is more than adequate to meet Telstar objectives. With a required baseband response of only 5 mc, it was possible to realize the additional baseband gain by simply increasing the interstage impedances in that amplifier.

While the basic method of automatic frequency control used in the TH equipment has been retained, increasing the peak deviation to 10

mc has necessitated extensive modifications in the AFC circuits. Requiring the FM deviator to operate satisfactorily with television signals for 405-, 525-, and 625-line systems further complicated the problem.

Referring to Fig. 2, the average frequency of the deviator output is compared with the frequency of a crystal-controlled oscillator. The AFC IF amplifier and the reference oscillator are alternately gated off-and-on at an $18\frac{1}{3}$ cps rate. (The reason for selecting this particular frequency will be discussed later in this section.) During one half of the gating period only the deviator output is effectively connected to the AFC discriminator; the dc output of the discriminator is proportional to the difference between the average frequency of the deviator and the center frequency of the discriminator. During the other half the reference oscillator is connected to the discriminator, and the dc output is then proportional

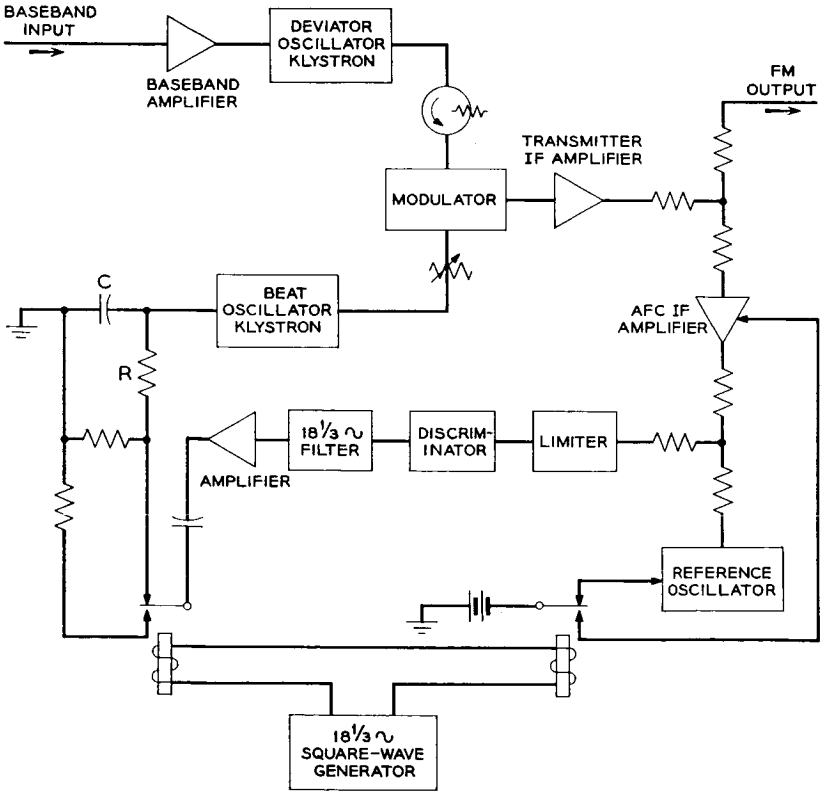

Fig. 2 — Block diagram of the FM deviator.

to the difference between the oscillator frequency and the discriminator center frequency. As a result, the AFC discriminator output contains an $18\frac{1}{3}$ cps square wave whose peak-to-peak average amplitude is proportional to the frequency difference between the reference oscillator and the average frequency of the deviator output. The function of the AFC limiter is to equalize signal amplitudes at the input to the discriminator. The bandpass filter following the discriminator effectively allows only the fundamental component of the $18\frac{1}{3}$ cps square wave to be amplified. At the output of the audio amplifier, the $18\frac{1}{3}$ cps sine wave is rectified in a synchronous detector and filtered. The dc signal is applied to the repeller of the beat-oscillator klystron with the proper polarity to reduce the frequency difference between the reference oscillator and the deviator output. Gating of the AFC IF amplifier and reference oscillator and the use of synchronous rectification eliminate the need for dc amplification and make the AFC loop insensitive to small drifts in the center frequency of the AFC discriminator. The open-loop gain of the AFC system is, typically, 36 db.

In the absence of modulation, frequency errors are in general the result of drifts in the klystron center frequencies. With modulation, the instantaneous frequency of the FM signal is continuously changing, and nonlinearities in the AFC discriminator characteristic will contribute terms to the average discriminator output that are not linearly related to the average frequency of the FM signal. To achieve comparable linearity at the increased peak deviation, the original AFC limiter-discriminator was replaced with the wideband limiter and discriminator of the TH FM terminal receiver.[5] Between 64 and 84 mc the first-order nonlinearity of the wideband discriminator is less than 2 per cent.

In gated AFC systems, objectionable "flicker" interference often arises as the result of beats between the harmonics of the gating frequency and low-frequency components of the television signal or power supply ripple. To make the FM deviator compatible with the 50-cps field rate of European television and the 60-cps U.S. standard, a gating frequency of $18\frac{1}{3}$ cps was chosen. Five-cps beats, developed between the 55-cps third harmonic of the gating frequency and either field rate, are effectively suppressed by the RC filter at the output of the synchronous detector. In addition, the bandpass filter at the output of the discriminator provides more than 20 db of attenuation to 50- and 60-cps signals before rectification At maximum deviation the 5-cps interference is more than 60 db below the 50- or 60-cps modulating frequency.

The wideband characteristics of the IF amplifier, limiter, and discriminator in the AFC loop make possible a simple method of shifting the deviator frequency for two-way telephone transmission. It is only

necessary to substitute a 69.13- or 79.13-mc crystal in the reference oscillator, retune the oscillator, and adjust the beat-oscillator repeller supply so that the output of the synchronous detector is zero. The rest frequency of the beat-oscillator klystron is then 69 or 79 mc different from that of the deviation oscillator klystron.

1.3.3 *Modulator-Amplifier and Transmitter Carrier Supply*

The TH radio relay system provides the basic elements of the modulator-amplifier and the transmitter carrier supply. Detailed descriptions of this equipment and its performance are published elsewhere.[3,4] Modifications that affect operations are limited to the addition of the IF switch and the output power control system.

1.3.4 *Power Amplifier*

The power amplifier, including the power supplies and the TWT itself, is contained in five cabinets. Two of these are on the lower level of the antenna structure and contain the high-voltage rectifier and its controls. The other three are on the upper level and contain the high-voltage regulator, intermediate- and low-voltage supplies, and the TWT and RF equipment. This arrangement imposes the minimum space and weight requirements on the upper level of the antenna structure. In addition to the TWT heater and accelerator supplies, the intermediate- and low-voltage units include supplies for the solenoid focusing magnet, ion pumps, arc detector, and control and protective circuits. Water is supplied for cooling the TWT and also the dummy load. Air under pressure is brought into the cabinets for general cooling, supplemented where necessary by auxiliary blowers.

1.3.4.1 *The RF Circuit.* The M4040 TWT is described elsewhere in this issue.[6] Fig. 3 shows additional elements required in the RF path. Interposed between the modulator-amplifier and the TWT is the input circulator, the principal function of which is to provide isolation between the two for better impedance matching over the frequency band. In particular, as the input signal to the TWT passes through the tube, some small amount will be reflected at the sever (which is not a perfect match over the whole band). This power will reappear at the TWT input port with about 14 db amplification due to its passage through this first section of the TWT. If it undergoes a further reflection due to a mismatch at the modulator-amplifier output, a buildup will occur leading to oscillation and tube damage. A termination at the input circulator absorbs this reflected power, preventing regeneration.

At the output window of the TWT, a photomultiplier tube is mounted

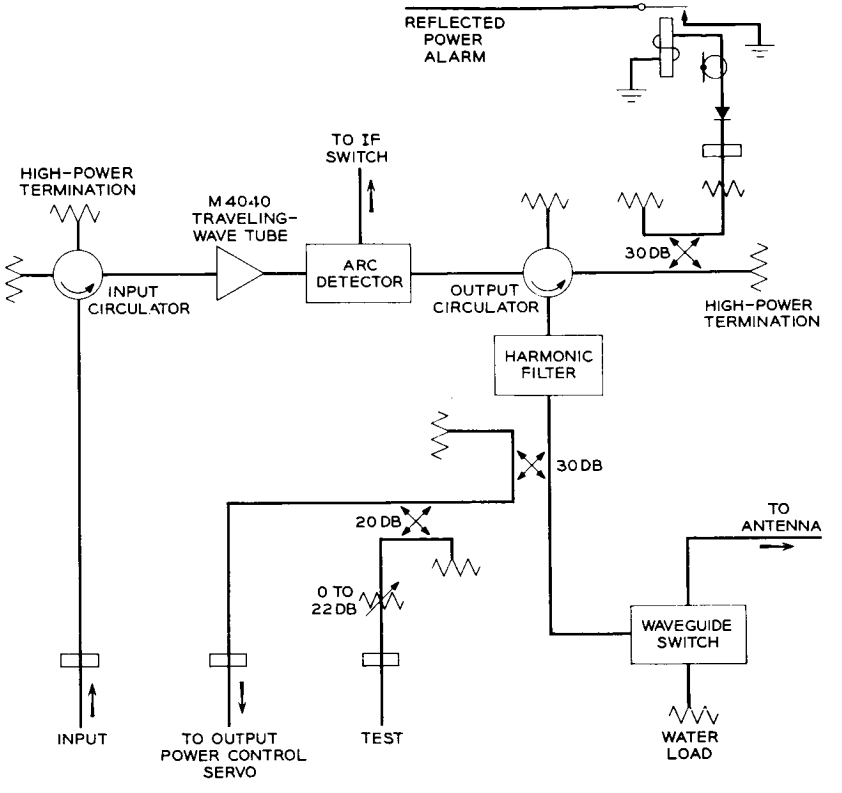

Fig. 3 — Block diagram of the power amplifier.

next to a small hole in the broad wall of the waveguide to detect any arcs that may develop in this region. Associated circuitry operates the IF switch, which removes drive from the tube, thus interrupting the arc.

A high-powered circulator is used in the output waveguide, again providing a minimum return loss of 14 db over the band to prevent oscillations in the output section due to excessive reflected power. In addition, one of the branches is connected through a 30-db directional coupler and an RF attenuator to a detector which monitors reflected power. If this exceeds 50 watts, the detector output operates a meter relay which opens the IF switch and removes the drive.

Following the output circulator, a harmonic filter reduces the second harmonic output of the transmitter, which may be only 25 db below the fundamental. To meet interference objectives, the filter is designed for 50-db minimum harmonic discrimination. To meet transmission

objectives, the filter has 0.5-db maximum insertion loss and 30-db minimum return loss over the band of 5925 to 6425 mc

Following the filter is a directional coupler and a waveguide switch and water load. The coupler is part of the output power control system, described in Section 1.3.5. The switch and water load permit all transmitter tests to be performed with the output disconnected from the antenna.

1.3.4.2 *DC Power Supplies*

(*i*) *TWT Heater Supply.* AC heater operation tends to cause small but measurable amounts of amplitude and phase modulation of the M4040 RF output. To eliminate these effects, a simple dc heater supply, consisting of a transformer, bridge rectifier and filter capacitor, is provided. A variable autotransformer on the power amplifier control panel determines the ac input to the power supply, and hence, the heater voltage. Normally, the heater supply is operated continuously to extend tube life and promote efficient outgassing. Meter relays connected to the primary of the heater supply cause high voltages to be turned off if the TWT heater current falls below a preset value.

(*ii*) *High-Voltage Beam Supply.* This supply, shown in Fig. 4, furnishes a regulated output of 0 to 20 kv at up to 1.5 amperes from 3-phase ac power at 50 or 60 cps. Its regulation for load changes from 1 to 1.5 amps, up or down, and/or line changes of ± 15 per cent, is better than 0.1 per cent peak-to-peak. Ripple and noise at rated load is less than 0.1 per cent peak-to-peak. The supply was designed with depressed collector operation of the TWT in mind for the future, so both plus and minus leads may be isolated from ground. Because of the requirement for regulated operation over the whole range of voltage from 0 to 20 kv, the supply was built with a motor-driven variable autotransformer to control the high-voltage applied to the rectifier, the output of which is further regulated by an electronically controlled series regulator tube. A limited degree of tracking between the autotransformer and the series tube control voltage is provided automatically.

The negative lead of this supply is fed to the TWT cathode at about 17 kv. The positive side, or ground end of the supply, is fed over separate leads to the collector and through the body-current sensing circuit to the body of the TWT. Regulated output voltage and collector and body current are monitored by meters on the control panel.

There are certain trouble conditions affecting the traveling-wave tube which might cause its destruction unless the high voltage is removed

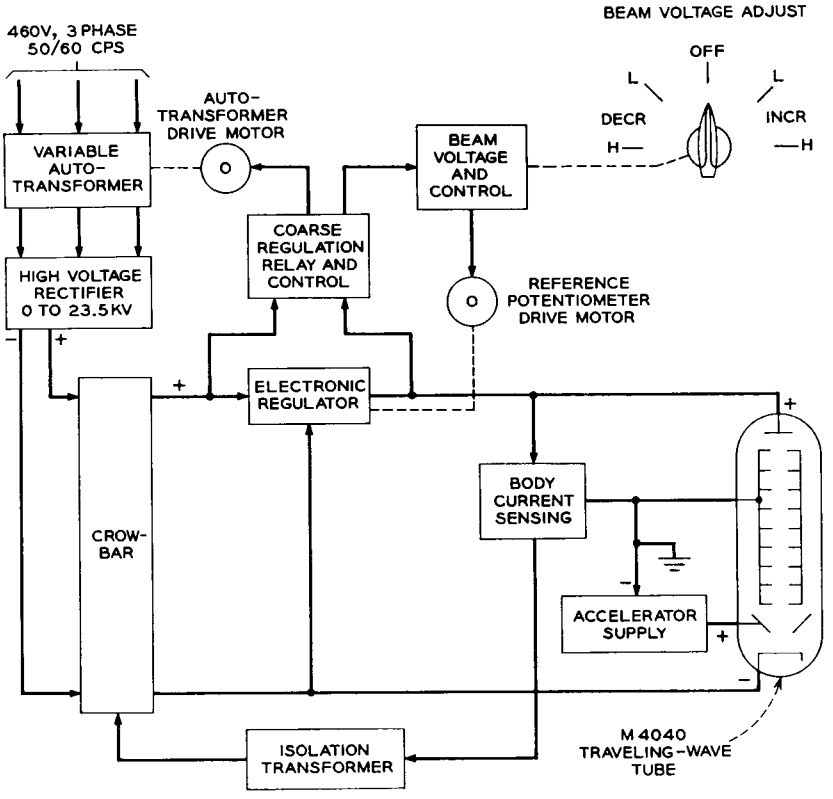

Fig. 4 — Block diagram of the high-voltage beam supply.

within a fraction of a millisecond. Protection of this sort is provided by the "crowbar" circuit, which can be operated by excessive TWT cathode current or body current. The crowbar tube is a type 5563A mercury vapor thyratron. This particular tube can be controlled by a grid voltage change of only 100 volts; the more usual hydrogen thyratrons or ignitrons require control voltages of several thousand volts. Thus, a simple and fast-firing circuit can be used. When fired, the crowbar puts a short circuit across the high-voltage rectifier, reducing the output voltage of the regulator to a few hundred volts in about 20 microseconds. After a few milliseconds delay due to relay operate time, the excessive current drain on the high-voltage rectifier causes its own protective circuits to shut it down.

(*iii*) *The Accelerator Supply.* The accelerator supply consists of a solid-state bridge rectifier and two stages of regulation. The first stage is a

ferroresonant type of circuit, and the second stage is an electronic regulator. Line and load regulation and ripple measure less than 0.03 per cent. Variation of output voltage is controlled by a potentiometer across a voltage regulator tube reference supply. The ferroresonant first stage has a voltage control on the same shaft so that the two stages can be made to track. Under normal operating conditions the output voltage is adjusted to 600 volts. The output current monitor in the supply is part of the protective circuitry in the power amplifier. If the accelerator current becomes excessive, the beam supply and all intermediate-voltage supplies, except those for the ion pumps, are disabled.

1.3.4.3 *Cooling.* Deionized and filtered water is supplied to cool the M4040 TWT and the dummy load. Flow is set at about 18 gallons per minute and valved to the various using areas. Pressure switches are used as part of the protective system as an indication of proper flow in the TWT, the high-powered circulators, and the solenoid focusing magnet. If one or more of these flows are below a minimum, interlocks prevent the application of all but TWT heater voltage and the ion pump supplies.

In addition to the normal flow of filtered air through the cabinets, a spot blower is used to keep the TWT waveguide flanges cool, and another blower is used for the series tube in the beam regulator. A vane switch in the air stream of this latter blower is in the interlock circuit, again preventing the application of all but the heater, ion pump and solenoid voltages.

1.3.4.4 *Operating Interlocks, Controls, and Monitoring Devices.* Because of the experimental nature of the Telstar program, a greater ability to control voltages is necessary than would be expected of a commercial system. The manner of applying dc power to the TWT requires that the heater voltage be raised and lowered by carefully controlled amounts and that accelerator voltage and high voltage be applied in steps. Furthermore, the tube must be protected against arcs in the waveguide; excessive feedback or return power in the tube itself; overheating of the body, sever or collector; inadequate water flow to the body or the solenoid; and various over- or under-voltage or current conditions. The following sections describe some of these features.

(*i*) *Control Panel.* Operating controls for the power amplifier portion of the ground transmitter are located on a panel of the control bay. This control panel contains the power switches, the visual monitoring meters, status indicating lamps, alarm lamps and adjustment controls.

The status lamps indicate upper-level and lower-level standby power, heater on, plate ready, plate on, beam ready, beam on, beam adjust disable, and antenna/dummy load switch positions. The alarm lamps

indicate such conditions as open circuit breakers, open interlock circuits, TWT water on or off, TWT over-temperature, over-current and under-current and over-voltage in certain circuits, high reflected RF power and RF drive disable. An audible alarm rings if the RF drive to the TWT is removed during normal operation. In addition to overload relays, additional protection is provided for the TWT by meter relays which will operate on out-of-limit readings to open the interlock protection circuit. Operation of the interlock protection circuit will remove power from the TWT.

(*ii*) *Circuit Protection and Operations Monitoring.* Individual circuits and functions are protected by 32 circuit breakers on a panel in the power bay in the upper level (there are additional circuit breakers in the beam rectifier control bay in the lower level). Elapsed time meters and operations counters are provided for heater, plate, and high-voltage monitoring.

1.3.4.5 *Mounting Arrangements and Maintenance Philosophy.* The equipment layout was planned with two particular considerations in mind: maintainability and personnel safety.

As much preventive maintenance and trouble analysis as possible is to be done in place, since bench maintenance facilities in the rotating structure are limited. To accommodate the objective of in-cabinet maintenance, sub-units in the control bay (20-kv regulator) are designed with test points of interest accessible from one side of the chassis, which is then mounted so that this side faces the front (or back) of the cabinet. Metal doors provide access to front and back of this cabinet and of the power bay (miscellaneous rectifiers), and inner plexi-glass panels prevent accidental contact with dangerous voltages. Small holes in these panels permit screwdriver adjustment to be made, or the insertion of a probe to some test points. In the case of the 20-kv regulator cabinet, opening these plexi-glass doors will operate interlocks, dropping the system back to the heaters-only condition, and will ground all high-voltage points with gravity-operated shorting bars. Most of the circuitry in this cabinet can be tested without high voltage being turned on, and in almost every case, troubles can be localized to the component requiring replacement without exposing maintenance personnel to undue risk.

The cabinets have been designed with RF shielding at the front and rear doors and some other openings, in order to keep the possibility of interference to the lowest possible level. Consideration of corona from high-voltage leads resulted in rounded corners and large-radius bends for potential corona sources. The cabinet containing the traveling-wave tube and its associated water-cooling, waveguide and RF measuring and monitoring gear was designed to isolate that part of the equipment

which might "leak" RF. The TWT and the leads going to it which carry much of the high voltage, and the arc-detector and photomultiplier, are all in a metal-enclosed box, with the customary shorting bar for the 20-kv supply. Water valves and gauges are in a compartment to the rear of this, and temperature-monitoring pyrometers and RF-monitoring equipment in a compartment next to it. The doors to these two compartments are not interlocked. The traveling-wave tube bay, the control bay (20-kv regulator) and the power bay (intermediate voltage supplies) are of aluminum and are mounted in the upper structure near the end of the horn; the beam rectifier control bay and the beam rectifier bay are of steel, and are mounted below on the rotating platform.

1.3.5 *Transmitter Control*

Off-on control of the ground transmitter output centers around the IF switch. The switch consists of an IF diode gate[8] and a switch control circuit. In the off state the insertion loss of the switch is more than 85 db; there is essentially no input to the power amplifier. In the on state the insertion loss is 1.5 db, and the motor-driven attenuator in the modulator-amplifier effectively determines the output of the transmitter. In order to protect both equipment and personnel from hazardous operating conditions, the IF switch control circuit is inhibited by an extensive chain of relay and switch contacts. The chain encompasses the local and remote operating positions, the waveguide switch and protective circuitry associated with the power amplifier, and the motor-driven attenuator in the modulator-amplifier, as well as the antenna elevation indicators. An auxiliary connection exists between the arc detector in the power amplifier and the IF switch control circuit. It enables the switch control circuit to open the IF gate in less than 5 microseconds after an arc in the 2-kw TWT.

Fig. 5 shows a diagram of the output power control system. The arc detector, output circulator and harmonic filter have been omitted for simplicity. In loop 1 the input power to the RF detector remains essentially constant. Any change at this point unbalances the input to the difference amplifier, operates the polar relay and causes the shaded-pole servo motor to increase or decrease the attenuation of the AGC attenuator until the output of the M4040 TWT changes sufficiently to restore the RF detector input to its nominal value. As a result, the loop automatically compensates for compression in the input-output characteristic of the M4040 TWT and for changes in the RF output of the 5-watt TWT. The output of the transmitter is directly related to the attenuation of the reference attenuator and the manual attenuator.

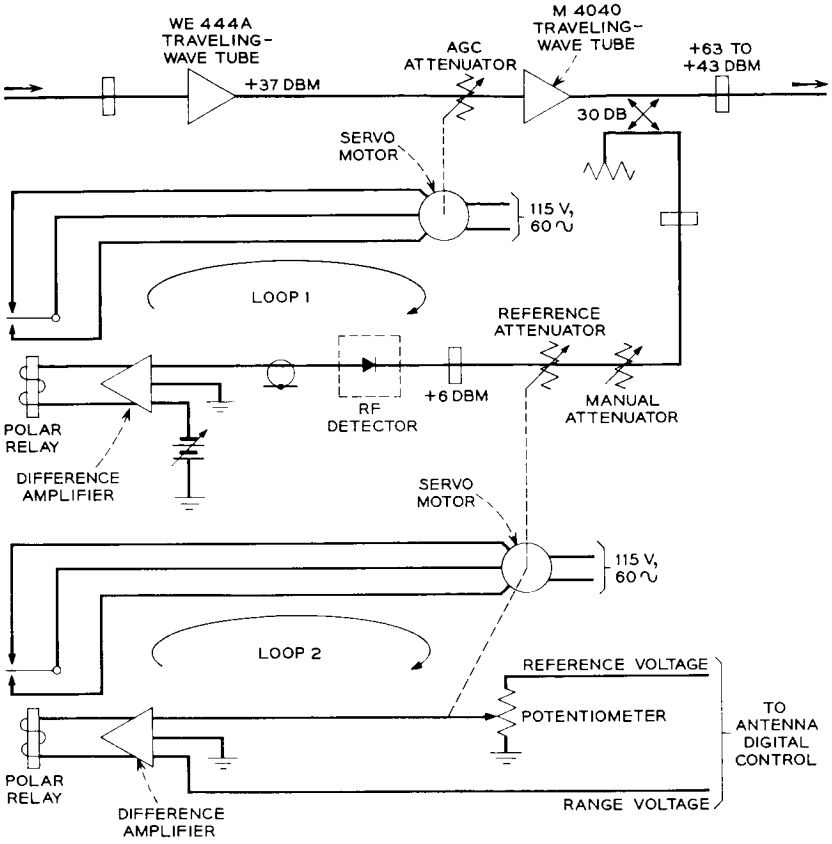

Fig. 5 — Output power control servo.

The control limits of loop 1 are 2 kw and 0.02 kw, equivalent to a 20-db variation in free-space path loss or a 10:1 variation of slant range.

The reference attenuator and hence the transmitter output are controlled by loop 2. The method of generating the two analog inputs to loop 2 is described elsewhere.[9] One is a fixed reference voltage; the second is proportional to the logarithm of the slant range or, in other words, free-space path loss. Expressed mathematically,

$$V_{\text{RANGE}} = 0, \qquad R < 0.1R_{\text{MAX}} \tag{1}$$

$$= V_{\text{REF}} \log_{10}\left(\frac{R}{0.1R_{\text{MAX}}}\right), \qquad 0.1R_{\text{MAX}} < R < R_{\text{MAX}} \tag{2}$$

$$= V_{\text{REF}}, \qquad R_{\text{MAX}} < R, \tag{3}$$

where R is the actual slant range and R_{MAX} is the maximum slant range at which it is possible to achieve a particular input power to the satellite. Since the transmitter is limited to 2 kw, the maximum slant range corresponding to a particular satellite input is determined by free-space path loss and transmitting and receiving antenna gains. For slant ranges equal to or greater than the maximum defined above, the voltage representing range is equal to the reference voltage; the reference attenuator in loop 1 and the potentiometer in loop 2 are set for maximum attenuation and resistance, respectively. As the slant range decreases, the voltage representing slant range also decreases. The inputs to the difference amplifier in loop 2 are no longer equal, and the servo motor adjusts the potentiometer to restore the equality. In so doing the attenuation in loop 1 and, consequently, the transmitter output are reduced. Since the loss in db of the reference attenuator and the resistance of the potentiometer are essentially linear functions of mechanical rotation, the decrease in transmitter output just equals the reduction in free-space path loss. As a result, the power incident on the satellite remains constant. In operation, a small second-order term is added to (2) to compensate for a slight nonlinearity in the attenuation vs mechanical rotation characteristic of the reference attenuator. With this addition, it is possible to maintain the signal incident on the satellite constant to within ± 0.5 db. The major portion of this error can be attributed to the dead space associated with the polar relays.

The IF switch and the output power control servo are interconnected with the ground station control console (GSCC) to permit remote operation of the transmitter from that location. Between passes, the transmitter output is connected to the water load and an out-of-service indication is displayed at the GSCC. Upon completion of pre-pass checks, the transmitter output is switched to the antenna and control is transferred from the local operating position to the GSCC. By activating appropriate switches, the console operator may choose any one of three operating conditions, provided the antenna elevation exceeds 5 degrees. These conditions are carrier off, standby, and carrier on. As long as the antenna is pointing below the horizon, however, the IF switch cannot be closed. The AGC attenuator is automatically positioned for maximum attenuation, independent of the output power control servo, and a carrier off indication is displayed on the GSCC. For antenna elevations above the horizon but less than 5 degrees, the choice is restricted to carrier off or standby. In the latter case, the IF switch is closed. However, the AGC attenuator is still positioned for maximum attenuation so that the radiated power is limited to approximately 0.2 watt. The standby condition is normally used during the pre-pass system checks

with the satellite simulator at the test tower. For antenna elevations above 5 degrees, no restrictions exist. In the carrier on condition, the IF switch is closed and the AGC attenuator is under control of the servo system.

1.4 *Equipment Features*

As stated earlier, the high-voltage beam rectifier and associated controls are located on the lower level of the antenna structure. Fig. 6 shows the arrangement of the units of the transmitter mounted on the upper level. Cabinet doors have been temporarily removed. The transmitter carrier supply and modulator amplifier are located in the two pull-out bays on the left. To the right of the modulator-amplifier are the three remaining units of the power amplifier. The first cabinet contains the M4040 TWT and RF circuitry; the second cabinet contains the series tube regulator and crowbar circuits and the power amplifier control panel; and the third contains the circuit breaker panel and intermediate- and low-voltage supplies. The FM deviator is mounted in the cabinet on the extreme right. Each of the cabinets is 6 feet high and 3 feet deep. The combined width of the four cabinets and the two pull-out bays is $18\frac{1}{2}$ feet. The weight of the six units is approximately 6000 pounds.

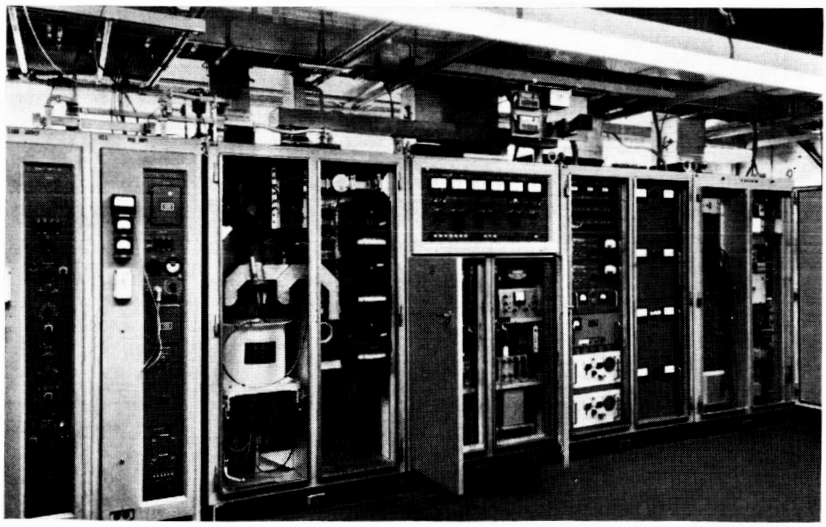

Fig. 6 — The ground transmitter.

II. THE RECEIVING SYSTEM

2.1 *General*

One of the major differences between a conventional microwave receiver — as used, for instance, in such ground-based microwave systems as TD2 and TH — and the ground receiver of the Telstar system, lies in the tremendously improved noise behavior of the latter. By the use of low-noise antennas and masers, the total noise temperature of satellite ground receivers can be made 100 to 200 times lower than for conventional receivers. The noise characteristics of the Telstar receiver are superior in still another respect. Present thinking calls for the use of wideband transmission methods, such as high-index FM, in order to keep the transmitter power in the satellite at a realistically low level. Such high-index systems necessarily work close to the threshold of detection. By the use of the FM with feedback (FMFB) principle, it is possible to extend the threshold of noise improvement in the Telstar system by about 4 to 5 db compared with the standard method of FM demodulation. This allows operation of the transmitter in the satellite with only one third the power otherwise required.

This part of the paper emphasizes the low-noise features of the receiver and describes the circuits responsible for such operation. An overall description of the receiver is given in Section 2.2. The pertinent operational characteristics of the maser, the parametric amplifier, and the FMFB receiver are described in Section 2.3. A description of the diplexer and other waveguide equipment required to connect the transmitter and receiver to the same antenna is found in Section 2.4. Various system noise measurements are presented in Section 2.5. Circuits of a more conventional type and those taken from the TH or TD2 microwave system, such as converters, IF amplifiers, and carrier supplies, are not described.

2.2 *Receiver Description*

2.2.1 *The Transmission Circuits*

A block diagram of the ground receiver is shown in Fig. 7. This equipment is located in the upper equipment room on the horn antenna structure. The received 4-kmc, left-hand circularly polarized signal from the satellite, after being picked up by the horn-reflector antenna, is guided toward the maser by a low-loss waveguide diplexer. The diplexer

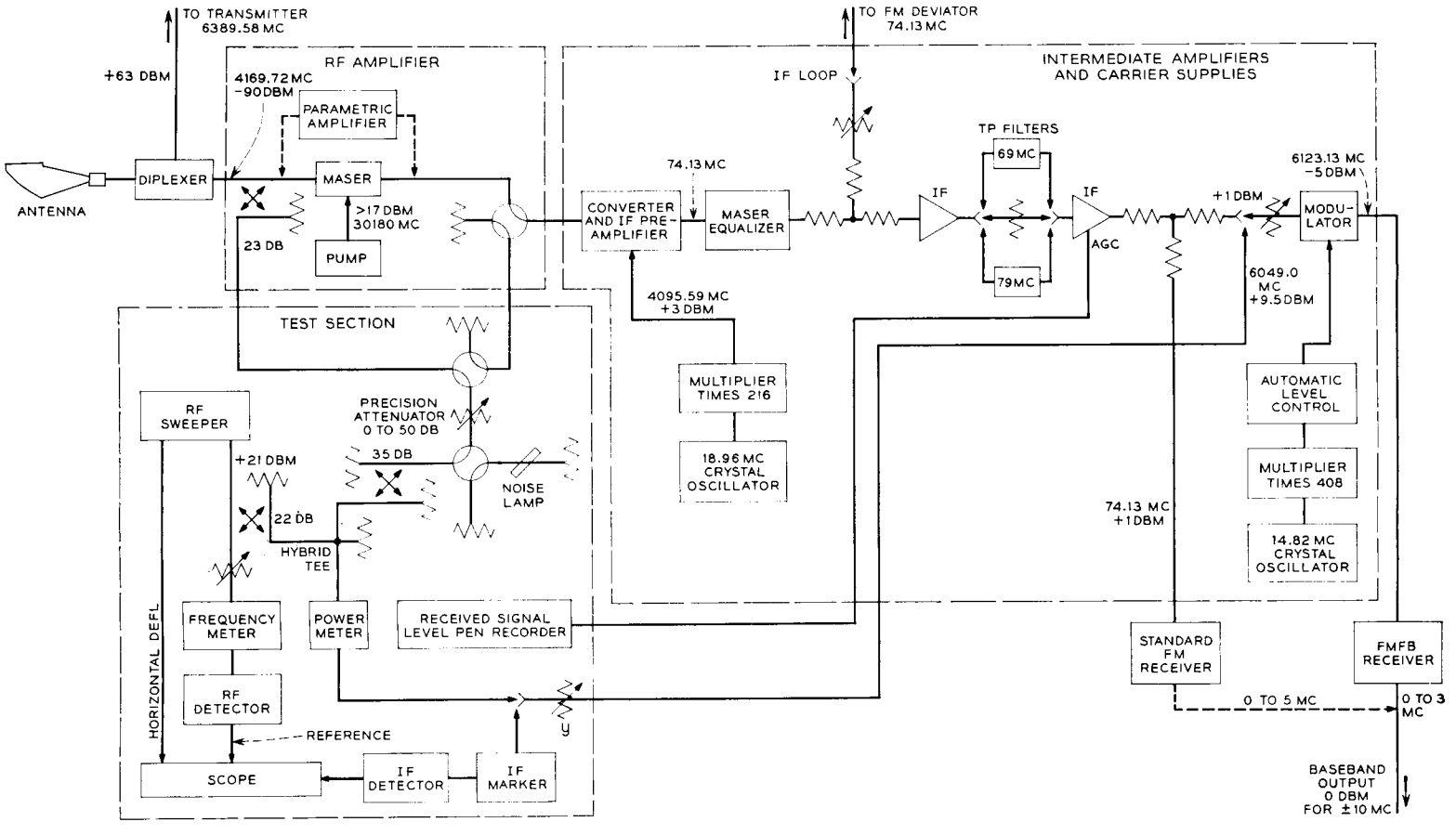

Fig. 7 — Block diagram of the ground receiver.

also accepts the high-power 6-kmc signal from the transmitter and feeds it to the same horn-reflector antenna, from where it is launched right-hand circularly polarized. The maser, operating at the temperature of liquid helium (4.2° Kelvin), has a gain of 42 db and a 3-db bandwidth of 16 mc. The receiver bandwidth is widened to the necessary 25 mc by the insertion of a maser equalizer at IF directly after the frequency converter. The 42-db gain of the maser is high enough to make the noise contribution of the following frequency converter negligible. Total noise temperature of the receiver measured at the input of the maser with the antenna pointed toward zenith is 32°K on a clear day. The maser requires for its operation a "pump" which supplies a frequency-stabilized microwave carrier of 30,180 mc at a power greater than 17 dbm.

It is also possible to use a broadband (60-mc) low-noise parametric amplifier instead of the maser for evaluation in the system.

The signal from the maser is changed to an intermediate frequency of 74.13 mc in a frequency converter. A crystal-derived carrier of 4095.59 mc serves as the local oscillator signal. A low-noise preamplifier and two more IF amplifiers bring the signal power up to a level of +1 dbm, which is held constant by an automatic gain control circuit in the second amplifier.

The transmission characteristic of the converter and IF circuits combined is flat and drops only 0.25 db at the edges of the 25-mc band. Except for the case where the parametric amplifier is used, the over-all transmission is limited by the combination of maser and maser equalizer. For TV transmission this bandwidth is 25 mc at the half-power points, and for two-way telephony it is reduced to 3 mc by the insertion of a special filter ahead of the last IF amplifier. This telephone filter is centered either 5 mc above or below the normal IF frequency of 74.13 mc, depending on the transmitting frequencies chosen in the two participating satellite ground stations. The insertion of the telephone filter is the only step necessary for changing the receiver from television to two-way telephone operation.

To the output of the last IF amplifier can be connected either a standard (conventional) FM receiver or an FMFB receiver after suitable frequency translation. The input frequency of the FMFB receiver is at 6123.13 mc for reasons explained under Section 2.3.3. A balanced diode modulator, together with a crystal-derived carrier of 6049.0 mc, translate the 74.13 mc signal to the required 6123.13 mc.

2.2.2 *The Test Equipment*

In addition to the basic transmission circuits just described, the Telstar ground receiver contains special test equipment for fast and precise measurements of noise temperature, transmission characteristics, gain and received signal level. This equipment is shown in the block called test-section of Fig. 7. It includes an RF sweeper which can be swept over 60 mc anywhere in the 3700- to 4200-mc range, a power meter for 4 kmc and 74 mc with an accuracy of a few tenths of a db, a waveguide noise lamp, a precision waveguide attenuator, an oscilloscope, and a pen recorder. A number of waveguide switches allow the distribution of either the 4-kmc carrier or the noise signal to either the input of the maser or the input of the converter. The output, for test purposes, is taken at the +1 dbm IF point.

The AGC voltage of the IF amplifier is a function of the received 4-kmc signal level and is recorded on a pen recorder. A wealth of information can be obtained from such recordings. Several examples of received level recordings are given in a companion paper.[10] The recorder is calibrated before each pass with a 4170-mc signal from the RF sweeper, which is applied to the input of the maser at the levels of −80 and −90 dbm. Absolute accuracy of the recording is about ±1 db. A second recorder of received level is located on the ground station control console in the control building. Its expanded range, going as low as −110 dbm, allows the personnel tracking the satellite to check whether the autotrack system has locked on the main beam and not on a sidelobe of the horn-reflector antenna. The recording also helps an experienced operator to easily discover troubles in the communications part of the system.

Whereas it is possible to test the entire receiver at Andover by means of an "RF loop" which includes the transmitter and the transponder on the test tower, it is often simpler to test important parts of the receiver in the "IF loop" (Fig. 7) which interconnects transmitter and receiver at intermediate frequencies. In this case, random noise from the input of the receiver can be injected into the communications channel for noise and threshold tests. For such tests the antenna should be pointed at the zenith to ensure stable noise power.

In addition to the integrated test equipment shown in Fig. 7, other specialized test sets are used to maintain all the circuits of the receiver on a routine basis. Tests to be performed include the measurement of IF-to-IF and baseband-to-baseband transmission characteristics, discriminator sensitivity and linearity, and IF and RF return loss. The

receiver can also be left in continuous and unattended operation due to the provision of alarm circuits with remote indication.

2.3 *Circuits for Low-Noise Amplification and Demodulation*

2.3.1 *The Maser*

The heart of the receiver is the low-noise maser amplifier which is described in detail in a companion paper.[11] The single-tuned (or equalized) maser, as described in this reference, was used in the receiver rather than the low-gain stagger-tuned version. This choice resulted in a substantial saving of equipment by eliminating a low-noise second-stage RF amplifier. The single-tuned maser has a gain of 42 db and a half-power bandwidth of 16 mc. At a bandwidth of 25 mc, the maser gain is still 35 db. The noise contribution of the converter with its 12-db noise figure or 4300°K noise temperature, referred to the input of the maser, amounts to a negligible 0.27°K at midband and to 1.36°K at the band edges. The stagger-tuned maser, on the other hand, has a flat gain of about 27 db, and the frequency converter would contribute 8.6°K unless the maser were followed by a low-noise second-stage RF amplifier, such as a traveling-wave tube or a parametric amplifier. The terminal noise temperature of the maser alone is 3.5°K.

The relatively low level at which a maser begins to saturate fortunately does not pose a problem in a satellite communications system, as can be seen from the following. The ruby maser shows a one-db drop from its small signal gain at an output level of about −40 dbm. The single-tuned maser, therefore, will begin to saturate at a single-carrier input level of −82 dbm. The highest expected received signal level is about −75 dbm, at which the gain of this maser is 3.5 db below the maximum. If, instead of a single carrier, a signal with the same power but a flat spectrum of 25 mc, resembling an actual communications signal, were applied to the maser, the saturation effects would be smaller. The automatic gain control circuit of the IF amplifier compensates not only for the variations in received signal level but also for the changes of maser gain due to saturation. Saturation also causes a widening of the maser transmission characteristic. This effect changes the transmission by only a few tenths of a db up to input levels of −75 dbm and can therefore be neglected for all practical purposes.

The saturated maser, unlike an electron tube or transistor amplifier, does not show signs of instantaneous nonlinearity, which would give rise to intermodulation or signal clipping. The maser acts much like an

extremely linear amplifier followed by a voltage divider containing a thermistor whose resistance is changed by the power in the amplified signal. As in this thermistor circuit, the maser gain reacts to a change in level very slowly, with a time constant of about 0.1 second.

The extremely low instantaneous nonlinearity predicted by maser theory was also confirmed experimentally. For this purpose, two strong signals of equal power at frequencies f_1 and f_2 were applied within the passband of the maser, and the third-order intermodulation products $2f_1 - f_2$ and $2f_2 - f_1$, falling again into the maser passband, were measured. If both signals f_1 and f_2 were at the level of -85 dbm, which is possible during two-way telephony operation, the intermodulation terms would be about 180 db lower. It is clear that such low distortion levels are completely negligible. One is also led to the conclusion that the maser is the most linear amplifier in existence.

For the design of the waveguide diplexer, it was necessary to determine how much of the 6390-mc transmitting signal could reach the input of the maser without causing saturation or other effects. Whereas saturation is evident around -82 dbm for signals in the passband (4170 mc), signal levels as high as 2.5 watts (34 dbm) can be applied to the (impedance-matched) maser input at 6390 mc without causing intolerable distortions of the transmission characteristic. In the latter situation, however, the helium boil-off rate will be increased considerably. Because we have no control over the impedance match of the maser at 6 kmc, it is not advisable to apply interfering signal levels in excess of a few hundred milliwatts.

It is possible to saturate the maser from the output side as well. Due to balancing and filtering in the converter, the leakage of the 4095.59-mc local oscillator signal is low enough not to cause saturation of the maser.

The over-all receiver bandwidth is widened to the required 25 mc at the half-power points by inserting an equalizing filter at IF. A simple bridged T single-pole filter is used with a loss of 7 db at midband and 3 db at the 25-mc bandwidth. The resulting transmission characteristic has two peaks of about 0.3 db, 5 mc away from the center frequency.

The magnetic field of 3300 gauss which tunes the maser to a frequency of 4170 mc is provided by a permanent magnet. Because of the high tuning sensitivity of 2.4 mc per gauss, it is necessary to avoid large temperature variations of the magnet, which will change the magnetic field at a rate of 0.4 gauss per degree centigrade and will therefore lead to a temperature sensitivity of 0.96 mc/°C. It is very helpful in this respect that the temperature of the upper equipment room in which the

receiver is located is kept within a few degrees. It has further been found important that magnetic material like metal chairs should not be brought close to the maser to avoid detuning. It is even possible to notice the effect of the earth magnetic field, which amounts to about 0.16 gauss at Andover, Maine. When the horn antenna is turned in azimuth, the earth field will add or subtract from the maser field, and a slight tilting of the transmission characteristic can be observed. (See Fig. 19 of Ref. 10.)

The operation of the maser requires a supply of liquid helium and nitrogen. The handling of these cryogenic fluids has been simplified considerably over standard laboratory procedures by the availability of new 100-liter containers and transfer tubes. The maser accepts 10 liters each of liquid helium and nitrogen, and boil-off occurs in about 20 and 50 hours, respectively. No attempts were made to recover the expended helium gas because this was considered to be an interim situation which would be changed in time by the installation of a closed-cycle helium liquifier.

A ruby maser operating at a frequency of 4170 mc must be pumped with a signal at 30,180 mc. The pump power at the maser terminals should be greater than 50 milliwatts if the maser gain is not to drop more than about 2 db from its maximum. The pump frequency should remain within a few mc of the correct value to ensure maximum pumping efficiency and to avoid loss of gain. A reflex klystron serves as the source of pump power. Good long-term frequency stability is provided by the AFC circuit shown in Fig. 8, which has the following features: (*i*) the reference cavity is made low Q in order to produce a peak-to-peak separation of 30 mc in the Foster-Sealey type waveguide discriminator, (*ii*) a wideband (100 kc) dc amplifier stabilized by a mechanical chopper is used, and (*iii*) the repeller of the klystron is operated at about ground potential. The so-often unreliable voltage translation from ground potential to the high dc potential of the repeller is therefore avoided. This requires operation of the klystron shell at a high potential and makes the use of a high-voltage waveguide choke necessary. The RC circuit between the dc amplifier and the klystron repeller determines the stability of the feedback loop.

2.3.2 *The Parametric Amplifier*

A parametric amplifier[12] can be inserted into the system instead of the maser for evaluation of its performance in a satellite system or as a back-up for the maser. The amplifier consists of two cascaded stages of

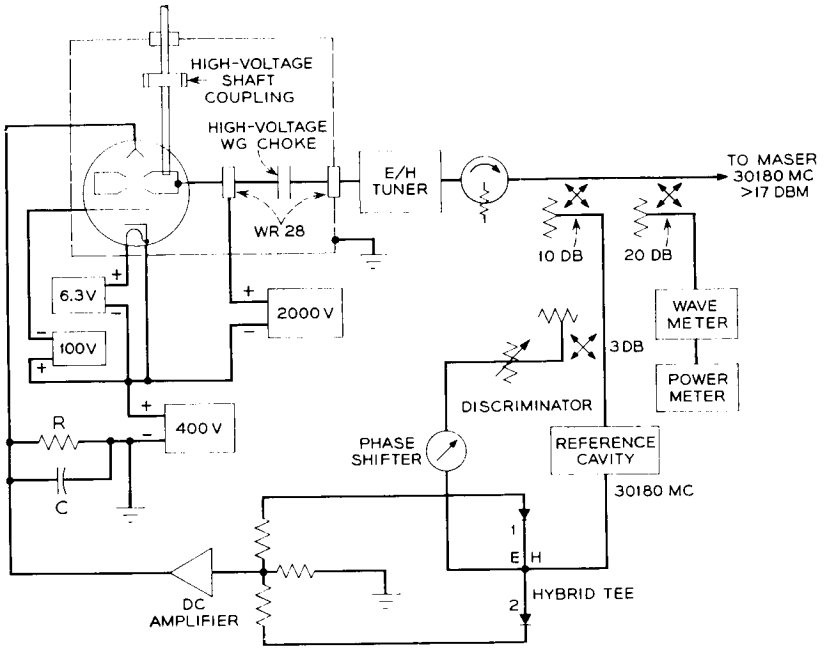

Fig. 8 — Circuit diagram of the maser pump.

similar design. The first amplifier is operated at liquid nitrogen temperature (77°K) and has a gain of 20 db, while the second works at room temperature with a gain of 18 db. The over-all gain of 38 db is therefore close to the 42 db of the maser. The room temperature parametric amplifier with its noise temperature of about 130°K serves as a buffer against the 4300°K noise of the converter circuit. The total noise temperature of the parametric amplifier, including converter, is about 50°K.

The bandwidth of the amplifier is 60 mc at the half-power points. It is obvious that no equalizing filter is needed at IF as in the case of the narrower maser. The over-all 3 db bandwidth of the ground receiver is then 32 mc as determined by the narrower waveguide filters and IF circuits. Saturation in this parametric amplifier, as expressed by a one-db drop from maximum gain, sets in at an input level of −50 dbm. It has been found that intermodulation is no problem for the typical satellite signals of −85 dbm. If a 6390-mc signal is applied to the input of the amplifier at a level greater than 0 dbm, then its 4-kmc transmission will be affected. A band rejection filter can be built into the first parametric amplifier, which raises the tolerable 6-kmc level to about 17 dbm without causing an increase in the noise temperature of the amplifier.

The good over-all stability of this parametric amplifier is due mainly to the stable design of the 23-kmc pump source. The same source is used to drive both stages of the amplifier. Refilling of the dewar with liquid nitrogen is required only every 10 days.

2.3.3 *The FMFB Receiver*

An FMFB receiver is part of the ground receiver. It serves to extend the threshold of noise improvement by 4 to 5 db over that obtained with a standard FM receiver. The feedback circuit is capable of demodulating high-index FM signals with peak frequency deviations of ± 10 mc. The circuit can be used for the reception of television, telephone multiplex and other types of signals.

An integral part of any FMFB receiver is a voltage-controlled oscillator. Such an oscillator should have good modulation linearity, high modulation sensitivity, small signal delay, and good long-term frequency stability. All these features were found in a 6-kmc reflex klystron. This made it necessary to enter the circuit at a frequency of 6123 mc, as indicated in Fig. 7. No further circuit details will be given here; the reader is referred to a companion paper[13] for a detailed description of the FMFB receiver.

2.4 *Diplexer and Associated Waveguide Circuits*

2.4.1 *The 4 kmc - 6 kmc Diplexer*

The waveguide circuit which allows the connection of the 6-kmc transmitter and the 4-kmc receiver to the same horn-reflector antenna is shown in Fig. 9. Although at present this diplexer is only required to work properly over a 25-mc band around the transmitting frequency of 6390 mc and the receiving frequency of 4170 mc, it was designed to handle a much wider band of frequencies. Several components are capable of operating over the full 4-kmc and 6-kmc common carrier bands, extending from 3700 to 4200 mc and from 5925 to 6425 mc, respectively. Other parts are more narrow-band, but studies are in progress to make the circuit work over the full 500 mc of the two common carrier bands.

Returning to Fig. 9, the 2-kw (63-dbm) signal from the 6-kmc transmitter arrives at the diplexer from the left in a rectangular waveguide and with horizontal polarization. The signal travels essentially unchanged over a waveguide transition and through the polarization coupler. The 6-kmc signal which leaks through the coupler into the arm towards the maser is at least 25 db lower. The polarizer then transforms

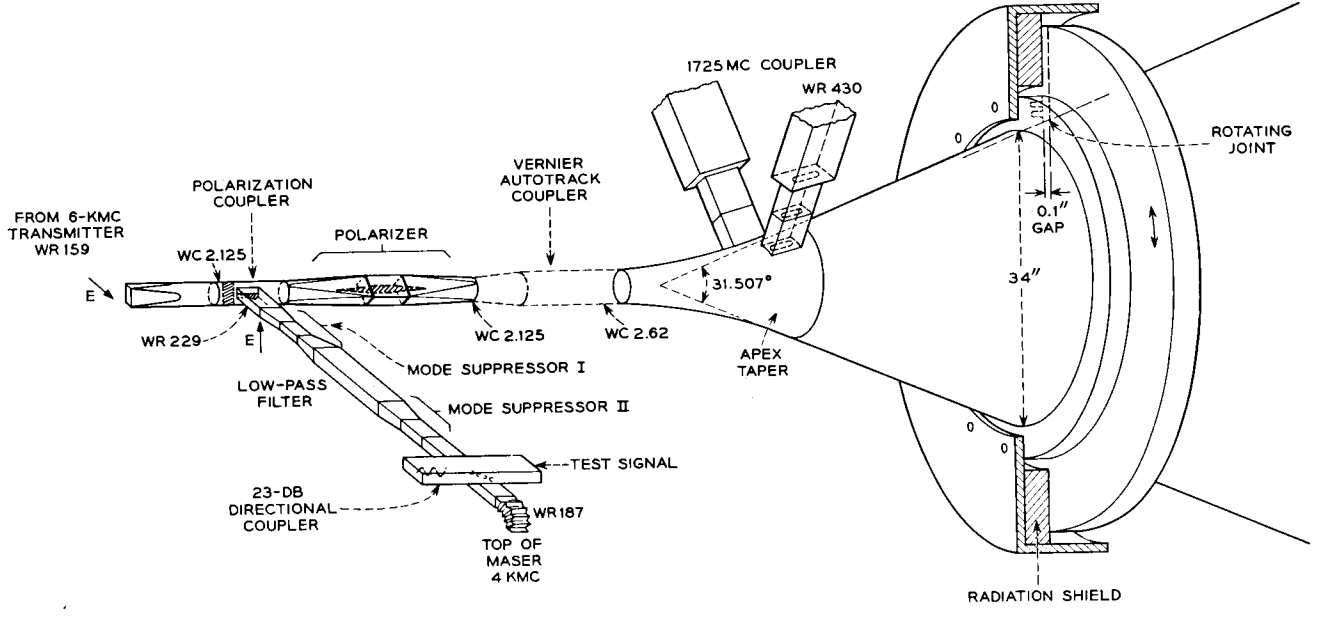

Fig. 9 — Sketch of diplexer and associated waveguide circuits.

the linearly polarized 6-kmc signal into circular polarization for launching by the antenna.

The 4-kmc signal from the antenna, after going through the polarizer, appears as a vertically polarized wave which is guided through the polarization coupler with little loss into the rectangular waveguide leading to the maser. The polarization coupler is of the same type as used in Project Echo, but is designed to work over both the 4- and 6-kmc common carrier bands.[14]

The diplexer was designed under the assumption that the 6-kmc signal level seen at the 4-kmc output terminal shall never exceed 0 dbm. This level is considerably below the value which is acceptable for the maser. It was chosen to allow the use of different types of parametric amplifiers. (See Section 2.3.2.) The diplexer therefore has to provide a total of 63 db of isolation for the 6-kmc signal. With a minimum guaranteed loss of only 25 db in the polarization coupler, additional loss is introduced by a waveguide low-pass filter. This filter was originally designed for the TD2 microwave system, working in the 4-kmc common carrier band, to suppress leakage from the TH system (6-kmc band). The filter has more than 60 db of attenuation for the fundamental mode, but negligible loss for the TE_{20} mode at 6 kmc. It also has an insertion loss of less than 0.09 db over the 4-kmc band. Generators of TE_{20} modes are the polarization coupler and the directional coupler on the maser side. Two mode suppressors were therefore inserted as shown in Fig. 9, consisting of a short piece of narrow-width (1.79-inch) rectangular guide and associated transitions. Each suppressor has little loss at 4170 mc but more than 40 db of attenuation for the TE_{20} mode at 6390 mc. With these precautions, the isolation of the diplexer is found to meet the 63 db isolation with a substantial margin.

The 23.35-db directional coupler at the maser is used for measuring the receiving system noise temperature and for gain and transmission measurements. A short piece of flexible waveguide connects the waveguide circuit to the top flange of the maser.

Because it is necessary to transmit a right-hand circularly polarized wave at 6 kmc and to receive a left-hand circular wave at 4 kmc, a polarizer is inserted between the polarization coupler and the antenna. The polarizer, suitable for operation at 4 and 6 kmc, is shown in Fig. 10 together with a plot of its performance in terms of axial ratio. For pure circular polarization to exist at the output of the polarizer, it is necessary for the field components parallel and normal to the dielectric plate to be equal in magnitude and 90° out of phase. If a differential loss or a deviation from 90° exists, the wave will be elliptically polarized, and

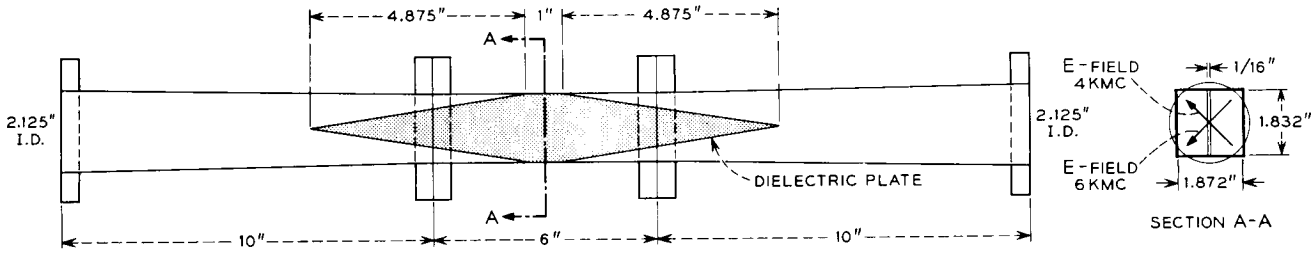

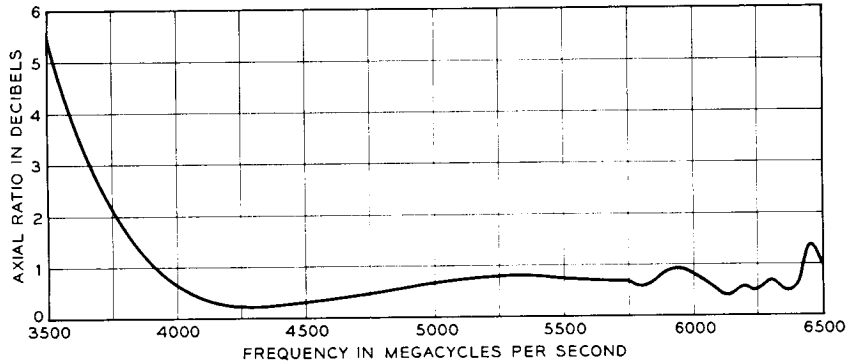

Fig. 10 — The polarizer.

the ratio of major to minor axis, the axial ratio, will be greater than 0 db. Fig. 11 shows how the axial ratio depends on the phase difference and on the differential loss between the two field components. The differential loss was kept below 0.01 db in the polarizer of Fig. 10 by using an extremely low-loss dielectric plate. A phase difference close to 90° is maintained from 4000 to 6500 mc in the polarizer shown. This was made possible by making use of the fact that a dielectric plate in a square waveguide produces a differential phase versus frequency characteristic which is opposite to the one obtained in a nonsquare guide. By locating the dielectric plate in a slightly nonsquare guide, a compensation over a wide frequency range is possible. As a consequence, the axial ratios plotted in Fig. 10 are found to be quite low over a frequency range of 2500 mc.

If imperfect polarizers are used in a system, they will cause a transmission loss. Fortunately, these losses are quite small and amount to only a few tenths of a decibel for the polarizer of Fig. 10 when working with a satellite whose axial ratio is lower than 4 db.

The diplexer is well matched over wide frequency bands at 6390 and

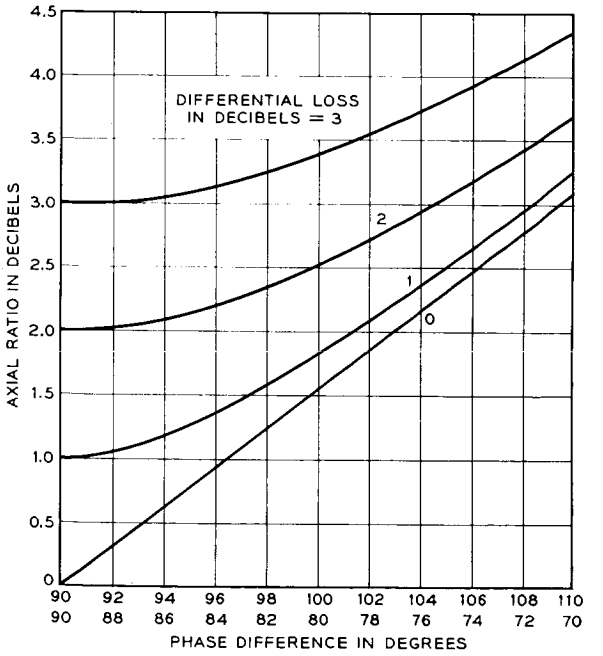

Fig. 11 — Dependence of the axial ratio of a polarizer on differential loss and phase difference.

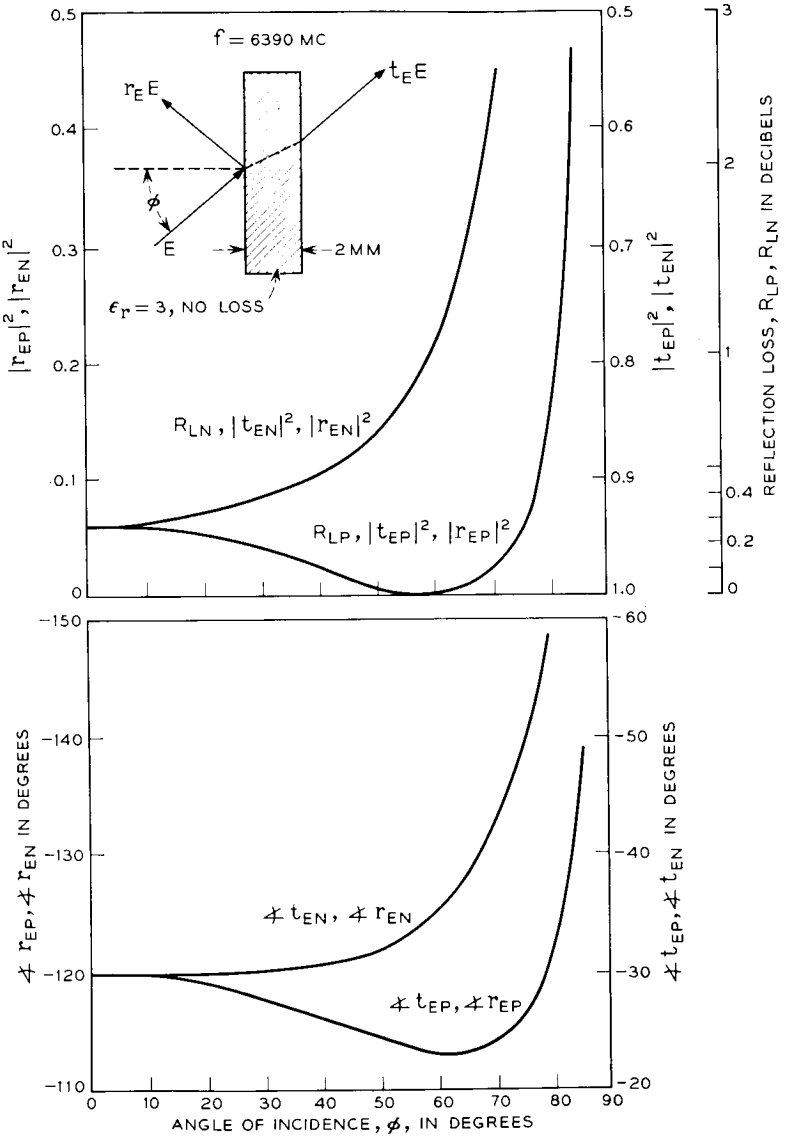

Fig. 12 — Reflection and transmission coefficients of the (lossless) radome at 6390 mc.

4170 mc, and the return losses at the three diplexer terminals are 30 db or higher.

2.4.2 *Effect of the Radome on the Operating Characteristics of the Diplexer*

The 4- and 6-kmc signals are affected in a number of ways by the radome which surrounds the horn-reflector antenna. The possible effects on the operating characteristics of the diplexer will be investigated here. The radome, for instance, will reflect the right-hand circularly polarized transmitted wave as a left-hand circular wave which, after being picked up by the horn antenna, will be directed towards the maser by the polarization coupler. The isolation of the polarization coupler, and in turn the isolation of the diplexer, could be reduced by this reflection. Measurements were made in the laboratory to determine the dielectric constant of the radome material. The power reflection $|r_E|^2$ and transmission $|t_E|^2$ coefficients and their phase angles were then calculated as a function of the angle of incidence Φ. Electric fields parallel (index P) and normal (index N) to the plane of incidence were considered. The results are shown in Figs. 12 and 13 for 6390 and 4170 mc, respectively. According to Fig. 12, the power reflection coefficient of the radome at 6390 mc, averaged over the possible angles of incidence from 8° to 52° and parallel and normal polarization, amounts to about 0.065, which corresponds to a return loss of only 12 db.

Only if all the reflected components from the radome appeared in-phase over the aperture of the antenna could a return loss of 12 db be seen at the apex of the horn. This obviously is impossible. The response of the antenna to reflections from the radome is very similar to its far-field response far away from the main beam. Measurements have indicated that the return loss of the radome as seen from the apex is much greater than 46 db. This figure is considerably higher than the 25 db of isolation provided by the polarization coupler. It can therefore be concluded that the isolation of the diplexer is not affected by the radome.

The radome material can also change the axial ratio of the circularly polarized signals and, therefore, affect the characteristics of the polarizer in the diplexer. The circularly polarized signal arriving at the radome can be decomposed into two linearly polarized waves which can be assumed to be parallel and normal to the plane of incidence. The curves of Figs. 12 and 13 through the voltage transmission coefficients t_{EP} and t_{EN} then tell how much differential loss and phase error is introduced by the radome. For angles of incidence up to 20° for 4170 mc and up to 12° for 6390 mc, no differential effects can be found. At 52°, the highest

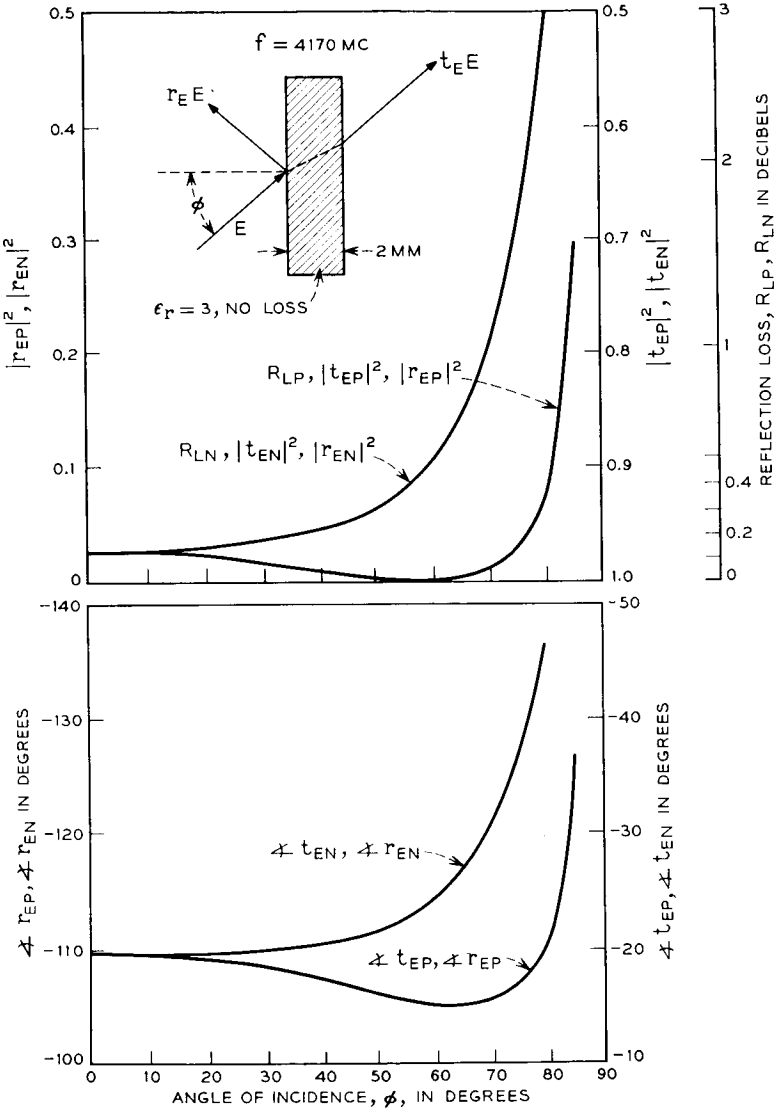

Fig. 13 — Reflection and transmission coefficients of the (lossless) radome at 4170 mc.

possible angle for the Andover horn, the differential losses amount to 0.30 and 0.65 db and the phase errors to 6.50 and 9° for the 4170- and 6390-mc frequencies, respectively. Using Fig. 11, this results in axial ratios of 1.08 db and 1.52 db for the two frequencies. Fortunately, only

a very small part of the energy is radiated (or received) at angles as high as 52°, and no significant loss of signal will result from the degradation of axial ratio by the radome.

2.4.3 *Other Waveguide Circuits*

Following the polarizer shown in Fig. 9, an autotrack coupler is inserted into the line to the antenna. Its purpose is to extract, over narrow-band coupling slots, the TE_{11} and the TM_{01} modes which are generated in the horn antenna by the 4080-mc beacon signal from the satellite. The TM_{01} mode, which propagates freely in the 2.62-inch circular waveguide of the coupler, is completely reflected in the taper leading to the smaller sized polarizer guide. The autotrack coupling section has about 0.01 db of loss for the 4170-mc signal and does not affect transmission of the 6-kmc signal. A complete description of this coupler is contained in a companion paper.[15]

A taper whose impedance varies exponentially with length connects the 2.62-inch circular waveguide to the 31.507° conical apex section of the antenna. The 12.25-inch long taper has a calculated return loss of more than 40 db for the TE_{11} mode and more than 30 db for the TM_{01} mode over the frequency range of 3700 to 6500 mc.[16]

The 1725-mc transmitting signal used in NASA's Project Relay is coupled to the antenna in the conical section directly following the apex taper. Two 1725-mc signals of equal amplitude and 90° phase difference are coupled at right angles into the horn. The phase difference is such as to give a signal right-hand circularly polarized in space. The hybrid Tee and the associated waveguide used to produce the two driving signals are not shown in Fig. 9. The coupling slots are longitudinal and are located at a point where the circumferential wall current at 1725 mc has the first maximum. This maximizes the coupling for the TE_{11} mode and keeps excitation of the TM_{01} mode at a low level. The coupling slots are backed by two-cavity bandpass filters, giving a maximally flat transmission with a 60-mc bandwidth. The filters are built in a small-sized waveguide (4.0 by 0.9 inch) to reduce the number of undesired modes which might be excited at 4 and 6 kmc. Insertion loss at 1725 mc is less than 0.1 db. The filters also act as transformers into the conical section of the antenna and into the larger-sized waveguide WR430, which is used for the rest of the installation. Return loss of the coupler, including the hybrid Tee splitting arrangement, is better than 16 db over a 14-mc band centered at 1725 mc. The coupler has no measurable effect on the transmission of 6390- and 4170-mc signals. The noise introduced into the system by the coupler at 4 kmc is dependent on the

losses in the iris located in the apex taper. By proper mechanical design of this iris, it was possible to reduce this noise contribution to less than 1°K.

A rotating joint is located at a cone diameter of 34 inches. This rather large diameter and a gap width of 0.1 inch simplify the electrical design of a joint which has to work at 6390, 4170, and 1725 mc. A double choke is used and optimized at 4170 mc. Measurements have indicated that for gap widths up to 0.5 inch, and with absorbing material covering the outside of the joint, the 4-kmc noise contribution was still below 1°K. A radiation shield of the form shown in Fig. 9 was put around the outside of the joint in order to keep the radiated energy at 6390 or 1725 mc below the Bell System safety limit for continuous exposure of 1 milliwatt per cm^2 at all points outside the gap.

2.4.4 *The 4-kmc Waveguide Losses and Noise*

The importance of using low-loss waveguide components in a low-noise system will now be explained. It can be shown that the noise introduced by a matched circuit with a power transmission coefficient a amounts to

$$T = T_R(1 - a) = T_R(1 - 10^{-A/10}),$$

where $A = -10 \log a$, the insertion loss in decibels, and T_R is the temperature of the circuit in degrees Kelvin. With T_R taken to be 290°K, the formula leads to the helpful approximation $T = 66.8$ A, if $A < 0.5$ db. For each tenth of a decibel loss, the noise will therefore increase by about 6.7°K. For a total loss of 1 db, the exact formula gives a temperature of 59.7°K. If one considers that the noise from all the nonwaveguide sources together amounts to about 20 to 30°K in a station like the one at Andover, it becomes clear that the waveguide losses should not exceed a very small fraction of a decibel.

It is enlightening to determine the effect of an additional 0.1 db of loss on the signal-to-noise ratio of a receiver with 26°K over-all noise temperature. We find that the added 6.7°K of noise is equivalent to an increase in the receiver noise power of one db. With the signal down only by 0.1 db the signal-to-noise ratio is degraded by 1.1 db. The effect of the loss is therefore 10 times greater on noise than on signal level. The situation becomes reversed, however, in cases where A is higher than a few db (very lossy waveguide circuits or high rain attenuation). The noise temperature then reaches 290°K asymptotically.

The waveguide components of Fig. 9 were measured with a dual-

TABLE II — LOSS AND NOISE OF THE WAVEGUIDE CIRCUIT AT 4170 MC

Waveguide Unit	Loss (db)	Noise Temperature °Kelvin
Autotrack coupler	0.010	0.67
Polarizer	0.021	1.40
Polarization coupler	0.007	0.47
Mode suppressor I	0.021	1.40
Low-pass filter	0.085	5.67
Mode suppressor II	0.016	1.07
23-db directional coupler, including coupling loss	0.030	2.00
Flexible waveguide	0.023	1.54
Total	0.213	14.22

channel insertion loss test set which gave an accuracy of a few thousandth of a db. Because noise is generated only by the absorptive part of the insertion loss, the loss due to reflections should normally be taken into account. However, the very high return losses (30–40 db) of the components made it possible to neglect the reflection losses for all practical purposes. Table II lists all the waveguide parts which contribute to the noise at 4170 mc.

No contributions from parts to the right of the autotrack coupler in Fig. 9 are shown because they are negligible. The noise temperatures shown in the table were calculated using the above formula. A more direct determination of the over-all waveguide noise temperature was made by using the maser as a low-temperature reference. The result was within 1°K of the above given figure of 14.22°K.

2.5 *System Noise Temperature*

2.5.1 *Method for Measuring Noise*

Those parts of the receiver which are important for the determination of the receiving system noise temperature are shown in Fig. 14. The noise energy coming from the sky, the radome, the antenna, and the waveguide circuits is lumped into a single term $kT_{IN}B$. It is assumed here that B is the receiver noise bandwidth of about 29 mc. Noise from a noise lamp can be injected through a 23.35-db directional coupler into the signal path ahead of the maser. With the noise lamp turned off, we can write for the noise power at the output of the IF amplifier:

$$N_{OFF} = kBg_M g_{IF} (T_{IN} + cT_R + T_M) + kBg_{IF} (f - 1)T_R .$$

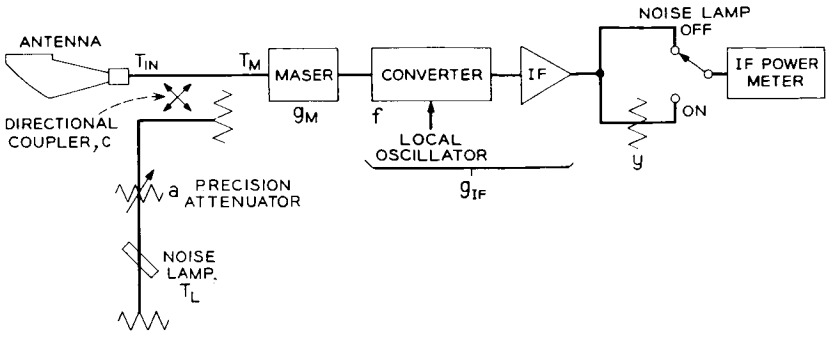

Fig. 14 — Circuit essential for the measurement of the noise temperature of the receiving system.

The g's are power gains, T_R is the room temperature, taken as 290°K, c is the coupling factor of the directional coupler ($=1/216$), and f is the noise factor of the converter ($=15.85$ or 12 db). TM is the temperature of the maser alone, amounting to 3.5°K. Effects like imperfect impedance matches, finite directivity of the directional coupler, and differences in noise bandwidth between the maser and the IF amplifier were neglected because they are very small. If we introduce the new term

$$T_{SYS} = T_{IN} + cT_R + \frac{f-1}{g_M} T_R + T_M,$$

meaning the receiving system noise temperature measured at the input terminals of the maser, the noise power can be written as

$$N_{OFF} = kBg_M g_{IF} T_{SYS}.$$

With the noise lamp turned on, the noise power at the output of the IF amplifier, after going through an attenuator with power loss coefficient y, is found to be

$$N_{ON} = kB \frac{g_M g_{IF}}{y} [T_{SYS} + ac(T_L - T_R)]$$

where T_L is the temperature of the noise lamp, amounting to about 9500°K, and a the power transmission coefficient of the precision attenuator. The noise due to the insertion of attenuator y is neglected because its loss is small and the product $g_M g_{IF}$ is high. In the course of a noise measurement, the two noise powers N_{OFF} and N_{ON} are made equal by adjusting the precision attenuator. The setting of the precision attenua-

tor will depend on, among other variables, the value of attenuator y, which can be changed in one-db steps. We then find for the system temperature:

$$T_{SYS} = \frac{ac}{y - 1}(T_L - T_R).$$

The maximum error of a noise measurement amounts to about ± 0.35 db or ± 8.5 per cent, with T_L contributing 0.2 db; $y - 1$, which includes short-term amplifier gain variations, 0.1 db; and the combination of a and c, 0.05 db. The improved accuracy of the noise lamp temperature over the 0.5 db of the commercial units was obtained by directly measuring the temperature of the lamp with the maser as a low-noise amplifier.

2.5.2 *Results of Noise Measurements*

Measurements of the system noise temperature made at Andover for different elevation angles of the antenna are shown in Fig. 15. The noise at zenith on a clear day is 32°K for the system containing a maser and is about 85°K with the parametric amplifier replacing the maser. The noise increases towards the lower elevation angles due to the higher noise originating in the atmosphere. When the antenna beam hits the ground, the noise increases abruptly to a value of about 235°K. This temperature depends on the actual temperature and the reflection coef-

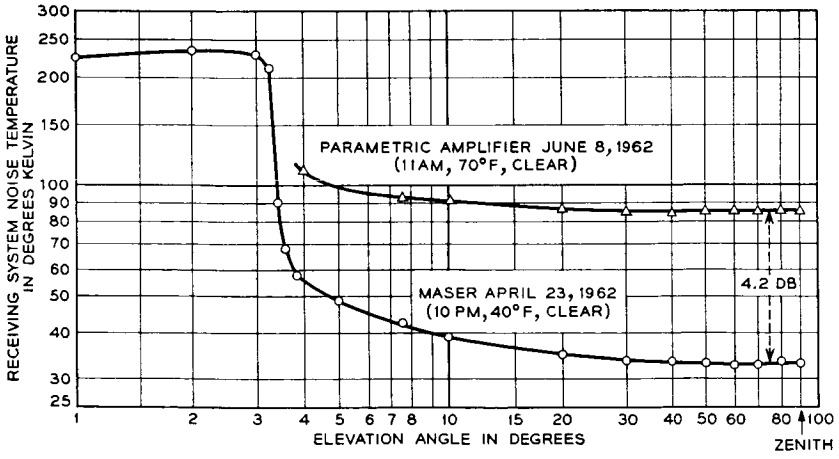

Fig. 15 — Receiving system noise temperature as a function of antenna elevation — clear day data. Azimuth = 142°.

ficient of the ground and on the losses of the signal through the radome and the waveguides. Knowing all these parameters, except the reflection coefficient of the ground, we find for the latter a value of 0.165 at 4170 mc. The sharp increase of the noise at the horizon was used to plot the radio horizon, which then was compared with the far optical horizon. The two coincided within about 0.1° for all regions where the far horizon was not hidden behind nearby obstacles.

The noise distribution shown in Fig. 15 was measured many times and was never found to vary more than one or two degrees on clear or cloudy days. During periods of rain or snow, vastly different noise temperatures were observed. Fig. 16 shows three typical curves. During a heavy rain (curve number 1), high noise values were found, with fast variations occurring in the region from 50° to 90° elevation. Variations at zenith over a period of about 15 minutes ranged from 68° to 126°K. Zenith temperatures between 70°K and 100°K are quite common during periods of moderate rain.

Curve 2 shows a case of light rain, and curve 3 was taken during a light and wet snowfall. The high noise temperatures found near the zenith (curve 3) are clearly due to the presence of the radome on which more snow has accumulated near the top than on the sides. Even curves

CURVE	DATE	LOCAL TIME	WEATHER
1	MAY 24, 1962	10:30 TO 11:30	HEAVY RAIN
2	SEPT 5, 1962	15:00 TO 15:20	LIGHT RAIN
3	OCT 26, 1962	07:10 TO 07:30	LIGHT WET SNOW

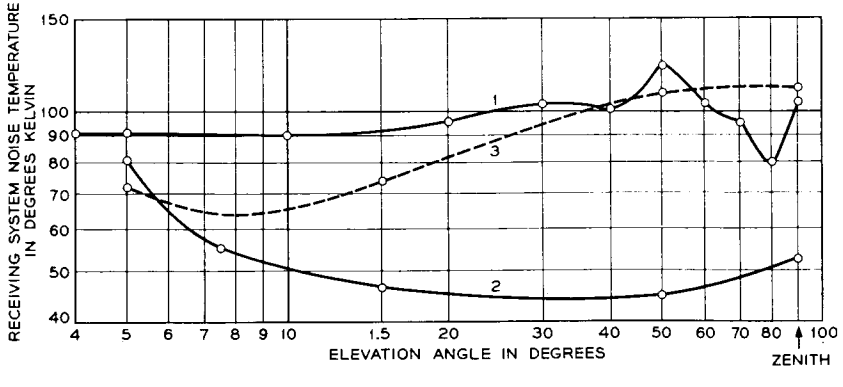

Fig. 16 — Receiving system noise temperature as a function of antenna elevation — rain and snow data. Azimuth = 142°.

1 and 2 show more noise at the higher angles than at, for instance, 15° elevation. This may again be due to some "accumulation" of rain on the top of the radome, but is also due to increased reflection of ground noise into the antenna aperture by the higher portions of the inner radome surface. The latter will become clearer in a moment when the electrical characteristics of the radome are described. The highest zenith system temperature observed to date in Andover due to rain is 135°K and 160°K due to snow. Within about half an hour after the end of a rainfall, noise temperatures close to the dry values of Fig. 15 can be found.

Similar measurements of noise during rain and snow, made at the Holmdel and Whippany, N. J., locations of Bell Laboratories, but without a radome, show a completely different character. Noise temperatures tend to be considerably lower, especially during snow, and they always seem to be lowest at zenith.

2.5.3 *Contributors to System Noise*

Table III gives a breakdown of the system noise into the different contributors. The values for the dry atmosphere were taken from measurements made at Holmdel.[17] The zenith temperature of 2.6°K of this reference appears reduced to 2.4°K by the total loss of 0.36 db in the radome and the waveguides. The contributions of antenna sidelobes, waveguides, maser and second stage are constant and amount to 19.2°K. They were discussed above with the exception of the antenna sidelobes. The horn-reflector antenna is probably the antenna with the lowest possible noise. If operated without a radome, all sidelobes and backlobes

TABLE III — CONTRIBUTORS TO SYSTEM NOISE

	Elevation			
	90°	30°	15°	7.5°
Dry atmosphere	2.4°K	4.8°K	9.2°K	18.4°K
Antenna sidelobes Waveguide circuits Maser Second stage	1.0 14.2 3.5 0.5		19.2°K	
Dry (wet) radome absorption	3 (12)	3 (12)	3 (12)	3 (12)
Dry (wet) radome scattering	7.4(18.5)	6.0(15.0)	4.1(10.2)	1.4(3.5)
Total (dry, measured)	32.0 °K	33.0 °K	35.5 °K	42.0 °K

will not contribute more than about 1°K if the antenna is pointed at least one degree above the horizon.

The effect of the radome on system noise is two-fold. First, the absorption of 4170-mc energy by the radome material is a measure of the noise it spontaneously emits at the same frequency; and second, the inner surface of the radome will reflect (scatter) ground noise into the antenna aperture. In order to investigate the first effect, it was necessary to know the loss characteristics of the radome. Laboratory measurements on dry and wet radome samples first gave values for the dielectric constant and the loss tangents. Calculations were then made to determine the power reflection $|r_E|^2$ and power transmission $|t_E|^2$ coefficients and the absorption transmission coefficient $a = |r_E|^2 + |t_E|^2$. The absorption loss in decibels is $A = -10 \log a$ and would amount to 0 db for the lossless material shown in Figs. 12 and 13. The results of the present investigation are shown in Figs. 17 and 18. If we consider again a maximum variation of angle of incidence from 8° to 52°, we find 3° and 12°K as rough averages for the absorptive noise in the dry and the wet case. It should be kept in mind that the data for the wet radome are based on tests made in the laboratory and that they cannot be completely representative of the conditions encountered in the field where the amount of wetness will vary with the rate of rain and possibly the position on the radome. The tests also showed that the dielectric constant and the loss tangent of the wet material decayed rapidly within minutes and later more slowly towards the "dry" values.

The scattering effect of the radome is difficult to determine by calculation. The noise values shown for dry radome scattering in Table III are therefore equal to the amount of noise which could not otherwise be accounted for. The higher scattering at high elevation angles is due to the particular antenna-radome geometry,* and to a certain extent is also dependent on the area surrounding the radome. The ground effects were determined by rotating the antenna 360° in azimuth and observing the change in zenith temperature. Values ranging from 31° to 35°K were found. The data presented in Figs. 15 and 16 and in Table III were taken at an azimuth of 142° (boresight tower).

The scattering effect of the wet radome was found by multiplying the dry values with the ratio of wet-to-dry power reflection coefficients as given in Figs. 17 and 18. This ratio is about 2.5 over a large range of

* Experiments with antennas whose apertures remain always vertical to the diameter of a spherical radome indicate that scatter-noise is minimum at zenith. Such a geometry is impractical for the horn-reflector antenna, however.

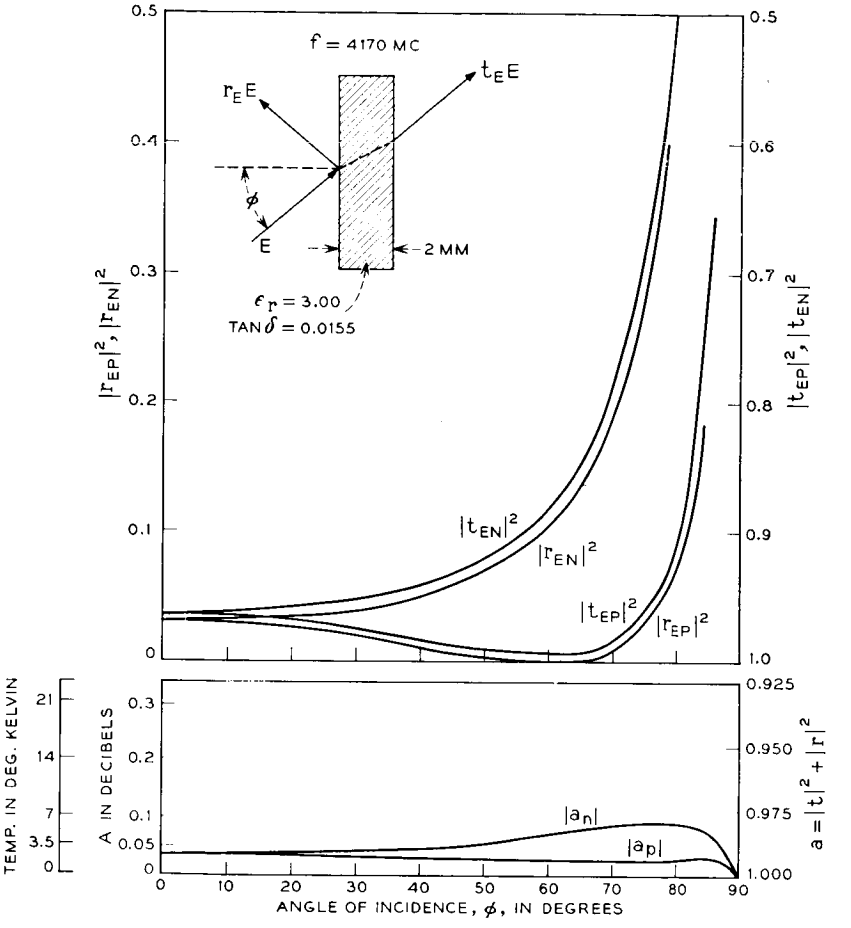

Fig. 17 — Reflection, transmission and absorption transmission coefficients of the dry radome at 4170 mc.

angles of incidence. Wet radome scattering is considerably larger at zenith than at lower angles. This explains the higher noise readings at zenith than at 15° elevation.

Recently, the diplexer of Fig. 9 was operated without the low-pass filter. It was found that one of the polarization couplers built had an isolation peak of 47 db in a narrow band around 6390 mc. This value of isolation allows unperturbed operation of the maser. The system temperature could thereby be reduced by 5°K, or to 27°K at zenith.

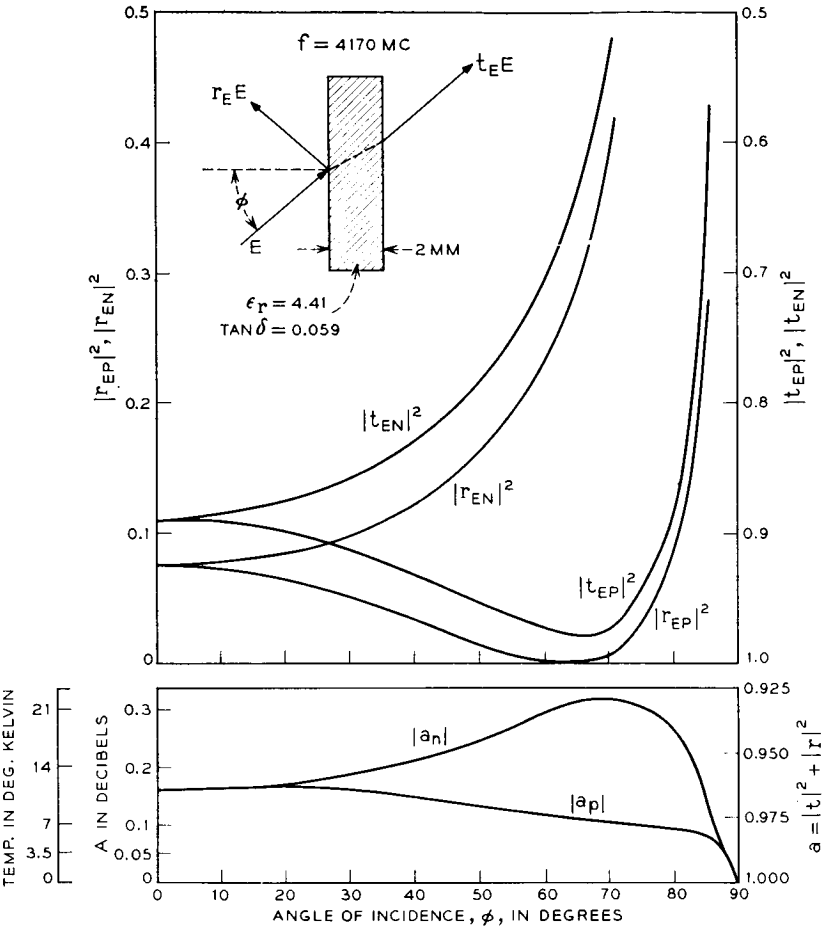

Fig. 18 — Reflection, transmission and absorption transmission coefficients of the wet radome at 4170 mc.

2.5.4 *Other Possible Sources of Noise*

A satellite communications system can be affected by extra-terrestrial noise sources, which is the case on such rare occasions when the satellite passes in front of one of these sources. The strongest source of noise at 4 kmc is the sun, followed by the moon and a number of radio stars. When the antenna is pointed at the center of the galaxy, a few extra degrees of noise will be introduced.

A measurement was made of the receiving system noise at and near

the sun. The antenna was pointed in the path of the sun, which then drifted through the antenna pattern. The result is plotted in Fig. 19. Over an angle of about 0.4°, which is a little less than the 0.5° diameter of the sun, a maximum temperature of 17,000°K is maintained, representing an interfering noise signal of −81 dbm. If we compare this signal with the signal from the satellite, which is in the range of −75 to −100 dbm, it is clear that communications would be disrupted during this time. The drop in noise shown in Fig. 19 is as expected from the radiation diagram of the antenna. Only one degree away from the center of the sun, the noise has dropped to an operationally acceptable 65°K.

The actual temperature of the sun at 4170 mc is higher than the measured 17,000°K by about 1.6 db, or equal to 24,500°K. The 1.6 db is made up of 0.04 db atmospheric loss, 0.15 db radome insertion loss, 0.21 db waveguide loss, and 1.2 db loss due to the finite width of the antenna pattern.

The temperature of the moon was measured on May 10, 1962, 10:00

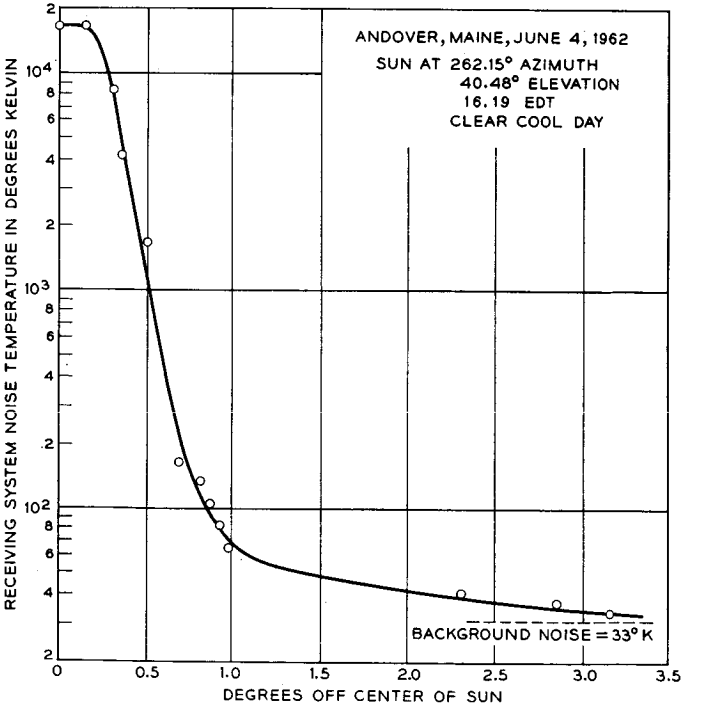

Fig. 19 — Receiving system noise temperature near the sun.

p.m. EDT. The maximum system temperature was found to be 195°K. If we subtract from this figure 34°K of system background noise and add 1.66 db due to the same type of losses mentioned before, we find for the temperature of the moon 236°K. The moon will produce a noise power in the communications channel of −100.5 dbm and therefore can affect the satellite link if the received signal level is lower than −95 dbm.

A search was also made for man-made sources of noise and interference. Such signals would be strongest close to the horizon. The measuring equipment included the receiver followed by a narrow-band IF amplifier which allowed the detection of signals down to −130 dbm. This is about 20 db lower than the normal broadband noise level of the receiver. No noise or other interfering signals could be detected. This is clearly a result of the topography of the Andover site.

III. ACKNOWLEDGMENTS

A number of people have contributed to the development of the transmitter and receiver for the Telstar ground station. The efforts of G. S. Axeling in the design of the receiver waveguide circuits are particularly acknowledged. W. Gabel, G. D. Hohmann and W. S. Irvine contributed to the power amplifier design, and J. Schill was largely responsible for the FM deviator.

REFERENCES

1. Hoth, D. F., O'Neill, E. F., and Welber, I., The *Telstar* Satellite System, B.S.T.J., this issue, p. 765.
2. Shennum, R. H., and Haury, P. T., A General Description of the *Telstar* Spacecraft, B.S.T.J., this issue, p. 801.
3. Sproul, P. T., and Griffiths, H. G., The TH Broadband Radio Transmitter and Receiver, B.S.T.J., **40**, November, 1961, pp. 1521–1568.
4. Susen, C. P., and Degan, J. J., The TH Radio Microwave Carrier Supply System, B.S.T.J., **40**, November, 1961, pp. 1569–1586.
5. Houghton, E. W., and Hatch, R. W., FM Terminal Transmitter and Receiver for the TH Radio System, B.S.T.J., **40**, November, 1961, pp. 1587–1626.
6. Collier, R. J., Laico, J. P., Helm, G. D., and Striny, K. M., The Ground-Station Traveling-Wave Tube, B.S.T.J., this issue, Part 3.
7. Houghton, E. W., and Drazy, E. J., Test Equipment for the TH Radio System, B.S.T.J., **40**, November, 1961, pp. 1717–1743.
8. Giger, A. J., and Low, F. K., The Automatic Protection Switching System of TH Radio, B.S.T.J., **40**, November, 1961, pp. 1665–1715.
9. Githens, J. A., and Peters, T. R., Digital Equipment for the Antenna Pointing System, B.S.T.J., this issue, Part 2.
10. Hatch, R. W., Bennett, S. B., and Kinzer, J. P., Results of the *Telstar* System Communication Tests, B.S.T.J., this issue, Part 2.
11. Tabor, W. J., and Sibilia, J. T., Masers for the *Telstar* Satellite Communications Experiment, B.S.T.J., this issue, Part 3.

12. Uenohara, M., Chruney, M., Eisele, K. M., Hanson, D. C., and Stillwell, A. L., A 4-gc Parametric Amplifier for the *Telstar* Satellite Communication Experiment, B.S.T.J., this issue, Part 3.
13. Giger, A. J., and Chaffee, J. G., The FM Demodulator with Negative Feedback, B.S.T.J., this issue, p. 1109.
14. Ohm, E. A., Project Echo Receiving System, B.S.T.J., **40**, July, 1961, pp. 1065–1094.
15. Cook, J. S., and Lowell, R., The Autotrack System, B.S.T.J., this issue, Part 2.
16. Tang, C., unpublished work.
17. De Grasse, R. W., Hogg, D. C., Ohm, E. A., and Scovil, H. E. D., Ultra-Low-Noise Antenna and Receiver Combination for Satellite or Space Communication, Proc. National Electronics Conference, **15**, October, 1959, pp. 370–379.

Page intentionally left blank

The FM Demodulator with Negative Feedback

By A. J. GIGER and J. G. CHAFFEE

(Manuscript received March 22, 1963)

This paper describes the design and theory of operation of the wideband FM demodulator with feedback (FMFB receiver) used at the Andover, Maine, earth station for Telstar satellite communications tests. Performance data for the FMFB receiver indicate a clear advantage over the conventional FM receiver in many cases. The principal advantage lies in the ability of the FMFB receiver to raise the threshold at which "breaking" occurs for TV and other wideband signals.

I. INTRODUCTION

The FM demodulator with negative feedback (FMFB)* is an outgrowth of an FM receiver circuit first described in 1937.[1] A demodulator of this type was used during the communication tests with the Echo I satellite, which started in August, 1960.[2] Compared with a conventional or standard FM demodulator, the principal advantage to be derived from this circuit is its ability to improve the threshold at which "breaking," resulting from excessive noise, will occur.

The receivers mentioned above were capable of demodulating a single 4-kc voice channel. Since it was required that the Telstar system be capable of handling television and other wideband signals, the design of feedback receivers became a problem of much greater complexity as a consequence of the relatively wide baseband.

The FMFB receiver to be described in this paper is used in the Andover ground station for the reception of wideband signals from the Telstar satellite.[3] A different FMFB receiver, described elsewhere,[4] was used in the Holmdel station during Telstar experiments. The basic elements of the feedback receiver are shown in the block diagram of Fig. 1. The incoming RF signal is combined in a mixer with the output of a

* Sometimes called "FM feedback receiver" or "frequency compression demodulator."

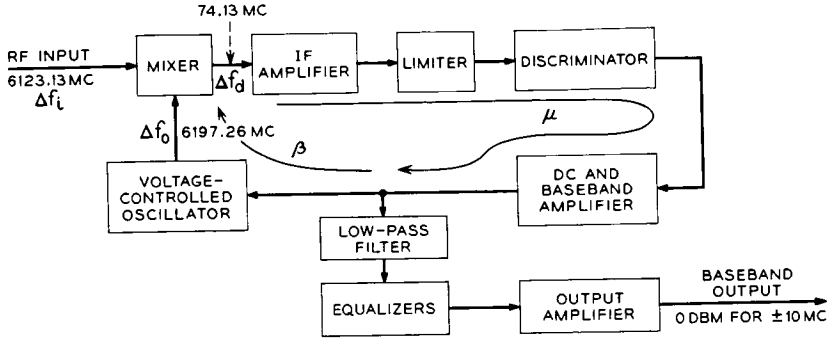

Fig. 1 — Block diagram of FMFB receiver.

voltage-controlled oscillator (VCO) to produce an intermediate-frequency signal. The frequency modulation which has been imparted to this signal, after going through an IF amplifier and a limiter, is then demodulated by the discriminator. The recovered baseband signals are amplified in the dc-and-baseband amplifier and are fed back to the VCO in such a way as to reduce significantly the instantaneous frequency difference between the two signals going into the mixer. The modulation index of the IF signal is thereby diminished. If this reduction is substantial, the resulting FM wave will occupy a much narrower band than the incoming RF signal. This makes it possible to restrict the bandwidth of the IF amplifier. In a sense, the feedback receiver can be considered as a "tracking" filter whose bandwidth is substantially narrower than that required to transmit the complete incoming FM wave; being narrower, the receiver is more immune to incoming noise.

The baseband signal to be fed to the output terminal of the receiver is taken from the input to the VCO and then passed through a low-pass filter, amplitude equalizers, and an output amplifier. The amplitude equalizers correct for deviations in the closed-loop transmission characteristics which are present at low and at high frequencies.

II. THEORY OF THE FMFB RECEIVER

2.1 *Operation above the Breaking Point*

The operation of the FMFB receiver is well understood in the region where the input carrier-to-noise ratio is large, which means well above the breaking point. For analytical purposes, it is convenient to represent the RF and IF circuits in the feedback loop by the baseband analogs

which are valid for FM signals. Simplified analog circuits are normally used which are accurate only for low-index FM signals. Such analogs do not describe the nonlinear distortions of the FM signal which are actually produced in the RF and IF circuits. Nevertheless, they are good enough for a linear analysis above threshold.

The FMFB circuit can then be represented as a conventional feedback circuit with the $\mu(s)$ and the $\beta(s)$ paths defined as in Fig. 1. The mixer is the element which forms the instantaneous difference between the frequencies of the incoming and the fed-back RF signals, i.e., $\Delta f_d = \Delta f_i - \Delta f_o$. The expression $\mu\beta$ is called the open-loop transmission characteristic. It is of fundamental importance in the design of a feedback circuit, since it determines the stability of the loop through its effect on the closed-loop transmission characteristic

$$\frac{\Delta f_o(s)}{\Delta f_i(s)} = \frac{\mu\beta}{1 + \mu\beta} = \frac{\mu\beta}{F}, \tag{1}$$

where $F = 1 + \mu\beta$ = feedback. In any practical wideband FMFB circuit, $\mu\beta$ is a function consisting of many poles and zeros. Analytical methods and actual measurements, together with the optimizing procedures given by Bode,[5] have been used here to design and shape the feedback loop.

The fact that so many stages (or poles) are necessary makes the design of a truly wideband FMFB circuit very difficult. The design problem is reminiscent of the one found in building amplifiers with maximum gain-bandwidth product, to which is added the complicating requirement of holding the over-all phase shift well below 180°. The problem was approached by carefully selecting each part of the FMFB circuit to have as little phase shift and as much gain as possible. In addition, it is advantageous to use high-level signals at the two inputs of the mixer of Fig. 1. This reduces the amount of amplification required inside the loop and can therefore be considered to be the same as obtaining gain without phase shift. This method is limited mainly by the power handling capabilities of the circuits.

In the circuit of Fig. 1 the transmission factor $\beta(s)$ is associated with the VCO alone. In the design to be described in Section III, the VCO consists of a reflex klystron whose transmission characteristic can be assumed to be a constant. The over-all input-output characteristic of the FMFB receiver is therefore obtained by multiplying the closed-loop transmission characteristic with the characteristics of the low-pass filter and the equalizers.

The signal-to-noise ratio (SNR) at baseband for a conventional FM

receiver for carrier-to-noise ratios (CNR) at RF well above breaking is known to be

$$\text{SNR} = \frac{3}{2} m^2 \frac{B}{b} \text{CNR}, \tag{2}$$

where B = RF bandwidth, b = baseband width, and m = modulation index. The RF and baseband transmission characteristics are assumed to be rectangular. It has been shown in Ref. 6 that (2) remains unchanged for an equivalent FMFB receiver. The feedback receiver, therefore, has no noise advantage if operated above the breaking or threshold point. This point, characterized by a certain CNR, is reached when the FM noise improvement given by (2) can no longer be obtained. The breaking point shall be loosely defined here as the CNR where the actual SNR has dropped 1 db below the value given by (2).

2.2 *Operation near the Breaking Point*

No theory is at present available which completely describes the behavior of an FMFB receiver near the threshold of noise improvement. Enloe[6] has introduced a two-threshold concept which has given good results in practical cases. Strictly speaking, the results of Ref. 6 are valid only under the assumption of an unmodulated carrier. We shall use this concept here in order to find simple mathematical expressions for the open-loop and the closed-loop threshold. Relations will then be derived for the optimum amount of feedback and the upper limit of the threshold improvement. These results are then compared with actual measurements taken under various conditions of modulation.

2.2.1 *The Open-Loop Threshold*

Under the assumptions that the incoming carrier is unmodulated and that the VCO generates a steady carrier (open loop), the CNR after the narrow-band IF amplifier (of bandwidth B_{IF}) in the loop will be greater than that at RF (bandwidth $B > B_{\text{IF}}$). Since FM discriminators break at about the same CNR, it can be seen that the insertion of the narrow-band filter results in a threshold improvement over a standard, wide-band FM receiver. The breaking point of a conventional FM receiver varies slightly with the ratio B_{IFN}/b (or B/b). B_{IFN} is the noise bandwidth of the IF filter, and we assume it to be 20 per cent higher than the 3-db bandwidth B_{IF}. B is assumed to be the 3-db bandwidth as well as the noise bandwidth. The empirical formula

$$\mathrm{CNR}_0 = \left[250\left(\frac{B_{\mathrm{IFN}}}{2b} - 1\right)\right]^{\frac{1}{3}} \tag{3}$$

was found to approximate well the breaking points shown in Fig. 9 of Ref. 6. The expression gives good results for B_{IFN}/b as low as 2.5. The threshold, as measured in the RF band B, then appears at

$$\mathrm{CNR}_1 = \mathrm{CNR}_0 \frac{B_{\mathrm{IFN}}}{B} = \frac{B_{\mathrm{IFN}}}{B}\left[\left(250\left(\frac{B_{\mathrm{IFN}}}{2b} - 1\right)\right]^{\frac{1}{3}}\right]. \tag{4}$$

Despite the fact that we consider the threshold under conditions of no modulation, we shall introduce here the modulation index $m = \Delta f/b$, where Δf is the peak frequency deviation caused by full sine-wave modulation at the top baseband frequency b. We can now express B in new terms, employing the so-called Carson's rule

$$B = 2(1 + m)\, b. \tag{5}$$

Under the assumption of uniform feedback F over the band b, the 3-db bandwidth of the IF filter in the loop should be $B_{\mathrm{IF}} = 2[1 + (m/F)]\, b$. Using these relations and $B_{\mathrm{IFN}} = 1.2\, B_{\mathrm{IF}}$, we can rewrite (4) in terms of m and F only

$$\mathrm{CNR}_1 = 1.2\, \frac{1 + (m/F)}{1 + m}\left\{50\left[1 + (6m/F)\right]\right\}^{\frac{1}{3}}. \tag{6}$$

2.2.2 *The Closed-Loop Threshold*

The CNR at which the closed-loop threshold occurs is directly proportional to B_c, which is equal to twice the closed-loop noise bandwidth at baseband. If we again measure the second threshold in the RF bandwidth B, we find by using equation (1) of Enloe's paper

$$\mathrm{CNR}_2 = 4.8\, \frac{B_c}{B}\left(\frac{F - 1}{F}\right)^2. \tag{7}$$

In order to obtain values for B_c, the open-loop characteristic $\mu(s)\cdot\beta(s)$ has to be specified. The Bode-type open-loop characteristic,[5] which provides constant feedback F up to a baseband frequency b and from there on a constant phase, can be considered to be near optimum for our purposes. It will be used for the following derivation. Although not strictly realizable in practice, this characteristic can be approximated by a technique, also due to Bode, which employs the so-called step and fillet. Fig. 8 of Ref. 6 has curves which give B_c as a function of the phase

margin with F as parameter. A phase margin of 50° is considered to be near optimum, because it minimizes B_c over a wide range of F. The empirical relation $B_c = 2bF^{0.8}$ was found to agree well with these curves for a phase margin of 50°. With this relation and (5), we can write (7) in the following form:

$$\mathrm{CNR}_2 = 4.8 \frac{F^{0.8}}{1+m}\left(\frac{F-1}{F}\right)^2. \tag{8}$$

2.2.3 *Optimum Feedback and Upper Limit for Threshold Improvement*

It can be seen from (8) that an increase in feedback F will increase the closed-loop threshold, mainly due to the increase in B_c. Equation (6), on the other hand, indicates a decrease in threshold with increasing feedback. For a certain value of F, the two thresholds will therefore be equal. Such an operating point will tend to optimize the over-all threshold of the FMFB receiver. Equations (6) and (8) were equated and the result is plotted in Fig. 2 as F_{OPT} in decibels versus the modulation index $m = (B/2b) - 1$. For a practical range of m from 3 to 10, we find feedback values varying over the narrow range from 14.2 to 18.2 db.

We can now determine the improvement I which an FMFB receiver provides over the threshold of a standard FM receiver. The standard

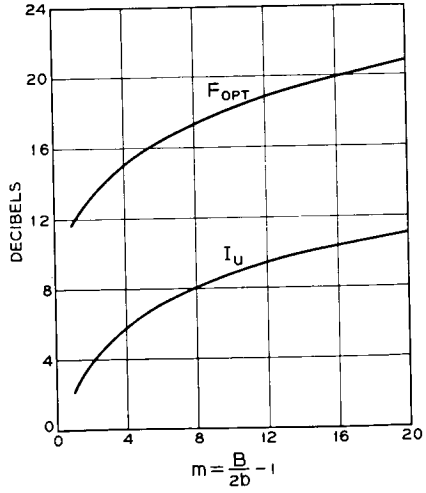

Fig. 2 — Optimum feedback F_{OPT} and upper limit of threshold improvement I_u.

receiver has a threshold given by (3) if B_{IFN} is replaced by B. Using (5), the threshold becomes

$$CNR_3 = \sqrt[3]{250\, m}. \tag{9}$$

Inserting $F_{OPT}(m)$ into either (6) or (8) yields CNR_{OPT}. The improvement is therefore

$$I \leqq \frac{CNR_3}{CNR_{OPT}}. \tag{10}$$

The equals sign indicates an upper limit I_u for the improvement, which could be reached only if the two thresholds occurred abruptly and independently of each other. This will most likely not be the case and the improvement will always be below this upper limit. I_u was calculated using the values of F_{OPT} previously found. The result is plotted as a second curve in Fig. 2. In the range of $m = 3$ to 10, upper bounds for the improvement reach from 4.9 to 8.8 db.

2.2.4 *Comparison with Measured Results*

We shall now compare the formulas derived above with measurements made on the FMFB receiver which are described in Section IV. The pertinent measured quantities are: $B = 25$ mc, $b = 2$ mc, $B_{IFN} = 7$ mc, $F = 15$ db (at 0.5 mc) and $B_c = 15$ mc. Then we find from (4) and (7), $CNR_1 = 2.05$ db and $CNR_2 = 2.90$ db, respectively. Therefore, the closed-loop threshold is governing by the small margin of 0.85 db. This is not quite optimum, and the design could be improved by a slight widening of the IF filter in the loop. Since the over-all threshold of the feedback demodulator is above either of the two thresholds, it must be greater than 2.9 db. It actually occurs at 4.5 db, as indicated by point A on curve 1 of Fig. 12 (Section 4.3.2). It can also be seen from this figure that the threshold is adversely affected by the application of modulation, especially at the higher baseband frequencies. We also wish to compare the measured results with the optimum design. Using (5), we obtain $m = 5.25$, and from Fig. 2 we find an optimum value for the feedback of $F_{OPT} = 16$ db and an upper limit for the threshold improvement of $I_u = 6.65$ db. The optimum setting of F was experimentally found to be the aforementioned 15 db at 0.5 mc. From Fig. 12, the threshold improvement amounts to 4.5 db, equal to the difference between points A and B. It can therefore be concluded that the actual design of the FMFB receiver has come to within 1 db of the calculated F_{OPT} and within 2.15 db of I_u.

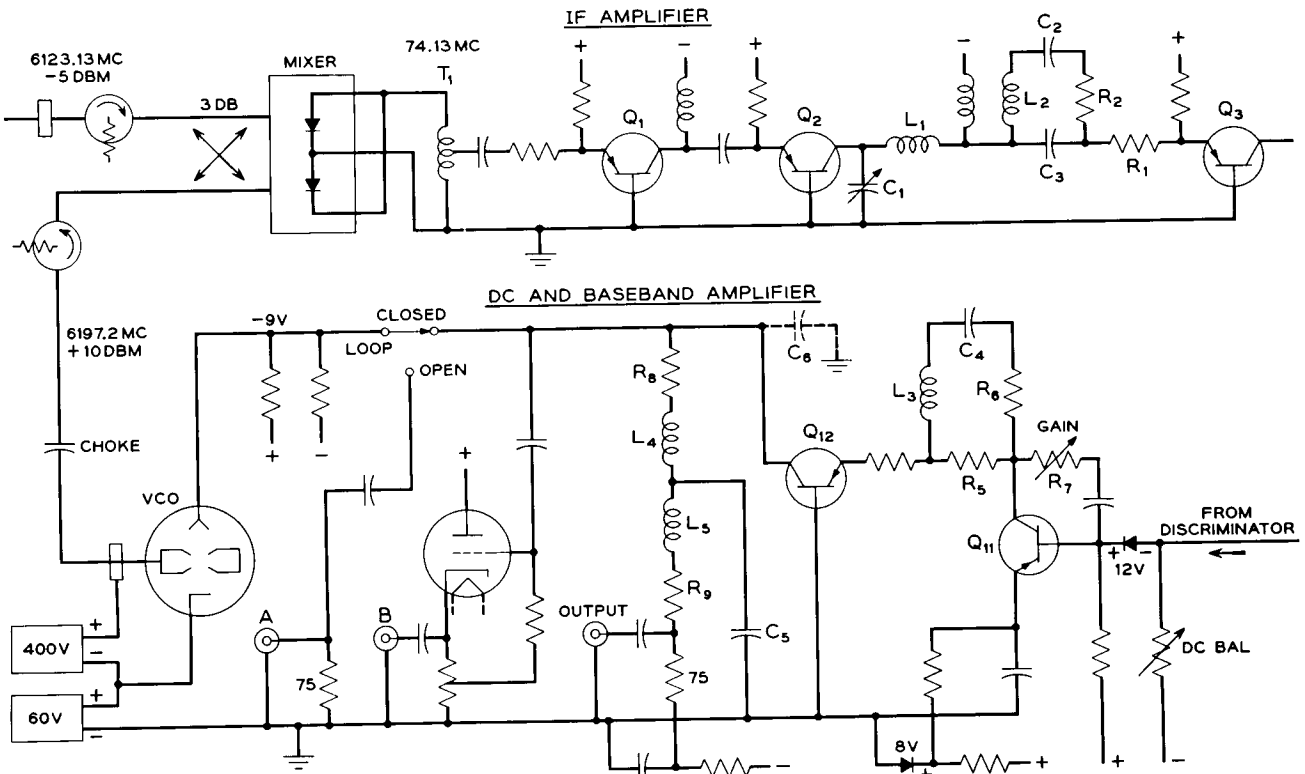

Fig. 3 — Circuit diagram of mixer, IF amplifier, VCO and dc-and-baseband amplifier.

III. CIRCUIT DESCRIPTION

Simplified schematic diagrams of the feedback receiver are shown in Figs. 3 and 4. For simplicity, conventional filtering and power supply circuit details have been omitted.

The decision to use a microwave frequency as the input to the feedback circuit was dictated by the choice of a 6-gc reflex klystron for the VCO (Fig. 3). A klystron gives very little signal delay, has good modulation sensitivity, and its linearity is excellent. The klystron used is a modified version of the WE450A tube, in which the modulation sensitivity was increased from 1.5 to 5.0 mc/volt by altering the operation from the 2-3/4 to the 3-3/4 mode, decreasing the loaded Q slightly and changing the repeller geometry.*

The repeller capacitance of only 3 pf tends to keep the delay or phase shift in the driving circuit at a low value. A second, although very small, source of delay is found in the klystron itself. It is estimated that the modulating signal is delayed by the total travel time of the electrons in the repeller field. Since the tube is working in the 3-3/4 mode, this time is about 0.6 ns at the operating frequency of 6197 mc. No delay is produced by the cavity resonator, however. The nonlinearity of the klystron is very low and amounts to a change in modulation sensitivity of less than 4 per cent at a frequency 10 mc away from midband. Since the feedback in the receiver tends to reduce the nonlinear effects of the other circuits, the klystron can be considered the main source of nonlinear distortion. Since this klystron is sensitive to a small degree of mismatch, an isolator is provided between its output and the input to the mixer. The isolator has a signal delay only slightly greater than a straight piece of waveguide of the same length.

In order to maintain the driving transistor circuits at ground potential, the negative terminal of the repeller bias source is grounded. Consequently the cavity of the klystron is at high potential, necessitating the use of an insulating waveguide choke.

The mixer is a version of the receiving modulator used in the TH radio system, modified to operate efficiently at higher local oscillator and input levels. The mixer is designed to deliver the 74-mc IF signal into a 75-ohm unbalanced load. Since the emitter of the grounded-base transistor Q_1 has a much lower impedance, a broadband autotransformer (T_1) having a 2:1 turns ratio[7] is inserted, which partly corrects this mismatch. These transformers have a bandwidth of about 150 mc.

* This modification was carried out at the Allentown Laboratories of Bell Telephone Laboratories.

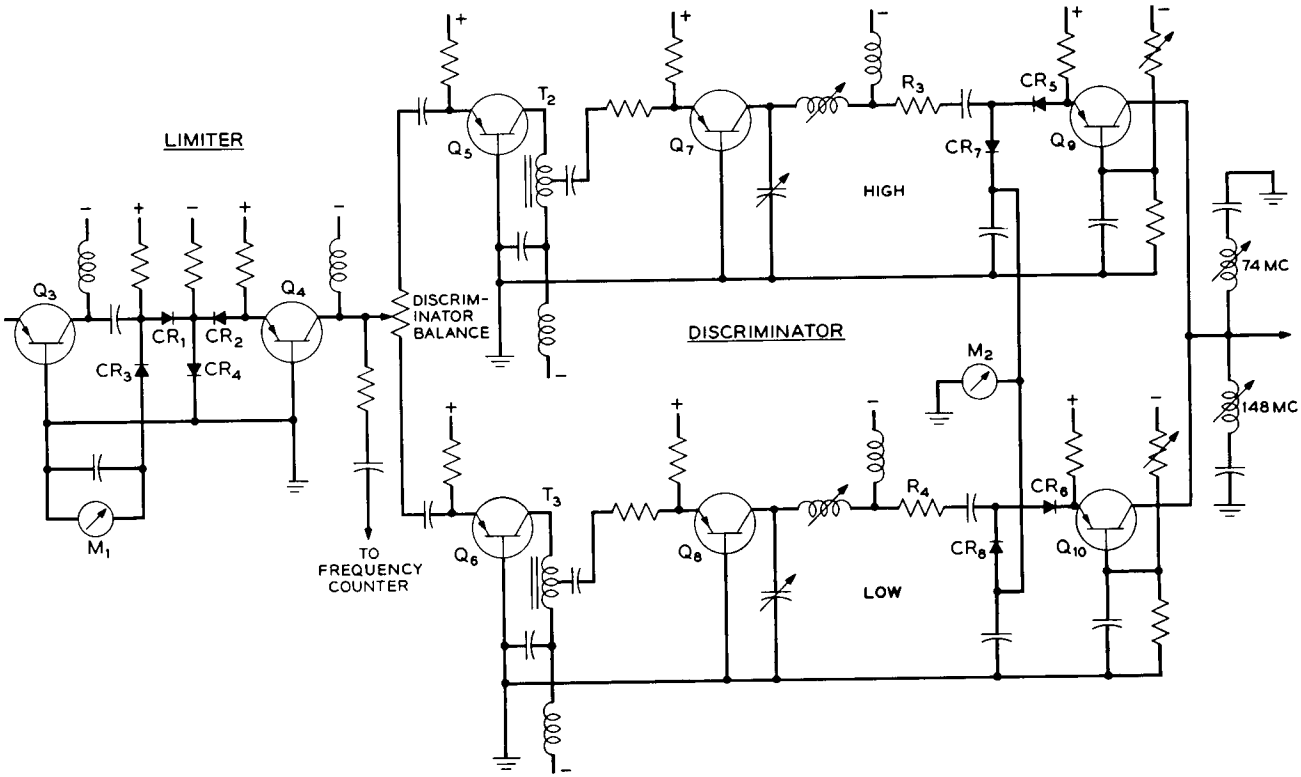

Fig. 4 — Circuit diagram of limiter and discriminator.

Diffused-base germanium transistors with alpha cutoffs above 500 mc were used throughout the circuit.

It was found that the relatively high impedance of the narrow-band IF filter network in the collector circuit of transistor Q_2 produced marked variations in the input impedance of this stage in the vicinity of resonance, even with a transistor having an $r_b'C_c$ product as low as 10 ns. In order to provide a suitable termination for the secondary of autotransformer T_1, it was necessary to introduce a buffer stage, represented by the first transistor, Q_1, to mask this effect.

The network shown in the output of the second transistor (Q_2) provides a bandpass transmission characteristic which limits the noise power delivered to the limiter-discriminator.

In the choice of a filter suitable for use at this point, several factors must be taken into consideration. From the standpoint of noise rejection, the use of a highly selective bandpass structure would be advantageous. However, such a filter would introduce a prohibitive amount of delay into the feedback loop. A simple single-pole network, on the other hand, has a much more favorable phase characteristic, but its effective noise bandwidth is 1.57 times the bandwidth between half-power points. The circuit shown is a compromise between these extremes. The tuned circuit formed by elements C_1, L_1, and R_1 alone would constitute a one-mesh filter circuit adjusted to resonate at the center of the IF band. The addition of a similar tuned circuit formed by elements C_2, L_2, R_2, loosely coupled to the first circuit through the mutual impedance of capacitor C_3, leads to a more nearly flat-topped transmission characteristic, shown in Fig. 5 by solid lines. For comparison, the characteristics of the one-mesh circuit of the same 3-db bandwidth are given by the dashed curves of Fig. 5. Although the two gain curves are superimposed in the figure, the two-mesh circuit produces a current gain which is 3 db greater than that of the one-mesh circuit. Note that the asymptotic phase shift with respect to midband is 90° for both circuits. The noise bandwidth of the two-mesh circuit is 7 mc, which is only 25 per cent higher than its 3-db bandwidth. The current gain is about 24 db. All the current gain in the IF amplifier is achieved by means of stable passive circuitry, with the common-base transistors acting as impedance transformers.

The common-base stage Q_3 feeds the IF signal to the series-type diode limiter which is shown in Fig. 4. Diodes CR_1 and CR_2 are normally conducting except at the peaks of the input wave. Diodes CR_3 and CR_4 normally do not conduct, except when diodes CR_1 and CR_2, respectively, are nonconducting.

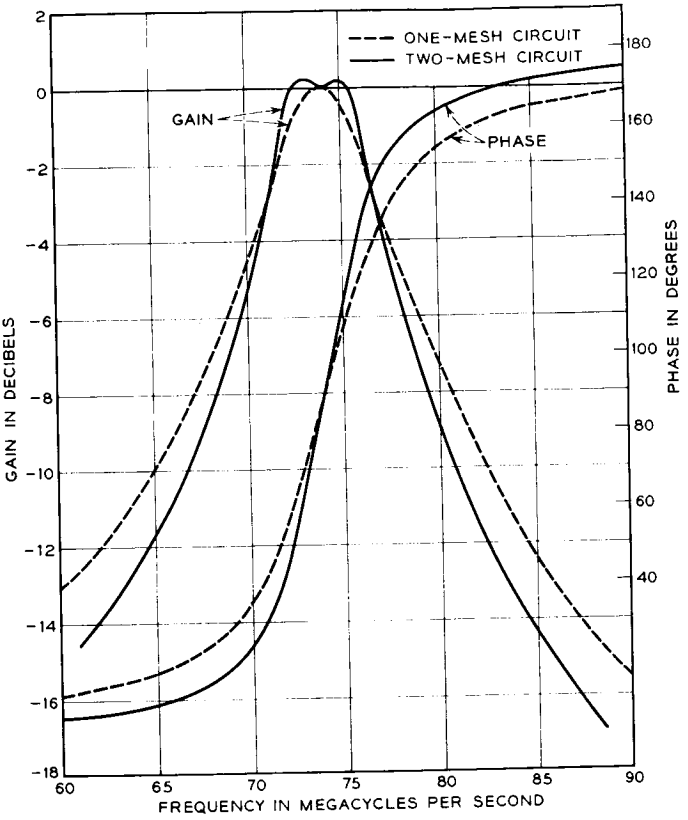

Fig. 5 — Gain and phase characteristics of narrow-band IF filter.

The limiter has no reactive elements and its impedance level is extremely low. This makes it a wideband circuit which exhibits very small signal delay. Envelope variations appearing on the input wave are reduced about 22 db by the circuit.

A dc meter M_1 in series with diode CR_3 serves as a convenient means for adjusting and monitoring the input to the limiter. The level is generally adjusted (by changing the 6123-mc input signal) so that clipping takes place about 3 db below the peaks of the IF signal.

Current delivered by the limiter is divided into two equal parts which are then subjected to 6 db of current gain in transformers T_2 and T_3 before being applied to the two inputs of a balanced discriminator. This discriminator consists of two simple resonant circuits connected to the collectors of transistors Q_7 and Q_8. One circuit is tuned to a frequency

12 mc above and the other a similar amount below the center frequency of the IF band. Damping of each circuit is adjusted by resistors R_3 and R_4 for a bandwidth of about 24 mc, so that the current gain of each branch is equal to 7 db at 74 mc.

When the incoming signal is frequency-modulated, frequency deviations give rise to amplitude variations within the two tuned circuits. These are detected by diodes CR_5 and CR_6. Diodes CR_7 and CR_8 provide a dc return in each case. These dc currents return to ground through a differential meter M_2, which gives a zero indication at midband when the two currents are equal. In order to avoid unequal biasing of diodes CR_5 and CR_6 by the emitter voltages of transistors Q_9 and Q_{10}, a bias is applied to the bases of these two transistors to make the resulting emitter voltages equal to zero.

The output of the discriminator is taken from the collectors of transistors Q_9 and Q_{10} and delivered to the dc-and-baseband amplifier shown in Fig. 3. Amplitude variations occasioned by noise will tend to cancel in the output line, thus supplementing the smoothing action of the amplitude limiter. Series-resonant circuits in the output line shunt to ground the 74- and 148-mc components which remain after the detection process.

The dc-and-baseband amplifier provides gain for the demodulated signal and delivers it to the repeller of the klystron as well as to the outgoing video line. Automatic center frequency control is accomplished by providing dc coupling within the amplifier.

In order to achieve adequate gain and phase margins within the feedback loop, it is necessary to control the open-loop gain characteristic over a wide range of frequencies — a problem common to all feedback amplifiers. This shaping of the loop has in general followed the techniques proposed by Bode.[5] The main correcting network is located in the collector circuit of transistor Q_{12} (Fig. 3). The part of the circuit consisting of C_6, R_8, and L_4, with return to ground over the large capacitor C_5, has a transmission peak at 30 mc which ensures the presence of the correct "Bode step" in the open-loop transmission characteristic. Below 30 mc, the gain of the last stage decreases and eventually rises again to a constant value at about 1 mc because of the presence of another shunt peaking network L_5, R_9, and C_5.

The common-emitter stage Q_{11} provides some minor shaping by means of the local feedback circuit consisting of R_7 together with R_5, R_6, C_4, and L_3. Increased gain is obtained for the "Bode fillet" at 1.25 mc, which is the resonant frequency of the series circuit R_6, C_4, L_3. The gain of Q_{11} otherwise is very flat up to about 40 mc, and can be

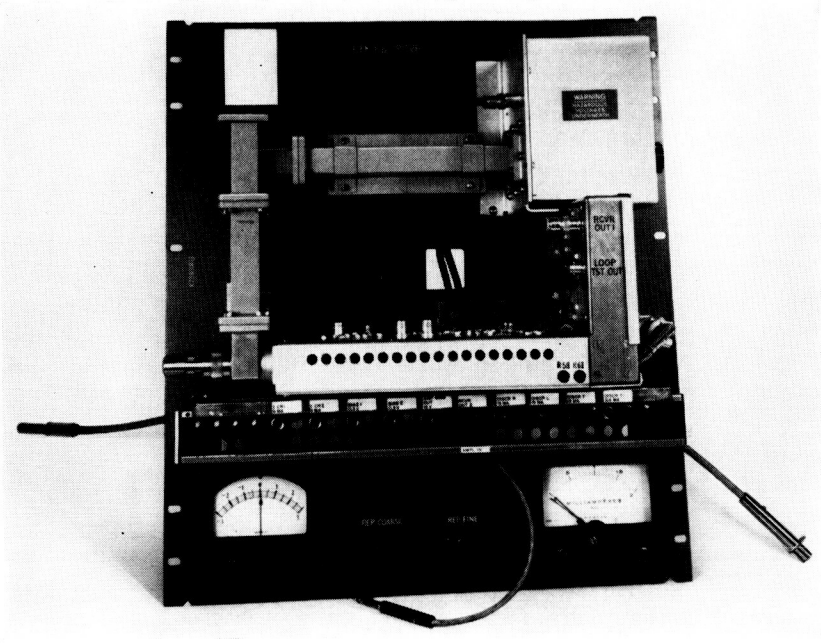

Fig. 6 — Photograph of FMFB receiver.

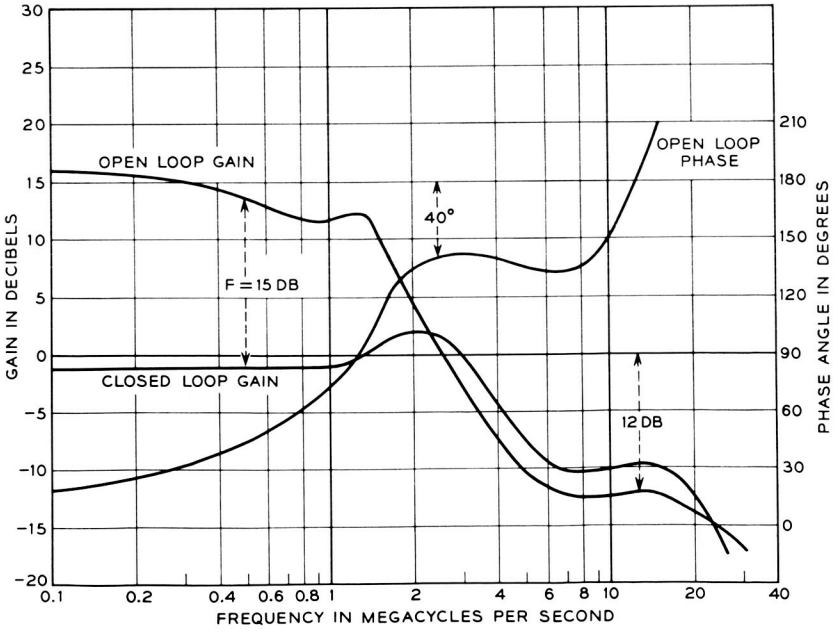

Fig. 7 — Open- and closed-loop transmission characteristics.

varied by R_7 over the range of 2 to 12 db. The normal setting is around 6 db, which results in a feedback of 15 db at 0.5 mc.

The gain characteristic of the loop is also well controlled down to dc by various circuits — not separately described — in the dc-and-baseband amplifier.

Baseband signals to be delivered to the outgoing line are taken from a 75-ohm impedance point within the main equalizing network. Transmission to this point differs markedly from the actual loop characteristic at frequencies above the usual baseband, in that frequencies higher than 3 mc are greatly attenuated. This effect is symbolized by the low-pass filter shown in Fig. 1.

The actual open-loop performance is measured by opening the loop with the switch in Fig. 3, applying baseband signals to the repeller at point A, and observing the voltage which appears at the collector of Q_{12}. Since this is a relatively high-impedance point, a cathode follower is permanently connected to the collector. The cathode impedance of this device is sufficiently low that standard low-impedance measuring devices can be connected at point B. The closed-loop characteristic is likewise measured at point B, with the loop switch in the closed position and a frequency-modulated 6123-mc signal applied to the input of the mixer.

A photograph of the FMFB receiver is shown in Fig. 6. The box housing the klystron (VCO) is shown on the upper right. The mixer on the lower left is attached to the horizontal part of the chassis, which contains the IF amplifier, limiter and discriminator. The dc-and-baseband amplifier is located in the vertical part of the chassis. The equalizers and the output amplifier are not shown in the photo.

IV. MEASUREMENTS

4.1 *Transmission Characteristics*

Gain and phase characteristics of the open loop are shown in Fig. 7. With the feedback F set to 15 db at 0.5 mc, the phase and gain margins are seen to be 40° and 12 db, respectively. Not shown in the figure is the transmission characteristic below 100 kc. Towards the very low frequencies the loop gain is permitted to increase slowly, so as to obtain about 5 db of additional gain at 15.75 kc. This is advantageous from the standpoint of television signals.

The gain with the loop closed is also shown in Fig. 7. In this case, a reflex klystron was used as the source of the 6123-mc FM signal. The closed-loop characteristic exhibits the typical region of gain enhance-

ment in the vicinity of the open-loop gain crossover. This region is strongly affected by the gain in the feedback loop. More gain would increase the transmission bulge around 2 mc, and in turn increase the closed-loop noise bandwidth. Less gain would cause insufficient frequency compression in the loop. With a feedback of 15 db, the closed-loop noise bandwidth at baseband was found to be about 7.5 mc, or $B_c = 15$ mc.

Since the effect of the gain enhancement around 2 mc is also seen at the useful output terminal of Fig. 3, a compensating high-frequency equalizer is included ahead of the output amplifier, as indicated in Fig. 1. The increase of gain in the open loop below 50 kc affects the closed-loop characteristic by about 1.3 db. A low-frequency equalizer makes the transmission flat to about 0.2 db down to a few hundred cycles. Transmission to the output of the output amplifier is shown in Fig. 8.

4.2 *Excess Phase Problems*

The problem of excess phase will now be dealt with in some detail because of its importance to present and future wideband feedback receivers. The term "excess phase" is used to indicate phase shift in excess of the theoretically determined minimum phase associated with the open-loop transmission characteristic. An obvious contribution to excess phase arises from the physical dimensions of the loop structure itself. In the present instance it is estimated that this can account for a delay of about 3.5 ns. In terms of phase, this would introduce a linear phase shift

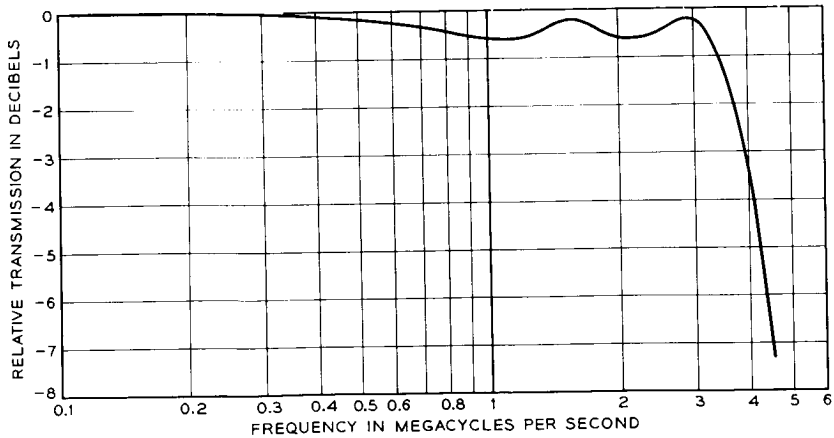

Fig. 8 — Over-all transmission characteristic.

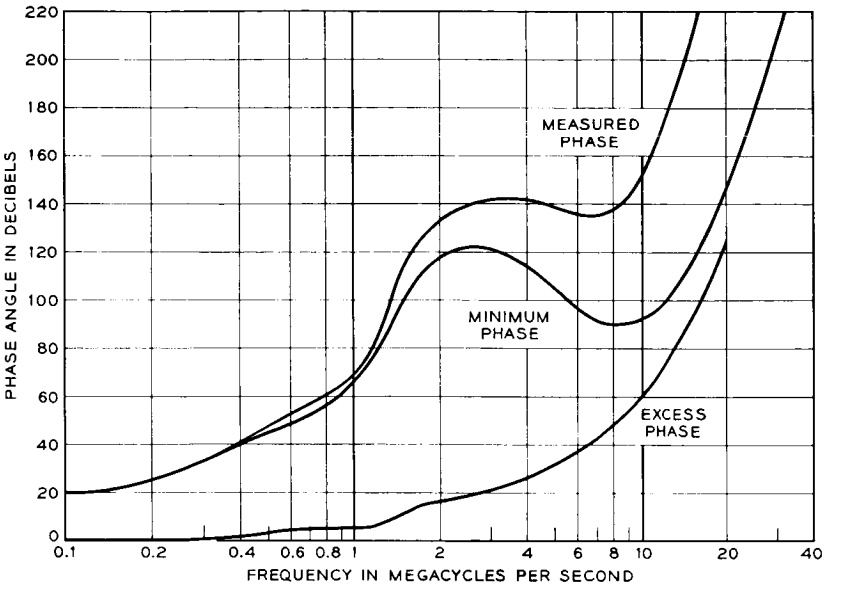

Fig. 9 — Measured and computed minimum phase characteristic of the open loop.

amounting to 1.27 degrees per megacycle. Though not negligible, the restriction thus imposed upon loop performance is rather small. Actually, a much greater amount of excess phase has been observed. This is illustrated in Fig. 9, which shows the computed minimum phase characteristic based upon the measured open-loop transmission. This curve is an approximation because of some degree of uncertainty regarding the cutoff performance at very high frequencies, in the region between 30 and 100 mc. However, conditions at these rather remote frequencies have only a minor influence upon the region of greatest interest.

Shown for comparison is the measured phase characteristic. The difference between these two curves closely follows the linear law of about 6 degrees per megacycle. This is five times as great as that estimated from the physical dimensions of the feedback loop. Several additional sources have been identified. Transistors are known to introduce a measure of excess phase. Measurements made at intermediate frequencies with a single common-base stage, such as is used at many points within the receiver, show excess phase amounting to about 0.2° per megacycle. Since there are in effect eight such stages within the loop, the total contribution of 1.6° per megacycle is not negligible.

TABLE I — SOURCES OF EXCESS PHASE

Source	Estimated Phase
Loop dimensions	1.3°/mc
8 common-base stages	1.6°/mc
Limiter	0.5°/mc
Common-emitter stage	2.0°/mc
Total	5.4°/mc
Measured	6.0°/mc

Considerable excess phase is associated with the common-emitter stage Q_{11} of the baseband amplifier. This amounts to about 2° per megacycle.

The limiter was found to have an essentially linear phase characteristic which, allowing for the input and output transistors, indicated a phase contribution of 0.5° per megacycle. Negligible phase shift is caused by the estimated 0.6 ns of delay in the klystron.

Adding these several contributions, we can account reasonably well for the difference between the minimum phase and the observed open-loop performance as indicated in Table I.

4.3 *Measurements near Threshold*

In order to obtain a better insight into the rather complicated mechanisms responsible for the performance near threshold, several types of measurements were performed on the FMFB receiver and on a conventional or standard FM receiver. The latter was taken from the TH radio system.[8] In order to produce the desired CNR's near threshold, flat thermal noise of 25-mc bandwidth was mixed with the FM signal at the intermediate frequency of 74 mc. This signal was then directly applied to the standard FM receiver, but translated to 6123 mc in a modulator for application to the FMFB receiver.

4.3.1 *Baseband Noise Spectra*

Baseband noise spectra were measured for CNR's ranging from 0 to 22 db. For this purpose, a sensitive analyzer with a 4-kc bandwidth was connected to the output of the receivers and readings were taken over the range from 100 kc to 5 mc. The solid curves of Figs. 10 and 11 show samples of these measurements taken on the standard and the FMFB receivers, respectively, for the case where the carrier is unmodulated. The noise readings were corrected where necessary so as to simu-

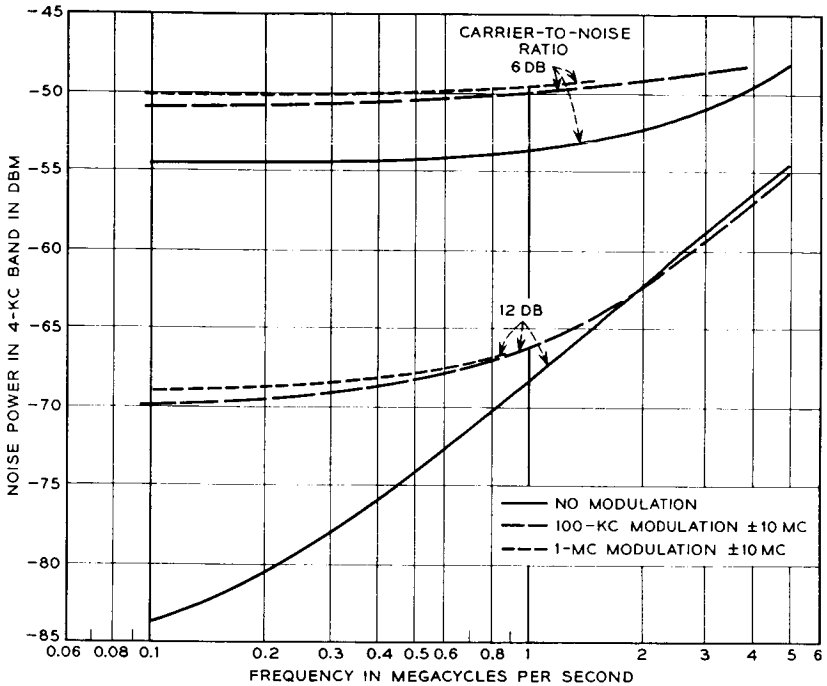

Fig. 10 — Noise spectra for standard FM receiver.

late absolutely flat receiver gain characteristics from 100 kc to 5 mc. At the higher CNR's, and for frequencies above a few hundred kilocycles, the spectra show the typical triangular characteristic of FM noise. When the CNR is decreased, the noise rises much faster at low frequencies, to produce ultimately the fairly flat noise spectra which were calculated by S. O. Rice[9] for the standard FM receiver. It has been known for some time that the baseband noise increases to some extent when modulation is applied to the FM carrier,[10] but the literature on the subject is very sparse. It was therefore decided to measure noise spectra in the presence of full ±10-mc sine-wave modulation. Such measurements are of somewhat limited practical value, because a single tone will only rarely be transmitted with the maximum frequency deviation. This is the case, however, in a number of TV test patterns, especially the "multiburst" pattern. Occasionally, such a situation may also arise in live TV signals for short periods of time. Examples of the results of modulation measurements are also shown in Figs. 10 and 11. A drastic difference exists between the standard and the FMFB re-

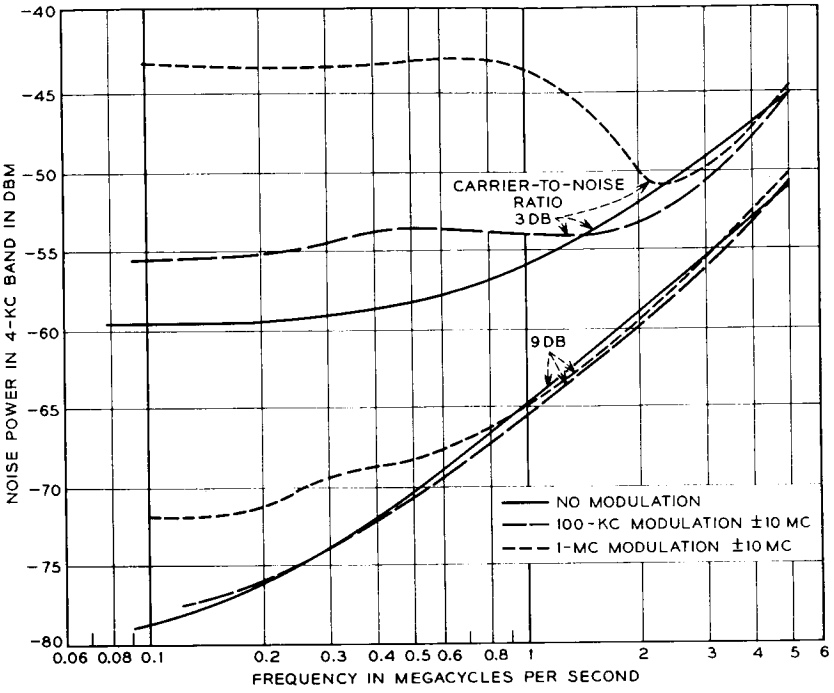

Fig. 11 — Noise spectra for FMFB receiver.

ceiver. The former shows an increase in noise which is nearly independent of the modulating frequency. The FMFB receiver, on the other hand, is little affected by a 100-kc modulating signal but much more so by a 1-mc signal, especially at low CNR's. The strongest effect of the modulation is seen at the low-frequency end of the noise spectrum, particularly in the case of the standard FM receiver at high CNR's.

4.3.2 *Threshold Curves*

The behavior of an FM system above and around the threshold region is often described by plotting the ratio of the signal power to the total noise power (SNR) in a baseband b, as a function of the CNR at RF in the bandwidth B. The total noise power in a 2-mc baseband was first determined for the case of no modulation by integrating a set of curves, of which the solid ones in Figs. 10 and 11 are a part. The result is shown in Fig. 12 as curves 1 and 3.

When modulation is applied, two effects are to be noted. One is the

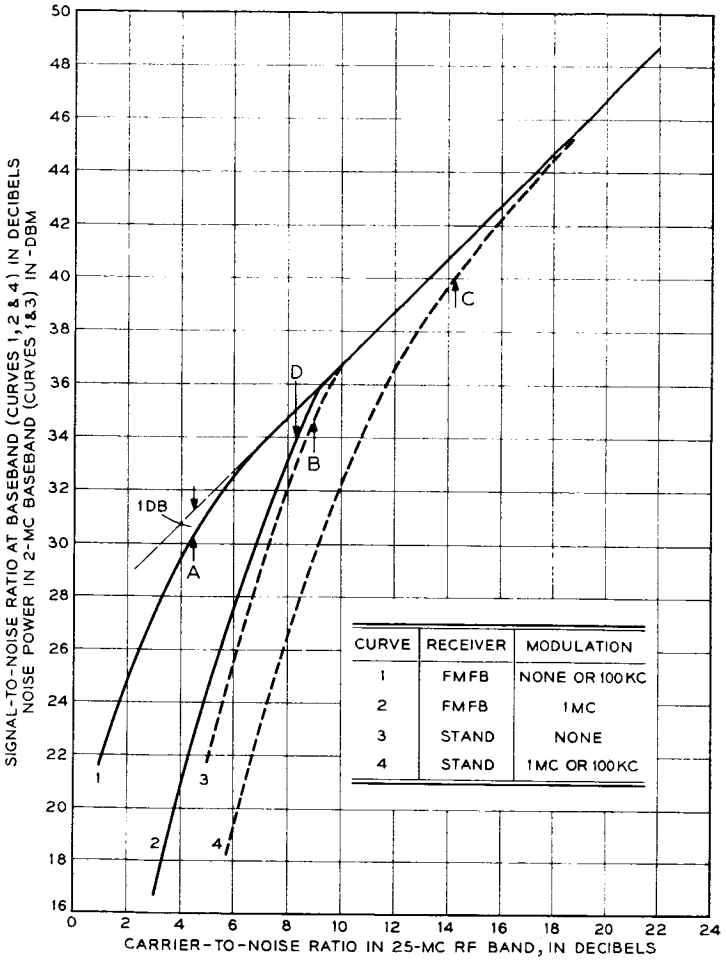

Fig. 12 — Signal-to-noise ratio at baseband.

increase in noise mentioned above. The other is a reduction in recovered signal level when the CNR is rather low. These effects shall be called noise increment and signal reduction, respectively. Noise increments for various CNR's were obtained by integrating spectra such as those shown in Figs. 10 and 11 for the case of full modulation. The results are shown in Fig. 13 for the two types of receivers. The increment is actually negative under some conditions — meaning that the total baseband noise is slightly less than for the case of the unmodulated carrier. This can be seen from the modulation curves of Fig. 11.

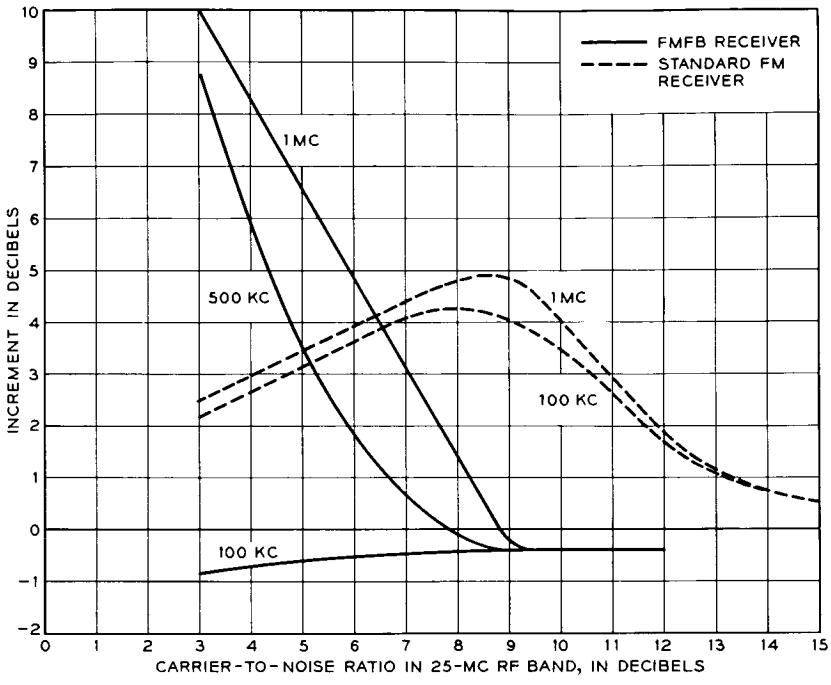

Fig. 13 — Noise increments.

Signal suppression was determined with the aid of a selective analyzer tuned to the signal frequency as the CNR was varied. Fig. 14 shows the performance which was observed.

The actual SNR in the 2-mc baseband can now be determined. The

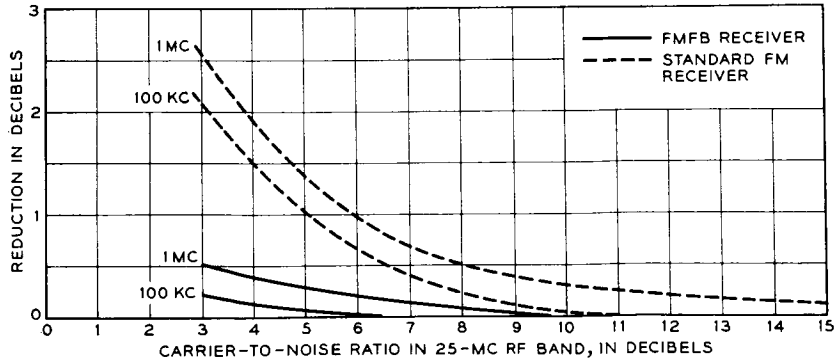

Fig. 14 — Signal reduction.

results are given in Fig. 12 as curves 1, 2, and 4. A few simplifications were made in this figure. Curves 1 and 4 are accurate only for no modulation and 1-mc modulation, respectively, and the 100-kc curves would actually be a few tenths of a db higher. Slight differences of about 0.5 db between the actual curves 1 and 3 and the calculated curve at high CNR's were neglected and made equal to the theoretical value given by equation (2).

The curves of Fig. 12 show clearly the advantage of the FMFB receiver over the standard receiver in the threshold region. An advantage of 4.5 db is obtained for the case of no modulation by taking the difference between the threshold points A and B. For 100-kc modulation the threshold improvement is 9.8 db ($C - A$), and for 1 mc it is 5.9 db ($C - D$). Curves similar to 3 and 4 were calculated by Rice.[10] No theory is yet available which would produce curves 1 or 2 for the FMFB receiver.

The threshold situation for actual signals such as TV and carrier multiplex requires further exploration by subjective tests and noise loading measurements, respectively. Such tests are described in the following two sections.

4.3.3 *Television Threshold Tests*

Fig. 15 shows the results of TV threshold tests. The peak-to-peak deviation produced by the television signal (including the sync pulse) was set to be 14 mc. An aural subcarrier at 4.5 mc, which deviated the main carrier by 2.8 mc peak-to-peak, was also transmitted. The television spectrum was restricted on the transmitting side by the insertion of a well-equalized 3-mc roll-off filter. Fig. 15 shows that the television patterns are still recognizable down to very low CNR's, especially when the FMFB receiver was used. A large number of subjective tests have shown threshold improvements of about 4 to 5 db. These pictures, as well as all the data described above, were taken with the FMFB receiver adjusted for a feedback of 15 db at 500 kc and its discriminator balance set for equal numbers of white and black noise dots. The 15-db figure was found to be a good compromise, giving a small enough closed-loop bandwidth (and therefore low noise) and still enough feedback to make high-frequency breaking due to lack of feedback not too conspicuous. A live TV picture occasionally contains very strong high-frequency components which show up as sharp vertical lines. Since there is not enough feedback available to keep the frequency deviation within the passband of the narrow IF filter, the signal at the discriminator will be below the breaking point at the deviation peaks. Breaking

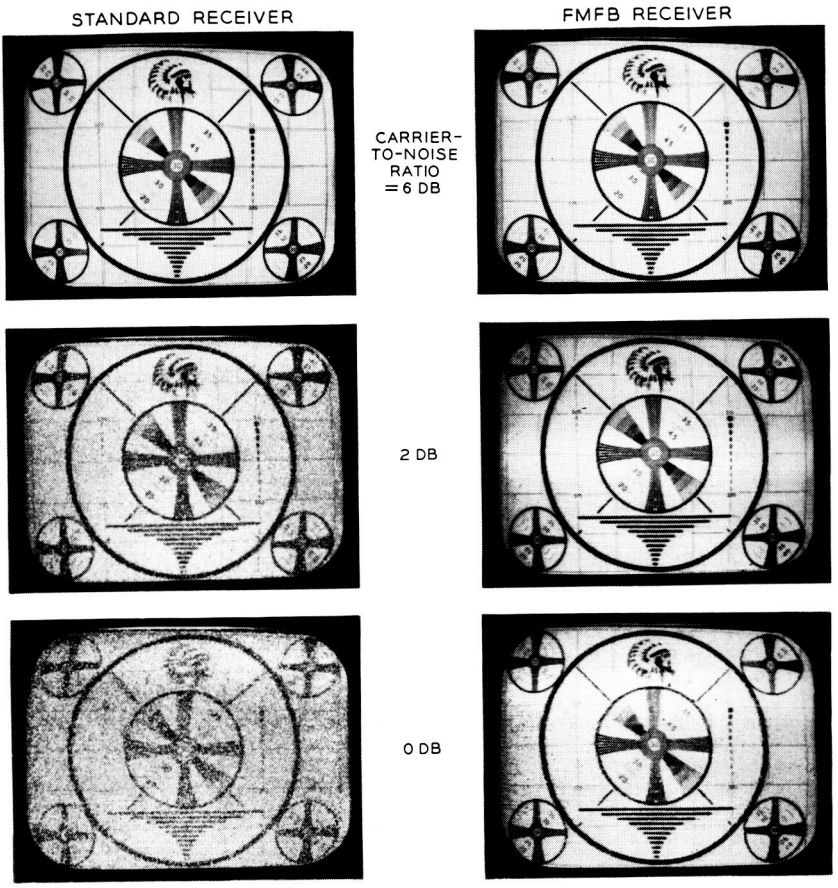

Fig. 15 — TV threshold tests.

which starts at a white peak produces a trailing black dot, and correspondingly a black peak generates a white noise dot. The nonrandomness of this breaking process makes it appear as a characteristic "sparkling" on the screen. It should be mentioned that the sparkling effect is not responsible for the strong increase in noise shown in Fig. 13 for 500 kc and 1 mc. Randomness of the noise in this case is still maintained, as observed on the oscilloscope.

The foregoing description makes it clear that TV pre-emphasis should not be used in a system containing the FMFB receiver of the present design. It is even desirable to insert a baseband roll-off filter in the transmitter in order to restrict the high-frequency components of the picture.

Tests with TV pre-emphasis were made, and it was found that the sparkling effect was strongly enhanced. This is due to the fact that the relatively short bursts of noise which cause the sparkle are integrated or lengthened in the de-emphasis network.

The FMFB receiver has also been tested with color TV signals. The behavior near threshold was found to be excellent if program material was transmitted, but rather poor if the color-bar pattern was used.

4.3.4 *Noise Loading Tests*

Tests were made to describe the behavior of the two types of receivers in the threshold region under conditions of a simulated telephone load. The telephone multiplex signal is simulated for this purpose by a noise signal with a flat spectrum, which in turn frequency modulates the RF carrier. Tests were made with 120, 240, and 600 channels. The noise-power ratio was measured at the receiver outputs in a number of frequency slots as a function of the total rms frequency deviation. The

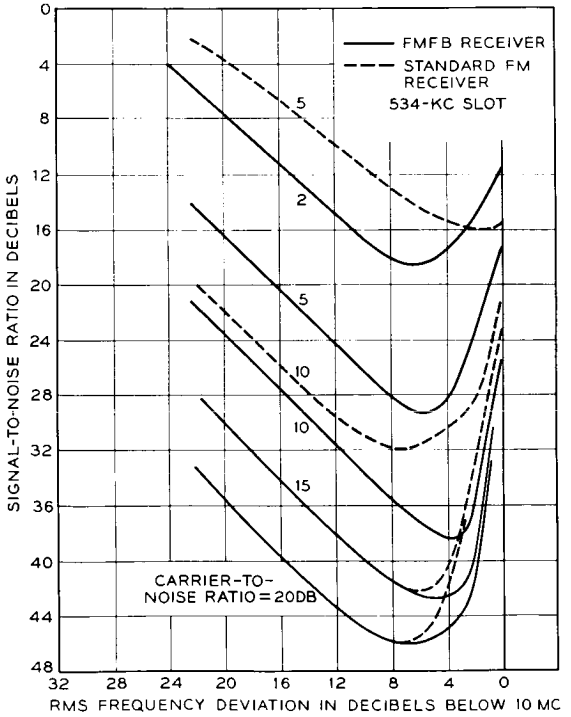

Fig. 16 — 240-channel noise loading.

noise-power ratio is the ratio of signal-plus-noise to noise, with the noise consisting of thermal and intermodulation noise. This ratio is essentially equal to the SNR for values greater than 10 db. Conditions existing in the vicinity of the threshold were established by injecting a 25-mc band of noise into the signal path. The bandwidth of the signal path exceeded the noise bandwidth by about 10 mc. Nonlinear distortions due to band limitations preceding the FM receivers were therefore reduced.

Fig. 16 shows results of 240-channel noise loading tests with a noise spectrum extending from 60 to 1052 kc and the test channel located at 534 kc. The FMFB receiver was found to have slightly more random noise, which is believed to be due to the $1/f$ noise generated in the transistors of the feedback circuit. In Fig. 16 the excess noise effect was subtracted from the original data of the FMFB receiver. Fig. 16 shows a clear advantage of using the FMFB receiver. For 600 channels the SNR should be greater than 31 db, which is consistent with recommendations of CCIR for satellite systems. This corresponds to 40 dbrn at the zero

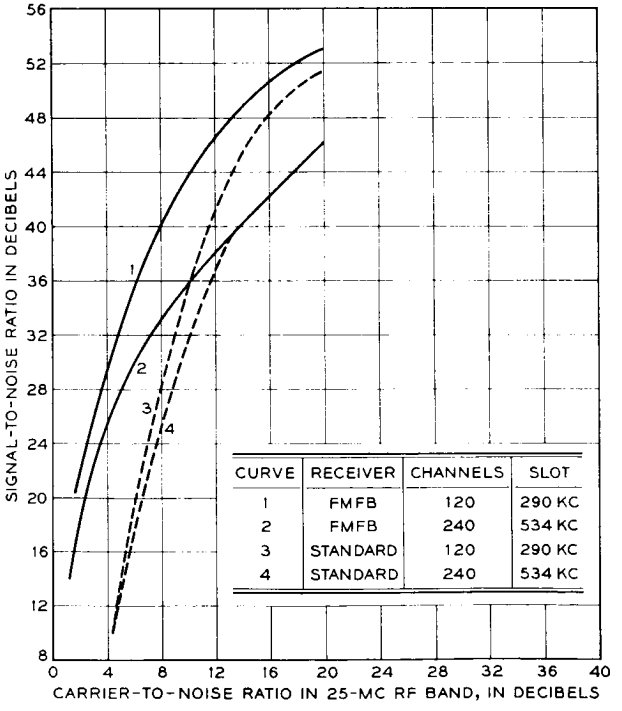

Fig. 17 — Noise loading tests; threshold region.

transmission level point. Curves were also taken at 70 and 1002 kc. They are not different in character, except that the values for SNR are higher for 70 kc and lower for 1002 kc than the ones given in Fig. 16.

With 600-channel noise loading, intermodulation in the feedback receiver begins to appear at lower modulation levels. This is due to the insufficient amount of feedback available in the circuit at higher frequencies. No useful advantage can be obtained from the present FMFB receiver in this case.

In order to show the behavior near threshold more clearly, the curves of Fig. 17 were plotted. They show the SNR in a channel as a function of the CNR at RF. An rms frequency deviation 8 db below 10 mc, or 4 mc, was chosen for these curves. The curves will eventually reach a horizontal asymptote at high CNR's. The noise will then be entirely due to intermodulation. Threshold improvements of about 4 to 5 db can be observed in Fig. 17.

V. ACKNOWLEDGMENT

The authors wish to acknowledge the help of H. A. Gifford in building and testing the FMFB receiver.

REFERENCES

1. Chaffee, J. G., United States patent 2,075,503, granted March 30, 1937; see also Chaffee, J. G., The Application of Negative Feedback to Frequency Modulation Systems, Proc. I.R.E., **27,** May, 1939, pp. 317–331.
2. Ruthroff, C. L., FM Demodulators with Negative Feedback, B.S.T.J., **40,** July, 1961, pp. 1149–1156.
3. Giger, A. J., Pardee, S., Jr., and Wickliffe, P. R., Jr., The Ground Transmitter and Receiver, B.S.T.J., this issue, p. 1063.
4. Ruthroff, C. L., and Bodtman, W. F., Design and Performance of a Broadband FM Demodulator with Frequency Compression, Proc. I.R.E., **50,** December, 1962, pp. 2436–2445.
5. Bode, H. W., *Network Analysis and Feedback Amplifier Design,* D. Van Nostrand Company, Inc., New York, 1945.
6. Enloe, L. H., Decreasing the Threshold in FM by Frequency Feedback, Proc. I.R.E., **50,** January, 1962, pp. 18–30.
7. Ruthroff, C. L., Some Broadband Transformers, Proc. I.R.E., **47,** August, 1959, pp. 1337–1342.
8. Houghton, E. W., and Hatch, R. W., FM Terminal Transmitter and Receiver for the TH Radio System, B.S.T.J., **40,** November, 1961, pp. 1587–1626.
9. Rice, S. O., Statistical Properties of Sine Wave Plus Random Noise, B.S.T.J., **27,** January, 1948, pp. 109–157.
10. Rice, S. O., Noise in FM Receivers, *Time Series Analysis,* ch. 25, ed. H. Rosenblatt, John Wiley & Sons, New York, 1963.